5

MARTIN MARIETTA ENERGY SYSTEMS LIBRARIES

3 4456 0059314 1

ORNL-2806
Health and Safety
TID-4500 (15th ed.)

HEALTH PHYSICS DIVISION ANNUAL PROGRESS REPORT

FOR PERIOD ENDING JULY 31, 1959

CENTRAL RESEARCH LIBRARY
DOCUMENT COLLECTION
LIBRARY LOAN COPY
DO NOT TRANSFER TO ANOTHER PERSON
If you wish someone else to see this document, send in name with document and the library will arrange a loan.

OAK RIDGE NATIONAL LABORATORY
operated by
UNION CARBIDE CORPORATION
for the
U.S. ATOMIC ENERGY COMMISSION

Printed in USA. Price $3.50. Available from the
Office of Technical Services
Department of Commerce
Washington 25, D.C.

LEGAL NOTICE

This report was prepared as an account of Government sponsored work. Neither the United States, nor the Commission, nor any person acting on behalf of the Commission:

A. Makes any warranty or representation, expressed or implied, with respect to the accuracy, completeness, or usefulness of the information contained in this report, or that the use of any information, apparatus, method, or process disclosed in this report may not infringe privately owned rights; or

B. Assumes any liabilities with respect to the use of, or for damages resulting from the use of any information, apparatus, method, or process disclosed in this report.

As used in the above, "person acting on behalf of the Commission" includes any employee or contractor of the Commission, or employee of such contractor, to the extent that such employee or contractor of the Commission, or employee of such contractor prepares, disseminates, or provides access to, any information pursuant to his employment or contract with the Commission, or his employment with such contractor.

ORNL-2806
Health and Safety
TID-4500 (15th ed.)

Contract No. W-7405-eng-26

HEALTH PHYSICS DIVISION ANNUAL PROGRESS REPORT

For Period Ending July 31, 1959

K. Z. Morgan, Director

DATE ISSUED

OCT 23 1959

MARTIN MARIETTA ENERGY SYSTEMS LIBRARIES
3 4456 0059314 1

OAK RIDGE NATIONAL LABORATORY
Oak Ridge, Tennessee
operated by
UNION CARBIDE CORPORATION
for the
U. S. ATOMIC ENERGY COMMISSION

CONTENTS

WASTE DISPOSAL RESEARCH AND ENGINEERING 1

Low-Level Waste Water Treatment 1
- Evaluation of Plant Performance 1
- An Experimental Procedure for Optimizing Treatment Efficiency 3

Disposal of ORNL Liquid Wastes 7
- Studies of Soil Disposal Facilities 7
- Clinch River Studies 9
- Development of Improved Well Probe 9
- Soil Column Studies 10

Burial of Solid Wastes 12
- Studies of Burial Areas in Melton Valley 12
- Explorations of Potential Burial Sites in Bear Creek Valley 16

Ecological Research 16
- White Oak Lake Bed Studies 16
- Forest Studies 37

Sorption and Retention by Clay Minerals 54
- Mix Formulations for Sintering 55
- Cesium Fixation by Ion Exchange 57
- Characterization of Fixation Mechanism 59

Disposal in Salt Formations 66
- Thermal Calculations 66
- Structural Properties of Rock Salt 69
- Materials Study 76
- Model Experiments 81
- Field Salt Disposal Experiments 85
- Cooperation with Other Agencies 98

Disposal in Deep Wells 98
- Cooperation with Other Agencies 98
- Laboratory Studies 99

Hazards Evaluation of Tank Storage 106
- Tank Storage 107
- Basic Premises 107
- Site Parameters 108
- Activity Distribution 110
- Power Generation 112
- Hazards Evaluation 112

Related Cooperative Projects 118
- Geologic and Hydrologic Studies by the U.S. Geological Survey 118
- Testimony at Joint Congressional Committee Hearings 118
- Review of Backflow Preventers for Protection of ORNL Water Supply 118
- Review of ORNL Waste Disposal Practice 119
- Preliminary Observations on Aerosol Emissions from High-Level Liquid Wastes During Storage 119
- NS "Savannah" Hazard Study 119
- Editorial Staff 119
- American Standards Association Sectional Committees 120
- American Public Health Association Committee on Radiological Health 120
- AEC Ecological Review Committee 120
- ORSORT Course in Physical Geology 120

RADIATION PHYSICS AND DOSIMETRY 121
Dosimetry Applications 121
Ichiban Project 121
Glass Dosimetry 123
Measurement of Leakage Radiation from Critical Assemblies 125
Blood Na^{24} Studies 125
Dosimetry of the Y-12 Accident 127
Theoretical Physics of Dosimetry 133
The Behavior of Plasma at Ionic Resonance 133
Occurrence of Vavilov-Cerenkov Radiation in a High-Temperature Plasma 133
Thermal Neutron Flux Depression 133
Radiation of Photons by Films Bombarded by Charged Particles 136
Image Force at a Metal Surface from the Hydrodynamic Theory of the Free Electron Gas 138
Monte Carlo Calculations of the Penetration of Weapons Radiation in Air 141
Physics of Tissue Damage 142
Rochelle Salt Radiation Damage 142
Thermoluminescence Studies of Ferroelectrics 143
Radiation Aging and Information Theory 146
Experimental Physics of Dosimetry 150
Electron Capture in O_2 150
Pulse-Height–Energy Curve of Anthracene for Monoenergetic Electrons and the Energy Intercept 153
Plasma Light Experiment 155
Measurement of Electron Flux in Media Bombarded by X Rays 156
Measurement of Electron Stopping Power at Low Energies – Scattering Effects 163
Studies on Personnel Dosimeters 167
Angular Response of a Partially Shielded Cylindrical Dosimeter 170
Dosimetry Techniques 173
Threshold Detector Program 173
Dosimetry Program for Criticality Accidents 175
Radsan Fast Neutron Dosimeter Developments 175
Assistance to Other Installations 183
Gamma Dosimetry Developments 184
INTERNAL DOSIMETRY 185
Applied Radiobiology 185
Inhalation Studies 185
Aerosol Project 186
Distribution and Excretion Studies 191
Instrumentation 192
Autoradiographic Studies 194
Internal Dose Estimation 194
Inorganic Analysis of Human Tissue 194
Dose to Gastrointestinal Tract from Ingested Radionuclides 200
Dose to the Gonads from Radionuclides Present in Food or Water 201
Internal Dose Handbooks 206

EDUCATION, TRAINING, AND CONSULTATION 208
AEC Fellowship Program 208
Other Activities 208
PUBLICATIONS 209
PAPERS 211
LECTURES 214

HEALTH PHYSICS ANNUAL PROGRESS REPORT

WASTE DISPOSAL RESEARCH AND ENGINEERING

LOW-LEVEL WASTE WATER TREATMENT

K. E. Cowser H. J. Wyrick D. A. Gardiner[1]

Evaluation of Plant Performance

The amount of radioactivity released to White Oak Creek from ORNL during 1958 was the lowest annual discharge on record.[2] This reduction of radioactivity can be attributed to the operation of the process waste water treatment plant.

The rate of flow through the plant is kept constant at 300 gpm. About 20 gpm is added to this flow by the three chemical feeders. During the first five months (September 1957 through January 1958) the plant was operated only five days a week and 4.3×10^7 gal of process waste amounting to 34% of the total volume was treated. In the next 14 months, with continuous operation, 17.6×10^7 gal of waste was treated, accounting for 62% of the total. Process waste that is not treated is selectively diverted to the settling basin and generally has a low concentration of radioactivity; however, in several instances process waste was released without treatment because of the limited capacity of the treatment system. The efficiency of treatment is determined by radiochemical analyses of composite samples of the plant influent and of the effluent. As shown in Table 1, Sr^{90}, Cs^{137}, and total rare earths are the major contributors to the gross radioactivity in the waste.

The percentage removals and the amounts of individual radionuclides removed are listed in Table 2. During the first six months, various amounts and combinations of lime and soda ash were fed; therefore, over-all plant efficiency varied. Since March 1958 the stoichiometric amount of lime and 200 ppm of excess soda ash have been added to the waste. Strontium removals during this interval averaged 84% and were as high as 94% during some weeks. Total rare earths were removed as efficiently as the strontium.

Lime-soda softening is not effective in removing cesium. Prior to the continuous addition of clay (Grundite[3]), which was begun in September 1958, cesium removals were erratic ranging from zero removal to 42% removal, and were probably influenced by the amount of silt in the equalization basin. The addition of 100 ppm of Grundite resulted in an average removal of 80% of the cesium, while at 150 ppm, 85% of the cesium was removed. Cobalt removal averaged 67%. Ruthenium removal averaged 58%. The reduction of gross radioactivity is dependent on the radionuclide composition of the waste and the types and amounts of chemicals that are fed. Through September 1958 the removal of gross radioactivity averaged 66%; since then the average removal has been 85%.

A total of 104 curies of Sr^{89} and Sr^{90}, 124 curies of total rare earths, 66 curies of Cs^{137}, 10.9 curies of Co^{60}, and 5.9 curies of Ru^{106} were removed. The radionuclides removed were associated with the calcium carbonate and magnesium hydroxide precipitate resulting from the addition of lime and soda ash and with clay. For the first 19 months of operation 641,000 gal of sludge containing an average of 51% solids by volume was transferred by trailer truck to waste pit No. 3.

The plant cannot treat all of the waste. To optimize the removal of radionuclides from the total volume of waste, it is necessary to treat that portion of the waste having the greatest concentration of radioactivity. Continuous operation of the plant began in February 1958; since that time, 62% of the process waste was treated while 72% of the strontium in the total waste stream was removed. This indicates that the waste treated had a higher concentration of strontium than waste diverted to the settling basin.

Weekly composite samples were analyzed for calcium hardness and total hardness as well as for strontium and total rare earths. The percentage removals of strontium and total rare earths were plotted as functions of the residual calcium in the plant effluent (Figs. 1 and 2). As calcium residuals increase, the percentage removal of strontium decreases, and the apparent relationship is expressed as a coefficient of correlation of −0.74; the 95% confidence limits are −0.57 and −0.86. Similarly, the coefficient of correlation between calcium residuals and total rare earths is −0.66, with 95% confidence limits of −0.45 and −0.79. The real meaning of these relationships

---

[1] Mathematics Panel, ORNL.

[2] *Operations Division Quarterly Report, October–December 1958*, ORNL CF-58-12-147, p 75.

[3] Produced by the Illinois Clay Products Company, Joliet, Illinois. It contains 65 to 75% illite, 10 to 20% kaolinite, and 5 to 15% quartz.

Table 1. Concentration of Radionuclides in Treatment Plant Influent and Effluent

Monthly composite samples

Gross beta activity in units of counts/min/ml referred to second-shelf counting using an end-window Geiger counter; Sr^{89}, Sr^{90}, TRE, Cs^{137}, Co^{60}, and Ru^{106} in units of disintegrations/min/ml

Date	Influent							Effluent						
	Gross Beta Activity	Sr^{89}	Sr^{90}	TRE[a]	Cs^{137}[b]	Co^{60}	Ru^{106}[c]	Gross Beta Activity	Sr^{89}	Sr^{90}	TRE[a]	Cs^{137}[b]	Co^{60}	Ru^{106}[c]
1957														
September	110	41	280	220	240	30	80	36	5.2	34	23	210	13	74
October	64	13	200	200	180	23	33	21	3.7	55	48	150	18	34
November	160	16	210	180	150	13	70	20	3.2	43	36	120	3.8	12
December	70	12	190	210	130	17	33	14	1.9	32	27	80	3.0	11
1958														
January	77	16	310	250	180	17	40	36	4.1	80	66		3.9	14
February	46	16	140	170	150	14	21	20	5.0	45	57	90	6.2	12
March	77	17	270	300	170	12	23	21	2.6	42	37	110	3.6	8.0
April	79	13	260	280	170	15	15	24	2.1	42	40	100	3.9	4.0
May	94	15	340	340	320	25	24	39	3.4	73	67	320	9.6	7.3
June	89	14	260	260	300	17	17	39	2.3	43	38	320	5.6	13
July	140	21	520	400	480	20	10	63	3.2	81	55	500	5.8	7.1
August	140	26	380	390	700	14	45	65	4.0	57	45	690	5.1	13
September	220	48	480	530	740	50	23	51	10	100	100	380	14	14
October	120	16	330	520	630	29	6.6	19	1.9	36	150	130	5.2	1.0
November		46	300		650				7.9	52		160		
December	120	20	370	440	670	40	9.3	19	2.2	41	50	110	14	3.8
1959														
January	140	19	390	600	430	270	32	20	2.3	51	65	60	60	17
February	100	17	300	480	390	74	29	17	3.6	63	68	60	16	7.9
March	190	16	330	1200	250	49	67	19	1.9	39	66	41	18	19

[a] Total rare earths.
[b] The ratio of Cs^{137} to Cs^{134} is about 50:1.
[c] The ratio of Ru^{106} to Ru^{103} is about 10:1.

Table 2. Removal of Radionuclides by Treatment

Monthly composite samples

Date	Percentage Removal						Curies Removed				
	Gross Beta Activity	Sr^{89+90}	TRE*	Cs^{137}	Co^{60}	Ru^{106}	Sr^{89+90}	TRE*	Cs^{137}	Co^{60}	Ru^{106}
1957											
September	67	87	89	9.5	51	7.6	3.7	2.6	0.62	0.02	0.19
October	68	73	77	19	23	0	2.6	2.7	0.84	0.12	0
November	87	80	80	21	72	83	2.4	1.9	0.23	0.12	0.74
December	79	84	87	40	83	67	2.4	2.6	0.74	0.21	0.31
1958											
January	53	74	74		76	65	3.6	2.7		0.19	0.38
February	57	66	67	42	56	42	2.3	2.4	1.4	0.17	0.18
March	73	85	88	32	69	66	4.7	5.1	1.1	0.16	0.30
April	70	84	86	40	74	74	5.3	5.5	1.6	0.25	0.26
May	59	78	80	0	61	69	6.0	5.9	0	0.34	0.36
June	57	84	86	0	67	24	5.2	5.2	0	0.25	0.09
July	55	85	86	0	70	30	10	7.6	0	0.30	0.06
August	54	85	89	2.1	64	73	7.4	7.5	0.31	0.20	0.70
September	77	79	81	48	73	38	9.6	9.8	8.2	0.82	0.20
October	84	89	71	80	82	84	6.5	7.8	11	0.50	0.12
November**		82	85	84			5.0		8.5		
December	84	90	89	84	65	59	7.3	8.2	12	0.54	0.12
1959											
January	86	87	89	86	78	47	7.8	12	8.1	4.6	0.33
February	83	79	86	84	78	73	5.4	8.9	7.0	1.3	0.46
March	90	88	95	84	65	72	7.0	26	4.8	0.78	1.1
							Total 104	124	66	10.9	5.9

*Total rare earths.

**Based upon analyses of weekly composite samples.

can be determined only after the mechanisms of strontium and total-rare-earth removal are established. Since a calcium determination can be made rapidly, it may continue to serve as a simple test to control the treatment process. There is no apparent relationship between the amount of calcium carbonate precipitated and the amount of strontium removed.

The cost of treatment for the initial 82 weeks was $39,800. This includes the cost of chemicals, a percentage of the total man-hours worked by Operations personnel, and the cost of utilities. Maintenance costs, analytical costs, and amortization of the plant are not included in this cost figure. During this 82-week period, 2.19×10^8 gal of waste was treated. The cost per 1000 gal of waste treated was 18¢.

An Experimental Procedure for Optimizing Treatment Efficiency

An experimental procedure was initiated for discovering the optimum combination of four treatment variables for removal of Cs^{137} and Sr^{90} from process wastes. Although not the primary purpose of this study, any insight that might be gained into the understanding of the fundamental processes of radionuclide removal would certainly improve the ability to remove cesium and strontium from the waste solution.

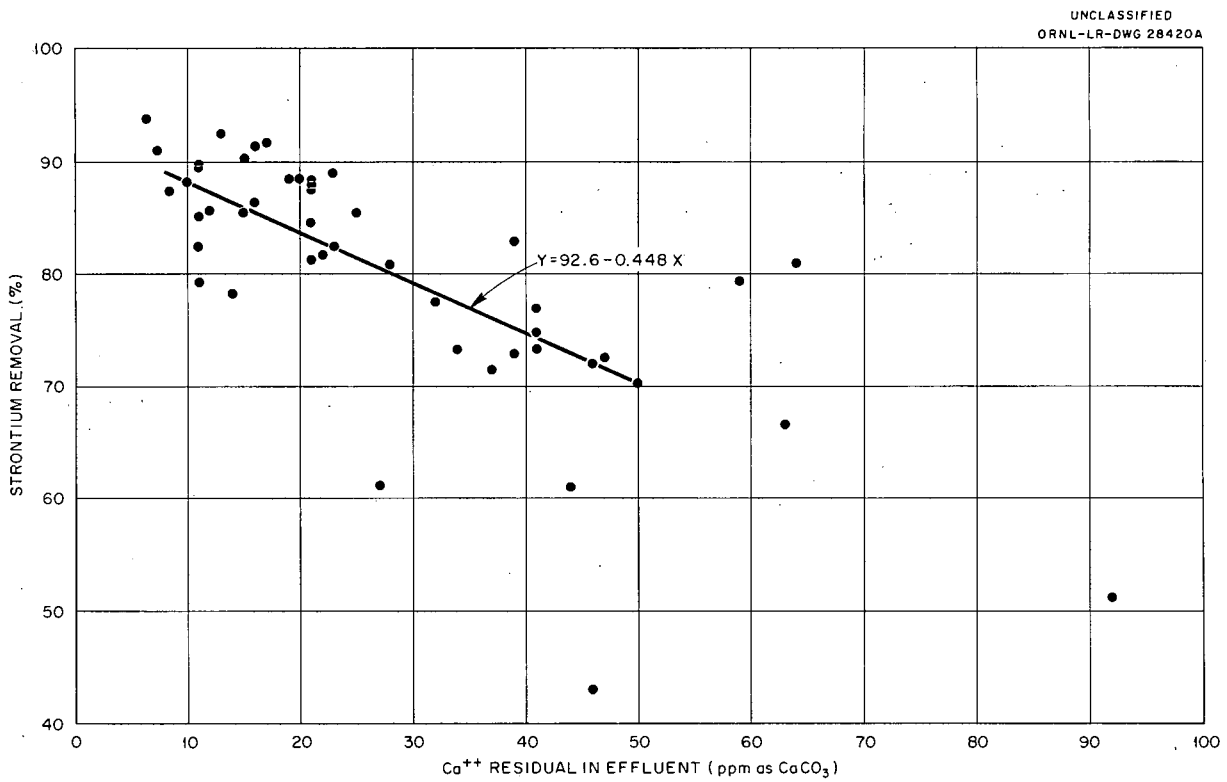

Fig. 1. Relation of Residual Calcium to the Removal of Strontium.

The experimental procedure is an application of a statistical technique, falling in the category of response surface methodology.[4] The treatment variables are clay (Grundite) dose, particle size of clay, proportion of lime stoichiometric requirement, and excess soda ash. Experimentation to date has been conducted in the laboratory using actual process wastes. The study is not yet complete.

In the first phase the wastes were treated by using five different combinations of the four variables according to a statistical pattern known as a simplex design. The ranges were:

Clay dose	50 to 200 ppm
Particle size	20–60 to 100–140 mesh
Proportion of lime stoichiometric requirement	$\frac{1}{3}$ to 1 (full)
Excess soda ash	0 to 375 ppm

[4]The earlier phases of this study were reported on at the Mathematics Panel Information Meeting, March 13, 1959.

The per cent removals of Cs^{137} and Sr^{90} were determined for each of the five treatment combinations and were found to vary from 46 to 88% for Cs^{137} and from 28 to 75% for Sr^{90}. Using linear regression techniques, the "paths of steepest ascent" for Cs^{137} and Sr^{90} were then estimated separately from these results. In this application, a path of steepest ascent describes a system for choosing combinations of the treatment variables such that experiments performed in accordance with this system would give greater increases in per cent removal than would experiments conducted with respect to some other system. It is the estimated shortest route to greater per cent removals.

The second phase of the study involved nine more experiments performed along the paths of steepest ascent for the two responses. It appeared that the path for Cs^{137} removal would be independent of lime requirement and excess soda ash and that the path for Sr^{90} removal would be independent of clay dose and particle size. The experiment run at the point farthest along the paths involved 310 ppm clay, 230–270 mesh size, full

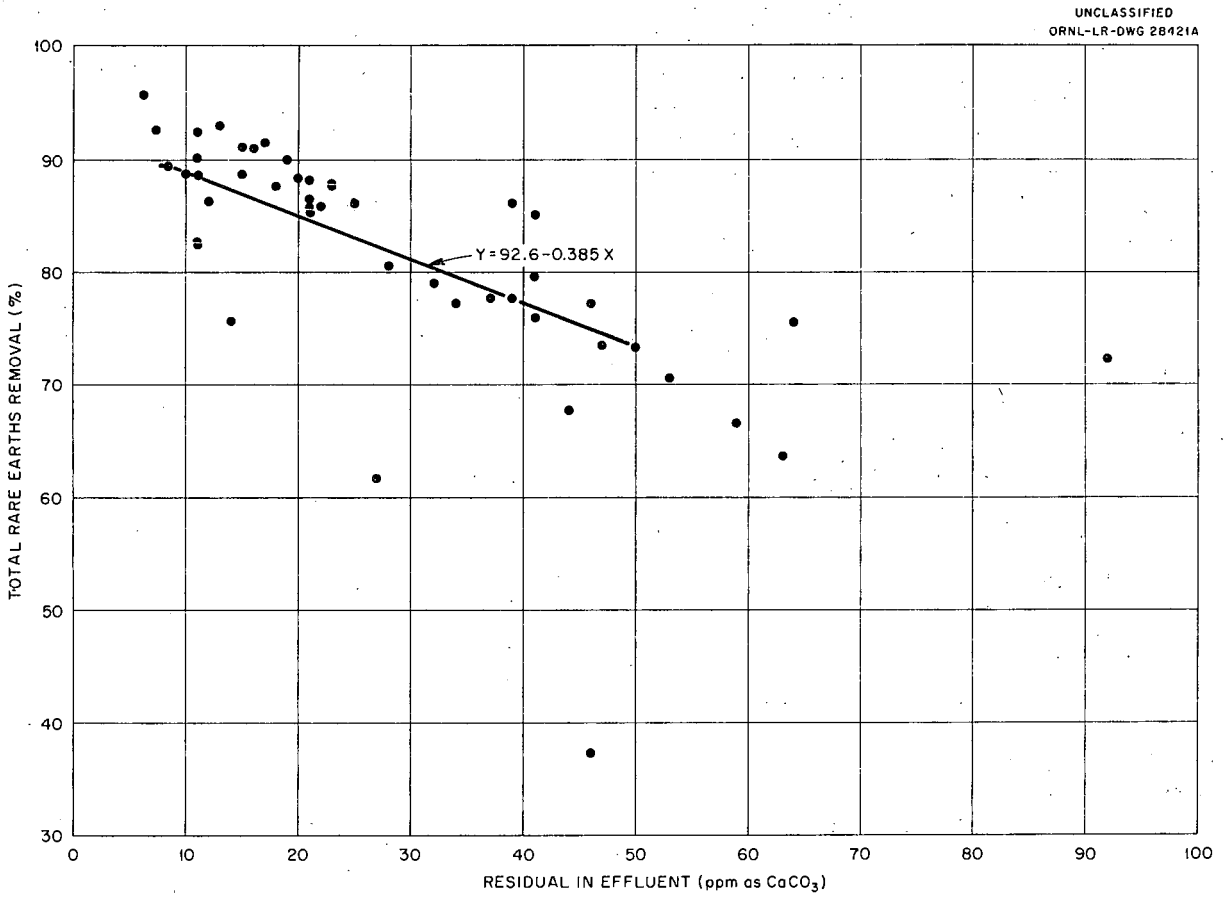

Fig. 2. Relation of Residual Calcium to the Removal of Total Rare Earths.

stoichiometric requirement for lime, and 455 ppm excess soda ash. The per cent removal of Cs^{137} increased from 71 to 95% along its path of steepest ascent and the per cent removal of Sr^{90} from 37 to 85% along its path.

The third phase of the study consisted of experiments run according to another simplex design for the purpose of re-estimating the paths of steepest ascent. The second simplex was performed with the following ranges for the four treatment variables:

Clay dose	300 to 450 ppm
Particle size	170–200 to 230–270 mesh
Proportion of lime stoichiometric requirement	1 to 2
Excess soda ash	460 to 600 ppm

The results of this experiment were gratifying from the standpoint of strontium removal but not from the standpoint of per cent removal of cesium. The largest per cent removal for Sr^{90} was 93%, an increase of 8% over previous experiments. However, the largest Cs^{137} removal was only 92%, or 3% less than previously observed.

The regression equations fitted to the results of the third phase of the study suggest that the level of excess soda ash has been overextended when considering the removal of Cs^{137}. The new path of steepest ascent calls for a decrease in excess soda ash from the neighborhood of 460 to 600 ppm. The equations show also that this decrease should have little effect on the removal of Sr^{90} if not carried too far. The levels of particle size should remain about the same, with slight increases in clay dose and proportion of lime stoichiometry.

A graphic summary of this series of experiments is given in Figs. 3 and 4. Figure 3 is a summary of the Sr^{90} per cent removal. It is plotted in the two-dimensional space of excess soda ash and

proportion of lime stoichiometric requirement only, because clay dose and clay particle size had little or no effect on strontium removal. The lower triangle represents the positions of the experiments of the first simplex design. The nine experiments along the first path of steepest ascent project to three points in the two-dimensional diagram and show the increase from 37 to 85% previously mentioned. The upper triangle represents the second simplex design with its generally higher per cent removals of Sr^{90}. The direction of the second path of steepest ascent is indicated.

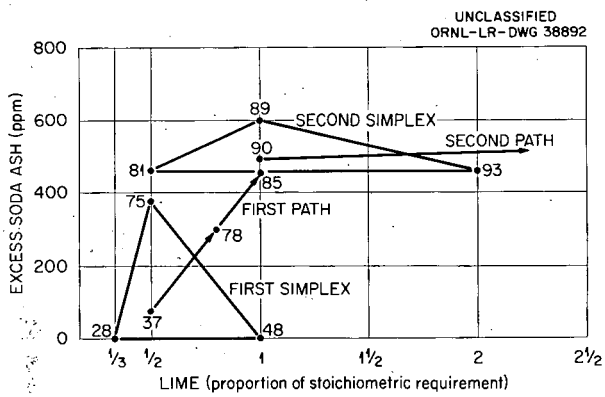

Fig. 3. Experimental Points Showing the Per Cent of Strontium Removal.

The summary of the Cs^{137} per cent removal is shown in Fig. 4. This is shown in three dimensions because during the third phase of the study it was found that only the effect of lime is negligible on the removal of cesium. The first simplex design is represented by the larger tetrahedron and the first path of steepest ascent by the three arrows, one at 75 ppm excess soda ash, one at 300 ppm excess soda ash, and one at 455 ppm excess soda ash. (The three arrows would project to one arrow if excess soda ash is considered negligible, as was earlier supposed.) The smaller tetrahedron, which is at higher levels of excess soda ash than previously, represents the second simplex design with its disappointingly low per cent removals. The second path of steepest ascent for Cs^{137} removal is shown by the arrow projecting from the second simplex. It is in the direction of smaller excess soda ash, larger clay doses, but relatively little change in mesh size.

Although the new paths of steepest ascent are calculated, no further experimentation has been done along these paths at this time. This experimentation will form the fourth phase of the study.

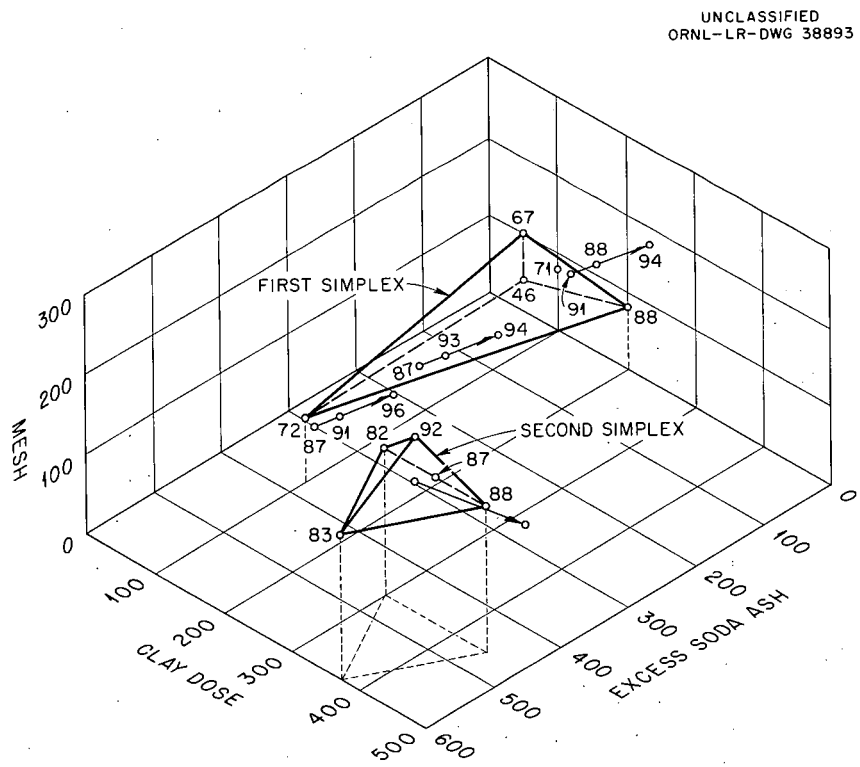

Fig. 4. Experimental Points Showing the Per Cent of Cesium Removal.

DISPOSAL OF ORNL LIQUID WASTES

K. E. Cowser

R. L. Bradshaw
E. R. Eastwood
D. G. Jacobs
T. F. Lomenick
F. L. Parker
H. J. Wyrick
M. A. Cobble[5]
D. W. Goodpasture[6]

Studies of Soil Disposal Facilities

Intermediate-level liquid waste is collected centrally at the Tank Farm, where it is neutralized prior to release to the waste pits. From June 1952 through December 1958, 1.17×10^7 gal of waste, containing about 158,000 curies of beta radioactivity, was pumped to the pits. The quantities of materials released are summarized in Table 3. While Cs^{137} and Ru^{106} continued to be the principal contributors to radioactivity in the waste, in 1958 there was a significant increase in the amounts of Sr^{90} and total rare earths (TRE). During this period approximately 10,000 curies of Sr^{90} and 9000 curies of TRE were released to the pits.

The importance of the increased amount of Sr^{90} in the wastes lies in the potentially hazardous contamination of the Clinch River. If all the waste released to the pits in 1958 had been released to the river, and if complete mixing had occurred, the maximum permissible concentration for drinking water for continuous occupational use would have been exceeded by a factor of 2. A continued increase in strontium amounts will increase this hazard potential. However, the pits have reduced significantly the potential hazard to the Clinch River, since the soil around the pits continues to retain the strontium and cesium.

In the waste pit area, Ru^{106} continues to be the only radionuclide identified in important amounts in any of the observation wells, surface seeps, and surface streams. The underground path of waste movement in the pit area is similar to that previously reported.[7] Figure 5 shows the fluctuations in concentration and the total transport of radioactivity for 1957 and 1958 in the streams east and west of the pits. By integration of the area under the total transport curve, it is estimated that 160 curies of Ru^{106} escaped from the pits into the bed of White Oak Lake in 1958. This is comparable to the estimated 200 curies of Ru^{106} released during 1957, particularly since the average concentration of Ru^{106} in the waste in 1958 was about half the average concentration for the period 1955–57. A similar inventory of the nonradioactive chemicals revealed that about 200 tons of nitrates escaped from the pits in 1958.

[5]Resigned December 1958. Presently at Monarch Equipment Company, Kingsport, Tenn.

[6]Student trainee, University of Tennessee.

[7]E. G. Struxness *et al.*, *H-P Ann. Prog. Rep. July 31, 1958*, ORNL-2590, p 6–26.

Table 3. Waste Disposal System Inventory[a]

	Pit 2	Pit 3	Pit 4	Total
Fission products released to pits, curies				
Gross beta emitters				158,000
Cs^{137}	30,400	43,600	10,900	84,900
Ru^{106}	8,800	11,500	1,900	22,200
Sr^{90}	500[b]	11,800	300	
Sr^{89}	60[b]	1,400	20	
TRE	<100[b]	20,000	<100	
Volume, thousands of gallons	4,866[c]	262	6,573	11,701

[a]Cumulative amounts of intermediate-level waste through December 1958.

[b]Curies in waste overflowed to pit 2 from pit 3 from June 1955 through December 1957.

[c]Includes 90,000 gal of nonradioactive chemical waste.

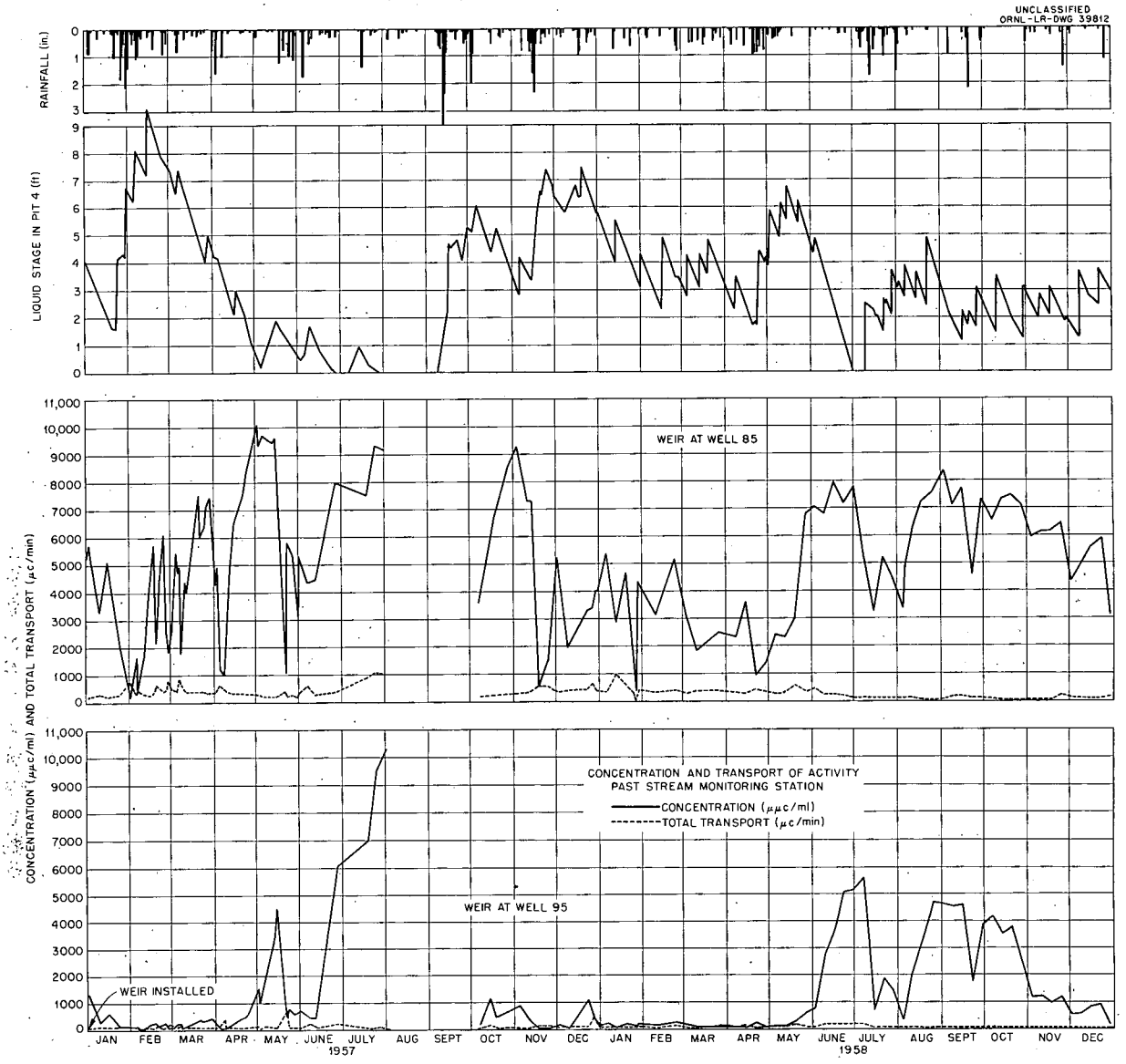

Fig. 5. Transport of Activity Past the Stream-Monitoring Stations at Wells 95 and 85.

As the wastes from the pit area move across the lake bed, additional amounts of ruthenium are removed. About 72 curies of ruthenium were released from White Oak Creek to the Clinch River during 1958; this compares with 60 curies released during 1957. With an average flow in the Clinch River of about 5600 cfs during 1958, the average concentration of ruthenium in the river with complete mixing would be 1.4×10^{-8} μc/ml. For the year, the ruthenium released to the river was calculated by H. H. Abee of the Applied Health Physics Section to be 3.5% of the maximum permissible concentration for drinking water for continuous nonoccupational use. Similarly, the amount of nitrates escaping from the pits would result in concentrations of the order of 0.04 mg/liter in the river.

Since the waste pit system would be inadequate if rates of seepage and evaporation were too small to handle the volume of liquid collected, it is desirable to evaluate the loss of liquid due to seepage and evaporation each year. During

1958, the calculated rates of seepage from pits 2 and 3 were 3400 and 700 gal/day, respectively, as compared with 3700 to 450 gal/day during 1957.

The differences in calculated rates of seepage for the two years are probably due to the inherent difficulties involved in estimating seepage. Seepage is determined as the net loss after accounting for waste pumpage, rainfall, and evaporation; any errors made in determining each of these, especially the volume of waste overflowed from pit 3 to pit 2 to pit 4, would be reflected. It seems unlikely that a change in permeability of the soil would account for the difference in rate of seepage.

With continuous records of liquid stage at pit 4 available, human errors in reading staff gages during periods of waste overflow to this pit are more likely to be detected. This is not the case when pit 3 is overflowed to pit 2; therefore, errors in determining the volumes overflowed between these pits would be expected. The combined rate of seepage from pits 2 and 3 is more representative of actual seepage; this was about 4100 gal/day during 1957 and 1958. Continuous records of liquid stage in pit 4 showed little change in the rate of liquid loss from this pit during this two-year period.

Clinch River Studies

The seepage from waste pits, as well as the effluent from the process waste water system, eventually finds its way into White Oak Creek and thence into the Clinch River. Therefore, it is necessary to determine the extent to which these streams can be safely used to assimilate these radioactive wastes.

With the assistance of the Surface Water Branch of the U.S. Geological Survey, background radiation, temperature, and velocity measurements above and below the confluence of White Oak Creek and the Clinch River were initiated in preparation for an intensive study of the dispersion, dilution, and uptake in this environment. The measurements are an extension of the work reported last year.[7] Further analysis of those data showed that, under the river conditions prevailing at the time of the test, complete dispersion was obtained at Clinch River Mile (CRM) 15.5 (Station C), 5.3 miles below the outfall of White Oak Creek into the Clinch River (at CRM 20.8).

A water level recorder was installed on the Clinch River at CRM 20.7, 0.1 mile downstream of the mouth of White Oak Creek. The measurements taken there will be correlated with the flow from Norris Dam and the elevation at Watts Bar Dam. This information will be used to determine the time of travel of a wave from Norris Dam to White Oak Creek during all river regimes.

Development of Improved Well Probe

Existing radiologging equipment at ORNL is inadequate for efficient monitoring of observation wells in the waste-pit area. Chief limitations of the existing trailer-mounted rigs are slow logging speed, insufficient mobility for the terrain, and equipment unreliability, partially due to age.[8] A survey of available loggers failed to reveal an instrument suitable for the needs at ORNL. Therefore, development of an improved instrument was undertaken,[7] a block diagram of which is shown in Fig. 6.

A cable reel and feed mechanism, based in part on a design developed by the New York Operations Office of the AEC, has been fabricated but not yet field tested. This unit, shown in Fig. 7, incorporates such features as an overload clutch, automatic log, retract and shutoff, resettable level-wind index, optional two-speed hand operation, and a wide range of automatic logging speeds. Power is supplied from a 12-v storage battery which should provide at least two 8-hr days of operation without recharging.

A simplified electronic unit utilizing the average current from four G-M tubes in the probe has been constructed and tested. This unit also operates from a 12-v storage battery and employs only one vacuum tube and one corona-type voltage-regulator tube. One charge will provide four to five 8-hr days of operation.

In Fig. 8 are shown the electronic unit (count rate meter and power supply), the recorder, and the G-M tube assembly. The G-M tubes and associated resistors and capacitors will be packaged in a 12-in.-dia probe.

The entire assembly, including the electronic unit, the reel assembly, the recorder, and the batteries, will be mounted on a frame for operation

---

[8] J. M. Garner and B. Kahn, *H-P Semiann. Prog. Rep. Jan. 31, 1954*, ORNL-1684, p 22.

UNCLASSIFIED
ORNL-LR-DWG 39804

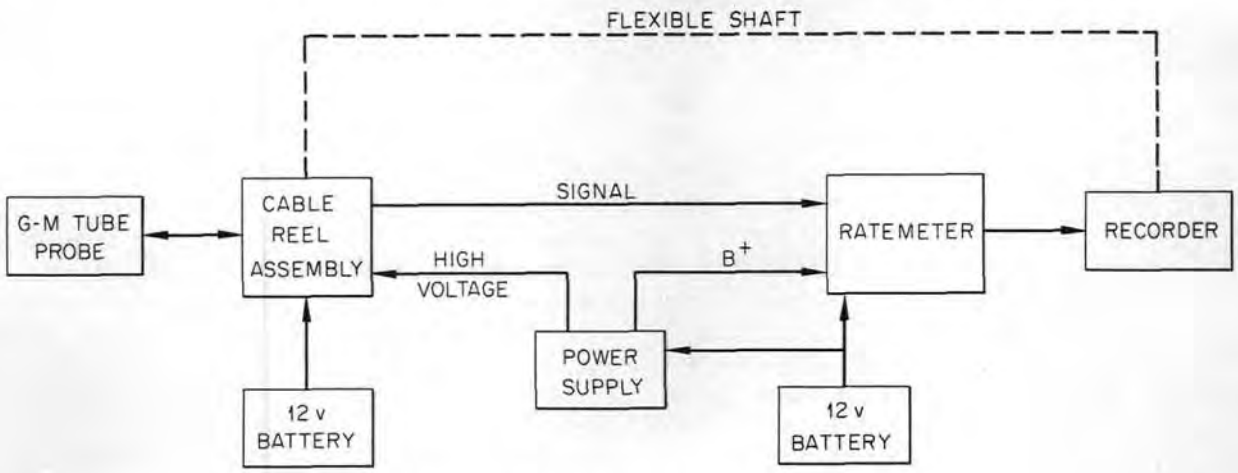

Fig. 6. Block Diagram of a Well Logger.

Fig. 7. Cable Reel Assembly.

from a Jeep station wagon; each unit will be separately demountable.

Soil Column Studies

While the waste pits have been used with success in disposing of large volumes of waste, difficulties are inherent in their operation and control. On the other hand a column containing one or several naturally occurring minerals, clay or otherwise, can offer material advantages for waste disposal. Columns may be operated under closely controlled conditions, thereby limiting the amount of fission products released to the general environment. Safeguards are easily incorporated into a soil column. Also, the location of fission products is defined by the configuration of the soil container; the contaminated soil is not subject to extraneous leaching conditions or wind action; the use of several selected sorptive materials increases the efficiency of removal of specific fission products; and, in a man-made column, the extent of waste-soil contact is greatly improved. Therefore, studies are in progress to obtain data needed for the design of a soil column system. These studies include investigations of the sorptive characteristics of various soil materials for the important radionuclides in ORNL waste, and the head-loss characteristics of these materials

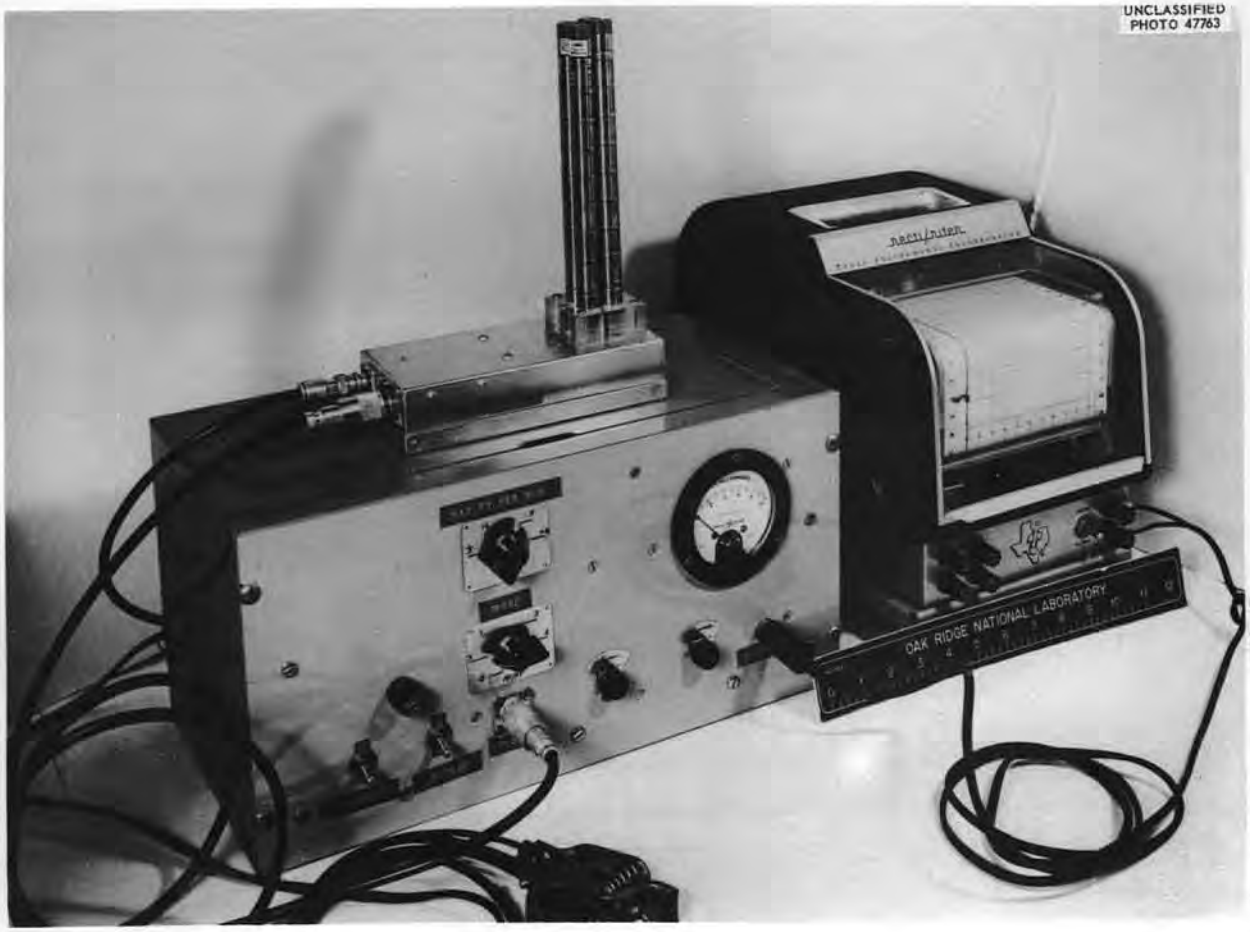

Fig. 8. G-M Tube Assembly, Rate Meter and Power Supply, and Recorder.

as a function of contact time and of volume of waste passing through the column.

A sample of the light-colored, weathered portion of Conasauga shale was collected, air-dried, and ground to pass a 20-mesh sieve. The cation exchange capacity was determined by the ammonium acetate method[9] and found to be 16.5 meq per 100 g. Increments of 0.23 *M* $NaNO_3$ solution containing the equivalent of 0.66 μc of Cs^{137} per milliliter were passed through 6-g portions of the shale. Results, as seen in Fig. 9, show the total amount of cesium retained by successive shale increments. Forty per cent of the total cesium activity remained in solution after 10 liters of waste was passed through the first 6-g increment of shale. Activity remaining was reduced to 17% by passing the effluent through a second increment of shale. Passage through the third, fourth, and fifth increments of shale reduced the activity remaining in solution to 6.9, 1.2, and 0.2% of the total activity, respectively. The capacity of the shale to retain cesium from this solution was found to be 670 μc of Cs per gram.

When the $NaNO_3$ concentration was increased from 0.23 *M* to 0.5 *M*, the saturation capacity dropped to 282 μc of Cs per gram. The selectivity coefficient, the Cs/Na ratio on the clay compared to this ratio in the solution at equilibrium, was approximately equal for both solution concentrations, indicating that in an $NaNO_3$ system, the Cs/Na ratio of the solution determines the capacity of the shale for cesium sorption.

[9] W. W. Skinner *et al.*, *Official and Tentative Methods of Analysis of the Association of Official Agricultural Chemists*, Assoc. Offic. Agr. Chemists, Washington, D.C., 1940.

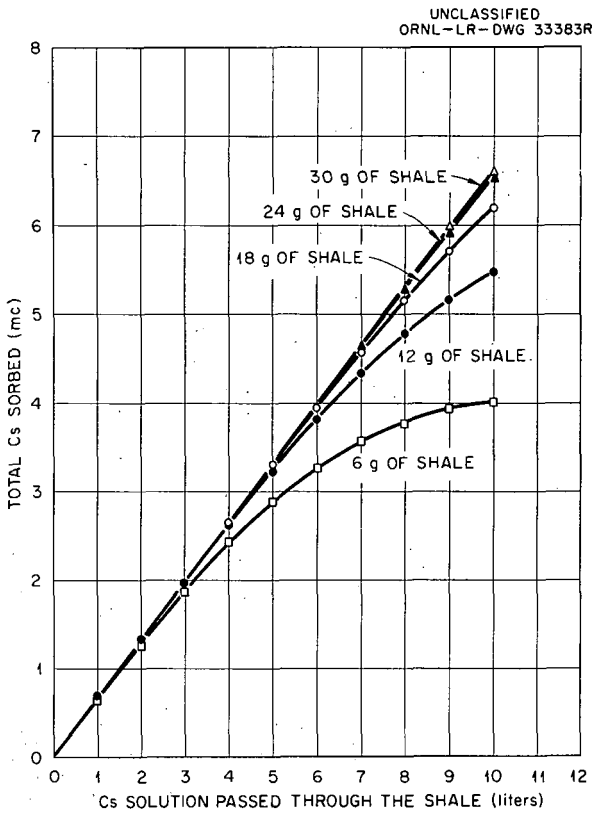

Fig. 9. Sorption of Cesium from Flowing Solutions by Conasauga Shale.

When 0.5 *M* NH_4NO_3 was employed as the carrier solution, the shale retained only 4 μc of Cs per gram. This extreme drop in the saturation capacity can be attributed to the ability of the NH_4 ion to compete effectively with cesium ions for the fixation sites.

A 1-in. glass column, 2½ ft in length, was charged with 12 in. (168.9 g) of 10–20 mesh Conasauga shale, prepared by air-drying, crushing, and screening. Immediately upon contact with distilled water the shale began to break down into smaller particles, and quickly caused the column to be plugged. This rapid breakdown points out the aggregate nature of Conasauga shale and the lack of stability that can be anticipated. The column was backwashed at rates ranging from 3 to 135 $ml \cdot min^{-1} \cdot cm^{-2}$; and although the higher backwash rates would be quite unrealistic on a plant scale, they were necessary to remove the bulk of the fines from the small column. Sixty-one grams of shale was washed from the column, leaving about two-thirds of the original bed depth.

The head-loss characteristics for downflow operation are shown in Fig. 10. The column was operated intermittently for 20 days with distilled water. Head loss through the shale increased during the first five or six days and then began to decrease, reaching apparent stability after 19 days. Continued breakdown and rearrangement of the particles probably account for the increased head loss through the shale with time. However, the reduction in the head loss that occurred after the sixth day is not readily explained, since a more drastic reduction of head loss would be anticipated if channeling began. Treatment of Conasauga shale with Arquad 18-50 (octadecyltrimethylammonium chloride), a soil stabilizer, increased the rate of breakdown of the shale. The difficulties encountered with operation of a column using Conasauga shale reduce the likelihood of this material's suitability as a sorptive medium. Therefore, other low-cost materials are being investigated in order to select those having suitable sorptive and hydraulic characteristics.

BURIAL OF SOLID WASTES

K. E. Cowser

T. F. Lomenick
H. J. Wyrick
M. A. Cobble[10]
W. M. McMaster[11]
R. M. Richardson[11]

Studies of Burial Areas in Melton Valley

The site of the new burial ground is in Melton Valley about 0.6 mile southeast of ORNL and on the Conasauga shale. The site is situated on the line of knobs underlain by more silty layers along the northwest side of Melton Valley. The topography is that typically developed on shale, with numerous steep-sided gullies, some of which are more than 10 ft deep. Within the site, elevations range from 765 to 875 ft, a maximum relief of 110 ft.

The principal types of rock of the disposal site are shale, siltstone, and limestone. There is no obvious distinction across the strike due to the gradational nature of the rock.

[10]Resigned December 1958. Presently at Monarch Equipment Company, Kingsport, Tennessee.

[11]U.S. Geological Survey.

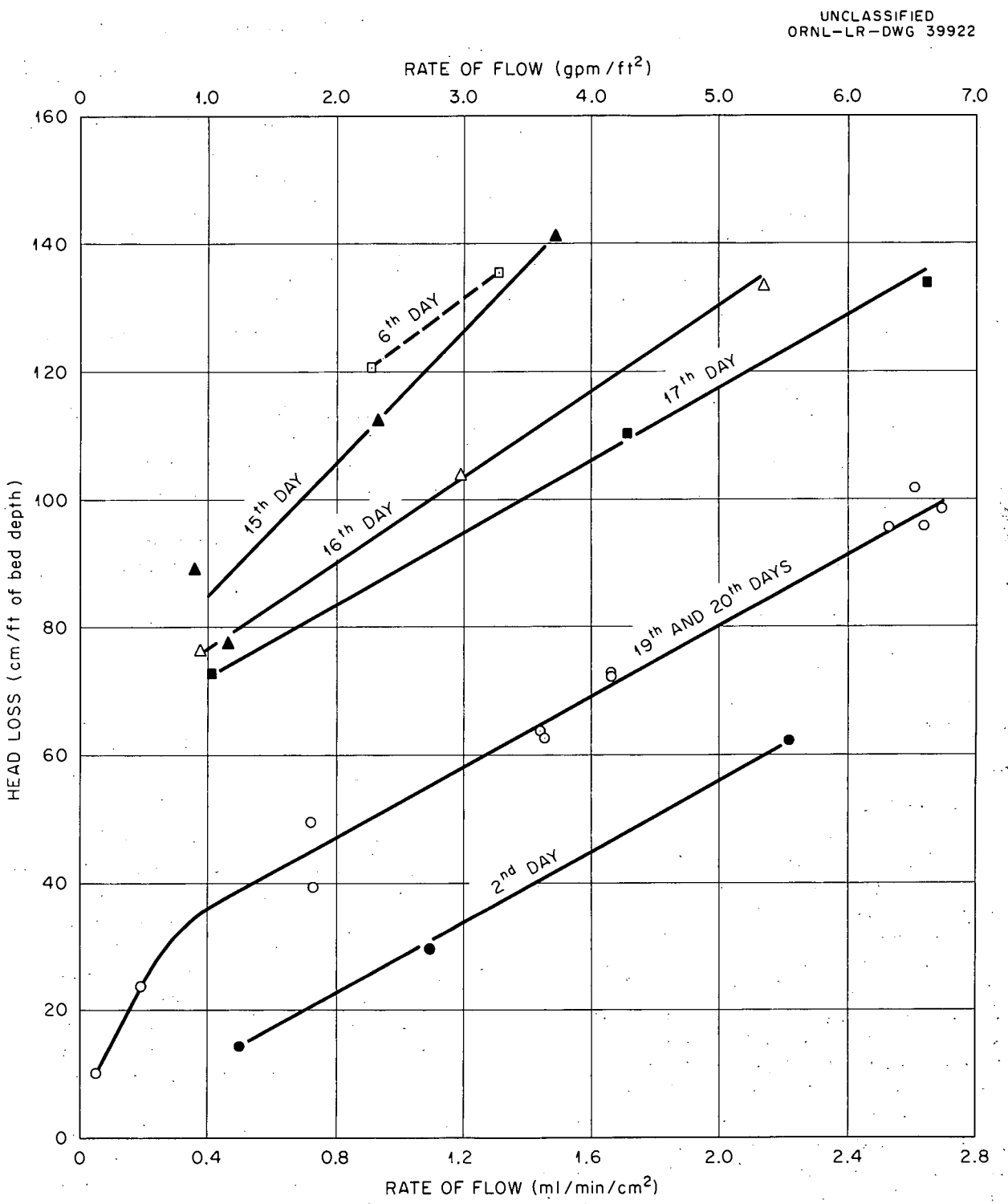

Fig. 10. Head-Loss Characteristics at Various Rates of Flow.

In the lower elevations northwest of the site the area is underlain by fairly pure multicolored shale. Siltstone and lenticular shaly limestone are present in minor amounts.

The amount of limestone and siltstone increases from northwest to southeast. Some of the siltstones are spongy and friable and represent layers of silty limestone from which the calcium carbonate has been leached. In places limestone can be seen to grade laterally into siltstone. The siltstone layers are interbedded with thin shales, most of which are olive green, with stained joint surfaces. The siltstone layers have well-developed joints which are usually open near the surface. Ground-water circulation in these layers is probably greater than in less silty layers where the joint surfaces are not so widely spread.

The weathered zone is thicker on the top of the knobs than at lower elevations. In areas of higher elevation auger holes were drilled to depths of 17 to 19 ft without encountering unweathered material.

The rock grades on the southeast into silty shale with thin layers of siltstone. The shale shows well-developed joints which are more closely spaced and tighter than those in the siltstones. Thin, lenticular beds of limestone appear and are interbedded with shale as the silt decreases to the southeast.

The southeasternmost zone contains limestone with interbedded shale. The limestone is mostly medium to dark gray, dense to crystalline, with irregular bedding planes; beds are up to 10 in. thick. Outcrops are relatively common in streams flowing across the strike. The lithology appears to be continuous along the strike.

The Conasauga shale is a structurally incompetent unit lying between the competent Rome formation and the Knox group. During deformation of the region, the shales, siltstones, and thin limestones were badly deformed. The beds generally dip to the southeast at a low angle, but many small structures and variations of dip and strike are present. Small anticlines and synclines are common. The thinly bedded, less silty shales are usually the most deformed of the lithologies.

Several small faults may be present which would have an influence on ground-water circulation, but evidence was insufficient to define their location.

A series of 45 auger wells were completed, and water-level measurements made about once a week beginning in May 1958. The auger wells range in depth from 5 to 21 ft. Although most wells located above an elevation of 800 ft are dry during the greater part of the year, water-level contours, developed from measurements of shallow wells during wet periods, show the water table as a suppressed replica of the surface topography. Churn wells are being installed to determine the occurrence and circulation of ground water at greater depths. Figure 11 shows the critical depth-to-water contours for the period from May 1958 through June 1959. In general, the values used to construct these contours are the minimum values observed for the 14-month period. Areas immediately adjacent to wells 144, 154, and 162 are believed to be subject to limited perched water conditions during periods of heavy rainfall. However, the rate of water-level decline following periods of recharge is rapid, averaging about 0.3 ft per day.

For most efficient use of the burial ground a plan of future disposal operations covering some reasonable period is necessary. To estimate the requirements of land usage, records of solid waste burial dating back to 1957 were analyzed. By linear extrapolation of these data estimates of the volumes of waste expected for the next 5½ years were made and are summarized in Table 4. Since the policy of segregating contaminated solids is followed, estimates of the volumes of alpha and beta-gamma wastes are included, namely, 1.2×10^6 ft^3 of alpha-contaminated waste and 1×10^6 ft^3 of beta-gamma-contaminated waste.

By use of the depth-to-water map, Fig. 11, the volume available for burial of solid waste can be determined. With the restriction that solid waste shall be buried 1 ft above the highest water level, the depth of burial in the area between the 6- and 11-ft depth-to-water contours is limited to 5 ft. Similarly, the depth of burial in the area between the 11- and 16-ft contours and above the 16-ft contours is limited to 10 and 15 ft, respectively. A 15-ft-deep trench is the maximum depth of burial due to the limitations of existing equipment. The volume available for disposal of solid waste in the outlined area is approximately 21×10^6 ft^3. The areas reserved for high-level waste and other special waste are not included in the calculations. Where the depth to water is less than 6 ft, these areas can be used for disposal of non-contaminated solids.

The total volume of a trench is not occupied by solid waste. A conservative estimate of the

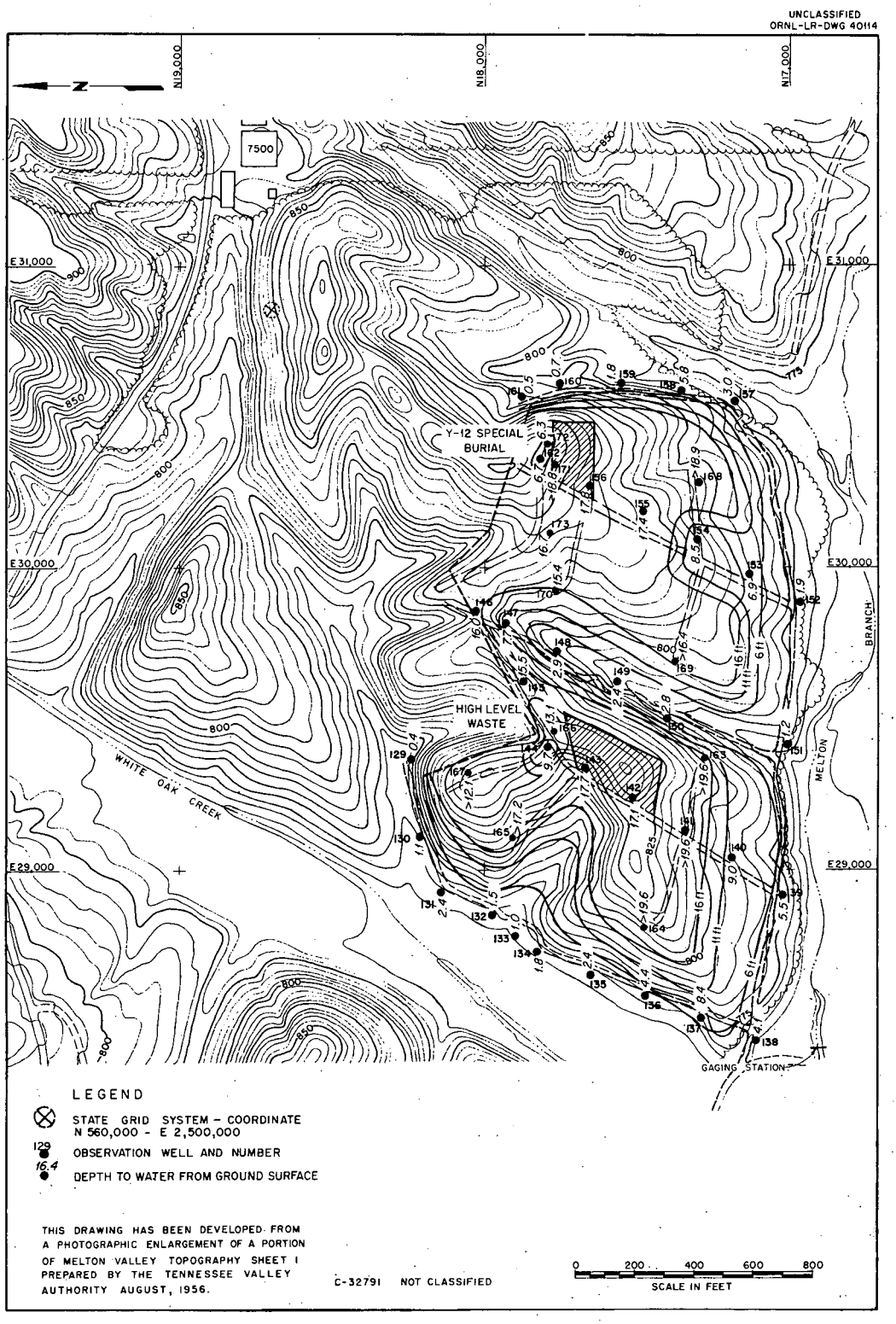

Fig. 11. Depth-to-Water Contours at New ORNL Burial Ground.

Table 4. Estimated Volumes of Solid Radioactive Waste for 1959 Through 1964

In thousands of cubic feet

Waste	1959 (last half)	1960	1961	1962	1963	1964	Total
Alpha	63	197	194	237	224	262	1177
Beta-gamma	77	163	173	186	193	201	993
Total	140	360	367	423	417	463	2170

occupied volume is 50%. For convenience of operation a trench width of 10 ft is normally employed, and a 5-ft spacing between trenches assures the integrity of each trench and a reasonable working area. Therefore, two-thirds of the available area would actually be employed. With these limitations, about one-third of the total volume in the burial ground will be occupied by solid waste. Considering all restrictions, the area east of the road along which wells 152 and 156 are located provides about 1.4×10^6 ft^3 of burial space; this should be ample for the alpha-contaminated waste expected over the next 5½ years. Similarly, east of the road along which wells 146 through 151 are located and west of the site for alpha waste burial about 2.2×10^6 ft^3 are available for burial of beta-gamma-contaminated waste.

To simplify and improve monitoring, a new trench design was adopted for the disposal of solid waste (see Fig. 12). The bottom of the trench, covered with 6 in. of gravel, is sloped to an asphalt-lined sump at one end in which a 6-in. perforated casing is installed. Any liquid entering the trench will flow through the gravel underdrain to the collecting sump, from which samples can be withdrawn and analyzed. After the trench is filled with waste, the void space around the contaminated material is backfilled with shale. A layer of shale near the top of the trench is compacted by tamping, providing a base for an asphalt cap as shown in Fig. 13. About 1 in. of asphalt is sprayed on the tamped shale; and after the asphalt hardens the remainder of the opening is backfilled with shale. The composition and amount of liquid collected in the sump will be used to evaluate the extent of leaching of radioactive materials from the waste and will serve as an indicator of the effectiveness of the asphalt cap in diverting rainfall.

Explorations of Potential Burial Sites in Bear Creek Valley

At the request of the Atomic Energy Commission, the U.S. Geological Survey is investigating several possible sites for the burial of low-level radioactive wastes in the eastern United States. One of the areas under consideration is the Oak Ridge reservation.

Available information suggested that Bear Creek valley, immediately west of the Y-12 Plant, is the most suitable area from geologic and hydrologic considerations for the burial of such waste. The valley is underlain by Conasauga shale, as is Melton Valley.

To further define the geology and hydrology of the area and to provide additional information necessary to evaluate the suitability of the site, a program of test drilling was begun in May 1959. This includes five core holes, approximately 3 in. in diameter and 200 ft deep, and ten churn drill wells, 6 in. in diameter and 150 ft deep. The test drilling will provide information on the character and thickness of the overburden and on the character and distribution of the bedrock. After completion, the wells will be pressure-tested to determine the location of permeable horizons and the amount of water they will accept.

To determine the position and range of fluctuation of the water table in the area, some of the wells will be equipped with continuous water-stage recorders. The remainder will be measured periodically.

To determine variations in the flow of Bear Creek and tributary springs, five stream-gaging stations have been established. Discharge measurements are made at these stations every month.

The chemical and radiochemical character of the ground and surface waters will be determined analytically.

Fig. 12. Gravel Underdrain System and Collecting Sump for Y-12 Special Waste.

Fig. 13. Asphalt Cap Over Backfilled Trench for Y-12 Special Waste.

ECOLOGICAL RESEARCH

S. I. Auerbach

R. M. Anderson	J. S. Olson
D. A. Crossley, Jr.	V. I. Dodson[12]
P. B. Dunaway	M. E. Pryor[12]
J. H. Marks	J. P. Witherspoon[12]

Ecological studies during the past year have been conducted in White Oak Lake bed and in the forest sites of the reservation. In this way the program is taking advantage of both the contaminated and uncontaminated features of the Controlled Area. Work in White Oak Lake bed emphasizes the uptake and food-chain transfer of Sr^{90}, Cs^{137}, and other radioisotopes within a unique, heavily contaminated system. The forest work is utilizing the uncontaminated areas for experiments on movement of tracer isotopes and for other studies on the dispersal and return of radioactive contaminants to the soil.

[12]Temporary employee.

White Oak Lake Bed Studies

Soils. – The general chemical characteristics of the lake bed soils showed little change over the last year. More extensive sampling in both the upper and the lower parts of the bed made possible a comparison of these two areas. The results (Table 5) suggest that the areas are sufficiently different in some of their chemical properties to warrant following them as separate systems. A detailed analysis and mapping of the radiation fields above the two parts of the bed demonstrated a profound difference in the air dose rates in the two areas, resulting primarily from differences in concentrations of Cs^{137} and Co^{60} in the soils.[13]

Part of the upper bed is receiving an input of Ru^{106}, stable Na, and as-yet-undetermined materials from the intermediate-level waste pits. This material is entering the bed via the east

[13]P. K. Lee and S. I. Auerbach, *Determination and Evaluation of the Radiation Field Above White Oak Lake Bed*, ORNL-2755 (1959).

Table 5. Comparison of Upper and Lower Lake Bed Soils

Values given are the means and the results of one- and two-tailed significance tests

Constituent	Analysis		Significance Tests	
	Upper Lake Bed	Lower Lake Bed	Two-Tailed, P	One-Tailed, P
Sr^{90}	0.0544 ± 0.0041 μc per 100 g	0.036 ± 0.00166 μc per 100 g	0.01–0.02	0.005–0.01
Cs^{137}	4.089 ± 0.4230 μc per 100 g	0.734 ± 0.1264 μc per 100 g	<0.001	<0.0005
Co^{60}	1.059 ± 0.1096 μc per 100 g	0.3068 ± 0.2468 μc per 100 g	0.02–0.05	0.01–0.025
Ca	36.007 ± 2.4556 meq per 100 g	20.097 ± 2.2990 meq per 100 g	<0.001	<0.0005
K	0.195 ± 0.0053 meq per 100 g	0.221 ± 0.0324 meq per 100 g		
Na	0.653 ± 0.321 meq per 100 g	0.0366 ± 0.0033 meq per 100 g		
P	3.50 ± 0.3066 ppm	2.04 ± 0.3792 ppm	0.001–0.01	0.0005
pH	7.53	6.67		

seep, which drains a portion of the waste pit area. The outfall from the seep is spreading over the bed in a delta fan pattern which is demarcated by the increased and variable air dose rates.[13] The movement of sodium is of particular significance for the future pattern of vegetation. The sodium levels in the upper lake (Table 5) already are much higher than those in the lower bed, and portions of the vegetation already have been eliminated in areas high in sodium. Continuation of this increase in sodium will result in the growth of salt-tolerant species (halophytes), which may be quite different from the species present on the lower bed.

Because the lake bed is part of the Laboratory's waste disposal system, there has been need for information on the budget of fission products contained in the lake bed soil. The establishment of the Interim Low-Level Analytical Laboratory in the Analytical Chemistry Division has made possible routine analyses of large numbers of samples. Because of its importance the budget of Sr^{90} was assayed first. Sixty-eight soil samples (0–6 in.) taken during 1956, 1957, and 1958 were analyzed for total Sr^{90}. The results are summarized in Fig. 14. The means for the upper and lower parts of the bed are plotted separately and connected by dashed lines, but a longer time will be needed to determine whether there is a difference in trend. Hence grand means also are shown with 95% confidence limits. Curve B was fitted visually. The data allow for either of two possibilities: (1) the trend of curve B applies to both parts of the bed, or (2) each part will have a different rate of loss.

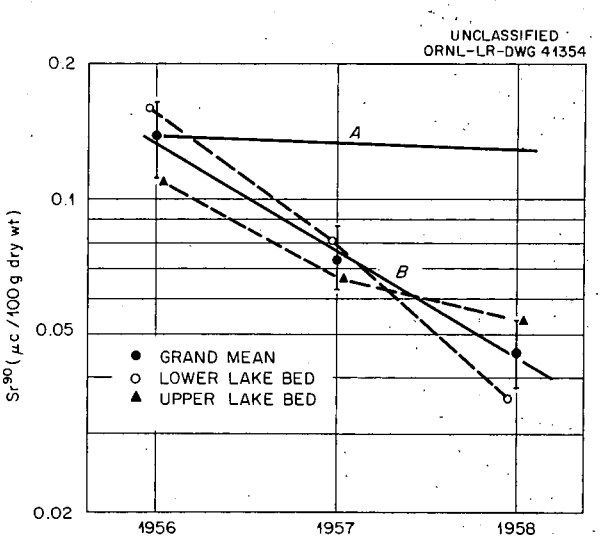

Fig. 14. Changes in Sr^{90} Budget in Upper and Lower White Oak Lake Bed. Curve A is loss due to radioactive decay.

If the first hypothesis is correct the trend line (curve *B*) suggests a 50% loss in 1.25 years. If this rate prevailed for 12.5 years, the amount remaining in the surface soil, barring recycling by the vegetation, would be reduced by three orders of magnitude to approximately 20 times current fallout levels, instead of the 1956 factor of 2.2×10^4. However, the data for 1958 suggest that the upper bed may be losing Sr^{90} at a slower rate than the lower bed. If this hypothesis proves to be valid, then differences in radionuclide content of the soils between the upper and lower bed would be increased. In either case it is possible that the rate of loss may decrease later, so that Sr^{90} could remain far above fallout levels for many decades.

The use of an improved soil core sampler last year made possible a better estimation of the soil mass per unit area. Based on one hundred 6-in. cores taken with this tool, the soil mass in the bed was estimated to range from 1.4 to 1.6×10^6 lb/acre to a depth of 6 in. Computations of the Sr^{90} budget based on this figure are summarized in Table 6. The basic data are concentrations in microcuries per 100 g of soil, dry weight. These were extrapolated to curies per acre and curies per 40 acres. Forty acres was chosen because this is the approximate area of the vegetated portion of the bed. Not included in this calculation is the area immediately above White Oak Dam. This area is partially under water most of the year.

A considerable portion of the Sr^{90} burden has been removed from the topsoil. To what extent the Sr^{90} has moved vertically to the water table and laterally to the creek has not been determined. Profile analyses in different parts of the bed will be made to determine the extent of vertical and lateral movement. Permanent core sampling stations will be set up to follow the loss of Sr^{90} from the topsoil. The discrepancies between the values reported this year and those of last year[14] for the earlier samples are probably due to the fact that previous analyses were done in various laboratories using different techniques. Similar budget analyses for the other fission products are under way.

Table 6. Changes in the Sr^{90} Budget of White Oak Lake Bed

Year	Soil Concentration		
	Microcuries per 100 g	Curies per Acre	Curies per 40 Acres
1956	0.1371 ± 0.0127	0.8876 ± 0.0823	35.5 ± 3.29
1957	0.0745 ± 0.0058	0.4824 ± 0.0375	19.3 ± 1.50
1958	0.0453 ± 0.0039	0.2933 ± 0.0252	11.7 ± 1.01

Native Vegetation. – The pattern of vegetation increased in complexity during the past year. The successional trend has been an increase in numbers of the trees (particularly willow) at the expense of the herbaceous vegetation. The sedge-rush community maintained about the same amount of coverage as in 1957. The predominant plant communities now present in the lake bed are: black willow (*Salix nigra* Marsh.); sedge-rush (*Carex* spp., *Juncus* spp.); smartweed-grass (*Polygonum* spp., *Echinochloa* spp.); grass [*Echinochloa colonum* (L.)]; Spanish needle (*Bidens* spp.); and lespedeza [*Lespedeza cuneata* (D.)]. The general pattern of vegetation in the ecology study grid is illustrated in Fig. 15. In addition to willow the most abundant new trees are sycamore [*Platanus occidentalis* (L.)], smooth sumac [*Rhus glabra* (L.)], and green ash (*Fraxinus pennsylvanica* var. *subintegerrima* Fern.). Tree growth has been rapid, averaging 3 ft per year.

Two aspects of the soil-to-plant movement of radionuclides were explored further this year. First, many of the species sampled[14] in 1957 were again sampled and analyzed for radionuclide content. The purpose of this phase was to evaluate the extent of radioisotope accumulation over a period of two growing seasons. Second, duplicate 0.5 m^2 harvests of some of the plant communities were taken to provide information on radionuclide accumulation per unit area of vegetation and soil. These data are useful in estimating the total annual turnover of radionuclides by different plant communities.

The plant taxa sampled for the first phase were *Solidago* spp., *Eupatorium serotinum* Michx., *Impatiens* spp., *Polygonum* spp., *Bidens frondosa* (L.), *Rhus* spp., *Salix nigra* Marsh., and *Fraxinus pennsylvanica* Fern. In addition samples of sycamore [*Platanus occidentalis* (L.)] and pokeberry [*Phytolacca americana* (L.)] were taken to

[14] S. I. Auerbach *et al.*, *H-P Ann. Prog. Rep. July 31, 1958*, ORNL-2590, p 31.

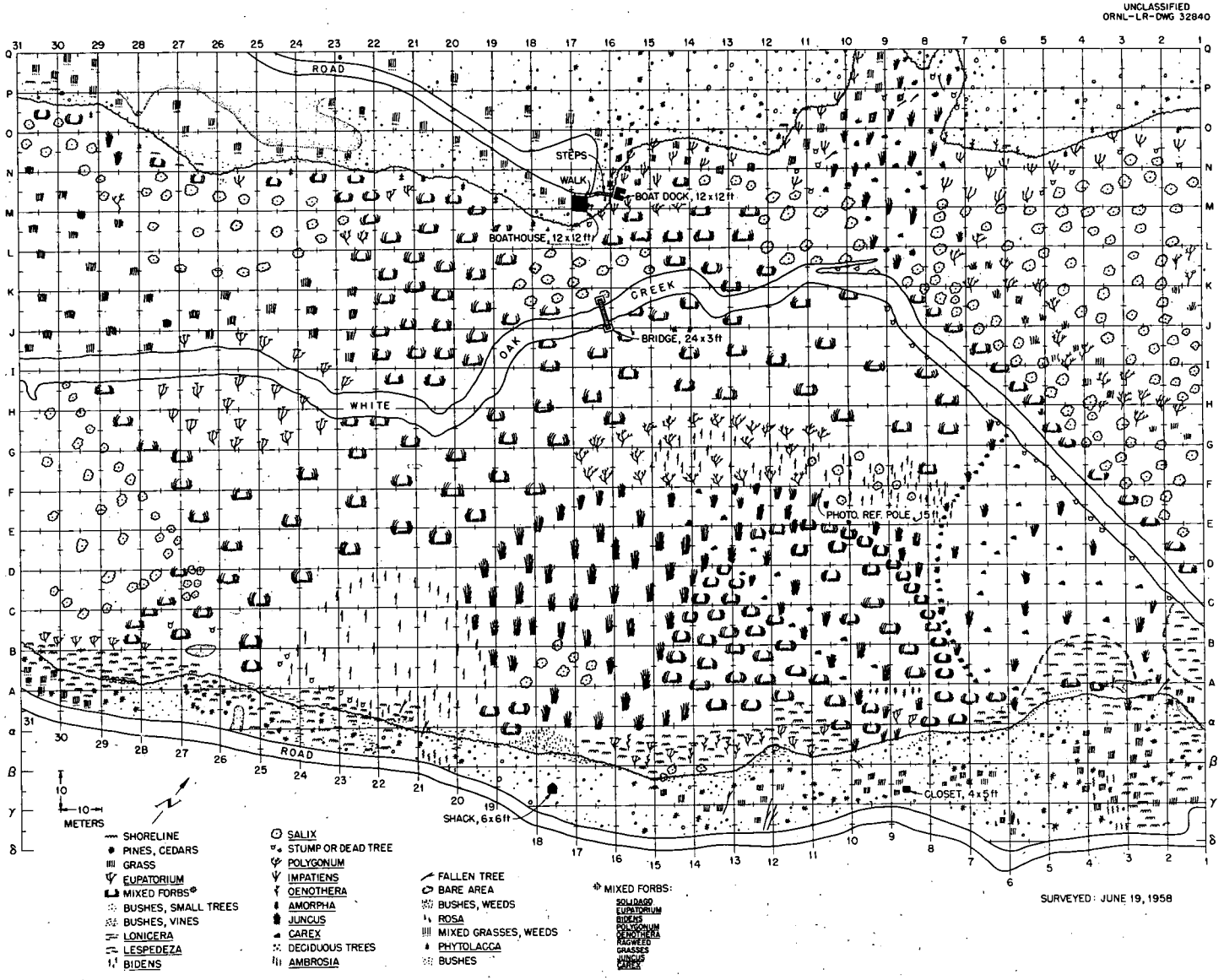

Fig. 15. Distribution of Vegetation in the Ecology Study Area of Lower White Oak Lake Bed, August 1958.

provide additional data for future comparisons. All samples were analyzed for Sr^{90}, Cs^{137}, Co^{60}, and the more abundant cations.[15]

Comparison of the Sr^{90} and Cs^{137} content of many of these species reveals that there are more similarities between 1957 and 1958 samples than differences (Table 7). Mean values for each plant part for the two years were tested for significance of difference by a *t* test.[16] However, variability of the lake bed samples was considerable and

[15] Acknowledgement is due S. A. Reynolds, T. H. Handley, C. L. Burros, W. R. Laing, and members of their respective groups in the Analytical Chemistry Division for performing these analyses.

[16] Statistical analyses were made by M. A. Kastenbaum, Mathematics Panel, ORNL.

Table 7. Comparisons of Radionuclide Content in Native Plant Species 1957 and 1958

In microcuries per 100 g

Differences are not significant unless indicated by asterisks

Species	Plant Part	Sr^{90}		Cs^{137}	
		1957	1958	1957	1958
Polygonum	Leaves	0.151	0.107		
	Stems	0.057	0.051		
Eupatorium					
Upper lake bed	Leaves	0.153	0.0745	0.012	0.042
	Stems	0.031	0.021	0.006	0.026
	Flowers	0.050	0.034	0.023	0.040
Lower lake bed	Leaves	0.062	0.121*	0.005	0.039
	Stems	0.021	0.030**	0.004	0.012
	Flowers	0.026	0.045**	0.008	0.025
Rhus					
Upper lake bed	Leaves	0.122	0.137	0.028	0.022
	Stems	0.095	0.139	0.009	0.020*
	Petioles	0.200	0.199	0.028	0.035
Lower lake bed	Leaves	0.111	0.151	0.005	0.003*
	Stems	0.094	0.232	0.003	0.004
	Petioles	0.159	0.410		
Solidago	Leaves	0.098	0.074	0.028	0.065**
	Stems	0.044	0.036	0.018	0.014
	Flowers	0.028	0.0318	0.040	0.052
Bidens	Leaves	0.042	0.099		
	Stems	0.033	0.028		
	Flowers	0.031	0.024		
Impatiens	Leaves	0.241	0.177		
	Stems	0.385	0.158**		
Fraxinus	Leaves			0.023	0.018
	Stems			0.007	0.013
	Petioles			0.023	0.027

*Significant at $P = 0.05$.

**Significant at $P = 0.01$.

the number of replicates was not great. Consequently, the degree of difference and the significance that is placed on this difference should be interpreted on the basis of the considerable variance in the samples. Nevertheless, the general trend over the past three years gives no indication of cumulative concentration. The four tree genera analyzed (*Rhus*, *Salix*, *Platanus*, *Fraxinus*) show no evidence of increasing accumulation in leaves or stems. Within this group, *Rhus* (sumacs) seem to be the most effective concentrators of Sr^{90}. On the other hand Cs^{137} and Co^{60} concentrations are much the same between the four genera. Consequently, even though sumacs have shallow, spreading roots this physical characteristic in itself would not account for the differences.

From a synoptic viewpoint, the most important general fact emerging from these studies is that the plants are maintaining the same concentrations of radionuclides, especially Sr^{90}, over a period of three years. This fact becomes particularly significant when the total accumulation of radionuclides per unit area is considered. Table 8 lists the total Sr^{90}, Cs^{137}, and Co^{60} per square meter of vegetation expressed as per cent of the total soil burden per square meter. Only one plant community – a legume (*Lespedeza cuneata*) – removed more than 1% of the soil burden of radionuclides. The per cent Cs^{137} accumulation was small even though in the first nine quadrats the concentration in the soil was high, ranging from 3 to 11 mc/m^2. Removal of Sr^{90} by the plants was far more effective, because Sr^{90} concentrations in the soil of the same quadrats ranged from 18 to 235 $\mu c/m^2$.

The possibility that increasing amounts of Sr^{90} are being tied up in the vegetation and undecayed litter can be ruled out at the present time because accumulation of strontium by the vegetation has been approximately the same since studies were started. The total Sr^{90} burden in vegetation on the 40 acres, using the highest values for accumulation per unit area, would be 150 mc. If it is assumed that equal quantities are contained in the two-year (1956 and 1957) accumulation of undecayed litter, then a maximum of 500 mc is bound in these compartments of the biological system. Most of the vegetation has a lower concentration, and this would be reflected in the litter. Since much of the 1956 litter has been decomposed and returned to the soil, the actual quantity in the vegetation is probably even less. Movement of Sr^{90} out of the litter may not be in equilibrium with the rate of income from vegetation for several more years. Yet decay rates on the lake-bed site are probably fast enough that high storage will not occur here.

Table 8. Accumulation of Radionuclides in 1 m^2 of Vegetation

Per cent of total soil burden of radionuclides

Quadrat No.	Plant Type	Sr^{90}	Cs^{137}	Co^{60}
1	Barnyard grass (*Echinochloa*)	0.12	0.017	0.003
2		0.004	0.0004	0.041
3		0.09	0.007	0.018
4		0.007	0.001	0.006
5		0.06	0.002	0.001
6		0.05	0.001	0.001
7	Smartweed (*Polygonum*)	0.69	0.006	0.019
8		0.93	0.015	0.048
9	Sericea (*Lespedeza*)	2.3	0.011	0.007
10		1.3	0.009	0.004
11	Begger-tick (*Bidens*)	0.62	0.006	0.006
12		0.54	0.041	0.006

As more Sr^{90} (and calcium) is leached out of the surface soil the possibility remains that the vegetation might translocate a relatively greater proportion of this fission product than it has the past three years. Under those circumstances a continuous replenishment of the surface soil in hazardous quantities might occur for several decades. In spite of the considerable loss of Sr^{90} in the past three years, there has not been any reduction in the hazard potential of the vegetation when considered from the food-chain aspect. In terms of strontium units (micromicrocuries of Sr^{90} per gram of Ca) the 1958 samples ranged from 8.0×10^4 to 7.0×10^5, which strongly suggests a long-term hazard for areas heavily contaminated

by this fission product unless effective means of depressing plant uptake or of removal from the soil are developed.

Agricultural Experiments. – Three species of forage crops, German millet (*Setaria italica*), sweet Sudan grass (*Sorghum sudanense* × *saccaratum*), and orange fodder cane (*Sorghum vulgare*), were planted in a randomized plot design in the lake bed agricultural plot. Three 30- by 50-ft blocks were laid out so that they spanned areas of high and low radionuclide contamination. Duplicate 4- by 4-ft plots were planted for each species in each block after being selected at random. Prior to seeding, ten 6-in. soil cores were taken in each of ten randomly selected plots in each block. These soil samples were analyzed for radionuclides and important nutrient cations. The mean values for these elements as well as the general chemical properties of the soil in each block are summarized in Table 9. Block III had the largest concentration of radionuclides, especially Cs^{137}. This block also had the greatest amount of exchangeable Ca and P.

Each species was harvested at maturity: German millet in August, sweet Sudan grass early in September, and orange fodder cane in the middle of October. All plots were clip-harvested to obtain the total yield per square meter (Table 10). The harvests were washed with mild detergent to reduce external contamination, dried at 105°C for at least 48 hr, ground in a Wiley mill, and then processed for chemical and radiochemical analyses.[15] For chemical analyses duplicate 1-g (dry weight) samples were wet-ashed with a mixture of nitric, sulfuric, and perchloric acids; the solutions were brought to volume; and cation determinations were made with a flame photometer. For radioanalyses single samples averaging 40 g (dry weight) were dry-ashed (450°C). The ash was then analyzed for gamma emitters spectrometrically. Upon completion of the gamma analyses duplicate aliquots of the ash samples were analyzed radiochemically for Sr^{90}.

The crops were compared within blocks and between blocks by means of analyses of variance. The results are summarized in Table 11. The concentration of radionuclides is significantly different statistically between the crop species and between the blocks. The concentrations of Ca, K, and Na were also significantly different between the crops but not between the blocks. German millet had the largest concentrations of radionuclides and Ca, K, and Na, whereas orange fodder cane had the smallest concentrations.

These differences in concentration are partly related to the crop yield. Millet had the lowest mean yield (Table 10), whereas fodder cane had the largest yield. Consequently some portion of the differences in concentration of these elements represents simple dilution by organic matter. In Fig. 16 the total radionuclide content per square meter of vegetation is plotted as a function of

Table 10. Yield of Forage Crops in White Oak Lake Bed Agricultural Plot

In grams per square meter (dry weight)

Block	Millet	Sudan Grass	Orange Fodder Cane
I	286	406	954
II	236	238	759
III	530	830	2358
Average	351 ± 79	491 ± 125	1358 ± 330

Table 9. Concentrations of Radionuclides and Chemical Properties of Soil Plots in White Oak Lake Bed Agricultural Plot – Summer, 1958

Values are means per block

Block	Sr^{90} (μc per 100 g)	Cs^{137} (μc per 100 g)	Co^{60} (μc per 100 g)	Ca (meq per 100 g)	K (meq per 100 g)	Na (meq per 100 g)	P (ppm)	pH
I	0.0253	0.279	0.125	17.7	0.339	0.333	2.10	6.95
II	0.0206	0.256	0.093	16.9	0.310	0.325	2.36	7.05
III	0.0305	0.948	0.151	21.2	0.276	0.267	3.17	7.39

yield for Sr^{90}, Cs^{137}, and Co^{60}. The grand means are plotted with 67% confidence limits; curves were fitted by connecting the grand means and zero axes. The crop mean for Sr^{90} yield is the same irrespective of plant yield, indicating the dilution effect. For example, millet had approximately one-fourth the yield of orange fodder cane (Table 10) and four times as much Sr^{90} per gram of plant (Table 11). While the curves for Cs^{137} are quite similar to those for Sr^{90}, the data for the blocks suggest a somewhat different relationship between fission product concentration and plant yield. The plants in block III had the greatest yield for all three species and also the highest concentration of Cs^{137} in comparison with the plants in the other blocks (Tables 10 and 11). Block III also had the highest concentration of Cs^{137} in the soil (Table 9), which suggests that

Table 11. Summary of Concentrations of Elements in Three Species of Forage Plants in White Oak Lake Bed

Values given are means of four replicates

Element	Block	Millet	Sudan Grass	Orange Fodder Cane	Degree of Significant Difference	
					Between Crops	Between Blocks
		$\times 10^{-2}$	$\times 10^{-2}$	$\times 10^{-2}$		
Sr^{90}, μc per 100 g	I	6.35	7.20	1.30		
	II	6.07	3.60	1.65	Highly significant	Significant
	III	5.45	3.42	1.67		
Cs^{137}, μc per 100 g	I	2.17	1.52	0.72		
	II	2.67	1.77	1.00	Highly significant	Highly significant
	III	2.90	3.05	1.87		
Co^{60}, μc per 100 g	I	1.07	0.30	0.08		
	II	1.47	0.47	0.08	Highly significant	Highly significant
	III	1.10	0.17	0.09		
Ca, g per 100 g	I	36.5	31.5	15.1		
	II	52.2	28.2	15.9	Highly significant	Not significant
	III	42.7	29.2	6.97		
K, g per 100 g	I	161.0	126.5	37.0		
	II	117.7	59.0	42.5	Highly significant	Significant
	III	122.5	64.5	37.7		
Mg, g per 100 g	I	14.5	12.6	11.0		
	II	10.5	14.3	12.5	Not significant	Not significant
	III	8.7	17.5	9.5		
Na, g per 100 g	I	4.43	1.06	0.79		
	II	2.53	0.80	0.62	Significant	Not significant
	III	1.88	1.19	0.69		

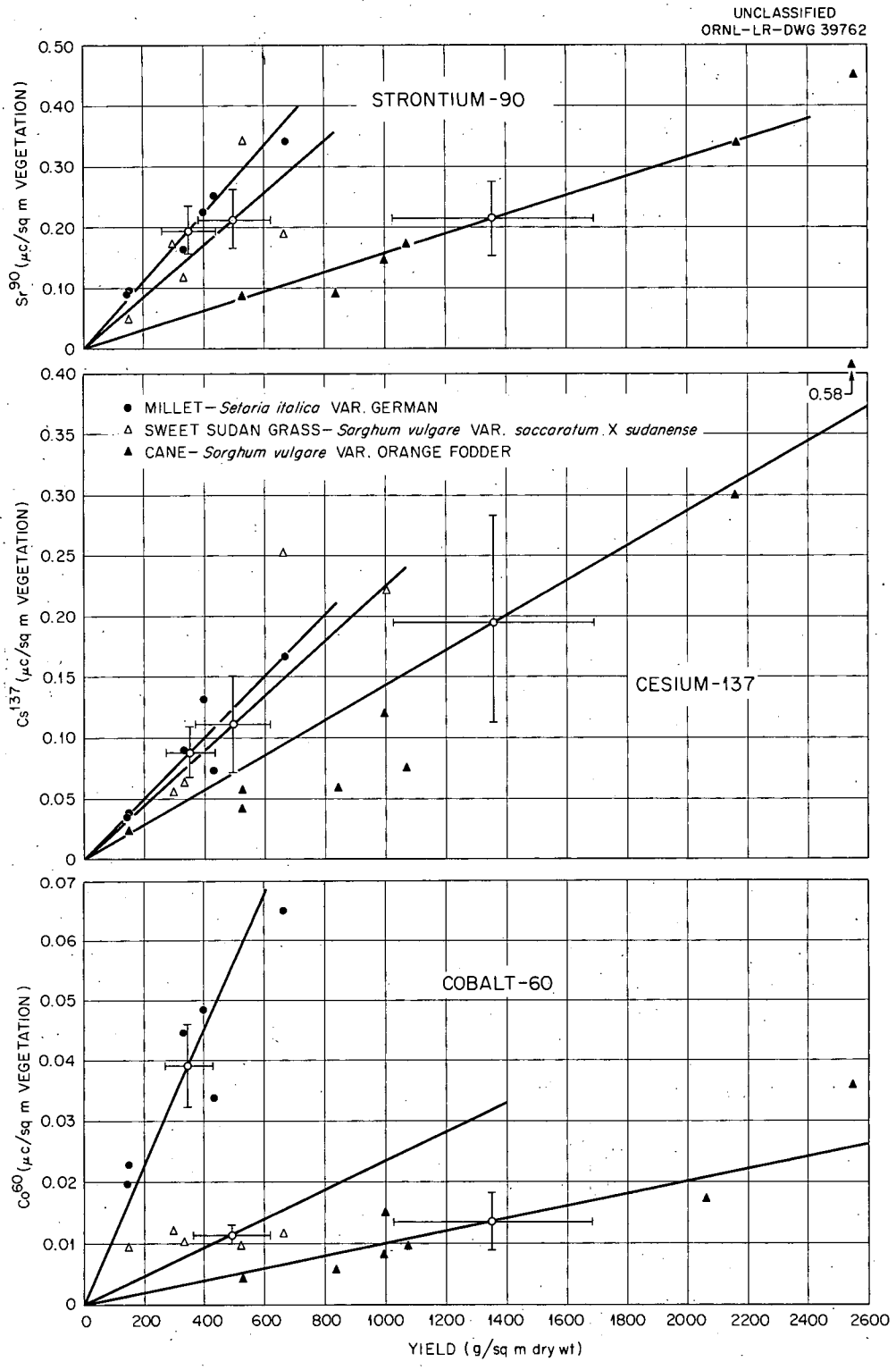

Fig. 16. Relationship Between Total Accumulation of Radionuclide Per Unit Area and Yield of Vegetation.

the concentration of fission products in the soil is also reflected in the amount accumulated by vegetation.

The bottom set of curves in Fig. 16 for Co^{60} indicates the effect of species physiology on the accumulation of radionuclides. The Co^{60} concentration in millet is significantly greater than in the other two species irrespective of yield and concentration in the soil.

Evaluation of the turnover of fission products by vegetation in a given ecosystem cannot minimize the effects of the following factors: (1) the concentration of fission product in the soil, (2) the physiological control of nutrient uptake by the various species populations, (3) the productivity (yield) of the different species populations comprising a vegetation unit.

Insect Studies. – The sampling regimen for insects on vegetation of the lake bed, initiated in 1956,[17] was continued in 1958. The three major objectives of the sampling are: (1) to discover how quickly insects invade the lake-bed vegetation, (2) to estimate the weight of insects per unit area (biomass), and (3) to obtain data on the accumulation of fission products by these insects. This sampling program is providing an estimation of the role of the insects in the environmental cycling of fission products.

Samples have been taken in three vegetation types: sedge-rush, smartweed, and willow. Generally, the insect communities in each of these areas were composed of a few dominant species during the first year the vegetation became established on the lake bed (1956 for sedge-rush and smartweed, 1957 for willow). In the herbaceous communities during subsequent seasons the trend has been for these dominant insect species to become less numerous and for additional insect species to appear. However, the willow insect community is still dominated by one group.

In the sedge-rush vegetation type, 1956 samples revealed a community dominated by two leafhopper species, two grasshopper species, a predaceous lygaeid bug, and a number of fly species. Numbers of these insects accounted for about 80% of the insects collected. In 1957 these groups of insects (leafhoppers, grasshoppers, true bugs, and flies) were still the most abundant, but no species was clearly dominant (i.e., of such abundance as to greatly exceed the other species in numbers of individuals). About 50–60% of the insects collected belonged to these groups. In 1958 the insect community was similar to that of 1957.

The smartweed vegetation type supported in 1956 a community dominated by a plant bug (*Lygus lineolaris*), bees, and flies. About 70% of the insects collected belonged to these groups. In 1957 other plant bugs, leafhoppers, bees, and flies were the most numerous, but many additional insect species appeared. All these groups were less numerous in 1957 than in 1956, and still less numerous in 1958.

The willow vegetation type was dominated by a single species of flea beetle, *Chalcoides fulvicornis* (Fab.), during the first year the willow insects were sampled (1957). A variety of other insect species was present but none was abundant. The 1958 samples revealed a very similar community, consisting of many insect species but still dominated by the flea beetle. The numbers of the flea beetle were greater in 1958 than in 1957.

Evidently, then, the insects characteristic of the sedge-rush and smartweed vegetation types required two or more seasons to develop, with the greatest change in the composition of the insect fauna occurring between the first and second seasons. Little change occurred in the willow insect community. Changes in the abundances of the vegetation types themselves may be reflected in these changes in their insect communities. The sedge-rush association maintained about the same amount of coverage on the lake bed during the period of study, but smartweed decreased in abundance and willow increased markedly. The expanded willow habitat available to the insects in each season may be responsible for the continued high populations of the dominant flea beetle in that community.

A sampling method has been developed for the estimation of the numbers and weights of insects per square meter of vegetation. Briefly, this method involves a series of replicated sweeps with an insect net which was checked against the results from a box trap. The box trap (Fig. 17) was a portable plywood box open at the bottom, standing 5 ft high, and covering 1 m^2. On one side was a plastic funnel, to which a killing jar could be attached. When the box was dropped over the vegetation, many insects were attracted

[17] R. M. Anderson *et al.*, *H-P Ann. Prog. Rep. July 31, 1957*, ORNL-2384, p 21.

Fig. 17. Insect Box Trap for Use in Smartweed Area.

to the light visible through the plastic funnel and were collected in the jar. Ten rapid consecutive sweeps through the vegetation with an insect net yielded about the same number of insects as were caught in the box trap. Both methods were used in estimation of biomass of insects.

A summary of the biomass estimates is given in Table 12 for the three vegetation types and for the years 1956–58. While the means for 1958 are higher than those for 1957, the differences between the years are not significant statistically. For the smartweed and sedge-rush areas, an average of 239 mg/m^2 was obtained for these years. Estimates similar to those in Table 12 were obtained by Cross[18] for old-field areas in Georgia. Estimates of biomass of insects on willow could not be checked against the box trap. By 1958 the willows had reached such size that the ten-sweep method for estimating biomass of insects was no longer applicable.

For the biomass samples a correlation coefficient r of 0.26 was obtained for numbers of insects per sample vs weights of samples. This correlation, although highly significant statistically, is too low to permit prediction of weights of samples from numbers of insects in samples.

Previous estimates of radionuclide content of insects on White Oak Lake bed were based on the biomass samples.[19] In order to refine these estimates, larger samples were taken in 1958. Samples were analyzed by gamma spectrometry for Cs^{137}, Ru^{106}, and Co^{60}, and then by radiochemical methods for Sr^{90} (ref 15).

[18] W. H. Cross, *The Arthropod Component of Old Field Ecosystems. Herb Stratum Populations with Special Emphasis on the Orthoptera*, unpublished doctoral dissertation, University of Georgia, 1956.

[19] S. I. Auerbach *et al.*, *H-P Ann. Prog. Rep. July 31, 1958*, ORNL-2590, p 38.

Table 12. Biomass (Dry Weight) of Herbivorous Insects on Vegetation Growing on White Oak Lake Bed

In milligrams per square meter

Year	Sedge-Rush		Smartweed		Willow	
	Mean	Standard Error	Mean	Standard Error	Mean	Standard Error
1956			192	38		
1957	197	34	202	26	88	9
1958	273	78	330	92		

Figure 18 shows a gamma scan for insects, plants, and soil of White Oak Lake bed. In the samples of insects, Cs^{137}, Co^{60}, and Ru^{106} were present in detectable amounts, with Cs^{137} concentrations being the highest; Sr^{90} also was detected by radiochemical methods.

Table 13 presents the Cs^{137} and Sr^{90} concentrations in six groups of insects. Of these, *Conocephalus* and *Melanoplus* are grasshoppers, *Systena* is a flea beetle, bees include a number of species, *Chauligognathus* is a soldier beetle, and Hemiptera-Homoptera includes mostly aphids and leafhoppers. Transfer of nuclides from plant hosts to these insect species is illustrated in Table 14. The Cs^{137} concentrations in the insects are very similar to the plant concentrations. Only in the case of insects feeding on *Juncus* is there a marked discrepancy between insect and plant concentrations of Cs^{137}. Since *Juncus*, a rush, has a low growth form, it is possible that plant values for this species include some soil contamination and thus are high. In any case it is evident from Table 14 that insects accumulate Cs^{137} to such extent that concentrations in plants and insects are quite similar.

In contrast, Sr^{90} concentrations in insects are nearly an order of magnitude lower than plant concentrations (Table 14). Still, the Sr^{90} concentrations in the insects are clearly related to concentrations in the host plants. The insects accumulate a larger amount of Cs^{137} than Sr^{90} in reference to the Cs^{137} and Sr^{90} in the host plants, and as a result, concentrations of these nuclides in insects are quite similar, although Sr^{90} concentrations are higher than Cs^{137} concentrations in the plants.

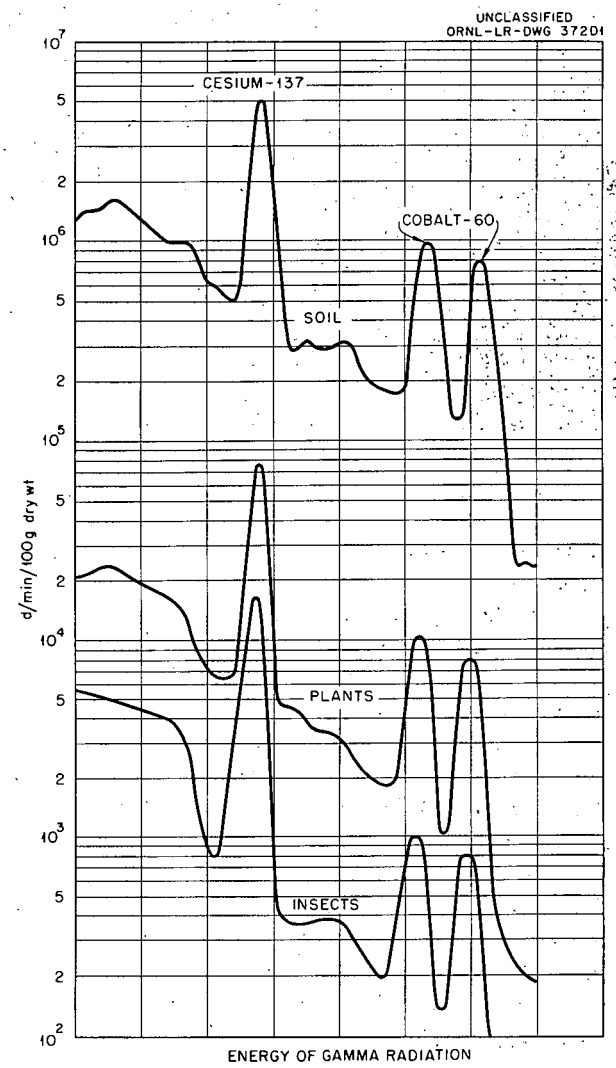

Fig. 18. Gamma Radioactivity in Soils, Plants, and Insects of White Oak Lake Bed.

Table 13. Concentrations of Sr^{90} and Cs^{137} in Insects Feeding on Vegetation of White Oak Lake Bed

Insect Species	Concentrations [$\mu c/g$ (dry wt)]	
	Cs^{137}	Sr^{90}
	$\times 10^{-4}$	$\times 10^{-4}$
Conocephalus	1.50	1.40
Systena	1.40	1.78
Bees	0.65	0.71
Chauligognathus	0.62	1.40
Melanoplus	0.59	0.10
Hemiptera-Homoptera	0.43	0.06

These data afford an interesting example of the interplay of biological materials in the environmental cycling of fission products. White Oak Lake bed soils contain more Cs^{137} than Sr^{90}, but native vegetation accumulates higher concentrations of Sr^{90} than Cs^{137} (by a ratio of approximately 7 to 1). In the herbivorous insects, however, the process is reversed, and Cs^{137} and Sr^{90} concentrations become approximately equal.

Accumulation and Excretion of Cs^{137} by Grasshoppers. – Knowledge of the rates of accumulation and excretion of radionuclides is essential to the interpretation of field data collected in areas such as White Oak Lake bed, where environments have become contaminated with fission products. Accordingly, a series of laboratory experiments was performed with adults of *Romalea microptera* (Beauv.), the eastern lubber grasshopper (Fig. 19).

Bean plants were used as the primary food source for the grasshoppers. Introduction of Cs^{137} into the grasshoppers' food was accomplished by injecting 1 μc of $Cs^{137}Cl$ (0.2 ml of aqueous solution) directly into the stems of the plants. Autoradiography showed that the cesium moved readily throughout all parts of the plant. For some of the uncontaminated feedings, native plants (*Polygonum* spp.) were substituted for the bean plants, since the grasshoppers required more plant food than could readily be grown.

A model 810 Baird-Atomic gamma scintillation detector with a 2- by 2-in. well crystal was used for estimation of Cs^{137} in grasshopper tissues and

Table 14. Transfer of Cs^{137} and Sr^{90} from Plants to Insects

Values are in units of 10^{-4} microcurie per gram (dry weight)

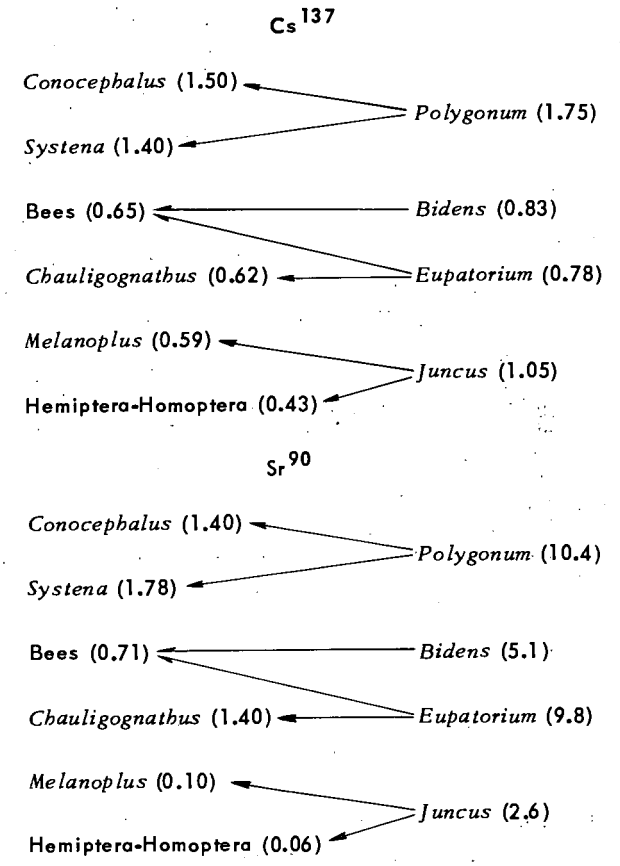

in living grasshoppers. Though living grasshoppers were too large to fit into the well, satisfactory counting (at 5% efficiency) was achieved by placing the grasshoppers in cellophane sleeves which held them in position on top of the crystal. The efficiency for this method was established by injecting known amounts of Cs^{137} into the abdominal cavities of test insects; experimental insects were subsequently counted in the same geometry.

A biological half life of about four to five days was estimated for Cs^{137} in *Romalea*. This estimate was obtained by isolating several individuals which had reached high body burdens and measuring their radioactivity at about 12-hr

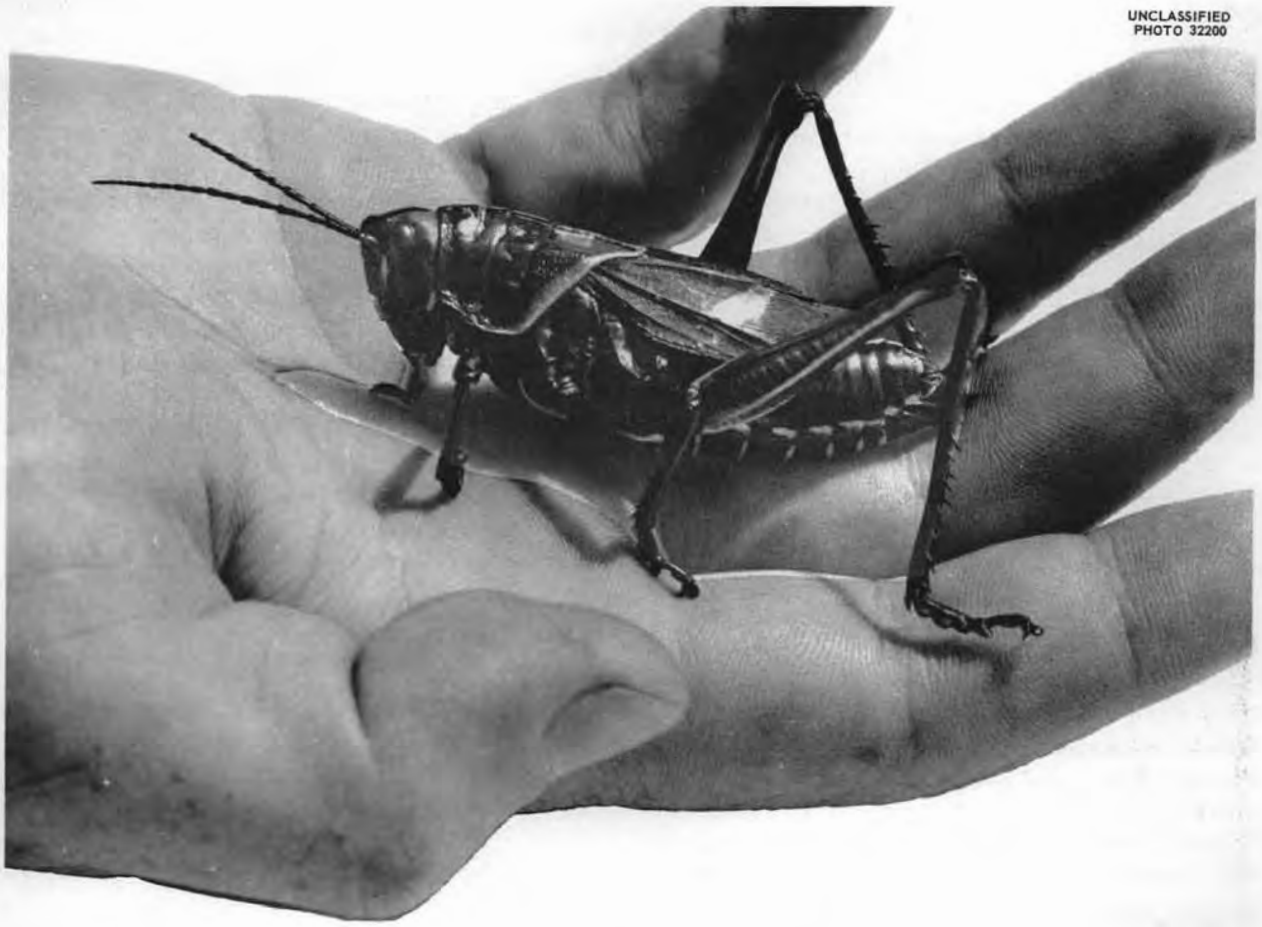

Fig. 19. *Romalea microptera* (Beauv.).

intervals. The results are shown in Fig. 20, where the average body burdens of five individuals are plotted as a function of time. While the four- to five-day rate is theoretically an effective half life, the physical half life of Cs^{137} is so long (about 33 years) that physical decay is of no significance in these measurements.

The accumulation of cesium by the grasshoppers was followed in three cages of sixteen grasshoppers each. Individual grasshoppers were identified by numbers painted on their backs. Bean plants containing 2 μc of Cs^{137} were placed in cage I on every second day, so that the average dose per grasshopper was 0.125 μc. Those in cage II received this dose every fourth day, and those in cage III every eighth day. In cages II

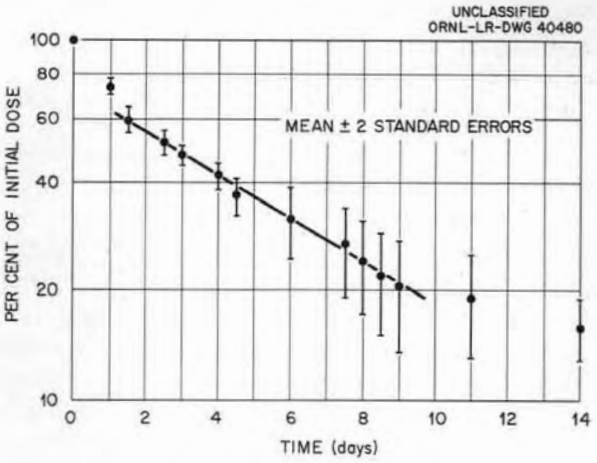

Fig. 20. Elimination of Cs^{137} by *Romalea*.

and III cesium-free plants complemented the feeding, so that each cage of grasshoppers was fed on every second day. All the food placed in the cages was consumed.

When the equilibration experiments were started, the grasshoppers already contained some Cs^{137} from preliminary trials. Those grasshoppers with the least body activity were placed in cage I and received the most cesium in food, while those with the most body activity were placed in cage III and received the least cesium. Grasshoppers in cage II had an intermediate level of body activity and were placed on the intermediate diet. In this manner equilibration with food was followed both as an increase (cage I) and a decrease (cage III) in whole-body activity of the grasshoppers.

Results for cage III are illustrated in Fig. 21, which shows the mean whole-body activity of the grasshoppers as a function of time. The expected values were calculated from the equation

$$Q_t = Q_0 e^{-\lambda t} ,$$

where Q_t is the whole-body activity at time t, Q_0 is the initial whole-body activity, λ is $0.693/T_b$, and T_b is the biological half life. A T_b of four days was used in these calculations. The observed values show reasonable agreement with the expected ones for about four weeks, after which time the grasshoppers began to die. Seemingly death was not the result of the experimental treatment, since control grasshoppers also began to die at about this time. The grasshoppers became lethargic several days before death, and did not feed or eliminate to any extent; thus, their observed radioactivity tended to remain constant. Accordingly, considerable deviation between expected and observed values at the end of the experiment could be anticipated. The standard error, shown in Fig. 21, became larger at the end of the experiment because the number of grasshoppers in the cage was reduced by deaths to 3.

Grasshoppers in cage II showed little change in whole-body concentration of Cs^{137} with time. The concentrations in the grasshoppers were almost at equilibrium with the food dosage when the equilibration experiments were started, so that little change in concentration could be expected.

Figure 22 shows the results from cage I, where grasshoppers received 2 μc in bean plants every second day. These grasshoppers had the lowest

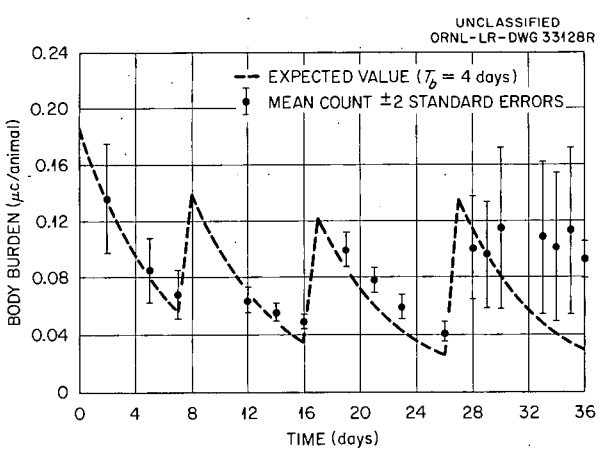

Fig. 21. Total Body Activity in *Romalea*, Cage III: 2μc of Cs^{137} Every 8th Day.

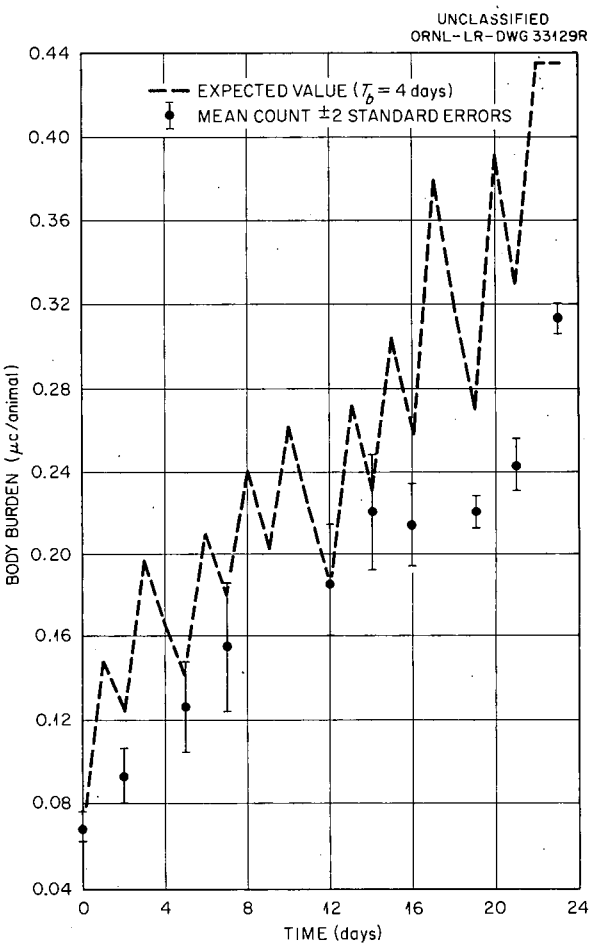

Fig. 22. Total Body Activity in *Romalea*, Cage I: 2 μc of Cs^{137} Every 2nd Day.

initial level of body activity. The curve for expected values in Fig. 22 shows distorted periodicity due to an occasional missed feeding. Also, the grasshoppers in this cage began to die after the first week, and difficulty was experienced in attempts to adjust the dose so that the amount per grasshopper remained constant. Agreement of observed with expected results is not good, but is reasonable for the first two weeks. In the latter part of the experiment the whole-body activities of the grasshoppers tended to remain constant, as did those in cage III. Presumably this stability of whole-body concentrations was also due to the cessation of feeding and elimination prior to death.

The Cs^{137} concentrations in a grasshopper species such as *Romalea microptera* feeding on vegetation in a contaminated area evidently would come into equilibrium rapidly with the concentration in the vegetation. The time required to reach equilibrium was not measured directly in our experiments; however, the time required to reach 50% of the equilibrium value is the same as the time required to eliminate 50% of the body activity (under conditions of constant intake and constant percentage elimination). Thus, the half time for 50% accumulation would be about four days, and equilibrium would be approximated ($^{31}/_{32}$ of the final value) after five such half times.

Analyses of grasshopper tissues and the use of autoradiograms showed that most of the ingested cesium is concentrated in the soft tissues. Table 15 presents the results of tissue analyses for four specimens of *Romalea microptera*. Muscular tissue, the digestive tract, and the reproductive organs contained much more cesium than did the exoskeleton.

Small-Mammal Program. – The long-term studies initiated in December 1957 on small mammals[20] are continuing. Information is accumulated mainly by live-trapping and the capture-recapture procedure, with information being recorded for each individual at first capture and for as long as it reappears. The mammals caught are examined in the field, and are then released at the point at which they were captured. Examination consists in noting species, animal number, sex, weight, age, point of capture, conditions of external genitalia, and related information. Information from the field data sheets is transferred to IBM cards. The populations are checked throughout the year. If possible, each main study area is trapped each week.

Emphasis on field trapping has been on two areas, one in the ecology grid area of White Oak Lake bed and the other in an old field near the confluence of White Oak Creek and the Clinch River. The earlier trapping areas in the lake bed (WOL-1 and WOL-2) were too small for the accumulation of data over a long term. It was possible in the summer of 1958 to enlarge the study area to about 7½ acres (WOL-3). All three of these areas are in that part of the grid area

[20] S. I. Auerbach *et al.*, *H-P Ann. Prog. Rep. July 31, 1958*, ORNL-2590, p 41.

Table 15. Cesium-137 Activities in Body Tissues of Four *Romalea microptera*

Tissue	Activity (μc/mg)				Mean of Sample Weights (mg)
	Male Cage II	Male Cage III	Female Cage II	Female Cage III	
	$\times 10^{-6}$	$\times 10^{-6}$	$\times 10^{-6}$	$\times 10^{-6}$	
Testes	258	320			20
Ovary				24	35
Eggs			135	10	600
Muscle	72	184	311	29	65
Digestive tract	178	248	705	26	450
Exoskeleton	3	5	2	3	100
Residue	66	87	138	15	700

to the south of White Oak Creek. On the north side of the creek is another area (WOL-4), about 4½ acres, which is trapped occasionally to gain additional information about mammals of the lake bed and to check the importance of the creek as a barrier to movement. The old-field area contains 10 acres and, being uncontaminated, serves as a comparison for the White Oak Lake bed.

Seasonal fluctuations of the dominant small mammals of White Oak Lake bed and the old field are indicated in Fig. 23. Both of these areas are in early herbaceous stages of plant succession during these studies. Plant succession was rapid on the lake bed for the first two years after the lake was drained. A young pine plantation was removed from the old-field area just prior to the beginning of studies on that area, and the openings left by the removal operation are still in the process of being occupied by plants. Consequently, the fluctuations in populations should be considered along with two main factors – season and plant succession. So far, only one species, the house mouse [*Mus musculus* (L.)] of the lake bed area, has been lost during succession. The white-footed mouse [*Peromyscus leucopus* (Raf.)] should be regarded as a marginal visitor of both areas, except during the early history of the lake bed, when this species ranged out on the bed with the house mouse. The dominant small mammals for the past year were cotton rats (*Sigmodon hispidus* Say and Ord) and rice rats [*Oryzomys palustris* (Harlan)] on the lake bed and pine mice [*Pitymys pinetorum* (LeConte)] and harvest mice [*Reithrodontomys humulis* (Audubon and Bachman)] on the old field (Fig. 23).

More detailed dynamics of the populations of three species are illustrated in Fig. 24. The high point in January is probably somewhat artificial since, owing to floods and other causes, only one night of trapping is represented and several individuals from nearby flooded areas are probably represented here. For the sake of brevity, in the following discussions on populations, weights, and home ranges only the cotton rats of the lake bed will be considered. Similar data exist for other species. The cotton rats had a clearly discernible nonbreeding period from January through March during which only one female was palpably pregnant. A puzzling aspect of the January-through-May period was the increase of individuals in spite of the cessation of births. Part of the explanation was better survival of the young born in the fall and early winter, but immigration from surrounding areas probably was involved also. Adult females outnumbered the adult males from August through November. From January through April the males were more numerous.

Field weights of mammals are important in that approximate ages may be determined, pregnancies can be followed, and physical conditions are often indicated (for instance, after a severe injury or illness the weight of an individual drops). Some weight curves for cotton rats are shown in Fig. 25. The data of Meyer and Meyer[21] were for caged rats with food available at all times. The curve for the spring-born rats starts with young which were born in the traps, freed, and retaken later. The rest of the curve was compiled from data for many other rats. No litters were born in the traps in the fall. The curve for the rats born in early fall was formed by plotting the weights of young individuals which were first taken in late fall and which continued in the area for over three months. It may be seen that the rats in the field increased in weight more slowly than the laboratory-reared animals, but this is not surprising in view of the abundance of food and lack of exercise for the latter. A more surprising aspect was the markedly slower increase in weight of the individuals born in early fall in contrast to the spring-born rats. Also, beginning in the last part of February the weights of the rats born in early fall began to level off or decline, with a sharp drop occurring in the last part of March and the first part of April, but the weight increase was rapid in the last part of April and during May. The animals born in late fall exhibited a similar pattern of growth. A decline and sharp drop in weight were also noted for heavier individuals at about the same time. Decreasing abundance and quality of food coupled with low temperatures probably contributed greatly to depletion of fat reserves and consequent loss of weight. A peculiar phenomenon is evident in Fig. 24: the 51-to-100-g weight group of cotton rats persisted and even increased in numbers from January through April, even though there was no recruitment from the group weighing 50 g or less; in May the numbers of the 51-to-100-g group

[21] B. J. Meyer and R. K. Meyer, *J. Mammalogy* 25, 107–29 (1944).

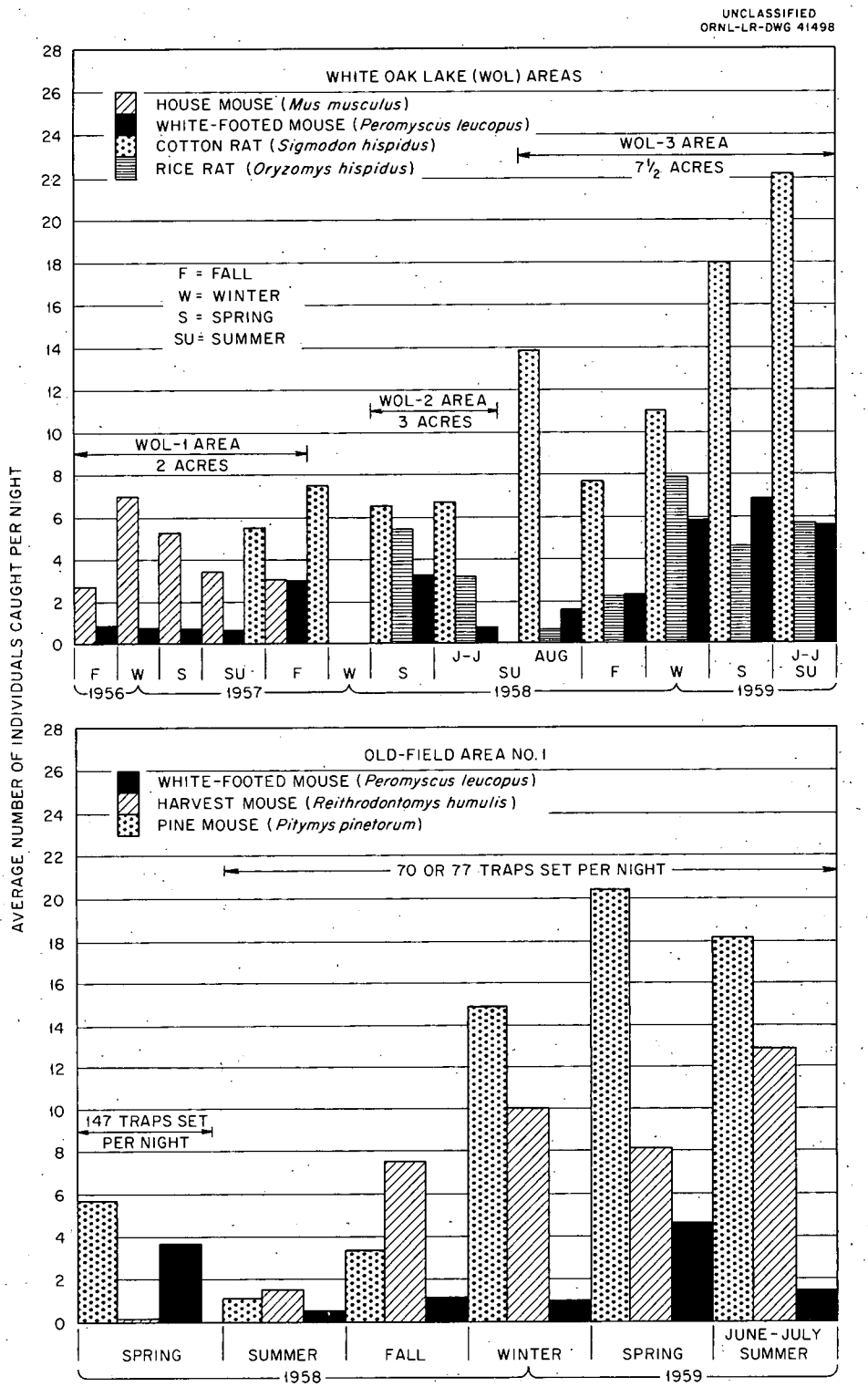

Fig. 23. Average Number of Dominant Small Mammals Caught per Night in the Old-Field and White Oak Lake Bed Areas.

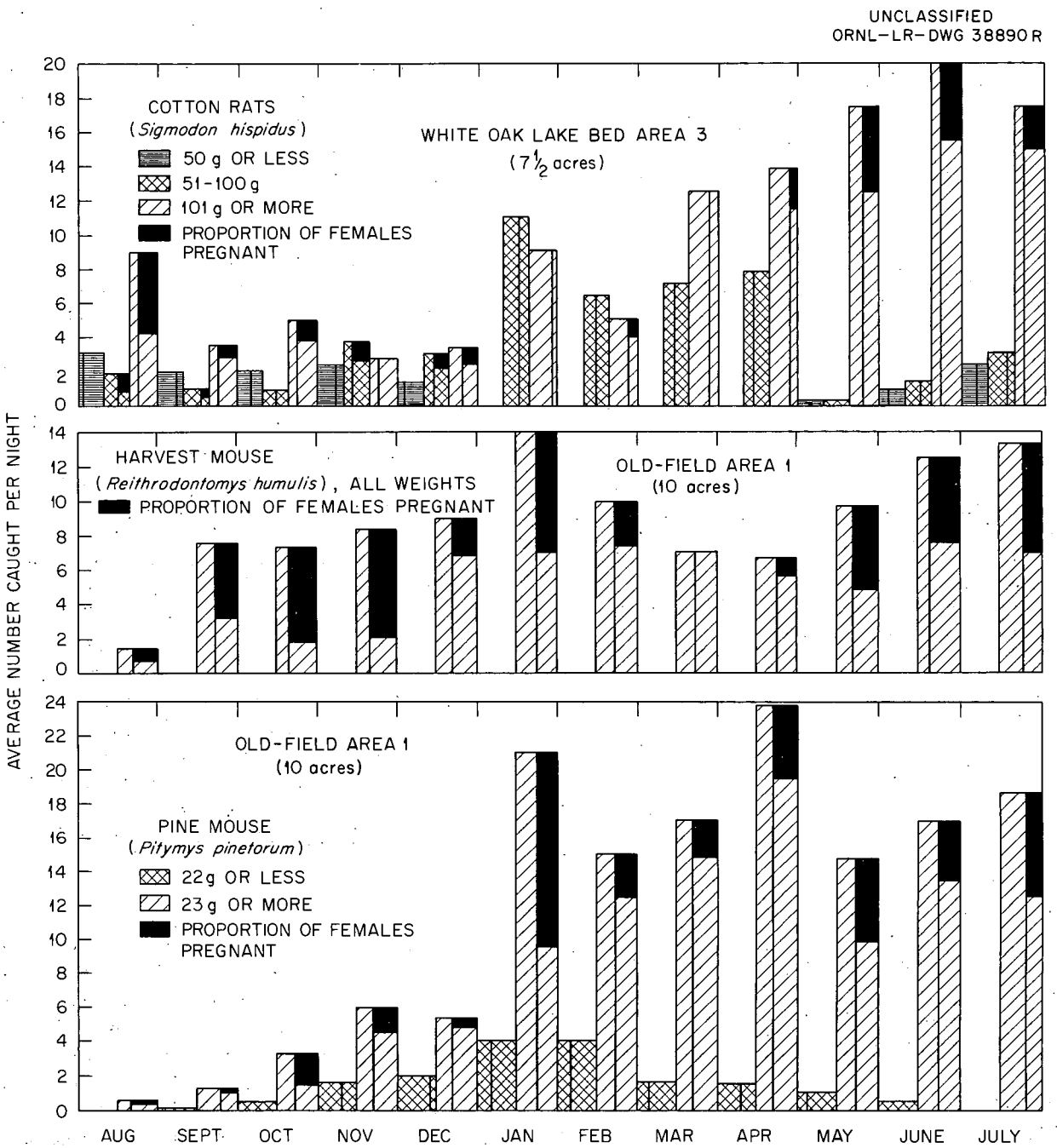

Fig. 24. Average Number of Three Species Caught per Night in Two Areas, 1958–59. The vertical lines within the bars indicate the proportion of males to females.

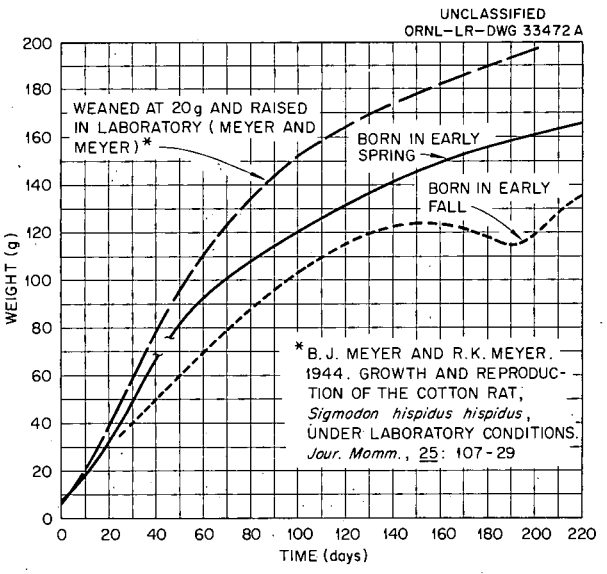

Fig. 25. Male Cotton Rats – Weight vs Time.

dropped precipitously. The slow rate of growth and the weight drop of the younger rats, especially those born in the late fall, probably explains in large part the persistence of the 51-to-100-g group through time. The rapid rise of weights in May was reflected in the virtual disappearance of this group as its members passed into the over-100-g weight group.

It is necessary to know the home ranges of individuals in an area to understand some of the activities of the individuals. The home range of an animal is an established area within which the animal moves during its everyday activities. These ranges are estimated by plotting boundaries about points at which captures are made (Figs. 26 and 27). The home ranges of adult females during the indicated time (Fig. 26) were well defined, with little overlap. The later histories of two of these ranges are interesting. Part of the range of No. 53 nearest the creek was seldom utilized by cotton rats. After the disappearance of No. 5, No. 53 abandoned this northern part of her range and extended her range into part of the area formerly occupied by No. 5. Similarly, after the disappearance of No. 4, No. 22 extended her range into part of the former range of No. 4, abandoning the eastern part of her own range. The home ranges of the adult males (Fig. 27) were not well defined and showed considerable overlap, because most of the males were located in what was apparently a choice part of the area for cotton rats. Trips of up to 350 ft or more were often made to far parts of the area. Two interesting facts emerge from the home range information. One is that cotton rats may occupy a home range for a relatively long time (for example: Nos. 17 and 18, males, for over six months; No. 22, female, over seven months; and No. 53, female, over ten months). The other is that the limits or boundaries of the ranges are not necessarily fixed but may be somewhat amoeboid.

Knowledge of home ranges is important in estimating external and internal doses received by individuals in a heterogeneously contaminated area such as the lake bed. A study of the radiation field over the lake bed[22] showed that, in general, in the 10-m-grid area the amount of radiation is highest near the creek and lessens toward the shores (Fig. 28). By considering the radiation field in relation to home range, it is possible to estimate the average amount of external radiation to which a resident animal is exposed for a given time. For instance, during the times indicated on Fig. 26 it was estimated that cotton rat No. 22 was exposed to external radiation of ~18 r/month, while No. 44 was exposed to ~3 r/month. When No. 53 altered her home range, she was exposed to ~9 r/month, rather than ~13 r/month.

The long-term studies on field populations will continue during the coming year. In addition, analyses will be made of radioactive materials in small mammals from the lake bed, and irradiations will be started on small mammals from radioactive and nonradioactive areas.

Forest Studies

Introduction. – A chemical and radiochemical study of natural vegetation reveals radioactive contamination outside the local areas (such as the waste pits and White Oak Lake bed) which are affected by disposal of processed wastes; such contamination is ascribed partly to local fallout and partly to regional fallout. More fundamentally, this study involves the gathering and organizing of information which is needed for predicting the future movements of isotopes in natural ecosystems, particularly forests.

These studies therefore include analyses of the elements which influence the movements of the

[22] P. K. Lee and S. I. Auerbach, *Determination and Evaluation of the Radiation Field Above White Oak Lake Bed*, ORNL-2755 (1959).

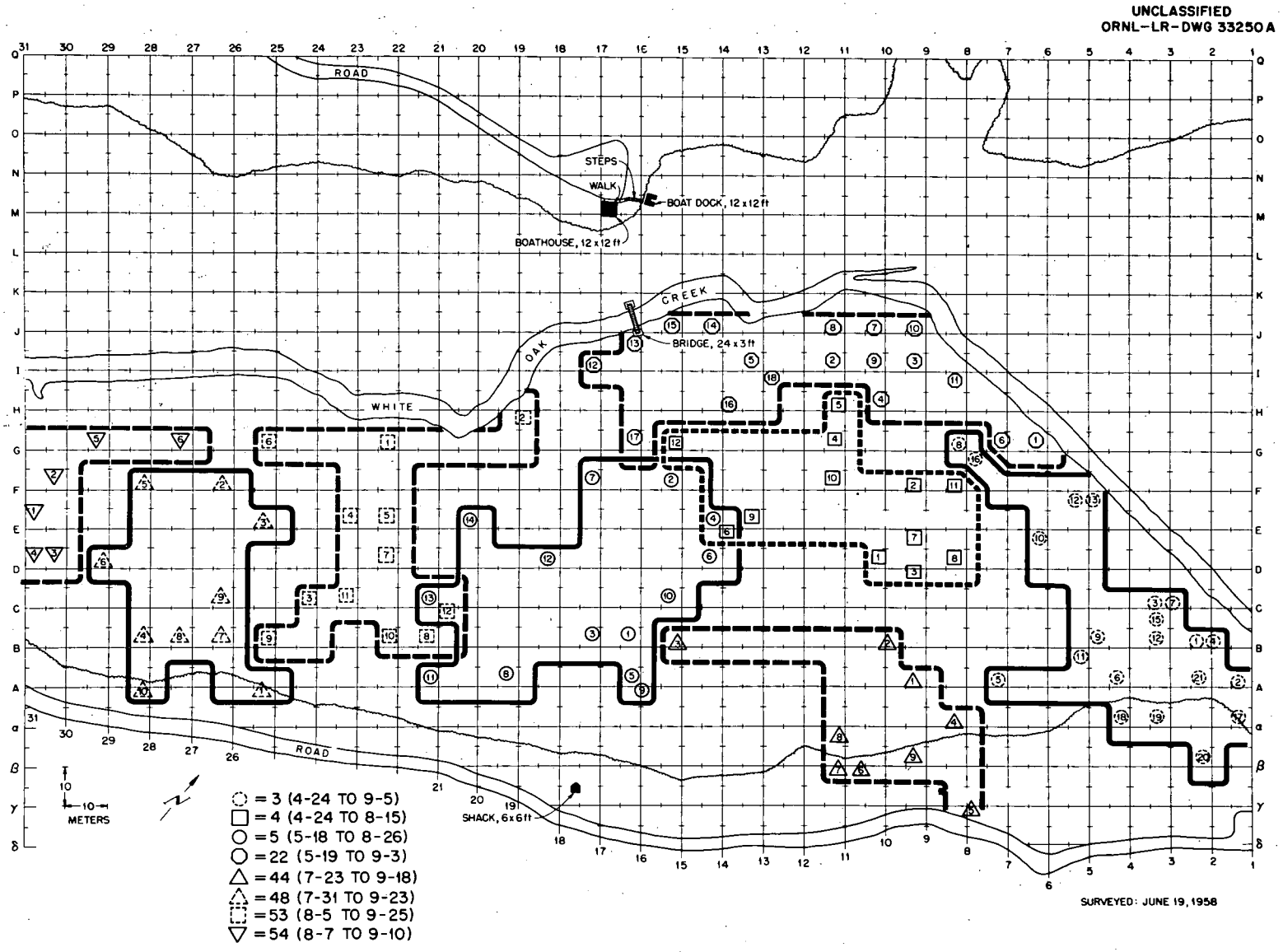

Fig. 26. Home Ranges of Adult Female Cotton Rats – White Oak Lake No. 3 Area, April–September 1958. Numbers inside symbols indicate sequence of capture.

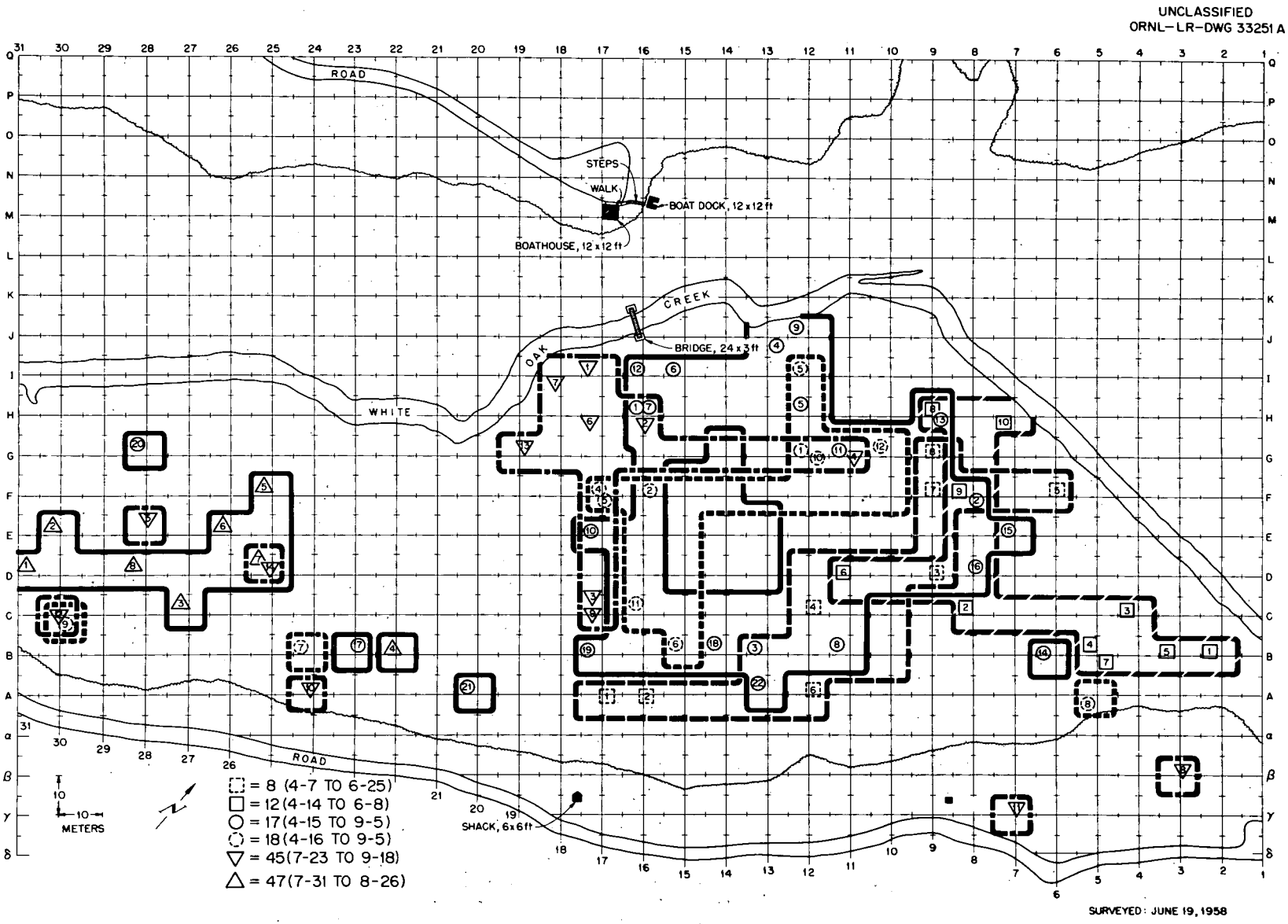

Fig. 27. Home Ranges of Adult Male Cotton Rats – White Oak Lake No. 3 Area, April–September 1958. Numbers inside symbols indicate sequence of capture.

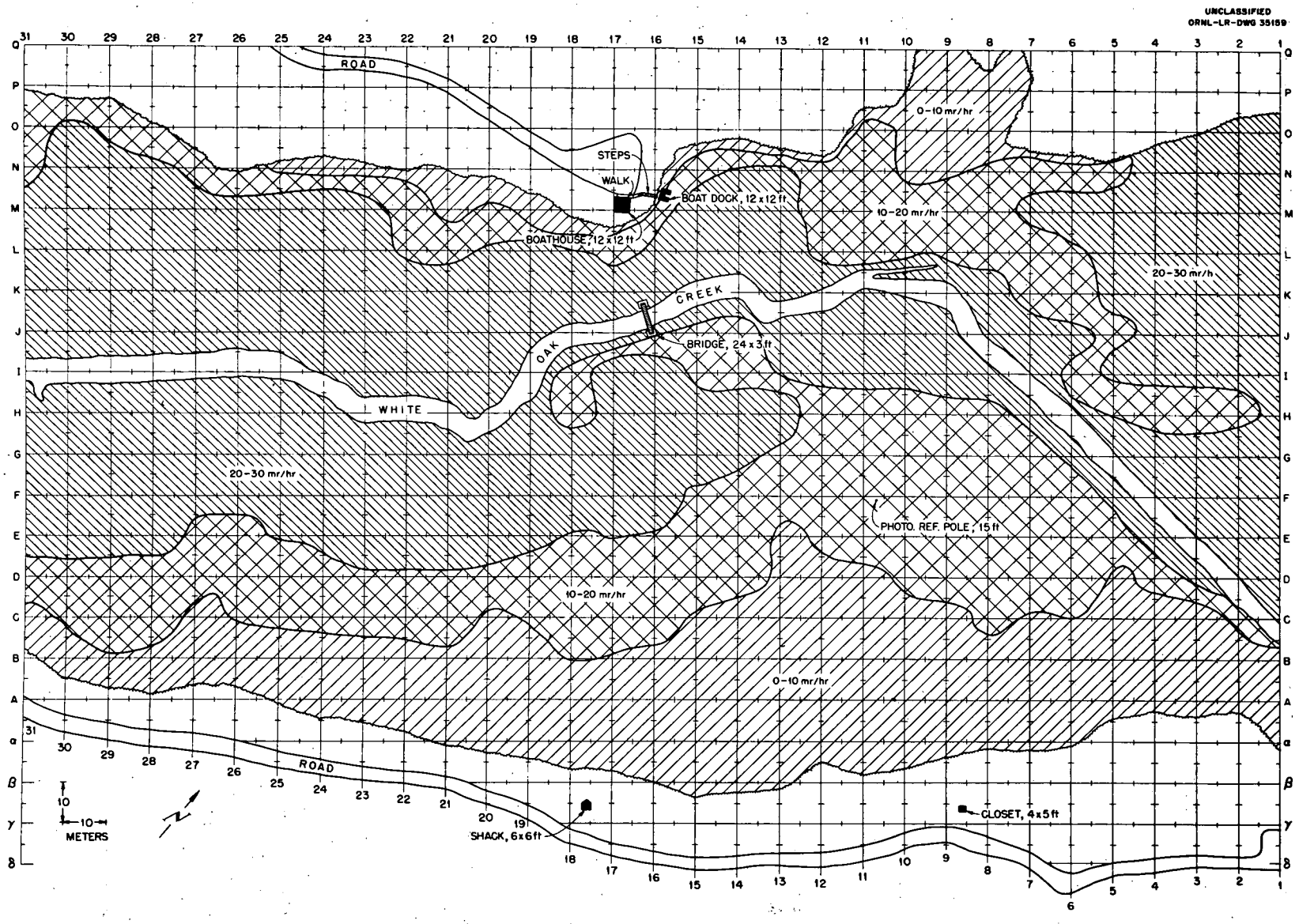

Fig. 28. Radiation Field 25 cm Above Surface of Ecology Study Area (10-m Grid of Lower White Oak Lake Bed).

radioisotopes, as well as tracer experiments and other investigations indicating the directions and rates of isotope movement.

Forest ecosystems cover much of the land area of the eastern United States, contribute most of its living and dead organic matter, and appear to provide the main natural reservoir of present and future radioactive contamination. The types of trees and forests currently being used for research at or near Oak Ridge include representatives of several broad forest regions of eastern North America, growing in several climatic, geologic, and physiographic habitats.

The abundant shortleaf, Virginia, and loblolly pines are among the dominant species of all but the coastal zone of the southern forest (Fig. 29). Deciduous trees typical of the central, as well as southern, forests are even more common, occurring in pure stands or mixed with pines. Evergreens such as hemlock and white pine, which are most widespread in the northern forest, extend into the Oak Ridge area; they are more abundant in nearby mountains. Even spruce and fir forests, somewhat resembling the Acadian and Boreal forests of Canada, are present on the coolest summits of the Great Smoky Mountains.

Several of these kinds of forests can be found on contrasting sites which may modify the parameters of chemical movement. The Oak Ridge reservation is typical of the Appalachian Ridge and Valley province in being crossed by several geologic formations, which support soils of varying levels of calcium, strontium, and other elements that would influence the equilibrium concentrations of isotopes in organisms and soils. Unusually low concentrations of basic elements are to be expected in the Cumberland province a few miles to the west and north, and in the older Appalachian province to the east. Such a variety of combinations of biological and physical factors thus make the Oak Ridge area particularly suitable for long-term research on the cycling of isotopes.

Predictions of isotope movement require, first, the development of theoretical models which relate the several stages in the cycles of the individual elements and, second, the estimation of the parameters of these models for forests in contrasting habitats. The theoretical work on models should apply in principle to nutrient cycles of forests in general. Background information bearing on the uptake phase of the cycle is provided, first, by analyses of the composition of forests and, second, by tracer experiments of isotope movement within trees. Air-borne dispersal of contamination is considered, first, in relation to amounts of fallout that reach the leaves from sources such as smokestacks and, second, in relation to dispersal of leaves around a contaminated tree. The return of radioisotopes into the soil is being studied in relation to the general rates of litter breakdown in contrasting forests and by tracer experiments using the litter from trees which have been inoculated with isotopes.

Development of Theoretical Ecological Models. – Mathematical analysis of schematic models or "circuit diagrams" of ecosystems is more than an expedient device for expressing the movement of particular radioactive contaminants from one compartment of the system to another. The parameters describing the rates of cycling of major and minor elements through the system express the fundamental characteristics and organization of the system as a whole.

Figure 30 illustrates the general movement of organic matter from the tree canopy to the "forest floor" to the mineral soil itself. Since the movement of many elements and radioisotopes will be closely related to the rate of carbon movement, some implications for problems of radioisotope contamination may be obtained from very preliminary evaluation of certain parameters from data in the literature.

A model was proposed by Jenny[23] in which I, the annual income of litter to the forest floor, is constant and occurs as a sudden increment of organic matter each autumn (Fig. 31). Assume for simplicity that the annual loss from the forest floor is a constant fraction k' of the new and old forest floor which has already accumulated; then the fraction of litter remaining after time t would be e^{-kt}. When annual income approximately equals annual loss, that is,

$$I = k'\mathfrak{I} \quad , \qquad (1)$$

then $\mathfrak{I}$ will have approximated an asymptotic total value T, and the ratio I/T will provide an estimate of the rate parameter k'. The natural logarithm

[23] H. Jenny, S. P. Gessel, and F. T. Bingham, *Soil Sci.* 68, 419–32 (1949).

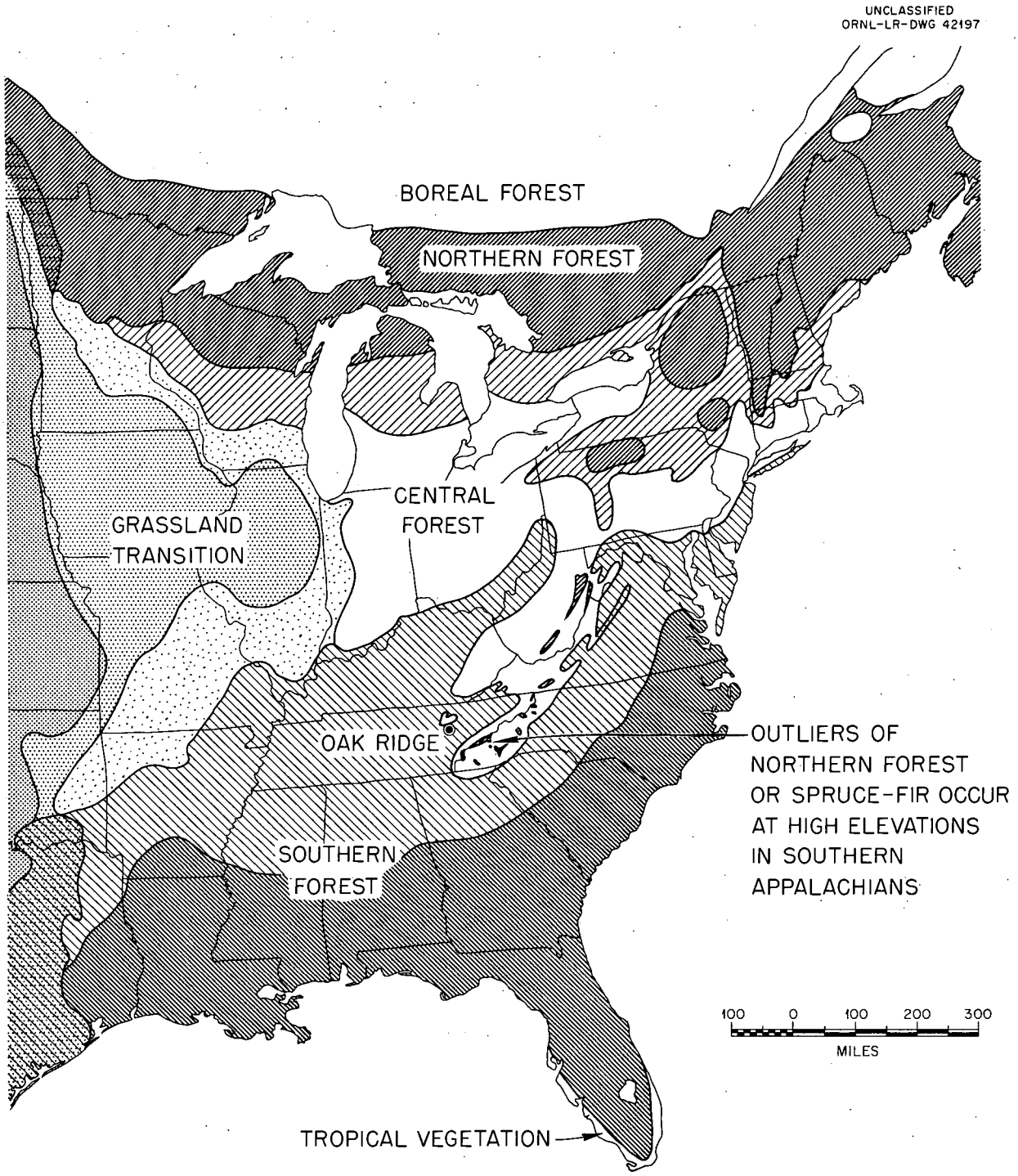

Fig. 29. Forest Zones of Eastern North America Having Different Potential Isotope Contamination Problems.

of $(1 - k')$ provides an estimate of the parameter $-k$ in the exponential equation for the decay of litters which takes place between episodes of litter fall (long dashed line in Fig. 31). The same parameter k described the exponential accumulation toward the asymptotic value T (short dashed line):

$$\mathfrak{F} = \frac{I}{k'}(1 - e^{-kt}) \quad . \qquad (2)$$

In the case of Fig. 31, which was chosen to approximate conditions of many forests of the southern region of the United States, k' is near $\frac{1}{4}$, $k = 0.288$, and the computed half time for either litter decay or accumulation is 2.4 years. In Fig. 32, a family of curves shows the theoretical trend of forest floor accumulation in forests of varying productivity. In Figs. 33 and 34 are families of curves corresponding with the same levels of productivity, but with markedly slower rates of litter decay. Decay or turnover parameters have been estimated from data on I and T reported for cooler forest regions.

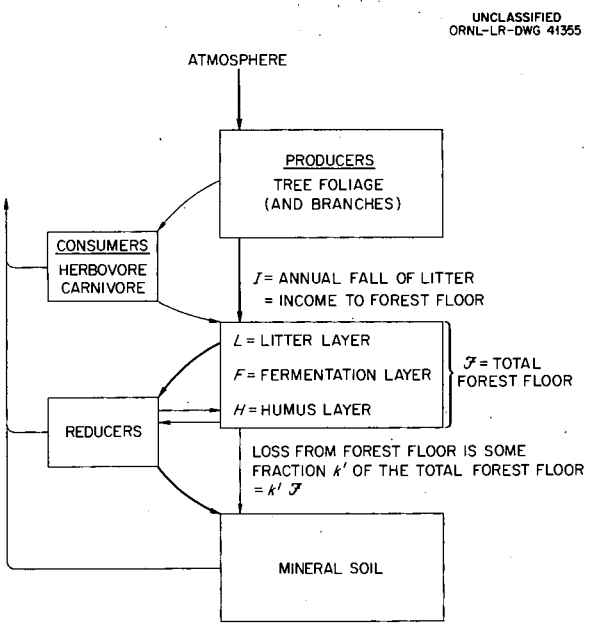

Fig. 30. Simplified Block Diagram for the Flow of Carbon Through a Forest Ecosystem.

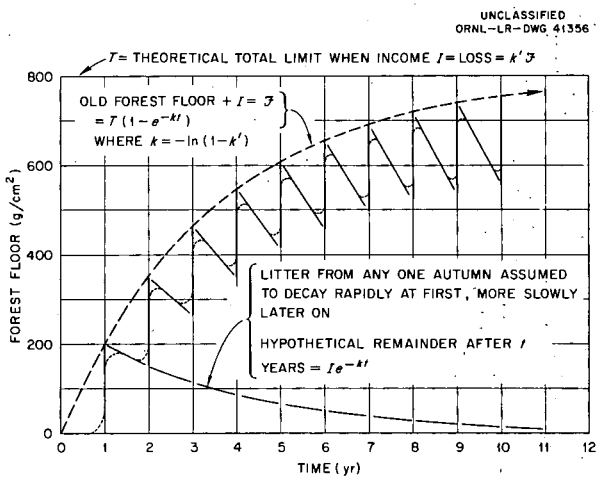

Fig. 31. Diagram of Income, Loss, and Net Accumulation for an Idealized Deciduous Forest. Income $I = 200$ g/cm^2; fraction decayed each year $= k' = \frac{1}{4}$.

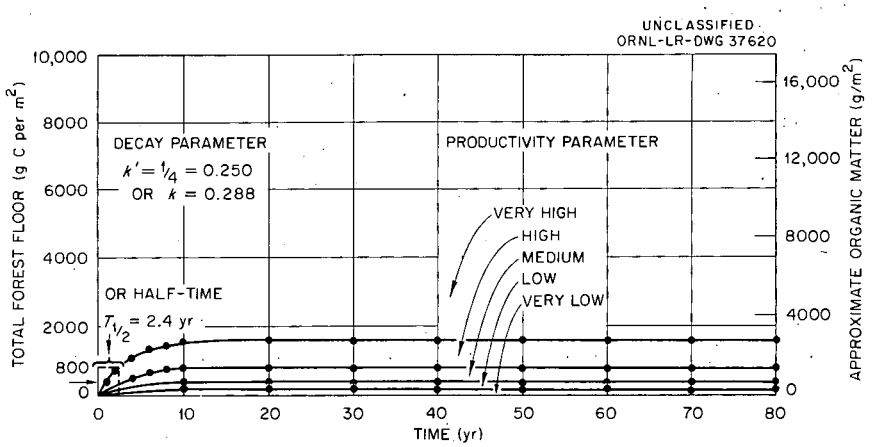

Fig. 32. Simplified Curves Describing the Theoretical Annual Maximum Values for Forest Floor, for Forests with Rapid Decay Rate and Varying Productivity.

Such striking differences in rates of turnover of carbon should be correlated with differences in movements of certain radioisotopes, even though not exactly proportional to them. In the case of tropical and subtropical forests, radioisotopes would move rapidly and provide considerable risk of internal contamination by way of the food chain. In forests around Oak Ridge, movement would also be fairly rapid, but several years might be required before we could assume that isotope concentrations were in equilibrium, with income balancing biological disintegration as well as physical decay (Figs. 31 and 32).

Many of our northern forests would have k' nearer to $1/16$ (half time of 10.7 years), shown in Fig. 33; it might take several decades for equilibrium to

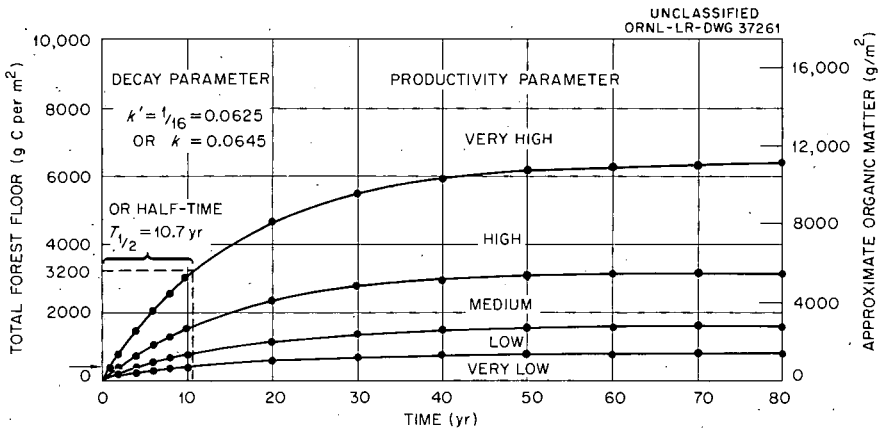

Fig. 33. Simplified Curves Describing the Theoretical Annual Maximum Values for Forest Floor, for Forests with Intermediate Decay Rate and Varying Productivity.

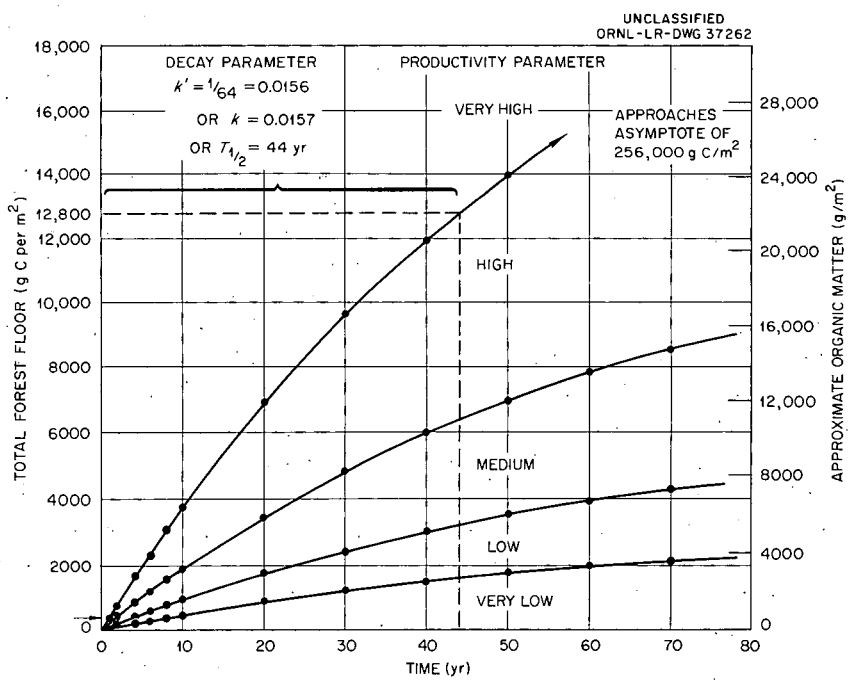

Fig. 34. Simplified Curves Describing the Theoretical Annual Maximum Values for Forest Floor, for Forests with Slow Decay Rate and Varying Productivity.

be attained. In the extreme Boreal forests, and in mountainous and boggy areas elsewhere, decay would be even slower, as typified by the example for $k' = 1/64$ (half time of 44 years) in Fig. 34. If there were a continuing source of contamination in such an area, relatively higher concentrations of activity would build up at the ground surface than would occur in warmer regions, where incorporation (and perhaps fixation) in the soil would be more rapid. (The probability of effects from external radiation might accordingly be higher in such cool regions.) Because of the holdup of isotopes in the raw litter, dangers of internal contamination via the food chain might be decreased here, unless the ecosystem had some means of recycling specific isotopes much more rapidly than it cycles the bulk of the organic matter.

Analysis of Forest Growth. – This phase of the forest studies seeks basic information needed for the interpretations of certain phases of the forest work. First, methods are being developed for estimating the total mass of living material (biomass) and annual productivity in terms of mass per unit area (including the litter-production parameter I in the model discussed previously). Such information is far more scanty for forests than for herbaceous ecosystems because of the bulk of the former. Second, the samples which are harvested and weighed are also used for chemical analyses. These can be converted to estimates of the mass of various elements per unit area of forest land.

Shortleaf pine (*Pinus echinata* Mill.) has been chosen for testing of methods because of its importance in the natural vegetation succession around Oak Ridge, because of studies already under way on the litter fauna and isotope movement in pine litter,[24] and because of operational advantages of working with such an evergreen as a "test organism." This work was started in the new solid-waste burial ground located on the Conasauga shale belt in Melton Valley, where forest clearing was already under way.[25] Furthermore, chemical and radiochemical analyses of the original forest trees, prior to waste burial in the vicinity, would be especially desirable here as standards for comparison in case of possible future changes resulting from contamination.

Trees were felled and the trunks sectioned at regular intervals (Fig. 35). Cross-sectional slabs were taken so that volume measurements of the total trunk could be converted onto a weight basis. Branches were sorted into diameter classes (Fig. 36) and weighed in the field. Sample branches from each size class were immediately cut into fractions of varying stem diameter. The last full year's growth was clipped from the small boughs (less than ½ in. in diameter). Dry weight was measured on both new and old needles and twigs. Root systems for a few trees were extracted as completely as possible.

So far, over 30 pines, up to 12.6 in. in diameter, have been harvested, along with a larger number of small red cedars and deciduous trees which occur with them. Data are being prepared for analyses by IBM computers.

The results should provide an adequate study of the mass of material on a representative area. Furthermore, the regressions of bark, branch foliage, and perhaps root weight on the readily measurable variables of diameter and crown should provide a preliminary basis for indirectly estimating the mass in forest areas which cannot be harvested.

Exploratory semiquantitative spectrographic analyses[26] of separated groups of elements were made on the silica residue, acid and basic sulfide precipitates, ammonium carbonate–8-hydroxyquinoline precipitate, and residual solution of composite leaf samples from three trees (Table 16). Table 16 also shows that the content of several elements increases during the aging of pine needles, from the end of the first growing season to the end of the second (Al, Ba, Fe, Na, Si, Sn, Sr, and Ti in Table 16).

Less refined semiquantitative analyses on total ash from leaf litter of several species of deciduous trees growing on the several geologic belts of the Oak Ridge reservation indicate generally higher values for calcium, strontium, and several other basic elements and lower values for certain elements like aluminum and manganese. Such differences, combined with information from the

[24] *ORNL Status and Progress Report, August 1958*, ORNL-2595, p 33.

[25] The cooperation of W. H. Felknor and D. Brogan of the Operations Division in arranging for help on tree cutting is acknowledged.

[26] J. A. Norris and L. J. Brady of the Analytical Chemistry Division provided these analyses.

Fig. 35. Slab Sample of Trunk of Shortleaf Pine Removed for Analysis.

literature, confirm the expectation that a more extensive sampling and analytical program will be essential for a basic understanding of the chemistry of forest ecosystems.

Translocation of Tracer Radioisotopes in Trees. – Five dogwood trees [*Cornus florida* (L.)] growing on four geologic formations in the Oak Ridge reservation were inoculated with a mixture of Sr^{85} and Ca^{45} tracers. The purpose of this experiment was to compare movement of Sr and Ca within these trees. One of these trees was injected with a triple-tag solution (0.1 *N* KCl) containing Sr^{85}, Ca^{45}, and K^{42}. The 1.5-Mev gamma rays of K^{42} made it possible to measure vertical movement of the carrier solution in the trunk shortly after inoculation. Leaf samples were collected and counted in a gamma well-type scintillation detector before the K^{42} had time to decay ($t_{1/2}$ = 12.44 hr), and again after one week, when K^{42} was reduced to 10^{-4} of its original value. At this time gamma counts could be considered as Sr^{85} (Table 17). The difference between the first and second count was the K^{42} activity, since there was negligible decay of the Sr^{85} ($t_{1/2}$ = 65 days) in one week's time.

Figure 37 shows the pump and pressure tank used for injecting and flushing the isotope from Tygon tubing through a pipe in a $\frac{3}{8}$-in. hole near the base of the trees.[27] A survey meter was used to trace the movement along a spiral path up the trunk and along each of the several major forks.[28] Readings of 1 mr/hr were obtained at a height of 1 m in 20 min. A reading of 20 mr/hr was obtained on the top branch of the tree at 3 m after only 5 hr. Most of the activity was gone after the first week, as expected for K^{42}. Subsequent decreases in activity indicated a slow upward translocation as well as radioactive decay of the Sr^{85}. The four trees which were inoculated

[27] A. E. Dimond and E. M. Stoddard of the Connecticut Agricultural Experiment Station provided useful suggestions on tree inoculation. D. Brogan of the Operations Division aided in the preparation of the inoculation apparatus.

[28] D. A. Fraser and C. A. Mawson, *Can. J. Botany* 31, 324–33 (1953).

Fig. 36. Shortleaf Pine Branches Sorted by Size Classes Before Weighing on Scales Suspended in Background.

with Sr^{85} and Ca^{45} without K^{42} showed no such rapid movement as that indicated by the K^{42}, but had the same slower upward movement of activity as was observed in the later stages of the experiment just described.

Leaves collected only 30 min after inoculation had significant K^{42} and Sr^{85} activity at a height of 60 cm, but not higher, confirming the estimate of rates shown by the survey meter. Leaves collected from the branches which were most directly in line with the pathways of direct movement had high concentrations of radioisotopes after 5 hr. Much lower activities (K^{42} but no Sr^{85}) were found in branches which were not along such a direct line. High potassium activity in the topmost branch of the tree implied that the inoculation solution had moved rapidly, but total absence of strontium activity in these samples indicated that this isotope was moving more slowly than its carrier solution. Twenty-one days after inoculation, samples from various parts of the crown of this tree and the other trees had high gamma activity, whose identity as Sr^{85} was confirmed by the 0.51-Mev peak of the gamma spectrum.

Because weak beta rays of Ca^{45} (0.25 Mev) are readily absorbed by matter, assays of leaf samples are more effective than field monitoring for tracing Ca^{45}. Disks of leaves collected 21 days after inoculation were counted in planchet holders of a gas-flow proportional counter having a window thickness of only 0.15 mg/cm^2. These samples clearly demonstrated the presence of high Ca^{45} activity in the upper part of the trees. Because this kind of assay is affected by self-absorption of the leaves, more quantitative measurements are currently being made on oxalate precipitates of calcium and strontium in a proportional counter,

Table 16. Spectrographic Analysis of New and Old Pine Needles

	1-Season Needles	2-Season Needles
Ash/sample	0.0309	0.0390
Grams of ash	0.9589	0.9454
(Ash/sample)/g ash	0.0322	0.0412
Analysis,* ppm		
Ag	0.3	0.4
Al	1600	2000
As	Trace ?	Trace ?
Au	Trace ?	Trace ?
Ba	16	40
Bi	0.01	0.01
Cs	<6	<8
Cr	3	3
Cu	20	25
Fe	280	430
Li	3	6
Mn	>130	>160
Mo	2.7	0.1
Na	100	160
Nb	0.06	?
Ni	13	9
Pb	12	15
Rb	6	8
Si	4900	8500
Sn	7	16
Sr	47	88
Ti	12	47
Zn	38	50
Zr	0.03	0.04

*Based on oven-dry weight of needles; Ca, Mg, and K are being analyzed by other methods.

with corrections for self-absorption, and also by beta liquid scintillation counting.

A similar difference between rapidly moving Rb^{85} and slowly moving Ca^{45} was noted by Fraser and Mawson,[28] although their experiments dealt with single isotopes in separate trees instead of mixtures of isotopes in a single tree. Garnaga[29] also noted relatively slow uptake of Ca^{45} by branches of apple trees.

[29] K. S. Garnaga, p 120–27 in *Tagged Atoms in the Study of Plant Nutrition . . .* , USSR Academy of Science, AED-tr-3376 Biology and Medicine.

The movement of divalent strontium and calcium ions thus seems to be consistently slower than that of monovalent potassium and (in Fraser and Mawson's work) rubidium ions. A plausible interpretation of this lag might be that the tagged divalent ions are more readily exchanged for untagged ions on the exchange sites within the tree. They would be able to move up the tree in detectable quantities only after a significant proportion of the exchange sites in the wood had in turn become labeled. Meanwhile the more rapid movement of K^{42} may have been aided first by a lesser affinity for the exchange sites available, and second by the large amounts of unlabeled potassium carrier in the original KCl solution. The difference in rate between these ions would then explain why the four trees in which the potassium was not labeled should only show the slower movement which seems to be characteristic of strontium and calcium.

Continuing studies aim to determine whether the ratio of radioactive strontium and calcium or the ratio of either tracer to the concentrations of carrier element in the trees or associated soils varies significantly from one geologic belt to another.

Foilage Contamination by Fallout. – Significant radioactive contamination on leaves of trees which were not inoculated with isotopes and which were not near the areas directly affected by waste disposal operations indicates the importance of fallout in the Oak Ridge area. The following preliminary analyses identify the main isotopes in this fallout and suggest the extent to which these can be attributed to local sources of contamination.

Ash samples of leaves collected in November 1958 were analyzed six months later by gamma spectrometry (Table 18). The fission products contributing most of the activity were the parent-daughter pairs of intermediate half life: Zr^{95}-Nb^{95} and Ce^{144}-Pr^{144} (Table 18). Since Zr^{95} has a half life of only 65 days, the values given in Table 18 represent only about 10% of the activity at the time of collection – about 200 to 500 $\mu\mu c$ per gram of dry leaf material. Cerium-144, with a half life of 285 days, is now the major contributor to leaf activity of most samples and presumably will remain so for several years.

Table 18 includes preliminary gamma spectrometric analyses for new and old pine needles

Table 17. Gamma Activity in Dogwood

Total activity inoculated: Ca^{45} 2.18 mc
Sr^{85} 0.79 mc
K^{42} 4.0 mc

Solution 0.1 *N* KCl adjusted to pH 5 injected May 4 at peak of bloom

Branch Sample	Location	Time After Tagging	Distance from Source (cm)	Sr^{85} (d/min)	K^{42} (d/min)
A	Lower trunk branches	30 min	60	140	33,994
B	Lower crown branches	30 min	130	*	*
C	Upper crown branches	30 min	266	*	*
D	Branches from four forks	5 hr	115	*	281
E			110	124	27,558
F			140	11,237	430,562
G			210	*	2,844
H	Top of tree	5 hr	330–480	*	2,697
H	Selected top branchlet	5 hr		*	18,301
I	Composite branch sample	22 hr		*	4,193

*No activity detectable above background.

and branches from the forest growth samples (new burial ground) described earlier. Lower Zr^{95}-Nb^{95} values are due partly to the longer period for decay and perhaps partly to the time of their collection, which preceded the last weapons tests of October 1958. Cerium values in pine needles fall within the same range of variability as those in deciduous leaves. It is not clear whether the higher Cs^{137} in old needles and branches might be due to a longer period available for contamination from rainfall, or whether they indicate a local source of contamination through dust or aerosols from the nearby White Oak Lake bed or the liquid waste pits. Ruthenium-106 and rhodium-106 were below detectable limits in all samples shown in Table 18. With the exception of one sample the long-lived Cs^{137} and Sr^{90} (and associated Y^{90}, which probably constitutes the main trivalent rare earth in Table 18) are near or below the lower limit of detection (~ 10 $\mu\mu$c per gram of dry weight).

If the spectrographic analyses given in Table 16 prove to be acceptable, a tentative estimate of the specific activity of zirconium in new pine needles at the time of collection (October 1, 1958) was about 1 mc per gram of zirconium, while that of niobium would be about 0.5 mc/g. The specific activities for the pure isotopes Zr^{95} and Nb^{95} are more than 10^7 times as great as these values. This means that there were 10^7 times as many stable atoms of zirconium and niobium than there were of the radioactive atoms – in spite of the exceedingly low levels of these minor elements in the general composition of the plant as shown in Table 16.

Samples of fresh leaves were collected between June 10 and June 13, 1959, in order to decide whether the origin of some of the fallout warranted further investigation, and to determine if different species of leaves differed in the extent of their contamination. Table 19 shows differences due to both species and location, including three locations on the Oak Ridge reservation (one mile west, one mile north, and four miles northeast of the X-10 stacks) and one location 30 miles east of the reservation.[30]

[30]Acknowledgement is due S. A. Reynolds, T. H. Handley, C. L. Burros, W. R. Laing, and members of their respective groups in the Analytical Chemistry Division for performing these analyses.

Fig. 37. Technique for Inoculating Trees with Tracer Isotopes. Isotope is first poured into lower part of plastic tubing, which is then connected to pressure vessel for pumping.

Table 18. Fallout Contamination, Autumn 1958

In micromicrocuries per gram of dry leaves

Leaf Species	Zr^{95}-Nb^{95}	Ru^{106}	Cs^{137}	Ce^{144}	TRE	Sr^{90}
Deciduous leaves						
Mulberry	22	<11	7	38	~13	~9
Sugar maple 1	22	<11	<2	28	<6	<5
Sugar maple 2	19	<15	<3	35	~9	~9
Sugar maple 3	20	<22	<4	11	~7	~4
Oak, Shumard	49	<11	<2	37	~6	~6
Oak, scarlet	18	<68	<7	3	<5	<5
Beech	18	<23	<5	37	~41	~39
Sycamore	21	<11	<2	30	<4	<9
Shortleaf pine						
New needles	4	<20	5	16		
Old needles	<13	<20	17	44		
Branches	<4	<20	13	24		

Zirconium-95 and niobium-95 are present at all locations, at concentrations below those recalculated from Table 18 for last autumn's fallout activity, which suggests that they are being contributed by regional fallout. Old needles seem to have had the opportunity of accumulating more than young needles, and higher values were noted for rough leaves (mulberry, red maple) than for smooth ones (redbud, tulip tree).

By contrast I^{131} was found to contribute one to several hundred micromicrocuries per gram to leaves one mile downwind from the X-10 stacks and very low activities in other locations (Table 19). The two days preceding sampling had had northeasterly and east-northeasterly winds, whereas the prevailing winds from the opposite directions would lead one to expect the highest fallout to the northeast of the Laboratory. Unlike the longer-lived Zr^{95}, I^{131} ($t_{1/2}$ = 8 days) had to be contributed by ORNL. This inference subsequently has been confirmed by air monitoring of the isotopes production stacks with charcoal filters[31] which indicates that approximately 10^4 curies of I^{131} was released in each of two successive weeks in July 1959. Continuing studies of the iodine contamination are under way.

Some Ru^{106} seems to be contributed by the regional fallout 30 miles from the Laboratory (Table 19) and also in other samples recently obtained from outside Tennessee. Nevertheless, the higher concentrations in the valley next to ORNL indicate that some Ru^{106} is of local origin.

Cerium-144 is detectable in the range of 10 to 200 $\mu\mu c$ per gram in most samples, although the precision for estimating this fission product is relatively low in isotopic mixtures. Cesium-137 was barely above the limits of detection in a few samples and its distribution showed no clear geographic pattern. Cobalt-60 may be responsible for some higher energy gamma rays which are present, but the quantity is not sufficient for estimation.

Comparisons of the values in Tables 18 and 19 with those reported from the vicinity of the liquid waste pits[32] shows that the latter Zr^{95}-Nb^{95} values fall in the same general range, when

[31] W. Thornton and J. Youngblood of the Health Physics Division, personal communication.

[32] S. I. Auerbach *et al.*, *H-P Ann. Prog. Rep. July 31, 1958*, ORNL-2590, p 46–47.

Table 19. Fallout Contamination on Fresh Leaves, June 1959

In micromicrocuries per gram

Species	Zr^{95}-Nb^{95}				I^{136}				Ru^{106}			
	SW1[a]	N1[b]	NE4[c]	E30[d]	SW1	N1	NE4	E30	SW1	N1	NE4	E30
Shortleaf pine												
Old needles	68	82	72	188, 36	106	8	*e*	*e*	28	52	*e*	117, 21
New needles	16	14	*f*		121	*e*	*f*	*f*	137	*e*	*f*	*e*
Dogwood	23	28	15	36	211	13	*e*	*e*	141	90	16	21
Red maple	43	49	22	27	232	7	22	11?	*e*	22	*e*	19
Mulberry	43	*f*	17	*f*	545	*f*	9	*f*	71	*f*	*e*	*f*
Sycamore	20	21	*f*	*f*	391	6	*f*	*f*	32	6	*f*	*f*
Redbud	9	*f*	11	*f*	32	*f*	10	*f*	15	*f*	15	*f*
Oak												
Post	16	12	*f*	28	170	3	*f*	7?	13	15	*f*	21
White	7	*f*	*f*	8	*e*	*f*	*f*	7?	*e*	*f*	*f*	16
Red	*f*	*f*	*f*	44	*f*	*f*	*f*	*e*	*f*	*f*	*f*	7
Southern red	*f*	*f*	*f*	20	*f*	*f*	*f*	5?	*f*	*f*	*f*	17
Tulip tree	*f*	*f*	12	9	*f*	*f*	4	11?	*f*	*f*	10	8

[a] 1 mile southwest of ORNL, Bethel Valley.

[b] 1 mile north of ORNL, edge of Bear Creek valley.

[c] 4 miles northeast of ORNL, patrol road to Y-12.

[d] Bays Mountain and vicinity, 30 miles east of ORNL. Questionable iodine values here are near lower limits of detection.

[e] Isotope not detectable in presence of other activity.

[f] No sample available for analysis.

allowance is made for decay between collection and analysis. Thus regional fallout from weapons tests provides the explanation for this portion of the foliage contamination. As reported last year,[32] the Ru^{106} is taken up directly from ground water by some of the trees; the Cs^{137} and Co^{60}, which have not yet been detected in ground water, may result from particulate contamination carried by wind from bare ground and water surfaces at the pit site.

Patterns of Leaf Dispersal by Wind. – The rapid terminal velocity of tree leaves, compared with the deposition velocity of fallout particles, makes the usual meteorological models for turbulent dispersal of air contamination inappropriate for predicting the pattern of dispersal of contaminated leaves. The weights of leaves from sample plots along the 16 compass directions around an isolated sycamore tree in a grassy field in Bethel Valley, a few weeks after leaf fall, nevertheless indicate a pattern of the same general type as would be predicted from knowledge of wind frequencies and velocities from these directions.

These weights suggest that approximately 44% of the leaves fall within the quadrant from north-northeast to east, in the lee of the southwest winds which prevailed during the 40 days of leaf fall, as is usual for the Oak Ridge area in autumn. The map on Fig. 38 clearly shows the secondary direction of movement which was favored by northeasterly and east-northeasterly winds. The very slight dispersal at right angles to this axis is predictable from the low frequencies and velocities of northwesterly and southeasterly winds.

Approximately 75% of the leaves from this tree fell within a radius of only 10 m from the tree. Outside this radius the density of leaves decreased abruptly. The distance for average leaf density to decrease by half (a "half distance"

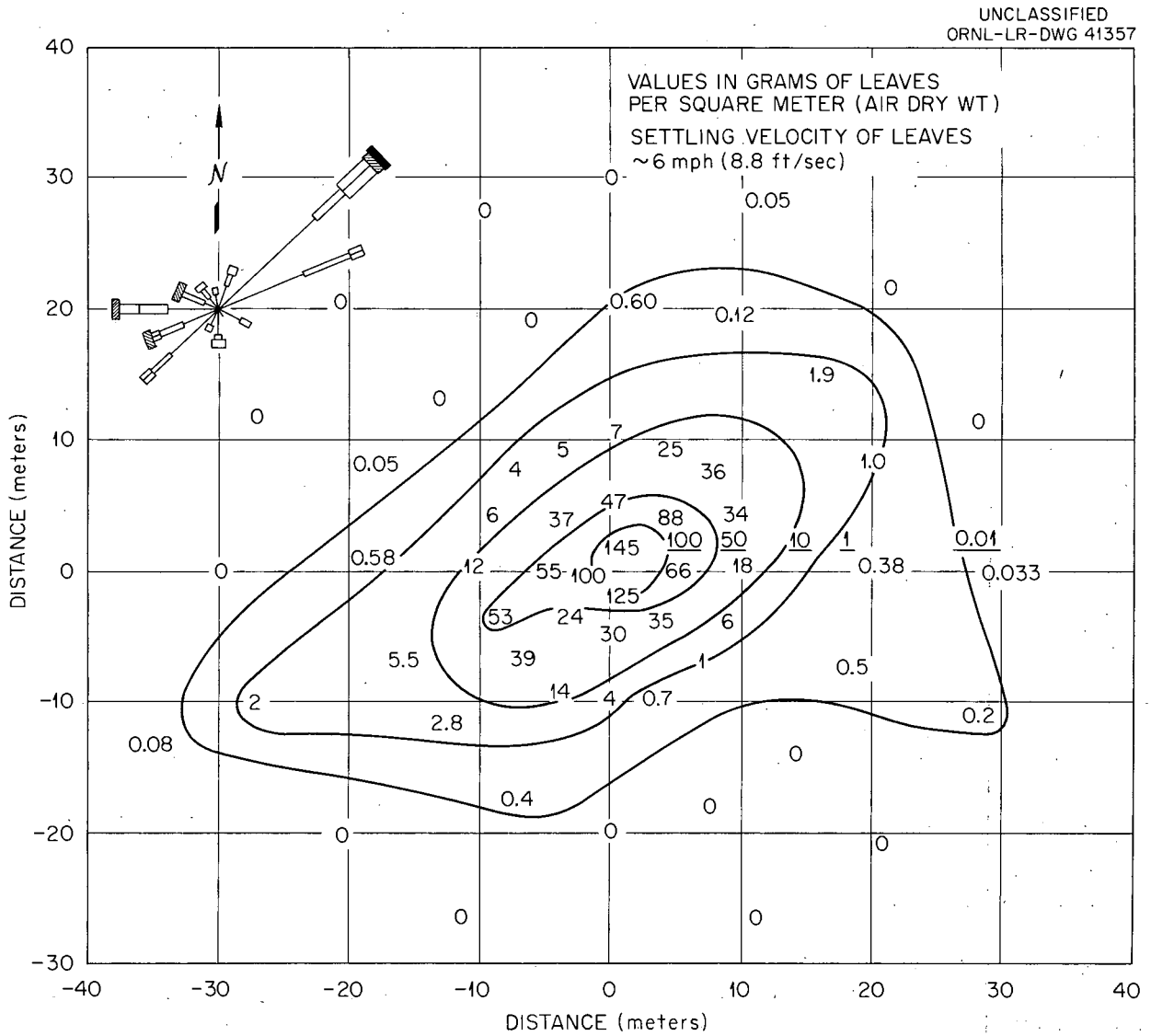

Fig. 38. Dispersal of Leaves Around a Sycamore Tree, Bethel Valley, East of ORNL.

for dispersal) appeared to be 4 m for the southwesterly direction and only 2 m for the other directions. Very few individual leaves were observed on the sample plots or elsewhere outside a radius of 30 m. While the probability for long-distance contamination for a large area appears to be very low, spot contamination around individual leaves could nevertheless be appreciable. In the present case, opportunities for lengthy secondary movement of leaves by wind were poor, but smoother ground could lead to much wider dispersal than that represented by this example.

Rates of Litter Breakdown in Contrasting Forests. – The model for the balance of income and decay of forest litter showed how rates of leaf and humus disintegration may be important factors limiting the return of isotopes to the mineral soil. To estimate these rates, nylon net bags containing 50 g of litter from each of five deciduous tree species were placed on top of the "F" layer of the forest floor in each of three conifer and three deciduous forests. These forests were located in the Oak Ridge Controlled Area and at two altitudes of the Great Smoky Mountains, in cooperation with R. Shanks of the University of Tennessee.

The weight losses shown in Table 20 are significant after only five months (January–May) and should be much greater after a full year. As

Table 20. Per Cent Weight Loss of Deciduous Leaf Litter from Nylon Net Bags in Deciduous and Conifer Forests at Three Elevations

Species of Leaves	Oak Ridge, 800 ft		Great Smoky Mountains National Park			
			3500 ft		5200 ft	
	White Oak	Pine	Cove Hardwoods	Cove Hemlock	Beech Gap	Spruce-Fir
Mulberry	32.8	31.8	40.5	27.7	34.1	25.2
Sugar maple	15.4	11.7	19.15	10.6	15.5	7.4
Shumard oak	11.5	16.7	17.4	11.2	14.3	5.2
White oak	11.0	17.3	16.7	11.0	12.7	5.2
Beech	7.6	8.9	10.8	5.8	8.8	

expected, decay of leaves was slower at 5200 ft elevation than at 3500 ft in the Smokies. Also, in evergreen spruce-fir and hemlock forests, decay was slower than in the deciduous forests. In the pine forests at Oak Ridge, decay was more rapid than in the mountain conifer forests. However, in the white oak forest in the Controlled Area, decay rates were in some cases lower than those for the nearby pine forest and for the mountain deciduous forests. This slower decay may be related to the rapid drying of litter in lowland deciduous forests. These results suggest the need for suitable recording of moisture as well as temperature of the forest floor habitat where the microflora and microfauna are active in decay.

Table 20 also shows differences in decay rate between species of leaves. Breakdown of mulberry leaves was four times as rapid as that of beech. Sugar maple and two species of oak consistently had intermediate rates of litter decay.

Preliminary chemical analyses indicate that the most rapidly decaying leaves are also the ones having highest contents of calcium and strontium. The difference in decay rate, combined with the difference in composition, implies a very considerable difference in the role of different trees in their rate of return of these elements to the soil. Such species differences, as well as geologic and climatic differences between the forest zones of Fig. 29, will be important in predictions which need to be made about environmental contamination.

Another experiment on the decay of pine litter has been started with needles from a tree inoculated with Ru^{106}. Other isotopes (Co^{60}, Ca^{45}, Sr^{85}) have been incorporated into tree leaves for tracer studies of the movement of isotopes after they are incorporated into the soil. This stage of movement will thus complete the biogeochemical cycle: uptake from the soil, which was considered for the White Oak Lake bed, and the return of isotopes to the soil.

SORPTION AND RETENTION BY CLAY MINERALS

T. Tamura

F. S. Brinkley D. G. Jacobs
B. L. Houser O. M. Sealand

Clays may be utilized in several ways to contain fission product wastes. By heating mixtures of waste and clay that contain appropriate fluxes, fission products can be fixed in the resultant durable and insoluble matrix. A second method of utilizing clay minerals for waste disposal is to take advantage of their ion exchange or sorptive property. By contacting the waste solution with the clay material, the fission products can be sorbed from solution, immobilizing the cationic fission products and lessening the probability of contamination of the environment. These two methods of using clays were investigated and the results are discussed here.

Mix Formulations for Sintering

One of the advantages of using clays to form durable and insoluble ceramic masses (sinters) is the pre-existence of a bond between silicon and aluminum through a common oxygen. This fact would be of little or no consequence if the firing temperature of the mix ensured complete fusion of the materials. However, with a peak temperature of 850°C and 1 hr of heating at this temperature as the conditions of firing, it was felt that the initial form of the material would affect the retention of fission products by the sinter. Tests were therefore designed to check this hypothesis; leaching of cesium from the sinters was used as the basis for evaluating sinter quality, since this element was found to be most difficult to fix.[33]

The results of several tests using clay and synthetic samples are shown in Table 21. From samples 1 and 2, it is apparent that the aluminosilicate (clay) is superior to the oxide ingredients. Comparing the results from samples 2, 3, and 4, it may be concluded that the alumina is not completely incorporated in the sinter; in fact, the formation of soluble aluminate is suggested by the high alumina content in the leaching solution.

After the superiority of clays in forming sinters under the limited conditions of firing was established, the influence of different clay minerals on the quality of sinters was tested. Several representative clays were used; their effectiveness for retaining cesium is shown in Table 22. The final weight of the sinter was the basis for the selection of the amount of clay to use. Two of the more promising materials appear to be illite and Conasauga shale. The latter was found to contain illite as the major mineral component; most of the later experiments used Conasauga shale as the source of clay.

Lack of uniformity of sinters is one of the problems in evaluating sinter quality. One of the relationships which became apparent from several firing runs was the increase in the cesium concentration in the leachate with increasing pH of the leachate. This relationship is plotted in Fig. 39. Several reasons for this type of relationship could be offered. One reason for the high pH is that the sodium (from the sodium nitrate waste) did not fuse completely with the clay. Thus, sodium oxide would be present in the sinter; when this was contacted with water, sodium hydroxide could have been formed.

If the inference regarding the incomplete reaction between the clay and sodium oxide is correct, the use of a fluxing agent is indicated. Boric acid was selected as a fluxing agent because it has the additional property of improving the durability of glasses.[34] Varying amounts of boric acid were substituted for clay; the results obtained from sinters prepared from Conasauga shale are shown in Table 23. Within the range of concentration of boric acid used, the ability of the sinters to retain cesium was improved. It was noted also that the sinters containing as low as 2% B_2O_3 are massive

[33] W. J. Boegly, Jr., *et al.*, *H-P Ann. Prog. Rep. July 31, 1958*, ORNL-2590, p 71, esp 72.

[34] J. Enss, *Glastech. Ber.* 5, 449 (1928).

Table 21. The Retention of Cesium as Influenced by the Form and Amount of Alumina in the Mix

Sample No.	Type*	Composition (g)						pH of Leachate	Leachate Composition (ppm)				Cesium Leached (%)
		Al_2O_3	SiO_2	Fe_2O_3	MgO	K_2O	Total		Na	Si	Al	K	
1	Clay	20.7	41.0	3.68	2.28	4.88	72.54		46.0	9.2	3.3	2.0	0.13
2	Synthetic	20.7	41.0	3.68	2.28	4.88	72.54		28.1	7.6	165.0	55.0	1.10
3	Synthetic	2.50	54.9	5.05	2.93	6.61	71.99	11.20	80.0	21.0	20.0	34.0	0.20
4	Synthetic	2.07	41.0	3.68	2.28	4.88	53.91	11.80	250.0	33.0	60.0	73.0	0.31

*The clay was illite. The chemicals added to the synthetic samples were in the form of oxides or nitrates.

Table 22. The Influence of Clay Type on the Retention of Cesium

	Material				
	Fithian Illite	Conasauga Shale	Wyoming Bentonite	Georgia Kaolin	Arizona Bentonite
Initial weight of clay used, g	80.0	80.2	85.8	87.3	97.2
Final weight of sinter, g	83.7	83.9	86.1	85.0	84.4
Cesium leached, %	0.13	0.13	0.27	0.42	0.47
pH of leachate	10.4	10.0	11.1	9.63	10.7
Leachate composition, ppm					
Na	50	34	180	150	65
Si	22	25	54	10	39
Al	5	6	7	4	5
K	8	3	1	1	1

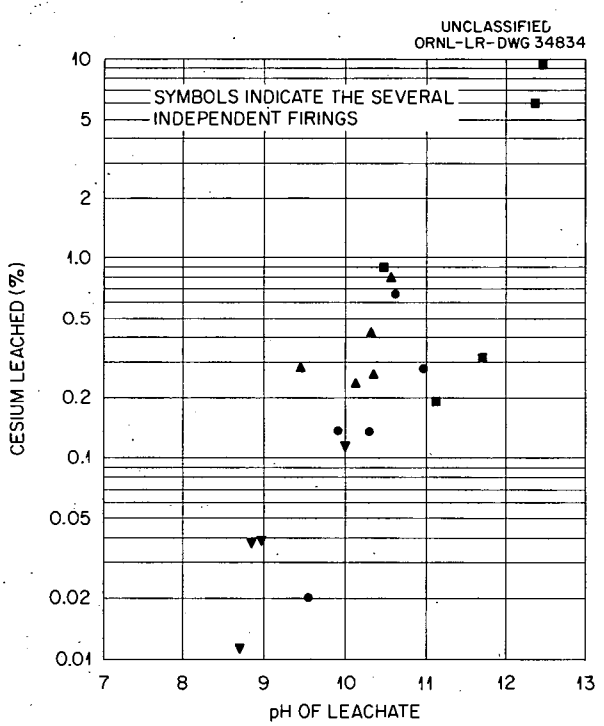

Fig. 39. Relationship of pH and the Amount of Cesium Leached from Sinters Prepared by Several Independent Firings.

and harder than those without borate. At 17.1% B_2O_3 the sinter was well fused; however, chemical analysis showed that the silica and alumina in this sinter were relatively more soluble. This indicates that the silicate framework has been weakened by an excessive amount of borate. The deleterious effect of excessive borate content has been demonstrated previously by Enss.[34]

An operational difficulty encountered with the production of sinters using Conasauga shale has been expansion of the heated mass, causing overflow of the container. Tests designed to investigate the mechanism of this phenomenon have not proved conclusive. However, it has been possible to prevent the rise during the formation of the sinter by substituting kaolinite clay for the shale. With kaolinite the preparation of uniform and homogeneous sinters is more difficult. Therefore the effects of boric acid additions, clay-solution ratio, and particle size on leaching have been more difficult to evaluate quantitatively. These difficulties, and perhaps the inconsistent results, may have been caused by improvised repairs on the firing furnace which resulted in uneven heat distribution. Further studies on sinters will be made after a better furnace is designed and installed.

Table 23. The Effect of Boric Oxide on the Retention of Cesium by Sinters

	Sample Number			
	1	2	3	4
Conasauga shale, wt %	87.9	83.6	79.3	70.6
B_2O_3, wt %	0.0	4.2	8.5	17.1
Na_2O, wt %	10.9	11.0	11.0	11.1
Cesium leached, %	0.11	0.04	0.01	0.03
pH of leachate	10.0	9.0	8.8	8.9
Leachate composition, ppm				
Na	38	22	1	4
Si	16	7	4	10
Al	5	4	2	8
K	3	2	1	4

Cesium Fixation by Ion Exchange

In the previous annual report a hypothesis was presented that emphasized the role of structure in cesium sorption.[35] Following tests performed on synthetic micas which verified the importance of the 10-Å *c*-axis spacing of the minerals, vermiculite was treated with neutral KCl to convert the 14-Å *c*-axis spacing to 10 Å. This treatment resulted in exhibition by the mineral of a higher specific affinity for cesium, verifying again the importance of the 10-Å spacing. Sorption of cesium by the potassium vermiculite increased by about 85% even though the exchange capacity was reduced from 60 meq per 100 g to 10 meq per 100 g. Greater detail and implications of these findings are reported elsewhere.[36]

Although montmorillonite showed some improvement in ability to sorb cesium after treatment with KCl, it was felt that greater improvements could be demonstrated if the *c*-axis spacing could be reduced to 10 Å. The KCl treatment had reduced the *c*-axis spacing of montmorillonite from 15 to 12 Å. The 12-Å spacing is evidence of a monolayer of water between the silicate sheets (the *c* axis of the clay). Although the monolayer of water can be removed by oven drying at 100°C, montmorillonites have a strong tendency to rehydrate. Any benefit that might be derived from heating would be nullified if the clay were brought into contact with the waste solution.

It was felt that heating montmorillonites to temperatures that would result in irreversible collapse of the lattice would favorably influence cesium sorption from waste solutions. Although it is known that high temperatures reduce the ion exchange capacity of clays, earlier studies with synthetic micas and vermiculite had shown that ion exchange capacity was not the dominant factor in cesium sorption.

Samples of montmorillonite (Wyoming bentonite) containing sodium, calcium, and potassium as saturating cations were heated to various temperatures up to 800°C. Sorption of cesium from 6 *M* $NaNO_3$ solutions was followed as a function of the temperature to which the clay was subjected and of solution-clay contact time. The effects of heating and time on the sorption of cesium are shown in Fig. 40 for the potassium montmorillonite. Below 600°C the amount of cesium sorbed is not

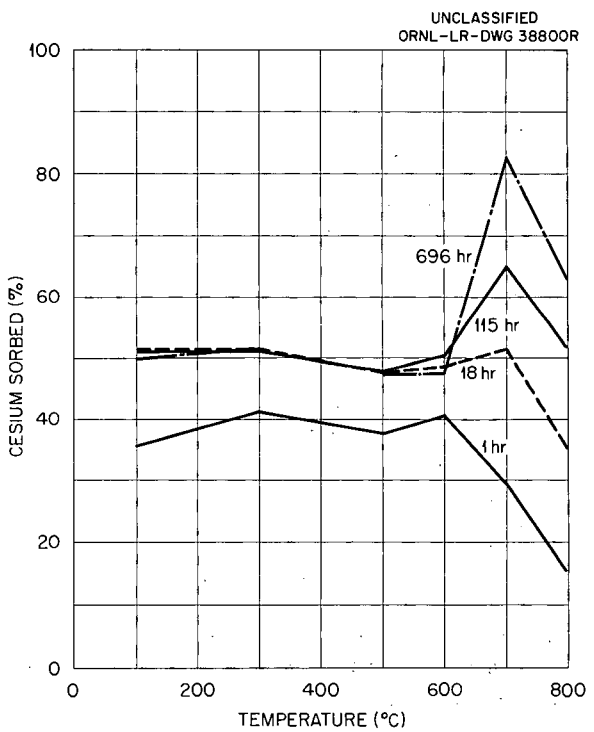

Fig. 40. Sorption of Cesium as Influenced by Heating of Potassium Montmorillonite and Solution-Clay Contact Time.

[35] W. J. Boegly, Jr., *et al.*, *H-P Ann. Prog. Rep. July 31, 1958*, ORNL-2590, p 76.

[36] T. Tamura and D. G. Jacobs, "Structural Implications in Cesium Sorption," submitted to *Health Phys.*

affected by heating; this behavior implies that rehydration of the lattice occurred even after heating to 600°C for 3 hr. The lower degree of sorption after 1-hr contact time is evidence that equilibrium was not established within this period. Samples heated to 700°C will sorb more cesium than samples heated to any other temperature, provided sufficiently long contact time has elapsed. Sampling showed that the cesium sorption increased from 30% after 1 hr to 82% after 696 hr. The lower sorption for the sample heated to 800°C may be explained on the basis that at this temperature the layer lattice structure has been destroyed and new phases introduced.

Another interesting relationship found after heating the montmorillonite is the change in the ion exchange capacity. The exchange capacity plotted as a function of temperature in Fig. 41 was determined by calcium saturation of the mineral followed by sodium acetate leaching and Versene titration of the leached calcium.[37] A sharp decrease in exchange capacity resulted from heating potassium and sodium montmorillonite at 700°C; the samples heated at this temperature also showed an increase in cesium sorption. With calcium montmorillonite the sharp decrease in exchange capacity occurred at 600°C; it is significant that the maximum sorption for cesium by calcium montmorillonite also occurred after heating to this temperature. These tests show that the influence of the structural factor is more important than the ion exchange capacity.

The important consideration from the standpoint of theory and the mechanism of sorption is whether it can be shown by more direct evidence that structure is the controlling parameter. X-ray diffraction studies were made on the clays by using the oriented-specimen technique. The purpose of the study was to check whether irreversible collapse of the lattice had occurred, on heating, at any specific temperature. The clays were therefore glycerol-solvated in order to expand the lattice most effectively; the spacing as shown in Fig. 42 may not represent the degree of expansion existing in water alone. Although the spacings appear to be relatively constant even when the clays have been heated to 700°C, the relatively low intensity of the maxima and the broader peaks suggest that some of the layers were irreversibly collapsed.

[37] M. L. Jackson, *Soil Chemical Analysis*, Prentice-Hall, Englewood Cliffs, N.J., 1958.

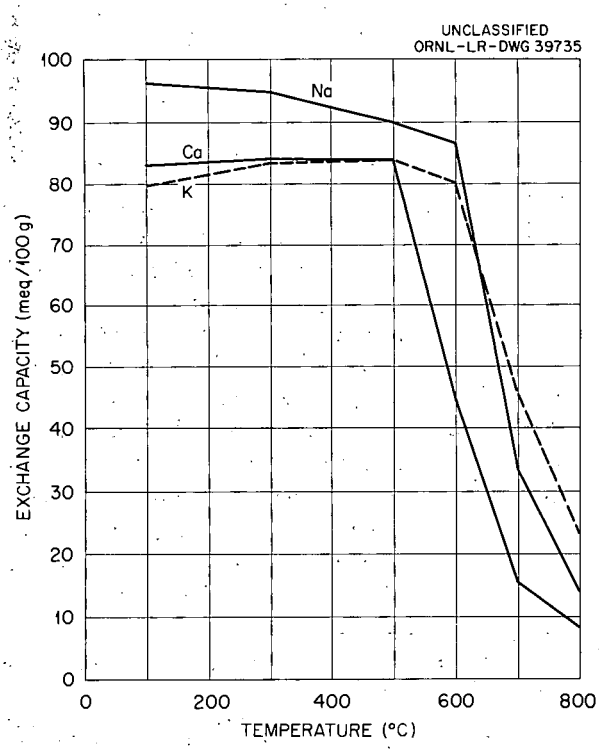

Fig. 41. Effect of Heating on the Ion Exchange Capacity of Montmorillonite (Wyoming Bentonite).

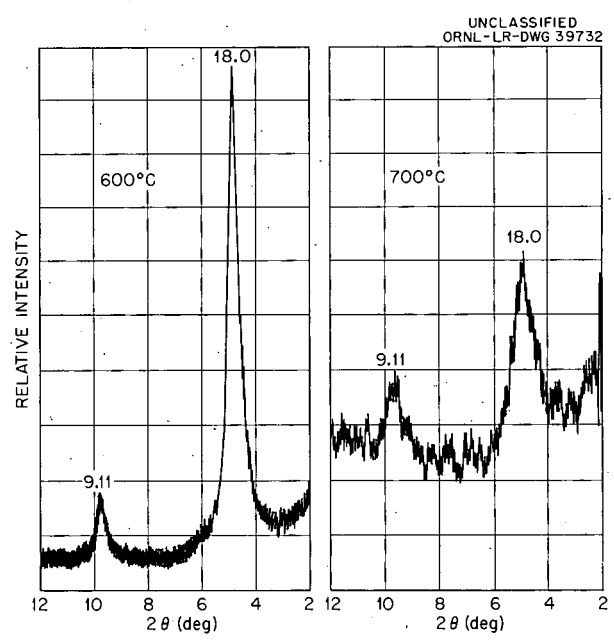

Fig. 42. X-Ray Diffraction Diagram for Potassium Montmorillonite (Wyoming Bentonite) After Heating.

Further studies are in progress on the determination of diffraction maxima without additions of glycerol.

The strong time dependence of cesium sorption by the montmorillonite heated to 700°C is suggestive that irreversible collapse to 10 Å was responsible for the increase in sorption. Time studies on synthetic mica that exhibits a 10-Å *c*-axis spacing showed that cesium sorption was greatly influenced by the mica-solution contact time (Fig. 43). Sorption data reported for illite (*c*-axis spacing of 10 Å) also showed that the amount of cesium sorbed was dependent on the contact time.[35] It is also evident from Fig. 43 that, when vermiculite was treated to produce a 10-Å *c*-axis spacing, the resultant product was sensitive to the time factor. These observations strengthen the concept that it is the irreversible collapse to 10 Å that caused an increase in cesium sorption by montmorillonite, rather than the formation of active amorphous material after heating. Formation of new phases would reduce the specificity for cesium, according to the data shown in Fig. 40. The reduced capacity of the sample heated to 800°C may be caused by the destruction of part of the sample; the net increase in the sorption as a function of time is due to the undestoryed part of the sample.

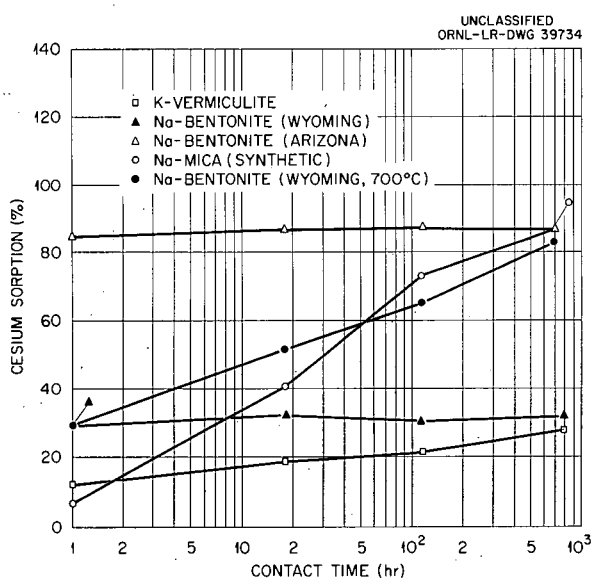

Fig. 43. Effect of Contact Time on the Sorption of Cesium by Several Materials.

A desirable physical change was noted in the montmorillonites heated to 700°C. The highly dispersing characteristic of montmorillonite was almost completely eliminated; a well-aggregated solid was formed when the clay was suspended in water (Fig. 44). In column applications of clay minerals for waste treatment, plugging caused by dispersion of the clay is undesirable. Similarly, the use of clays to remove cesium from low-level treatment plants would be more attractive if clays would settle to the bottom rather than be suspended in the water. Dispersion of the clays would result in the loss of the particles to the effluent stream. The aggregation of the montmorillonite and the increased affinity for cesium by heating are desirable features discovered during this phase of study.

Since clays do not show high specificity for strontium in waste solutions,[38] studies were made with materials whose structure would favor the sorption of strontium. A material which should show some affinity for strontium is rock phosphate. Comparative tests made with Florida pebble phosphate, Tennessee phosphate, illite, and vermiculite showed that the phosphates were definitely superior to the clay minerals. Results also show that the phosphates are much more effective at high pH (about 11) than when neutral. Further tests are being considered; the approach will be oriented towards understanding the mechanism of sorption by these materials.

Characterization of Fixation Mechanism

In the preceding discussion on cesium fixation by ion exchange, the range of cesium concentrations was limited to that expected in high-level wastes. For more complete understanding of the system, a greater range of cesium concentrations was investigated; in addition, the basis for comparing different clays was changed from equal weights to equal milliequivalents. Reference clay minerals, whose properties are described in detail elsewhere,[39] were obtained from Ward's Natural Science Establishment. In addition, samples of vermiculite were obtained from the Zonolite Company, Traveler's Rest, South Carolina.

---

[38] W. J. Boegly, Jr., *et al.*, *H-P Ann. Prog. Rep. July 31, 1958*, ORNL-2590, p 78.

[39] P. F. Kerr *et al.*, *Reference Clay Minerals, American Petroleum Institute Research Project 49*, Columbia University, New York, 1949.

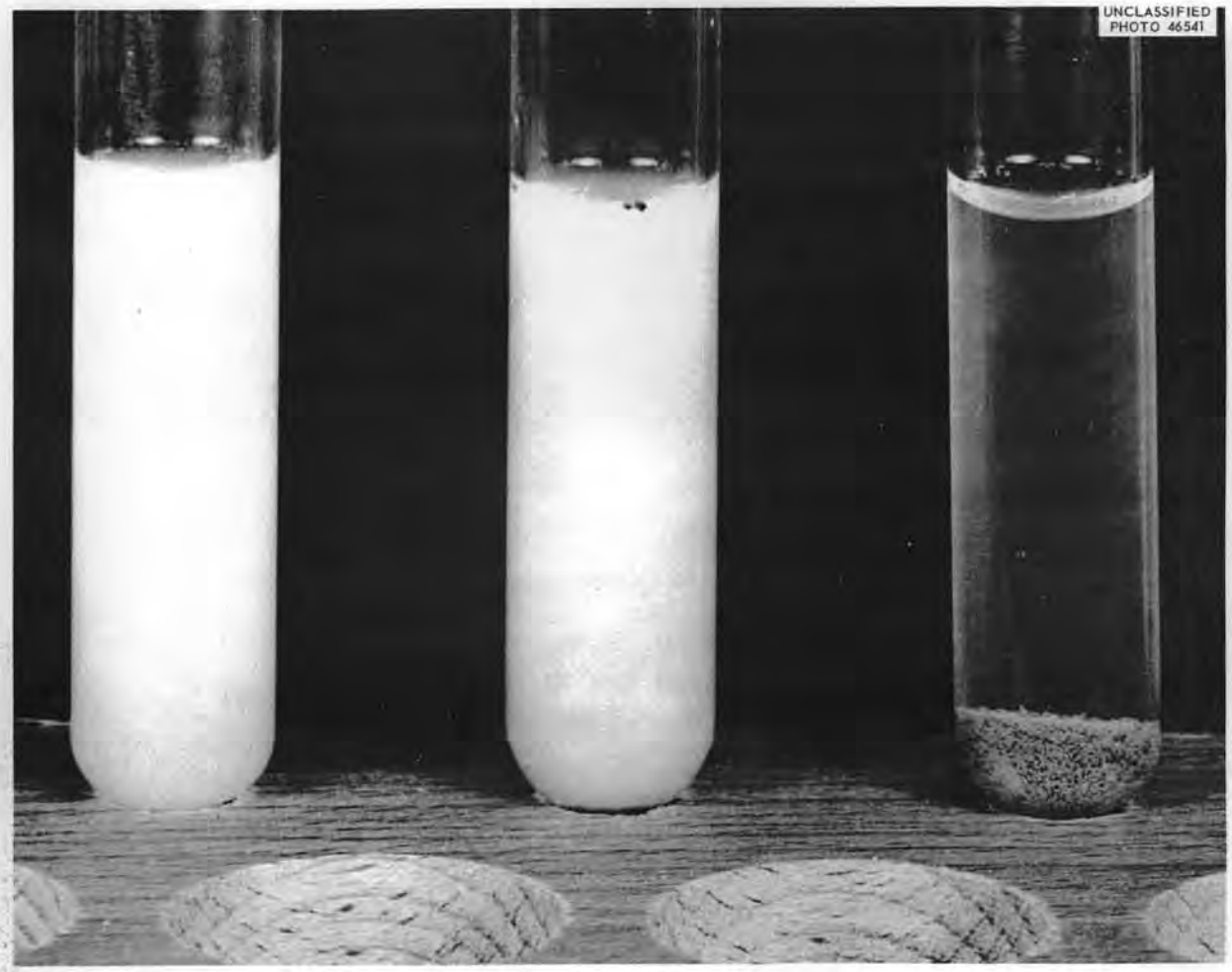

Fig. 44. Physical Characteristics of Montmorillonite After Treatment. From left to right: natural montmorillonite, potassium montmorillonite, and potassium montmorillonite heated to 700°C.

In the case of cesium sorption studies on the reference clay minerals, portions of the clays representing 1 meq of cation exchange capacity (CEC) were weighed into bottles containing 100 ml of tagged $CsNO_3$ solution of the desired concentration. After sufficient time for completion of the exchange reaction, 1-ml aliquots were removed for counting and a known amount of a complementary cation (Na^+, K^+, Rb^+, NH_4^+, H^+, Ca^{++}, or Al^{+++}) was added to each bottle. This was repeated for each complementary cation concentration desired. The amount of cesium sorbed by the clay was computed by comparing the initial and final counting rates of the supernatant.

Typical curves of sorption obtained in 0.1 *M* HCl are shown in Fig. 45. It can be seen that the sorptive behavior of kaolinite is nearly identical to that of Arizona bentonite on the basis of equivalent exchange capacity. However, it must be noted that 6 g of kaolinite was required for 1 meq CEC while only 0.68 g of Arizona bentonite represented the same CEC. The sorption curve for Wyoming bentonite appears to belong to the same family of curves, differing only in amplitude. The sorption curve obtained for illite differs from the other sorption curves and is reminiscent of cesium sorption curves obtained for Conasauga shale. The similarity of the curves illustrates the importance of clay mineralogy in controlling sorptive behavior of sediments.

The sorption curves obtained for Arizona bentonite, kaolinite, and Wyoming bentonite are readily

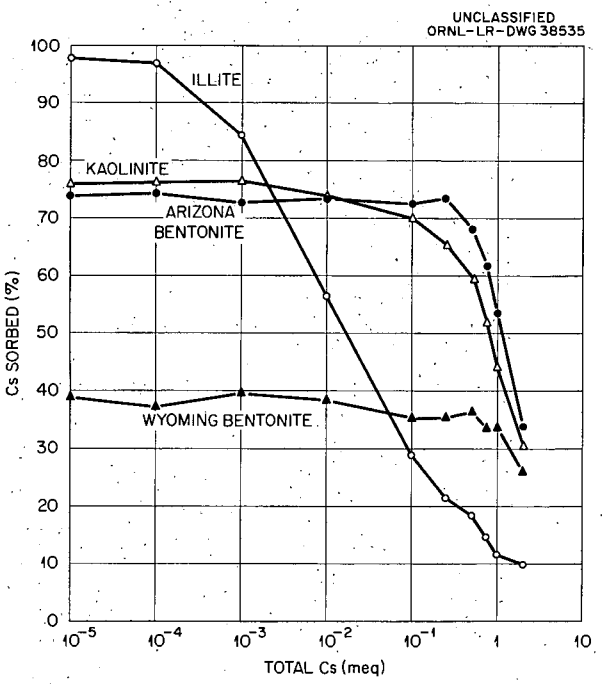

Fig. 45. Sorption of Cesium from 0.1 *M* HCl by Various Clays (1 meq Cation Exchange Capacity).

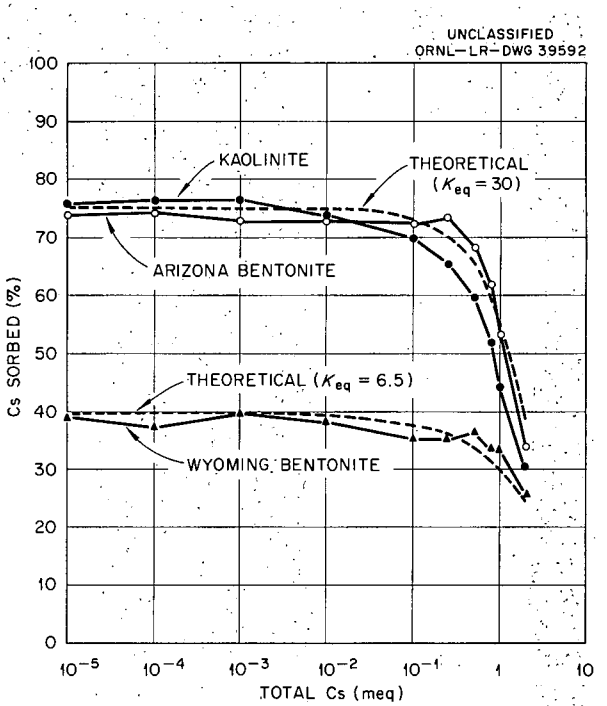

Fig. 46. Description of Cesium Sorption from 0.1 *M* HCl Based on Mass Action.

reconstructed by assuming a single equilibrium coefficient for the entire range of cesium concentration (Fig. 46). In the case of the expanding 2:1 layer lattices, as well as the kaolinitic type of lattice, the entire surface of the clay is accessible to nearly all exchangeable cations and the exchange surface may be considered uniform, at least for the concentration ranges investigated. The affinity of these surfaces for cesium compared to hydrogen may be attributed to the ability of the dehydrated cesium ion to closely approach the charged surface of the clay mineral, partially penetrating the open hexagonal network of oxygen atoms and forming covalent bonds with the surrounding six oxygen atoms.

The sorption curve for illite, however, cannot be easily reconstructed on the basis of a single equilibrium coefficient, as clearly demonstrated in Fig. 47. A second approximation, assuming a small number of exchange sites highly selective for cesium, allows computation of a curve that fits the observed data more closely. Mathematical manipulation could improve the fit of the theoretical curve to the observed data, but the case presented demonstrates satisfactorily the interpretation that is necessary for this type of behavior.

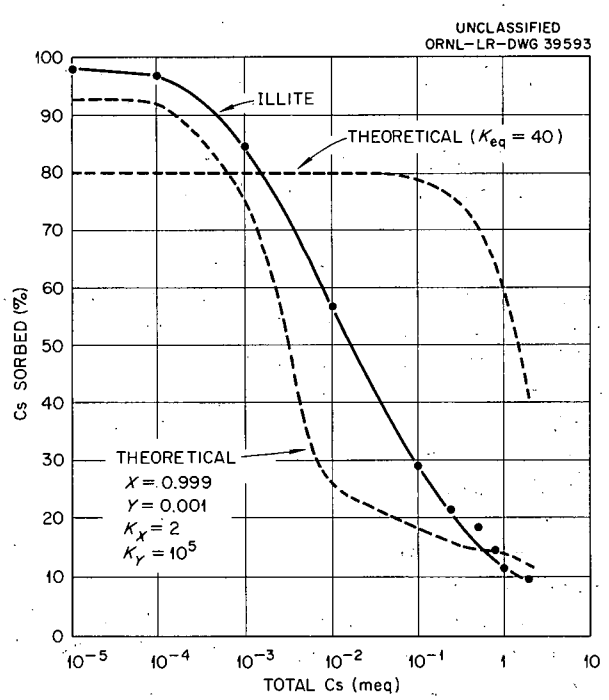

Fig. 47. Description of Cesium Sorption by Illite from 0.1 *M* HCl Based on Mass Action.

Based on the crystal structure of the illite lattice, an argument can be made permitting prediction of exchange sites highly selective for cesium.[36] The open hexagonal network of oxygen atoms constituting the basal surface of the 2:1 layer lattice clay minerals is of the exact size and configuration for the accommodation of cesium ions. In the case of the collapsed illite lattice, the cesium ion would be completely surrounded by 12 oxygen atoms. The basal surface of the collapsed lattice is not completely accessible to all cations in the system; therefore cesium sorption by illite must occur at the edges of the clay platelets. These sites would prefer cesium for steric reasons, and the cesium would be held there with high affinity. Other exchange sites, not lying between the basal surfaces, would not be expected to exhibit a high affinity for cesium. Potassium held at internal regions of the interlayer spacing by illite is probably only very slowly displaced by cesium, since the lattice is not freely expandable. If the process of internal displacement of potassium is very slow compared to the sorption of cesium at the edges of the lattice, then a quasi equilibrium may have been obtained.

So far we have considered only the clay minerals that exist either in an expanded or in a collapsed state. The clay mineral vermiculite normally exists in an expanded state (14-Å *c* spacing) with hydrated magnesium ions occupying the interlayer exchange sites. However, it is possible to collapse the lattice by saturating the exchange sites with potassium, forming a pseudoillite.

Vermiculite was treated by refluxing with 1 *M* NaCl or KCl and elutriating with ethanol (95%) until a negative test for chloride was obtained. X-ray diffraction showed that upon potassium treatment the (001) spacing of the vermiculite was reduced from 14.2 to 10.3 Å, indicating conversion of the vermiculite to an illitic structure. Sodium treatment caused a portion of the basal spacing to be reduced from 14.2 to 12.2 Å, corresponding to the loss of a layer of water of hydration. That the interlayer potassium ions in collapsed lattices are not easily exchangeable was evidenced by a drop in the exchange capacity, as determined by calcium titration.[37] The exchange capacity was reduced from 60.2 meq per 100 g of vermiculite to 16.7 meq per 100 g upon potassium saturation.

Two grams of vermiculite was used for sorbing cesium from 0.1 *M* NaCl. The data obtained from this sorption series are shown graphically in Fig. 48. As predicted from structural considerations, the potassium-treated vermiculite, now of illitic structure, exhibited a cesium sorption curve nearly identical to that of natural illite. An explanation of the behavior of the sodium-treated vermiculite is not so apparent at first glance. However, application of the structural considerations outlined above leads to a very good explanation for the complex curve observed. The behavior of the curve in the very dilute cesium concentration range is possibly due to biotite impurity in the vermiculite sample. Thus the really interesting portion of the curve is that region representing concentrations greater than 10^{-2} meq of cesium per 100 ml. As the total cesium concentration is increased a greater portion of the exchange complex is satisfied by cesium. Cesium, behaving much like potassium, causes a collapse of the vermiculite lattice; this results in an increased affinity of the vermiculite for cesium. This increase in cesium

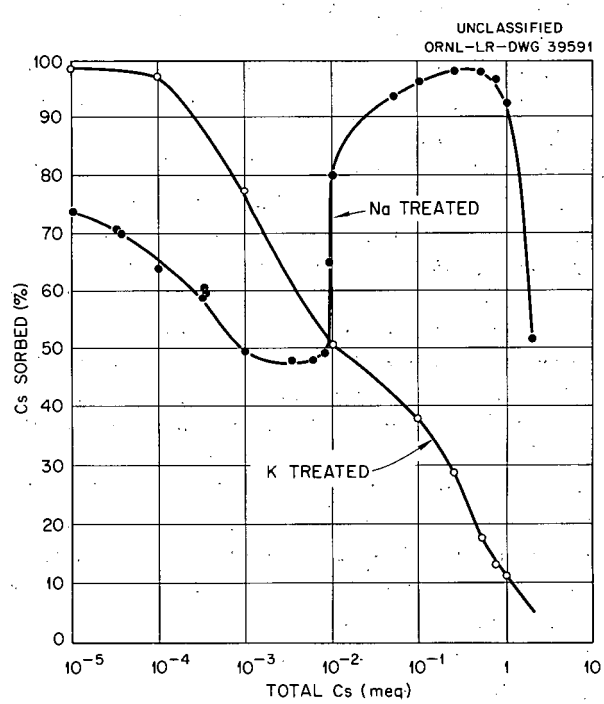

Fig. 48. Sorption of Cesium from 0.1 *M* NaCl by Vermiculite.

sorption, accompanied by an increased number of exchange sites highly selective for cesium, continues until the number of cesium ions in the system exceeds the total number of available exchange sites.

Because of the peculiar changes in the cesium sorption properties of vermiculite upon structural collapse of the lattice induced by sorption of potassium or cesium, it was felt that intermediate levels of potassium saturation might lead to an interesting correlation between sorption curves and structural response. It was felt that in this way it might be possible to determine whether a critical degree of saturation of the exchange complex was necessary for complete collapse of the vermiculite lattice or whether collapse, accompanied by increased affinity for cesium, might occur between platelets in a stepwise fashion.

Sodium-treated vermiculite was exposed to solutions containing various amounts of potassium nitrate tagged with K^{42}, which has a short (12.4 hr) half life. After contact for 2 hr the suspensions were centrifuged, and an aliquot of the centrifugate was counted for K^{42} activity. This allowed estimation of the amount of potassium sorbed by the vermiculite. Portions of the vermiculite were used for cesium sorption studies, two weeks being allowed for completion of the cesium exchange reaction and for decay of the K^{42}. Samples of the vermiculite were submitted for x-ray diffraction and for determination of the cation exchange capacity. The sorption of potassium is not easily reversible, as shown by the drop in exchange capacity with increasing sorption of potassium (Table 24). From the x-ray diffraction patterns (Figs. 49–54) it is seen that lattice collapse occurs continuously rather than in an abrupt single collapse at a critical concentration of sorbed potassium.

Figure 55 shows the cesium sorption curves obtained for vermiculite having various levels of potassium saturation. Collapse of a few platelets by treatment with small amounts of potassium results in improved cesium sorption from very dilute cesium solutions. In the more concentrated ranges of cesium the sorption of cesium is reduced by an amount dependent on the degree of previous potassium saturation. Although x-ray diffraction indicates complete collapse of the lattice at about 60% potassium saturation, the sorption results

Table 24. The Change of Measurable Exchange Capacity of Vermiculite with Potassium Treatment

Sample	Potassium Sorbed (meq per 100 g)	Exchange Capacity (meq per 100 g)
1	0	60.2
2	4.8	55.9
3	17.6	31.8
4	22.1	25.4
5	34.7	18.1
6	35.9	15.1
K-saturated		16.7

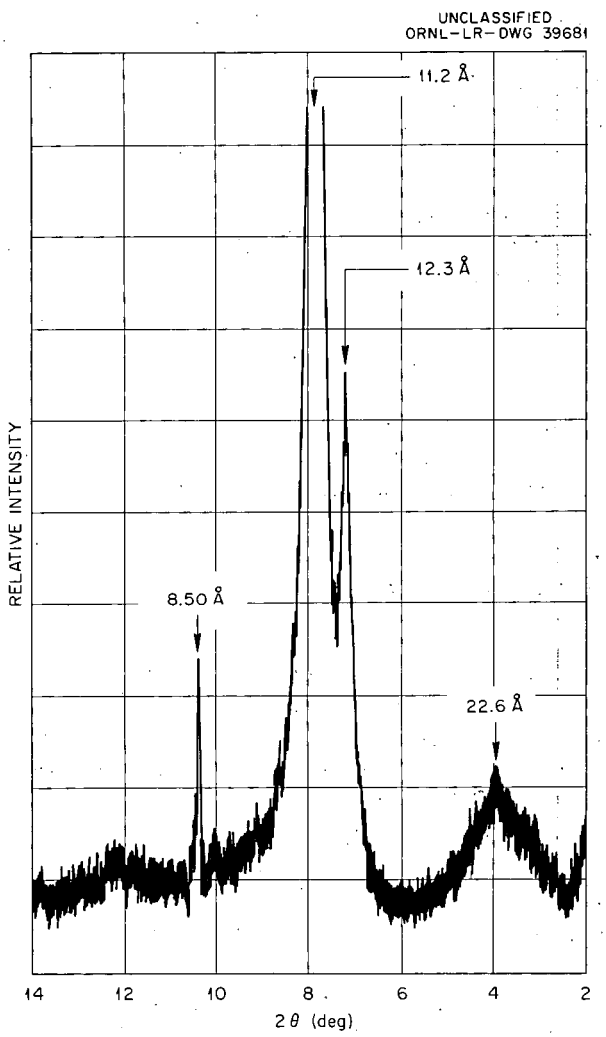

Fig. 49. X-Ray Diffraction Pattern of Sodium-Saturated Vermiculite.

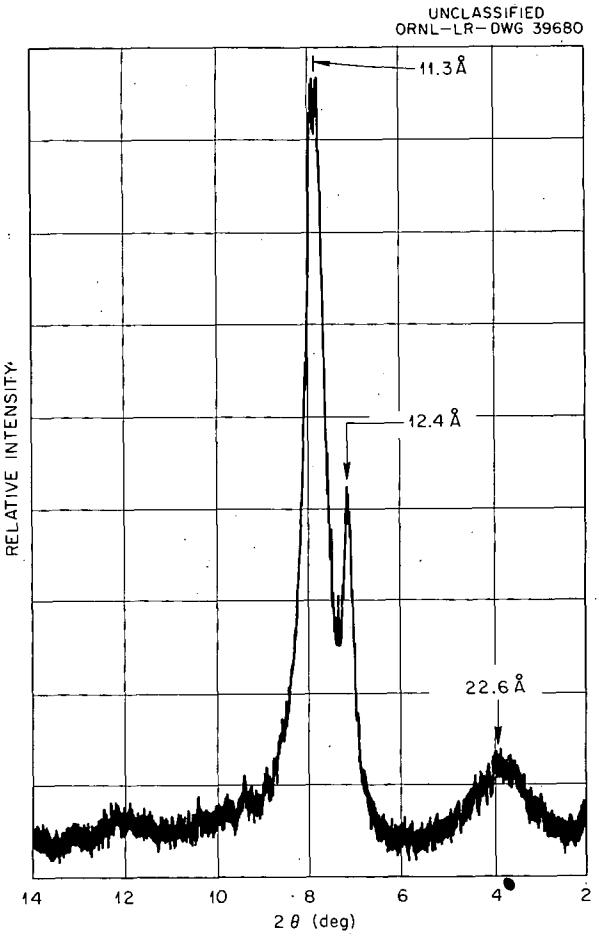

Fig. 50. X-Ray Diffraction Pattern of Vermiculite, 8% Potassium Saturated and 92% Sodium Saturated.

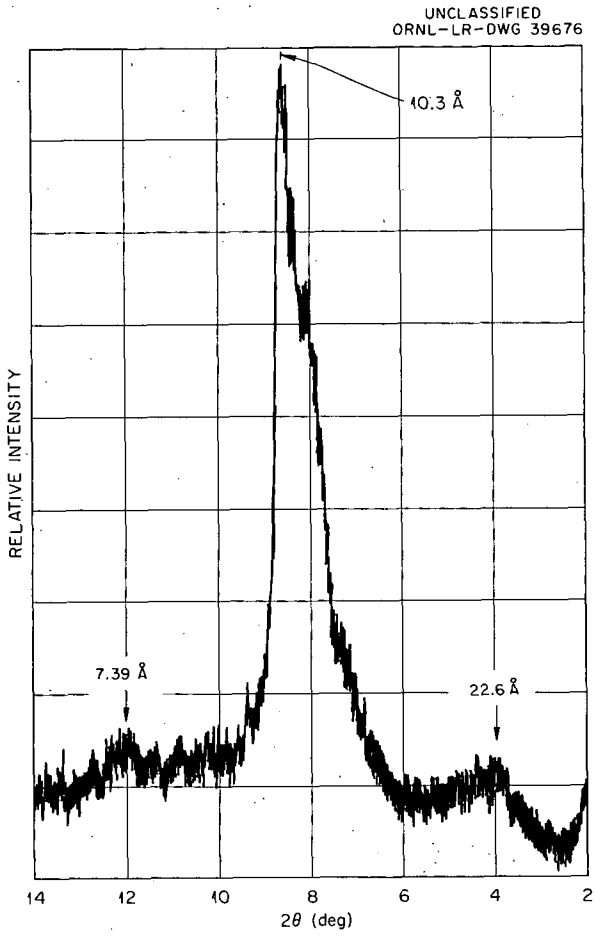

Fig. 51. X-Ray Diffraction Pattern of Vermiculite, 30% Potassium Saturated and 70% Sodium Saturated.

show that even higher degrees of potassium saturation do not so completely collapse the lattice as to prevent additional interlayer fixation of cesium. Even the supposed 100%-potassium-saturated vermiculite shows a slight suggestion of interlayer cesium fixation indicating that all platelets were not previously collapsed.

It seems obvious that although the structure of the basal surface of the clay minerals combined with a collapsed *c* spacing of the lattice is requisite for cation fixation, the fixation process for previously collapsed minerals is slightly different from that for minerals that collapse during the fixation process. In the cases of illite, potassium-treated vermiculite, micas, and fluorophlogopites the "fixed" cations were merely held with a high affinity by exchange sites at the edges of the interlayer spacing. In the case of vermiculite, on the other hand, the cations are physically entrapped by collapse of the lattice in a true fixation process. For this reason nearly all of the interlayer exchange sites of vermiculite are available for cation fixation, while only the exchange sites along the outer edges of the interlayer spacing of illite have the capability of fixing new cations introduced to the system. This accounts for the observation that the fixation capacity of vermiculite is several times that of illite even though the interlayer charge of vermiculite is less than that of illite.

These studies with the various clay minerals on the characterization of ion exchange reactions of cesium have implications beyond the immediate

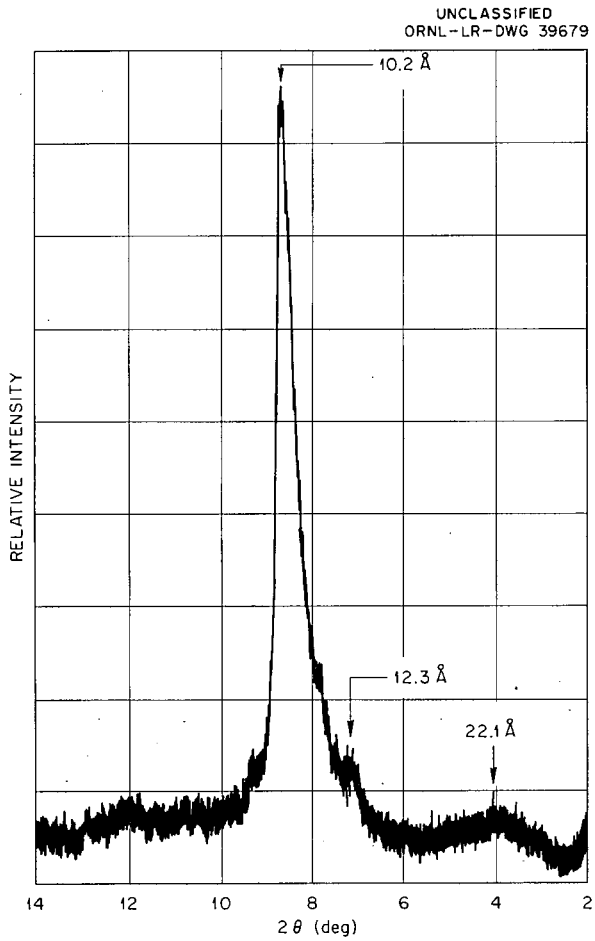

Fig. 52. X-Ray Diffraction Pattern of Vermiculite, 37% Potassium Saturated and 63% Sodium Saturated.

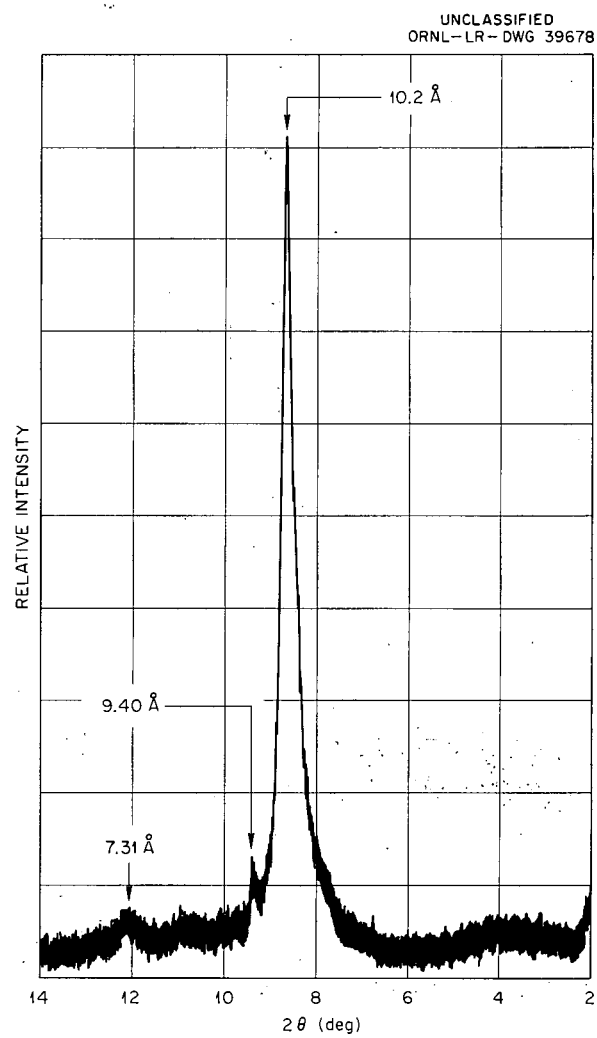

Fig. 53. X-Ray Diffraction Pattern of Vermiculite, 55% Potassium Saturated and 45% Sodium Saturated.

application to waste disposal techniques. For example, the observation that 60% potassium saturation showed x-ray diffraction maxima at only 10 Å reveals the limitations of using x-ray techniques alone for mineral characterization. Furthermore, the resolution of the further fixation capability of the 60%-saturated mineral by the radiochemical Cs^{137} technique permits quantitative characterization of the true mineral character. This is indeed a powerful method for the proper identification of minerals in soils and sediments.

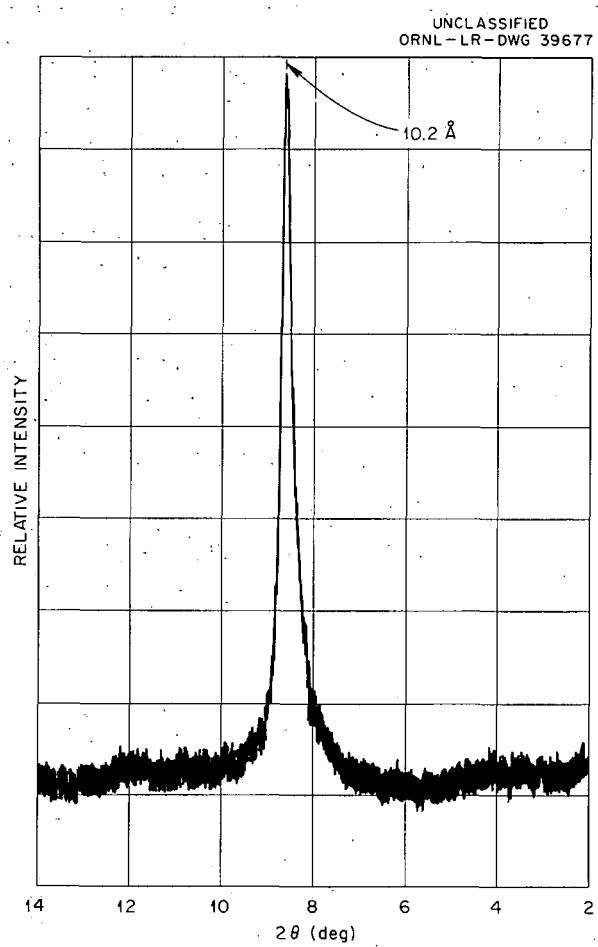

Fig. 54. X-Ray Diffraction Pattern of Vermiculite, 60% Potassium Saturated and 40% Sodium Saturated.

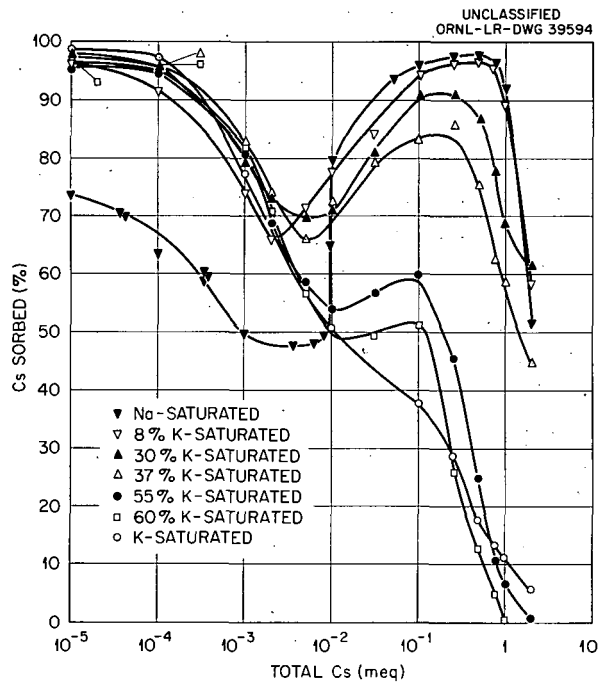

Fig. 55. Effect of Degree of Potassium Saturation on Sorption of Cesium from 0.1 *M* NaCl by Vermiculite.

DISPOSAL IN SALT FORMATIONS

F. L. Parker

W. J. Boegly, Jr.
R. L. Bradshaw
E. R. Eastwood
F. M. Empson
L. Hemphill
O. H. Myers
J. Crowell[40]
B. D. Gunter[40]

The problem of radioactive waste disposal in cavities in natural salt formations has been characterized as that of "the degree to which the structural properties of salt are affected by chemical interaction, pressure, temperature, and radiation. . . ."[41] This report covers some of the theoretical considerations and laboratory investigations of these factors. Theoretical studies indicate that the temperature of radioactive wastes stored in salt cavities can be kept within acceptable limits by controlling the age of the wastes and the size of the cavity. Laboratory work shows essentially no chemical interactions between the present-day wastes and rock salt. Additionally, radiation has little effect on the structural properties or thermal conductivity of rock salt. However, all the information necessary for the design of the field-scale radioactive experiment cannot be obtained theoretically or by laboratory tests, because theoretical solutions require a number of simplifying assumptions, and laboratory tests of disturbed geological materials are not conclusive for field application. Preliminary field tests are designed to provide information on the effects of heat and chemical interaction on the structural integrity of the salt, the movement of nuclides from the cavity into the surrounding salt, and the migration of the cavity itself.

Thermal Calculations

The plasticity and structural strength of rock salt are dependent upon temperature and pressure.

[40] AEC Fellow in radiological physics.

[41] F. L. Parker *et al.*, *H-P Ann. Prog. Rep. July 31, 1958*, ORNL-2590, p 78.

The pressure imposed on the system is a function of the stratigraphy, the percentage of salt excavated, the configuration of the excavation, and the thickness of the overburden. Temperature in a cavity is a function of its depth, size, shape, the rate of heat production of the stored material, and thermal conduction in the surrounding salt. The heat production rate, approximated from Fig. 56, is given as a function of decay time, assuming 800 gal of waste per metric ton of uranium, irradiated for 10,000 Mwd/ton at 33 Mw/ton specific power.[42]

If a limit to the temperature rise within a cavity and the surrounding space is established, then the time-space-temperature distribution can be calculated for various sizes and shapes of the cavity and for heat production rates of the wastes stored within the cavity. The maximum permissible temperature that would not produce drastic physical changes in a salt cavity has been set at 200°F.[43]

The possible sizes and shapes of cavities and the heat-production rates of wastes are so numerous that a few simplifying assumptions were necessary:

1. Only spherical shapes would be investigated so that an analytical solution would be facilitated.
2. Diameters of the spheres would be limited to 10 and 20 ft, since it has been shown previously[44] that larger spheres, containing wastes generating heat at a rate of 2 $Btu \cdot hr^{-2} \cdot gal^{-1}$, would exceed the permissible limit of 200°F.

[42] J. O. Blomeke, *Status Report on the Disposal of Radioactive Wastes*, ORNL CF-57-3-114 (Rev.), p 68 (June 25, 1957).

[43] F. Birch, *Thermal Considerations in Deep Disposal of Radioactive Wastes*, NAS-NRC 588, p 9 (July 1958).

[44] F. L. Parker, L. Hemphill, and J. Crowell, *Status Report on Waste Disposal in Salt Formations*, ORNL-2560, p 30 (Jan. 29, 1959).

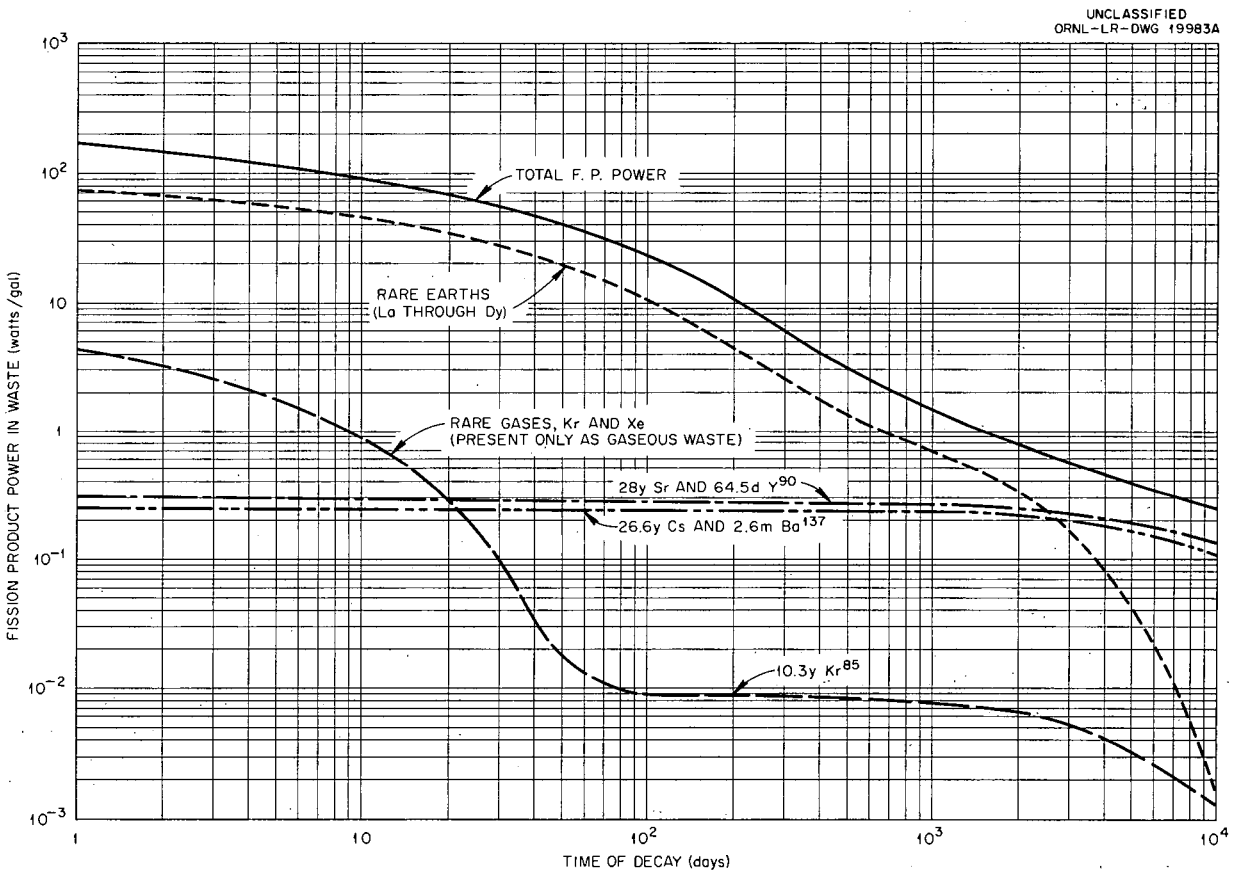

Fig. 56. Fission Product Power in Waste as a Function of Decay Time. Basis: 800 gal waste per metric ton uranium, irradiated 10,000 Mwd/ton at 33 Mw/ton specific power.

3. Wastes considered would be limited to those described by Fig. 56 and cooled for 1, 6, and 11 years.
4. Waste-filled cavities would be located in an infinite body of salt.
5. Thermal conductivity, density, and specific heat of the salt and the wastes would be constant and independent of changes in temperatures.
6. Heat would be lost by conduction only.
7. Phase changes would not occur in the wastes or in the salt.
8. Convective currents would not develop in the wastes.
9. All beta and gamma energy would be absorbed in the wastes.

All assumptions, except the extent of salt, are on the safe side; that is, the calculated temperatures would be higher than those actually achieved. In the absence of convective currents in the wastes a temperature gradient from the center of the cavity to the interface of the salt and the waste would be produced. If convective currents were present, the temperature would be more uniform throughout the sphere. However, for cavities of the size considered, the edge temperature in the conduction case would approach the more uniform temperature that would be achieved if convective currents were present.

Statement of Problem. – A mathematical statement of the spherical problem is:

$$\frac{1}{\alpha_1}\frac{\partial T_1}{\partial t} = \frac{\partial^2 T_1}{\partial r^2} + \frac{2}{r}\frac{\partial T_1}{\partial r} + \frac{Q(t)}{K_1} \quad (0 \leq r < a,\ t > 0), \quad (1)$$

and

$$\frac{1}{\alpha_2}\frac{\partial T_2}{\partial t} = \frac{\partial^2 T_2}{\partial r^2} + \frac{2}{r}\frac{\partial T_2}{\partial r} \qquad (r > a,\ t > 0), \quad (2)$$

where subscripts 1 and 2 refer to the heated sphere and to the infinite body, respectively, T is temperature, t is time, r is radial distance from the center of the sphere, a is the radius of the sphere, K is thermal conductivity, α is thermal diffusivity, and $Q(t)$ is heat generation per unit time per unit volume.

Initially, the wastes and salt are considered to be at zero temperature. Boundary conditions are such that the temperature and heat flux are continuous at the interface, and the temperature remains finite both at the center of the sphere and at infinity. Then by the use of Laplace transforms and Duhamel's theorem the following equations are obtained. The temperature inside the cavity is

$$T_1(t) = \int_0^t \sum_{i=1}^{N} A_i \frac{e^{-\lambda_i(t-\tau)}}{2C_2}\left\{\operatorname{erf}\left(\frac{a-r}{2\sqrt{\alpha_2\tau}}\right) + \operatorname{erf}\left(\frac{a+r}{2\sqrt{\alpha_2\tau}}\right) - \sqrt{\frac{4\alpha_2\tau}{r^2\pi}}\left[e^{-(a-r)^2/4\alpha_2\tau} - e^{-(a+r)^2/4\alpha_2\tau}\right]\right\} d\tau, \quad (3)$$

and outside the cavity

$$T_2(t) = \int_0^t \sum_{i=1}^{N} A_i \frac{e^{-\lambda_i(t-\tau)}}{2C_2}\left\{\operatorname{erf}\left(\frac{r+a}{2\sqrt{\alpha_2\tau}}\right) - \operatorname{erf}\left(\frac{r-a}{2\sqrt{\alpha_2\tau}}\right) - \sqrt{\frac{4\alpha_2\tau}{r^2\pi}}\left[e^{-(r+a)^2/4\alpha_2\tau} - e^{-(r-a)^2/4\alpha_2\tau}\right]\right\} d\tau, \quad (4)$$

where N is the number of fission products; A_i is the heat generation per unit time per unit volume for the ith fission product and λ_i is the disintegration constant of the ith fission product as

$$\sum_{i=1}^{N} A_i e^{-\lambda_i t}$$

is substituted for $Q(t)$; C is the specific heat per unit volume ($C = K/\alpha$); t is a variable of integration; and erf is the error function. For rock salt, K_2 equals 2.07 Btu·ft^{-1}·hr^{-1}·(°F)$^{-1}$, α equals 0.07 ft^3/hr, and C^2 equals 29.7 Btu·ft^{-3}·(°F)$^{-1}$.

Summing the integrals of the decay curves of all fission products contributing to heat generation would be arduous. Therefore, the total fission product power, as shown on Fig. 56 is approximated by six exponentials: the decay curves for Cs^{137}-Ba^{137}, Sr^{90}-Y^{90}, long-lived and short-lived components of the rare earths, and long-lived and short-lived components of the remainder of the fission products.

Results. – Equations for the temperatures both inside and outside the cavity were numerically

integrated on the IBM-704. The results are shown in Table 25 and Figs. 57 and 58.

For the 10-ft-dia sphere and one-year-old waste (Fig. 57), it is seen that the maximum rise in temperature at the center of the sphere is 530°F at 1000 hr and at the surface of the sphere 315°F at 1500 hr. In Fig. 58 the maximum temperature rise for six-year-old waste at the center of the sphere is 100°F at 4500 hr and at the surface 65°F at 7000 hr. As interpolated from the curves and Table 25, two-year-old wastes stored in a 10-ft-dia sphere would reach a peak temperature of 200°F in less than five months. The same wastes could not be stored in 20-ft-dia spheres without boiling.

These results are substantially the same as the calculations of Birch[43] and Schecter,[45] who considered only temperature-time distributions for the conduction and convection cases. For a sphere of 5-ft radius, Schecter found a drop of 35% from the center-of-the-sphere temperature in the conduction case to the uniform sphere temperature in the convection case. Our calculations for spheres of this size show a 40% reduction from center temperature to surface temperature in the conduction case, or little difference between surface temperature in the conduction case and sphere temperature in the convection case.

It may be concluded that the thermal problem in salt disposal will cause no serious difficulties if the size of the cavities and the age and dilution of the wastes are controlled.

Structural Properties of Rock Salt

The rock salt surrounding waste-filled cavities will be subjected to certain stresses induced by elevated temperatures and pressures and by radiation. The response of crystal aggregates of rock salt to temperature, pressure, and radiation was investigated to determine the stress-strain relationships and the creep rate.[46] Stress-strain relationships were used to determine the compressive strength, modulus of elasticity, yield strength (0.2% offset), and apparent elastic limit.

[45] R. S. Schecter and E. F. Gloyna, "Temperature Rise in Underground Storage Sites for Radioactive Wastes," *Ind. and Eng. Chem.*, prepublication copy (Mar. 1, 1958).

[46] B. D. Gunter, *The Effect of Gamma Irradiation on the Mechanical Properties of Rock Salt*, thesis, Vanderbilt University, in press.

Table 25. Maximum Temperature Rise of Radioactive Wastes Stored in 5- and 10-ft-Radius Spheres

Age of Fission Products (years)	5-ft-Radius Spheres			10-ft-Radius Spheres		
	Distance from Center of Sphere (ft)	Temperature (°F)	Time (hr)	Distance from Center of Sphere (ft)	Temperature (°F)	Time (hr)
1	0	527	1,000	0	1733	2,000
	2.5	470	1,500	5.0	1533	2,000
	5.0	317	1,500	10.0	983	3,000
	10.0	122	3,000	20.0	335	7,000
	50.0	8.0	20,000	100.0	15.6	60,000
6	0	102	4,000	0	368	7,000
	2.5	91	5,000	5.0	331	7,000
	5.0	64	7,000	10.0	227	10,000
	10.0	28	10,000	20.0	94	20,000
	50.0	32	40,000	100.0	>8	150,000
11	0	66	7,000	0	245	10,000
	2.5	60	7,000	5.0	221	15,000
	5.0	43	10,000	10.0	153	15,000
	10.0	19	15,000	20.0	66	30,000
	50.0	2	60,000	100.0	>7	>150,000

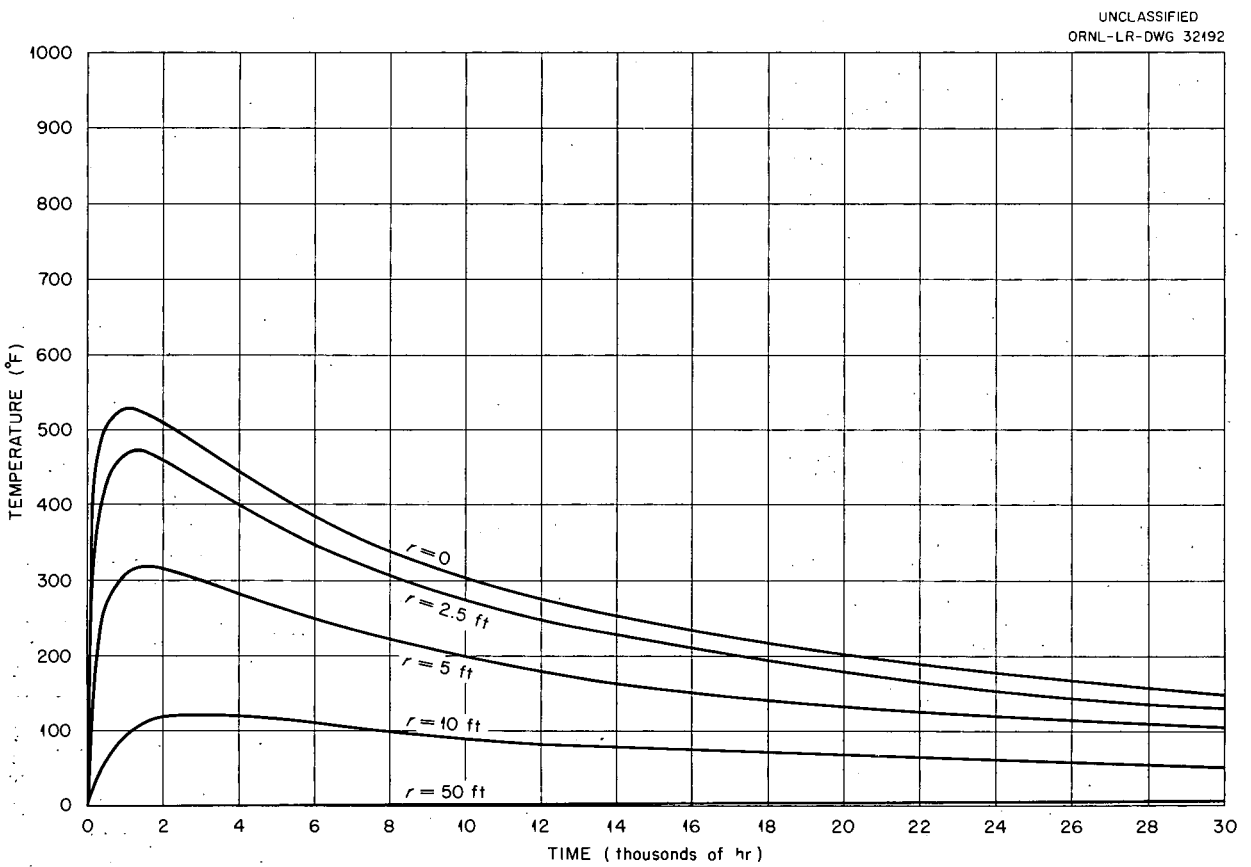

Fig. 57. Temperature Rise in a One-Year-Old Waste – Sphere of 5-ft Radius, Surrounded by an Infinite Bed of Salt.

Experimental Procedure. – The American Society of Testing Materials has no standard procedure for the testing of rock-salt aggregates. Consequently, the test procedures for wood and stone were investigated and the more pertinent provisions applied to the testing of rock salt.[47] Two-inch cubes of salt, randomly selected, were used as test specimens. Specimens of dome salt were machined from a large block taken from the Morton Salt Company's mine at Grand Saline, Texas. Specimens of bedded-deposit salt were machined from a block taken from the Carey Salt Company's mine at Hutchinson, Kansas. The purity of the dome salt was greater than 98% NaCl and that of the bedded salt was 95% NaCl.

Machined specimens were irradiated in the Cobalt Storage Facility of the Operations Division at ORNL. Approximately 200,000 curies of Co^{60} in aluminum-clad cylinders are stored in a 1-ft^3 chamber below ground level to produce an exposure dose rate of 3.2×10^6 r/hr, as measured with a ceric sulfate chemical dosimeter.

Specimens were tested with the assistance of the Mechanical Testing Section of the Metallurgy Division at ORNL. A 120,000-lb-capacity Baldwin-Tate-Emery universal testing machine was used for load application. Deformation was measured by a bell-crank-anvil extensometer. This apparatus automatically plotted a total load vs total deformation curve, which was then reduced to a stress-strain diagram.

Stress-Strain Relationships of Unirradiated Bedded and Dome Salt at 20°C. – Three specimens each of dome salt, bedded salt loaded parallel to the planes of stratification, and bedded salt loaded perpendicular to the planes of stratification were tested in order to establish a control with which

[47] I. H. Cowdrey and R. G. Adams, *Materials Testing*, p 14, Wiley, New York, 1945.

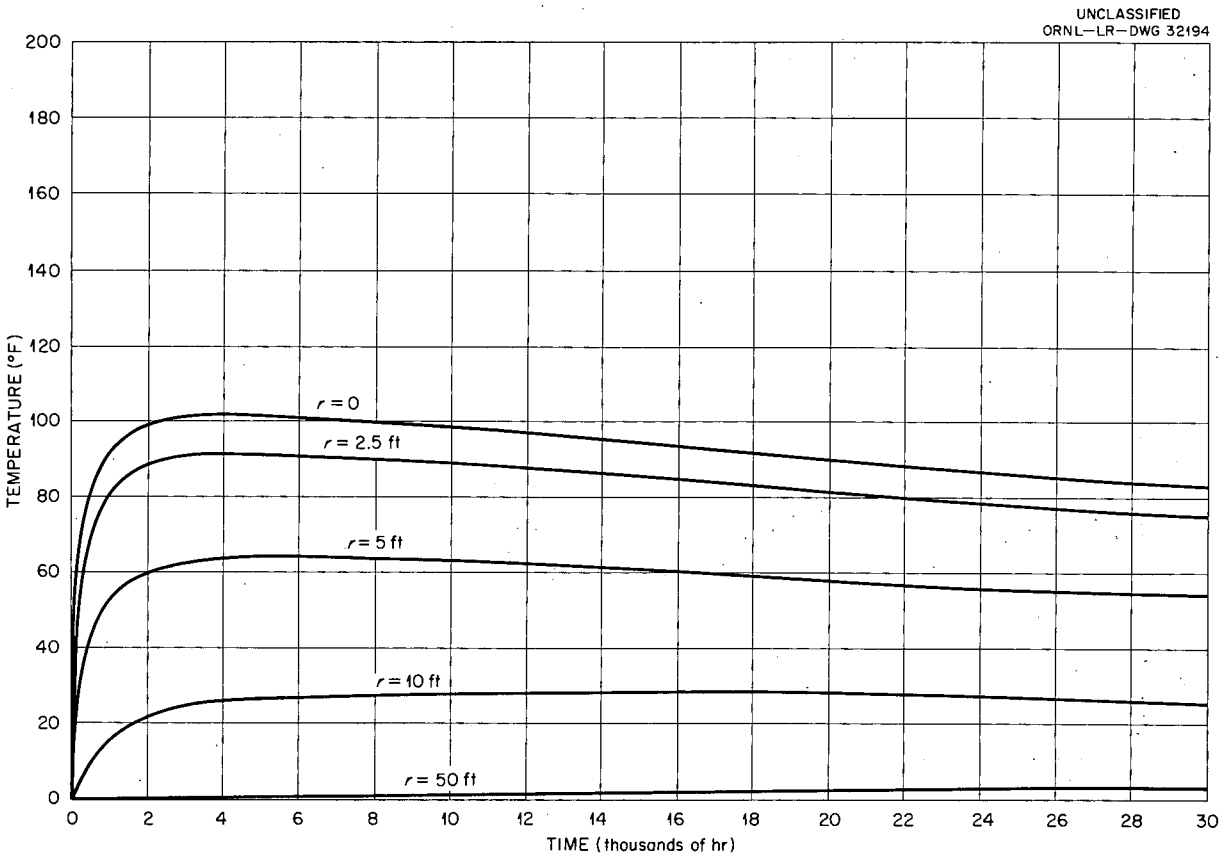

Fig. 58. Temperature Rise in a Six-Year-Old Waste – Sphere of 5-ft Radius, Surrounded by an Infinite Bed of Salt.

to compare irradiated specimens. The results of these tests are shown graphically in Fig. 59 and in tabular form in Table 26.

Dome salt has greater compressive and yield strengths than bedded salt. Previous work with synthetic crystals indicated that small amounts of impurities increased the tensile strength of salt. However, the results for synthetic and single crystals are not applicable to aggregates of crystals.[48] The binding strength between crystals becomes an important factor in the strength of the aggregates. The presence of other substances in the specimens, such as anhydrite and shale, is partially responsible for the greater variation exhibited by the bedded salt (the mined block of bedded salt was interstratified with anhydrite and shale bands of various thicknesses). Dome salt, although neither isotropic nor homogeneous, is much more uniform with respect to impurities than bedded salt.

Bedded salt appears to be slightly stronger when loaded parallel to planes of stratification than when loaded perpendicular to planes of stratification.

Creep Tests of Unirradiated Bedded and Dome Salt at 20°C. – The creep rate resulting from the application of a constant load of 2500 psi for 100 min is shown in Fig. 60. After an initial rise, due mostly to elastic compression, the strain increases very slowly with time. As in the stress-strain tests, dome salt is strongest (least creep under the same load conditions) and exhibits the least variation from sample to sample. Bedded salt loaded parallel to the planes of stratification is again stronger than bedded salt loaded perpendicular to the planes of stratification.

[48] F. L. Parker, L. Hemphill, and J. Crowell, *Status Report on Waste in Natural Salt Formations*, ORNL-2560, p 39 (Aug. 14, 1958).

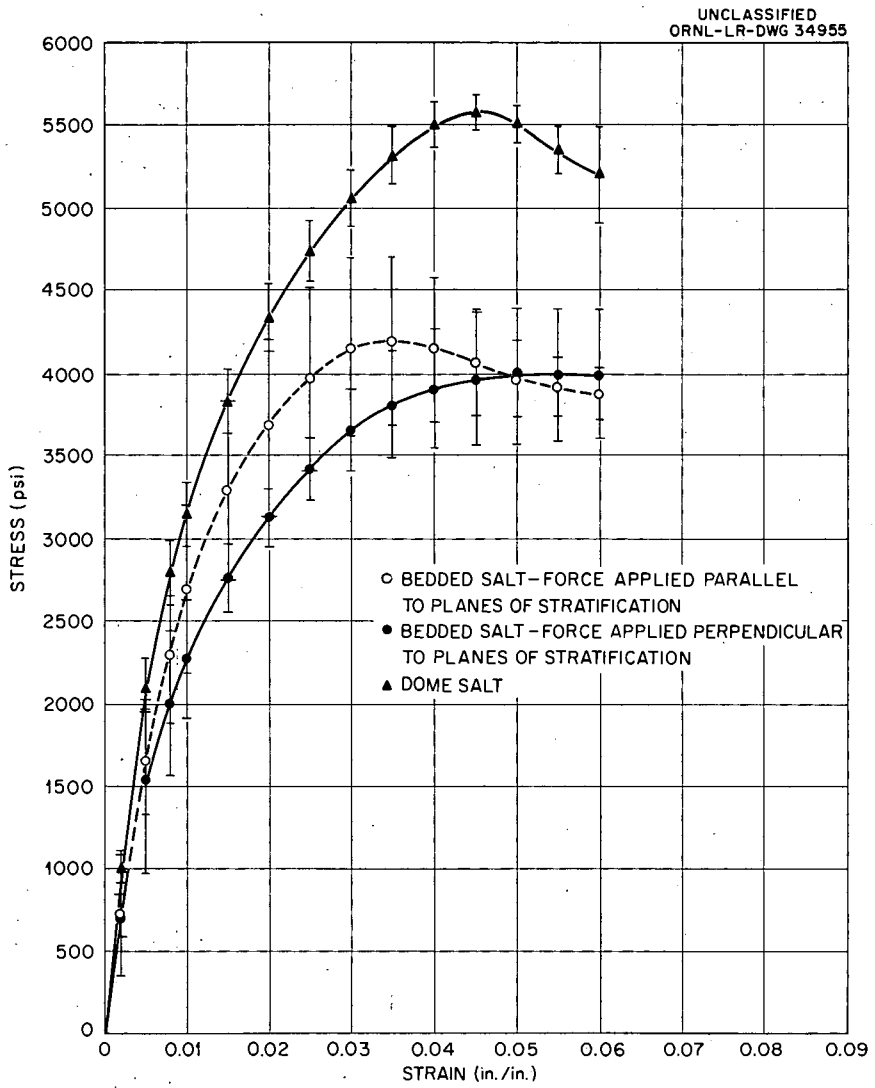

Fig. 59. Compression Test of Unirradiated Salt at Room Temperature.

Stress-Strain Relationship at 20°C of Irradiated Bedded Salt Loaded Parallel and Perpendicular to the Planes of Stratification. – Bedded salt samples were irradiated for periods sufficient to give exposure doses of 10^6, 10^7, 10^8, and 5×10^8 r, assuming a dose rate constant with time.

The stress-strain curves of irradiated bedded salt are shown in Figs. 61 and 62, and the data are given in Table 26. From Figs. 61 and 62 it is seen that there is very little difference in the stress-strain relationship up to a stress of 2000 psi. The compressive strength increases with exposures up to 10^8 r, where a statistically significant decrease is observed.

The expected decrease in the modulus of elasticity is observed only at 5×10^8 r. At 10^6 r the modulus of elasticity, yield strength, and apparent elastic limit are slightly lower than for the unirradiated specimens.

Creep Rate at 20°C of Irradiated Bedded Salt Loaded Parallel and Perpendicular to the Planes of Stratification. – The effect of radiation on the rate of creep was investigated by testing three specimens exposed to 5×10^8 r. These results were compared with those for unirradiated salt (Figs. 63 and 64).

Very little difference in the creep rate can be seen between the irradiated and unirradiated salt.

Table 26. Physical Properties of Rock Salt

All results have been rounded off to the nearest 100 psi and the standard deviations to the nearest 50 psi

Type of Salt	Exposure Dose (r)	Compressive Strength (psi)	Yield Strength (psi)	Apparent Elastic Limit (psi)	Modulus of Elasticity (psi)
			At 20°C		
					$\times 10^6$
Bedded, parallel*	0	4200 ± 500	2500 ± 300	1900 ± 300	0.35 ± 0.06
	10^6	4500 ± 500	2500 ± 150	1900 ± 200	0.32 ± 0.06
	10^7	4600 ± 400	2700 ± 250	2100 ± 200	0.35 ± 0.02
	10^8	4600 ± 150	3400 ± 250	2800 ± 200	0.36 ± 0.09
	5×10^8	3500 ± 50	2700 ± 200	2000 ± 300	0.39 ± 0.07
Bedded, perpendicular**	0	4000 ± 400	2300 ± 300	1700 ± 200	0.36 ± 0.17
	10^6	3800 ± 500	1800 ± 250	1400 ± 250	0.35 ± 0.10
	10^7	4100 ± 400	2300 ± 500	1800 ± 500	0.38 ± 0.04
	10^8	4000 ± 400	2400 ± 500	1900 ± 300	0.38 ± 0.06
	5×10^8	3500 ± 400	2400 ± 300	1900 ± 250	0.37 ± 0.11
Dome	0	5600 ± 100	2900 ± 150	2000 ± 100	0.50 ± 0.05
	10^6	5300 ± 100	2900 ± 150	2000 ± 300	0.51 ± 0.12
	10^7	5100 ± 200	3000 ± 100	2100 ± 300	0.62 ± 0.06
	10^8	4100 ± 200	2700 ± 100	1800 ± 200	0.48 ± 0.04
	5×10^8	3600 ± 500	2600 ± 200	1900 ± 50	0.59 ± 0.12
			At 200°C		
Bedded, parallel	0	3900 ± 200	1600 ± 200	1400 ± 100	0.09 ± 0.01
	5×10^8	3400 ± 400	1900 ± 250	1800 ± 250	0.12 ± 0.02
	0	3600 ± 100	1600 ± 100	1500 ± 150	0.11 ± 0.01
	5×10^8	3300 ± 400	2100 ± 150	1800 ± 100	0.13 ± 0.01
Dome	0	3600 ± 500	1900 ± 150	1600 ± 200	0.14 ± 0.01
	5×10^8	3100 ± 300	2300 ± 150	1800 ± 200	0.16 ± 0.01

*Bedded salt, force applied parallel to the planes of stratification.
**Bedded salt, force applied perpendicular to the planes of stratification.

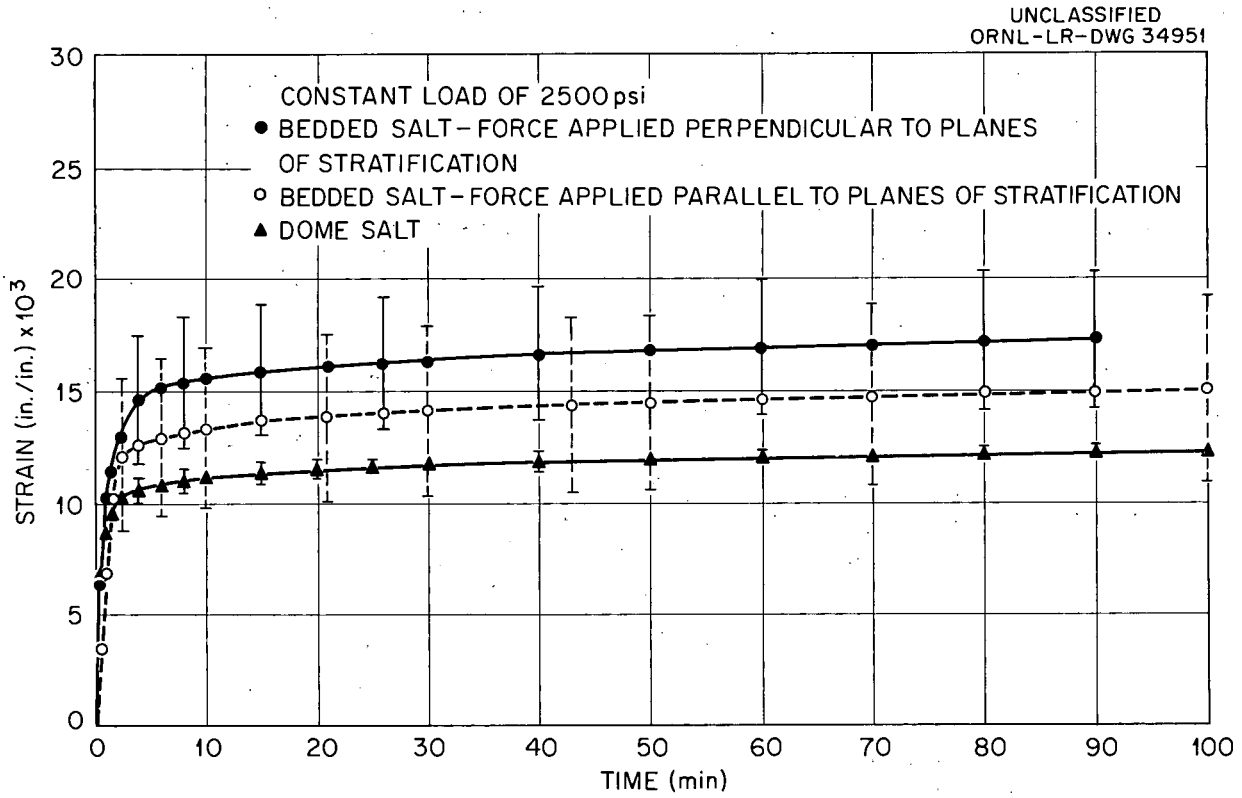

Fig. 60. Creep Test of Unirradiated Salt at Room Temperature.

Only a little over a thousandth of an inch strain separates the two curves when the force is applied parallel to the planes of stratification. The unirradiated salt actually shows less strain than the irradiated specimen for the same case. If the modulus of elasticity is increased, the irradiated salt should show less strain. However, two of the irradiated specimens developed cracks during the test, resulting in a wide variation in results and probably causing the greater strain. The results were as expected for the blocks where the force was applied perpendicular to the planes of stratification.

Stress-Strain Relationship at 200°C of Irradiated Bedded Salt Loaded Parallel and Perpendicular to the Planes of Stratification. – The expected rise in temperature of the salt surrounding waste-filled cavities suggests the need for determining the structural properties of irradiated and unirradiated salt at elevated temperatures. Three specimens each of bedded salt, unirradiated and exposed to 5×10^8 r, were tested at a temperature of 200°C. The results are given in Figs. 65 and 66 and in Table 26 (note that the strain scale has been changed in Figs. 65 and 66). As expected, the plasticity increases quite rapidly with temperature, with a maximum deformation of 25%. Also, the modulus of elasticity, yield strength, and apparent elastic limit are lower than at room temperature. As in the room temperature tests, the stress-strain response of irradiated material (dose 5×10^8 r) rises much faster initially and falls off more rapidly than the stress-strain response for the unirradiated specimens. This gives, as at room temperature, an increase in the modulus of elasticity, yield strength, and apparent elastic limit and a decrease in compressive strength.

Conclusions. – On the basis of these tests, unirradiated dome salt is consistently stronger than unirradiated bedded salt. Under both static and creep loading conditions the unirradiated bedded salt appears to be stronger when loaded parallel to the planes of stratification than when loaded perpendicular to the planes of stratification, though the difference is within the statistical variation of the tests. Radiation causes only minor changes,

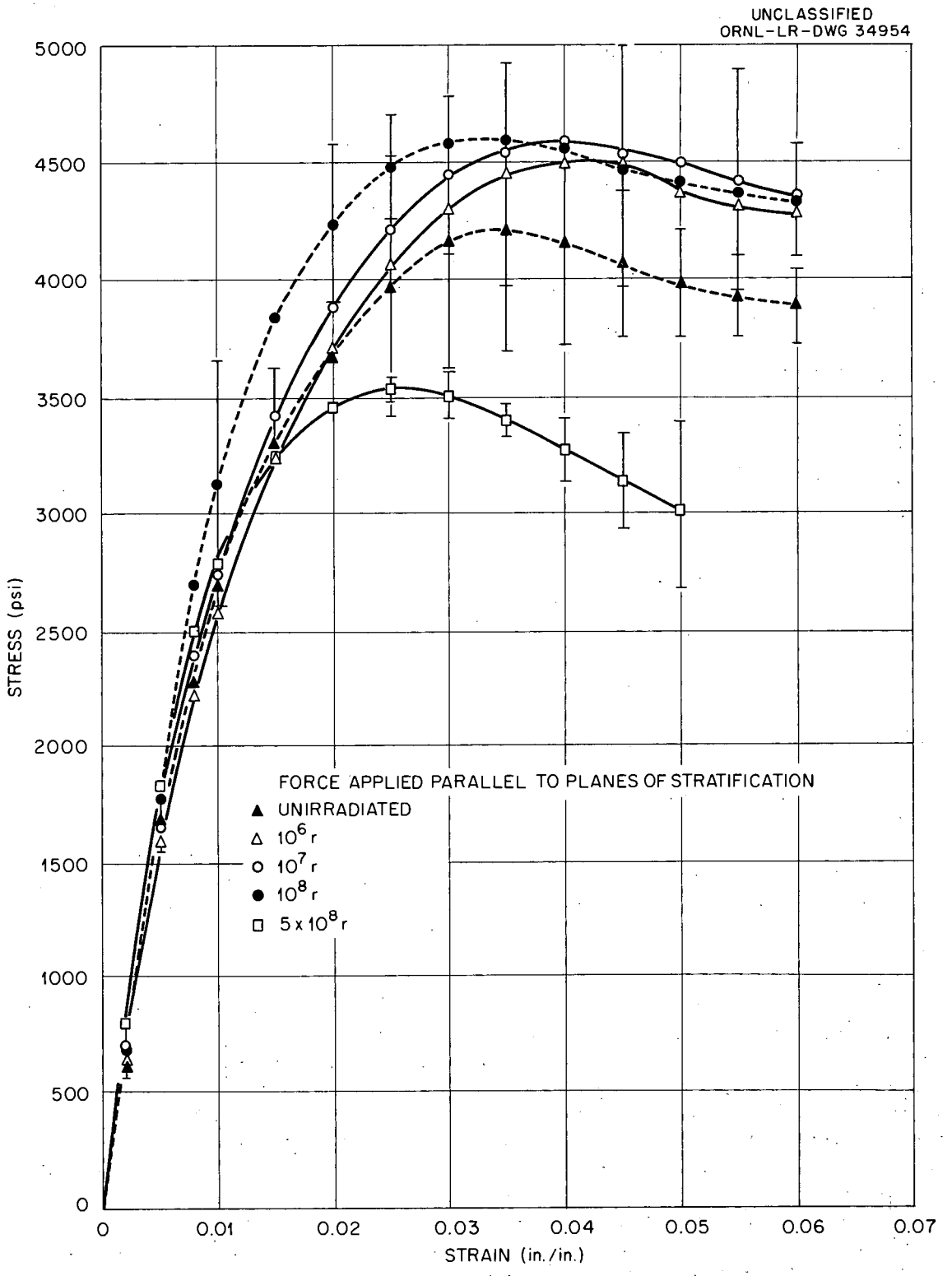

Fig. 61. Compression Test of Bedded Salt at Room Temperature.

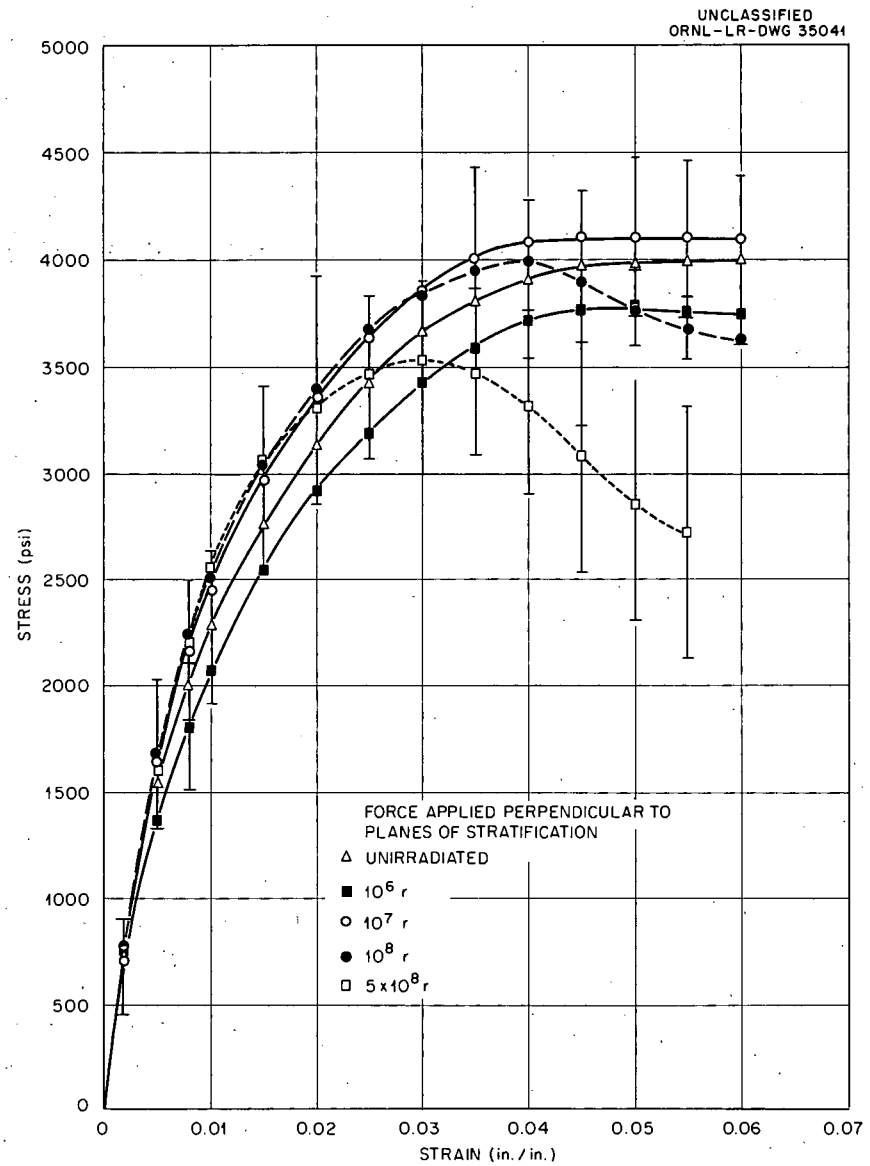

Fig. 62. Compression Test of Bedded Salt at Room Temperature.

if any, in the structural properties of salt. The more important changes are: (1) a statistically significant decrease in the compressive strength at an exposure dose of 5×10^8 r, (2) an apparent increase in the modulus of elasticity at an exposure dose of 5×10^8 r, and (3) an apparent increase in the yield strength and apparent elastic limit at all exposure doses except 10^6 r. Therefore, it appears that the effects of radiation on the structural properties of rock salt are minor.

Materials Study

Cover Materials. – In standard practice both Purex and acid aluminum nitrate waste solutions are safely contained in austenitic stainless steel vessels. However, when these solutions are saturated with NaCl, the resulting solutions and vapors are extremely corrosive. The corrosiveness, in the case of Purex waste, is similar to that of aqua regia; in fact the two mixtures contain the same

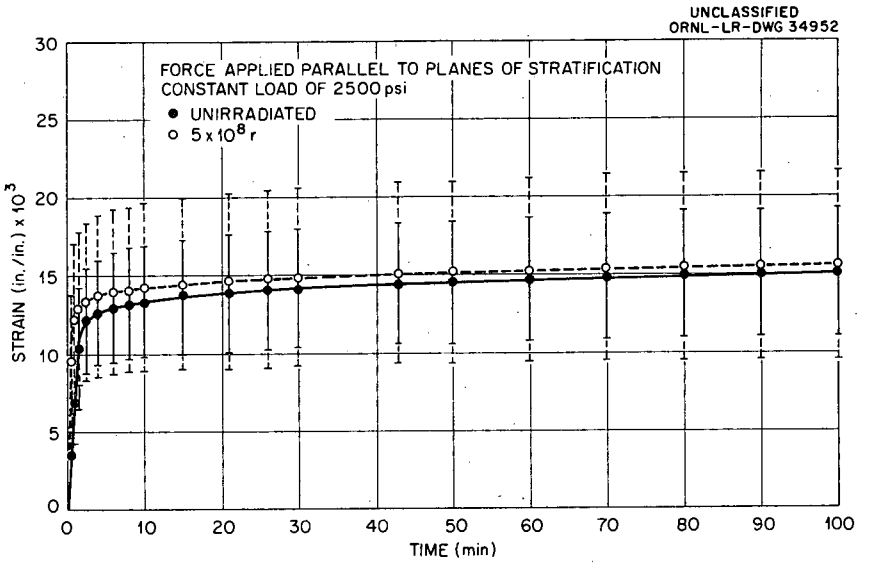

Fig. 63. Creep Test of Bedded Salt at Room Temperature.

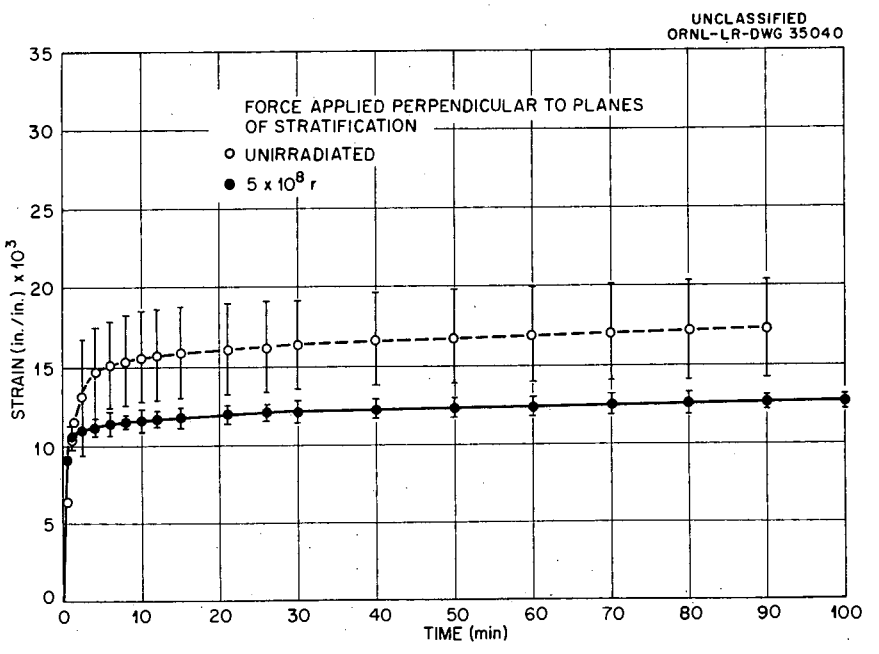

Fig. 64. Creep Test of Bedded Salt at Room Temperature.

ions, and both produce free chlorine, nitrogen dioxide, and nitrosyl chloride. The free chlorine and the acid mixture dissolve most base metals and several noble metals, such as gold and platinum. Previous work by Battelle Memorial Institute, in connection with the Darex process development, showed that titanium and Haynes 25 alloy were resistant to HNO_3-HCl mixtures in an HCl atmosphere.

Samples (1- by 3-in. coupons) of these materials, as well as several conventional stainless steel alloy samples, were obtained and exposed to salt-saturated solutions of acid aluminum nitrate and Purex wastes. A complete list of the materials,

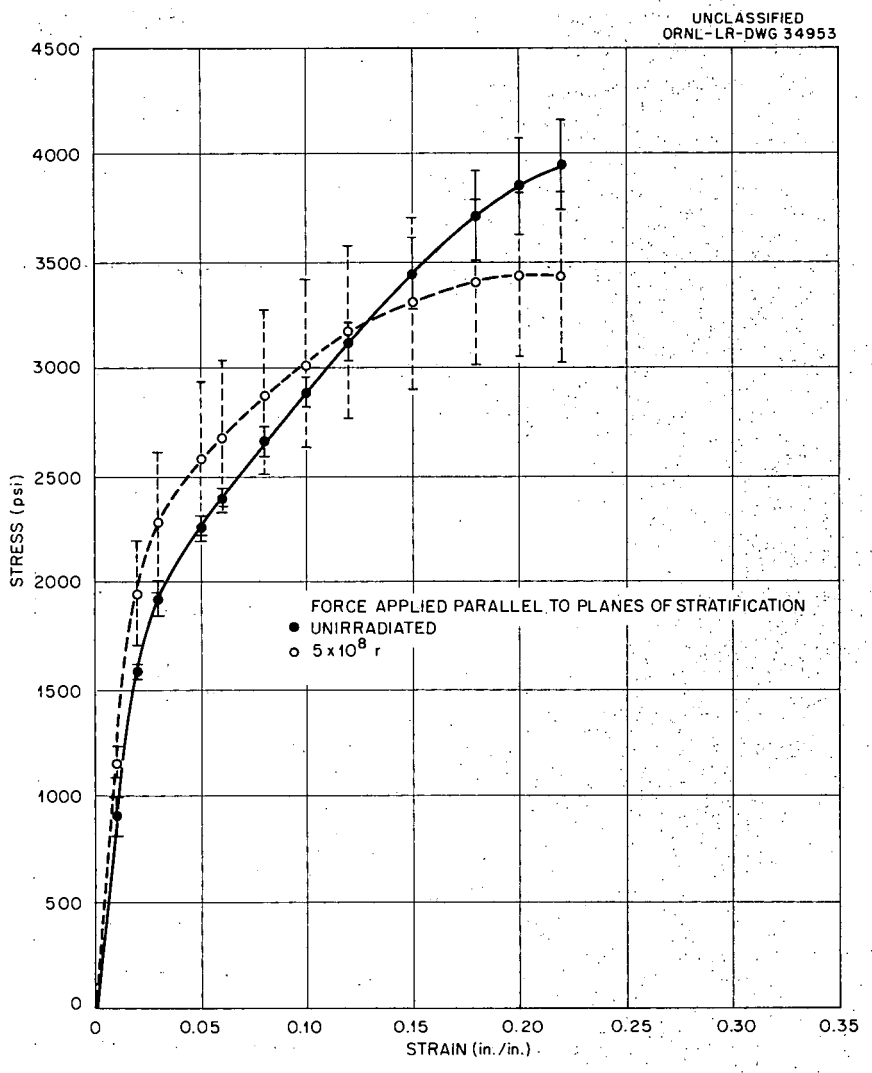

Fig. 65. Compression Test of Bedded Salt at 200°C.

exposure times, temperatures, and corrosion rates are listed in Table 27. Also listed in Table 27 are several organic materials which were corrosion-resistant to the solutions.

All the materials listed showed negligible corrosion in contact with salt-saturated neutralized solutions of Hope and Purex waste. However, all the samples exposed to salt-saturated acid Purex waste, with the exception of titanium and Haynes 25, either dissolved immediately or showed severe corrosion within 48 hr. Tantalum, not listed in Table 27, was tested and found to be corrosion-resistant to all the solutions, but the uncertainty of the fabrication properties of tantalum precluded its use in this program. Further specialized testing of welded specimens of titanium and Haynes 25 showed that both materials are subject to slightly increased corrosion rates in the welded areas.

Graphite and Teflon were not susceptible to corrosion by any of the salt-saturated waste solutions. Polyvinyl chloride also demonstrated corrosion resistance but is subject to swelling and discoloration. Teflon, though corrosion-resistant,

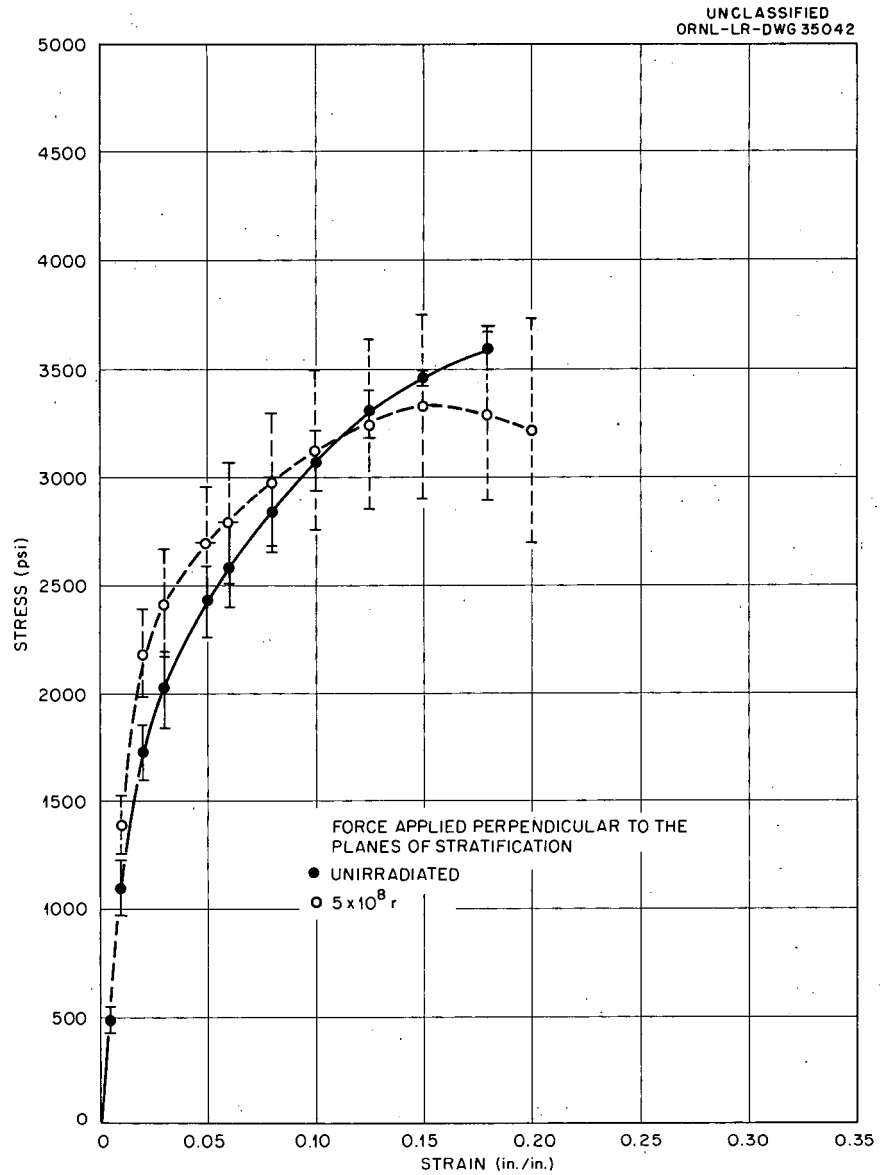

Fig. 66. Compression Tests of Bedded Salt at 200°C.

is subject to certain restrictions because of its difficult fabrication properties and limited structural strength. Based on these studies, Haynes 25 was selected as the material for the cover, and Teflon for the gaskets and seals.

Waste Solution Preparation. – The waste solutions for the field experiments, 3000 gal of neutralized Purex and 3000 gal of acid Purex, were prepared under ORNL supervision by Associated Sales and Supply Company, St. Louis, Missouri. The chemical composition of typical Purex waste as well as a suggested composition of simulated Purex waste has been reported.[49] The final composition of the neutralized waste is largely determined by the composition of the acid waste and by the NaOH used in neutralization. Simulated

[49] W. J. Lacy, *Manual for the Preparation of Simulated Fuel Reprocessing Waste Solution*, ORNL CF-58-4-45 (June 20, 1958).

Table 27. Corrosion Data in Salt-Saturated Simulated Waste

All samples partially immersed except as noted
Samples at 80°C (and higher) under refluxing conditions

Material	Corrosive Medium (salt-saturated)	Approximate Temperature (°C)	Exposure (days)	Corrosion Rate (in./year)	Remarks
410 SS	Hope	22	238		Failed
	Hope, neutralized	22	238	Negligible	
	Purex–7 *M* HNO_3	22	238		Failed
	Purex, neutralized	22	238	Negligible	
316 SS	Hope	22	238	Negligible	
	Hope, neutralized	22	238	Negligible	
	Purex–7 *M* HNO_3	22	238		Failed
	Purex, neutralized	22	238	Negligible	
347 SS	Hope	22	238	0.0025	
	Hope, neutralized	22	238	Negligible	
	Purex–7 *M* HNO_3	22	238		Failed
	Purex, neutralized	22	238	Negligible	
Inconel	Hope	22	238	0.013	
	Hope, neutralized	22	238	Negligible	
	Purex–7 *M* HNO_3	22	238		Failed
	Purex, neutralized	22	238	Negligible	
INOR	Hope	22	238	0.008	
	Hope, neutralized	22	238	Negligible	
	Purex–7 *M* HNO_3	22	238		Failed
	Purex, neutralized	22	238	Negligible	
Hastelloy C	Purex–7 *M* HNO_3	22	139	0.0004	
	Purex–7 *M* HNO_3	80	19		Failed
Haynes 25	Purex–7 *M* HNO_3	80	77	0.0007	Stamped sample
	Purex–7 *M* HNO_3	80	34	0.00147	Sample cut from sched 40 pipe
	Purex–7 *M* HNO_3	80	34	0.004	Sample from sched 40 pipe containing butt weld
	Purex, neutralized	80	77	Negligible	Stamped sample
Titanium	Purex–7 *M* HNO_3	80	63	0.0008	
	Purex, neutralized	80	63	Negligible	
	Purex–7 *M* HNO_3	22	127	Negligible	
Teflon	Purex–7 *M* HNO_3	100	70		No change; slight weight gain
Polyvinyl chloride (unplasticized)	Vapor above Purex–7 *M* HNO_3	80	24	Negligible	Approx. 1.4% weight gain without apparent swelling
Polyvinyl	Purex–7 *M* HNO_3	80	21	Negligible	Totally immersed in medium; 1% gain without apparent swelling
Graphite	Purex, neutralized	80	30		No corrosion; slight weight gain
	Purex–7 *M* HNO_3	80	30		No change; no weight loss during use of graphite as electrode in heating experiments

acid Purex has a specific gravity of 1.304 at 24°C, free mineral acidity of 8.4 moles/liter, and acid deficiency of 7.4 moles/liter.

Since it is necessary to saturate both the acid Purex and neutralized Purex solutions with NaCl prior to placing them in the experimental cavities, a minimum of 20% free volume was reserved in each container. Due to the corrosive nature of the acid Purex solution, 15-gal polyethylene carboys in steel drums were used for shipping containers. Neutralized waste was shipped in 55-gal black iron drums.

Model Experiments

To evaluate the design of components of the field equipment, small-scale models of the field tests were operated in salt blocks taken from the Carey mine and the Grand Saline salt mine in Texas.

The first model, a 7.5 × 7.5 × 9.5-in.-deep cavity, one-twelfth scale, in a 2-ft^3 block of salt from Grand Saline, was filled with 6 liters of salt-saturated, synthetic, neutralized Purex waste and was covered with a flat sheet of ½-in.-thick Teflon. Thermocouples in the liquid and the salt, a quartz-sheathed electric resistance heater, and a reflux condenser were placed in the block.

The test was run for two months, during which time a "bridge" of pure recrystallized salt 2 in. thick completely covered the cavity above the waste liquid. Below the liquid level there was no apparent chemical interaction other than the deposition of a hydrous iron oxide film approximately 1/16 in. thick. Above the liquid interface there was dissolution of the side walls, and later recrystallization above the liquid surface. The temperature in the wastes was not uniform, and the quartz-sheathed electrode was partially dissolved by the neutralized waste.

This model test showed that while Purex wastes could be contained in salt, a different cover design (to prevent condensate dissolution of the salt) and more uniform heating of the waste were required.

A second model experiment was operated to test improved methods of heating. Stainless steel, tantalum, and graphite electrodes were tested. The graphite electrodes proved to be more corrosion-resistant than stainless steel, and an insulating film did not form on the graphite electrode surface as on the tantalum electrodes. Therefore graphite was chosen as the electrode material for electrolytic heating of the solution.

The experiment was operated for three weeks under widely varying conditions at temperatures above boiling. The test proved that it is possible to electrolytically heat the neutralized waste with graphite electrodes. Concurrently, the areal power distribution with two electrodes per electrical pole was obtained (Fig. 67); with four electrodes per pole, the power distribution will be much more uniform. In model experiments with acid waste solution there was essentially no temperature variation in the horizontal plane. If the electrodes had no resistance there would be no variation in the power input in the vertical plane in the acid waste experiment.

Equation (5), which takes into account the electrode resistance, is used to calculate the vertical power distribution. The equation is exact except that the effective resistance per unit depth of solution, R_S, is not constant as a function of depth when there is a temperature variation with depth:

$$I_E(X) = I_0 \cosh \frac{R_E}{R_S} X - \frac{E_0}{R_E R_S} \sinh \frac{R_E}{R_S} X \ , \quad (5)$$

where

X = depth in solution,

$I_E(X)$ = current in the electrodes at point X,

I_0 = input current,

E_0 = input voltage (at zero solution depth),

R_E = effective resistance per unit length of the electrode insulation,

R_S = effective resistance per unit depth of solution (assumed constant with depth).

Figure 68 shows the calculated power distribution in acid waste in a 10-in.-square salt cavity and the temperature distribution obtained with this power input. The calculated power distribution for the 7½-ft-square field cavities is also shown.

The curve for the neutralized waste applies only to the sludge phase, and no current flow in the supernatant is assumed. This curve indicates that electrode resistance is negligible in the neutralized solution. For the 7½-ft-square acid experiment, the variation in power input from top to bottom is less, due to lower current density in the electrodes, than in the 10-in. experiment; thus the temperature differential will probably be less.

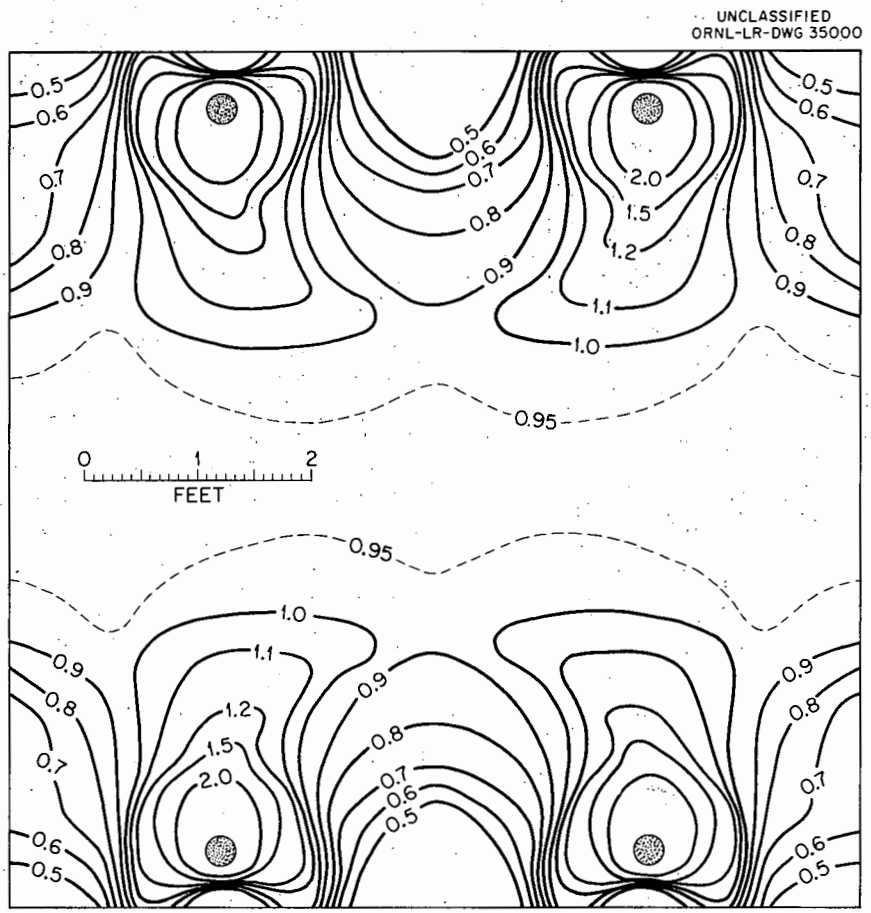

CONSTANT POWER PRODUCTION CONTOURS
ARBITRARY POWER SCALE

Fig. 67. Power Distribution with Four Electrodes.

The curves shown depict the power distribution in the entire acid solution and in the neutralized sludge. There will also be some power dissipation in the electrodes above these levels. For the cases of interest the distribution of the total power input is indicated in Table 28.

Another series of experiments using acid Purex wastes in a 24-in.-cube salt block at one-tenth scale was made to determine gas production, to find a satisfactory gas seal, and to evaluate a cover designed to be corrosion resistant.

The experiment, assembled and ready for operation, is shown in Fig. 69. The graphite electrodes, by which electrolytic heating is accomplished, may be seen on opposite sides. Teflon-sheathed thermocouples are installed in the cavity and stainless-steel-sheathed thermocouples in the salt block. The glass reflux condenser discharges the uncondensed gases to polyethylene bags. The titanium cover rests in the annular groove around the cavity. The cavity is sealed from the atmosphere by filling the groove with saturated brine solution. During operation the block and cover are insulated with approximately 2 in. of glass fiber mat.

The experiment was operated for 20 days, during which time the temperature of the solution in the cavity was between 80 and 85°C for four days. Off-gases collected during early operation at lower temperatures were largely air and nitrogen oxides (less than 1%). During operation in the range 80 to 85°C the nitrogen oxide concentration increased to 12%. Saturated brine solution in the annular groove proved to be unsatisfactory as a gas-tight seal because of its evaporation and the need for frequent replenishment. When brine was added,

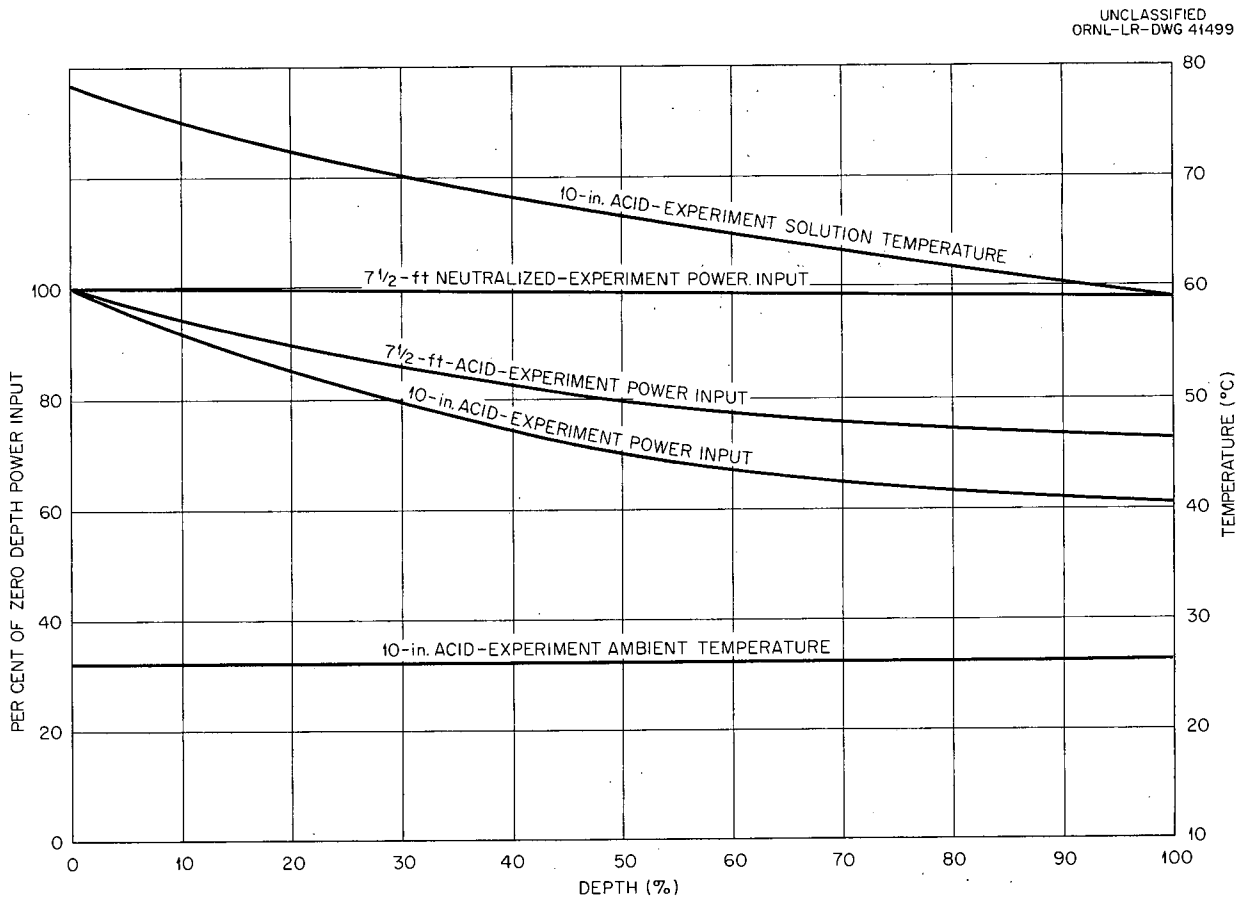

Fig. 68. Solution Power Input per Unit Depth as a Function of Depth.

Table 28. Effective Power Input – Model Experiments

Experiment	Solution Input (Electrolytic Plus Electrode) (w)	Electrodes Above Solution (w)	Total (w)
10-in. acid	245	46 (air)	291
7½-ft acid	14,870	1530 (air)	16,400
7½-ft neutral	14,100	510 (supernatant) 435 (air)	15,045

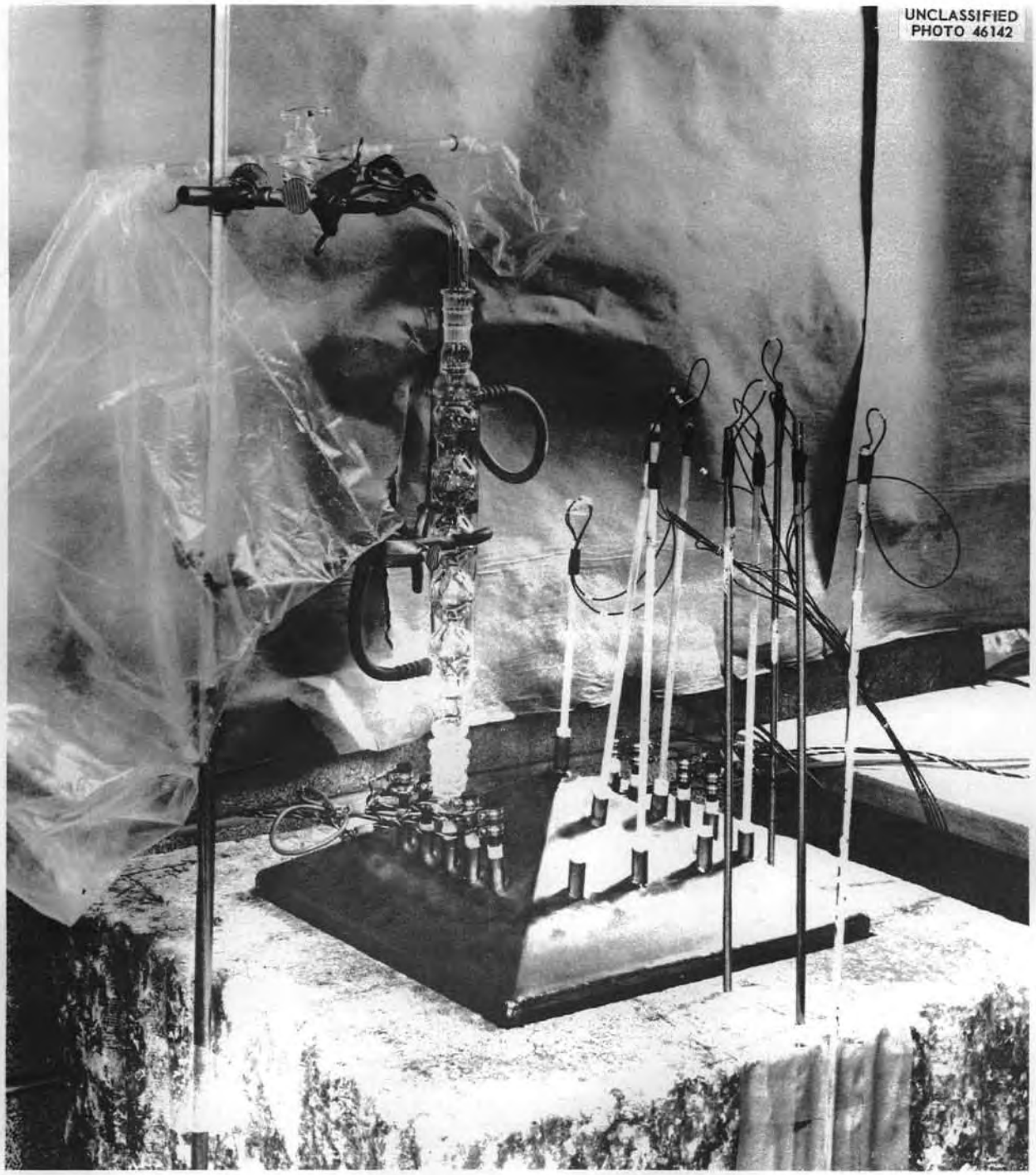

Fig. 69. Experimental Setup – Model No. 3.

the trench filled with recrystallized salt. When water was added, the trench enlarged by dissolution of the salt.

When the experiment was terminated and the cover removed, a large amount of recrystallized sodium chloride was found in the bottom of the cavity. When the crystals were removed, it was found that the dimensions of the lower part of the cavity were unchanged. However, deep undercutting had occurred at the liquid level, becoming less pronounced with increasing depth and diminishing to no undercut at approximate middepth.

The experiment was repeated for 16 days to evaluate G-E silicone fluid [SR-96 (100)] as a gas seal. The silicone did not evaporate but migrated over the surface of the salt into the cavity. When the experiment was concluded and the equipment disassembled, the cavity contained a large amount of silicone polymer.

Dissolution of the upper part of the cavity wall had continued, with recrystallization of the material in the bottom of the cavity. Figure 70 shows one-half of the block after the rerun experiment. The sharp undercut at the liquid level had progressed about 1½ in. The inner apron of the metal cover effectively protected the extreme upper edge of the cavity in the vapor space. These tests showed that acid wastes could be electrolytically heated and that a titanium cover was corrosion-resistant to the waste vapors.

A final one-tenth-scale model experiment in a 24-in. salt block showed that a dry gas seal of sand, silica gel, and charcoal was satisfactory.

Field Salt Disposal Experiments

In the laboratory it is practically impossible to reproduce the conditions that exist in a natural rock salt formation. Samples removed from the formation go through a process of stress relief which is violent enough in some cases to shatter the samples. Even if the samples are not shattered, there is some alteration of the physical properties of the rock. If the overburden pressure is reapplied, the induced stresses will not be the same unless the sample is completely elastic, which is not true of geologic materials. Therefore it is necessary to conduct field experiments before a prototype disposal facility can be designed.

Experimental Design. – Information can be obtained in a field experiment on (1) the structural integrity of the cavity, (2) the migration of nuclides from the cavity, (3) the migration of the cavity, (4) thermal gradients inside and outside the cavity, and (5) gas production. The first tests with synthetic wastes and simulated fission product decay-heating will be followed by tests with actual radioactive wastes.

Site Selection. – During the past year, the Geotechnical Corporation of Dallas (a Laboratory subcontractor) investigated operating salt mines in the northeastern quadrant of the U.S. The investigation was limited to this area because it seemed likely to be the general location of the first commercial fuel-reprocessing plant. Some of the mine owners were amenable to the use of their mines for the field tests, since the first tests would not involve the use of radioactive wastes. There were a number of advantages in using mined-out space for these tests, for example, the immediate availability of a test site, a competent work force with the necessary equipment available to excavate the cavities, and the necessary auxiliaries such as shaft, hoist, electrical power, and railroad sidings.

The Carey Salt Company mine (Hutchinson, Kansas), Fig. 71, satisfied the requirements of a good test site, that is, favorable geology and adequate facilities in the mine. Accordingly, the Laboratory entered into contractural arrangements with the Carey Salt Company for the use of an unoccupied section of their mine to carry out these experiments. Geotechnical Corporation core-drilled in the Carey mine to find the most favorable location for the test cavities. The area selected for the first test is shown in Fig. 72.

Engineering Design. – The test facility for the first experiment consists of two 7.5-ft-square by 10-ft-deep cavities in the floor of the mine, off-gas covers, off-gos collection equipment, heaters, power recorders and controls, and instrumentation (see Fig. 73). The size of the cavities was selected so that the surface area, when the cavity is filled to a 7.5-ft depth, will be equal to that of a 10-ft-dia sphere. Thus thermal data from the theoretical heat calculations can be correlated with thermal data from the experiments. The operating level of the Carey mine is about 640 ft below the earth's surface, and all equipment must be fabricated to sizes that can be brought down the mine shaft. This restriction limits the dimensions of any equipment to about 5 by 6 ft. The equipment will be reassembled and installed in the experimental area in the mine.

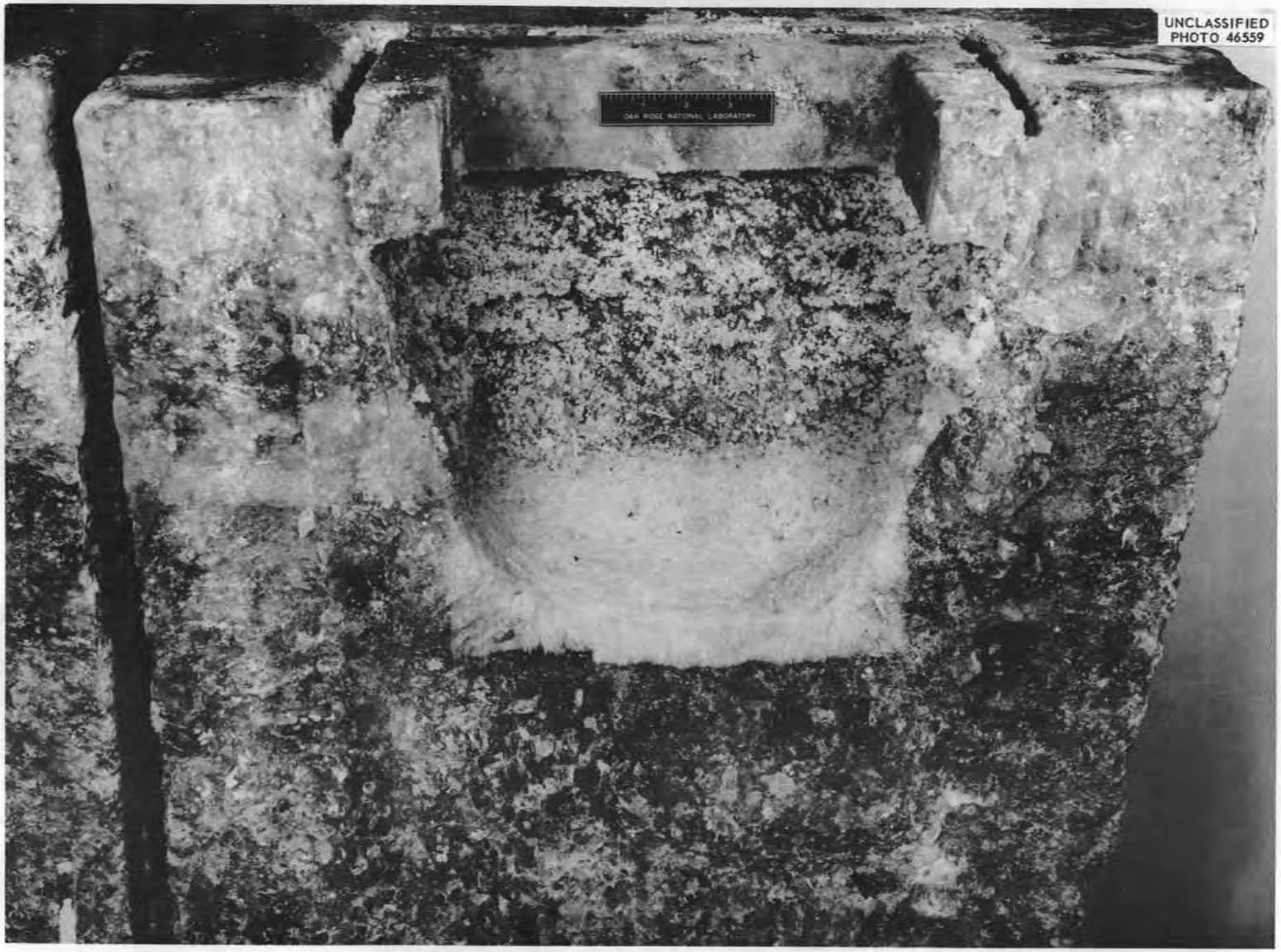

Fig. 70. Cross Section of Block – Model No. 3.

UNCLASSIFIED
ORNL-LR-DWG 41500

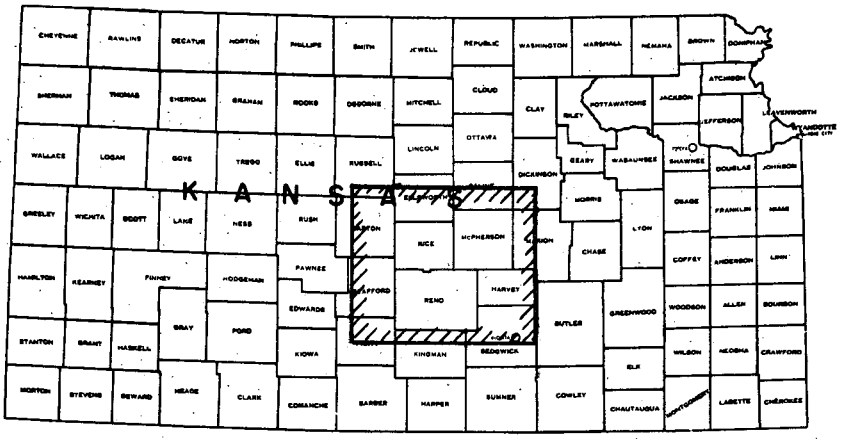

Index Map Showing Location of Area Included in Map Below.

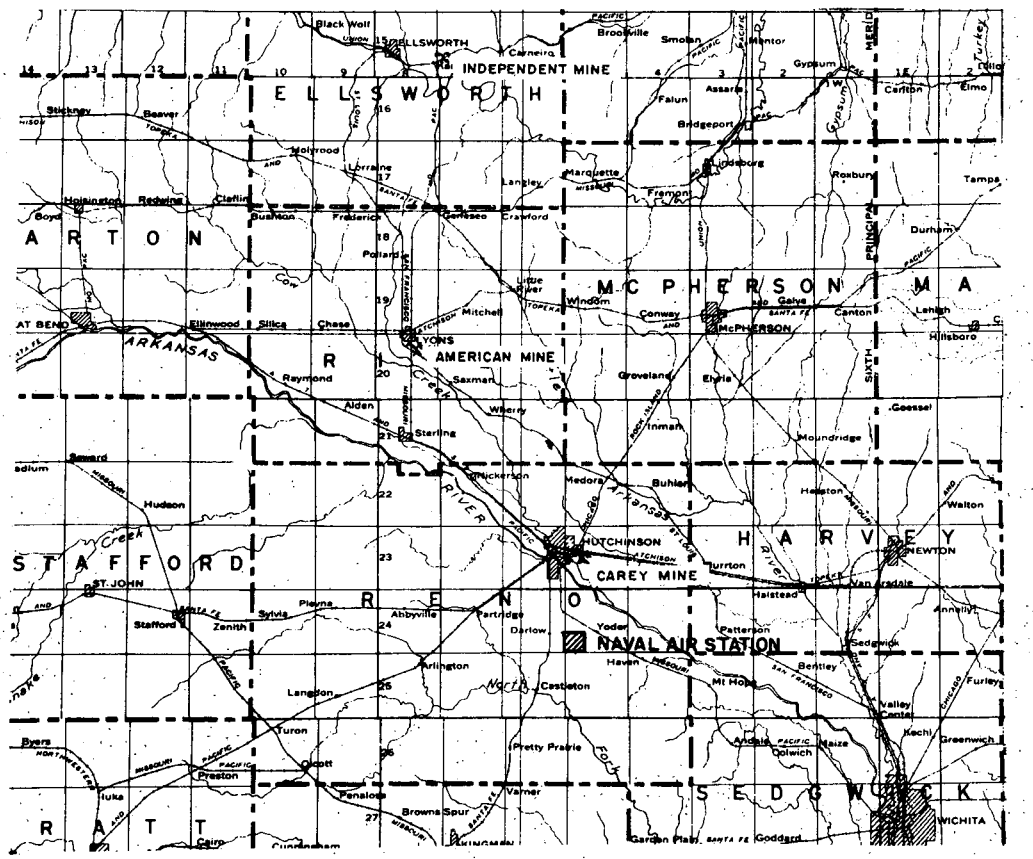

Fig. 71. Map of Central Kansas Showing Location of Carey Salt Mine.

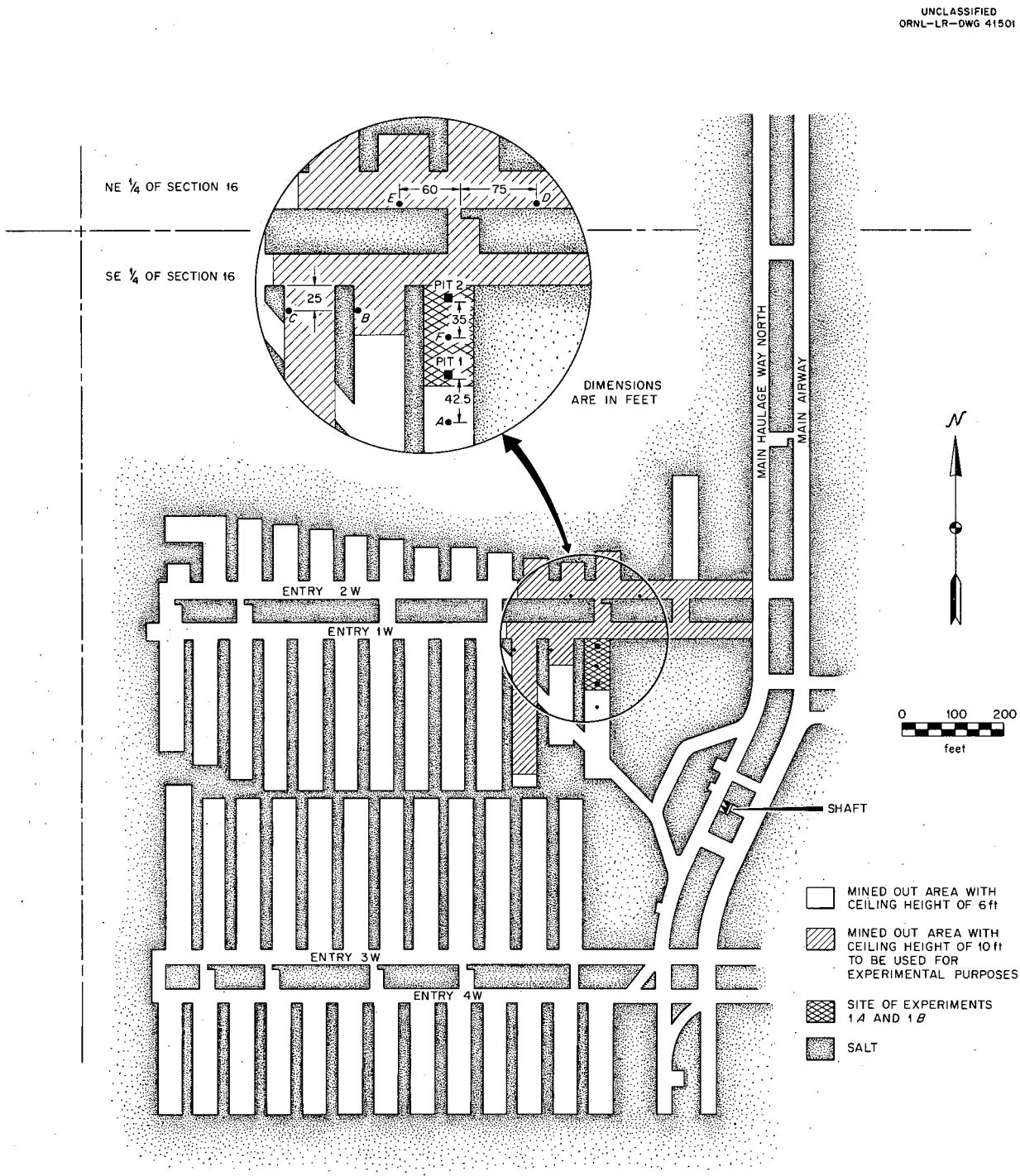

Fig. 72. Plan of Carey Salt Mine Showing Area Selected for First Test.

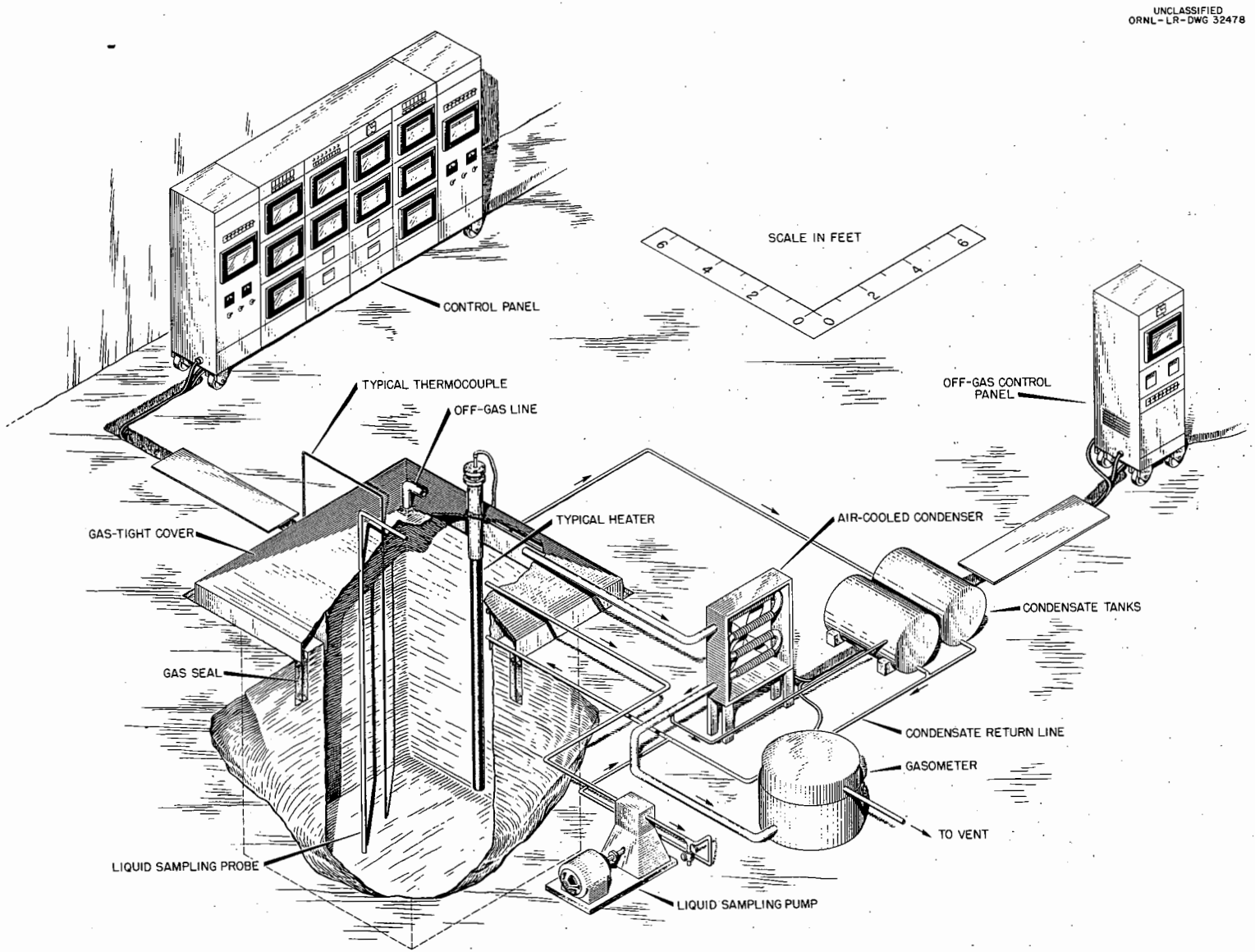

Fig. 73. Proposed Salt Field Experiment.

Off-Gas Covers. – In order to collect and analyze the off-gases released from the heated waste-salt mixture, a gas-tight cover will be placed over each cavity. These covers are pyramidal in shape and are 10½ ft on each edge and 4 ft high (see Fig. 74). They are equipped with an off-gas outlet, thermocouple holes, liquid-level probe assemblies, heater connections, a condensate collector, and aprons for side-wall protection. The covers, fabricated in half sections, are made of Haynes alloy No. 25 (cobalt, chromium, and tungsten).

Off-Gas Containment. – In order to prevent the escape to the mine atmosphere of the gases produced by chemical interaction and by heating the salt-saturated waste in salt, a dry seal composed of 4 in. each of sand, silica gel, and activated carbon will be placed in the peripheral trench in which the metal cover is supported. This seal will not be gas-tight; however, it will provide a high resistance to gas flow and will possess sufficient surface area for adsorption. During the operation, the vapors will condense on the sand, thus removing water. The noncondensible gases such as NO_2, Cl_2, and NOCl will be sorbed by the water-saturated sand and silica gel, or by the activated carbon.

Most of the water vapor–gas mixture will flow from the off-gas outlet in the metal cover through an air-cooled condenser to a liquid-nitrogen cold trap. The water vapor will be removed in the air-cooled condenser, and the remaining gases will be condensed in the liquid-nitrogen trap.

Instrumentation. – Instruments for the experiment include thermocouples; moisture probes; off-gas, liquid level, and pressure measuring devices. All thermocouples (60 for each experiment) record on one 144-point Brown Data Logger recorder (see Fig. 75). The moisture probes (12 for each experiment) are used to detect the penetration of moisture through the salt; when moisture is present the conductivity of the probe is changed and a signal is given. Alarms are provided for the detection of high temperature, high off-gas pressure, power failure, and moisture penetration. The alarm system is telemetered to the surface, where visual and audible signals are provided in the night watchman's quarters and the mine office. An intercommunications system is also provided. The control panel for liquid-level measurement and off-gas pressure is shown in Fig. 76.

Simulation of Fission Product Heating. – In neutralized Purex waste there is a precipitate which, after heating, occupies approximately 30% of the solution volume. In the actual case the major portion (90–99%) of Sr^{90} and the rare earths are in the precipitate, producing a concentrated heat source in the bottom of the container. Acid Purex waste has no precipitate, and the fission

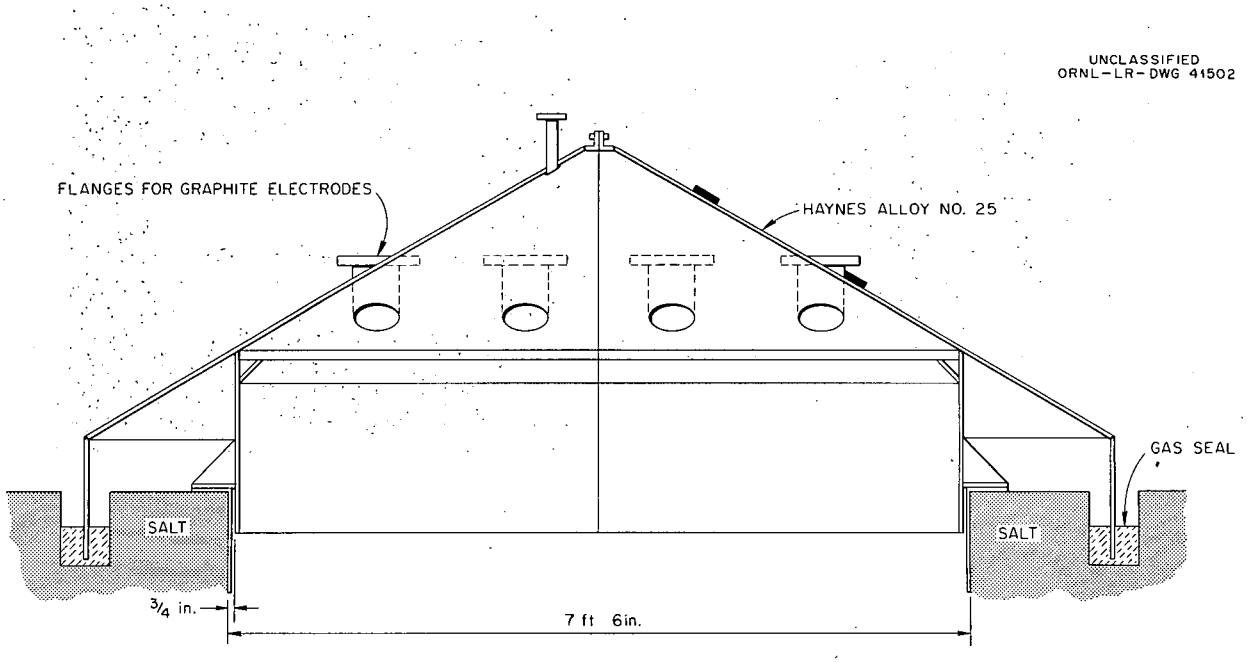

Fig. 74. Cavity Cover for Field Experiment.

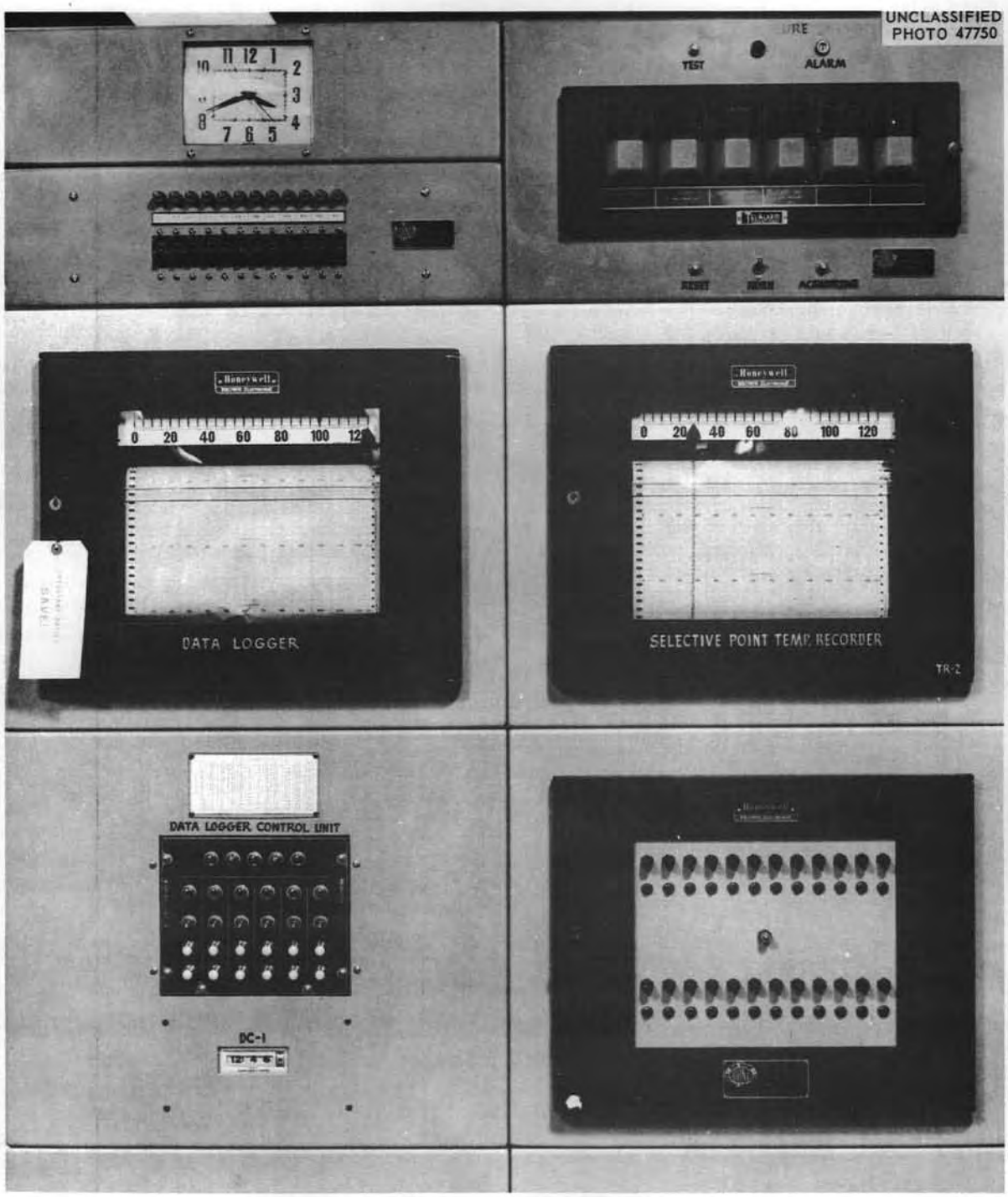

Fig. 75. Instrument Panel for Field Experiment.

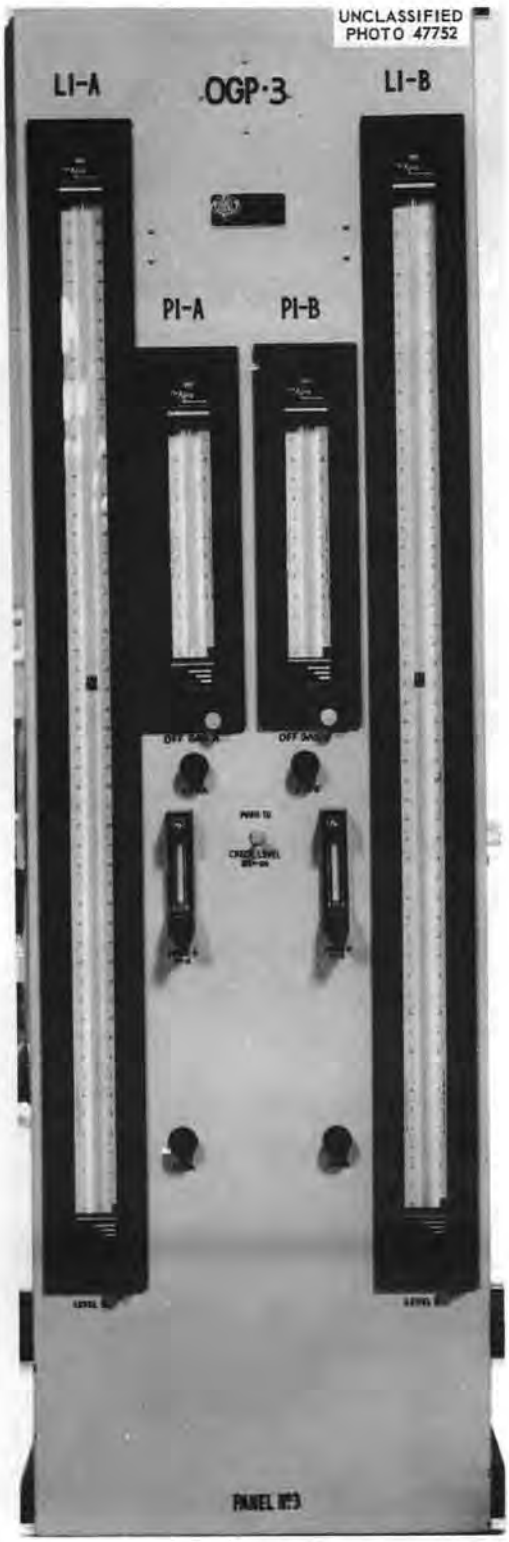

Fig. 76. Control Panel for Liquid-Level Measurement and Off-Gas Pressure in Field Experiments.

products are uniformly distributed. Thus, to simulate fission product heating in the field experiments, it is necessary to produce uniform heating in the acid waste and concentrated heating in the sludge of the neutralized waste.

Uniform heating may be achieved electrolytically by means of flat-plate electrodes on opposite walls of the salt cavity. An a-c voltage applied between the electrodes results in a heat-producing current flow through the solution. Due to corrosion problems with acid waste and poor thermal convection in neutralized sludge, resistance heating is not feasible.

While plate electrodes would be ideal, practical considerations favor the adoption of four vertical graphite electrodes per electrical pole, that is, eight per cavity in the field experiments. Electrodes for the 7½-ft-square cavities are 4 in. in diameter and 12.3 ft long.

Graphite electrodes will be used in an identical manner for neutralized and acid wastes, with the exception that electrodes in the neutralized waste will be insulated over the upper three-fourths of their length (in the solution) to provide concentrated heating of the settled sludge. Insulation will be by means of a fused Teflon tape.

Power Supply. – The measured resistivities of the salt-saturated waste solutions are shown in Table 29. The neutralized waste has a resistivity greater than acid waste by a factor of 2 to 3, and the resistivities change by a factor of 2 to 3 over the range of temperatures which will be experienced. In addition, the comparative effective resistance of the neutralized waste cavity will be about twice as great as indicated by this table, since the electrodes will be exposed only to the sludge.

To supply an input of 15 kw, with an adequate safety margin under all operating conditions, two identical power supply units which have ratings of 3000 amp ac at output voltages from 5 to 20 v and 1500 amp from 10 to 40 v were obtained.

Table 29. Waste Solution Resistivity

Salt-Saturated Solution	Resistivity (ohm-cm)	
	20°C	80°C
Acid	2.4	1.2
Neutralized precipitate	6.8	2.6
Neutralized supernatant	6.2	2.4

A preset power input to follow a particular fission product power decay scheme will be maintained, in the face of solution resistance and line voltage changes, by means of a recording, controlling wattmeter feeding a saturable reactor in the power supply.

Current will be conveyed from the supply to the electrodes by means of two ¼- by 6-in. bus bars. At each electrode, connection will be made by means of copper tubing inserted in an oversize hole in the electrode end. The hole will then be filled with Cerrolow 117, which will be liquid under operating conditions, assuring a low-resistance contact.

Site Preparation. – On March 9, 1959, field work was initiated in the Carey mine to prepare the site for the first field experiments. The area around each cavity was leveled to provide a uniform bearing surface for the off-gas covers. The room containing the two cavities was whitewashed to provide better illumination, and all loose salt and rock was removed from the ceiling. Prior to excavating the two large cavities, a core was drilled in the corners of each cavity. A plot of the cores from these holes is shown in Fig. 77 (their locations are indicated in Fig. 72). After core-drilling, the cavity excavation was started by means of drill holes spaced on 3-in. centers around the perimeter of the cavities. These holes were drilled to an 18-in. depth and the material then removed down to 12 in. with jack hammers. Figure 78 shows the first 12 in. of salt and anhydrite being removed from the No. 1 pit. After removing this upper layer, the holes were then drilled and the salt removed in 12-in. increments. This procedure was followed until the 10-ft depth

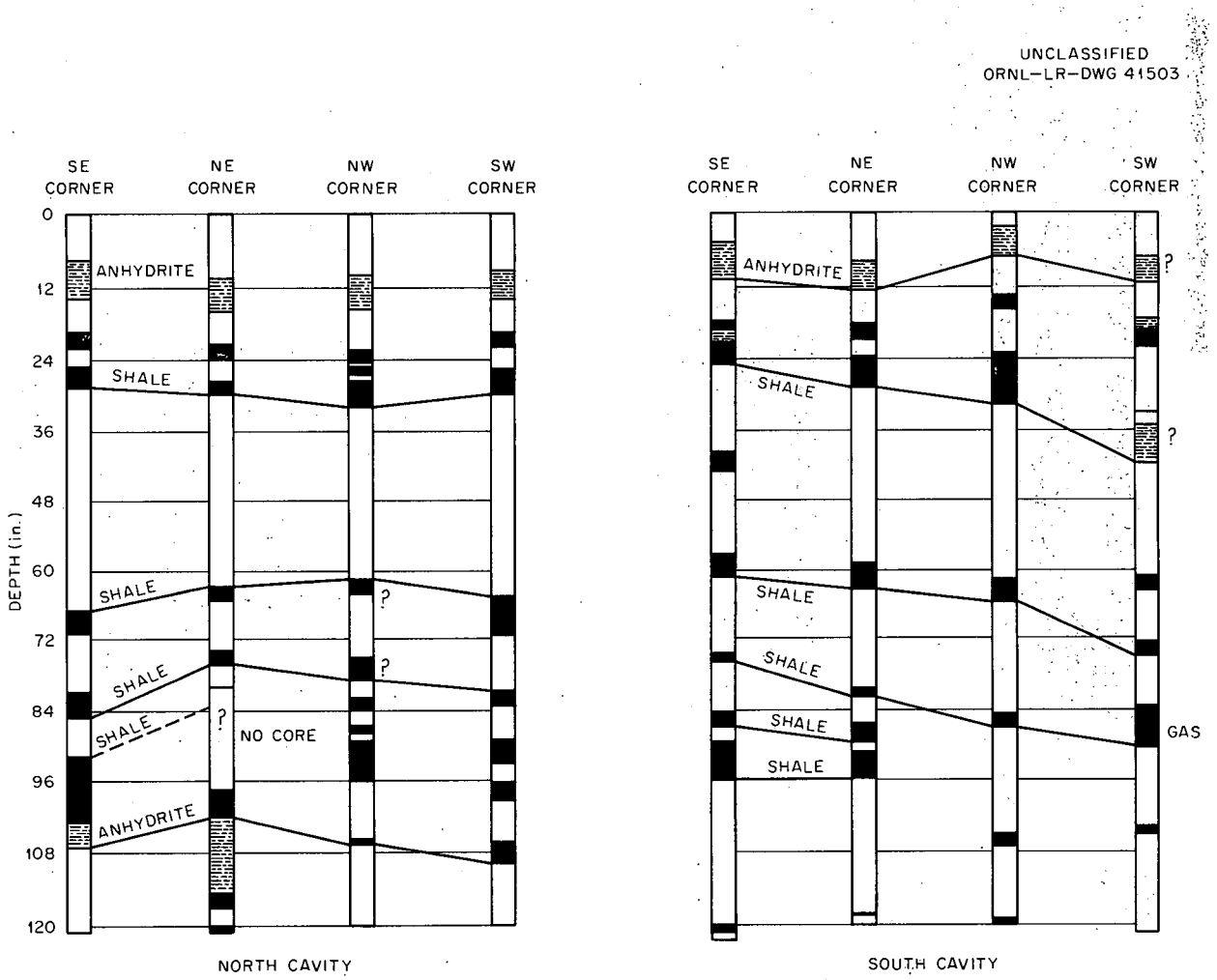

Fig. 77. Core Logs from Corners of Field Cavities Showing Anhydrite and Shale Bands Interstratified with Salt.

Fig. 78. Removal of First 12 in. of Salt and Anhydrite from the Field Cavity.

was reached. At this point the walls were smoothed by means of special tools until the deviation from the required dimensions was less than ½ in. Table 30 compares the distribution of salt, anhydrite, and shale in the cavity walls as determined by chemical analysis and x-ray diffraction. The average salt concentration is 72% for pit No. 1 and 78% for pit No. 2. However, in vertical distribution, shale, salt, and anhydrite bands differ in continuity and thickness (Figs. 79 and 80). Selected samples of the material were examined by x-ray diffraction for quartz, vermiculite, illite, and kaolinite.

After the cavity had been excavated the gas-seal trenches were cut. The side walls of the seal trenches were not smoothed, since irregularities were not critical.

Subfloor Exploration in the Mine. – The cores taken at the four corners of each cavity indicated that a greater amount of shale and anhydrite was present than in the original cores. Gas pockets were also encountered during these drillings. As a result, additional cores were drilled to define the extent of the gas pockets and the slope and thickness of the shale beds in the vicinity of the experimental cavities. The logs of these core holes indicate that the anhydrite and upper shale bands are continuous, but, at depths below 3 ft, the width of the shale bands varies.

Because of the voids and cracks in the lower salt and shale layers, as shown by the appearance of gas and by the loss of drilling fluid during coring, the cavities were filled with brine in an attempt to seal the cracks and permeable shale layers. A decrease in the water level in pit No. 2 and a corresponding increase in pit No. 1 indicated that there was a hydraulic connection between the pits. Core holes between the two pits showed that the connection was not a straight line and, further, that it was about 8.5 ft below the floor of the mine. Further core drilling and explorations will be conducted in an attempt to define the depth, size, and location of this connection. The presence of the interconnection does not rule out the use of this location for experimental purposes. It does, however, require that liquid levels in each pit be kept equal to prevent flow of waste from one cavity to the other.

Small-Scale Cavity Experiment. – Since the subfloor of the Carey mine is not pure salt, the pattern of heat dissipation will be different from that predicted by theoretical calculations. Therefore two one-fifth-scale models of the field experiment will be run in the 6-ft layer of pure salt (in a pillar of

Table 30. Distribution of Anhydrite, Shale, and Salt with Depth in the Walls of the Field Cavities

Determined by chemical analysis and x-ray diffraction*

Sample Depth (in.)	Distribution (%)					
	Halite	Anhydrite	Quartz	Kaolinite	Illite	Vermiculite
			Pit No. 1 (South)			
7–10	25–50	25–50			Est <10	
10–12	0–25	25–50				0–25
21–23	25–50	Est <10	Est <10		0–25	0–25
37–39	50–75	Est <10	Est <10	Est <10	0–25	
51–53	75–100	Est <10				
62–63	0–25		Est <10	0–25	25–50	Est <10
73–74	25–50	0–25	Est <10	Est <10	0–25	
84–87	0–25	25–50	Est <10	Est <10	0–25	
91–91.5	75–100			Est <10		
104–106	75–100	Est <10		Est <10		
115.5–116	50–75	Est <10	Est <10		0–25	
			Pit No. 2 (North)			
9–13	25–50	25–50		Est <10	0–25	0–25
21–23	25–50		Est <10	0–25	0–25	
29–30	Est <10	Est <10	Est <10	0–25	0–25	0–25
67–69	0–25		Est <10	0–25	0–25	
83–84	25–50		Est <10	0–25	0–25	
95–100	0–25		Est <10	0–25	25–50	0–25
104–106	0–25	50–75				
118–120	75–100	Est <10				

*X-ray analysis by T. Tamura.

the cavity chamber) above the existing mine floor. The data from these experiments will be correlated with the thermal calculations and scale factors computed. To determine the effect of shale and anhydrite bands on temperature distribution, another small cavity will be tested in the mine floor.

Operating Procedures. – After the equipment is installed and tested, 7000 gal of synthetic waste (saturated with salt) will be transferred to the two test cavities. When the temperature of the waste solution has reached ambient mine temperature, the heaters will be turned on and the power varied to correspond to a predetermined fission product decay function representative of a given waste type.

Temperatures in the cavity (above and below the liquid level) and in the salt surrounding the cavity will be measured and recorded continuously. Also, heater power and electrical conductivity of the surrounding salt will be recorded continuously. Periodic samples of cavity solution, condensate, and off-gases will be withdrawn and analyzed. Routine preventive maintenance of the recorders and power controls will be performed at regular intervals.

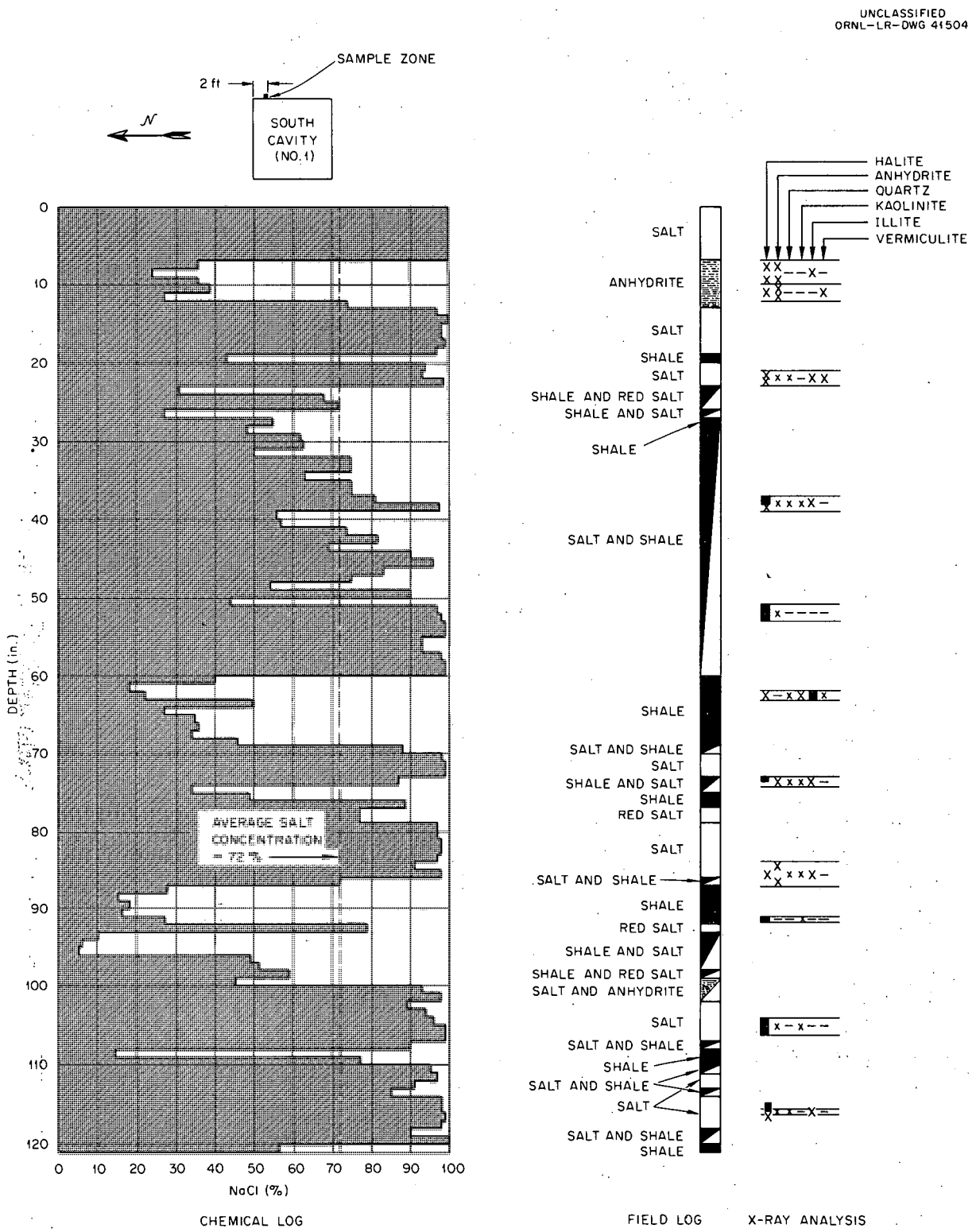

Fig. 79. Mineral Analysis of East Wall of South Cavity (No. 1), Carey Salt Mine.

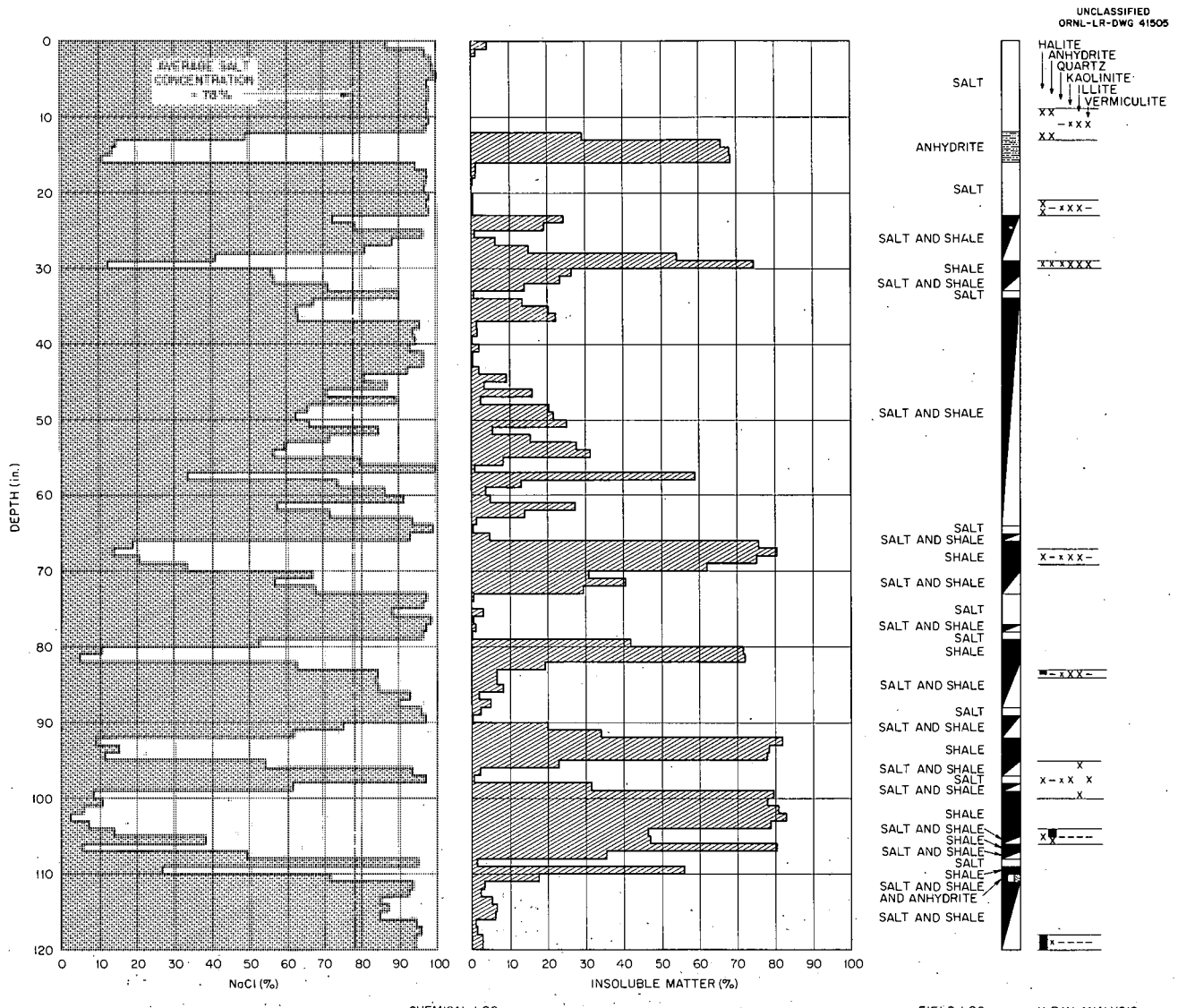

Fig. 80. Mineral Analysis of West Wall of North Cavity (No. 2), Carey Salt Mine.

The peak temperature in the solution (~80°C) is expected to occur in approximately five months. Once the solution temperature levels off, the heaters will be turned off, and the solution will be cooled to ambient temperature. The covers will be removed and the cavities emptied. The empty cavities will be filled with rock salt, and the equipment will be used in future tests as indicated.

Cooperation with Other Agencies

Discussions were held with F. Birch of Harvard University on the stability of rocks as a function of temperature. As an outgrowth of these discussions he analyzed the thermal problems of the deep well and salt disposal methods; the results were published.[50]

Irradiated samples of rock salt were tested on Birch's thermal conductivity apparatus. The salt samples were somewhat irregular, so absolute values of the thermal conductivity were not obtained; but relative values showed that irradiation has only a small effect upon thermal conductivity of rock salt.

Cores from the Carey mine were furnished to R. Kulstead of the University of Kansas to aid in the preparation of a stratigraphic map of the area. In addition, a detailed mineralogic analysis of the cores will be made. A graduate student of Kulstead's is measuring the creep of the pillars under widely varying conditions at the Carey mine and at the American Salt Company mine at Lyons, Kansas.

A group under the direction of E. Gloyna of the University of Texas will measure the creep in the pillars in the room where the cavities have been excavated and compare these with the creep measured in an undisturbed area.

Through the cooperation of Stringfield, Waesche, Richardson, and Young, of the U.S. Geological Survey, a literature search has been made for information on the physical properties of salt and on the location and extent of salt deposits in the United States; an annotated bibliography of salt deposits throughout the world was prepared. In addition, the Geochemistry and Petrology Branch of the Geological Survey is making a detailed mineralogic examination of the salt core from the Hutchinson Naval Air Station. The Ground Water Branch further cooperated by making a survey of four areas in the arid west for possible use as experimental sites for the field program (see later section, "Related Cooperative Projects").

A group under the direction of L. Obert of the Applied Physics Laboratory, U.S. Bureau of Mines, will make strain measurements around the cavities. These tests will be correlated with tests of the University of Texas. The stress in the pillars will be determined before and after the waste disposal tests are run.

DISPOSAL IN DEEP WELLS

W. de Laguna — O. M. Sealand
F. M. Empson — W. J. Lacy[51]

Cooperation with Other Agencies

The American Petroleum Institute (API) Committee issued its report[52] in the fall of 1958, and this report will be published in the report of the hearings on waste disposal of the Joint Congressional Committee on Atomic Energy. The API group felt that even though there would be many difficulties, disposal of waste into deep wells shows sufficient promise to justify further investigation, and they suggest research which should be undertaken. Although conservative, the report suggests the possibility of the direct injection of fairly fresh acid waste directly into the ground, relying on massive dilution to prevent plugging or undue temperature rise. The general design of the wells and equipment for such an operation is shown by diagram. Specifically mentioned as problems requiring further study are adsorption of radioactive materials by the solid matrix of the disposal reservoir, definition of suitable reservoirs for permanent confinement of the waste, dissipation of heat, corrosion of the well casing, and plugging of the disposal well. The last two, the group felt, were largely economic problems, not fundamental to the success or safety of the operation but of importance in determining design, operating procedures, and cost.

The Committee suggested that the detailed local knowledge required to evaluate the geology of potential disposal sites might be obtained, in part at

[50] "Thermal Considerations in Deep Disposal of Radioactive Wastes," *Natl. Acad. Sci. – Natl. Research Council* Publ. No. 588.

[51] Resigned March 1959; presently at Research and Development Division, Office of Civil Defense Mobilization, Battle Creek, Mich.

[52] American Petroleum Institute, *Problems in the Disposal of Radioactive Wastes in Deep Wells*, Dallas, Texas, October 1958.

least, from the American Association of Petroleum Geologists (AAPG). Discussions with the AAPG and the U.S. Geological Survey suggested that the Survey's plan to make broad regional studies of the geological problems of waste disposal could be supplemented by a number of detailed reports on small specific areas. These reports would be prepared by geologists who were personally familiar with the areas.

Laboratory Studies

The API Committee report suggested several areas of study which should be undertaken. Included among them were the problems of well plugging, interaction of radioactive nuclides with the solid matrix, and dissipation of heat. The progress being made on these problems in the laboratory is discussed below.

Complexing of Wastes. – Neutralization of the acid wastes, either in a tank or in the ground, produces precipitates of aluminum, iron, or zirconium depending on the type of waste. Attempts to pump waste containing these precipitates into a well would quickly result in plugging. In general three or possibly four alternatives are suggested. One possibility is to neutralize the waste on the surface and filter out the precipitate, which would then be disposed of separately. As suggested by the API Committee, the acid waste could be pumped into the well and diluted at the well bottom with such large volumes of water that the precipitates would be widely scattered through the disposal formation without serious loss in permeability. A third alternative is to restrict the use of deep-well disposal to low- or intermediate-level wastes which are low in dissolved solids but which may be produced in large volumes. A fourth method is to complex the metal ions in the waste so that they will remain in solution even when the waste is neutralized. Citric acid, for example, is being used successfully in complexing iron in low concentrations in the water injected into oil sands for secondary recovery of oil. Other reagents suggested for complexing include the Versenes, tartaric acid, and oxalic acid.

The results of laboratory tests on complexing Purex, Darex, and SIR wastes are presented in Table 31. Calculations were made on the quantity of complexing agent necessary for preventing precipitation at a pH of 7 to 8.5 and on the cost

Table 31. Complexing of Fuel Reprocessing Wastes

Neutralization accomplished by addition of concentrated NaOH up to pH 7–8.5

Waste Type	Complexing Agent	Quantity per Gallon of Waste (lb)	Cost (¢/gal)*
Purex, 1 M	Citric acid	0.39	12
	Tartaric acid	0.10	5
	Oxalic acid	0.42	8
	Versene	1.71	34
Darex (10% waste, 90% H_2O)	Citric acid	1.28**	38**
Darex (undiluted)	Tartaric acid	1.00	50
SIR	Citric acid	1.19	5.7
	Tartaric acid	0.25	12.5

*Assumed price of complexing agent (per lb)

Citric acid	30¢
Tartaric acid	50¢
Oxalic acid	20¢
Versene	20¢

**Per gallon of undiluted waste.

of each reagent.[53] Purex waste was complexed at lower costs with tartaric acid (5¢ per gallon) and oxalic acid (8¢ per gallon); the moxt expensive complexer for Purex waste is Versene (34¢ per gallon).

Darex waste was effectively complexed with citric acid and with tartaric acid. This was the most difficult waste to handle as it has the highest iron content. It was necessary to dilute the waste (10% Darex–90% water) to effect complexing with citric acid. The reagent cost is 38¢ per gallon of undiluted waste. Tartaric acid complexed undiluted Darex waste at a cost of 50¢ per gallon. Oxalic acid and Versene were not effective.

Reagent cost for complexing SIR waste was approximately 6¢ per gallon for citric acid and 12½¢ for tartaric acid. The SIR waste has not been effectively complexed with oxalic acid or Versene.

It should not be assumed that actual waste disposal operations would be faced with costs per gallon for complexing comparable with those shown in the table. The laboratory work is primarily of interest in showing that complexing can prevent precipitation from such concentrated solutions when they are neutralized. In actual disposal operations it is probable that the bulk of the inert solids would be removed by filtration or centrifuging, and that complexing would be used as a final operation to remove the last of the suspended solids. This would make the first separation step less critical, and therefore easier and cheaper, and the amounts of reagent required for complexing would be greatly reduced. Some waste solutions, low in dissolved solids, might be complexed directly. The choice of method would be determined by economic considerations.

In order to evaluate the stability of these complexes when subjected to radiation, samples of complexed waste were exposed in the cobalt storage facility to doses of 7.7×10^7 and 1.5×10^8 rads. The observations following the irradiations are shown in Table 32. Purex solutions were complexed with citric acid and with tartaric acid. The lower dose resulted in a darkening of the yellow solution. The higher dose produced further darkening and a trace of precipitate. Additional precipitate formed after four weeks in the samples exposed to 1.5×10^8 rads.

Darex waste, the concentrated as well as the diluted solution, was complexed with tartaric acid. No change could be observed in the opaque solutions after the lower dose. After an absorbed

[53] Calculations based on prices of reagents reported by *Chemical and Engineering News* in 1958. No attempt was made to establish lower prices for larger purchases which might be secured through negotiation.

Table 32. Effects of Irradiation of Complexed Waste Solutions

Cobalt in storage: 158,000 curies
Dose rate: 7.7×10^7 rads/day

Solution	Complexing Agent	Effects	
		After 24 hr, 7.7×10^7 Rads	After 48 hr, 1.5×10^8 Rads
Purex, 1 *M*	Citric acid	Darkened	Precipitate
	Tartaric acid	Darkened	Precipitate
Darex, concentrated	Tartaric acid	No change	Turbidity
Darex (10% waste, 90% H_2O)	Tartaric acid	No change	Precipitate
SIR	Citric acid	No change	No change
	Tartaric acid	No change	Slight turbidity

dose of 1.5×10^8 rads, no solids were observed, but a precipitate developed in the diluted Darex after a four-week period.

No effect was observed on SIR waste complexed with citric acid and with tartaric acid when exposed to radiation at this level. However, the tartaric acid–complexed solution exposed to the higher dose developed slight turbidity after four weeks.

As a preliminary evaluation of the compatibility of complexed waste with an aquifer, sequestering agents were added to 2-liter quantities of waste. The wastes were neutralized with caustic, and the complexed wastes were diluted to 18 liters with tap water. These solutions were then passed through a 1½-in.-dia by 10-ft-long glass column packed with quartz sand containing 2% limestone. The rate of flow was 30 ml/min, or about 2.6 cm/min superficial velocity. Exploratory tests indicated that at a pH of less than 8, some gas formation occurred in the sand. When the neutralization was carried to a pH of about 8.5, there was no observable interaction or change in the permeability of the synthetic aquifer. This procedure was carried out with Purex waste complexed with citric acid and tartaric acid, with diluted (10%) Darex waste complexed with tartaric acid, and with SIR waste complexed with citric acid and with tartaric acid.

Sequestering agents show promise as a treatment for waste prior to injection into geologic formations. Other complexing agents remain to be tested.

Slurry Tests for Strontium Removal. – The jar-test results reported here show the amount of strontium removed from a typical neutral Purex solution by various clay minerals. Results shown in Fig. 81 indicate the sorption of strontium from 150 ml of 6 *M* $NaNO_3$ solution containing 40 mg/liter of strontium carrier.

The materials studied included: (1) Conasauga shale, (2) Fithian illite, (3) New Mexico kaolinite, (4) montmorillonite (Wymoing bentonite), (5) North Carolina vermiculite, and (6) Utah halloysite. The effectiveness of these materials for strontium sorption ranged from Conasauga shale, the best, to halloysite, the poorest, in the order listed above.

Comparison of the amount of strontium removed by these materials to the amount of cesium removed under similar test conditions indicates that about one-third as much strontium as cesium is removed by the same weight of clay material. However, the specific activity of Sr^{90} is 1.5 times greater than the specific activity of Cs^{137}, and the net result is that for each curie of strontium sorbed 2 curies of cesium is sorbed.

Coagulation studies of the removal of radiostrontium from water revealed that pH played a major role. Therefore, three series of slurry jar tests were made to determine the effect of pH on the removal of strontium from a 1 *M* sodium-neutralized Purex-type waste by Conasauga shale. The range of pH values studied was from 5.2 to 11.5, using from 1 to 20 g of shale, 150 ml of solution. The results in Fig. 82 show that the higher the pH, the greater the amount of strontium sorbed on the same weight of shale. At pH values above 11.5 little effect due to pH was observed.

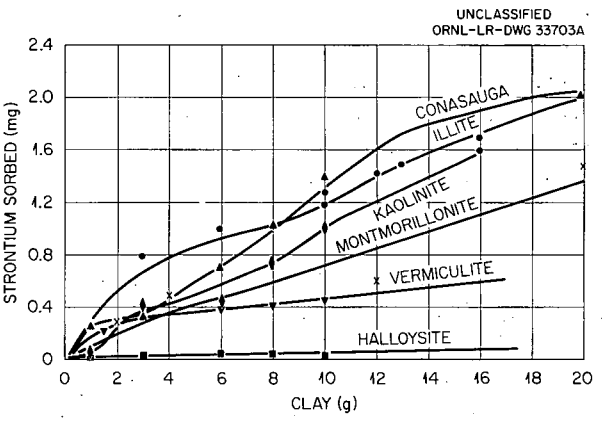

Fig. 81. Sorption of Strontium from 6 *M* $NaNO_3$ Containing 40 mg of Strontium per Liter.

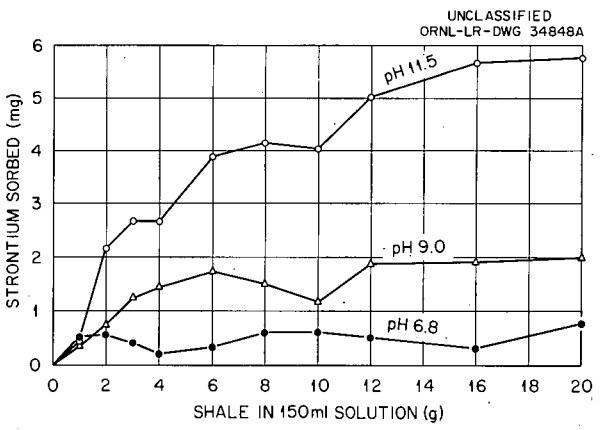

Fig. 82. Effect of pH on the Removal of Strontium (6 mg) from 1 *M* Sodium Solution by Conasauga Shale.

The results indicated that (1) increasing the weight of shale gave increasing amounts of strontium sorbed but with diminishing returns, and (2) high pH values resulted in proportionately greater amounts of strontium being sorbed.

Other investigations included a study of the removal of strontium by various clay minerals from a 1 *M* sodium solution and the effect of mixtures of calcium carbonate and clay on the amount of strontium sorbed. In the first test 8–20 g of illite sorbed 1.5–2.2 mg of strontium, while the same amount of Wyoming bentonite sorbed 1.0–1.2 mg of strontium. When 10% of calcium carbonate was added to the clay, 0.4–0.9 mg of strontium was sorbed by illite, and 0.6–1.0 mg of strontium was sorbed by the Wyoming bentonite. The same jar-test procedure using halloysite showed no change in the amount of strontium sorbed when calcium carbonate was present. However, it should be mentioned that the amount of strontium sorbed by 20 g of halloysite from a 1 *M* Na^+ solution containing 40 mg of Sr per liter was 0.9 mg. This is much lower than the amount of cesium sorbed and lower than the amount of strontium sorbed by most clays.

The results shown in Fig. 83 indicate that calcium carbonate decreases the amount of strontium sorbed by illite and bentonite clays but has no detectable effect on the normally low capacity of halloysite. Therefore, the presence of limestone within the sandstone-clay mixture of the disposal formation will help to decrease the sorption and chromatographic separation of strontium from the 1 *M* sodium-neutralized Purex-type waste solution.

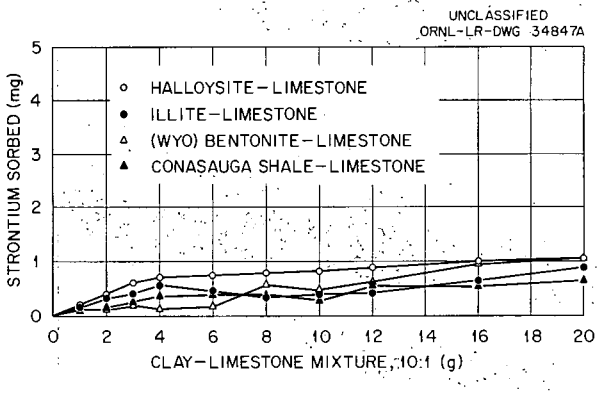

Fig. 83. Plot of the Amount of Strontium Sorbed from 150 ml of 1 *M* Sodium-Neutralized Waste Containing 40 mg of Strontium per Liter.

Effect of Citrate Ion on Sorption of Strontium and Cesium by Clays. – Figure 84 shows the sorption of cesium and strontium on four types of clay materials from a neutralized, complexed, and diluted waste solution. The four types of clay materials used were (1) Wyoming bentonite, (2) illite, (3) illite and limestone, and (4) Conasauga shale. The solution was 1 *M* Purex waste that had been complexed with citric acid, sodium-neutralized (pH 7.5), and diluted 1:9 with 1 *M* sodium chloride solution.

The cesium sorption was equal to or slightly less than the amount of cesium that would be sorbed from this solution if citric acid were not added. However, the amount of strontium sorbed was less by about a factor of 3 when the waste was complexed with citric acid. These data indicate that under the test conditions citric acid does not noticeably affect the sorption of cesium but does depress the sorption of strontium. This conclusion agrees with the general theory of chelation; that is, the higher the valence the greater the degree of chelation. Therefore, it can be assumed that some of the strontium in the waste solution was chelated by the citric acid and was therefore not available as a cation for sorption or exchange with the replaceable ions of the clay material. The monovalent cesium and the relatively high concentration of sodium ions, also present in the waste solution, were not complexed by the citric acid and were not sorbed.

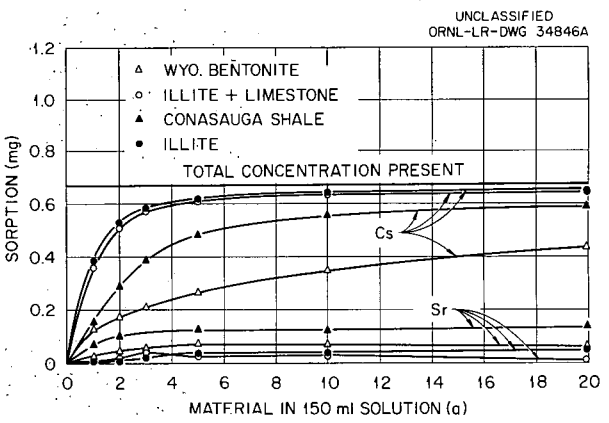

Fig. 84. Sorption of Cesium and Strontium on Various Materials from a Citric Acid–Complexed 1 *M* Sodium-Neutralized Purex Waste Solution That Had Been Diluted 9:1 with 1 *M* Sodium Chloride.

Core Studies. – Several cores of Berea sandstone were obtained from the Crystal Lake Laboratories of the Pure Oil Company[54] for preliminary testing and technique development. The method of mounting cores consisted of coating the outside with an epoxy resin and, after allowing the resin to harden, securing the two Plexiglas or stainless steel end plates with four brass tie rods (see Fig. 85).

Waste solution was pumped through the core by using a Lapp Pulsafeeder[55] driven by a $\frac{1}{20}$-hp electric motor. The solution was 1 *M* sodium-neutralized, citric acid–complexed Purex waste which had been diluted 1:9 by using a 1 *M* sodium chloride solution. The solution contained 4.0 mg/liter of cesium and about 15,000 counts/min/ml of Cs^{137}.

[54]Pure Oil Co. obtained the cores from Silica Chemicals, Inc., Amherst, Ohio.

[55]Product of Lapp Insulator Co., Inc., Le Roy, N.Y.

The coated Berea core had an effective volume, which is equal to the total volume minus the volume occupied by the resin, of 388 cc. The void volume, 87.6 cc, was determined by filling the interstitial spaces with distilled water. The porosity was 22.6%. Chemical analyses of two different samples of Berea cores are shown in Table 33.

A photograph of the experimental setup is shown in Fig. 86. The solution was pumped through the core at a rate of about 25 ml/hr. Samples of the effluent were taken for every 50 ml and counted in the well-type scintillation counter and 1024 scaler.

The results are shown in Fig. 87, which is a plot of Cs^{137} radioactivity in the effluent vs the cumulative volume of waste solution passed through the core. The solution was made up in two batches of 2 liters each; in the first batch the concentration of radiocesium was 15,000 counts/min/ml; in the second, 17,000 counts/min/ml. The results

UNCLASSIFIED
PHOTO 45709

Fig. 85. Method Used in Mounting Berea Sandstone Cores.

Table 33. Analysis of Berea Sandstone*

Constituent	Per Cent	
	Sample 429	Sample 1931
Ca	1	Trace
Mg	0.4	None
SiO_2	86	88
Al_2O_3	1	1.3
Fe	1.5	4
CO_2	0.71	0.88
Ignition loss	2	0.95
Clay content (approx)**	5	4

*A nonswelling type.

**Reported by the Crystal Lake Laboratories, Pure Oil Co., Crystal Lake, Ill.

show a breakthrough after 2900 ml of solution was passed through the core. The variations in effluent activity thereafter were due to the inability of the solution to reach equilibrium at that flow rate with so few theoretical plates remaining in the core.

The following is the cesium capacity of the core for this particular test solution:

1. Volume of feed = 2.5 liters;
   concentration of cesium = 40 mg/liter;
   10 mg of Cs sorbed per core.
2. Core volume = $388 \text{ cc} \times 3.53 \times 10^{-5} \text{ ft}^3/\text{cc}$
   $= 1.37 \times 10^{-2} \text{ ft}^3$.
3. Amount of Cs sorbed per cubic foot

$$= \frac{10 \text{ mg of Cs sorbed per core}}{1.37 \times 10^{-2} \text{ ft}^3}$$

$$= 730 \text{ mg of Cs per cubic foot.}$$

If the specific activity of the cesium in Purex waste were 40 curies/g, then 1 ft^3 of Berea sandstone would sorb about 5.3 curies of Cs^{137}.

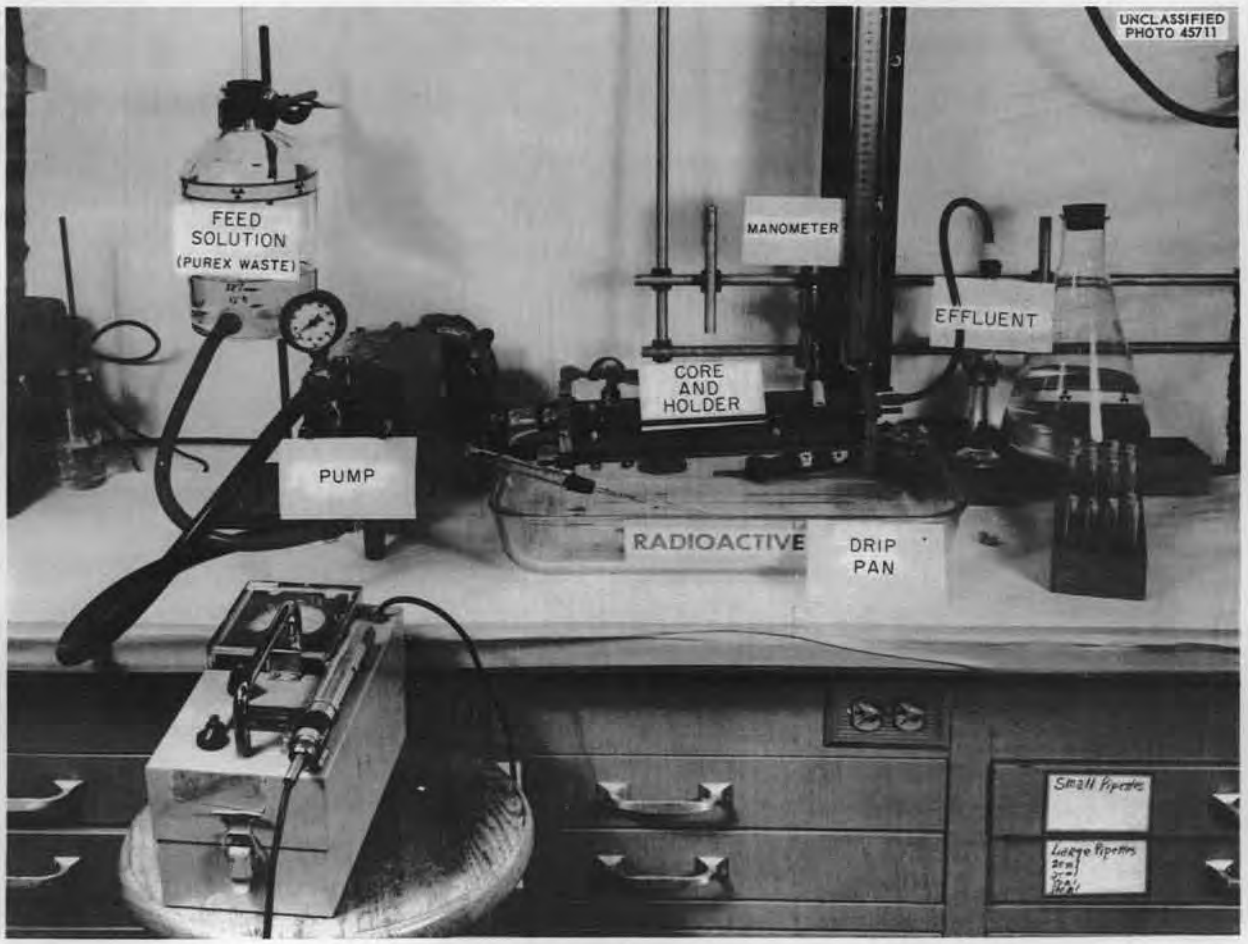

Fig. 86. Laboratory Setup for Core Testing.

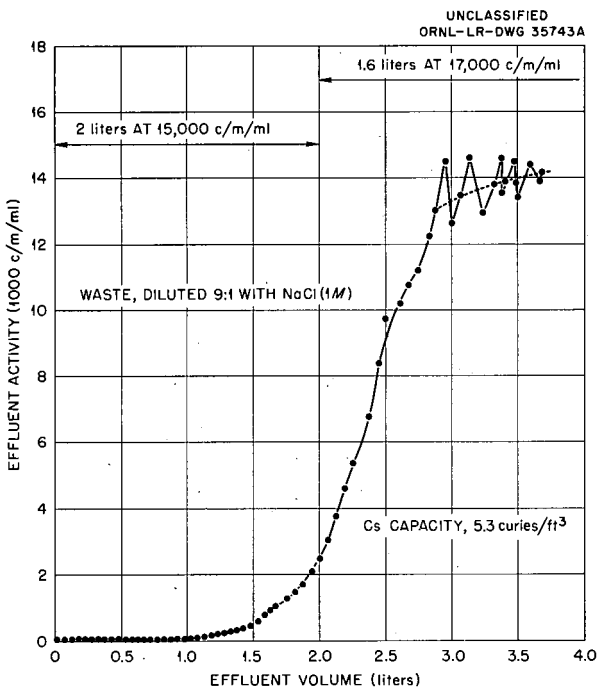

Fig. 87. Effluent Activity vs Volume of Purex Waste (Neutralized, Citrate Complexed) from Sandstone Core No. 1.

Calculation of the cesium capacity of a cubic foot of sandstone containing 5% illite clay using the same solution and based on the results of the jar test gave the following:

1. 0.35 mg of Cs per gram of illite at equilibrium (this was found to be 60% of capacity);
   100% capacity = 0.60 mg of Cs per gram.

Assume: 1 ft^3 of aquifer = 100 lb contains 5% illite-type clay; then

2. 0.60 mg of Cs per gram × 450 g/lb × 5 lb/ft^3
   = capacity for Cs per cubic foot
   = 1350 mg of Cs per cubic foot.

The capacity for cesium in the core was 730 mg/ft^3, while the jar-test capacity for cesium was 1350 mg/ft^3. This difference may be due to the clay mineral present in the core.

Throughout the test runs, no increase in head pressure was detected, no plugging of the leading face of either core was found, and both cores worked well at operating pressures of less than 80 psi.

In a second core test, using the same material and experimental techniques, the waste was diluted 30:1 with 1 *M* NaCl. The results of this test are shown in Fig. 88. Calculations of the amount of cesium sorbed per cubic foot of Berea sandstone from a 30:1 dilution of the waste solutions are as follows:

1. Retention (counts/min)
   = influent (counts/min) − effluent (counts/min);
   171.5×10^6 counts/min
   $= 237 \times 10^6$ counts/min $- 65.6 \times 10^6$ counts/min.
2. Effective weight of core
   = effective volume × specific gravity;
   1031 g = 491 cc × 2.1 g/cc.
3. Total amount of cesium sorbed in core

$$= \frac{\text{retention (counts/min)}}{\text{average influent count rate (counts/min/ml)}} \times$$

$$\times \text{ carrier concentration of cesium;}$$

$$1.39 \text{ mg} = \frac{17.2 \times 10^7 \text{ counts/min}}{2.7 \times 10^4 \text{ counts/min/ml}} \times$$

$$\times\ 0.00022 \text{ mg/ml.}$$

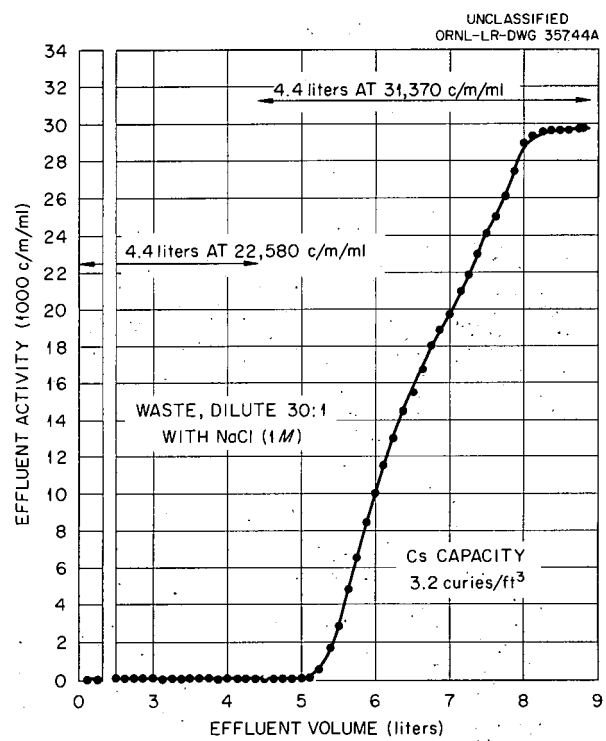

Fig. 88. Effluent Activity vs Volume of Purex Waste (Neutralized, Citrate Complexed) from Sandstone Core No. 2.

4. Effective volume of core in cubic feet
   = effective volume in cubic centimeters ×
   × number of cubic feet per cubic centimeter;
   1.73×10^{-2} ft^3 =
   491 cc × 3.53×10^{-5} ft^3/cc.
5. Then 1.73×10^{-2} ft^3 sorbed 1.39 mg of cesium.
6. One cubic foot would sorb 80 mg of cesium, and if the specific activity of the cesium in the Purex waste were 40 curies/g, this would equal 3.2 curies of Cs^{137} per cubic foot.

The cores were tested with Sr^{89} plus strontium carrier. The concentrations of carrier used were 4.4 and 1.33 mg of strontium per liter. The same test procedure was followed, except that counting was accomplished with an end-window-type G-M tube and 64 scaler.

Calculations, based on the amount of strontium removed from the test solution (9:1 dilution) and on the amount of strontium actually sorbed on various samples of the core, showed that 0.33 mg of strontium was sorbed in the core. Thus 1 ft^3 of this sandstone would sorb 2.4 curies of Sr^{90} (see Fig. 89). Similar calculations for the case of 30:1 dilution showed that 0.178 mg of strontium was sorbed. This is equivalent to about 1.9 curies of Sr^{90} per cubic foot of sandstone. These values assume the specific activity of strontium in the waste to be 80 curies/g. The results are shown in Fig. 90. Due to the length of time required to complete the experiment (nine days), a correction was made for the decay of Sr^{89} ($T_{1/2}$ = 53 days).

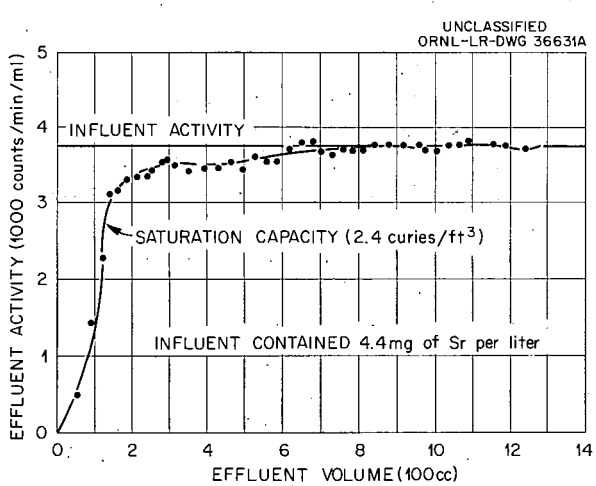

Fig. 89. Strontium Sorption from a 9:1 Dilution of 1 *M* Purex Waste on a Berea Sandstone Core.

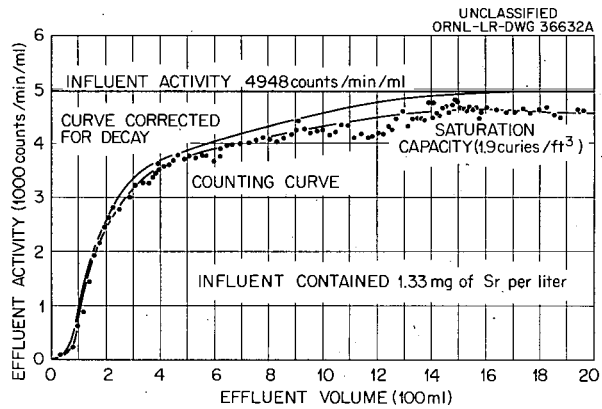

Fig. 90. Strontium Sorption from a 30:1 Dilution of 1 *M* Purex Waste on a Berea Sandstone Core.

A comparison of cesium sorption with strontium sorption from the same waste solution on sandstone cores shows that a 9:1 dilution sorbs 2.4 curies/ft^3 of Sr^{89} and 5.3 curies/ft^3 of Cs^{137}, while a 30:1 dilution sorbs 1.9 curies ft^3 of Sr^{89} and 3.2 curies/ft^3 of Cs^{137}. The results with jar tests (slurry tests) indicate that strontium removal by various clays is about one-third of cesium removal. The results of the core tests compared very favorably with the values obtained by slurry treatment. In the case of cesium sorption, the amount sorbed is dependent on the Na/Cs ratio. The amount of strontium sorbed is only slightly affected by the Na/Sr ratio.

HAZARDS EVALUATION OF TANK STORAGE

L. C. Emerson D. G. Jacobs
F. L. Parker R. M. Richardson

Economic studies suggest that the future nuclear power industry in this country will be developed around a few basic reactor types geographically dispersed throughout industrial regions. The partially spent fuel from these reactors will be chemically processed in one or, at most, a few multipurpose reprocessing facilities. In the interest of both safety and economy this plant must be located at or near the site of the disposal facility. Thus, it is quite likely that a single disposal facility will receive the first-cycle or high-level wastes from essentially the entire industrial nuclear power complex. It is possible, therefore, that different fuel types which give rise to chemically different waste streams will have to

be isolated within the disposal system. Even so, any portion of this system will contain wastes accumulated from many reactor-years of operation.

The ultimate success of any disposal technique will be measured in terms of the success with which the associated radiation hazards are held within acceptable limits. The analysis of the hazards is, in fact, the most important single study topic associated with the development of any disposal method. As will be shown, the power developed by the estimated Purex wastes in a typical disposal facility within the coming 10- to 15-year period will be some 4 Mw (thermal). This is comparable to the power level of many present-day reactors for which the hazard analysis has received the direct attention of teams of experts. Reactor hazards are perhaps more easily recognized because a single fuel loading is capable of releasing energy at a rate sufficiently high to destroy the containment system.

The power density in the highly concentrated wastes of the future will also be sufficiently high to destroy the container. While it is difficult to compare the hazard potential of reactors with that of high-level waste, it is possible to compare several factors upon which the hazard associated with both depends:

1. The power developed by the waste cannot be "turned off" as is the case at the first sign of trouble within a reactor.
2. Meltdown of a reactor core, in all likelihood, would terminate the fission process, thus stopping the power release. This is not so in a waste system, where a meltdown would merely redistribute the source of power.
3. The relative percentages of the long-lived and highly radiotoxic materials are much greater in the waste than in the reactor.
4. The normal state of the waste is liquid, which is much more easily dispersed in the environment than is the normally solid fuel of a reactor.
5. The dispersed wastes give rise to potential radiation hazards for hundreds of thousands of years, whereas in the case of dispersed reactor fuels the critical period is less than one thousand years.

Tank Storage

To those engaged in the field of waste disposal research the need is clear for thorough studies of the hazard potential of each proposed disposal method. Unfortunately, many of the more promising methods are still in the early laboratory stages, and their ultimate features are not sufficiently well defined to permit hazard analysis to proceed. In this interim period the storage of high-level wastes in underground tanks has become almost standard practice. In addition to its being essentially the only method available, tank designers can draw upon industry's wide experience in the underground storage of other liquids.

In view of the fact that tanks are being used to store present-day wastes and probably will continue to be used for some years, it was decided to initiate a series of waste-disposal hazard studies with a study of the hazards of tank storage. Additionally, a knowledge of those hazards associated with present-day storage methods is necessary in establishing the degree of effort to be made in the research and engineering programs associated with the more permanent disposal methods.

Basic Premises

The preliminary information upon which the hazard study is based was obtained from a concurrent study of the economics of tank storage made by the Chemical Technology Division of ORNL. In turn, that study was based upon a nuclear power industry predicted for the year 1970. The assumed distribution of reactor types and reprocessing methods was based on present-day knowledge but allowed for some additional development during the coming ten-year period.

Of the various assumed waste streams from the reprocessing facility neutralized Purex waste contains the highest concentration of fission products and transuranics, and for this reason the hazards associated with its storage are the object of this study. The characteristics of the reactors giving rise to this waste are shown in Table 34.

Early in the study it was recognized that little contribution could be made to the existing knowledge of the probability or mechanism of tank failures except to point out that tanks which are subject to the corrosion action of Purex waste, as well as to the intense radiation and heat over long periods, would be more prone to failure than those tanks used to store much less noxious materials. And it is significant that the record of failures of even the latter has been poor. It was therefore decided that the study should be limited to an investigation of the possible consequences of a

Table 34. Irradiation History of Purex Waste from Various Reactors*

Reactor Type	Irradiation History			
	Burnup	Power Density	Processing Rate (tons/year)	Purex Volume (gal/year)
				$\times 10^4$
U converter	10^4 Mwd/ton	28 Mw/ton		
Zr-clad UO_2			720	4.32
SS-clad UO_2			450	2.70
Fast breeder				
Core: SS-clad UO_2, 15% PuO_2	30%	1.5 Mw per kg of Pu	18	0.108
Blanket: SS-clad UO_2	8 kg of Pu per ton	~0	92	0.552

*Data developed by the Chemical Technology Division, ORNL.

tank failure and not to the probability or mechanism of the failure itself.

Preliminary investigations of the optimum tank size indicated that Purex wastes could be stored most economically in tanks of 4×10^5 gal capacity. Accordingly, the hazard study was based upon this figure. (Later studies have pointed out the difficulty of cooling a 4×10^5-gal tank with wastes of the concentration specified.)

Site Parameters

Site Selection. – For reasons of economy it would be advisable to locate the fuel reprocessing facility near the geographical center of the power reactor industry which it will service. As fuel element shipments via surface waterways provide the cheapest means of transportation, location of the reprocessing facility near one of the navigable rivers would be advantageous. For purposes of the economic study only a general area need be specified, whereas for the hazard analysis it is necessary to study a specific area. Even though such a choice is necessary it has the disadvantage that the completed study applies only to the one specific area studied and, in reality, does not answer the general question as to the safety of tanks.

The general area specified by the economic study lies in the Ohio River valley within one or two miles of the river between Cincinnati, Ohio, and Louisville, Kentucky. A specific site was chosen within this general area by reviewing the geologic and topographic features of various areas along the river. Desirable characteristics were isolation, proximity to the river, and suitable hydrologic characteristics.

The site chosen is located in Jefferson County, Indiana, about five miles southwest of Madison. Figure 91 shows the general location as well as the areas bordering the river which serves the facility.

Site Description. – The site lies on a broad plateau of low relief. The general elevation of the ground surface is about 790 ft, whereas the normal pool elevation of the Ohio River is 420 ft. The valley wall of the Ohio River is quite steep and is highly dissected by tributary streams which have cut deep, narrow valleys into the upland surface.

The site, about seven square miles in area, is bounded on the east by the river. It is readily accessible by water, rail, and highway. The only highway bridge across the river between Cincinnati and Louisville is located at Madison as are docking and terminal facilities. The climate would present no unusual problems.

The bedrock underlying the area consists of limestones and shales of various groups. These are essentially flat-lying with a slight westward dip. The bedrock surface is reasonably smooth, but as this rock is covered by glacial till, determination of its exact configuration would require test drilling.

Fig. 91. Geographical Locotion of the Hypothetical Tank Farm.

The thickness of the till deposits varies from 0 to 50 ft, with the maximum probably being found on the flat upland. The till is composed primarily of clay with some siliceous pebbles and scattered lenses of sand and gravel. Again, test drilling would be required to determine the thickness and composition at specific locations within the general site area.

Hydrologic Characteristics. – The physical properties of the glacial till that covers most of the area are markedly different from those of the underlying limestones and shales. For this reason the occurrence of ground water in the different rocks, which is controlled in part by porosity and permeability, is quite different. The glacial till is composed of unconsolidated material ranging in particle size from clay to coarse gravel. Although the permeability and porosity of the till are far from uniform, the granular nature of the material permits it to transmit water. The underlying limestones and shales are dense rocks devoid of primary openings, and in these rocks ground water occurs in openings generally developed along bedding planes and joints. These openings are frequently enlarged by the solvent action of moving ground water. The existence of such openings capable of transmitting water in the underlying limestones in the area is indicated by the numerous sinkholes and springs and several caves shown on the topographic map of the site and its vicinity.

The source of ground water in the area is rainfall, a part of which seeps down through the mantle rock to the water table and then moves laterally toward points of discharge at lower altitudes along the bluffs of the Ohio and in the valleys of the tributary streams. Determinations of the permeability of the till at the site have not been made, and information on the slope of the water table is not available. However, information on similar areas indicates that the rate of ground-water motion in the till at the site is probably less than a foot per day.

Water in the underlying limestone, as in the till, moves under the influence of gravity from points of higher elevations to points of discharge at lower elevations. The openings in the limestone are larger than those in the till, and hence the rate of ground-water movement in the limestone is much faster. It is probable that water in the limestone underlying the site moves at the rate of 1 ft/min or more.

Activity Distribution

Fission Products. – In all cases consideration of a two-member decay chain was sufficient to describe the growth and decay of the fission products. The activity in the influent waste stream was calculated for the important fission products by using the standard equations,

$$N_1(t,T) = \frac{P}{\lambda_1} f_1(t,T)$$

and

$$N_2(t,T) = \frac{P}{\lambda_2 - \lambda_1}\left[f_1(t,T) - \frac{\lambda_1}{\lambda_2} f_2(t,T)\right] ,$$

where

$$f_j(t,T) = [1 - \exp(-\lambda_j t)] \exp(-\lambda_j T),$$

N_j = atoms of jth type per unit mass of fuel,

P = production rate in the reactor in atoms per ton of fuel,

λ_j = decay constant of jth type,

t = irradiation time,

T = cooling time.

Because the time required to fill the tank is comparable to, and in some cases exceeds, the half lives of many of the important isotopes in the waste stream, it is necessary to take into account the decay of these isotopes during the five-year filling period. This was done by solving the two differential equations describing the rate of change of the number of atoms, A, present in the tank at time τ, during the filling period. These equations are:

$$\frac{dA_1}{d\tau} = R\, N_1(t,T) - \lambda_1 A_1(t,T,\tau)$$

and

$$\frac{dA_2}{d\tau} = R\, N_2(t,T) + \lambda_1 A_1(t,T,\tau) - \lambda_2 A_2(t,T,\tau) ,$$

where R is the rate at which fuel is processed. The solutions to these equations are found to be

$$A_1(t,T,\tau) = \frac{R}{\lambda_1} N_1(t,T)\,[1 - \exp(-\lambda_1 \tau)]$$

and

$$A_2(t,T,\tau) = \frac{R}{\lambda_2} N_2(t,T)\,[1 - \exp(-\lambda_2 \tau)] + \frac{R}{\lambda_2 - \lambda_1} N_1(t,T) \left\{ [1 - \exp(-\lambda_1 \tau)] - \frac{\lambda_1}{\lambda_2} [1 - \exp(-\lambda_2 \tau)] \right\} .$$

By standard methods the activity in curies at any storage time following the filling period was computed. The calculations were carried out for each of the important fission products, and the results are shown in Fig. 92.

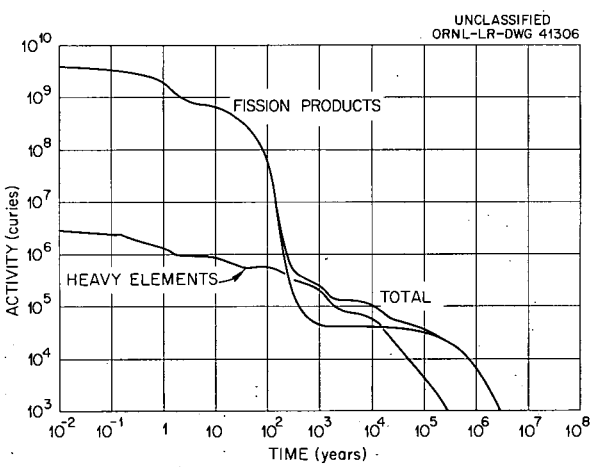

Fig. 92. Fission Product and Transuranic Activity.

As a small fraction of the Purex waste results from the processing of the core and blanket of the fast breeder reactors it is necessary to apply a 12% correction to the values calculated. This correction was obtained from the ratio of the production rates of the gross isotopes in the fast breeder reactors and the uranium converter reactors, as determined by the Chemical Technology Division. In some cases (e.g., Sr^{90} and Cs^{137}) specific values for the nuclides were available.

In the absence of specific information regarding the chemical processing methods it was decided not to attempt any adjustments in the individual contributions which reflect varying efficiencies in the process. Thus, the quantities shown represent an upper limit of the activity which would be present in an actual situation. The only obvious discrepancy in this regard is the inclusion of I^{129}. In all probability this element would be removed during the fuel dissolution process and consequently would not be present in the waste. Its inclusion does not affect the power generation or the hazard for times less than a few hundred thousand years. Its presence in the waste could be of concern at long times, since its long half life coupled with its high thyroid radiotoxicity would tend to prolong the necessary storage time beyond the period at which the more commonly recognized hazards disappear.

Transuranics. – In a detailed consideration of the hazards associated with the storage of high-level waste it is necessary to elevate the contribution of the heavy elements. In general, the contribution of these materials to the hazard potential of the waste stream representing a single reactor is negligible because the amount of the material present is small. However, in the waste stream from a reprocessing plant handling fuels from a large reactor complex the amount of material is no longer small; and, after considering decay during the filling period, the contribution to the hazard is no longer negligible. Even more revealing is a look at the proportion of the various contributors to the hazard at times following the decay of materials such as Sr^{90} and Cs^{137}. The transuranics contribute the majority of the power for all times greater than 400 years and the majority of the activity starting at about 400 years and lasting for a period of approximately 20,000 years. Considering the ratio of the activity to the maximum permissible concentration for drinking water as a measure of the hazard potential, the transuranics are the major contributor between 400 and 10^5 years.

The concentration of the heavy elements in the effluent waste from the reprocessing plant was determined by using analog computer solutions to the differential equations describing the in-pile growth and decay.[56] As in the case of the fission products, a two-member chain was sufficient to account for all of the important contributors during the storage period. If the rate, I, at which the activity, C_j, is introduced into the tank is known, then the activity present at the end of the filling

[56] J. O. Blomeke, *The Buildup of Heavy Isotopes During Thermal Neutron Irradiation of Uranium Reactor Fuels*, ORNL-2126 (December 1956).

period, τ, may be determined. In the case of a one-member chain the differential equation and its solution are quite familiar:

$$\frac{d\,C_1(\tau)}{d\tau} = I - \lambda_1\,C_1(\tau)\ ,$$

and

$$C_1(\tau) = \frac{I}{\lambda_1}[1 - \exp(-\lambda_1\tau)]\ .$$

In the case of a two-membered chain the differential equation takes a slightly different form, but the solution again is straightforward:

$$\frac{d\,C_2(\tau)}{d\tau} = \lambda_2[C_1(\tau) - C_2(\tau)]\ ,$$

and

$$C_2(\tau) = \left\{[1 - \exp(-\lambda_2\tau)] - \frac{\lambda_2}{\lambda_2 - \lambda_1}[\exp(-\lambda_1\tau) - \exp(-\lambda_2\tau)]\right\}\ .$$

The fast-breeder correction was made in the same manner as was done previously. The activity as a function of the storage time is shown along with the activity of the fission products and the total activity in Fig. 92.

Power Generation

The heating of the waste solution within the tank will necessitate the inclusion of an efficient cooling system to prevent boiling of the solutions. Experience has shown that cooling will be necessary for at least the first several hundred years of storage.[57] Forced and natural convection would keep the solution temperature uniform throughout the tank, thus permitting an even distribution of cooling. In case of failure of the tank in a manner permitting the escape of a fraction or all of the contents to the surrounding soil the heat problem would be much more severe. In any event consideration of this and other allied problems necessitates a knowledge of the heating rate of the waste.

The volume of the waste is sufficiently large that the deposition of gamma-ray energy at any point other than within the waste volume may be neglected. This greatly simplifies the calculation, since it admits the assumption that the distribution of the absorbed power is the same as that of the released power.

Calculations were carried out for the heating rate over the same periods of time as those calculated for the activity. The results are shown in Fig. 93. The relative contribution of the transuranics to heating (like their contribution to the radioactivity) is insignificant up to about 400 years. However, for times in excess of 400 years the relative contribution of the transuranics to the power is much greater than to the curies present. This is a direct result of their greater energy per disintegration.

Hazards Evaluation

To obtain a valid analysis of the hazards resulting from a specific accident involving the loss of waste solution from a storage container it would be necessary to know the conditions under which the loss occurs. These conditions would include (among others neither available nor necessary to a general study) the liquid loss rate, amount, location, temperature of the escaping material, etc. In addition to this information, complete geologic, hydrologic, and atmospheric characteristics of the site and its immediate environs would have to be known. However, for the purposes of this study it is entirely satisfactory to make reasonable assumptions regarding the type of accident and then to measure the safety of tank storage in terms of

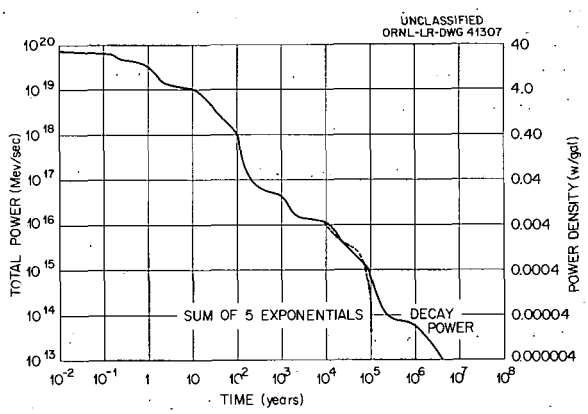

Fig. 93. Heat Source from Radioactive Decay.

[57] E. A. Coppinger and R. E. Tomlinson, *Heat Problems in the Disposal of High Level Radioactive Wastes*, TID-7517, part 1b (October 1956).

the consequences of the hypothetical release. In the study conducted to date this has been the procedure followed.

The only type of accident so far considered has been the sudden release of the entire contents of the tank at a point below the surface of the ground. The occurrence of an accident of this type is entirely within the realm of possibility. A release of this magnitude could result from such obvious causes as earthquakes or sabotage as well as from explosions resulting from chemical reactions or internal pressure buildup.

Interaction of Waste with Local Soils. – In the following treatment the interactions between the elements in the waste with the soil are considered as the waste moves away from the site of the release in the direction of the drainageways. Initially, these interactions would be of considerable importance since they would determine the physical distribution of the radiocontaminants. The till is unconsolidated, thus allowing a uniform flow pattern rather than the formation of channels, as well as a very high efficiency of contact between the waste solution and the minerals of the formation. In addition, till deposits generally contain substantial amounts of micaceous minerals which have a high affinity for some of the important fission products.

The neutralization of acid Purex waste results in a precipitation of $Fe(OH)_3$ which removes approximately 40% of the bulk of the waste. The precipitate scavenges the majority of the trivalent rare-earth fission products as well as 90 to 99% of the strontium. Because the distribution of cesium between the liquid and solid portions of the waste is relatively uniform, only 60% of the cesium in the tank can be considered mobile. The $Fe(OH)_3$ precipitate may be a further aid in limiting ground and surface water contamination, since it would tend to plug the pores of the till formation and prevent rapid percolation of the waste solution, thus increasing the efficiency of the till for removing fission products.

The till formation would be instrumental in retarding the movement of the fission products from the tank site into surface drainageways, thus reducing the amount of stream or river contamination. However, the fission products that are retained by the till would be expected to move into drainageways over an extended period of time. This subsequent movement, which might result from ionic desorption, microbial activity, the action of growing plants, erosion processes, or temperature increases, would proceed at a much slower rate and would present much less of a hazard.

It is possible to examine a number of cases of predicted behavior for some of the isotopes. Two of the most important are Sr^{90} and Cs^{137} because of their long half life, high yield, and high radiotoxicity. They can be considered as representative of the cationic materials. Ruthenium does not behave primarily as a cation, and it must be considered that approximately 90% will move through the till and into surface drainageways.

The exchange capacity of the till was assumed to average 10 meq per 100 g. (Laboratory analysis of samples of till from Madison, Indiana, at a later date indicated a value of 12.3 meq per 100 g.) The contact between the waste solution and the till was assumed to be 100% efficient. The distribution factors used in the calculations were 10 for strontium and 100 for cesium.

Case I: All of the Till Contacted by the Waste Solution Becomes Saturated. – At saturation the Cs/Na ratio of the sorbed ions will be 100 times the ratio of these ions in the equilibrium solution. This means that 4.8×10^8 g of till must be contacted by the waste solution if all the cesium in the mobile portion of the waste is to be sorbed. Assuming a bulk density of 1.5 g/cm^3 for the till, this would amount to 1.1×10^4 ft^3. In the case of strontium 1.1×10^5 ft^3 of till would be required for removal, since the distribution factor assumed for strontium is a factor of 10 less than that assumed for cesium.

These estimates of the amount of till necessary for removal of these isotopes are low, because all of the till contacted by the waste solution will not become completely saturated. As the concentration of the fission product in the waste solution is decreased, the amount sorbed by the till will decrease. The shape and slope of the sorption front is important in determining just how effectively the till is saturated. The character of the sorption front is dependent on the distribution factor, the efficiency of contact, and the rate of percolation compared with the rate of the exchange reaction.

Case II: Exponential Removal of Fission Products. – The other extreme in the fission product distribution can be obtained by assuming that a given amount of till will remove a given percentage

of fission product from solution. This is a valid assumption since the fission products occupy a negligible portion of the total number of exchange sites. When the amount of cesium in solution is equal to the amount of cesium sorbed on the till, the distribution factor (DF) is represented by the ratio of sodium in solution to the sodium in the shale. Because the cesium constitutes a negligible portion of the total exchangeable ions on the till, the number of equivalents of till necessary to reduce the cesium concentration in half is given by

$$\text{equivalents exchange capacity} = (Na)_0/DF \quad .$$

Four hundred thousand gallons of neutralized Purex waste (5.3 M Na^+) contains 8×10^6 equivalents of Na^+. However, only 2.4×10^5 gal of the waste is mobile; so 4.8×10^8 g of till would be required to remove one-half of the cesium. This is the same amount calculated above that would be required to remove all of the cesium if completely saturated. A second portion of till of the same dimensions as the first would remove one-half of the remaining cesium. For strontium, the values would be the same as given for cesium except that they would be increased by a factor of 10.

Figure 94 shows how the amount of fission product sorbed by the till would increase as successive increments of waste solution pass through the formation. The limiting case, of course, occurs when an infinite number of solution increments are passed through infinitely small increments of the till. When this occurs, the front of the sorption curve extends over such a small linear distance that the till can be considered to be completely saturated up to the point where it was last contacted by the fission product (i.e., case I).

These cases represent the two extremes. The true distribution of fission products would lie somewhere between the two extremes, depending on the rate at which the waste solution percolates through the formation.

River Contamination. – It seems evident that the wastes will not enter into the Ohio River as a single sudden dose but undoubtedly as a more continuous flow. The ground water system will act as an averaging reservoir so that the large quantities of fission products will be payed out of the reservoir at a relatively constant rate and over a substantial period of time. This is due to

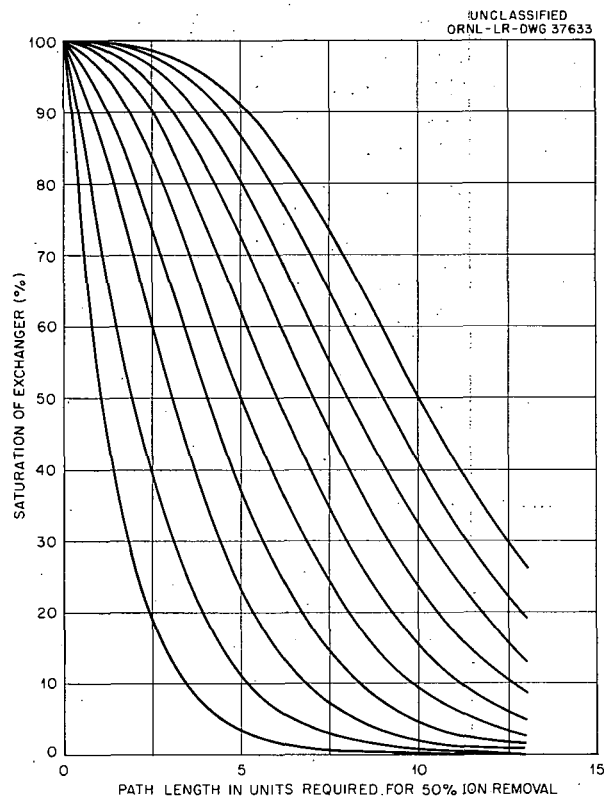

Fig. 94. Sorption Front Movement as Successive Increments of Solution Are Passed Through an Exchanger.

the fact that the site will be some distance back from the river and the ground water velocities are such that mixing will take place prior to discharge.

A detailed analysis of the fate of contaminants released to the river would require a knowledge of the hydraulics, temperature, velocity, and pollution distribution in the river. This information unfortunately is not available, as the most recent survey of the river by the Corps of Engineers is that of 1911–12. Surveys since that time have taken place only in the areas of the river where silting occurred. The Public Health Service in its comprehensive report of 1942 dealt with the pollution load and possible means of reducing this load. Detailed cross sections of the various streams were not included in this report. The annual reports of the U.S. Geological Survey of surface-water runoff have been of help in establishing the mean, maximum, and minimum flows of record. They also tell the velocity profiles at the gaging stations. Unfortunately there is no gaging station between Cincinnati and Louisville.

The substance of the above is that the data are so nebulous that a sophisticated analysis is unwarranted and simple dilution factors may be used to calculate the concentrations downstream from the point of entry. Since the continuous release is postulated, then the dispersion according to hydraulic flows and involving such parameters as cross-sectional areas, velocity, and eddy diffusivity really only operates on the tail of the contaminant cloud. In this study the simple flow rates shown in Table 35 are used.

Table 35. Ohio River Downstream Flow Rates

Location	Flow Rate (cm^3/sec)		
	Average	Maximum	Minimum
	$\times 10^9$	$\times 10^{10}$	$\times 10^8$
Louisville, Ky.	3.2	3.1	1.2
Evansville, Ill.	3.8	4.0	
Metropolis, Ill.	7.4	5.2	5.8
Memphis, Tenn.	12.9	5.6	22.4
Vicksburg, Miss.	15.8	5.9	28.2

Assuming complete dilution in the river the concentration at any point and at any time may then be determined only if the rate at which the material is introduced into the river is known. This in turn depends upon the rate and direction of ground water movement as well as upon the previously discussed interactions between the waste and the soil. In a detailed analysis each chemical element would have to be treated separately with the result being that the calculation of river concentrations would be a tremendous and time-consuming task. In addition, the lack of knowledge of the significant factors governing the transport of subsurface waters does not justify such detailed treatment. Even the use of simplified models which attempt to describe the introduction of the radiocontaminants to the river is open to serious question. About the best that can be hoped for is an idea as to the upper and lower limits of the river concentrations under reasonable conditions.

An upper limit to the concentration may be obtained by assuming that the tank contents are introduced directly into the river in a short time period. While this case represents one of the more severe accidents conceivable, in that the contamination of the river would reach disastrous levels, the accident itself is not entirely improbable. If the tank rupture were to occur under conditions that permitted channeling in the till, then it would be possible for the waste solution to come in intimate contact with the underlying bedrock which is already known to contain relatively large openings. Such an accident would afford minimum contact between the waste and the unconsolidated till while possibly introducing the waste directly into openings in the limestone. The high flow rates in limestone cavities could move the waste from the tank site to the river in a matter of hours.

A less severe accident can be postulated by assuming that the contents of the tank are emptied into a ground water reservoir which feeds either directly into the river or into a surface stream which empties into the river. The mathematical model representing this case can be simplified by assuming that the tank contents drain into the reservoir instantaneously and that the contaminants mix intimately with the water within the reservoir. Additionally, no credit is taken for ion exchange or other processes which deplete the concentration of contaminants. In this case the equation of continuity is

$$\frac{dA}{dt} = -(f + \lambda)\, A \quad ,$$

where

$\frac{dA}{dt}$ = rate of change of the activity within the reservoir with time,

f = fractional leakage rate of the reservoir,

λ = effective decay constant of the wastes.

The solution to this equation when multiplied by f/F, where F is the flow rate of the river, yields the concentration in the river at time t and at the point corresponding to the value of F,

$$\text{river concentration} = \frac{f}{F} A_0 e^{-(f+\lambda)t} \quad .$$

The concentrations at Louisville, the first city downriver, have been calculated for various values of f and are shown in Fig. 95. In this as well as in the following discussions it is assumed that the tank rupture occurs after the tank has been filled but before decay has depleted the activity.

The maximum permissible concentration of the radiocontaminants in drinking water is also strongly

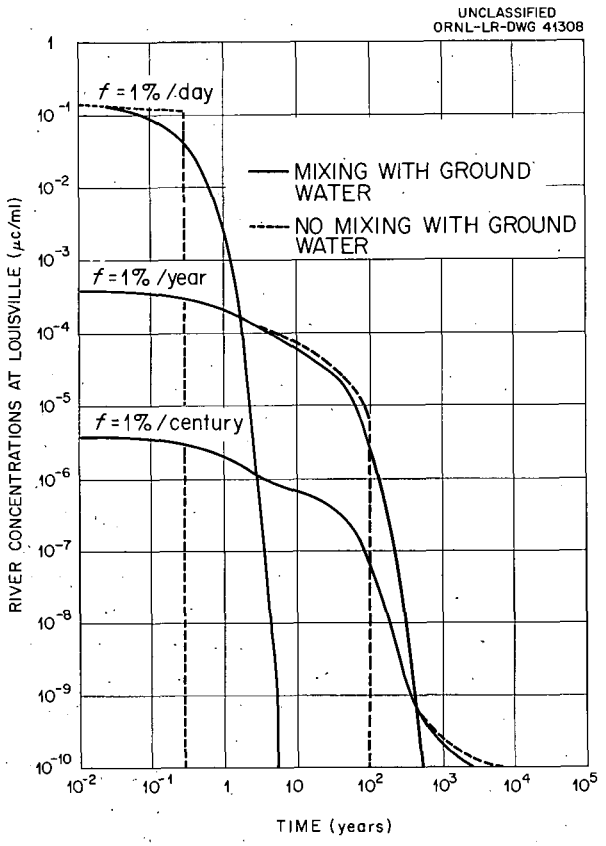

Fig. 95. River Contamination at Louisville.

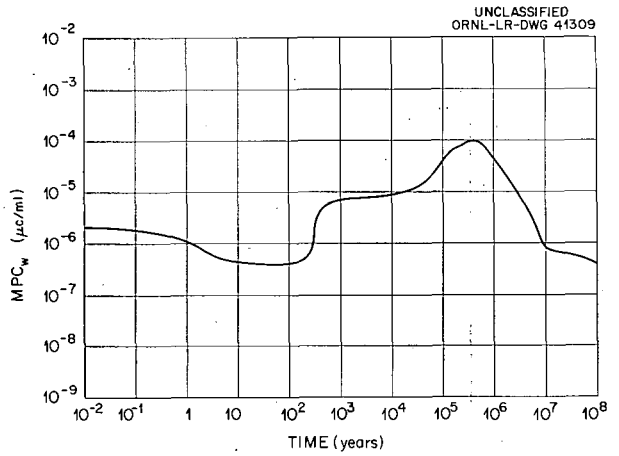

Fig. 96. Maximum Permissible Concentration in Water of Radiocontaminants vs Time.

time-dependent since the composition of the mixture continues to change with time. This time-dependency is exhibited in Fig. 96, in which the value of the quantity

$$\frac{\sum_i A_i}{\sum_i A_i (\mathrm{MPC}_w)_i^{-1}}$$

is plotted against time. Here A_i is the activity of the ith radioisotope in the tank at time t, and $(\mathrm{MPC}_w)_i$ is the maximum permissible concentration of the ith radioisotope for the population living in the neighborhood of a controlled area.[58] This quantity represents the maximum permissible concentration in the river over long periods of time. Its use in the analysis of the accident described can be justified only in an attempt to describe the general seriousness of the incident.

An identical model, but one which does not allow for mixing with the ground water, is also easily handled. The river concentrations based on this model are also shown in Fig. 95. In both cases the transit time to the river is assumed negligible. This assumption would be valid for the case of transit through the limestone channels, thus disallowing contact with the till.

The ratio of the river concentration under the stated conditions to the effective MPC_w for the mixture is plotted against time in Fig. 97. These values are somewhat higher than would be observed following an accident similar to that assumed. In other words, there are several factors of safety which have not been taken into account in the preceding analysis. The most important of these is the neglect of the removal of the radiocontaminants by ion exchange within the till and of the mechanical filtering action of the soil.

Subsurface Heating. – The decontamination of the waste solution by the till gives rise to an additional problem which could easily be more serious than any yet discussed. This is the problem of local heating which results from the energy released by the waste while confined within a small volume. In fact, the more effective the soil is in decontaminating the waste the more serious is this problem.

For the purpose of estimation of the temperatures which could be attained within the volume of soil

[58] *Maximum Permissible Body Burdens and Maximum Permissible Concentrations of Radionuclides in Air and in Water for Occupational Exposure*, Natl. Bur. Standards (U.S.), Handbook No. 69 (1959).

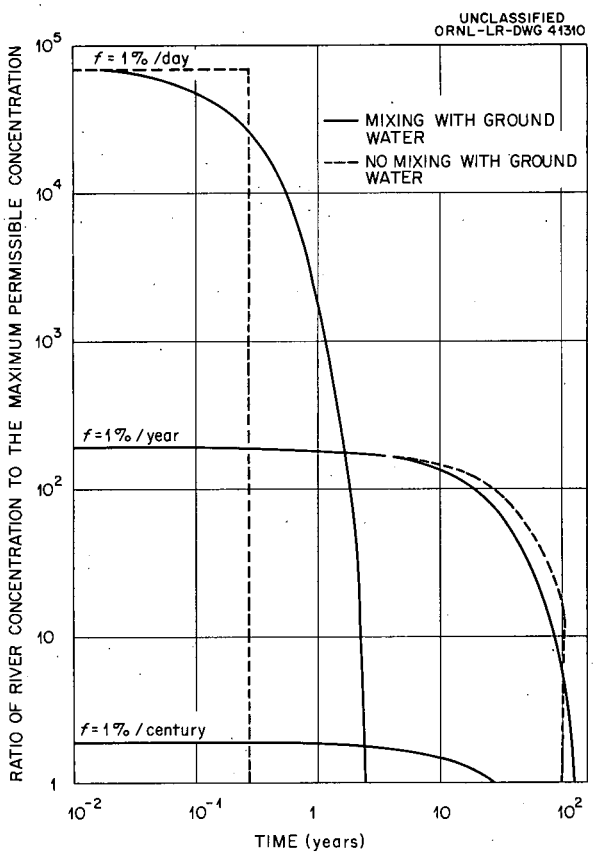

Fig. 97. Ratio of the River Contamination to the Maximum Permissible Concentration.

containing the radioactive materials it is necessary to make several assumptions regarding the physical distribution of activity. As a large fraction of the activity exists in insoluble form within the tank it is obvious that these materials will be mechanically trapped by the soil near the site of the release. Ion exchange would further add to the concentration of activity in the same region. The worst case may be investigated by assuming that all the activity becomes entrapped by a volume of soil equivalent to the original waste volume, 4×10^5 gal. (A more valid estimation of the volume of soil required to retain all the activity by ion exchange is within a factor of 2 of the value of 4×10^5 gal used in the calculation.) To simplify the calculation the source was assumed to be homogeneously distributed within a spherical region of soil surrounded by an infinite region of uncontaminated soil. An analytic approximation to the power decay curve was obtained which fitted (within 2%) the calculated decay curve out to 10^4 years. The calculational technique used has been described previously.[59] The initial calculations, based on rather unrealistic assumptions (i.e., heat transfer by conduction alone and constant conductivities), indicated peak temperatures of 10^5 deg at the center of the source region. The maximum was reached about one year following the accident. A more detailed thermal analysis is under way.

Obviously, the assumptions upon which the calculations were based would fail to apply long before these temperatures were reached. However, the calculation does indicate that the temperatures reached will be well above the boiling point of water and perhaps would vaporize certain of the fission products and actually cause local melting of the soil and rock. The escaping steam would probably leave fissures in the surface of the ground through which some fission products could be expected to escape. More detailed considerations of this problem will be undertaken.

External Radiation Hazards. – In the analysis to date no consideration has been given to the external radiation hazards resulting from failure of the tank. As the soil cover provides adequate shielding of the activity, the radiation fields in accessible areas would not be expected to be serious unless the activity moved away from the original site of deposition. This could occur through subsequent movement within the ground water system or by various processes which would tend to bring the waste to the surface. As has been mentioned, vaporization of the source and entrainment in the water vapor from heated ground water could serve as transportation mechanisms. Another mechanism which will be considered is that of capillary action.

It is possible that the loss of the soil cover would lead to a significant local hazard. This could occur as a result of structural failure of the top of the tank followed by collapse of the soil cover. Sky shine would give rise to appreciable radiation fields extending away from the sides of the collapsed structure.

---

[59] F. Birch, *Thermal Considerations in the Deep Disposal of Radioactive Waste*, NAS-NRC, Publication 588.

RELATED COOPERATIVE PROJECTS

S. I. Auerbach
W. de Laguna
R. J. Morton
E. G. Struxness
Y. Feige[60]
R. M. Richardson[61]
K. E. Cowser
L. C. Emerson
F. L. Parker
E. T. Chanlett[62]
W. M. McMaster[61]

Geologic and Hydrologic Studies by the U.S. Geological Survey

A general-purpose geologic map of the Oak Ridge Reservation, which comprises about 59,000 acres, was completed. The map covers all of one and parts of four 7½-min topographic quadrangles on a scale of 2000 ft to the inch. The map and three accompanying cross sections show the distribution and attitude of the rock formations that underlie the area. The thickness and character of the geologic formations in the area are shown on a columnar section. A brief report has been prepared for publication.[63] The map and report provide information necessary for the selection of sites for waste disposal and other facilities, as well as for ecologic studies.

The exploration of potential sites for a burial ground for radioactive waste in Bear Creek Valley is described in the section, "Burial of Solid Wastes."

A geologic map, structure sections, and a report describing the geology of the new burial ground in Melton Valley were prepared. This work is also described in "Burial of Solid Wastes."

The work of the Geological Survey in behalf of the salt project is described in the section, "Disposal in Salt Formations." Five sites for possible field tests in the western United States were examined and reports prepared. A report describing the location and extent of salt deposits in the United States was published,[64] as well as an annotated bibliography on salt deposits throughout the world.[65] Also, a literature search for information on the physical properties of salt was made.[66] The Geochemistry and Petrology Branch is making a detailed study of the core from a well drilled at the Naval Air Station at Hutchinson, Kansas.

The Knoxville Office of the Surface Water Branch cooperated with the Division in making a series of velocity and temperature measurements in the Clinch River downstream from White Oak Creek. This work is described in the section, "Disposal of ORNL Liquid Wastes."

The Quality of Water Branch made complete chemical analyses of six oil field brines in support of the program on deep well disposal and analyses of ground water from wells in the new burial ground in Melton Valley.

In support of the programs on deep well disposal and sorption and retention by clay minerals, the Geochemistry and Petrology Branch made various analyses on a number of rock, soil, and clay samples.

A Jeep-mounted well-logging instrument developed by the Geophysics Branch was loaned to the Division for use in the monitoring of wells in waste disposal areas.

Testimony at Joint Congressional Committee Hearings

One member of the Section presented two oral statements in testimony at the "Public Hearings on Industrial Radioactive Waste Disposal," conducted by the Congressional Joint Committee on Atomic Energy in January and February 1959. One of these statements was on "Direct Disposal of Radioactive Wastes," and the other was on "Fixation and Ultimate Disposal." Others in the Section submitted five written statements on particular aspects of radioactive waste problems for publication in the printed record of the hearings.

Review of Backflow Preventers for Protection of ORNL Water Supply

During the past year there have been specific proposals that "reduced-pressure principle backflow preventers" be used in cross connections at various places in the Laboratory. The purpose

---

[60] Alien guest for one year from Israeli Atomic Energy Commission.

[61] U.S. Geological Survey.

[62] ORINS research participant, University of North Carolina.

[63] W. M. McMaster, *Geologic Map of the Oak Ridge Reservation, Tennessee* (to be published).

[64] W. G. Pierce and E. I. Rich, *Summary of Rock Salt Deposits in the United States as Possible Disposal Sites for Radioactive Wastes*, TEI Report-725, U.S. Dept. of Interior, Geological Survey (May 1958).

[65] W. B. Lang *et al.*, *Annotated Bibliography of Salt Deposits: A Supplement to U.S. Geological Survey Bulletin 1019-J*, TEI Report-712, U.S. Dept. of Interior, Geological Survey (January 1958).

[66] E. C. Robertson, R. A. Robie, and K. G. Books, *Physical Properties of Salt, Anhydrite, and Gypsum — Preliminary Report*, TEM Report-1048, U.S. Dept. of Interior, Geological Survey (August 1958).

was to reduce the cost of the present system of separation of potable and nonpotable water and to increase the degree of protection where backflow hazards now exist. Two members of this section were requested to obtain further information about the reduced-pressure devices and to advise regarding their acceptance and use at ORNL.

Available information was obtained and summarized, and a report was prepared which submitted recommendations based on this preliminary review.[67] It was recommended (1) that standard procedures for prevention of cross connections at ORNL be formulated and adopted, (2) that an improved program of cross connection control be established, (3) that backflow hazards be eliminated insofar as possible by the maintenance of positive separation of potable and nonpotable water pressure systems, and (4) that additional evaluation and testing of the reduced-pressure devices be considered.

It was necessary to obtain firsthand information concerning the reduced-pressure devices in places where they were developed, tested and evaluated, used extensively, and observed in actual use under a system of strict supervision. This was done at Los Angeles and at Los Alamos. The conclusions reached were that the reduced-pressure devices include features which make them more dependable than earlier devices but that additional testing, particularly with radioactive tracers, is essential before they should be approved for use in cross connections that involve health hazards at the Laboratory.

Review of ORNL Waste Disposal Practice

The Chief of the Health Physics Section of the Israeli Atomic Energy Commission, Y. Feige, spent six months with the Waste Disposal Research and Engineering Section studying waste disposal methods at ORNL. In collaboration with two members of this Section, a report, "Analysis of the Liquid Waste Disposal Practice at ORNL," is being prepared for publication.

Preliminary Observations on Aerosol Emissions from High-Level Liquid Wastes During Storage

The operation of the Fission Products Pilot Plant at the X-10 site requires the dumping of small volumes of high-level wastes to the Tank Farm. Tank W-6 has been receiving these wastes, in which a major component is Zr^{95}-Nb^{95}. Tank contents on occasions have risen to a temperature of 95°F. In the X-10 area, Zr^{95}-Nb^{95} has been found as a surface contaminant. In view of projected operations at the pilot plant, a preliminary investigation of aerosol emissions by entrainment was made during the summer of 1959. The primary purpose was to evaluate the hazard of air-borne contaminants from high-level waste tanks at ORNL.

Initial investigations indicated that the choice of analytical methods for characterizing the waste in tank W-6 was limited by the radioactivity in the sample. Study of the unit processes and flowsheets indicated the nature and sources of the wastes and the relationship of operations to certain intermittent dumps to tank W-6. The operational records of the pilot plant were given an initial examination. From these records it may be possible to determine whether an indicator ratio among the macroionic constituents can be used to characterize the waste.

Laboratory runs of simulated Purex waste showed that at temperatures above 90°C, condensate of vapor carry-over contains iron and nitrates. Equipment was assembled and calibration was begun to extend experimental runs to air-sweeping of the liquid surface. The range of temperatures and air volumes will be carried downward to establish a threshold for ionic carry-over in trap condensates, gaseous freeze-outs, and membrane filtrates.

NS "Savannah" Hazard Study

One member of the Section served as leader of the study group on the effects on the hydrosphere should an accidental release occur during the startup and operation of the NS "Savannah." The results of the study were presented before the Advisory Committee on Reactor Safeguards. The full report on the effects of releases to the environment is in preparation.

Editorial Staff

One member of this Section is serving on the staff of the newly created journal, *Technical Progress Review on Nuclear Safety*. This is a quarterly publication being prepared by ORNL at the request of the AEC. It is intended that this journal meet the needs for concise summaries of current developments in the field of nuclear safety.

---

[67] R. J. Morton, *Backflow Preventers for Cross-Connection Control at Oak Ridge National Laboratory*, ORNL CF-59-5-27 (May 7, 1959).

Each of the reviews will provide a technical abstract and evaluation on the latest findings in specific areas of this topic.

American Standards Association Sectional Committees

Three of the staff have served as members and have participated in the work of ASA Sectional Committee N5, "Chemical Engineering for the Nuclear Field," and ASA Sectional Committee Z54, "Industrial Use of Radiation." Two have served as members of subcommittee N5.2 on "Radioactive Waste Disposal," and one has served as a member of subcommittee Z54.9 on "Contamination Levels of Industrial Materials." During the year these staff members have attended meetings of the sectional committees and subcommittees and have contributed on problems assigned to working groups.

American Public Health Association Committee on Radiological Health

One person in the Section has continued as a member of and has attended two meetings of the Program Area Committee on Radiological Health of the American Public Health Association (APHA). This committee has the over-all responsibility for guidance of the Association in its policies and actions relative to radiological health and radiation exposure problems. Past work of the committee has included preparation of two publications for use by health workers and for distribution to the public; one is entitled "Public Exposure to Ionizing Radiation," and the other is "Radiological Health Practices – A Guide for Public Health Administrators." The current and future program of the committee includes redrafting of the statement by the APHA on "Public Health Policy on Radiological Health"; restudying existing state laws and developing a revised model law; and making recommendations to the Association regarding problems of radiation exposure from food and milk, selection and training of personnel for health programs, and public information bulletins to be developed by private agencies.

AEC Ecological Review Committee

The report of the Ad Hoc Ecology Advisory Committee to the Division of Biology and Medicine, AEC, Washington, D.C., on which one member of the staff served, was completed. The committee recommended that parallel and comparable ecological researches should be initiated on a long-term basis in the various soils, climatic regions, and vegetational regions of the earth. The report urged that permanent on-site reservations for long-time ecological studies should be established at the Argonne National Laboratory, Hanford Atomic Power Operation, National Reactor Test Site, Nevada Test Site, Oak Ridge National Laboratory, and the Savannah River Plant.

ORSORT Course in Physical Geology

One member of the section gave a six-week course in physical geology to a group of foreign students in the Oak Ridge School of Reactor Technology. Emphasis was placed on problems of reactor site selection. These included the ways in which the site may cause difficulties for the reactor (as in foundation weakness) and also the ways in which the reactor may cause difficulties at the site (as by contamination of surface- or ground-water supplies).

RADIATION PHYSICS AND DOSIMETRY

DOSIMETRY APPLICATIONS

J. A. Auxier
E. T. Arakawa
J. S. Cheka
W. W. Ogg
F. W. Sanders
C. H. Bernard[1]
W. T. Thornton[2]

Ichiban Project

Operation Hardtack II Experiments. – During Operation Hardtack II (fall of 1958) a detailed study was made of the neutron and gamma radiation dose distributions in facsimiles of typical Japanese dwellings exposed to nuclear bomb radiation. All framing was of typical Japanese type, but the walls and roof panels were composed of slabs of cement asbestos board rather than the mud-bamboo used in Hiroshima and Nagasaki. Comparative measurements of the neutron and gamma penetration of Japanese walls, Japanese roofs, and numerous domestic materials had been made to determine a suitable domestic substitute for the Japanese materials. Seven houses were exposed during two of the nuclear detonations and six during the last detonation. The arrangement of the houses for each event was such as to provide data on the dose distribution as a function of house size, orientation relative to ground zero, and mutual shielding. Figure 98 shows a typical arrangement of the houses. Figure 99 shows a typical instrument

[1]Research participant.

[2]AEC Radiological Fellow.

UNCLASSIFIED
PHOTO 47758

Fig. 98. Typical Arrangement of Houses for Operation Hardtack.

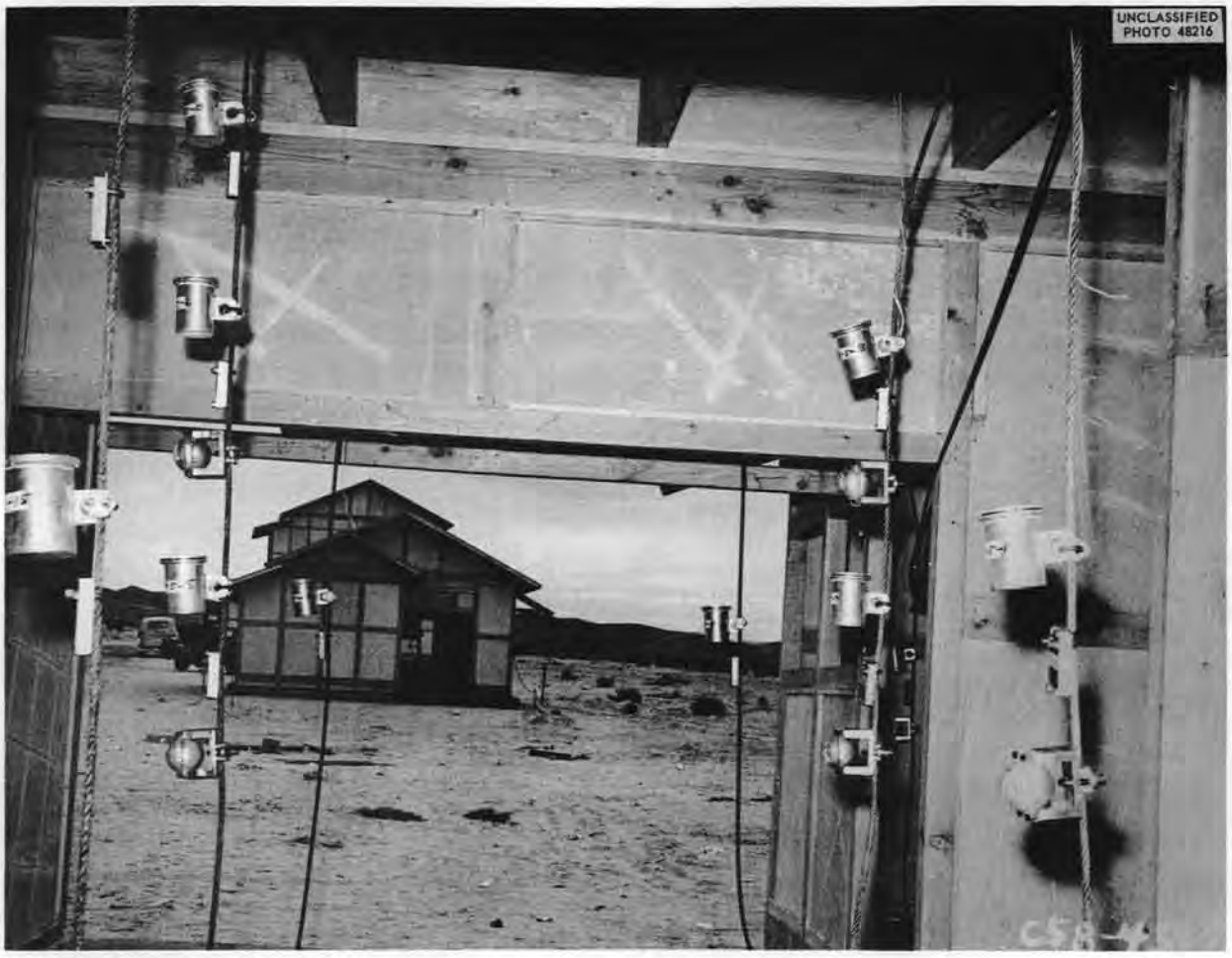

Fig. 99. Typical Instrument Installation in the Houses for Operation Hardtack.

installation; the instruments were suspended on cables to facilitate recovery after the detonation. Radiation measurements were made with threshold detectors[3,4] and chemical dosimeters[5] for neutrons and gamma rays, respectively.

In addition to the dose distributions in the houses, the field experiments included measurements of angular distribution and slab penetration such as those reported earlier.[6,7] The analysis of the data has not yet been completed.

The substitute-materials analysis comprised a series of measurements of the transmission characteristics for gamma and neutron radiation of various domestic building materials, with special emphasis on such materials as are available in slabs. The preference for slabs was based on efforts to minimize labor costs, which are a major item of cost in construction at the Nevada Test Site (NTS).

The measurements were made with both good and poor slab geometry. Figure 100 illustrates the apparatus used for measuring neutron penetration of Cemesto board, in this case positioned for "poor geometry" measurements.

Table 36 shows the results obtained on several materials tested, including a section of wall and a section of roof fabricated according to Japanese specifications. The measurements are given in terms of half thicknesses for the Co^{60} and Cs^{137}

[3] G. S. Hurst *et al.*, *Rev. Sci. Instr.* **27**, 153–56 (1956).

[4] P. W. Reinhardt and F. J. Davis, *Health Phys.* **1**(2), 169–75 (1958).

[5] S. C. Sigoloff, *Nucleonics* **14**(10), 54–56 (1956).

[6] J. A. Auxier *et al.*, *H-P Ann. Prog. Rep. July 31, 1958*, ORNL-2590, p 100–103.

[7] R. H. Ritchie and G. S. Hurst, *Health Phys.* **1**(4), 390–404 (1959).

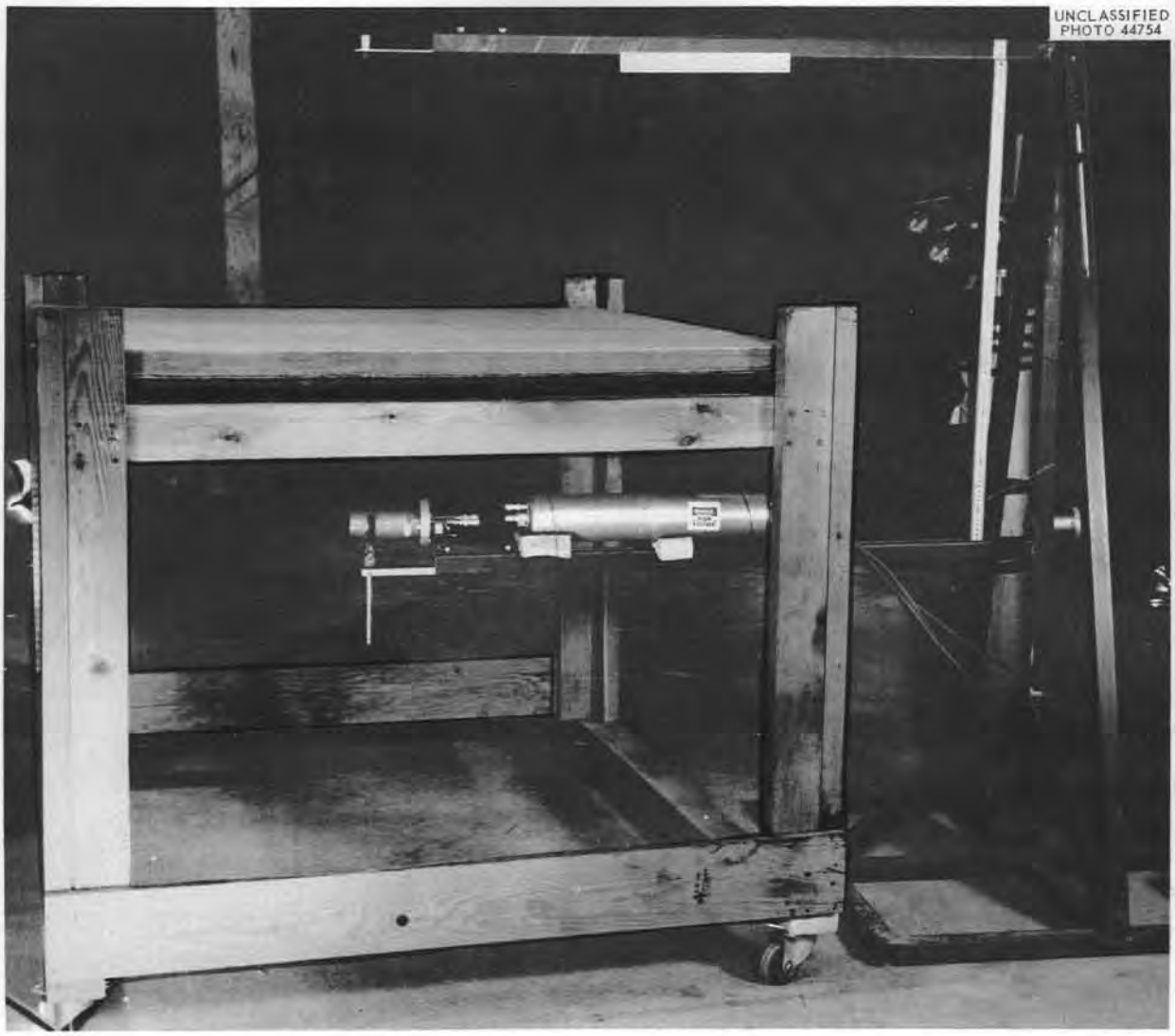

Fig. 100. Apparatus Used to Measure Neutron Penetration of Cemesto Board.

gamma radiation and Po-B neutrons. In addition, the relative attenuations for Co^{60} gammas and Po-B neutrons are given.

The data indicated that cement asbestos board best approximated the relative attenuation for both the Japanese wall section and roof section. This information, together with the results of measurements made in Japan for radium gamma attenuation[8] established the proper thicknesses to be used for the walls and roofs of the NTS structures.

Glass Dosimetry

Metaphosphate glass containing silver can be used as a gamma dosimeter in the range of five to several thousand rads. Small rods of the glass (1 mm in diameter by 6 mm long) and a convenient reader are commercially available.[9] Many properties of the system have been reported by Schulman[10,11] and others.[12–14] The glass composition, by weight, is 46% $Al(PO_3)_3$, 23% $Ba(PO_3)_2$,

[8] C. C. Sartain *et al.*, *H-P Ann. Prog. Rep. July 31, 1957*, ORNL-2384, p 89–91.

[9] Bausch and Lomb Optical Co., Rochester, N.Y.

[10] J. H. Schulman *et al.*, *J. Appl. Phys.* **22**, 1479 (1951).

[11] J. H. Schulman and H. W. Etzel, *Science* **118**, 184 (1953).

[12] N. J. Kreidl and G. E. Blair, *Nucleonics* **14**(3), 82–83 (1956).

[13] H. W. Etzel, R. D. Kirk, and J. H. Schulman, *Ra-Det* 8(2), 49 (1955).

[14] A. L. Riegert, H. E. Johns, and J. W. T. Spinks, *Nucleonics* **14**(11), 134–37 (1956).

Table 36. Building Materials and Their Radiation Attenuation Characteristics

Material	Half Thickness (g/cm^2)			Ratio, $\frac{Co^{60}}{\text{Po Neutrons}}$
	Co^{60}	Cs^{137}	Po Neutrons	
Wood	~36		8.7	4.14
Plywood	21.5	20.0	9.6	2.24
Roofing felt			7.4	
Roll roofing			13	
Cemesto	25.8	22.5	18.6	1.39
Gypsum board	22.2	23	20.1	1.10
Sand			44.4	
Brick	~24	~24	26.2	0.92
Concrete slab	21.4		23.0	0.93
Cement asbestos board*	23	19.5	21.2	1.08
Japanese wall section	24.5		24.0	1.02
Japanese roof section	19.8		17.8	1.11

*Johns-Mansville Transite.

23% KPO_3, and 8% $AgPO_3$. When the rods are exposed to ionizing radiation, loosely bound electrons are freed from negative ions and migrate through the glass. Some of these are trapped by interstitial silver ions to form a radiophotoluminescent or *F*-center. This type of *F*-center can be excited by ultraviolet light, and the electron returns to the ground state by the emission of a photon of about 6400 Å wavelength.

The dependence of the response of this system on photon wavelength has been reported.[14,15] The energy response for narrow beams of filtered x rays is shown in Fig. 101 for bare glass rods and for rods encapsulated in certain filters intended to improve the energy response. For broad energy spectra, such as the fission gamma-ray spectrum, the 20-mil Ta–15-mil Teflon filter is sufficient for measurements accurate to ±10%.

The fast-neutron response of the glass rods is, relative to gamma rays, negligible. Results of exposures to monoenergetic neutrons in the region

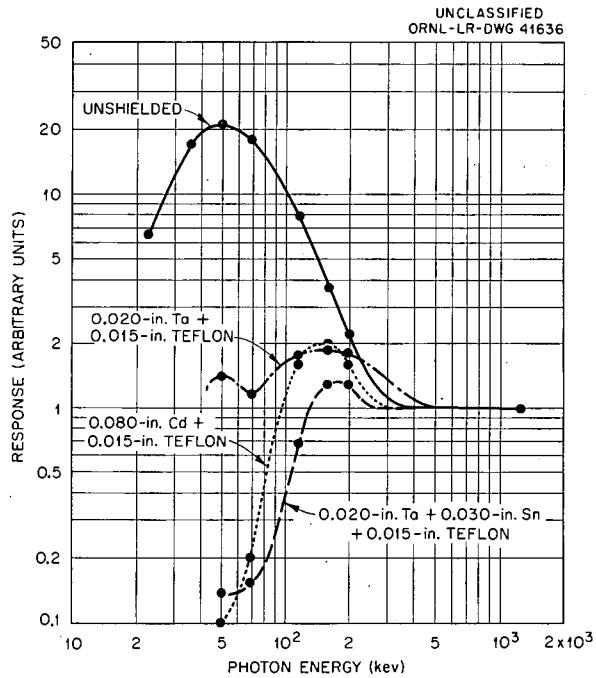

Fig. 101. Shielded and Unshielded Response of Silver Metaphosphate Glass Dosimeter.

[15] T. Brustad and T. Henriksen, *Brit. J. Radiol.* 31, 163 (1958).

of 0.5 to 1.5 Mev indicate an upper limit of response, relative to Co^{60} gamma radiation, of less than 1% (Fig. 102).

Glass rods enclosed in Li^6 cans of various thicknesses were exposed in the thermal column of the ORNL Graphite Reactor. Measurements were made of the thermal neutron flux in and near the Li cans and in the same locations without the Li cans. The response of the glass to thermal neutrons was then determined to be 1 roentgen equivalent per 5×10^9 thermal neutrons/cm^2. This response is sufficiently high to necessitate encapsulation in lithium for accurate measurement of gamma radiation coexistent with thermal neutrons. In general, the dimensions of the glass rods justify the use of lithium enriched in Li^6.

Measurement of Leakage Radiation from Critical Assemblies

For prompt determinations of the doses received by persons exposed to radiation from nuclear accidents, as much information should be readily available as possible. In criticality accidents, rapid dose determinations for inadequately monitored individuals require knowledge of the neutron-to-gamma dose ratios. If the neutron spectrum can be estimated, an analysis of the blood-sodium activation will permit an approximate calculation of the neutron dose. From a knowledge of the neutron-gamma ratio and the dose due to neutrons, the major exposure parameters can be determined using the method employed for the Y-12 criticality accident in June of 1958. A series of experiments to measure the ratio of the neutron and gamma dose rates and the neutron spectra generated by various types of critical assemblies has been initiated. Measurements completed include those for aqueous solutions of uranyl nitrate in three sizes of right circular cylindrical tanks: 22 in., 5 ft, and 9 ft. The data for the 22-in. tank were taken in the course of experiments for determining doses for the persons exposed in the Y-12 accident and have been reported.[16]

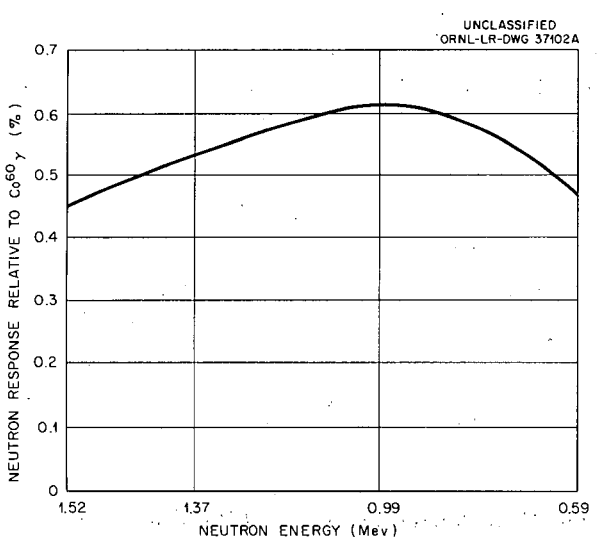

Fig. 102. Luminescent Response to Fast Neutrons as a Function of Energy.

With the cooperation of the Neutron Physics Division, measurements were made for the other tanks during the course of normal criticality experiments. This prescribed that the measurements be made at tank levels and concentrations that were not necessarily optimum for these measurements.

The 9-ft-dia tank had walls of $\frac{3}{8}$-in.-thick steel, and the base was supported 12 ft above a concrete floor. The base of the 5-ft-dia tank was supported 10.7 ft above a concrete floor, and the steel walls were $\frac{1}{8}$ in. thick. Measurements were made at points on radii at the half height of the solution and at points on a vertical arc having its center at the center of the solution. Some values obtained for gamma-to-neutron dose rate ratios for the two large tanks are given in Table 37.

Figures 103 and 104 show the neutron spectrum as determined by threshold detector methods[3,4] for the 5-ft tank and the 9-ft tank, respectively. The measurement position in each case was immediately adjacent to the outside of the tank and in the center plane of the solution; that is, at one-half the solution height.

Blood Na^{24} Studies

Determination of the concentration of Na^{24} in blood serum appears to be one of the most feasible methods of determining the neutron dose received by individuals involved in nuclear accidents. Using this method to estimate the neutron dose and using an experimentally determined ratio of gamma-to-neutron dose rates, it is possible to estimate the total dose.[16] In order to determine

[16] *Accidental Radiation Excursion at the Y-12 Plant, June 16, 1958*, Y-1234.

Table 37. Ratio of Gamma-Ray to Fast-Neutron Dose Rates for Leakage Radiation from Aqueous Solutions of Uranyl Nitrate Contained in Steel Tanks

Critical Assembly		Gamma-Neutron Ratios at Various Distances from Wall of Tank				
Diameter (ft)	Solution Height (in.)	1 m	2 m	3 m	4 m	5 m
5	18.5	3.36	3.00	2.76		
9	35.6	6.85	7.09	6.37	6.01	5.77
		Gamma-Neutron Ratios at Various Angles with Respect to Horizontal at 2.25 m from the Center of the Solution				
		0°	30°	45°	90°	
5	18.5	3.22	2.33	1.99	2.21	

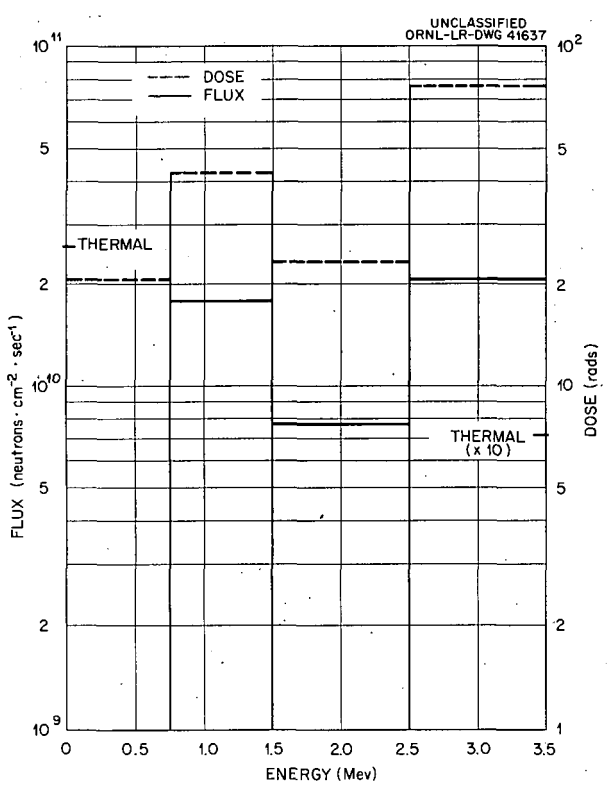

Fig. 103. Energy Spectrum and Dose Distribution for Neutrons from a 5-ft Tank with 18 in. of Solution, Measured in Contact with the Tank at the Solution Half-Height.

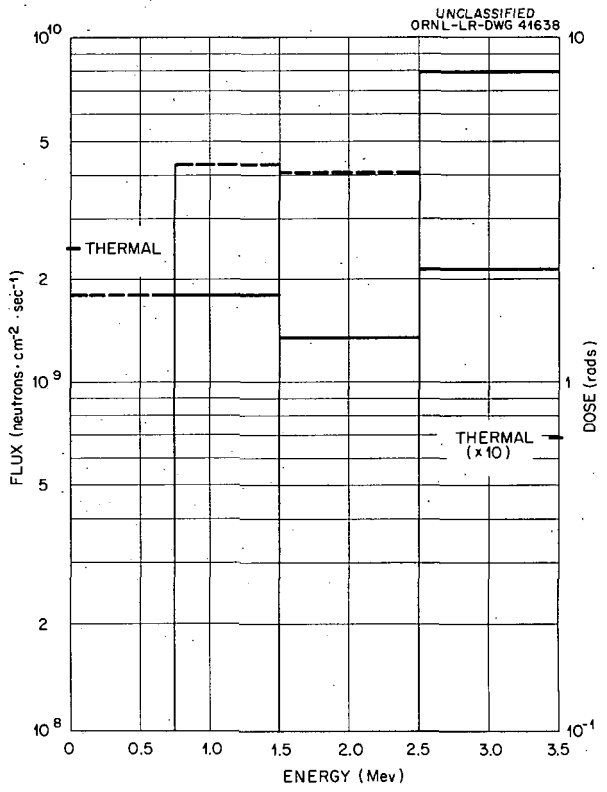

Fig. 104. Energy Spectrum and Dose Distribution for Neutrons from a 9-ft Tank with 90 in. of Solution, Measured in Contact with the Tank at the Solution Half-Height.

neutron dose by measurement of the Na^{24} concentration it is necessary to have a knowledge of the relationship between incident neutrons and neutron capture by Na^{23} in the body. This relationship depends upon several parameters such as neutron energy distribution, mass configuration, orientation of the body, and inhomogenous distribution of blood and other tissues in the body.

In order to avoid the inconveniences of prolonged experimentation with blood serum a simulated blood serum was tested. Burro blood serum containing 3.1 mg/ml of Na as determined by flame photometry was compared with a solution of NaOH in H_2O containing the same percentage of Na. Equal volumes of NaOH solutions and blood serum were irradiated by thermal neutrons in the slant animal tunnel and by fission neutrons in the west bunny tunnel of the ORNL Graphite Reactor. Figures 105 and 106 show that 4 hr postirradiation the gamma activity of energy greater than 2.0 Mev was essentially all from Na^{24}. Therefore, NaOH solution of the proper concentration can be used in experiments as a substitute for blood serum.

Samples of blood serum and NaOH solution placed in a phantom consisting of 607 parts H_2O, 250 parts sugar, 70 parts urea, 150 parts isopropyl alcohol, and 4.3 parts concentrated HCl in a polyethylene drum liner were exposed to fission neutrons. The container was a right cylinder 37 cm in diameter and 51 cm high with walls about 1.5 mm thick. The Na^{24} activities in samples of NaOH solution and blood serum exposed in equivalent positions in the phantom were found to be the same within 10%.

A sample of NaOH solution at the center of the phantom exposed to fission neutrons was found to have an activation, extrapolated to zero time, of 2.12×10^{-6} $\mu c \cdot ml^{-1} \cdot rad^{-1}$. In the Y-12 accident mockup experiment, burro blood was found to have 6.04×10^{-6} $\mu c \cdot ml^{-1} \cdot rad^{-1}$. This difference emphasizes the need for further study of the interrelationship of neutron energy, body size, body and organ configuration, and the distribution of blood and tissues in the body to sodium activation by neutrons.

Dosimetry of the Y-12 Accident[16]

An aqueous solution of enriched uranium accidentally flowed into a 55-gal drum in the Y-12 Area of Oak Ridge in June 1958. A prompt critical chain reaction was established in which about 10^{18} fissions occurred before the system finally became subcritical due to the addition of water.

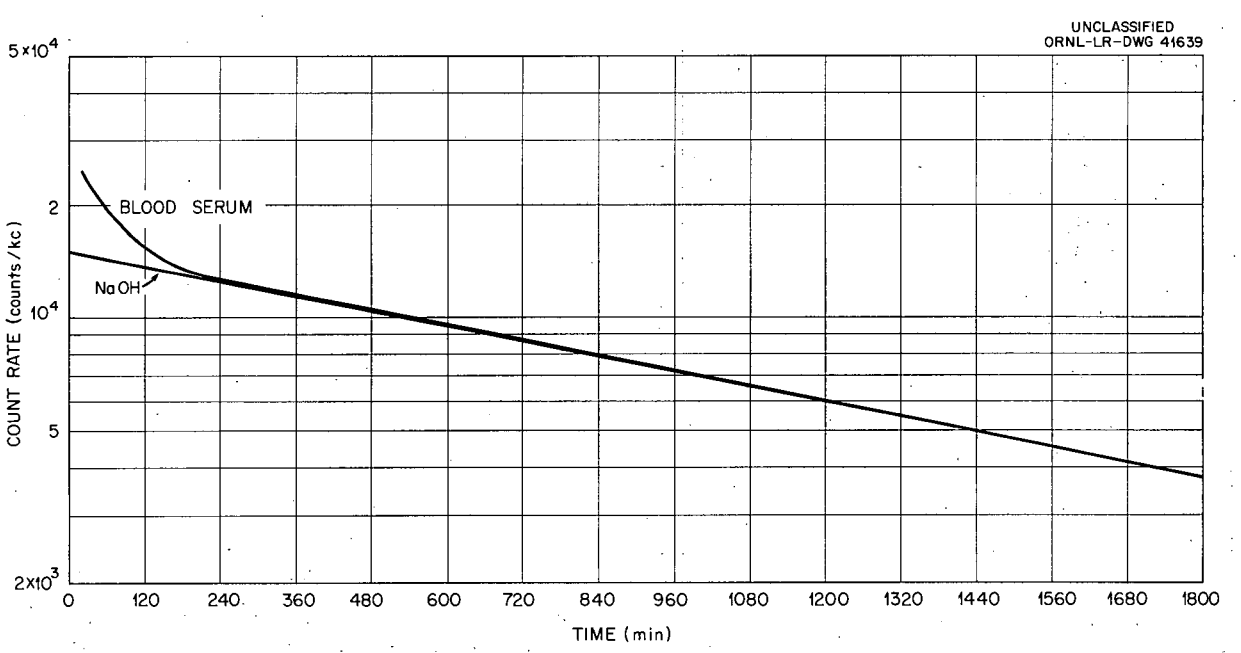

Fig. 105. Count Rates of Blood Serum and NaOH Solution Samples Irradiated by Thermal Neutrons in the ORNL Graphite Reactor Slant Animal Tunnel.

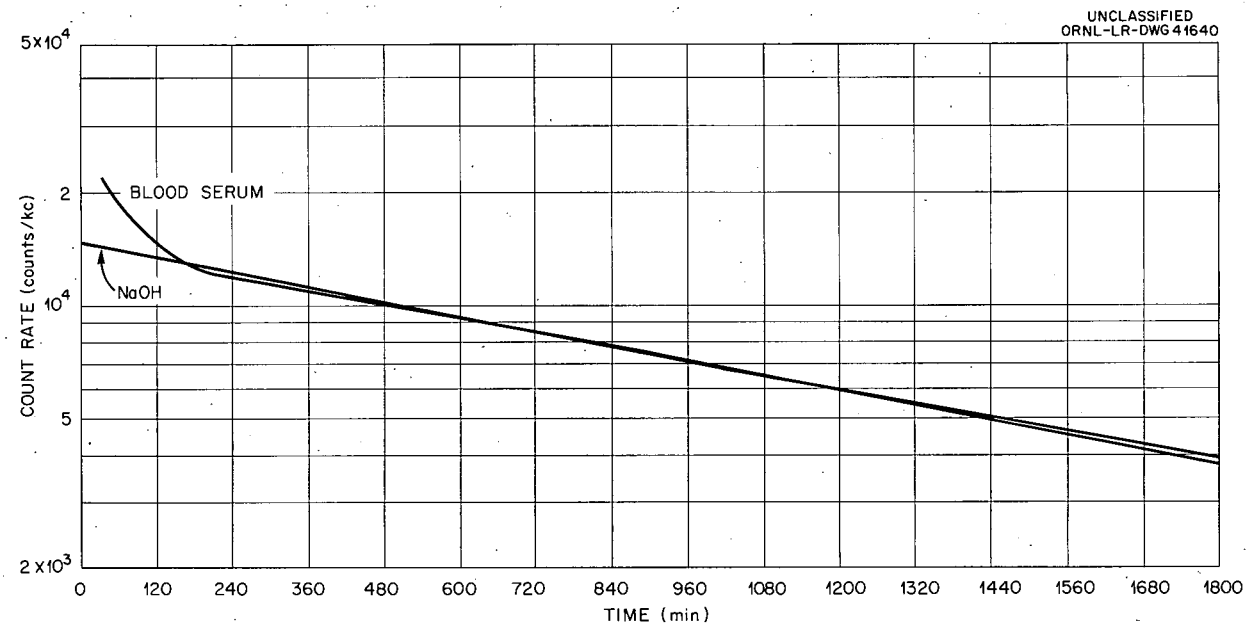

Fig. 106. Count Rates of Blood Serum and NaOH Solution Samples Irradiated by Fission Neutrons in the ORNL Graphite Reactor West Bunny Tunnel.

Eight individuals received appreciable doses of radiation during this excursion. A physical analysis of this accident has been reported by Callihan.[17]

Very early estimates of the doses received by the individuals, based on the total number of fissions which occurred, were unreasonably high. For example, the fast-neutron component of the total dose received by one employee was estimated to have been 1500 rads. This dose plus the gamma dose was much greater than his medical symptoms indicated. Therefore, it was assumed that the location of the personnel during a substantial fraction of their exposure time was not known and that fissions occurred over a time interval comparable with the exposure times. This, together with the fact that those exposed were not wearing personnel monitoring equipment (with the exception of an indium foil in the security badge), dictated that the evaluation of the doses be based on the activation of body elements. Experience at Los Alamos in the Pajarito accident[18] indicated that, of the body fluid methods, the formation of Na^{24} in blood may be the most reproducible measure of neutron exposure.

The final dose values inferred from the Na^{24} activity are believed to be reasonably accurate (approximately ±20%) and were obtained by the following procedure:

1. Blood samples were collected from the eight exposed employees and were counted for Na^{24} activity.
2. A burro was exposed to a steadily operating mockup of the liquid assembly in order to determine the relation between blood Na^{24} and the incident neutron dose. The ratio of gamma dose to neutron dose was also measured for this mockup assembly.
3. A parallel but independent determination of the neutron and gamma dose leaking from the assembly was made by calculation alone.

The human body is several mean free paths thick for neutrons. Consequently, the probability that a neutron will be captured as a thermal neutron is not a sensitive function of its initial energy. The body is approximately equivalent to the long counter used so much in neutron flux measurement. Calculations by Snyder and Neufeld[19] yield results from which the thermal capture probability as a function of neutron energy may be obtained for a

[17] D. Callihan and J. T. Thomas, *Health Phys.* 1(4), 363–72 (1959).

[18] L. H. Hempelmann, H. Lisco, and J. G. Hoffman, *Ann. Internal Med.* 36, 279–510 (1952).

[19] W. S. Snyder and J. Neufeld, *Brit. J. Radiol.* 28, 342 (1955).

30-cm slab phantom subjected to normally incident radiation. Figure 107 shows the capture probability vs E for a slab and for a cylindrical phantom. The results for the cylinder were obtained from the slab values by making approximate corrections for the boundary effect. A more accurate Monte Carlo calculation of this quantity for the cylinder is planned. It is important to note that the $\xi(E)$ curve is appreciably lower at thermal energy than it is over most of the fast portion of the spectrum, indicating that thermal buildup from room scattering may be unimportant in many cases.

Experimental Evaluation of the Dose. – To establish experimentally the relationship between the total first-collision dose and the blood sodium activation, a mockup of the critical assembly was constructed and operated as a low-power reactor in two experiments. Table 38 shows a comparison between the mockup assembly and the actual critical assembly.

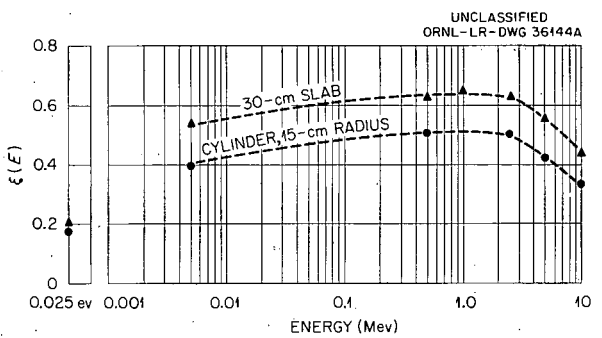

Fig. 107. Thermal Capture Probability for Unit Incident Flux.

Table 38. Comparison of the Mockup Critical Assembly with the Actual Critical Assembly

	Actual Critical Assembly	Mockup Critical Assembly
Diameter, in.	22	20
Height, in.	9.2	15
U^{235} concentration, g/liter	37.4	25.9
Total U^{235}, kg	2.1	2.00

The first experiment was designed to measure the ratio of gamma dose to neutron dose in the radiation field around the reactor. The assembly was operated at a power level of about 6 w for 11 min.

Figure 108 shows a schematic of the mockup experiment with the reactor tank surrounded by a larger tank shield. The gamma dose at point A, 6 ft from the center of the assembly, was measured with an ion chamber having carbon walls and containing CO_2 gas. The chamber was calibrated with Co^{60} radiation to read the first-collision gamma tissue dose in rads. Measurements of the neutron dose were made at the same distance using

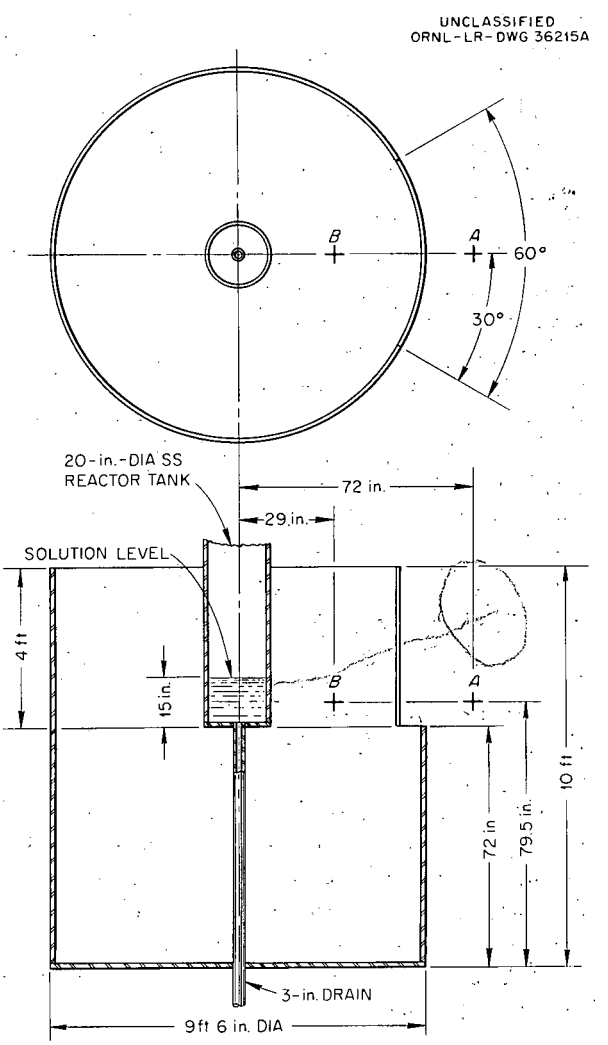

Fig. 108. Schematic Drawing of the Mockup Experiment.

the Radsan fast neutron dosimeter[20] which employs the absolute proportional counter.[21] (The neutron spectrum data could be used to correct the readings of the carbon wall–CO_2 gas chamber for its response to neutrons.) A gamma-neutron dose ratio of 3.3 was found.

Since this ratio is valid only for the reactor which had been running at constant power for about 3 min, a correction to the exposure conditions of the accident was necessary. The exposure conditions were taken to be (1) that a pulse of neutrons was emitted instantaneously and (2) that only the first 15 sec of the delayed gamma radiation was effective before the exposed people left the area. The experimental results of Maienschein, Peelle, Zobel, and Love[22] for the spectrum of delayed gammas were used to correct the measured ratio. The corrected ratio was found to be 2.8. The correction is insensitive to the way in which neutrons are generated during the exposure time of the people. For example, the assumption that the Y-12 accidental nuclear reaction occurred under steady power conditions for 15 sec and that those exposed were irradiated during a 15-sec period changes the results by only a few per cent.

In the second experiment with the mockup assembly, a burro was exposed so that the center of his body was located at point *A*, where the dose was measured in the first experiment. The burro was chosen as the experimental animal because he is comparable in size with man and because his blood sodium concentration is approximately the same as that of man.

The second experiment was conducted at a power level of approximately 300 w for 42 min, giving the burro a first-collision neutron dose of 48 rads. Blood samples were drawn and counted for Na^{24}.

These samples and samples from the exposed men were counted with a 2- by 4-in. NaI crystal as shown in Fig. 109. The polyethylene bottles containing whole blood with a small amount of heparin added to prevent clotting were placed on top of the crystal. Counting was done with an integral discriminator set at 0.66 Mev and 2.0 Mev.

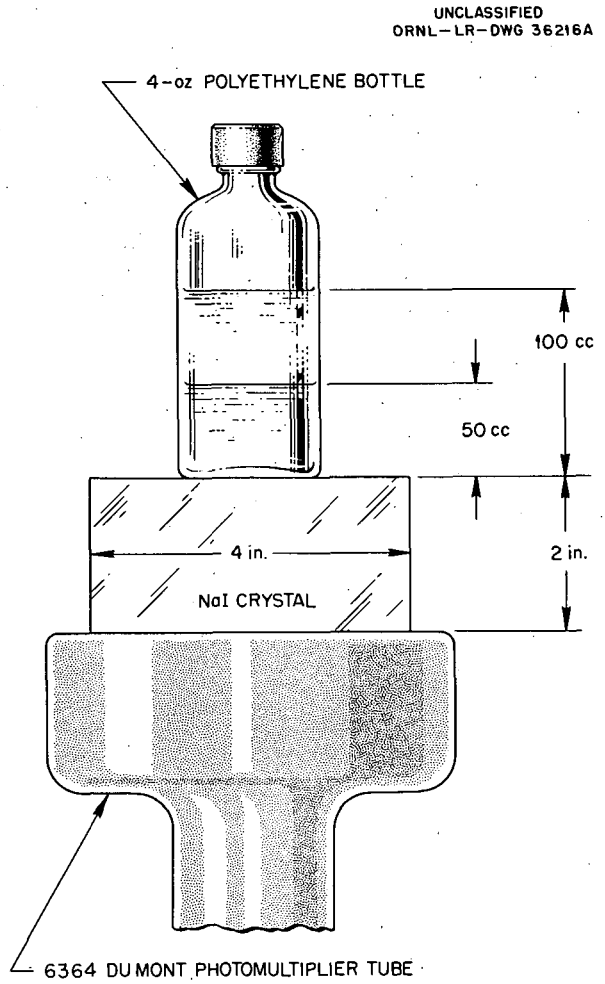

Fig. 109. Diagram Showing Blood-Counting Method.

The equipment was calibrated with 50-cc and 100-cc aqueous solutions of Na^{24}. The counting method is very sensitive; a dose of 1 rad can be detected easily with the present apparatus, and with minor improvements in counting techniques it should be possible to determine doses as low as 100 mrads.

The mockup experiment using the burro gives a direct determination of the conversion factors from Na^{24} concentration to neutron and gamma dose, if it is assumed that the neutron and gamma spectra, at distances at which the people were exposed, are the same as in the mockup.

During the exposure of the burro a series of threshold detectors were used to determine the fast-neutron spectrum. The neutron detectors (Au, Au + Cd, Pu^{239}, Np^{237}, U^{238}, and S^{32}) were

[20] E. B. Wagner and G. S. Hurst, *Rev. Sci. Instr.* **29**, 153 (1958).

[21] G. S. Hurst, *Brit. J. Radiol.* **27**, 353 (1954).

[22] F. C. Maienschein *et al.*, *Proc. U.N. Intern. Conf. Peaceful Uses Atomic Energy, 2nd, Geneva, 1958*, paper A/Conf.15/P/670 (1958).

exposed at approximately 29 in. from the center of the liquid assembly. From the experimental flux values the first-collision neutron dose was calculated at the position of the burro.

Calculations. – Following the accident the leakage spectra of the neutrons and the gamma rays were estimated. It is difficult to assess the accuracy of the methods employed to determine the fast-neutron leakage because of the complicated geometry of the actual assembly. However, the calculation agreed reasonably well with the measured spectrum. A more accurate calculation is planned in which stochastic methods will be employed. The leakage spectra were calculated under the assumption that the assembly could be considered spherical and that the distribution of nascent fission neutrons in the assembly can be adequately represented by the fundamental spatial distribution determined for a spherical reactor. The number of escaping neutrons in the Mev energy region was calculated by integrating over the volume source distribution using infinite medium penetration data for fission neutrons in water.[23] The low-energy end of the spectrum was calculated by multigroup methods. The resulting estimate of the escape spectrum is shown in Fig. 110. The ordinate in this figure is $EN(E)$, where $N(E)$ is the number of escaping neutrons per unit energy interval per fission in the sphere. From this curve the dose carried in the escaping field may be calculated, and from the $\xi(E)$ curve the Na^{24} concentration in the phantom may be determined. The dose (rads) per microcurie of Na^{24} per cubic centimeter of blood was found to be 1.95×10^5 compared with the experimental value of 1.67×10^5. Table 39 shows a comparison of the measured and calculated leakage spectra. The thermal component of the experimental spectrum is appreciably larger than the calculated value. The higher experimental value is probably caused by room scattering.

The leakage of gamma rays from the assembly was determined by using infinite-medium attenuation data and by considering three sources of

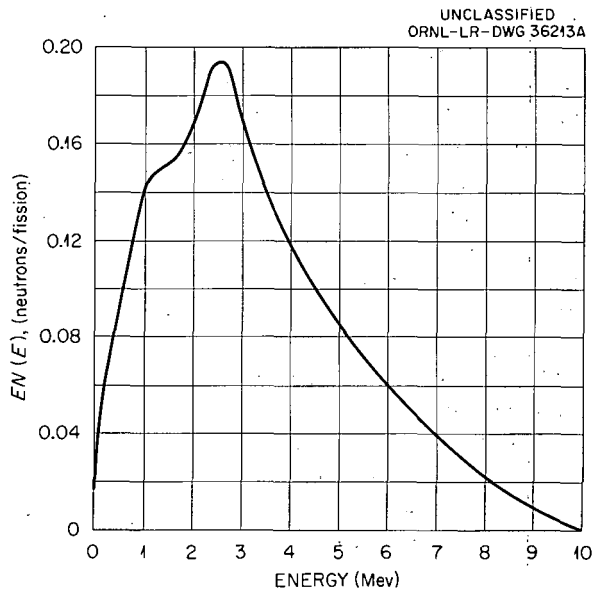

Fig. 110. Estimated Escape Spectrum.

[23] R. Aronson *et al.*, *Penetration of Neutrons from a Point Isotropic Fission Source in Water*, NYO-6267 (1957).

Table 39. Relative Flux Density of Neutrons for Various Energy Regions

Energy Range	Observed Flux Density (neutrons/cm^2)	Normalization of Flux Density	
		Observed	Theoretical
	$\times 10^{11}$		
Thermal	0.90	0.45	0.08
Total fast	2.0	1.00	1.00
0.5 kev to 0.75 Mev	0.25	0.125	0.30
0.75 Mev to 1.5 Mev	0.70	0.35	0.204
1.5 Mev to 2.5 Mev	0.58	0.29	0.246
>2.5 Mev	0.50	0.25	0.250

gamma radiation: (1) prompt fission gamma rays, (2) capture gamma rays from hydrogen and uranium capture, and (3) delayed gamma rays from fission. Figure 111 shows the spectra of prompt and delayed gamma rays. Integrating over the volume source distribution assumed for the sphere, the results shown in Table 40 are obtained. The variations between cases I, II, and III represent different delayed gamma distributions depending upon the actions of individuals after the alarm. Case II is believed to be the maximum gamma-neutron ratio for the exposed employees.

Table 41 shows a summary of the dose results for the eight exposed individuals and for the burro.

Table 40. Results of Gamma Dose Calculation for Three Individuals

Case No.	Dose $\left(\frac{\text{rad-cm}^2}{\text{fis}}\right)$				D_γ/D_n
	Prompt	Capture	Delayed	Total	
	$\times 10^{-9}$	$\times 10^{-10}$	$\times 10^{-10}$	$\times 10^{-9}$	
I	2.06	6.4	4.0	3.10	2.87
II	2.06	6.4	9.4	3.64	3.37
III	2.06	6.4	6.4	3.34	3.09

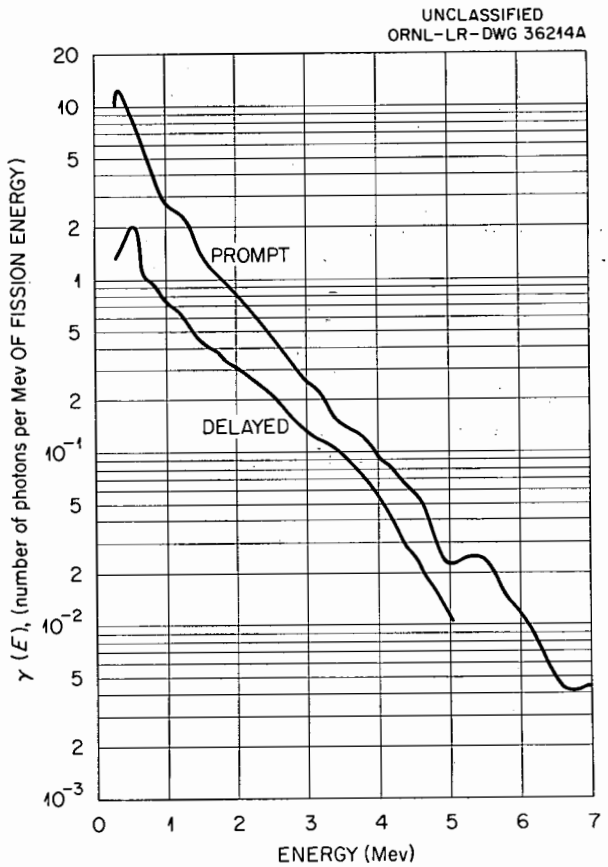

Fig. 111. Spectra of Prompt and Delayed Gamma Rays.

Table 41. Na^{24} Activation and Dose Values for Exposed Personnel

Employee	Na^{24} (μc/cc)	Neutron Dose (rads)		Gamma Dose (rads)		Total Experimental Dose (rads)
		Experimental	Theoretical	Experimental*	Theoretical**	
	$\times 10^{-4}$					
A	5.8	96	113	269	349	365
B	4.3	71	83	199	256	270
C	5.4	89	104	250	321	339
D	5.2	86	100	241	308	327
E	3.7	62	72	174	223	236
F	1.1	18	21	50.5	64.9	68.5
G	1.1	18	21	50.5	64.9	68.5
H	0.36	6.0	7.0	16.8	21.6	22.8
Burro	2.9	48				

*Using $D_\gamma/D_n = 2.8$.
**Using $D_\gamma/D_n = 3.08$.

THEORETICAL PHYSICS OF DOSIMETRY

J. Neufeld
P. H. Doyle[24]
H. B. Eldridge
R. H. Ritchie
W. S. Snyder
P. R. Flusser[25]

The Behavior of Plasma at Ionic Resonance

An electromagnetic wave having its wave vector parallel to the direction of the steady magnetic field H is attenuated in plasma very effectively when the frequency ω is equal to the ionic resonance frequency Ω_g of the plasma. A small localized periodic disturbance initiated in a plasma in thermodynamic equilibrium at $t = -\infty$ and having frequency $\omega = \Omega_g$ produces along the direction of the magnetic field a wave motion characterized by a complex wave vector

$$k \sim \left(\frac{\Omega_0 \Omega_g}{c^2 u_{0i}}\right)^{1/3} (\sqrt{3} + i) ,$$

where Ω_0 is the Langmuir frequency and u_{0i} is the mean thermal velocity of the ions in the plasma. The attenuation per wavelength at the resonance frequency is substantial, since

$$\frac{Im(k)}{Re(k)} = \frac{1}{\sqrt{3}} .$$

However, the attenuation per unit of length is not a maximum at ionic resonance, since it increases with increasing frequencies when ω passes through the resonance. This is shown by the fact that for $\omega = \Omega_g$ we have $Im(dk/d\omega) > 0$, since at resonance

$$Im\left(\frac{dk}{d\omega}\right) = \frac{K_1}{u_{0i}} + \left(\frac{K_2}{u_0^2 u_{0i}}\right)^{1/3} ,$$

where K_1 and K_2 are appropriate positive constants and u_0 is the velocity of the magnetohydrodynamic wave.

Occurrence of Vavilov-Cerenkov Radiation in a High-Temperature Plasma

Akhiezer and Sitenko[26] investigated the energy loss of a charged particle moving through a plasma at a velocity considerably lower than the mean thermal velocity of the electrons in the plasma and determined the component of the stopping power due to the transverse electric field produced by the plasma and acting upon the particle. The presence of such a component may in some instances be associated with the occurrence of the Vavilov-Cerenkov radiation. It is shown, however, that in this particular case the field surrounding the particle decreases very rapidly with the distance from the particle, and no radiation takes place.

Thermal Neutron Flux Depression

The question of the depression of the flux by an absorbing foil placed in a medium in which thermal neutrons diffuse is important in the standardization of neutron source strengths and fluxes and in the calibration of detectors (e.g., the Hurst neutron threshold detector system). Some theoretical work has been done on this problem,[27,28] but some confusion exists among experimenters both as to the proper way of making corrections for this effect and as to whether a given correction formula is superior to another one (e.g., the Bothe theory vs the Skyrme theory).

The flux depression problem may be stated briefly as follows: A foil of some specified shape is inserted into a medium in which there exists some (usually time independent) spatial distribution of neutrons in thermal equilibrium with the medium. The medium is characterized by a diffusion length L and a mean free path ℓ. Alternately the absorption cross section σ_a and the total cross section σ may be specified. If the activity of the foil is A atoms·cm^{-3}·sec^{-1}, the question is: what was the neutron flux ϕ_0 (neutrons·cm^{-2}·sec^{-1}) at the point of measurement before the foil was inserted?

Bothe[27] was the first to consider this problem in detail. He schematized the problem by assuming that the flux is originally constant at the value ϕ_0 everywhere throughout the medium and that first-order diffusion theory describes the transport of neutrons in a medium. He considered a disk-shaped foil, but his work applies (strictly) to the case of a small spherical detector.

---

[24] Consultant.

[25] Summer employee.

[26] A. I. Akhiezer and A. G. Sitenko, *Zhur. Eksptl. i Teoret. Fiz.* 23, 161 (1952); this paper appeared in English translation as British Atomic Energy Project Report AERE Lib/Trans. 759.

[27] W. Bothe, *Z. Physik* 120, 437 (1943).

[28] T. H. R. Skyrme, MS-91.

His result may be summarized as follows: if $\bar{\phi}(\tau, L)$ is the average flux in the foil, then

$$\frac{\bar{\phi}(\tau, L)}{\phi_0} = \frac{\frac{1}{\tau}\left[\frac{1}{2} - E_3(\tau)\right]}{1 + \left[\frac{1}{2} - E_3(\tau)\right] g_B(L/\ell, a)}, \quad (1)$$

where τ is the foil thickness in units of mean free paths for absorption in the foil and a is the radius of the foil. Explicit formulas are given for g_B in ref 27.

Skyrme treated the problem by transport-perturbation theory, employing essentially the same assumptions as above. He finds that

$$\frac{\bar{\phi}}{\phi_0} = \tau\left[1 - \tau\left(\frac{1}{2}\ln\frac{1}{1.78\tau} - \frac{3}{4} + g_S\right)\right], \quad (2)$$

which may be written

$$\frac{\bar{\phi}}{\phi_0} \cong \frac{1}{\tau}\left[\frac{1}{2} - E_3(\tau)\right]\left\{1 + \left[\frac{1}{2} - E_3(\tau)\right] g_S\left(\frac{L}{\ell, a}\right)\right\}^{-1} \quad (3)$$

to the same order of accuracy in which he worked. The quantity $g_S(L/\ell, a)$ is a function which is presented graphically by Skyrme for rather limited ranges of the arguments. Skyrme's work seems quite consistent and somewhat more convincing than that of Bothe, since he resorts to transport theory rather than diffusion theory, but it suffers from the uncertainty attending a perturbation approach when $\tau \sim 1$.

Since a good deal of confusion has arisen concerning the domain of applicability of these two solutions of the flux depression problem, it seems well worthwhile to consider a case which may be treated by transport theory and for which fairly exact numerical results for arbitrary τ's may be obtained. Such a solution serves as a common ground for the comparison of the theories of Skyrme and Bothe and also aids in the interpretation of experimental results in this field. The problem which has been treated is that of the flux depression in the neighborhood of a semi-infinite plane foil ($a \to \infty$) immersed in a diffusing medium. The idealization which will be assumed is (1) that thermal neutrons scatter isotropically in the laboratory system, (2) that their transport in matter is described by the one-speed neutron transport equation, (3) that there is initially a uniform distribution of the flux in a medium before the foil is inserted, and (4) that there is no scattering in the foil. The transport equation may be written in the following way for this problem. Let $\phi(x)$ be the flux at a distance x from the foil, where x is measured in units of total mean free path. If

$$\frac{\phi(x)}{\phi_0} \equiv 1 - f_0(x), \quad (4)$$

then

$$f_0(x) = \frac{\gamma}{2}\int_0^\infty f_0(x')\,dx'\left[E_1(|x - x'|) + E_1(x + x' + \tau)\right] + \frac{1}{2}\left[E_2(x) - E_2(x + \tau)\right], \quad (5)$$

where $\gamma = \sigma_S/\sigma$.

If the functional is defined as

$$F(f) = \int_0^\infty f(x)\,dx\left\{E_2(x) - E_2(x + \tau) + \frac{\gamma}{2}\int_0^\infty f(x')\,dx'\left[E_1(|x - x'|) + E_1(x + x + \tau)\right] - f(x)\right\}, \quad (6)$$

then it may be shown that $F(f)$ is an extremum when $f(x) = f_0(x)$ and that $F(f_0)$ is a lower bound to $F(f)$. Further,

$$\frac{\bar{\phi}}{\phi_0} = \frac{1}{\tau}\left[\frac{1}{2} - E_3(\tau) - \gamma F(f_0)\right],$$

so that the value of $\bar{\phi}/\phi_0$ obtained by using a trial function for f_0 has the true value of $\bar{\phi}/\phi_0$ as its lower bound. It was decided that a good trial function would be a sum of exponential functions of the form

$$f(x) \cong \sum_{i=1}^{n} A_i e^{-a_i x} ,$$

where the a_i are taken from spherical harmonics theory. This establishes a connection between simple first-order diffusion theory ($n = 1$) and allows convergence of the spherical harmonics series in this particular case to be tested. By this means the solution of the variational problem is reduced to the solution of a set of n linear simultaneous equations for the A_i:

$$\sum_{j=1}^{n} C_{ij} A_i = S_i ,$$

where the C_{ij} and S_i are simple algebraic functions of a_i, τ, and γ. Solving this set of equations, $\bar{\phi}/\phi_0$ may be expressed in the same general form as above; that is,

$$\frac{\bar{\phi}}{\phi_0} = \frac{\frac{1}{\tau}\left[\frac{1}{2} - E_3(\tau)\right]}{1 + \left[\frac{1}{2} - E_3(\tau)\right] g_v(\tau_1 L/\ell)} .$$

In this equation g_v is a function of τ, unlike the corresponding quantity in the Bothe and Skyrme equations.

In Fig. 112, g_v is plotted as a function of $1/n$, where n is the number of terms in the trial function for small and large values of τ when $\gamma = 0.5$. The convergence is reasonably fast here with a five-term trial function giving an error of $\sim$2%. For values of $\gamma \sim 1$, which are usually found in practice, the error to be expected for $n = 5$ is much smaller than this.

Taking $n = 5$, a number of values of g_v have been calculated on the Oracle as a function of τ for various values of L/ℓ. Generally it was found that for $\tau \ll 1$, g_v is approximately equal to $g_S(L/\ell, a \to \infty) \equiv g_S^{\infty}$, while for $\tau \gg 1$, g_v approaches a value only slightly larger than $g_B(L/\ell, \infty)$ asymptotically.

Figures 113–15 show $g_v(L/\ell, \tau)$ as a function of τ for various values of L/ℓ. The results for a rather large range of values of L/ℓ [2(2)20, 20(5)30] show that for the small values of τ ($\lesssim 0.2$) ordinarily used and for L/ℓ values commonly encountered in practice, g_S^{∞} instead of

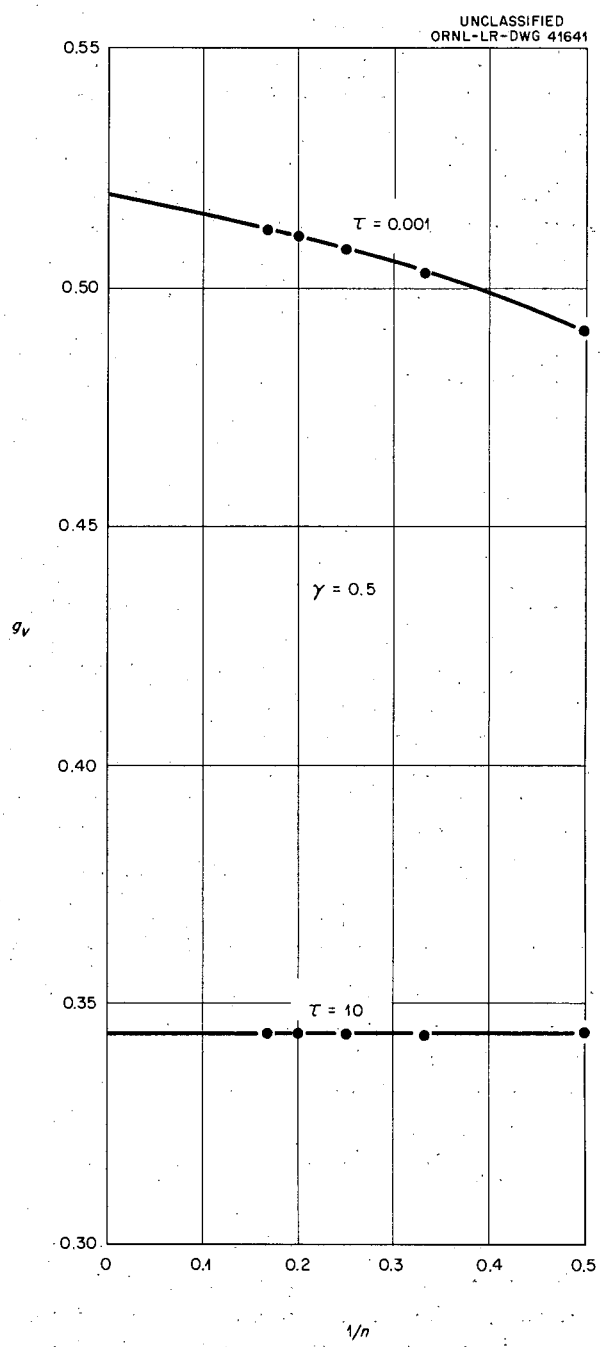

Fig. 112. Convergence of Trial Function.

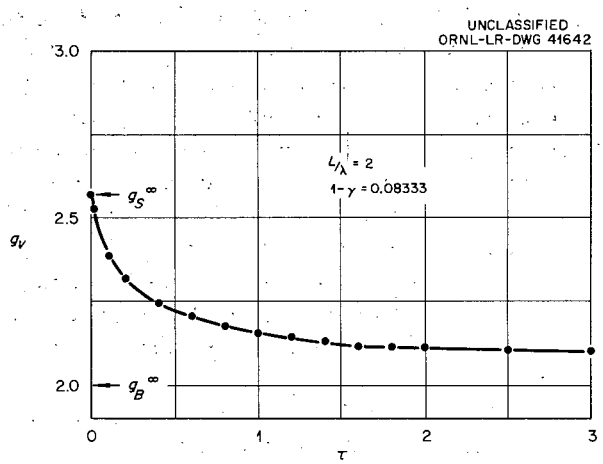

Fig. 113. Flux Depression Function vs Foil Thickness.

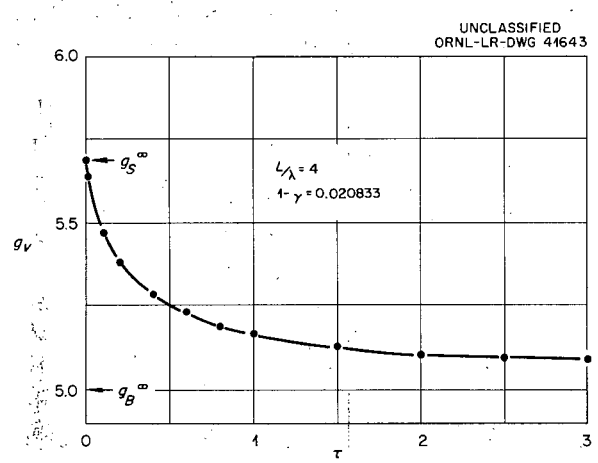

Fig. 114. Flux Depression Function vs Foil Thickness.

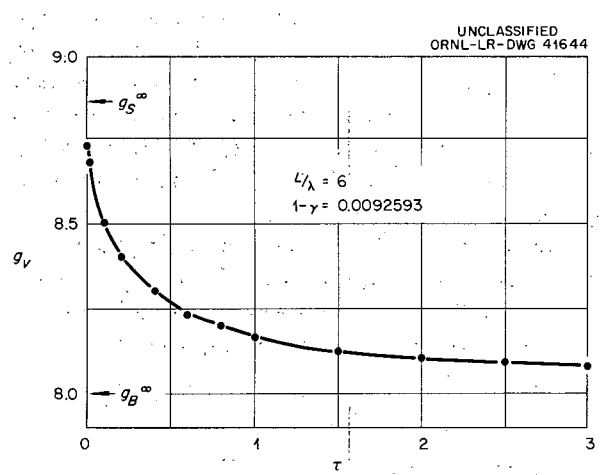

Fig. 115. Flux Depression Function vs Foil Thickness.

g_v may be employed with an error of less than 1% in ϕ/ϕ_0. If a finite disk-shaped foil ($a \neq \infty$) is involved, rather good results may be obtained by using Eq. (3), where

$$g_S\left(\frac{L}{\ell, a}\right) = D_1 - D_1'$$

is used in Skyrme's notation. The functions D_1 and D_1' are not evaluated by Skyrme as completely as might be desired. Consequently, g_S has been re-evaluated and is presented in the following form:

$$g_S = \frac{3}{2}\frac{L}{\ell}\left(1 - \frac{\ell^2}{L^2}\right) S\left(\frac{2a}{L}\right) - K\left(\frac{2a}{L}, \gamma\right) .$$

The Skyrme function $S(x)$ is presented in Fig. 116, and the function $K(S, \gamma)$ is plotted in Fig. 117.

Radiation of Photons by Films Bombarded by Charged Particles

One of the most interesting properties of a metal is the ability of its conduction electrons to sustain oscillations. They are capable of being excited coherently and can absorb energy in multiples of the plasma energy $\hbar\omega_p$, where ω_p is the characteristic "plasma" frequency. In

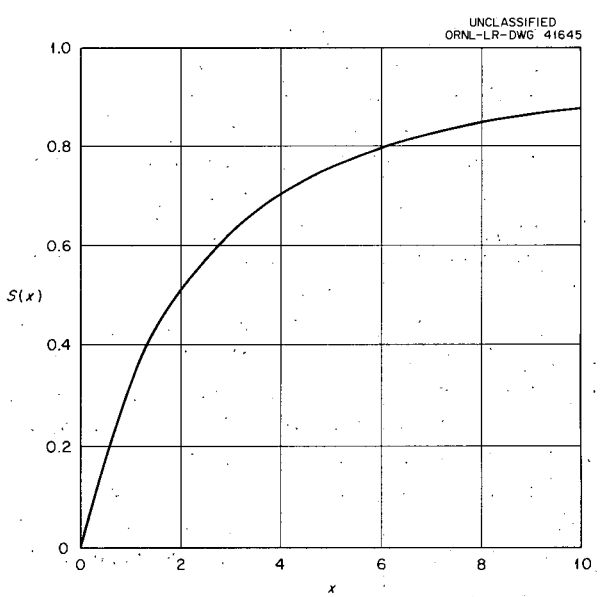

Fig. 116. The Skyrme Function

$$S(x) = 1 - \frac{4}{\pi}\int_0^1 \sqrt{1 - t^2}\, e^{-xt}\, dt .$$

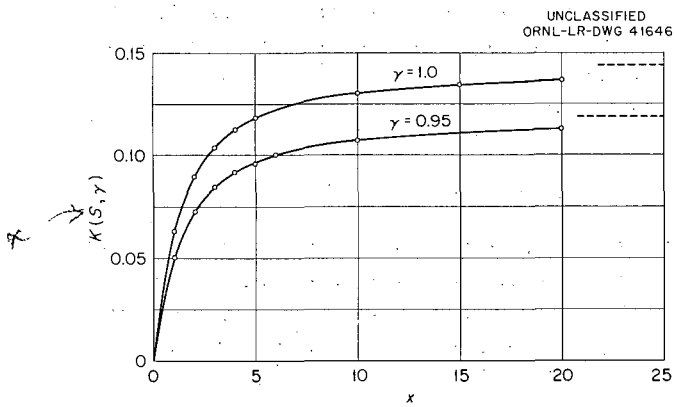

Fig. 117. $K(S)$ – Correction to Flux Depression Function for a Finite Foil.

the past several years many investigators have performed differential stopping experiments in which "characteristic losses" of electrons in solids have been observed. Fast electrons are allowed to penetrate thin foils, and their energy loss is determined. It is found that these losses occur in multiples of a fundamental loss unit which compares favorably with $\hbar\omega_p$ in metals. Since these losses are only a few volts in many thousands, high precision spectroscopy is required. Such studies have stimulated much work in the theory of many-body interactions in solids.

Ferrell[29] has suggested that a promising method of studying these losses is by looking for stimulated photon emission from metals at their characteristic frequencies. These photons may be easier to detect than the differential energy loss of the charged particles themselves.

Ferrell has discussed the physics of this emission process in a very illuminating manner and has evolved a theory which predicts the yield of these photons. However, his theory does not contain the effects of retardation in a consistent way and consequently is not complete. The "transition" radiation emitted by a charged particle in passing through a boundary between two dielectric media has been treated in a number of Russian papers.[30] The approach of these workers may be easily generalized to a complete classical treatment of stimulated emission from a finite foil having a realistic dielectric variation with frequency. It is well known that a fast-charged particle is equivalent, for many purposes, to a nearly "white" source of electromagnetic radiation. Hence this problem may be considered to be one of investigating the reflection and transmission by a metal of photons having the joint distribution in frequency and angle characteristic of a swiftly moving electric charge. In this viewpoint, the advantage of charged particles in such experiments lies in the fact that they are easily obtainable sources of high-energy photons of known spectral distribution.

An experimental arrangement which might be employed, then, is a metal foil a few thousand angstroms thick having electrons incident normally upon it. Maxwell's equations for the equivalent classical electrodynamical situation can be written as follows:

$$\overline{\nabla} \cdot \overline{H} = 0 \ ,$$

$$\epsilon(\omega)\, \overline{\nabla} \cdot \overline{E} = -4\pi e\, \delta(\overline{r} - \overline{v}t) \ ,$$

$$\overline{\nabla} \times \overline{E} = -\frac{1}{c}\frac{\partial \overline{H}}{\partial t} \ ,$$

$$\overline{\nabla} \times \overline{H} = \frac{\epsilon(\omega)}{c}\frac{\partial \overline{E}}{\partial t} - \frac{4\pi}{c}\, \overline{v}e\, \delta(\overline{r} - \overline{v}t) \ .$$

These equations must be solved in the three media, subject to the boundary conditions that the tangential components of $\overline{E}$ and $\overline{H}$ must be continuous at the surfaces. The form of the solution is sought which dominates at large distances from the foil, and the Poynting vector in this region as a function of angle with respect to the foil normal is calculated. The solution is similar to the solution of the famous problem, first solved by Sommerfeld, of the radiation from a dipole above a plane boundary.

It is found that $N(\omega)$, the number of photons of frequency ω emitted per unit frequency interval in the direction θ with respect to the foil surface, may be expressed in the following way:

$$N(\omega, \theta)\ d\omega\ d\Omega$$

$$= \frac{1}{137} \cdot \left(\frac{v}{c}\right)^2 \cdot \frac{d\omega}{\omega} \cdot f(\theta, \omega, \beta, t)\, d\Omega \ ,$$

where t is the foil thickness and f varies slowly

[29] R. A. Ferrell, *Phys. Rev.* 111, 1214 (1958).

[30] See, e.g., I. Frank and V. Ginsburg, *J. Phys. (U.S.S.R.)* 9, 353 (1945); G. M. Garibian, *Soviet Phys. JETP* 6, 1079 (1958).

with β and t. Although the photon distribution diverges as $\omega \to 0$, the total energy emitted is finite, as in the case of ordinary bremsstrahlung.

By integrating over the whole hemisphere of directions (in the case $t \to \infty$, $\beta = v/c \ll 1$) the curve given in Fig. 118 is found. The intensity distribution $\omega N(\omega)$ is plotted against ω, for an ideal metal with $\epsilon(\omega) = 1 - \omega_p^2/\omega^2$. Although there is a peak at the plasma frequency, there is clearly a large background of low-energy photons which might interfere with a measurement of the characteristic emission frequency. At low frequencies, a metal is a perfect reflector for low-energy photons. The incoming charge sets up an image charge in the metal which annihilates the real charge upon its entry into the metal. Hence for $\omega \ll \omega_p$ the pattern of radiation is roughly that of a charge at the surface decelerated normal to the surface. Figure 119 shows the angular distribution of this radiation at various frequencies. It is clear that an experimental apparatus designed to detect the characteristic frequency should sample photons in directions around the normal to the foil.

A detector which has a solid angle of 10^{-2} that of a sphere, located at an angle of 30° with the normal to the foil and accepting photons of energy $\hbar\omega_p$ (in the range $\Delta(\hbar\omega) = \pm 0.13\ \hbar\omega_p$) generated by 100-kev electrons striking an aluminum surface, should detect $\sim 2 \times 10^{-5}$ photon per incident electron.

The detection of coulomb-stimulated photon emission from metals seems a promising and practical method of studying characteristic electron losses in these metals.

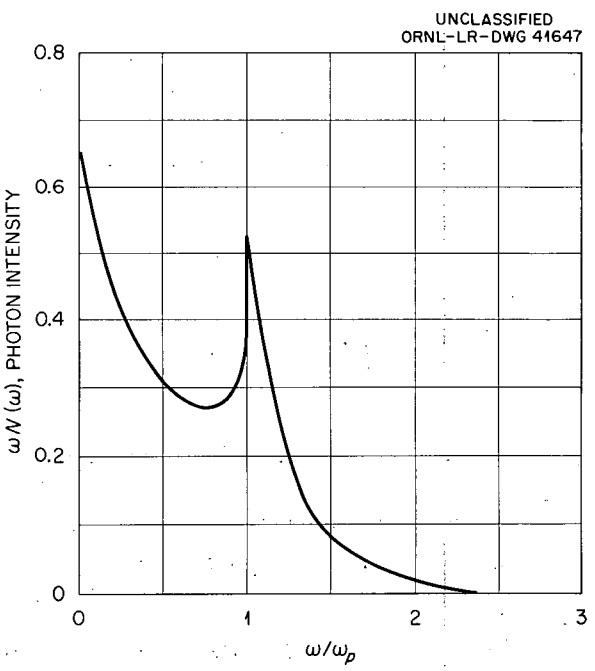

Fig. 118. Emitted Photon Intensity Integrated Over the Hemisphere.

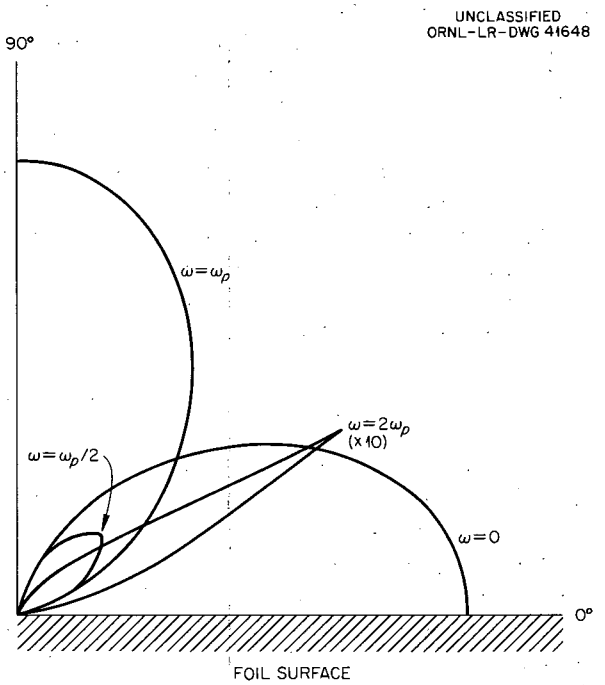

Fig. 119. Angular Distribution of Photon Intensity.

Image Force at a Metal Surface from the Hydrodynamic Theory of the Free Electron Gas

The image force acting on a charge lying outside a metal is of interest in the theory of the potential barrier encountered by an electron crossing such a surface. The form of the potential is of importance in the theory of the Schottky emission and thermionic emission as well as in the prediction of the reflection of monoenergetic electrons impinging on metals. Reflection calculations[31] are usually made by assuming that the

[31] See, e.g., L. A. MacColl, *Phys. Rev.* **56**, 699 (1939); L. W. Nordheim, *Proc. Roy. Soc. (London)* **A121**, 626 (1928); E. Guth and C. J. Mullin, *Phys. Rev.* **59**, 575 (1941); C. Herring and M. H. Nichols, *Revs. Modern Phys.* **21**, 185 (1949).

potential acting on an electron outside a metal is of the classical form for large distances but breaks down at a few angstroms from the surface. Bardeen[32] has given a quantum mechanical justification for the use of this image potential but has shown that this classical form of the potential is not valid at small distances from the surface. More recently, Sachs and Dexter[33] have calculated an approximate quantum mechanical correction to the classical image force theory using the Thomas-Fermi equations. They found a correction term to the classical image formula which gives approximate agreement with the result of Bardeen. Although they formulate a differential equation which could be solved to give the potential function continuously through the surface and into the metal, no solution of this equation is given.

The Bloch hydrodynamic equations for the free electron gas have been applied to the calculation of the stopping power of the statistical atom,[34] to the prediction of a universal photoelectric curve,[35] and more recently[36] to a treatment of surface oscillations in a metal foil. These equations may be applied also to the determination of the image potential. A complete description of the potential at points both in and outside the metal is obtained, and an analytical representation is presented below. The assumption is made that the electronic density decreases abruptly to zero in passing through the surface from the interior of the metal.

Suppose that the metal is confined to the region $z > 0$. Assume that there is a point charge located on the z axis at $-z_0$, outside the plasma. In the time-independent case, the linearized Bloch equations may be reduced to a single equation for n, the perturbation in the electron density, that is,

$$\nabla^2 n - \frac{1}{D^2} n = 0 \qquad \left(D^2 \equiv \frac{\beta^2}{\omega_p^2} \right), \tag{1}$$

while Poisson's equation for the electric potential reads

$$\nabla^2 \phi = 4\pi e [n + \delta(x)\,\delta(y)\,\delta(z + z_0)] \ , \tag{2}$$

subject to the boundary condition

$$\frac{\partial \phi}{\partial z} = 4\pi e D^2 \frac{\partial n}{\partial z} . \tag{3}$$

This last equation follows from the requirement that the component of $\bar{v} = -\bar{\nabla}\Psi$ normal to the surface shall vanish. In the above equations ω_p is the "plasma" frequency in the metal, while $\beta = 1/\sqrt{3}$ times the Fermi velocity.

If both n and ϕ are expanded in Fourier integrals in the x and y coordinates, then

$$n(x, y, z) = \frac{1}{(2\pi)^2} \int_{-\infty}^{\infty} dk_x \int_{-\infty}^{\infty} dk_y e^{i(xk_x + yk_y)} n(k_x, k_y | z|) \ .$$

Therefore

$$\left[\frac{d^2}{dz^2} - \left(K^2 + \frac{1}{D^2} \right) \right] n = 0 \ , \tag{4}$$

$$\left(\frac{d^2}{dz^2} - K^2 \right) \phi = 4\pi e \left[n + \delta(z + z_0) \right] \ , \tag{5}$$

$$\frac{d}{dz} \phi = 4\pi e D^2 \frac{\partial}{\partial z} n \quad (z \to 0+) \ , \tag{6}$$

where $K^2 = k_y^2 + k_y^2$. The source-free solution of Eq. (4), which is bounded as $z \to \infty$, may be written

$$n \left(\frac{k}{z} \right) = A\, e^{-\left(\sqrt{K^2 + D^{-2}}\right) z} \ ,$$

and employing the Green's function for Eq. (5) gives

$$\phi \left(\frac{k}{z} \right) = - \frac{2\pi e}{k} \left[e^{-K|z+z_0|} + \int_0^{\infty} e^{-K|z-z'|} n \left(\frac{K}{z'} \right) dz' \right] .$$

If the boundary condition (6) is imposed, the

[32] J. Bardeen, *Phys. Rev.* **58**, 727 (1940).

[33] R. G. Sachs and D. L. Dexter, *J. Appl. Phys.* **21**, 1304 (1950).

[34] F. Bloch, *Z. Physik* **81**, 363 (1933); *Helv. Phys. Acta.* **1**, 358 (1934).

[35] J. A. Wheeler and E. L. Fireman, unpublished manuscript.

[36] R. H. Ritchie, *Phys. Rev.* **106**, 874 (1957).

constant A may be evaluated. The potential outside the plasma is found by

$$\phi(\rho, z<0) = -\frac{e}{\sqrt{\rho^2 + (z+z_0)^2}} + \frac{e}{d}\int_0^\infty \frac{d\eta J_0(\eta\rho/D)\, e^{\eta(z+z_0)/d}}{\left(\eta+\sqrt{\eta^2+1}\right)^2}, \quad (7)$$

where $\rho^2 = x^2 + y^2$. The first term on the right side of Eq. (7) is the potential due to the point charge at $(0, 0, -z_0)$. The second term represents the potential in $z < 0$ due to electrons in the plasma in the region $z > 0$. To look at its behavior for $(z+z_0)$, $\rho >> d$, the integrand of ϕ_i is examined for $\eta << 1$. It is found that

$$\phi_i \rightarrow \frac{e}{\sqrt{\rho^2 + (z+z_0)^2}} .$$

This is the image potential which is found in the classical case of a point charge located approximately a distance z_0 from an infinite metal surface.

The image potential evaluated at the position of the point charge is, from Eq. (7),

$$\phi(0, -z_0) \equiv \phi_{\text{image}} = \frac{e}{d}\int_0^\infty \frac{e^{-2\eta z_0/D}\, d\eta}{\left(\eta+\sqrt{\eta^2+1}\right)^2}$$

$$= \frac{e}{2D}\sum_{n=0}^{\infty} \frac{(+1)^n}{n!}\left(\frac{z_0}{d}\right)^n \left[E_{n+2}\left(\frac{z_0}{D}\right) + E_{n+4}\left(\frac{z_0}{D}\right)\right],$$

where

$$E_n(x) = \int_1^\infty e^{-xu}\frac{du}{u} .$$

To obtain ϕ_{image} inside the metal, the procedure is as before except that $z_0 \rightarrow -z_0$ and there is a source term $1/D^2\ (z-z_0)$ on the right side of Eq. (4). It is found that

$$\phi(\rho, z>0) = -e\frac{e^{-\sqrt{\rho^2+(z-z_0)^2}/D}}{\sqrt{\rho^2+(z-z_0)^2}} - \frac{e}{D}\int_0^\infty \frac{\eta\, d\eta\, J_0(\eta\rho D)\, e^{-(z+z_0)\sqrt{1+\eta^2}/D}}{\sqrt{1+\eta^2}\left(\eta+\sqrt{1+\eta^2}\right)^2} .$$

As in the case of the infinite plasma, the potential in the neighborhood of a point charge at greater than a few angstroms from the surface is of the Debye screened form. The image potential is given by $\phi(0, z_0)$, that is,

$$\phi_{\text{image}} = -\frac{e}{D}\int_0^\infty \frac{\eta\, d\eta\, e^{-2z_0\sqrt{1+\eta^2}/D}}{\sqrt{1+\eta^2}\left(\eta+\sqrt{\eta^2+1}\right)^2}$$

$$= -\frac{e}{2D}\sum_{n=0}^{\infty}\frac{1}{n!}\left(-\frac{z_0}{D}\right)^n \left[E_{n+2}\left(\frac{z_0}{D}\right) - E_{n+4}\left(\frac{z_0}{D}\right)\right].$$

The form of the image potential is sketched in Fig. 120. For comparison the dotted line shows the simple classical image potential $\phi/e = -1/2z_0$.

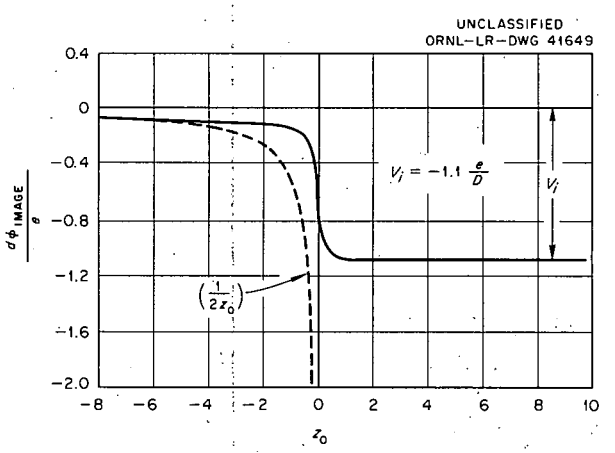

Fig. 120. Image Potential in the Neighborhood of a Metal Surface.

The discontinuity at $z_0 = 0$ arises from the Sommerfeld assumption that the potential in the neighborhood of a metal surface changes abruptly at the surface. The inner potential V_i has been taken to be $-1.1\ e/D$ in the case illustrated in Fig. 120. This result shows that the simple image potential is valid only at relatively large distances from the surface. The approximation, employed by MacColl,[37] that $\phi_{image} = -e/2z_0$ for z_0 larger than the value at which $-e/2z_0$ is equal to the inner potential, V_i, seems to be very unrealistic in view of the present results.

Monte Carlo Calculations of the Penetration of Weapons Radiation in Air

Extensive measurements of the transmission of neutrons and gamma rays from weapons at large distances in air have been made in the Ichiban Project.[38] The distribution in angle of both neutron and gamma-ray dose at various distances from weapons has been determined experimentally, and, in addition, neutron energy spectra have been obtained by the Hurst threshold detector techniques.

Some theoretical predictions of neutron and gamma transmission in an infinite homogeneous air medium are available.[39,40] A realistic approach to the calculation of the air-over-ground geometry appropriate to the experiments referred to above may be made by using stochastic methods. A neutron Monte Carlo code written at Los Alamos[41] has been modified to yield information pertinent to the Ichiban experiments. The source is assumed to emit monoenergetic neutrons isotropically at a point in air above a semi-infinite earth. The neutron flux is calculated on the surface of the interface at various distances from the source as a function of energy and of angle with respect to the source-detector line. The first collision dose as a function of the slant distance, R, and angle is calculated also. Preliminary results have been obtained by using this code. Figures 121–23 show the angular dependence of the dose with respect to the source-detector line at various distances on the interface from a point source of 7.0-Mev neutrons. The ordinates in the graphs give $2\pi D(\theta)$, where $D(\theta)$ is the dose per steradian, averaged over the angular intervals indicated on the abscissa. The strong forward peaking of the dose is clearly shown in these graphs.

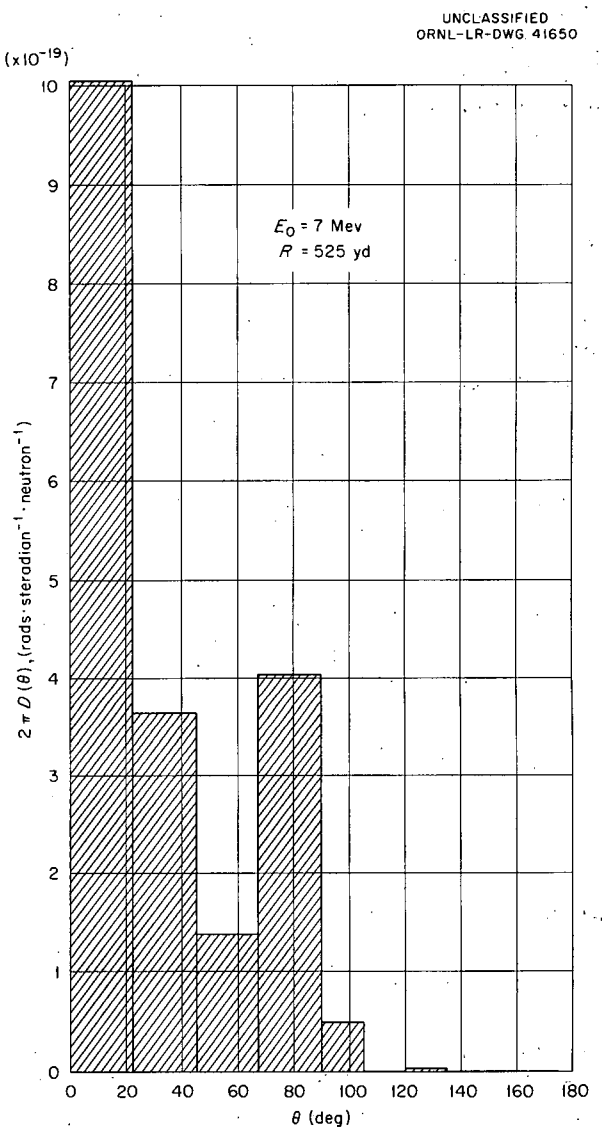

Fig. 121. Angular Distribution of Neutron Dosage.

[37] L. A. MacColl, *Phys. Rev.* **56**, 699 (1939).

[38] R. H. Ritchie and G. S. Hurst, *Health Phys.* **1**, 390 (1959).

[39] S. S. Holland and P. I. Richards, *J. Appl. Phys.* **27**, 1042 (1956).

[40] H. Goldstein and E. O. Wilkins, *Calculations of the Penetrations of Gamma Rays. Final Report*, NYO-3075 (June 30, 1954).

[41] W. Biggers and J. Pulos, unpublished work.

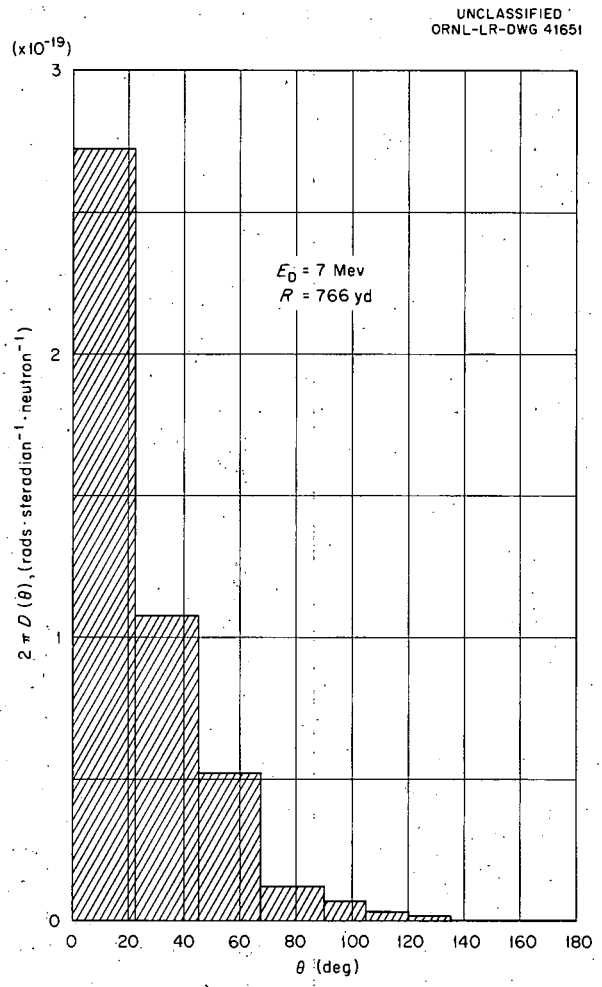

Fig. 122. Angular Distribution of Neutron Dosage.

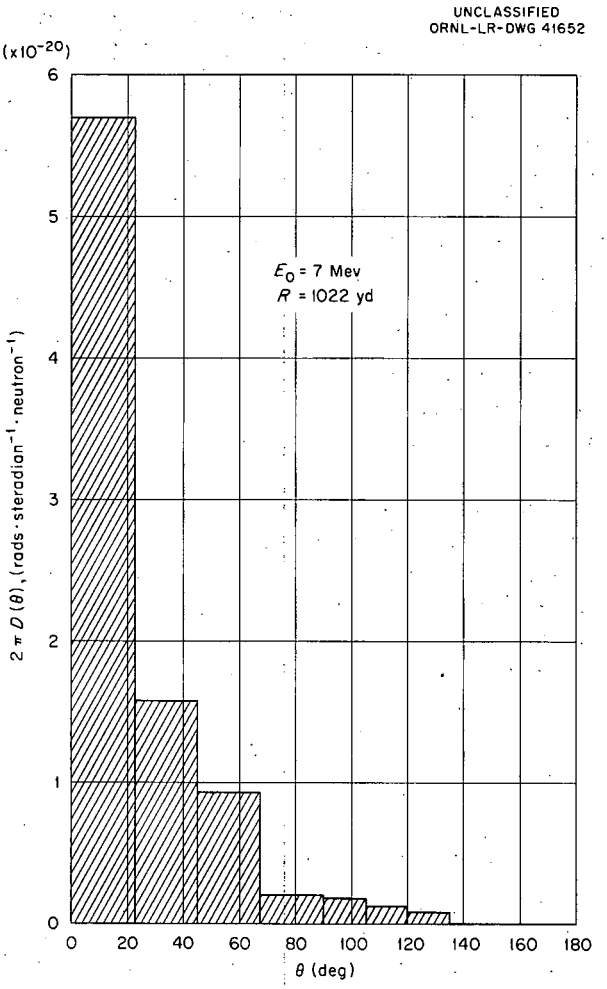

Fig. 123. Angular Distribution of Neutron Dosage.

PHYSICS OF TISSUE DAMAGE

H. P. Yockey[42] T. M. Sims[44]
D. R. Nelson[43] J. S. Mendell[45]
J. S. Gilliland[44]

Rochelle Salt Radiation Damage

The study of radiation effects on the ferroelectric properties of Rochelle salt ($NaKC_4H_4O_6 \cdot 4H_2O$) is nearly complete.[46] Rochelle salt crystals were irradiated with gamma rays and neutrons at both room and liquid-nitrogen (77°K) temperatures. The irradiated crystals were then sent to the Clevite Corporation for the ferroelectric measurements. Those crystals irradiated at liquid-nitrogen temperature were shipped in a special Dewar flask which kept the samples at 77°K.

Unirradiated Rochelle salt is ferroelectric between sharp temperature transitions (Curie points) at −17 and +24°C, while highly irradiated Rochelle salt loses its ferroelectric properties. Radiation causes the Curie-point temperatures to approach each other until the ferroelectric property is destroyed at a dose of between 1×10^6 and 3×10^6 r. The Curie temperature becomes

[42] Now at Aerojet General Nucleonics Corporation, San Ramon, Calif.

[43] Now at St. John's University, Collegeville, Minn.

[44] AEC radiological physics Fellowship student.

[45] Now at Rensselaer Polytechnic Institute, Troy, N.Y.

[46] H. H. A. Krueger *et al.*, "Effects of Radiation on the Ferroelectric Properties of Rochelle Salt" (to be published).

more diffuse as irradiation proceeds. The curve of logarithmic decrement vs temperature of the unirradiated crystal has a peak at 24°C, the upper Curie point, but no peak appears on the curve at the lower point. The curve of the irradiated crystal develops a peak at the lower Curie point at 10^4 r. These two peaks grow somewhat as the irradiation proceeds, follow the Curie points, and finally coalesce to a broad peak with a maximum at about 4°C.

The shear stiffness coefficient c_{44}^E reflects the behavior of the ferroelectric effect as manifested by the reciprocal of the dielectric constant. The coefficient c_{44}^E is almost unchanged until the dose reaches a value above 1×10^7 r. The results of the irradiations in the reactor were similar to those with the Co^{60} source; no effects specifically attributable to neutrons appeared. X-ray rocking curves found in a study of the crystalline structure by x-ray diffraction indicated a small increase in sharpness of the diffracted lines at 10^4 r but a steady broadening at higher doses. Such a broadening is usually attributed to an increase in disorder in the crystal lattice.

Thermoluminescence Studies of Ferroelectrics

Thermoluminescence is a well-known phenomenon that has been studied quite extensively in many substances. Thermoluminescence is usually defined as luminescence emitted by a substance when it is warmed, preferably at a slow constant rate, after having been subjected to some type of exciting radiation at low temperatures. Measurement of the light intensity emitted as a function of the substance's temperature yields what is commonly referred to as a "glow curve."

When a crystalline material is irradiated with ionizing radiation such as gamma rays, ionization occurs and electrons are excited into the conduction band. In this excited state, the electron moves freely through the crystal until it finds a position of lower potential energy. A position of lower potential energy is attained by one of two processes – recombination or trapping. The process of recombination occurs when an electron recombines with a positive hole or returns to the ground state. Trapping occurs when the electron assumes a metastable position with potential energy between those of the conduction and ground states. For each trap there is a characteristic energy of activation for release of the electron. When the electron receives enough energy E to leave its trap and again enter the conduction state, it soon returns to the ground state by recombination, yielding a quantum of light.

In order for an electron to be released from a trap of depth E it must absorb at least an amount of energy E. When a substance has been irradiated at low temperature and then warmed at a constant rate, maxima will be observed in the glow curve at temperatures corresponding to the trap depths present in the crystal. Randall and Wilkins give the following approximation for converting the maximum glow temperature to trap depth:

$$\text{trap depth} = 25\, kT \ ,$$

where k is Boltzmann's constant and T is the temperature in °K (ref 47) at which the glow peak occurs. Randall and Wilkins assume in their theoretical calculations that there is no retrapping and that the electron goes directly to a luminescent center. The temperature of the glow peak varies only slightly with the rate of warming.

Although many substances exhibit the property of thermoluminescence, only certain ferroelectrics have been investigated in this work. Because the properties and physical structures of certain ferroelectric substances are well known, some of these were chosen for radiation damage studies. In particular, Rochelle salt has been investigated for the effects of gamma rays and neutrons.[46] Thermoluminescence induced by gamma rays has been used as a tool to study the radiation damage mechanism in the following ferroelectrics: Rochelle salt, guanidine aluminum sulfate hexahydrate (GASH), and potassium dihydrogen phosphate (KDP).

The various substances were irradiated at liquid-nitrogen temperature (77°K) at the ORNL cobalt garden facility and at the cobalt irradiation facilities in Building 4501. The samples were either in the form of crystals or twice-recrystallized reagent-grade powders. The samples were placed in aluminum holders during the irradiation and during subsequent glow curve measurements.

---

[47] J. T. Randall and M. H. G. Wilkins, *Proc. Roy. Soc.* (*London*) A184, 372 (1945).

Measurement of the glow curve was accomplished by having the output of a 1P28 photomultiplier fed through an electrometer circuit (micromicroammeter model 410, made by Keithley Instruments, Inc., Cleveland, Ohio) to a strip-chart recorder while a simultaneous recording was made of the sample temperature. Figure 124 gives a vertical cross-section view of the sample holder and glow curve apparatus assembly.

Thermoluminescence glow curves were obtained in the temperature range from −196 to 0°C with a warming rate of 12°C per minute. The constant warming rate of 12°C per minute was normally maintained quite well within ±1°C, giving good reproducibility and facilitating the theoretical calculation of the electron trap depths.

Pure Rochelle salt single crystals irradiated with doses up to 3.5×10^6 r showed no detectable thermoluminescence. The less pure reagent-grade Rochelle salt powders did produce a glow peak at about −61°C that seemingly disappeared after two recrystallizations. Recently, work at higher sensitivity with a cooled photomultiplier tube has definitely established glow peaks at −61 and −11°C for aluminum oxide powder. It was recognized early in this work that the aluminum holders would have to be quite clean, especially free from organic contaminants. Since aluminum oxide was known to be thermoluminescent at higher temperatures, it was also suspected of being thermoluminescent at lower temperatures.[48] Many methods for removal of the aluminum oxide were tried without any giving 100% removal. In most cases the glow curve of the substance completely masked the background aluminum oxide glow peaks. A more detailed description of sample preparation and irradiation, equipment, obtainment of glow curves, etc., is given in two reports.[49,50]

Single crystals of guanidine aluminum sulphate hexahydrate (GASH) show a glow peak at −119°C which is concealed at high doses (3.5×10^6 r) by a much larger peak at −146°C. A low broad peak with a maximum at about −5°C was observed in GASH at doses of 10^5 to 10^6 r but is poorly resolved at higher doses. Figures 125–27 give a sequence growth of the −119 and −146°C GASH glow peaks for doses of 10^4, 10^5, and 10^6 r, respectively. Figure 128 is a photograph of the strip recording of the 3.5×10^6 r dose GASH glow curve.

Potassium dihydrogen phosphate (KDP) glow curves were obtained from both powder and crystal samples. Twice-recrystallized Mallinckrodt reagent-grade KDP with a grain size between 100 and 170 mesh was used for the powder samples.

The glow curve for KDP powder given a dose of 10^4 r exhibited two peaks, one at approximately −78°C and the other at approximately −146°C. The −78°C peak split into two distinct peaks with increasing dosage. Glow curves for two KDP single crystals, each exposed successively to 10^4, 10^5, and 10^6 r, gave fair correlation with the KDP powder curves.

Both powders and single crystals of KDP gave a glow peak in the vicinity of −146°C. The glow peak in the range −65 to −73°C for single crystals exposed to doses of 10^4 and 10^5 r may correspond to the −77°C peak for powder samples exposed to the same doses, although this peak for the single-crystal samples did not split with increasing dose as did that for the powder samples. This splitting in the case of the powder samples may be an impurity effect. Indication of a still higher temperature glow peak in the single crystals, around −10°C, was evident at 10^6 r but was probably due to aluminum oxide. The single crystals also exhibited a fairly prominent glow peak at around −120°C. This, however, may be due to thermoluminescence of ice which may have been formed on the crystals during cooling due to inadequate methods of eliminating moisture. More refined techniques than were used in this study would be necessary to determine conclusively whether this −120°C peak is actually a property of KDP.

Short-duration flashes of light were observed during the warmup of both KDP powders and single crystals. Similar spurious signals were superimposed on the glow curves of Rochelle salt and GASH. Flashes of the order of 10 msec duration were observed from Rochelle salt. These

[48] J. K. Reinhe and F. Daniels, *J. Phys. Chem.* 71, 629 (1957).

[49] J. W. Gilliland, Jr., *Thermoluminescent Studies of the Gamma-Irradiated Ferroelectrics Rochelle Salt and Guanidine Aluminum Sulphate Hexahydrate*, ORNL-2783 (Aug. 24, 1959).

[50] T. M. Sims, *Low-Temperature Thermoluminescence of Gamma Radiation of Potassium Dihydrogen Phosphate*, ORNL-2846 (to be published).

UNCLASSIFIED
ORNL-LR-DWG 36666A

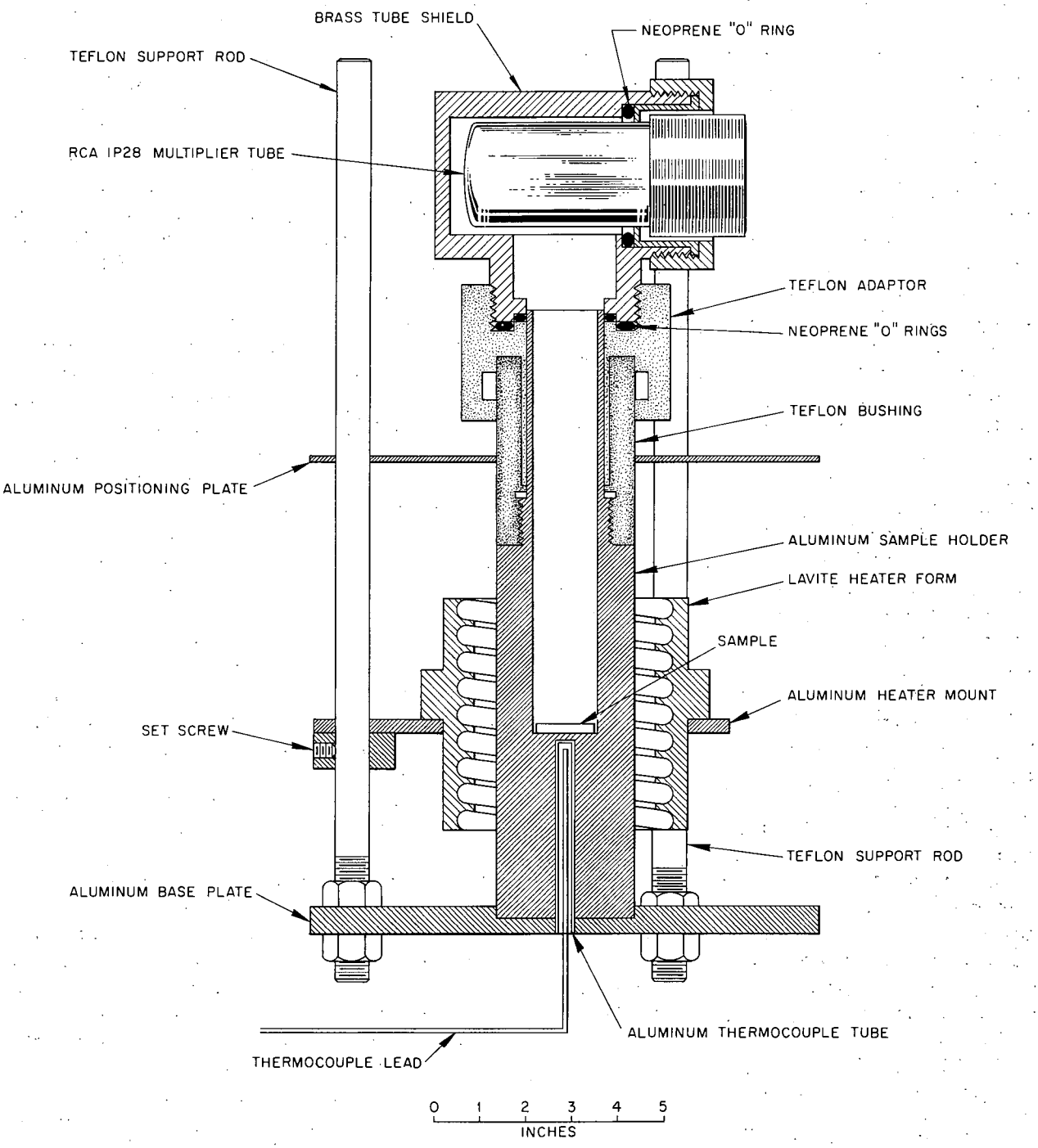

Fig. 124. Vertical Cross Section of Assembly for Thermoluminescence Measurements.

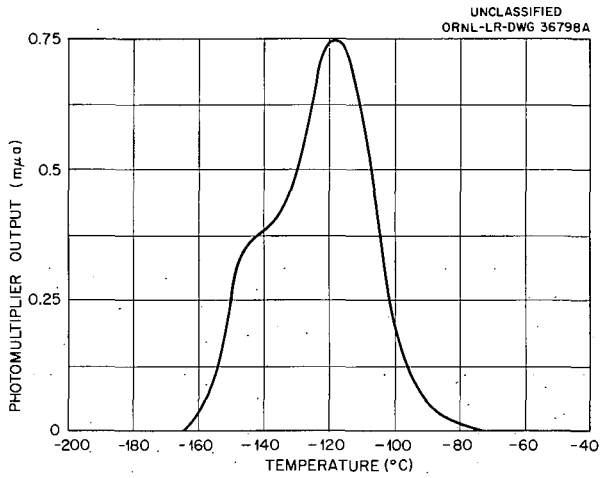

Fig. 125. Glow Curve of GASH, 10^4 r; Warming Rate = 12°C/min.

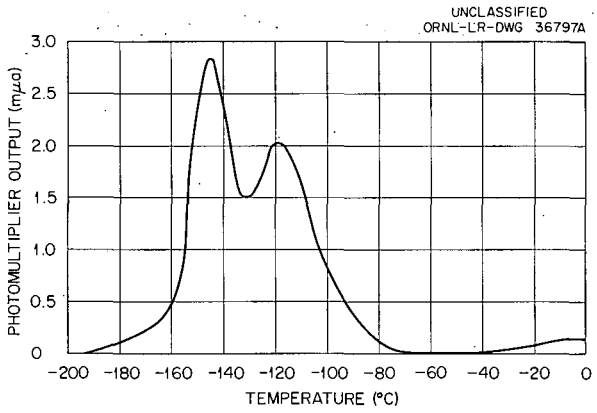

Fig. 126. Glow Curve of GASH, 10^5 r; Warming Rate = 12°C/min.

flashes are possibly due to triboluminescence caused by thermal expansion and the resulting fracturing of the crystals. An example of the superimposed flash signals can be seen on the glow curve of Fig. 127.

Calculations of electron trap depth according to the approximation of Randall and Wilkins[51] yielded depths of 0.28 and 0.34 ev for peaks of −146 and −119°C, respectively, in GASH. Trap depths of 0.28 and 0.43 ev were calculated for peaks of −146 and −77°C, respectively, in KDP.

Radiation Aging and Information Theory

The most usual mortality pattern exhibited by an ensemble of isogenic organisms, dying of natural causes or of radiation-induced causes, is

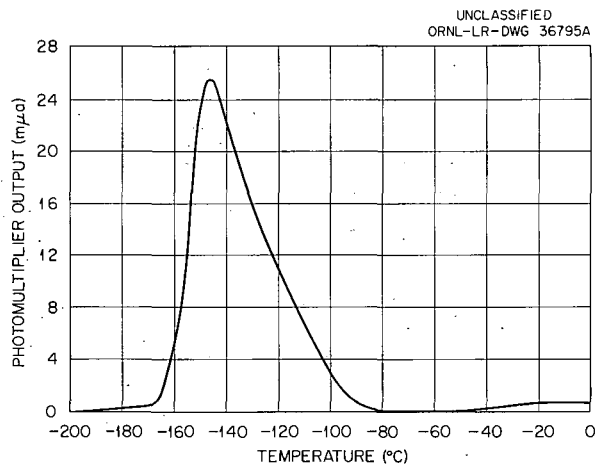

Fig. 127. Glow Curve of GASH, 10^6 r; Warming Rate = 12°C/min.

an asymmetric bell-shaped curve. The mortality curve of an acute irradiated ensemble will always be shifted (relative to a control ensemble) towards earlier times of death. The mortality curves of a chronically irradiated ensemble will be shifted and also compressed, that is, the duration between the first and last times of death will be reduced. Information theory has led to a very precise way of expressing these ideas.

In the derivation below we will assume that the measure of premature aging (days, weeks, etc.) is, to the first order, linearly proportional to the measure of dose (roentgen, rad, etc.). Then an acute irradiation is equivalent to a premature increase in age τ and chronic irradiation of duration t is equivalent to accelerated aging for a time $t^{(s)} = ct$.

Data are often tabulated as a sequence of n pairs (t_i, f_i), t_i being a time of death and f_i being the number of organisms dying at that time. We define:

$\bar{t}$ = the mean time of death,

m_2, m_3, m_4 = the second, third, and fourth moments of the mortality curve,

σ = the standard deviation (or dispersion),

β_1 = the skewness (or asymmetry),

β_2 = the kurtosis (or flatness).

[51] J. T. Randall and M. H. G. Wilkins, *Proc. Roy. Soc. (London)* A184, 372 (1945).

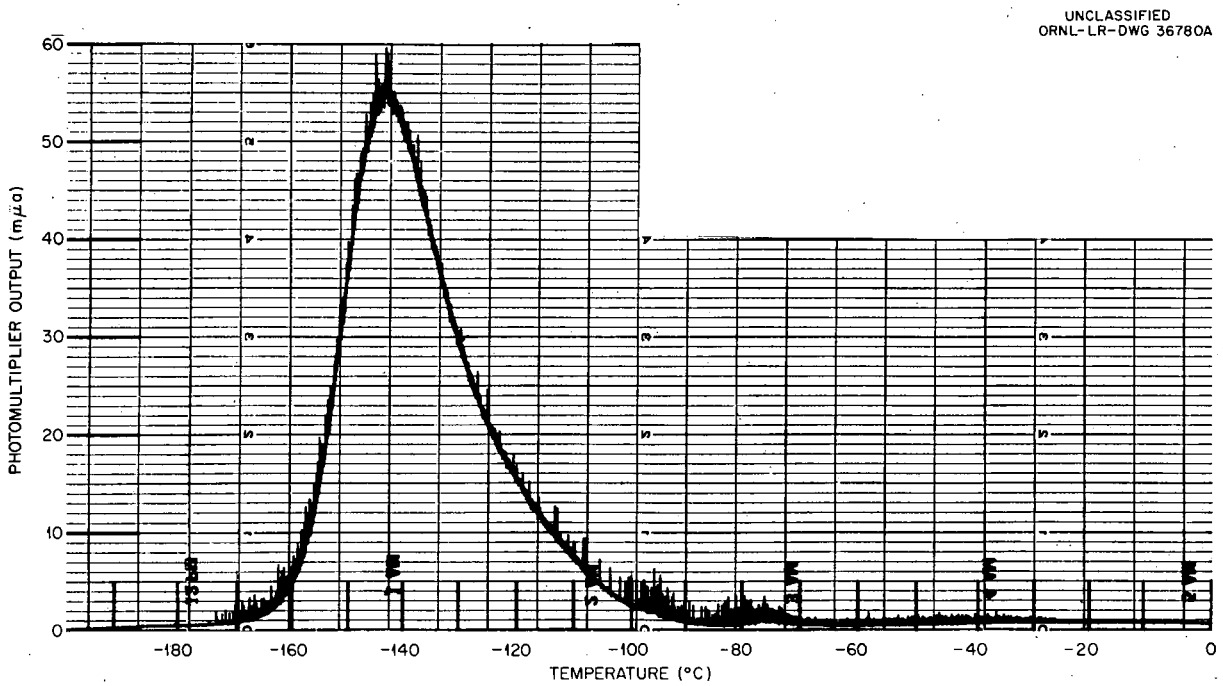

Fig. 128. Glow Curve of GASH, 3.5×10^6 r; Warming Rate = 12°C/min.

Or,

$$N = \sum^{n} f_i ,$$

$$\bar{t} = \frac{1}{N} \sum t_i f_i ,$$

$$m_2 = \frac{1}{N} \sum (t_i - \bar{t})^2 f_i ,$$

$$m_3 = \frac{1}{N} \sum (t_i - \bar{t})^3 f_i ,$$

$$m_4 = \frac{1}{N} \sum (t_i - \bar{t})^4 f_i ,$$

$$\sigma = \sqrt{m_2} ,$$

$$\beta_1 = \frac{m_3^2}{m_2^3} ,$$

$$\beta_2 = \frac{m_4}{m_2^2} .$$

Acute Case. – Values of $\bar{t}$, σ, β_1, and β_2 will be predicted and compared for control and acute irradiated ensembles:

$$\bar{t} = \frac{1}{N} \sum t_i f_i ,$$

$$\bar{t}^{(s)} = \frac{1}{N} \sum t_i^{(s)} f_i$$

$$= \frac{1}{N} \sum (t_i + \tau) f_i$$

$$= \frac{1}{N} \sum t_i f_i + \tau .$$

Therefore $\bar{t}^{(s)} = \bar{t} + \tau$, where τ is proportional to the acute dose:

$$m_2 = \frac{1}{N} \sum (\bar{t} - t_i)^2 f_i ,$$

$$m_2^{(s)} = \frac{1}{N} \sum_i [\bar{t}^{(s)} - t_i^{(s)}]^2 f_i$$

$$= \frac{1}{N} \sum (\bar{t} + \tau - t_i - \tau) f_i$$

$$= \frac{1}{N} \sum (\bar{t} - t_i)^2 f_i$$

$$= m_2 .$$

Similarly,

$$m_3^{(s)} = m_3 , \qquad m_4^{(s)} = m_4 .$$

Hence,

$$\bar{t}^{(s)} \neq \bar{t} ,$$

$$\sigma^{(s)} = \sigma ,$$

$$\beta_1^{(s)} = \beta_1 ,$$

$$\beta_2^{(s)} = \beta_2 .$$

Chronic Case. – Proceeding as before, and using $t^{(s)} = ct$:

$$\bar{t} = \frac{1}{N} \sum t_i f_i ,$$

$$\bar{t}^{(s)} = \frac{1}{N} \sum t_i^{(s)} f_i = \frac{1}{N} \sum c t_i f_i$$

$$= c \frac{1}{N} \sum t_i f_i$$

$$= c\bar{t} ;$$

and

$$\sigma = \sqrt{\frac{\sum (\bar{t} - t_i)^2 f_i}{N}} ,$$

$$\sigma^{(s)} = \sqrt{\frac{\sum [\bar{t}^{(s)} - t_i^{(s)}]^2 f_i}{N}}$$

$$= c\sigma .$$

Hence,

$$\frac{\sigma}{\bar{t}} = \frac{\sigma^{(s)}}{\bar{t}^{(s)}} .$$

It is easily seen that

$$\beta_1^{(s)} = \beta_1 ,$$

$$\beta_2^{(s)} = \beta_2 .$$

The limits of error of $\bar{t}$, σ, β_1, and β_2 have been tabulated.[52] Hence it is possible to determine whether the various parameters are equal within the limits of error.

A program of life-table analysis has been in progress for some time. Acute irradiation data from Operation Greenhouse, a nuclear detonation, have already been examined, and our results published.[53] The data of Neary, Munson, and Mole have been examined.[54]

An Example. – It is very interesting to find regularities in mortality curves, especially ones that are unnoticed until predicted by theory.

To test the hypothesis that $\sigma/\bar{t}$, β_1, and β_2 will remain constant (allowing for experimental fluctuations) from chronically irradiated group to chronically irradiated group, we define an idealized ensemble of organisms:

1. Its members must be derived from the same strain.
2. Its members must be of the same age.
3. Its members must contain an unbiased sample of the strain at each dose level.
4. Males and females must be studied separately.
5. Its members must suffer *exactly* the same dose at each *nominal* dose level.

Items (1) and (4) are required to guarantee genetic similarity. Item (2) is required because this is an aging experiment. Item (3) is required for reasons deeply rooted in the information theory.[53] Item (5) is required because a dispersion of doses at one nominal level will produce a spurious smearing of the mortality probability pattern.

The monograph by Neary, Munson, and Mole[54] includes not only raw data on rodent mortality but a detailed description of experimental design and dosimetry. Their experiment closely approximates our idealized experiment.

The mice were exposed to the ionizing radiations of a nuclear reactor for several years and may be

---

[52] K. Pearson, *Tables for Statisticans and Biometricians, Part I*, Cambridge University Press, New York, 1930.

[53] J. S. Mendell, *Some Evidence for the Uniform Radiation Life Shortening Predicted by Information Theory*, ORNL-2533 (June 26, 1958).

[54] G. J. Neary, R. J. Munson, and R. H. Mole, *Chronic Radiation Hazards: An Experimental Study with Fast Neutrons*, Pergamon Press, New York, 1957.

divided into ten groups of 45–50 mice each according to the sex, type of radiation, and dose: controls, gamma, neutron minimum, neutron medium, and neutron maximum.

We hypothesize that $\sigma/\bar{t}$ is constant (allowing for experimental fluctuations) from group to group. The relatively small number of mice used by Neary, Munson, and Mole at each dose level invalidates (we feel) any test of the constancy of β_1 and β_2.

Let V_1, with standard error S_1, and V_2, with standard error S_2, be the calculated values of $\sigma/\bar{t}$ for the different groups. Then, by hypothesis, the difference $V_1 - V_2$ is due to experimental fluctuations. According to theory the standard error of the difference, S_{1-2}, is equal to $\sqrt{S_1^2 + S_2^2}$ (ref 55). Hence, nonzero values of the parameter

$$Z = \frac{V_2 - V_1}{\sqrt{S_1^2 + S_2^2}},$$

by hypothesis, are due to experimental fluctuations.

If we believe that the differences $V_1 - V_2$ fluctuate normally about zero, then the probability that the two values are consistent, $p(Z)$, may be read from a table of the tails of the normal distribution.[56]

It is almost universally accepted that whether or not errors are normally distributed, a Z value exceeding 2 or 3 is an indication of inconsistency.

Calculated data are shown in Table 42. Values of Z and $p(Z)$ are shown in Table 43. The values for the females shown seem to support the hypothesis in a striking fashion, while those for the males seem just as strikingly to violate it. Evidently the question will remain open until further chronic irradiation data approximating the ideal experiment are obtained.

---

[55] A. G. Worthing and J. Geffner, *Treatment of Experimental Data*, Wiley, New York, 1953.

[56] G. U. Yule and M. G. Kendall, *An Introduction to the Theory of Statistics*, Griffin, London, 1948.

Table 42. Mean Time of Death, $\bar{t}$, for Rodents Subjected to Chronic Irradiation (Calculated Data)

Sex	Group	$\bar{t}$ ± Standard Error (days)	σ ± Standard Error (days)
Female	Control	818.7317 ± 21.547 (±2.63%)	137.9001 ± 15.233 (±11.05%)
	Gamma	787.0800 ± 19.727 (±2.51%)	139.9720 ± 13.947 (±9.89%)
	Neutron		
	Minimum	803.6735 ± 16.359 (±2.04%)	114.5155 ± 11.566 (±10.10%)
	Medium	758.9592 ± 19.074 (±2.51%)	133.5203 ± 13.485 (±10.10%)
	Maximum	511.500 ± 14.128 (±2.76%)	100.3084 ± 9.989 (±9.96%)
Male	Control	743.8723 ± 20.630 (±2.77%)	135.8713 ± 19.505 (±10.73%)
	Gamma	714.9149 ± 14.805 (±2.07%)	101.4174 ± 10.467 (±10.32%)
	Neutron		
	Minimum	676.7551 ± 23.438 (±3.46%)	164.0647 ± 16.571 (±10.10%)
	Medium	703.7000 ± 15.410 (±2.19%)	97.5957 ± 10.895 (±11.17%)
	Maximum	499.1633 ± 12.848 (±2.57%)	89.9345 ± 9.084 (±10.10%)

Table 43. Comparison of Values of Z and p for Groups of Irradiated Rodents

	Gamma	Neutron		
		Minimum	Medium	Maximum
		Females		
Controls	$Z = 0.36$	$Z = 1.18$	$Z = 0.32$	$Z = 1.06$
	$p = 0.719$	$p = 0.238$	$p = 0.789$	$p = 0.239$
Gamma		$Z = 1.52$	$Z = 0.04$	$Z = 0.70$
		$p = 0.131$	$p = 0.968$	$p = 0.484$
Neutron				
Minimum			$Z = 1.17$	$Z = 0.79$
			$p = 0.242$	$p = 0.430$
Medium				$Z = 0.83$
				$p = 0.407$
		Males		
Controls	$Z = 1.78$	$Z = 2.06$	$Z = 2.35$	$Z = 0.12$
	$p = 0.075$	$p = 0.039$	$p = 0.019$	$p = 0.90$
Gamma		$Z = 3.62$	$Z = 0.15$	$Z = 1.65$
		$p \to 0$	$p = 0.88$	$p = 0.10$
Neutron				
Minimum			$Z = 3.72$	$Z = 2.16$
			$p \to 0$	$p = 0.031$
Medium				$Z = 1.78$
				$p = 0.075$

EXPERIMENTAL PHYSICS OF DOSIMETRY

G. S. Hurst
T. E. Bortner
L. W. Cochran[57]
L. B. O'Kelly
R. D. Birkhoff
H. H. Hubbell, Jr.
W. G. Stone[58]
R. A. Finston[59]
P. L. Ziemer[59]
W. Happer, Jr.[60]

Electron Capture in O_2

Examples of Data. – Electron attachment in O_2-CH_4 and O_2-CO_2 mixtures has been studied using the method and apparatus described previously.[61] For each case the quantity determined is α, the probability of electron capture per centimeter of drift in the direction of the applied electric field and per unit (mm Hg) pressure of the attaching gas (oxygen).

The O_2-CH_4 mixtures were studied over an E/P range of 0.1 to 2.0 $v \cdot cm^{-1} \cdot (mm\ Hg)^{-1}$ and for total pressures from 400 to 800 mm Hg. Oxygen concentrations up to 30 mm Hg of oxygen in 400 mm Hg total pressure were used. Figure 129 shows α plotted against f_1P (oxygen pressure) for an E/P of 1.4. It is evident that α depends on both oxygen pressure and CH_4 pressure. Lines similar to these can be plotted for other values of E/P.

[57] Consultant.

[58] Now at Redstone Arsenal, Huntsville, Ala.

[59] AEC radiological physics Fellow.

[60] Summer employee.

[61] T. E. Bortner and G. S. Hurst, *Health Phys.* 1(1), 39–45 (1958).

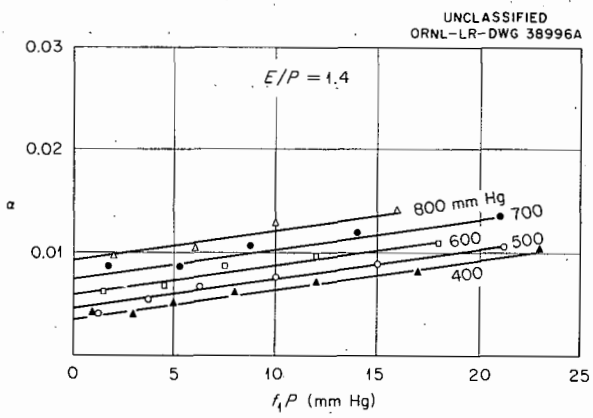

Fig. 129. Electron Capture in Oxygen-Methane Mixtures.

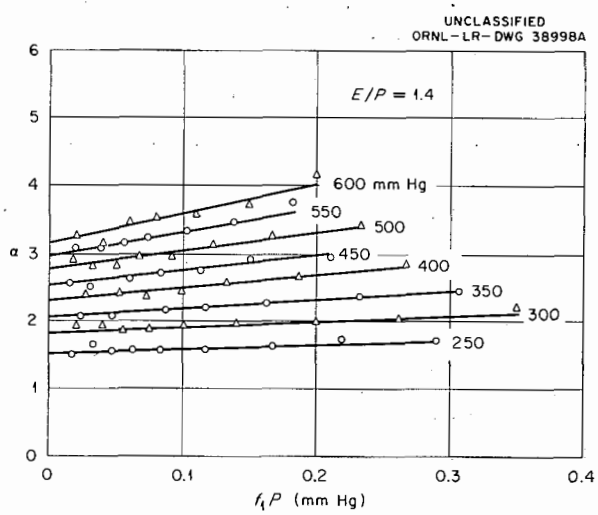

Fig. 130. Electron Capture in Oxygen–Carbon Dioxide Mixtures.

All the lines for a given E/P are very nearly parallel except at very low values of E/P, where the slope appears to increase as CH_4 pressure increases. The results seem to be interpretable by a method similar to that used for other gas mixtures.[62,63]

The O_2-CO_2 mixtures were studied over an E/P range of 0.1 to 3.0 and a total pressure range of 250 to 600 mm Hg. The minimum pressure that could be used in each case was determined by the stopping power of the gas since alpha particles were used as the source of electrons in the ionization chamber. Because of its great sensitivity to oxygen contamination, the maximum oxygen concentration that could be used with CO_2 was 0.42 mm Hg in 250 mm Hg total pressure. Figure 130 shows α plotted against f_1P for an E/P of 1.4. Again α depends on both total pressure and oxygen pressure; however, with this mixture the slopes of the lines increase as total pressure increases. The interpretation of the attachment process in O_2-CO_2 appears to be more complex than in the other gases studied and has not been completed.

An Improved Method for Measuring Electron Attachment. – The earlier method[61] used to study the process of electron capture to O_2 employed an alpha source to produce the free electrons. This imposes two limitations: (1) the number of electrons per pulse was limited to about 2×10^5, which in turn limited the amount of oxygen that could be used, and (2) a nonattaching gas at a pressure greater than that required to stop the alpha particles in the chamber had to be used. Neither of these difficulties appears in a new apparatus which employs a photoelectric surface and a pulsed ultraviolet light source for the generation of the pulses of electrons. In this method two identical ionization chambers are used, each receiving light from the same ultraviolet flash tube. One chamber contains a nonattaching gas, the other contains a mixture of the same nonattaching gas and O_2. The ratio of the pulse heights furnishes data from which the attachment coefficient is calculated. The double-chamber arrangement eliminates the uncertainty caused by fluctuation of the light output. The pulse heights are determined with an oscillator-ramp circuit in which the number of pulses recorded on a scaler is proportional to pulse height.

Figure 131 shows the general schematic diagram of the entire system. Each light flash is a complete event and there is no comparison of the pulse heights from one event to the next. The actual method of pulse-height comparison is shown in Fig. 132. By this method pulse heights in the two chambers are compared and the ratio read on the scalers.

Analyses of Results. – Complete analyses of results for electron capture in mixtures of O_2-Ar, O_2-N_2, and O_2-C_2H_4 are given in ORNL-2670.[62]

[62] G. S. Hurst and T. E. Bortner, *Capture of Electrons in Molecular Oxygen*, ORNL-2670 (July 6, 1959).

[63] G. S. Hurst and T. E. Bortner, *Phys. Rev.* 114, 116 (1959).

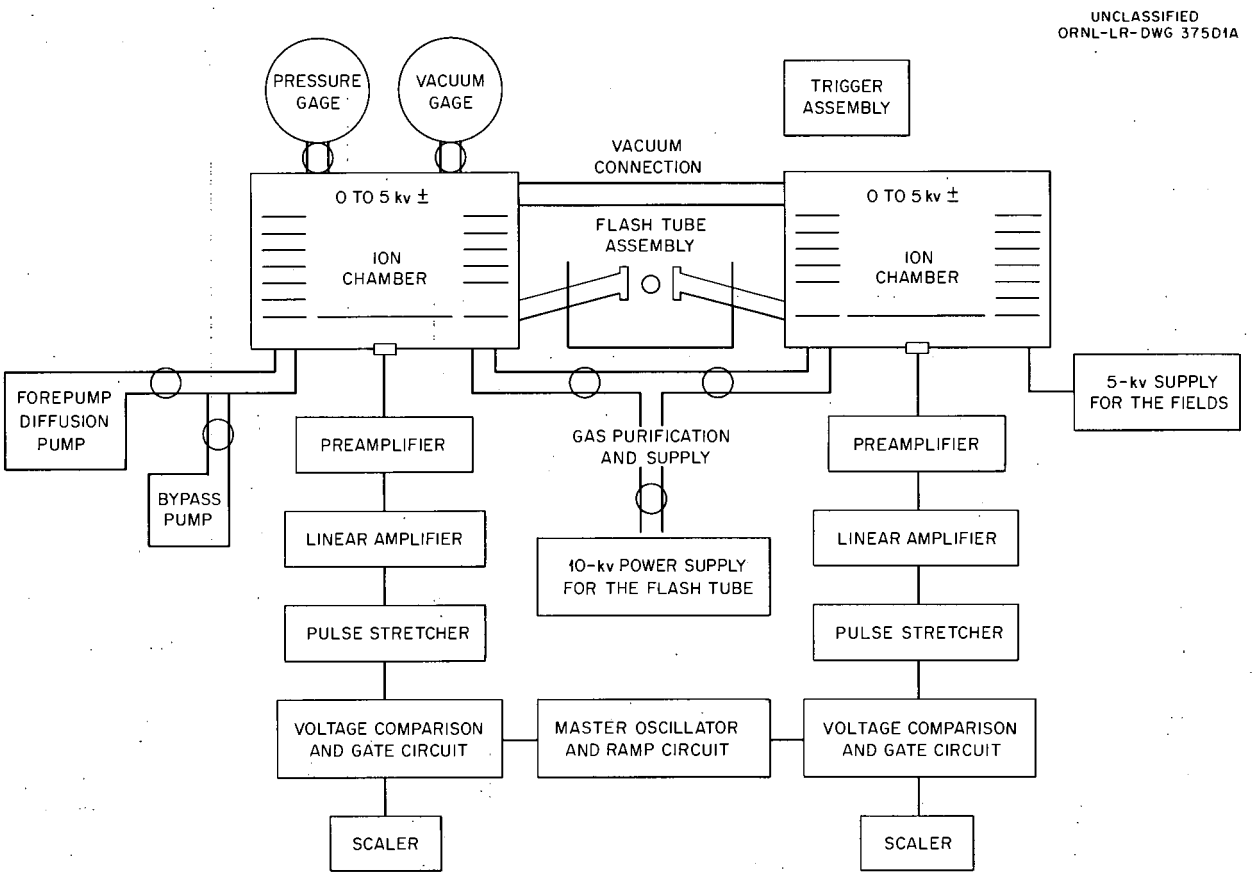

Fig. 131. Schematic Diagram for Measuring Pulse-Height Differential.

In the case of O_2-Ar, electron capture is due to the process $O_2 + e \rightarrow O^- + O$, since the energy of the electrons, even for $E/P < 0.5$, is large enough to produce dissociation. True pressure dependence for this case was not observed, but it was found that in the region of $0.3 \leqq E/P \leqq 0.5$, α decreased with increasing P_{O_2}/P_{Ar}. This implies that, in this region of electron energy, α is a decreasing function of energy, and that the mean electron energy decreases with increasing P_{O_2}/P_{Ar}.

For the case of O_2-N_2, α depends on the pressure of oxygen (f_1P) and the pressure of nitrogen (f_2P). The complete expression for α was found to be $\alpha = Af_1P + Bf_2P + Cf_1Pf_2P$. These results were interpreted in terms of an extension of the Bloch-Bradbury mechanism, where the initial capture leads to an unstable ion O_2^{-*}. An analysis of the results leads to the cross section for the collisional stabilization of O_2^{-*} by O_2 and by N_2; the values were found to be 3×10^{-15} cm^2 for O_2 and 6×10^{-17} cm^2 for N_2. The magnitude of the experimental constant C could not be understood on the basis of the usual gas kinetic theory for three-body collisions. It was suggested that the complex O_2^--N_2 is formed having a lifetime which is long compared to the vibration time of the molecule and to the time for electron emission from O_2^{-*}.

The results for α in the case of O_2-C_2H_4 mixtures were expressed as

$$\alpha = \alpha_0 + kf_2P \ ,$$

where α_0 and k are pressure independent and f_2P is the pressure of C_2H_4. These results were shown to be a special case of the detailed model used to explain the O_2-N_2 results. The physical interpretation of the results is as follows: the constant term α_0 arises from the fact that at the lowest C_2H_4 pressure all of the O_2^{-*} have been

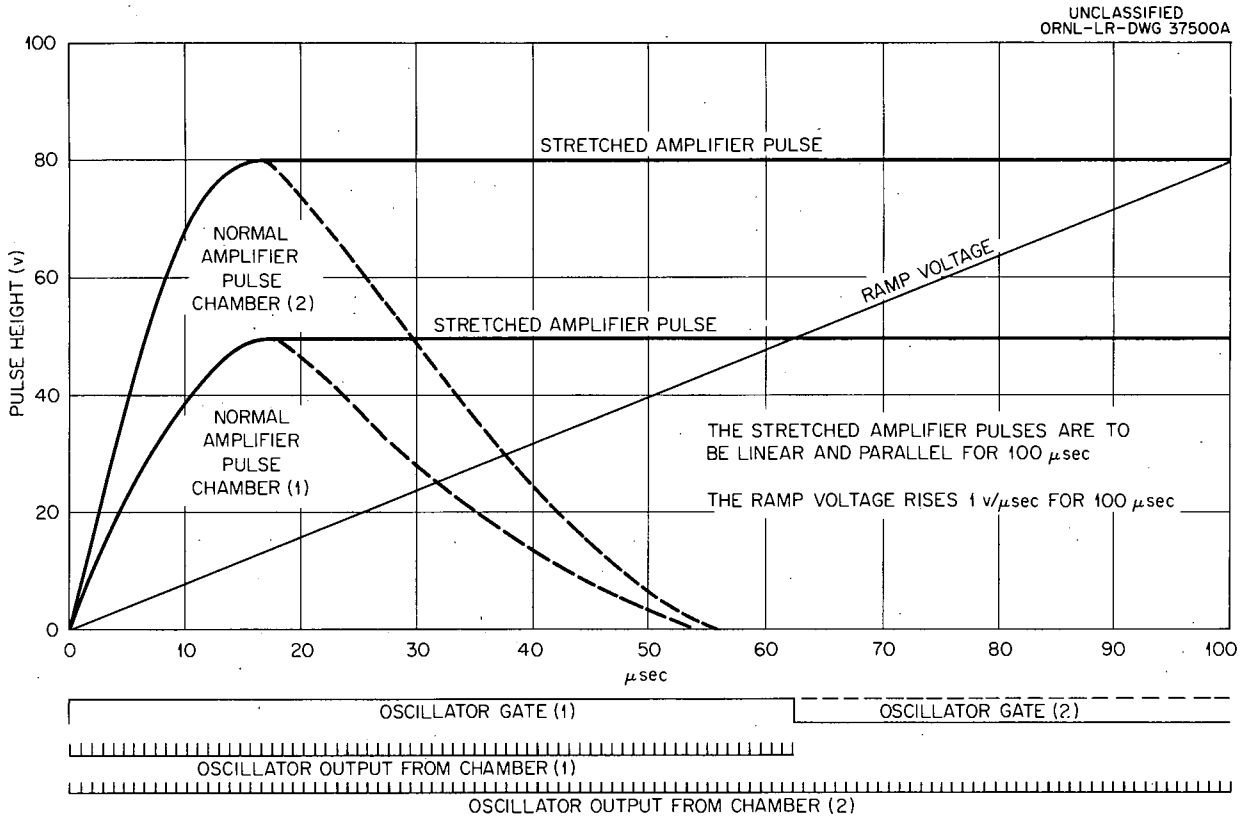

Fig. 132. Diagram of the Pulse-Height Differential by the Ramp Oscillator Method.

stabilized by collisions with C_2H_4 molecules. The term kf_2P arises as a result of direct formation of stable O_2^- by reactions of the type,

$$O_2 + e + C_2H_4 \rightarrow O_2^- + C_2H_4^T \ ,$$

where the T designates the transfer of energy to a C_2H_2 molecule.

Electron Agitation Energy. – In order to make a more complete interpretation of the mechanism of electron attachment in oxygen-gas mixtures, data are needed on the average energy of agitation of electrons in gases and gas mixtures. Accordingly, experiments have been initiated to make these measurements by employing the diffusion technique. An ionization chamber, similar in design to that of Huxley and Zaazou,[64] is being constructed for these experiments. Provisions are being made for orientation of the chamber in a suitable magnetic field to permit also the determination of electron drift velocities in a wider variety of gases and over a greater range of E/P values than is possible with the existing apparatus.

Pulse-Height–Energy Curve of Anthracene for Monoenergetic Electrons and the Energy Intercept

Recent work[65] on the response of anthracene to monoenergetic electrons has pointed up apparent discrepancies among the results of several investigators regarding the linearity of the pulse-height–energy relationship and the value of the intercept obtained by extrapolating the curve of pulse height vs energy to zero pulse height. In the latter case, Hopkins[66] obtained an intercept of 25 kev extrapolating from data in the Mev range,

[64] L. H. G. Huxley and A. A. Zaazou, *Proc. Roy. Soc. (London)* A196, 402–26 (1949).

[65] L. W. Johnston *et al.*, *Response of the Anthracene Scintillation Counter to Low Energy Electrons*, ORNL-2298; *Rev. Sci. Instr.* 28, 765 (1957).

[66] J. I. Hopkins, *Phys. Rev.* 77, 406 (1950); *Rev. Sci. Instr.* 22, 29 (1951).

whereas Johnston *et al.*[65] found a value of 4 kev from data taken at several tens of kilovolts. In the following, these results are shown to be compatible with each other and with the theory of Birks[67] on the scintillation process.

In Birks' theory the spatial rate of production of photons dS/dx is related to the spatial rate of energy loss dE/dx by constants of proportionality A and B in the following way:

$$\frac{dS}{dx} = \frac{A\ dE/dx}{1 + (kB\ dE/dx)}\ , \qquad (1)$$

where k is the capture probability of a damaged molecule, or quencher, relative to the capture probability of an undamaged molecule, or photon producer. According to Glocker,[68] Libby,[69] and Lane and Zaffarano,[70] the range of electrons with energies from 1 kev to 300 kev is proportional to the $\frac{5}{3}$ power of the electron energy, or

$$x = bE^{5/3}\ . \qquad (2)$$

This range-energy relationship may be differentiated and substituted into Eq. (1) to yield:

$$\frac{dS}{dE} = \frac{A}{1 + \left(\frac{3kB}{5b}E^{-2/3}\right)}\ . \qquad (3)$$

The quantity $3kB/5b$ may be evaluated from published values of the parameters kB and b. Birks has given a value of 7.15 cm air per Mev for kB; an average value for b from the references cited is 0.65 g·cm^{-2}·(Mev)$^{-5/3}$. The quantity $3kB/5b$, subsequently designated by α, is then

$$\alpha \equiv \frac{3kB}{5b} = \frac{3 \times 7.15\ \frac{\text{cm air}}{\text{Mev}} \times 0.001293\frac{\text{mg/cm}^2}{\text{cm air}} \times \frac{273}{288} \times \left(1000\ \frac{\text{kev}}{\text{Mev}}\right)^{2/3}}{5 \times 0.65\ \frac{\text{g/cm}^2}{(\text{Mev})^{5/3}}} = 0.81\ (\text{kev})^{2/3}\ .$$

Equation (3) may be integrated[65] immediately and the pulse height S is found to be

$$S = AE\left(1 - \frac{3}{\mu^2} + \frac{3}{\mu^3}\tan^{-1}\mu\right)\ , \qquad (4)$$

where $\mu \equiv E^{1/3}/\alpha^{1/2}$. For low energies the $\tan^{-1}\mu$ may be expanded in a Taylor's series so that

$$S \rightarrow AE\left(\frac{3\mu^2}{5}\right) = 0.6\left(\frac{A}{\alpha}\right)E^{5/3}\ . \qquad (5)$$

At high energies all terms vanish except the first and

$$S \rightarrow AE\ . \qquad (6)$$

Thus the response of anthracene is explained qualitatively as being linear at high electron energies but with some curvature at low energies.

A more quantitative comparison may be made on the following basis. Consider the slope of the pulse-height–energy curve at some point (S_1, E_1). The energy intercept E_i from elementary considerations will be

$$E_i = E_1 - S_1\left(\frac{dS}{dE}\right)^{-1}_{E_1}\ , \qquad (7)$$

and if the slope equation (3) is substituted into Eq. (7), then

$$E_i = E_1\left\{1 - \left[1 + \mu_1^{-2}\right]\left[1 - 3\mu_1^{-2}\left(1 - \mu_1^{-1}\tan^{-1}\mu_1\right)\right]\right\}\ , \qquad (8)$$

where $\mu_1 = E_1^{1/3}\alpha^{-1/2}$. This equation has been plotted in Fig. 133 for $\alpha = 1$. It may be seen that if the slope is evaluated in the region around 50 kev, then $E_i \cong 4$ kev. However, if the slope is

[67] J. B. Birks, *Proc. Phys. Soc. (London)* **A64**, 874 (1951).

[68] R. Glocker, *Z. Naturforsch.* 3a, 147 (1948).

[69] W. E. Libby, *Anal. Chem.* 19, 2 (1947).

[70] R. O. Lane and D. J. Zaffarano, *Transmission of 0–50-kilovolt Electrons by Thin Films with Applications to Beta-Ray Spectroscopy*, ISC-439, (December 1953).

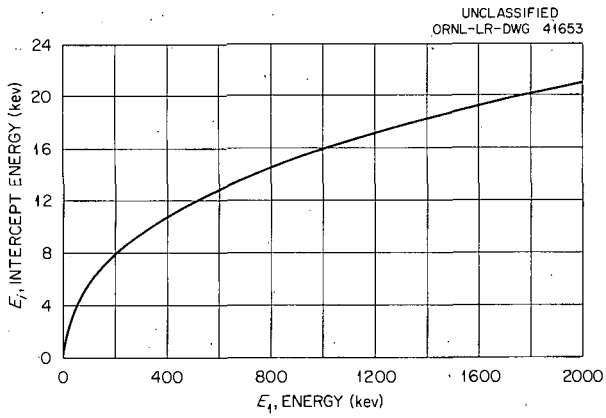

Fig. 133. Intercept of Extrapolated Pulse Height vs Energy Curve for Anthracene as a Function of the Energy.

taken in the neighborhood of 1.5 Mev, an intercept of about 20 kev is obtained in rather good agreement with Hopkin's value of 25 kev.

Plasma Light Experiment

The discrete energy losses suffered by fast electrons passing through thin metal foils were the object of both theoretical and experimental investigation in this laboratory several years ago.[71,72] The absorption was attributed to the excitation of the plasma of free electrons in the metal, though other workers have questioned whether such oscillations occur. A crucial experiment would be to observe light emitted by the decay of the excitation, since the wavelength and approximate intensity are predicted theoretically. First estimates showed that the measurement would require a spectrometer, of very high transmission, which was sensitive far into the vacuum ultraviolet. Decay of the 14.8-ev characteristic energy losses in aluminum observed by Blackstock would emit light at 837 Å. Ferrell[73] estimates that the light yield from a metal foil of optimized thickness would be approximately one photon per 1000 electrons bombarding the foil.

A preliminary experiment was performed to set an upper limit to the amount of light emitted at 837 Å from an aluminum foil bombarded by electrons of 0.69 Mev average energy. The apparatus used was a vacuum ultraviolet monochromator of the normal incidence reflection grating type with a 2.15×10^{-7} transmission at the wavelength of interest. This equipment was made available by C. Nelson of the Solid State Division. The plate exposure times were unfortunately limited to evenings and weekends due to the continuous use of the machine during working hours.

The source of bombarding electrons was a series of phosphorus-Bakelite plaques which had been irradiated in the ORR for five days at a thermal flux of about 10^{13} neutrons·cm^{-2}·sec^{-1}. This formed a source of an estimated 1.1-curie strength, giving $\sim 4 \times 10^9$ beta particles per second passing through the 5×12.5 mm area of the foil. The average energy of the P^{32} beta flux in a radioactive medium as calculated from the Spencer-Attix theory[74] is 0.69 Mev.

According to Ferrell the optimum thickness of an aluminum foil is $\lambda_{ex}/2$, where

$$\lambda_{ex} = \frac{2\pi}{\Delta k} = \left(\frac{v}{c}\right)\lambda_p \ .$$

Since our λ_p for aluminum is 837 Å and (v/c) for 0.69-Mev electrons is 0.904, $\lambda_{ex} = 757$ Å. Thus the optimum foil thickness is 380 Å or about 9 μg/cm^2. The metal for this ultrathin foil was plated directly upon the surface of the phosphorus-Bakelite source plaque by the vacuum evaporation technique. None of three 12-hr exposures under these conditions produced observable blackening on the plates. A lower limit to the amount of light detectable was obtained from the response of the photographic plates. These were special Kodak SWR plates made by the "Schumann Technique"[75] whereby the sensitive silver bromide particles are held in a minimum matrix of gelatin emulsion in order to limit the absorption of photons by the gelatin. Kodak[76] quotes an exposure (E) of 0.2 meter-candle-second (m-c-sec) to produce a

[71] A. W. Blackstock, R. H. Ritchie, and R. D. Birkhoff, *Phys. Rev.* 100, 1078 (1955); *Discrete Electron Energy Losses in Thin Metallic Foils*, ORNL-1910 (June 16, 1955).

[72] R. H. Ritchie, *On the Interaction of Charged Particles with Plasma*, ORNL-2697; submitted to the *Physical Review* for publication.

[73] R. A. Ferrell, "Predicted Radiation of Plasma Oscillations in Metal Film," *Phys. Rev.* 111, 1214 (1958).

[74] H. H. Hubbell, Jr., R. D. Birkhoff, and R. M. Johnson, *Radiology* 69, 268 (1957); *Pocket Ion Chambers for Beta Radiation Dose*, ORNL-2158 (Apr. 26, 1957).

[75] V. Schumann, *Akad. Wiss. Wien, Abt. IIa* 102, 625 (1893).

[76] *Kodak Photographic Plates for Scientific and Technical Use*, 7 ed., p 6, Eastman Kodak Company, Rochester, N.Y., 1953.

density of 0.6 above background fog. Thus, for a minimum observable darkening of 0.3 above background film fog the requisite intensity becomes

$$I_{min} = \frac{E}{t} = \frac{0.1 \text{ m-c-sec}}{43200 \text{ sec}} = 2.3 \times 10^{-6} \text{ m-c} .$$

If it is assumed that the conversion factor from lumens (in the region of maximum visibility) to watts applies in this region, then the minimum intensity may be expressed as:

$$I_{min} = 2.3 \times 10^{-6} \text{ m-c} \left(1 \frac{\text{lumen/m}^2}{\text{m-c}}\right) \left(10^{-4} \frac{\text{m}^2}{\text{cm}^2}\right) \left(1.61 \times 10^{-3} \frac{\text{w}}{\text{lumen}}\right) \times$$

$$\times \left(1.6 \times 10^{-19} \frac{\text{wsec}}{\text{ev}}\right)^{-1} \left(\frac{14 \text{ ev}}{\text{photon}}\right)^{-1} = 1.6 \times 10^5 \frac{\text{photons}}{\text{cm}^2 \cdot \text{sec}} .$$

That is, for a 12-hr exposure of this film, the minimum intensity of light which would be observable is 1.6×10^5 photons·cm^{-2}·sec^{-1} at the detector. Detection with the spectrometer and exposure time used would require an intensity of light in this wavelength region of 7.5×10^{11} photons·cm^{-2}·sec^{-1}.

Therefore, an order-of-magnitude limit on the efficiency of light production is that less than 100 photons are produced per beta particle passing through the foil. Since Ferrell's estimate was 10^{-3} photon per electron, we are still five orders of magnitude from being able to observe the light.

Methods for refinement of the experiment are available now which will result in an improvement of this limit by about nine or ten orders of magnitude. Exposure time may be increased by one or at the most two orders of magnitude. The electron flux through the foil can be increased from 4×10^9 from the radioactive source to a maximum in the range of 5×10^{14} electrons per second from a 100-μa beam out of our Cockcroft-Walton accelerator.

The use of a more efficient vacuum ultraviolet monochromator, such as the Seya-Namioka machine recently available in the Division, gives another factor of 300. Using a metal foil whose characteristic energy losses are at a lower voltage, the efficiency of the spectrometer may be improved by another order of magnitude, because the reflectance of the aluminum-surfaced grating is only about 0.04 at 837 Å, but is much higher in the near ultraviolet.

Using all of the above refinements, the limit on the efficiency of the light production process can be established down to approximately 10^{-8} photon per electron. This should be more than sufficient to determine spectral distribution of the light if the theoretical estimates of the intensity are correct.

Measurement of Electron Flux in Media Bombarded by X Rays

The previously reported[77-79] studies on the energy distribution of secondary electrons in an evacuated cavity in a medium bombarded by x rays have been continued. It is hoped that these studies may be an important preliminary to a more thorough understanding of the mechanism of biological damage.

The essential part of the apparatus consisted, as previously, of a parallel-plate chamber uniformly irradiated by x rays in an evacuated enclosure. Three improvements were made: first, the use of a much more sensitive and accurate measurement technique, second, the measurement of the electron flux over a wider energy range in a tissue-equivalent plastic as well as in copper, aluminum, and graphite, and third, studies of the variation in the flux spectrum and total yield of electrons as the x-ray voltage was varied.

In the earlier work the following expression was derived for the flux inside the material of electrons which have a kinetic energy above the bottom of the conduction band equal to the sum of the Fermi energy E_F, the work-function ϕ, and the applied potential V:

$$N(E_F + \phi + V) = \frac{1}{eAR} \left[-\frac{dI}{dV} - 2(E_F + \phi + V) \frac{d^2 I}{dV^2} \right] . \qquad (1)$$

In this expression, e is the electronic charge, A

[77] G. S. Hurst *et al.*, *H-P Ann. Prog. Rep. July 31, 1958*, ORNL-2590, p 137.

[78] D. R. Nelson *et al.*, *Measurement of Electron Flux in Media Bombarded by X-Rays*, ORNL-2151 (July 25, 1958).

[79] R. A. Finston *et al.*, *Measurement of Electron Flux in Irradiated Media by AC Methods*, ORNL-2732 (to be published).

the irradiated area of the plates, R the dose rate in the cavity, and I the observed current between the plates for an applied potential V. To calculate the flux, the two derivatives of the current-voltage curve of the chamber must be determined. The derivatives were originally evaluated numerically from a carefully measured $I(V)$ curve, but this process of taking derivatives greatly reduces the accuracy of the final result. The new method measures the second derivative directly by the use of the phenomenon of intermodulation distortion, similar to that which occurs in broad-band a-c amplifiers.

Suppose the chamber current is represented by

$$I = I(V) \quad . \tag{2}$$

Then let the applied voltage contain a d-c component, the chamber bias V_0, and two a-c components whose amplitudes are small compared to V_0 and of different frequencies, ω and α:

$$V = V_0 + a \sin \omega t + b \sin \alpha t \quad . \tag{3}$$

Assuming that I is an analytic function in the domain considered, we may represent it by a Taylor's series about the point V_0. If the resulting expression is expanded and like terms in ω and α are collected, the equation contains a d-c term, and terms in $\sin \omega t$, $\sin \alpha t$, $\cos 2\omega t$, $\cos 2\alpha t$, $\cos (\omega + \alpha)t$, and $\cos (\omega - \alpha)t$. The sum and difference frequencies represent the intermodulation distortion. The difference frequency is of particular interest, and its amplitude is given by the series:

$$I_{(\omega-\alpha)} = \frac{ab}{2}\left(\frac{d^2 I}{dV^2}\right)_{V_0} + \left(\frac{a^3 b}{16} + \frac{ab^3}{16}\right)\left(\frac{d^4 I}{dV^4}\right)_{V_0} + \dots \quad . \tag{4}$$

If the amplitudes a and b are sufficiently small, we may pass to the limit and then solve for the second derivative:

$$\left(\frac{d^2 I}{dV^2}\right)_{V_0} = \lim_{a,b\to 0} \frac{2}{ab} I_{(\omega-\alpha)} \quad . \tag{5}$$

Thus a measurement of the difference frequency permits the calculation of the second derivative needed in Eq. (1) for the electron flux. In the experiment, successive reductions in the product ab of the amplitudes produced proportional reductions in the amplitude of the difference frequency $I_{(\omega-\alpha)}$. Hence the process outlined converges satisfactorily.

In general, the various derivatives are related to the amplitudes of the corresponding harmonics present in the output by expressions like:

$$\frac{d^n I}{dV^n} = \lim_{a\to 0} 2^{n-1}\, n! \left(\frac{I_n}{a^n}\right) \quad . \tag{6}$$

In the experiment, however, it was more satisfactory and more accurate to obtain the first derivative by numerical integration of the experimental data for the second derivative. The fundamental response also contained a considerable residuum of pickup and capacitive current which was impossible to annul completely.

The energy resolution of the device considered as a spectrometer is the apparent energy spread which would be observed if monoenergetic electrons were released in the medium. It is usually defined as the width of the observed line profile at half height divided by the central energy of the measured distribution for such a monoenergetic flux.

In order to determine the expected energy resolution, let the monoenergetic electron flux be represented by a delta function,

$$N(V') = \delta(V' - V_1) \quad , \tag{7}$$

where V_1 is the energy of the electrons. The probable $I(V)$ curve and its derivatives, when measured by the techniques discussed, are first calculated. Then by a procedure similar to that used with the observed data, the $N(V)$ curve is calculated from these derivatives. The breadth of this $N(V)$ curve gives the instrumental energy resolution.

Consider first the energy resolution for measurement by the harmonics of a bias modulated by a single frequency. It was shown previously[77,78] that the net current $I(V)$ may be expressed as

$$I(V) = eAR\left[\int_0^V N(V')\, dV' + \int_V^\infty \left(\frac{V}{V'}\right)^{1/2} N(V')\, dV'\right] \quad . \tag{8}$$

If (7) is substituted into (8) the expected $I(V)$ curve may be calculated for monoenergetic electrons, and the derivatives may then be obtained from these equations. The results are plotted in Fig. 134.

Suppose an a-c modulation, $a \sin \omega t$, is superimposed on the applied spectrometer bias V_0, where a is small compared to V_0 or V_1. Then $I(V)$ is expanded in a Fourier series:

$$I(V) = \sum_{n=1}^{\infty} A_n \sin n\,\omega t + B_n \cos n\,\omega t \quad , \qquad (9)$$

where the coefficients are given by the usual expressions of the form

$$A_n = \frac{1}{\pi} \int_0^{2\pi} I \sin n\,\omega t \, d(\omega t) \quad . \qquad (10)$$

The integrations are carried out over two regions as indicated in Fig. 135. One region is that in which $(V_0 + a \sin \omega t) < V_1$ and the other occurs where $(V_0 + a \sin \omega t) > V_1$. The first and second harmonic amplitudes obtained from these integrations are then used to obtain the derivatives of $I(V)$. These derivatives when substituted in Eq. (1) give the following approximate expression for the response curve:

$$N(V_0) = \pm \frac{1}{V_1} \frac{\cos \phi}{\pi} \left[\frac{16(V_0/V_1)}{(a/V_1)^2} (\sqrt{V_0/V_1} - 1) \sin \phi + \frac{4\sqrt{V_0/V_1}\,(2 - 4/3 \cos^2 \phi)}{a/V_1} \right] , \qquad (11)$$

where

$$\phi = \sin^{-1} \left(\frac{V_1 - V_0}{a} \right) \quad . \qquad (12)$$

The positive sign applies for $V_0 < V_1$ and the negative for $V_0 > V_1$. The graph of this function in general coordinates, Fig. 136, shows that the width of the line profile at half height, the resolution, is 1.2 a/V_1 and the base of the line profile is $2a$. For the mathematically more complicated analysis of the energy resolution for the intermodulation frequency measurement, it can be argued that the base of the line profile $N(V_0)$ is no greater than $4a$, and that the energy resolution is no greater than 2.4 a/V_1, assuming that the amplitudes of the two modulating frequencies are each equal to a.

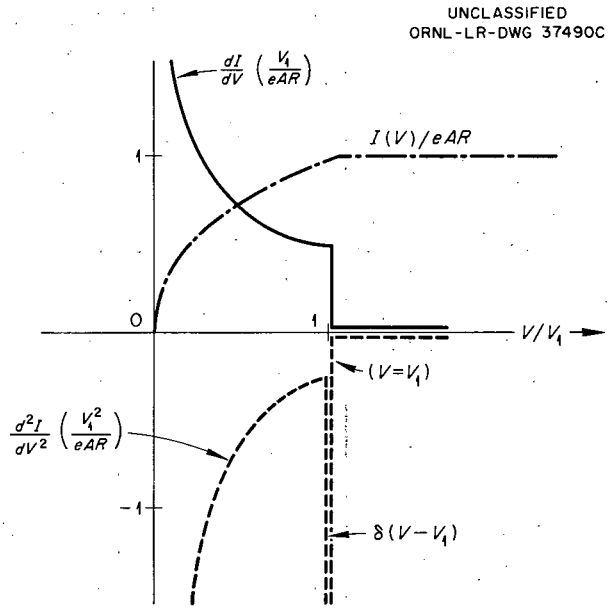

Fig. 134. Current-Voltage Curve and Derivatives for Monoenergetic Electrons.

A preamplifier of very low noise was used[80] because the small number of electrons with energies above 10 ev gave an $I(V)$ curve with little curvature and hence the intermodulation-signal amplitude was less than 5×10^{-14} amp. The input impedance was limited to about 10^8 ohms by the chamber plate and input capacitances. The noise from external sources was reduced as far as possible by careful shielding and by the use of shielded battery power supplies to remove hum and pickup, together with shock mounting of the system to reduce microphonics. Microphonic noise from the chamber plates necessitated shutting off the mechanical fore pump during measurements, and running the diffusion pump at low power to prevent bumping in the boiler. The preamplifier was mounted

[80] A detailed discussion of the noise problem in amplifier design is given in ref 79 and in the chapter by E. Fairstein, entitled "Electrometers and Amplifiers," in *Handbook of Instruments and Techniques* to be published under the sponsorship of the National Research Council Committee on Nuclear Science.

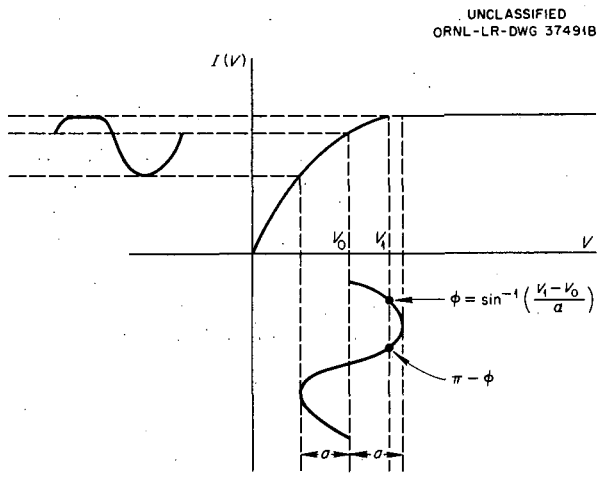

Fig. 135. Phase Angle Analysis for Monoenergetic Electron Line Profile.

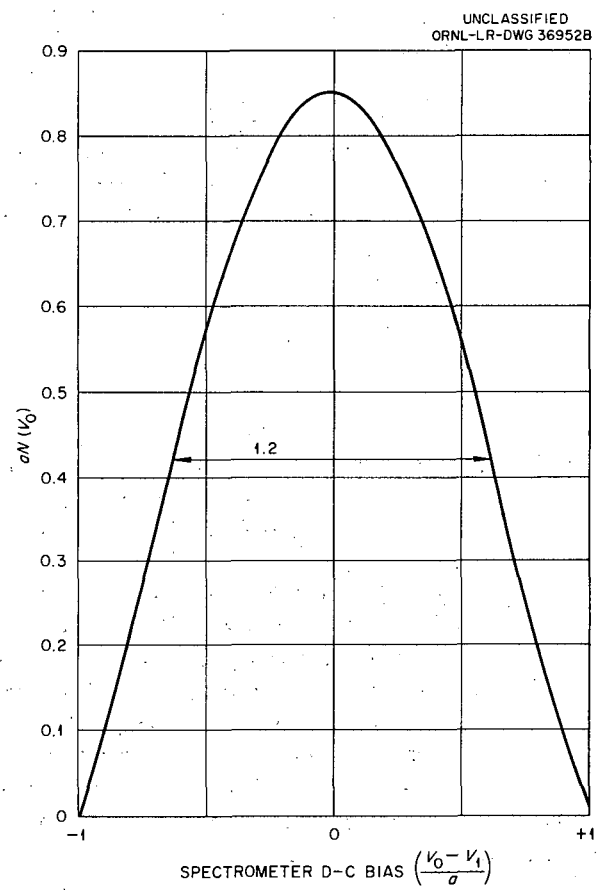

Fig. 136. Line Profile of Parallel-Plate Spectrometer for Monoenergetic Electrons.

beside the plates inside the vacuum system to allow short leads and thereby reduce pickup.

Inherent noise may arise in the amplifier from thermal agitation of electrons in the resistors, and from grid-current fluctuations, shot effect, and flicker effect in the input tube. The signal-to-noise ratio S/N is made as large as possible by minimizing each noise component.

Thermal-agitation noise and grid-current noise were both decreased by using as large an input capacitance as possible without making the input time constant longer than the period of the beat frequency signal to be detected. The long time constant also reduced the Schottky shot noise due to random variations in the electron stream within the first amplifier tube. A high transconductance in the input tube helped lower the shot noise, but the noise reduction thus obtained was limited by the fact that the mutual conductance of a tube increases with some power of the cathode emission current. Lowering the cathode current also lowered the grid current, and a lower grid current was accompanied by less noise resulting from its random variations.

The grid current was also reduced by operating the input tube at a low plate potential. The least grid-current noise occurred at the stable point in the curve of grid current vs grid voltage, at a potential about half a volt more negative than the floating grid point.

Flicker noise is apparently due to random changes in the work function of the tube cathode, and is independent of operating conditions.

The preamplifier circuit chosen is shown in Fig. 137. This is a modified cascode input with a constant-current pentode as a plate load. With proper choice of individual tubes for low noise and correct characteristics at the best operating points, the circuit gave good stability with a gain of the order of 100 or more.

The complete circuit is shown in Fig. 138. The two oscillators were tuned to 300 and 324 cps, respectively, and the signals fed through a mixing transformer of very high quality (General Radio type 941-A). A small variable capacitor formed one arm of a bridge and the parallel-plate chamber (spectrometer) formed the other. The capacitor was varied until the fundamental components were annulled in the measuring circuit, to prevent overloading of the preamplifier. The a-c output from the preamplifier at the difference frequency of

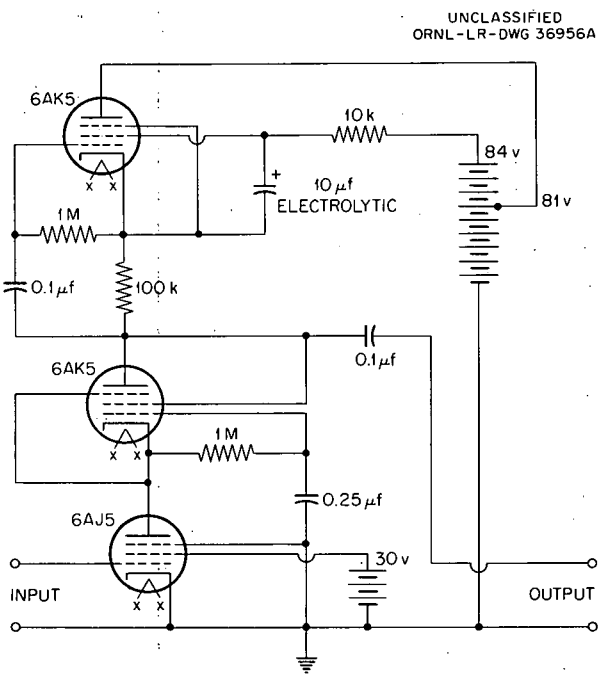

Fig. 137. Low-Noise Preamplifier Circuit.

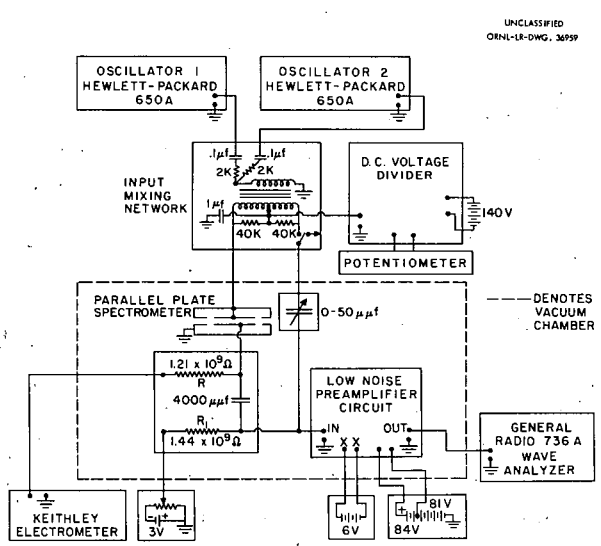

Fig. 138. Circuit Schematic Diagram for Measurement of Electron Flux in Media Bombarded by X Rays.

24 cps was measured on a General Radio wave analyzer with a 4-cps band width. The low beat frequency was chosen to give the highest possible input impedance with the necessarily rather large (45 $\mu\mu$f) capacitance in the spectrometer. The d-c current was measured with a Keithley model 410 micromicroammeter.

A typical measurement for the second derivative of the $I(V)$ curve is shown in Fig. 139. Except for the drop at very low voltages, this curve is quite similar to those obtained by Nelson *et al.*,[81] and the first derivative and $I(V)$ curve obtained by integration show even greater similarity to theirs.

The spectra of electrons released by x-ray bombardment are shown in Figs. 140–43, for copper, aluminum, graphite, and tissue-equivalent conducting plastic, respectively. It may be noted that for aluminum and graphite, x rays of the two energies gave practically indistinguishable spectra, which differences seem to exist for copper and the plastic. Above the range of measurements by Nelson *et al.*, the spectral shapes deviate appreciably from the empirical equation they found:

$$eN(E_w + V) = \frac{\alpha}{(\beta + E_w + V)^2} \quad . \qquad (13)$$

Also, the curves found by the a-c method fall off at very low energies, though this may be an artifact of the method.

With air in the chamber, the x-ray dose rate at a position between the plates was measured with a Victoreen Condenser r-Meter when all the absorbing and scattering materials were in approximately the same positions as during the experiment. The added absorption and scattering of the x rays by air should be negligible at the energies used between 50 and 250 kev.

The d-c current across the chamber is nearly constant above a d-c bias of 25 v. Figure 144 shows how this saturation current varies with the effective energy of heavily filtered x rays. The current per square centimeter per roentgen is

[81] D. R. Nelson *et al.*, *Measurement of Electron Flux in Media Bombarded by X-Rays*, ORNL-2151 (July 25, 1958).

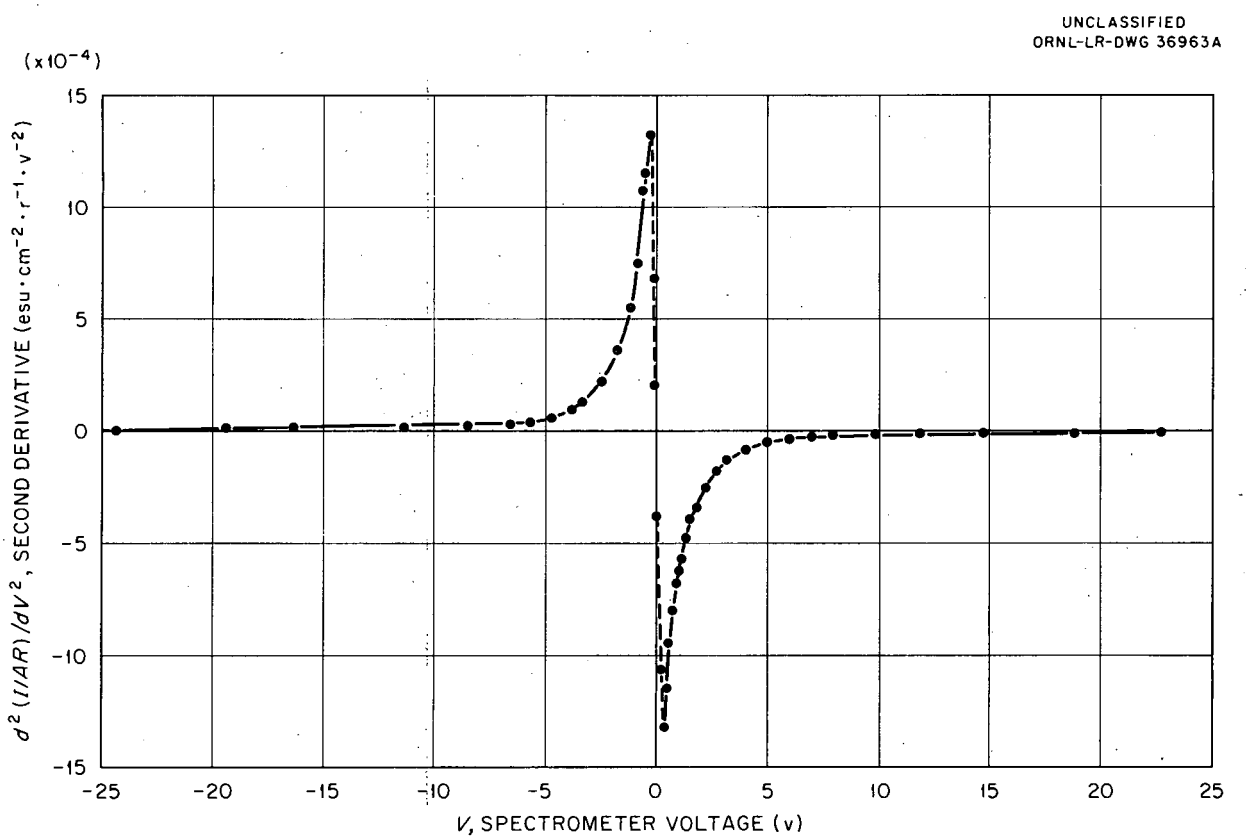

Fig. 139. Second Derivative of Current-Voltage Curve for Annealed Copper (250-kv Constant Potential X Rays).

nearly constant for graphite and tissue-equivalent plastic, but rises rapidly at lower energies for aluminum, and still faster for copper. Also, the yield per roentgen rises rapidly with atomic number in the photoelectric region below 100 kev.

The yield per absorbed rad may be calculated from these data by multiplying each point by the average absorption for that energy in the plates as used, using the spectra found by Villforth *et al.*[82] and the absorption coefficients given by Storm *et al.*[83] The procedure is not accurate, since the spectral range in the various beams is rather broad and the absorption, especially in copper, is a sensitive function of the x-ray energy below 100 kev. Also, with copper the beam after going through the two upper plates will be much more weighted on the high-energy side than that of Villforth. The resulting curves are shown in Fig. 145.

The significant feature of these curves is that the yield per absorbed rad is nearly constant for the several atomic numbers and over the range of energies measured, except perhaps in copper, possibly because of the error noted. We may say approximately that the net yield per rad absorbed in the plates is about 4×10^{-4} esu·cm^{-2}·rad^{-1} for the materials and energies investigated.

If we assume an average range for the secondary electrons of the order of 200 Å, we may calculate that roughly 100 ev is expended per secondary electron released in each of these materials. This is to be considered only as an estimate of order of magnitude, and more accurate data on the point would be desirable.

We feel that the investigation of the energy-flux distribution of secondary electrons released in a

[82] J. C. Villforth, R. D. Birkhoff, and H. H. Hubbell, Jr., *Comparison of Theoretical and Experimental Filtered X-Ray Spectra*, ORNL-2529 (July 1, 1958).

[83] E. Storm, E. Gilbert, and H. Israel, *Gamma-Ray Absorption Coefficients for Elements 1 Through 100 Derived from Theoretical Values of the National Bureau of Standards*, LA-2237 (1958).

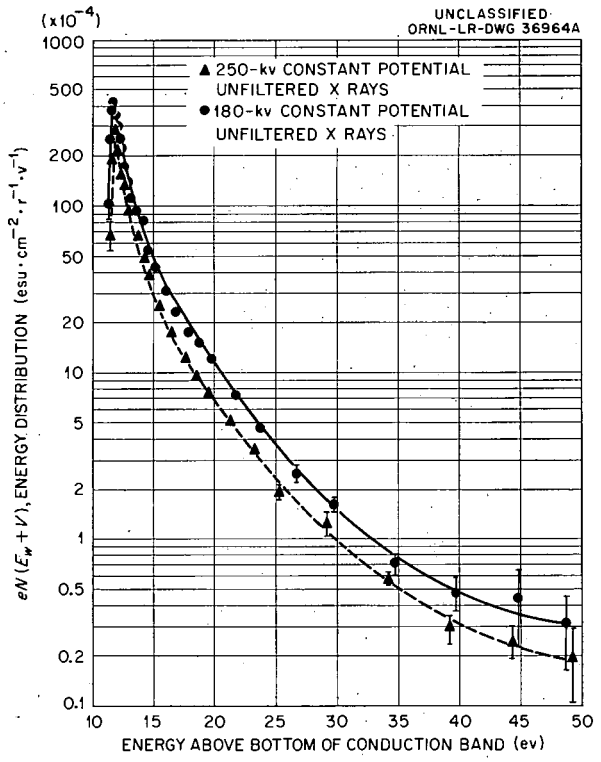

Fig. 140. Energy Distribution of Flux in Annealed Copper.

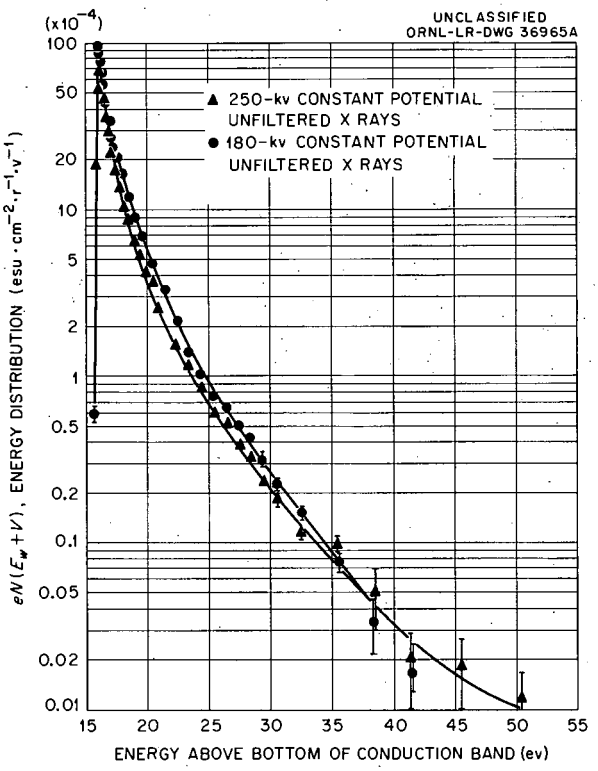

Fig. 141. Energy Distribution of Flux in Aluminum.

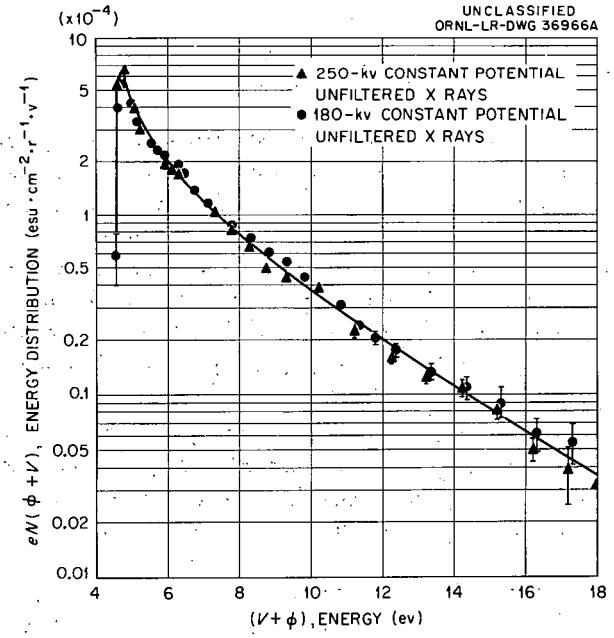

Fig. 142. Energy Distribution of Flux in Graphite.

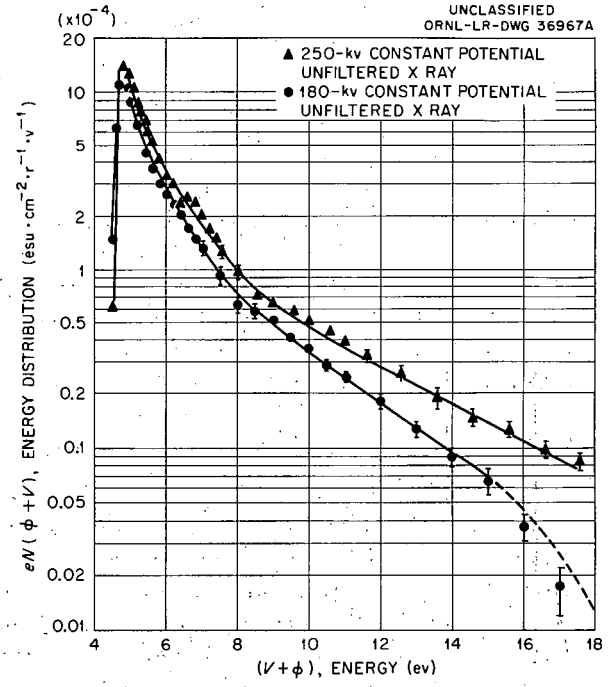

Fig. 143. Energy Distribution of Flux in Tissue-Equivalent Conducting Plastic.

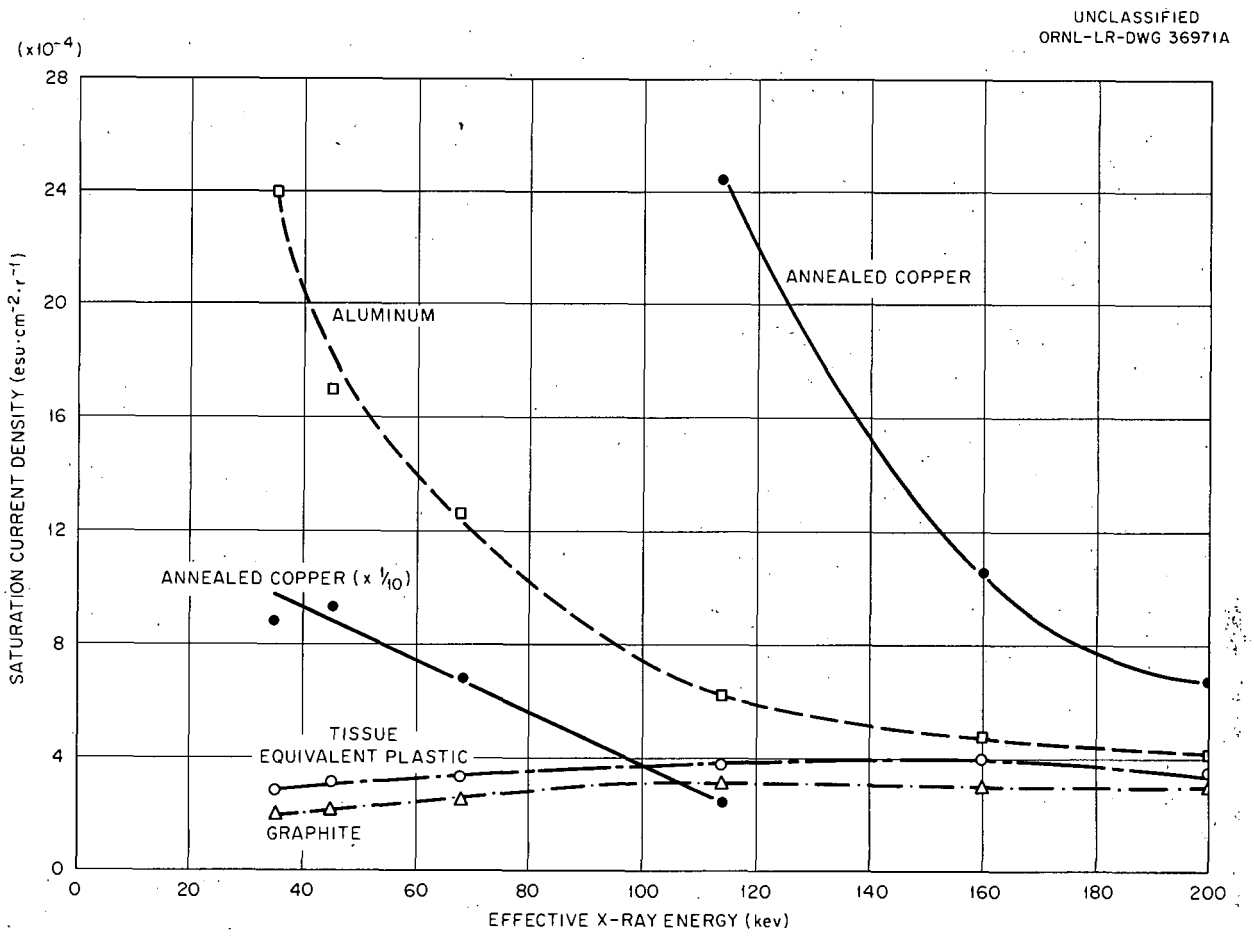

Fig. 144. Saturation Current Density per Roentgen for Heavily Filtered X Rays.

medium is an important first step in understanding the interaction of radiation and matter, and perhaps may shed light on the significance of the Relative Biological Effectiveness Factor. Further experimental and especially theoretical studies would be desirable.

Measurement of Electron Stopping Power at Low Energies – Scattering Effects

The studies described last year wherein the stopping powers of thin foils are measured calorimetrically have been extended to elements of higher atomic number. Because nuclear scattering increases with atomic number, increased attention must be paid to the influence of scattering on the experimental results.

It is well known[84] that electrons which emerge from thin foils at angles of the order of 90° or more from the direction of incidence have in general suffered only one large-angle scattering in the foil. If a fraction f of the incident beam scatters into an angular range between θ_1 and θ_2, where these are the angles subtended at the center of the foil by the copper ring on which the foil is mounted, it may be assumed that these electrons deliver all of their energy E to the system instead of the amount $\overline{\Delta E}_{exp}$ associated with a traversal of the foil. The foil and ring are then heated more than they should be, and an

[84] R. D. Birkhoff, *Handbuch der Physik*, vol 34, p 53, Springer, Berlin, 1958.

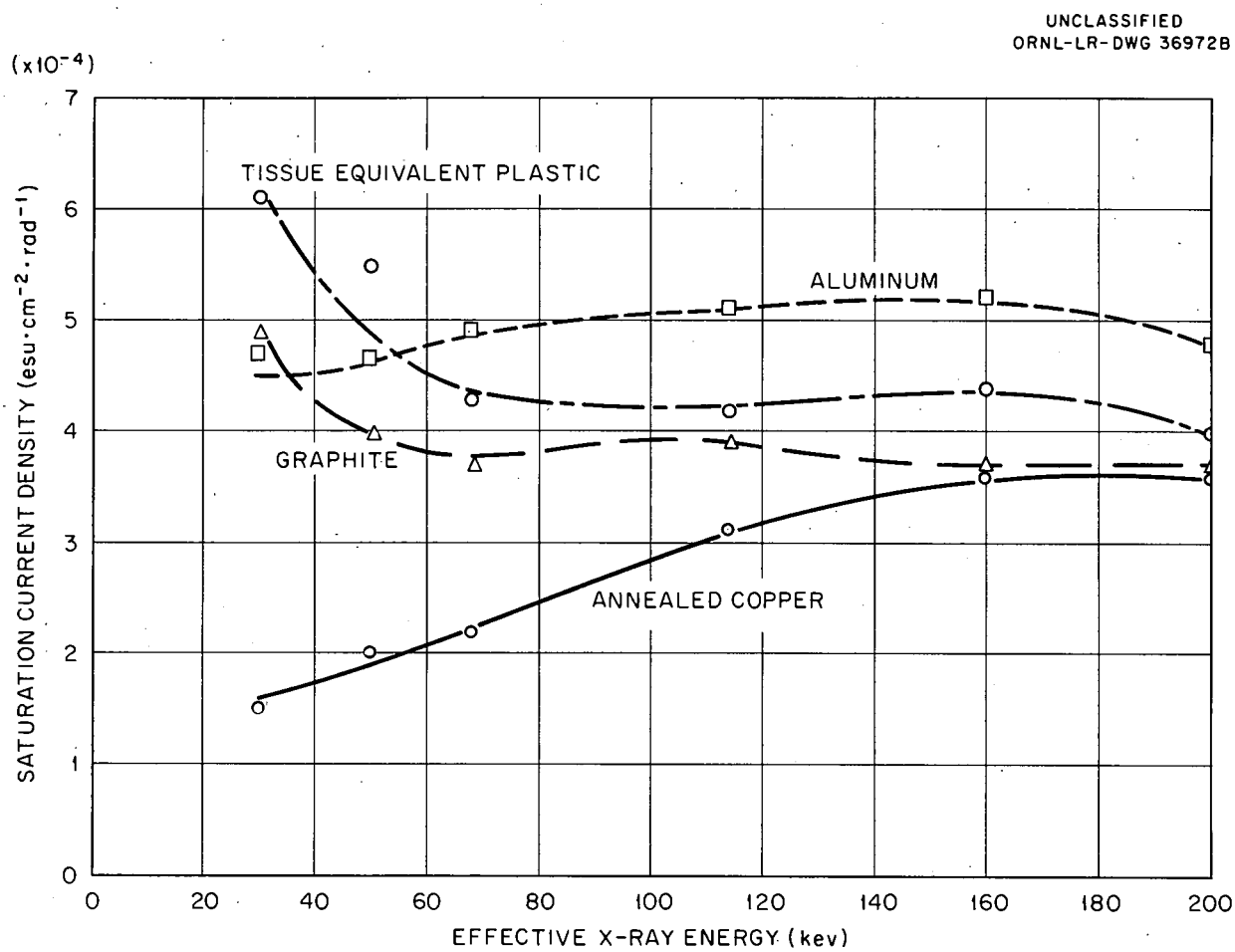

Fig. 145. Saturation Current Density per Absorbed Rad for Heavily Filtered X Rays.

evaluation of this heating leads to an apparent energy loss $\overline{\Delta E}_{app}$ which exceeds $\overline{\Delta E}_{exp}$. It is obvious that

$$\overline{\Delta E}_{app} = (1 - f)\,\overline{\Delta E}_{exp} + fE \quad , \qquad (1)$$

or that

$$\frac{\overline{\Delta E}_{app}}{E} = (1 - f)\,\frac{\overline{\Delta E}_{exp}}{E} + f \quad . \qquad (2)$$

This fractional apparent energy loss is plotted in Fig. 146 as a function of f for various values of the fractional experimental energy loss. A sensible limit to the amount of heating which may be permitted due to the beam striking the ring may be arbitrarily set such that foil and ring heating

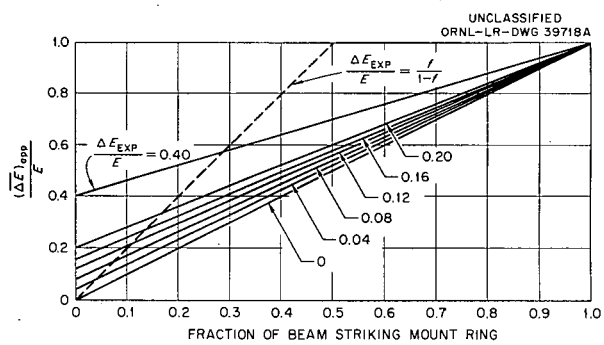

Fig. 146. Relation of Fractional Apparent Energy Loss of an Electron Beam Traversing a Thin Foil to That Observed Calorimetrically When Part of the Scattered Electrons Strike the Foil Mounting Ring.

are equal. In this case

$$\frac{\overline{\Delta E}_{\text{app}}}{E} = 2f \ , \tag{3}$$

and this limit is plotted also in the figure. If a point determined by the experimental $\overline{\Delta E}_{\text{app}}/E$ and the theoretical f lies above this line, the data may be considered meaningful; if it does not, the data should be rejected.

The values of f may be computed from single-scattering theory. The differential cross section for scattering through an angle between θ and $\theta + d\theta$ into a solid angle $d\Omega = 2\pi \sin\theta \, d\theta$ is, according to Rutherford,[85]

$$d\sigma(\theta) = \left[\frac{\pi Z^2 e^4 (1-\beta^2)}{2m_0^2 v^4}\right] \frac{\sin\theta \, d\theta}{\sin^4(\theta/2)} \ , \tag{4}$$

where Z is the atomic number of the scatterer, e, m_0, and v are the electronic charge, mass, and velocity, respectively, and $\beta = v/c$.

The value of f is obtained by multiplying this cross section by the number of atoms per square centimeter and integrating between θ_1 and θ_2. The more exact single-scattering cross section obtained by Mott[86] in the form of an infinite series has been evaluated recently on a digital computer by Doggett and Spencer.[87] The results are given as a ratio of the Mott to the Rutherford cross section, σ/σ_R. For a given energy and atomic number, the ratio changes only slowly over the angular range between θ_1 and θ_2 and an average value of the ratio may be used with little error. Thus the fraction f of the incident electron beam which strikes the ring is

$$f = \frac{\sigma}{\sigma_R} \times \frac{N_A \rho t}{A} \times \frac{\pi Z^2 e^4 (1-\beta^2)}{m_0^2 v^4} \times$$

$$\times \left[\frac{1}{\sin^2(\theta_1/2)} - \frac{1}{\sin^2(\theta_2/2)}\right] . \tag{5}$$

Besides the single nuclear scattering which causes an extraneous heating of the foil and ring, multiple nuclear scattering exists, which causes the path length in the foil to exceed the foil thickness. If, at some depth in the foil t', the electron moves to $t' + dt'$ while moving at an angle θ to the direction of incidence, then the actual path length dx is

$$dx = \frac{dt'}{\cos\theta} \cong dt'\left(1 + \frac{\theta^2}{2}\right) . \tag{6}$$

Now if the increased path length dl which results is defined by the relation

$$dx = dt' + dl \ , \tag{7}$$

it is apparent that

$$dl = \frac{\theta^2}{2} \, dt' \ . \tag{8}$$

If the foil may be considered as divided into slabs of thickness dt', wherein the contribution $\overline{\theta^2}$ to the mean squared scattering angle for the entire foil is the same, then

$$\overline{dl} = \frac{\overline{\theta^2}}{2} \, dt' \ , \tag{9}$$

and because of the additivity of Gaussian distributions, the over-all increase in path $\overline{\Delta l}$ is just

$$\overline{\Delta l} = \int_0^t dl = \frac{1}{2}\int_0^t \overline{\theta^2} \, dt' \ . \tag{10}$$

The mean squared scattering angle as calculated by Williams[88] is sufficiently accurate for this purpose and is given by

$$\overline{\theta^2} = t \, \frac{4\pi N Z(Z+1) \, e^4 (1-\beta^2)}{m_0^2 v^4} \times$$

$$\times \ln\left[4\pi Z^{1/3} (Z+1) \, Nt \left(\frac{\hbar}{m_0 v}\right)^2\right] \tag{11}$$

$$= \alpha t \ln(\delta t) \ ,$$

where N is the number of atoms per cubic centimeter and the numbers α and δ are defined as indicated.

[85] E. Rutherford, *Phil. Mag.* 21, 669 (1911); R. D. Birkhoff, *loc. cit.*

[86] N. F. Mott, *Proc. Roy. Soc. (London)* A124, 425 (1929); A135, 429 (1932).

[87] J. A. Doggett and L. V. Spencer, *Phys. Rev.* 103, 1597 (1956).

[88] E. J. Williams, *Proc. Roy. Soc. (London)* A169, 531 (1939); *Phys. Rev.* 58, 292 (1940).

By substituting Eq. (11) into Eq. (10) and performing the integration, one obtains

$$\overline{\Delta l} = \frac{\alpha t^2}{4} [\ln (\delta t) - 0.5] \quad . \tag{12}$$

The total path length $\overline{\Delta x}$ is then

$$\overline{\Delta x} = t + \overline{\Delta l} \quad . \tag{13}$$

It is again apparent that thin foils must be used because the increase in path length depends on the square of the foil thickness.

The stopping power of a 192-μg/cm^2 copper foil is shown in Fig. 147. The experimental points are shown after correction for scattering as described above. The extraneous heating due to scattering onto the foil mounting ring varied from a high of 50% of the foil heating at the lowest energy to a low of 33% at the highest energy. The increased path length due to multiple scattering varied from a high of 7.7% of the foil thickness to a low of 0.4%, again at the lowest and highest energies, respectively. The solid line is that given by the theory of Bethe, and the agreement is seen to be excellent.

In order to reduce the heating due to ring pickup, a new calorimeter design has been worked out in which the ring subtends only 1% as large a solid angle as the one used above. In this design the thermoelectric metals bismuth and antimony are vacuum evaporated onto a 1-mg/cm^2 Mylar film which has a hole punched in its center over which the foil may be placed. Preliminary tests indicate a much lower pickup, lower time constant, and higher sensitivity than the present design.

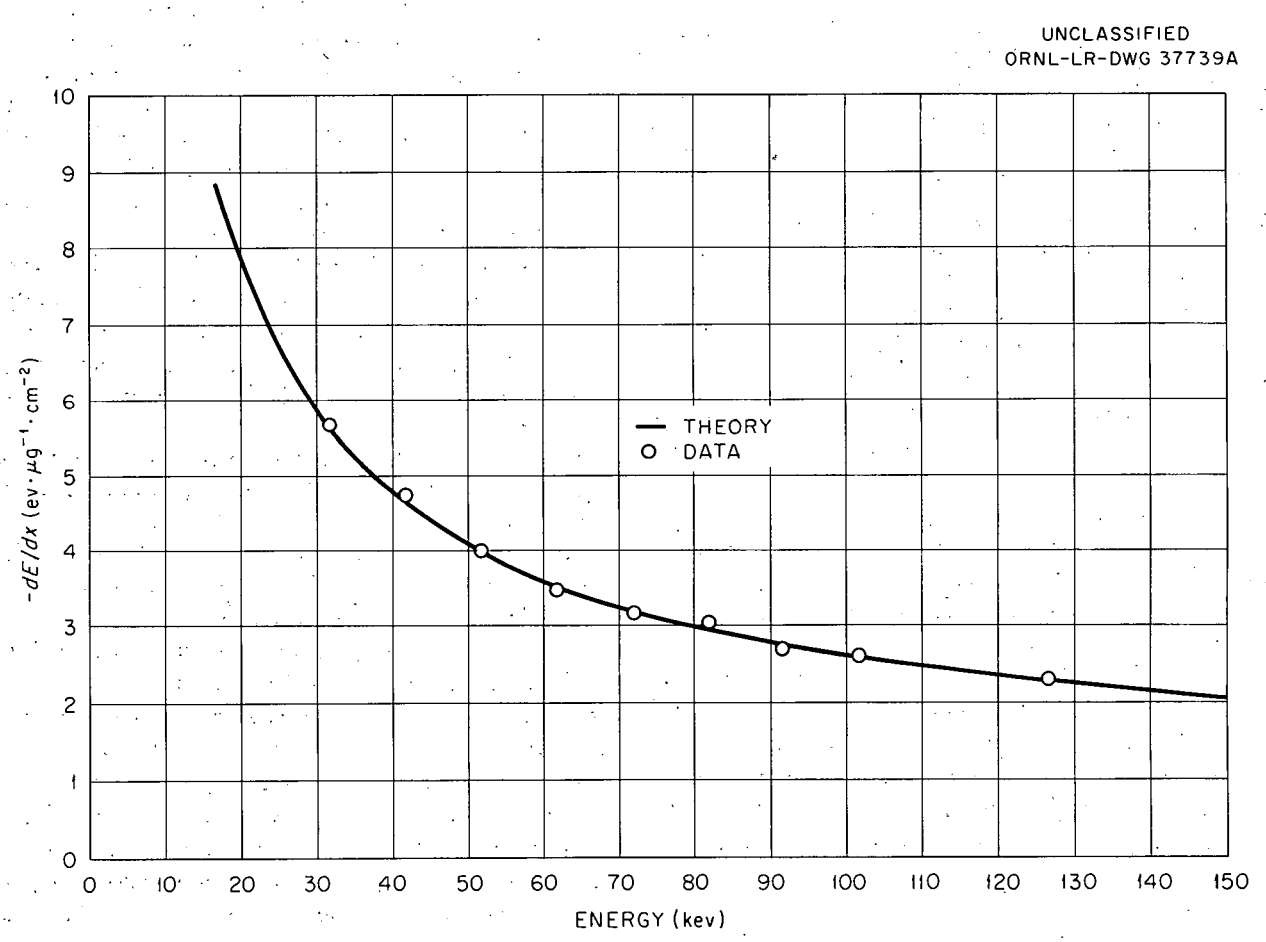

Fig. 147. Stopping Power of 191.8-μg/cm^2 Copper.

Studies on Personnel Dosimeters

The development of the wrist dosimeter described in the last progress report[89] led to further consideration of the design principles of ion chamber–electrometer dosimeters.[90] These results are summarized below under the general considerations of the requirements for satisfactory dosimetry of beta and gamma radiation, the consequences of the electrical properties of separable ion chamber–electrometer systems, the methods for minimizing the chamber dimensions, and the angular response of partially shielded cylindrical dosimeters.

The satisfactory design of any dosimeter requires a clear understanding of exactly what the dosimeter system is intended to measure. The simultaneous dosimetry of mixed radiations such as beta and gamma rays presents a particular problem because the requirements for correct dosimetry are different and partially conflicting for the two radiations. A reasonably satisfactory compromise is possible at some sacrifice in accuracy because in health physics one wishes to determine principally the percentage of the maximum permissible dose which an individual has received.

For penetrating radiation such as x rays and gamma rays up to 2 or perhaps 3 Mev the dose may be calculated by the use of the Bragg-Gray principle from measurements with a cavity ionization chamber. The principle states that the absorbed dose in a medium (the walls of the cavity) may be measured by the ionization produced in a small gas-filled cavity in the medium by the use of the relation

$$E_m = JW\rho \quad ,$$

where E_m is the energy absorbed in ergs per gram of medium, J is the measured ionization per gram of gas, W is the average energy in ergs expended by the radiation to produce an ion pair in the gas, and ρ is the ratio of the mass stopping power of the medium to that of the gas.

Two important restrictions must be placed on the use of this principle to determine the dose. First, W and ρ must be the same in the dosimeter as in air for all energies of radiation. Since these quantities do in fact depend on the radiation energy rather strongly in the x-ray region, the walls of the cavity must be made of materials having as nearly as possible the same average atomic number as air. The second restriction is that as many secondary electrons must be produced in each element of the inner walls as stop there, a condition which is referred to as "electronic equilibrium." This equilibrium is assured when the walls of the cavity have a thickness equal to the range of the most energetic secondary electrons produced by the radiation. On the other hand, the walls must not be thick enough to produce a significant attenuation of the radiation. These two requirements tend to be mutually exclusive for radiation of a wide range of energies, since walls thick enough to produce electronic equilibrium for 3-Mev gamma rays, about 1 cm of plastic, will attenuate 20-kev x rays to about 35% of their original intensity. In theory one always corrects for the chamber wall attenuation once the distance from the source exceeds the range of the secondary electrons, but this is impossible in dosimetry of unknown radiations. The cases mentioned are, of course, extreme, but illustrate the dilemma and show the maximum error which may occur. Approximate equilibrium may be attained over most of the common energy range with about 2 to 3 mm of plastic. This much shielding also reduces the error due to backscattered radiation, since the backscattered radiation is always softer and attenuated more in the shield than is the primary radiation.

For the dosimetry of beta rays, the rapid attenuation of the radiation in matter requires the use of very thin walls, in contrast to the thick ones needed in measuring gamma rays. Handbook 59 (ref 91) specifies (p 38) that the maximum permissible dose rate to the basal layer of the epidermis (defined as lying at a depth corresponding to 7 mg/cm^2) shall be 600 millirads per week. It is usually satisfactory to measure the dose in air, a measurement which can be made if the dosimeter walls have no more than 7 mg/cm^2 superficial density and are air equivalent. Since Handbook 59 allows only half the exposure to penetrating radiation that is permitted for nonpenetrating, a compromise design for the ionization chamber with 50%

[89] G. S. Hurst *et. al.*, *H-P Ann. Prog. Rep. July 31, 1958*, ORNL-2590, p 114.

[90] H. H. Hubbell, Jr., A. P. Hull, and R. D. Birkhoff, *A Small Wrist Dosimeter for Beta and Gamma Radiation*, ORNL-2730 (to be published).

[91] *Permissible Dose from External Sources of Ionizing Radiation*, Natl. Bur. Standards (U. S.) Handbook No. 59 (Sept. 24, 1954).

of the wall area having a thickness of about 2 mm and 50% having only 7 mg/cm^2 gives a dosimeter which, being only half as sensitive to beta rays, can be read in percentage of MPD (maximum permissible dose) to both types of radiation.

Personnel monitoring of large groups of people requires the use of inexpensive devices. The cost is greatly reduced by having the persons wear only the ionization chambers and using one electrometer to read the discharge of all the chambers. Any new chamber sensitive to beta radiation should therefore be designed to be charged and read on an available electrometer both to reduce costs and for greatest convenience. The type of string electrometer in common use is basically an electrostatic voltmeter with very low capacitance and a scale marked in milliroentgens. The characteristics to be considered in designing a chamber for use with a given electrometer are its sensitivity in volts per division (or volts per mr as it is marked), $S = \Delta v_m/\Delta D$, and its capacitance c.

An ion chamber (of capacitance C and volume V) is charged by first being connected to the electrometer; the two are charged to a predetermined voltage, v_m, marked "0 mr" on the scale. Then the chamber is removed, capped, and exposed to radiation which lowers its charge, and its voltage by Δv_c. It is then uncapped and reconnected to the electrometer, and the resultant voltage of the two becomes v_D. It can readily be shown from the conservation of charge that the sensitivity of the system is

$$S = \frac{V}{C + c}$$

in esu, or

$$S'\left[\frac{\text{volts}}{\text{milliroentgen}}\right] = \frac{V}{3(C' + c')}\left[\frac{\text{cm}^3}{\mu\mu f}\right]$$

in conventional units.

Two important conclusions can be drawn from this result: First, the final reading of the electrometer after a radiation exposure to the chamber is independent of the initial charging voltage at which the electrometer reads zero, as pointed out previously.[92] Second, the same sensitivity and calibration may be obtained for different chambers either by making the new chamber have the same volume, V, and capacitance, C, as that for which the electrometer was designed, or by varying V and C but keeping the ratio $V/(C + c)$ constant. This relaxation on the requirements for V and C gives an added adjustable parameter in chamber design so that an additional condition may be imposed, such as minimum dimensions or electric field above a predetermined minimum after discharge.

A further conclusion may be drawn from the electrostatic behavior of the system, namely, that the voltage change of the electrometer is only $C/(C + c)$ of that of the chamber. This result shows the desirability of low capacitance in the electrometer since the chamber voltage drops by $(C + c)/C$ of the drop observed on the electrometer. The lowest voltage of the chamber after discharge must still be adequate to produce saturation, so that none of the ions formed by the radiation can recombine.

A method for optimizing the dimensions of an ion chamber for fixed volume and capacitance was mentioned in the last annual progress report, to which reference has been made. More general techniques and restrictions have emerged from further study of this problem and will be summarized here[93] with illustrations from the cases of hemispherical and pillbox-shaped chambers, which appear to be the most suitable shapes for wrist wear.

In the simplest case, the volume and capacitance of the chambers may be made equal to those of the chamber for which the electrometer system was designed. For example, the Victoreen Minometer and pocket chamber, model 362, form such a pair and were convenient models for design. There are two equations to satisfy in each case – one for the sensitive volume and the other for the capacitance as functions of the dimensions: inner and outer radii for hemispheres, or radius and separation of the plane-parallel electrodes in a pillbox design, as indicated in Fig. 148*a*. They are:

Hemispheres –

$$V = \frac{2\pi}{3}(R^3 - r^3) ,$$

[92] H. H. Hubbell, Jr., R. D. Birkhoff, and R. M. Johnson, *Pocket Ion Chambers for Beta Radiation Dose*, ORNL-2158 (Apr. 26, 1957).

[93] A detailed discussion is given by E. Rutherford, *Phil. Mag.* 21, 669 (1911); R. D. Birkhoff, *loc. cit.*

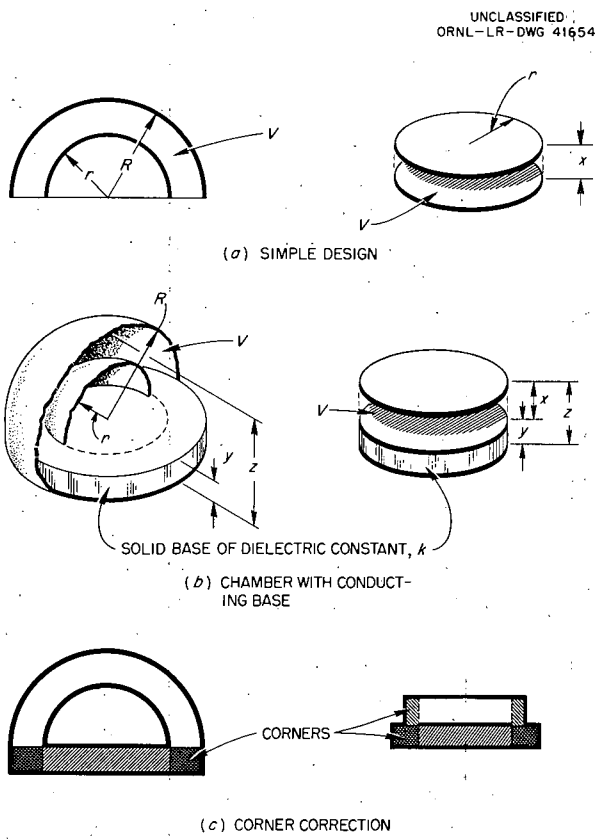

Fig. 148. Geometry of Hemispherical and Pillbox Ionization Chambers. Electrodes shown by heavy lines.

$$C = 2\pi\epsilon \frac{Rr}{R - r} ;$$

Pillbox Wrist Dosimeter –

$$V = \pi r^2 x ,$$

$$C = \frac{\epsilon \pi r^2}{x} .$$

The solution for the dimensions is unique in either case, and no additional requirements can be imposed.

However, electrostatic principles require that if the potential of the insulated electrode of the chamber is to change only because ionization by radiation has lowered its charge, the electrode must be completely surrounded by another electrode, usually at ground potential. This geometric requirement is satisfied for spherical or cylindrical electrodes with closed ends, but not for the simple hemispherical or pillbox arrangements. Therefore a metallic base connected to the grounded electrode is needed in order to isolate the insulated electrode. This base will have a capacitance to the insulated electrode. Furthermore, in order to avoid shielding of part of the sensitive volume from beta rays by the inner electrode, the grounded base must be separated from the inner electrode by a solid dielectric, so two additional adjustable parameters enter, the thickness and dielectric constant of the base. Hence two additional requirements may be imposed, such as a minimum value for the total thickness, and an electric field which exceeds a specified minimum everywhere in the sensitive volume even after full-scale discharge.

The capacitance equation thus contains two additional independent variables k and y as indicated in Fig. 148*b*:

Hemispheres –

$$C = \epsilon\pi \left(\frac{2Rr}{R - r} + \frac{kr^2}{y} \right) ,$$

Pillbox Wrist Dosimeter –

$$C = \epsilon\pi r^2 \left(\frac{1}{x} + \frac{k}{y} \right) .$$

The minimum thickness condition may be imposed by expressing the total thickness, z, as a function of the volume, capacitance, and dimensions, and by setting, for example, $dz/dr = 0$ or $dz/dx = 0x$. The resulting three equations for V, C, and the derivative may be solved simultaneously to obtain expressions for the dimensions in terms of the dielectric constant k, the capacitance units constant ϵ, and the given values of V and C.

The dielectric constant may be chosen so that the electric field after a chosen full-scale discharge, such as 200 mr, is still above a specified minimum value known to be sufficient to collect all the ions formed at any reasonable exposure rate. The electric field equations may be written to give this minimum value after discharge in terms of the initial electrometer charge voltage v_m and the exposure D in the form:

Hemispheres –

$$E_R = \frac{Cv_m - VD}{4\pi\epsilon r^2} ,$$

Pillbox Wrist Dosimeter –

$$E = \frac{Cv_m - VD}{Cx} .$$

It may well happen that the dimensions so calculated are inconvenient for a wrist dosimeter, or that a dielectric material both of sufficiently high insulation to prevent leakage and have the correct dielectric constant may not be available. Therefore it is convenient to use the sensitivity requirement mentioned above and allow other values of volume and capacitance. This gives an additional degree of freedom and permits the choice of convenient dimensions, or alternatively in the case of the pillbox design, permits one in principle to make a chamber having both minimum thickness and also minimum radius. Actually, however, the derivative equations for this case do not have a solution minimizing both dimensions of the pillbox simultaneously.

An additional problem arises from the fact that the outer electrode must completely surround the inner one. As a result, there are corners between the electrodes which add to the total capacitance, as indicated in Fig. 148*c*. The corrections can be calculated approximately from the published formula.[94] The calculation procedure outlined above for the optimum dimensions of the dosimeter chamber is very useful in guiding the design, but the resulting equations are quite complex algebraically and must be solved by numerical approximation methods. To add the corner-correction formula to the capacitance equation would hopelessly complicate the result. It is usually satisfactory to calculate the best dimensions without this correction, then calculate the correction, and use the sensitivity equation as a guide in modifying the dimensions to obtain the correct response with a given electrometer.

Angular Response of a Partially Shielded Cylindrical Dosimeter

Some cylindrical dosimeters have very thin walls and are partially shielded by a reinforcing structure. If the tops and sides of the dosimeter are unequally shielded the response of the dosimeter will depend upon the angle between the plane of the cylinder base and the direction of the incident radiation. For instance, a cylinder with unshielded top and opaque sides will admit all radiation incident perpendicular to the plane of the base, but none which is incident parallel to the base. If the fraction of the volume irradiated through the top and the fraction irradiated through the sides are known separately as functions of the angle of incidence, the total irradiated volume of a shielded dosimeter may be determined as a function of the angle of incidence. These fractions are derived below.

In the diagram, Fig. 149, θ is the angle between the direction of the incident radiation and the plane of the base of the cylinder, and ϕ is an angle in the plane of the base made with a line through the center of the base in the reference direction. If p is the radius, a plane at a distance $x = p \sin \theta$ from the axis of the cylinder and parallel to the reference direction forms the base of an infinitesimal rectangular volume element. It is convenient to consider two cases.

Case I:

$$\cos \phi \geqq \cos \phi_c \equiv \frac{h}{2p \tan \theta} ,$$

or

$$\phi \leqq \phi_c .$$

Case II:

$$\cos \phi \leqq \cos \phi_c ,$$

or

$$\phi \geqq \phi_c .$$

These two cases are illustrated in Fig. 149. Thus ϕ_c is the critical angle such that a ray incident at angle θ is parallel to the diagonal of the volume elements whose edges intercept the top of the cylinder at angles ϕ and $\pi - \phi$. The infinitesimal rectangular volumes have been divided into three regions in both cases. In case I it is obvious that region (1) will be irradiated through the side, while regions (2) and (3) will be irradiated through the top. Similarly in case II regions (4) and (5) will be irradiated through the side, while region (6) will be irradiated through the top.

In case I the infinitesimal volume element of region (1) is

$$dV_1 = \frac{h^2 p \cos \phi \, d\phi}{2 \tan \theta} ,$$

where h is the height of the cylinder. The volume

[94] *American Institute of Physics Handbook*, sec 5, p 17, McGraw-Hill, New York, 1957.

UNCLASSIFIED
ORNL-LR-DWG 41655

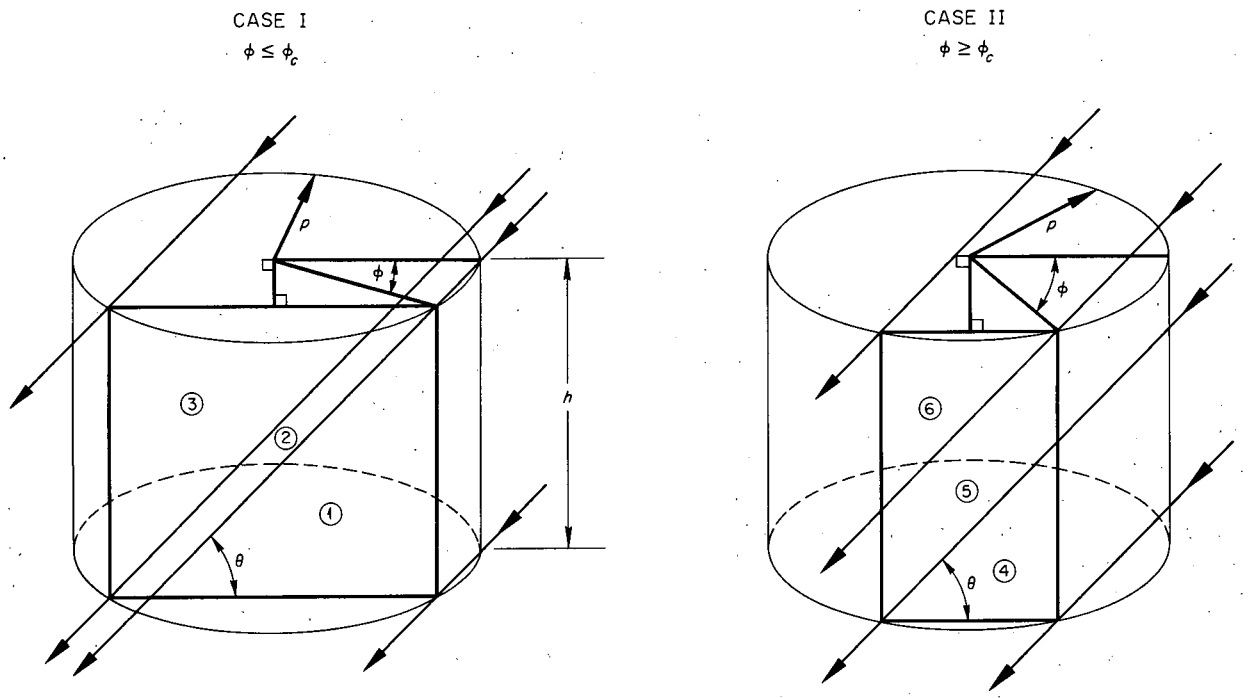

Fig. 149. Geometry for the Angular Response of a Partially Shielded Cylindrical Dosimeter.

element of region (2) is

$$DV_2 = \left[2p \cos \phi - \frac{h}{\tan \theta}\right] hp \cos \phi \, d\phi \ ,$$

and the volume element of region (3) is

$$dV_3 = dV_1 \ .$$

In case II the volume element of region (4) is

$$dV_4 = 2p^3 \tan \theta \cos^3 \phi \, d\phi \ ,$$

the volume element of region (5) is

$$dV_5 = 2p^2 \cos^2 \phi \, d\phi \, [h - 2p \cos \phi \tan \theta] \ ,$$

and the volume element of region (6) is

$$dV_6 = dV_4 \ .$$

Now the volume irradiated through the top will be

$$V_{top} = 2 \int_0^{\phi_c} (dV_2 + dV_3) + 2 \int_{\phi_c}^{\pi/2} dV_6 \ ,$$

and that through the side will be

$$V_{side} = 2 \int_0^{\phi_c} dV_1 + 2 \int_{\phi_c}^{\pi/2} (dV_4 + dV_5) \ .$$

The solutions of these integrals are

$$\frac{V_{top}}{\pi p^2 h} = \frac{2\phi_c}{\pi} + \frac{\sin 2\phi_c}{\pi} - \left(\frac{h}{p}\right) \frac{\sin \phi_c}{\pi \tan \theta} + \frac{4\pi \tan \theta}{\pi (h/p)} \left(\frac{2}{3} - \sin \phi_c + \frac{\sin^3 \phi_c}{3}\right)$$

and

$$\frac{V_{side}}{\pi p^2 h} = 1 - \frac{2\phi_c}{\pi} - \frac{\sin 2\phi_c}{\pi} + \left(\frac{h}{p}\right) \frac{\sin \phi_c}{\pi \tan \theta} + \frac{4 \tan \theta}{\pi (h/p)} \left(\frac{2}{3} - \sin \phi_c + \frac{\sin^3 \phi_c}{3}\right) \ ,$$

where

$$\phi_c = \cos^{-1} \frac{(h/p)}{2 \tan \theta} \ .$$

Note the dependence of the fractional irradiated

volumes on the parameter (h/p), the "tallness" of the cylinder. The functions

$$\frac{V_{\text{top}}\,[\theta,\,(h/p)]}{\pi p^2 h}$$

and

$$\frac{V_{\text{side}}\,[\theta,\,(h/p)]}{\pi p^2 h}$$

have been plotted in Fig. 150 for several values of the parameter (h/p) including $h/p = 0.521$, which applies to a beta dosimeter developed at ORNL. The two curves for any value of (h/p) represent, respectively, the fraction of the volume which received radiation through the top of the cylinder for an angle of incidence θ, and the fraction which received radiation through the side. The sum of the two ordinates at any θ must be unity.

If A_{top} is the unshielded area of the top and A_{side} is the unshielded area of the side, then the irradiated volume $V_{\text{eff}}(\theta)$ at an angle of incidence θ is

$$V_{\text{eff}}(\theta) = \frac{A_{\text{top}}}{\pi p^2}\,V_{\text{top}}(\theta) + \frac{A_{\text{side}}}{2\pi p h}\,V_{\text{side}}(\theta)\ .$$

Two assumptions must be made in order to use $V_{\text{eff}}(\theta)$ to determine the per cent of the radiation incident which is recorded in the cylindrical chamber: first, the "shielding" cover must contain a large number of holes whose dimensions are small compared with the dimensions of the cylinder, and, second, the diameter of the holes must be large compared with the thickness of the cover. These requirements are necessary in order that the transmission through any one hole vary at the same rate as the projection of its area on a plane perpendicular to the direction of incidence. This projection was used in deriving the formula for $V_{\text{eff}}(\theta)$. With these restrictions, the curves offer a convenient method of finding the angular dependence of the response of a cylindrical chamber.

UNCLASSIFIED
ORNL-LR-DWG 39502A

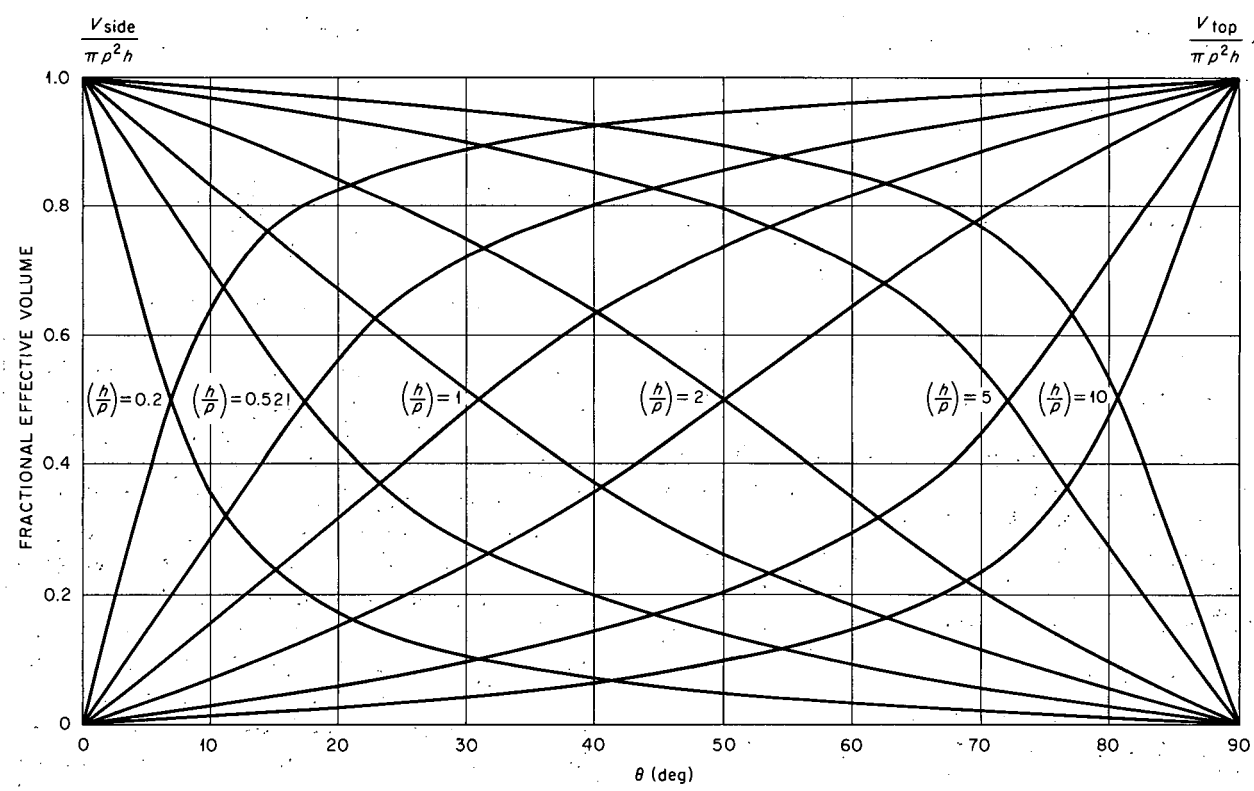

Fig. 150. Fractions of the Volume of a Cylindrical Dosimeter Which Receive Radiation Through the Sides and Top, Respectively.

DOSIMETRY TECHNIQUES

F. J. Davis R. M. Simmons
P. W. Reinhardt E. B. Wagner
J. Thorngate[95]

Threshold Detector Program

Molded Boron Shields. – Molded B^{10} spherical shields (Fig. 151) have been developed to replace the spherical boron-loaded shields[96] used with fission foil threshold detectors. The new type of shield, fabricated by the Norton Company, has a composition of 77% B^{10} and 23% C and is molded under high pressure and temperature conditions to a wall thickness of 1 cm, a density of 2.38 g/cm^3, and a B^{10} density of 1.66 g/cm^3. Two of the new shields and two of the old type with 1- and 2-cm wall thicknesses were loaded with fission foils. To compare their efficiency in the removal of thermal neutrons, these shields were exposed in the West Animal Tunnel of the ORNL Graphite Reactor; sulfur pellets were used for monitoring. With the energy spectrum of the neutron flux assumed to be the same for all the shields, a measure of the efficiency of the shields would be the ratio of the activity of the plutonium foil (which has a high thermal cross section) to that of the other foils. The ratios of the foil activities shown below indicate that the new type of shield is better than the old type of 1 cm thickness and equal to, if not better than, the old type of 2 cm thickness.

Type of Shield	Pu/U	Pu/Np	Pu/S
New	5.28	1.84	5.03
	5.11	1.74	
Old, 1 cm thick	6.68	1.98	6.20
Old, 2 cm thick	5.80	1.69	5.43

A large molded boron shield with wall thickness of 3.75 cm composed of 80 to 90% natural boron (18.8% B^{10} + 81.2% B^{11}) and carbon and having a density of 2.5 g/cm^3 was compared with the molded B^{10} shield. The removal of thermal neutrons was comparable for the two shields; however, the attenuation of fast neutrons by the large shield was of the order of 25%.

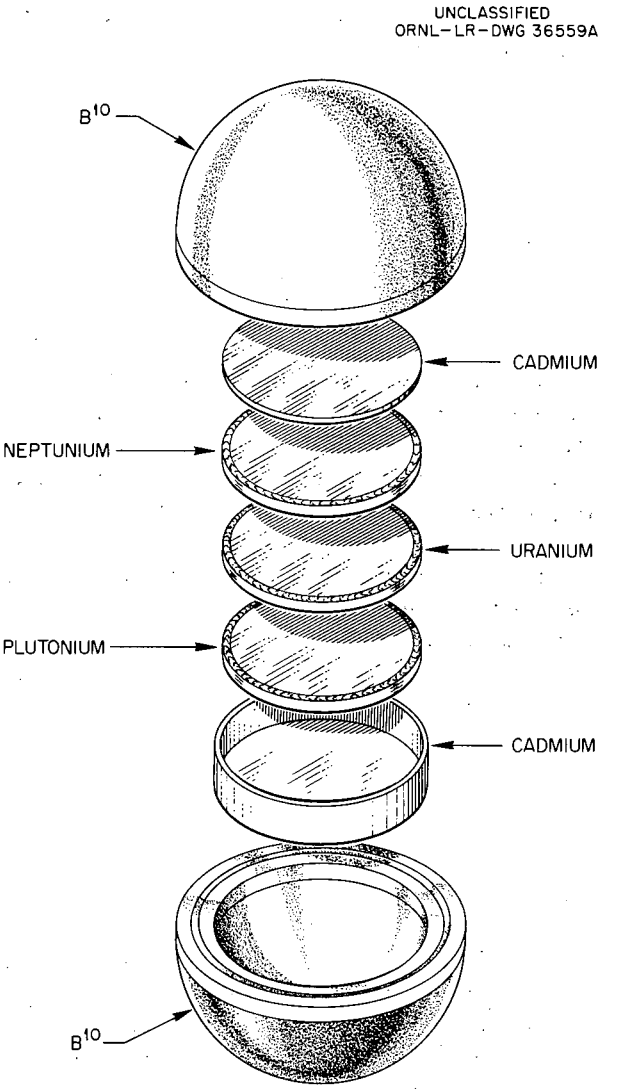

Fig. 151. Molded B^{10} Spherical Shields.

Simulated U^{238} and Np^{237} Foils. – The decay of the U^{238} and Np^{237} fission products is not identical with that from Pu^{239} (ref 97). If it is assumed that the deviation in the count rate of the fission products is proportional to the atomic mass of the parent atom, simulated foils of U^{238} and Np^{237} can be made up from mixtures of Pu^{239} and U^{235}. The advantage of the simulated foils is that they can be activated in a thermal column for easy calibration and study of decay curves. The amounts of U^{235} and Pu^{239} which give the same number of fissions in a given thermal flux can be easily calculated by setting the products

[95] AEC Radiological Fellow.

[96] G. S. Hurst *et al.*, *Rev. Sci. Instr.* **27**, 153–56 (1956).

[97] F. J. Davis *et al.*, *H-P Semiann. Prog. Rep. July 31, 1957*, ORNL-2384, p 113.

(fission cross section times the number of atoms) of each nuclide equal to one another:

$$\frac{\sigma_{Pu^{239}}}{239} \times W_{Pu^{239}} = \frac{\sigma_{U^{235}}}{235} \times W_{U^{235}} ,$$

$$\frac{W_{U^{235}}}{W_{Pu^{239}}} = \frac{235 \times \sigma_{Pu^{239}}}{239 \times \sigma_{U^{235}}} = \frac{235 \times 793}{239 \times 580} = 1.344 ,$$

where W is the weight of U^{235} and of Pu^{239} and σ is the thermal fission cross section of each, corrected for non-$1/v$ variation.[98] Therefore, a mixture of 1.344 g of U^{235} and 1 g of Pu^{239} should decay as Np^{237} does but have the effective thermal activation of a 2-g foil of Pu^{239}. To minimize corrections due to flux depression, the actual amounts used were one-twentieth of those given, so that the effective thermal activation was the equivalent of a 0.1-g Pu^{239} foil. Since U^{238} deviates one-fourth as much as U^{235}, the amounts used for the simulated U^{238} foil were 1.344/40 = 0.0338 g of U^{235} and 0.75 g of Pu^{239}. This foil also has the effective thermal activation of a 0.1-g Pu^{239} foil. In Fig. 152 are shown normalized decay curves (short exposure time) of these foils.

Exposure-Time Correction Factors. – The decay curve of the fission products depends on exposure time. The curves shown in Fig. 153 are flux correction factors which must be applied for exposure times longer than 5 min. These curves were obtained by exposing Pu^{239} foils for the various times shown and comparing their decay curves with a decay curve of a Pu^{239} foil exposed for 5 min. These correction factors are valid for the Np^{237} and U^{238} foils within experimental error.

[98] D. J. Hughes and J. A. Harvey, *Neutron Cross Sections*, BNL-325 (July 1, 1955); D. J. Hughes and R. B. Schwartz, *Neutron Cross Sections* (Supplement No. 1) BNL-325 (Jan. 1, 1957).

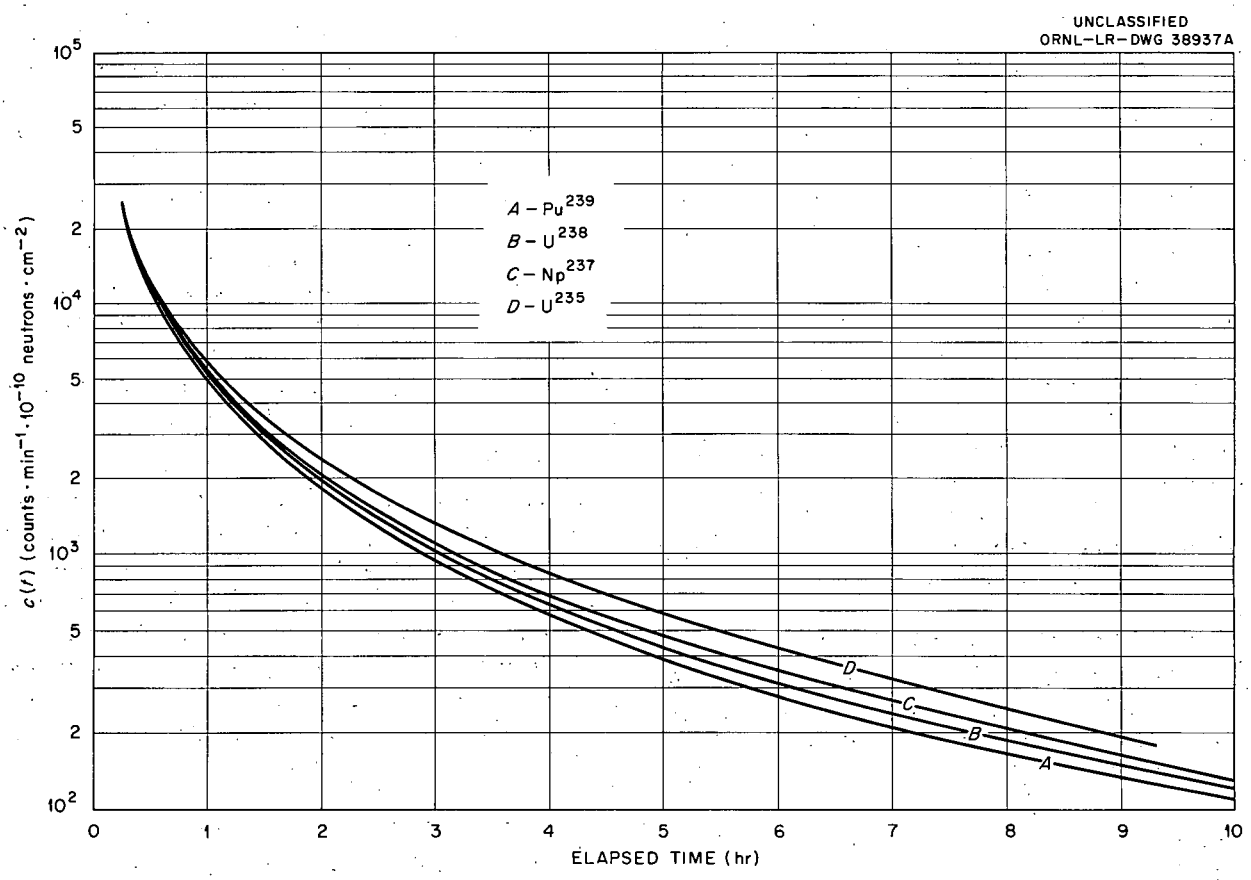

Fig. 152. Normalized Decay Curves for Fission Products.

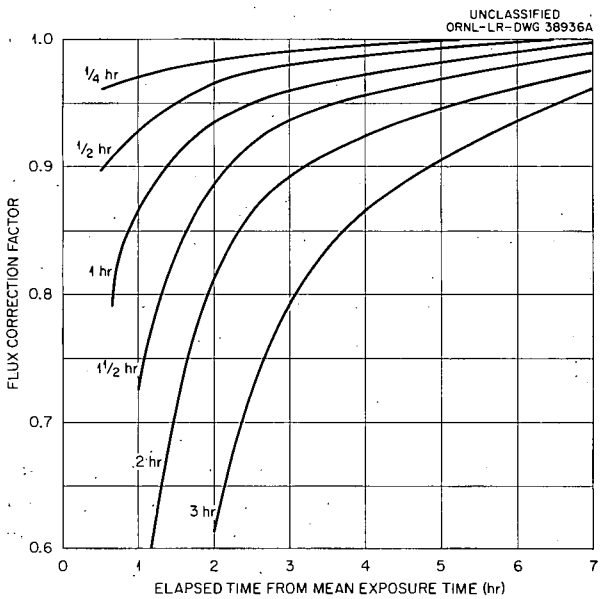

Fig. 153. Flux Correction Factors Necessary for Exposure Times Greater Than 5 min.

Dosimetry Program for Criticality Accidents

Dosimetry Units. – Five hundred dosimetry units are being assembled to be distributed to various AEC sites. Each unit consists of a neutron threshold detector assembly (shown in Fig. 154) as well as chemical gamma dosimeters contained in a lithium shield.

Scintillation Counter for Film Badge Sulfur. ORNL film badges now contain a 0.5-g sulfur detector. To obtain sufficient sensitivity to measure the P^{32} activity in the sulfur detector in the event of an incident, a low-background scintillation counter was developed (Fig. 155). The background of this counter in a lead shield (approximately 4 in. thick) is approximately 1 count per minute. If the sulfur is removed by burning,[99] a Godiva neutron exposure of 1 rad will give a count rate of 1.5 counts/min.

Radsan Fast Neutron Dosimeter Developments

The Health Physics Division and the Instrumentation Division through a joint effort have redesigned the Radsan[100] for commercial production. The redesign is essentially complete, and contract bids for commercial production of 10 units are being prepared by the Instrumentation Division.

Counter Gas Experiments. – It has been shown[100] that when cyclopropane is used as the counting gas in the neutron counter Q-1696, the counter anode voltage required is about 1000 v compared with the 2000 v needed when ethylene is used. The following advantages are attainable by lowering the high voltage: (1) a simpler high-voltage power supply, (2) a considerable reduction in noise, and (3) smaller preamplifier cables. Cyclopropane also appears to be less susceptible to gas impurities. A possible disadvantage of cyclopropane is that it "ingasses" into the polyethylene liner[100] and thus takes about 2 weeks to reach equilibrium pressure. This problem can be overcome by proper filling methods.

The effect of temperature on the neutron response of counter Q-1696 with ethylene and with cyclopropane gas has been determined by immersing the counters in a controlled-temperature water bath at a fixed distance from a Po-Be neutron source. Curves 1 and 2 in Fig. 156 show the variation in the neutron dose, as read on the Radsan, as a function of temperature. With a temperature change from 5 to 60°C the indicated dose changed 15% with ethylene and 17% with cyclopropane. Curves 3 and 4 in Fig. 156 show the results of the same experimental procedure except that before each neutron reading was taken the gain of the Radsan amplifier was adjusted so that the alpha source in the counter initiated the same response. Temperature dependence of the counter does not appear to be a serious problem since in practical use the Radsan gain and alignment are checked periodically.

Gamma Response and Energy Losses in the Fast Neutron Dosimeter.[101] – Since there has been some question and criticism[102] of the proportional counter method of neutron dosimetry on the basis that excessive fractions of the neutron dose are lost under the bias necessary for the discrimination of gamma rays, some basic data are given for x and gamma radiation with dose rates ranging from 1 to 100 r/hr.

---

[99] P. W. Reinhardt and F. J. Davis, *Health Phys.* 1, 173 (1958).

[100] E. B. Wagner and G. S. Hurst, *Rev. Sci. Instr.* 29, 2 (1958).

[101] E. B. Wagner and G. S. Hurst, *Health Phys.* 2(1) 57–61 (1959).

[102] I. I. Petrov, *Atomnaya Energ.* 3, 326 (1957).

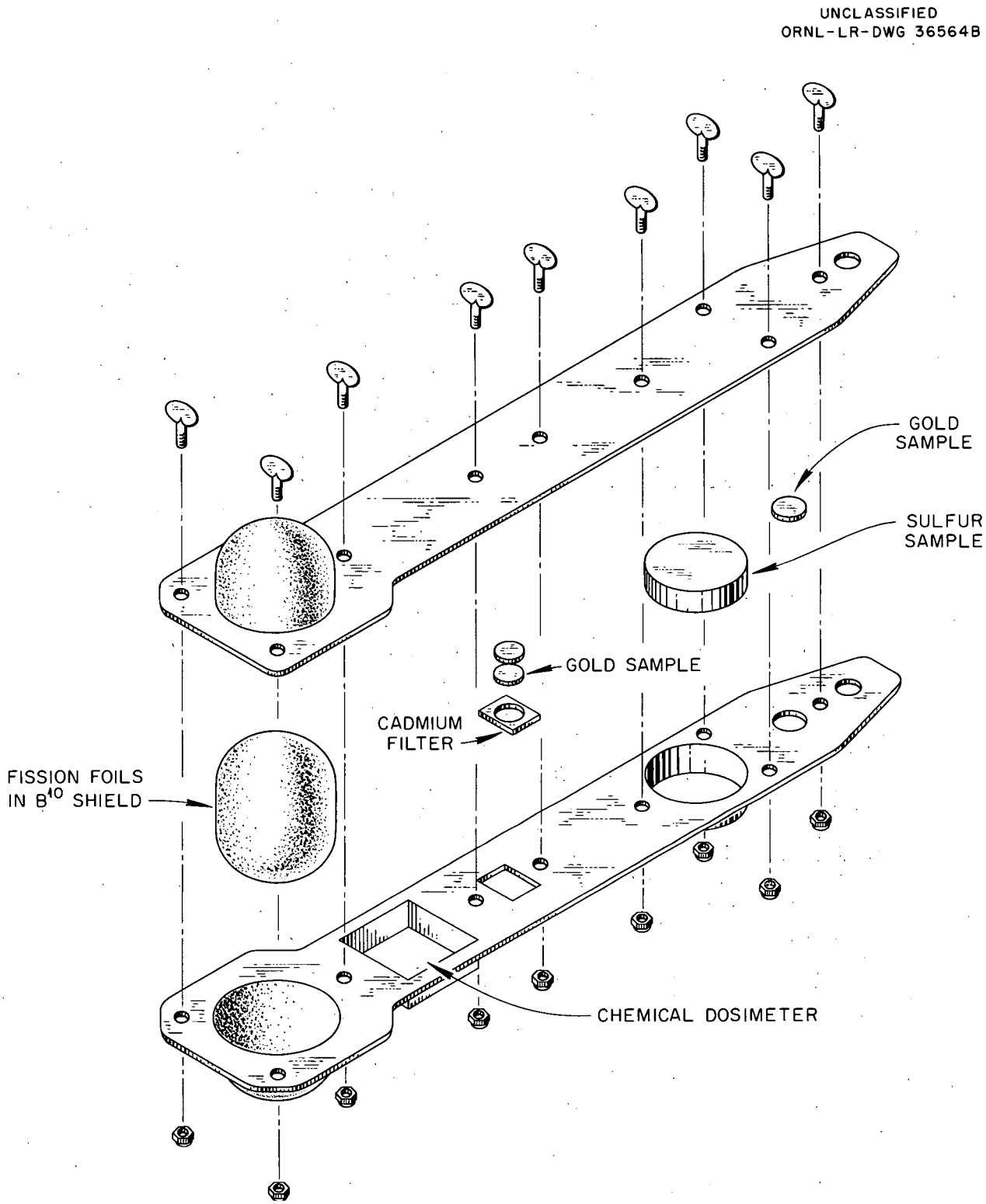

Fig. 154. Threshold Detector Placement Container.

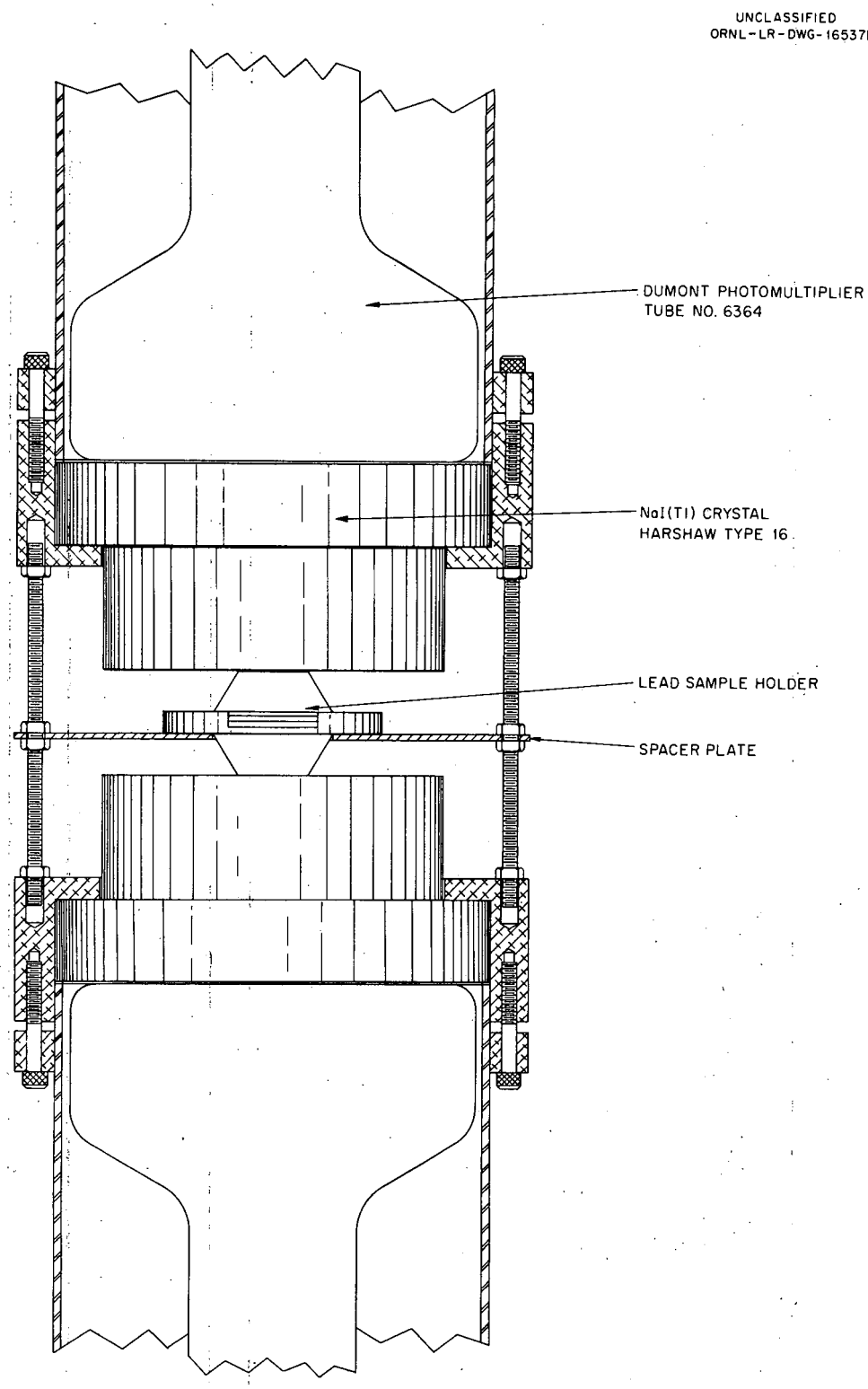

Fig. 155. Low-Background Scintillation Counter.

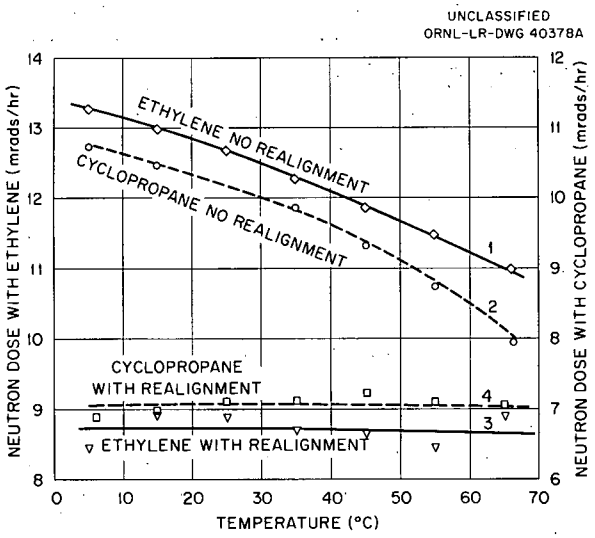

Fig. 156. Effect of Temperature on Neutron Responses of Counter Q-1696 with Ethylene and with Cyclopropane Gas.

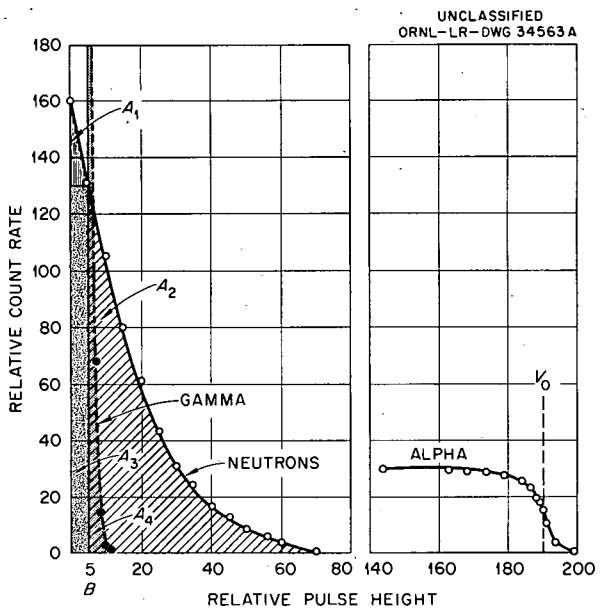

Fig. 157. Relative Count Rates for Gamma Rays, Fast Neutrons, and the Alpha Pu^{239} Calibration Source.

Figure 157 shows the relative count rates for gamma rays, fast neutrons, and the alpha Pu^{239} calibration source. The neutron dose is proportional to the area under the neutron curve ($A_1 + A_2 + A_3$); this may be measured directly (by utilization of the alpha source) in units of Mev per gram of ethylene and, hence, gives the tissue dose. For example, in Fig. 157 the alpha pulse height, V_0, is 190 v; thus 190-v pulses indicate an energy expenditure in the gas of 5.14 Mev. The area A_1 represents the part of the neutron dose which is lost under the bias, B (B = 5 v in the case shown in Fig. 157). The rectangular area A_3 is not lost under the bias, but is a part of the energy dissipated by protons making pulses larger than the bias. The area A_4 represents the gamma response for the particular gamma dose rate. Obviously, for a given dose rate, increasing B makes A_4 smaller but A_1 larger.

Two methods are used to determine $A_1 + A_2 + A_3$: (1) the direct graphical integration method and (2) the automatic pulse integration method. In the graphical method A_3 is included, and even A_1 can be estimated as will be shown later. The binary pulse integrators are designed to measure the area $A_2 + A_3$. In the case of the simple four-stage binary integrator,[100] it was shown that the integrator overestimates $A_2 + A_3$, thus partially compensating for the area A_1.

Basic data required for the determination of the fraction, f, of the energy lost as a function of neutron energy, E, and discriminator bias, B, have already been presented.[100] Values of f, defined as $f = A_1/(A_1 + A_2 + A_3)$ are shown in Table 44.

For 100-kve (kilovolt effective) x rays, 200-kve x rays, and 1.25-Mev Co^{60} gamma rays, the integral pulse height distributions were determined for radiation doses ranging from 1 to 100 r. Using these data, families of curves (Figs. 158–60) were plotted for the 100-kve x rays, 200-kve x rays, and Co^{60} gamma rays, showing counts per second as a function of pulse height.

Figures 161–63 show both the neutron data[100] and the x- and gamma-ray data. (In an independent experiment the combination procedure was validated; i.e., gamma intensities as high as 100 r/hr did not affect the pulse distributions due to fast neutrons or to the alpha calibration source.) Figure 161 shows the most severe case, that is, the combination of 0.5-Mev neutrons with 200-kve x rays. In Fig. 161 the neutron dose rate corresponds to 1 mrad/hr, and the gamma-ray dose rate to 1 and 5 r/hr. With 1 r/hr the gamma response becomes appreciable for $B \leq 0.20$ Mev, hence the fraction of the dose, f, which must be estimated by extrapolation is 32% (see Table 44). When the neutron dose is higher, a higher gamma dose rate

Table 44. Fraction, f, of Energy Spent by Recoils Losing Less than the Bias Energy, B, in the Counter

Bias		Fraction of Fast Neutron Energies							
Energy (Mev)	PHS (v)	0.5 Mev	1.0 Mev	2.0 Mev	3.5 Mev	4.8 Mev	14 Mev	Po-B	Po-Be
				$\times 10^{-2}$					
0.074	2.6	8.9	2.0	1.5	1.3	1.4	2.5	0.6	1.4
0.14	5.3	19.5	9.4	4.1	3.5	2.8	8.5	2.8	4.5
0.21	7.8	32.0	12.9	7.6	5.6	5.9	16.2	6.5	10.1
0.28	10.5	52.6	23.5	12.3	9.1	9.8	25.8	9.9	14.4
0.36	13.2	73.0	33.3	18.8	12.8	16.2	36.9	15.2	20.5

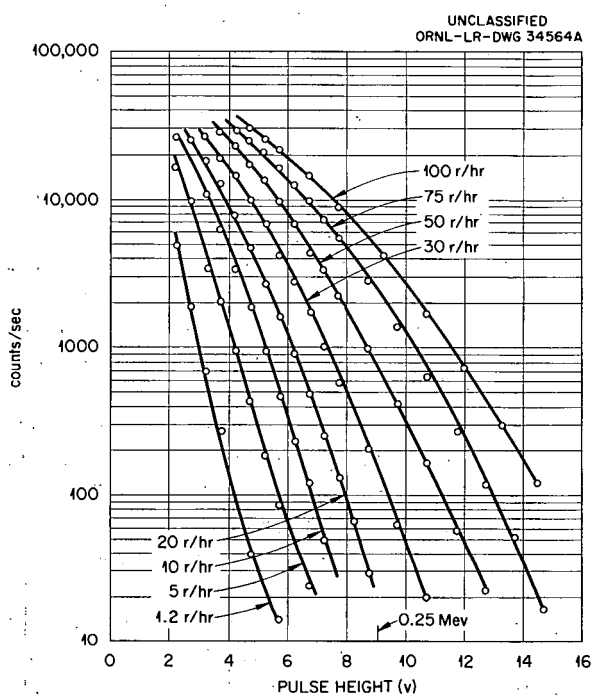

Fig. 158. Response of the Fast-Neutron Dosimeter to 100-kve X Rays.

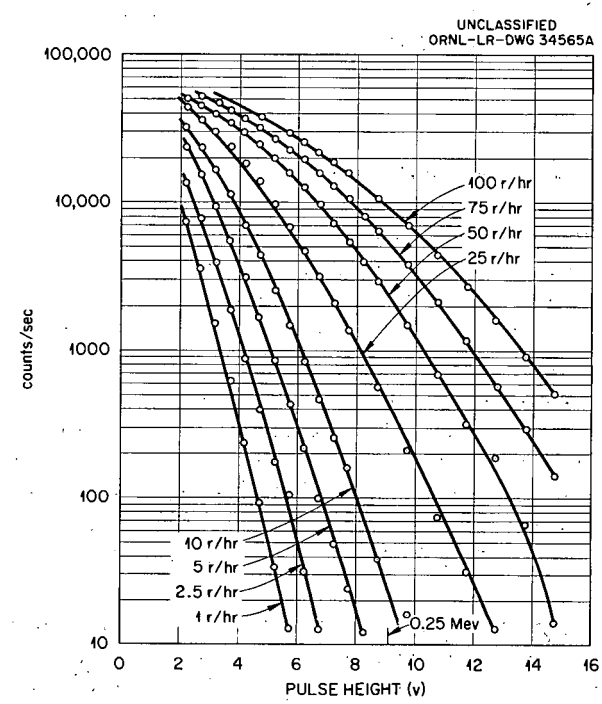

Fig. 159. Response of the Fast-Neutron Dosimeter to 200-kve X Rays.

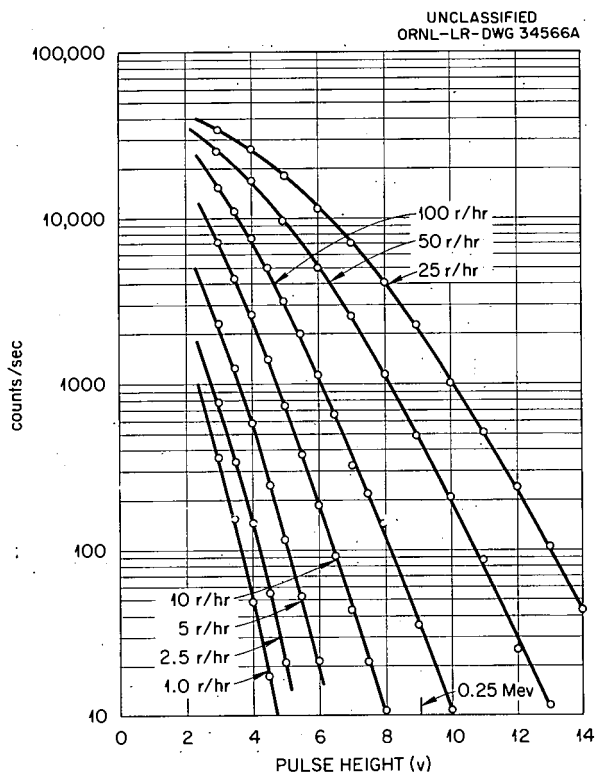

Fig. 160. Response of the Fast-Neutron Dosimeter to Co^{60} Gamma Rays.

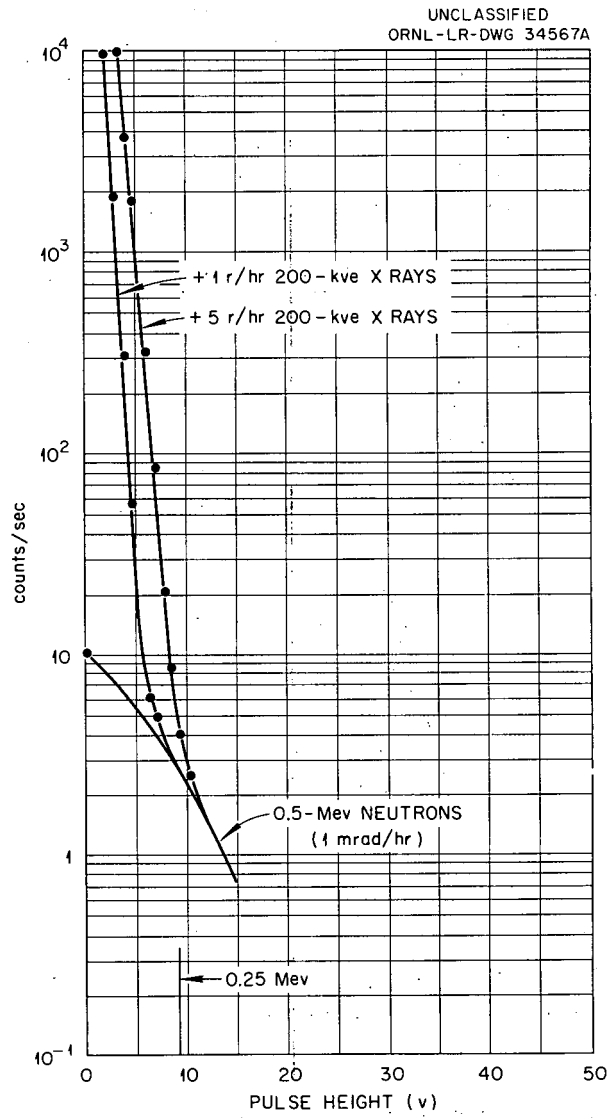

Fig. 161. Response of the Fast-Neutron Dosimeter to 200-kve X Rays Plus 0.5-Mev Neutrons.

may be tolerated (see Fig. 162). In limiting cases of this type it is recommended that the graphical method of determining the area under the neutron curve be used. In practice, low-energy x rays could be attenuated with high-Z materials without appreciable effect on the neutron dose. The above example, however, serves to define the limits of the proportional-counter method for separating the neutron dose from the gamma dose. Figure 163 shows a more typical case, that is, the Po-Be neutron spectrum mixed with Co^{60} gamma radiation.

The graphical method for determining the amount of energy lost under the bias involves (1) plotting the log of total count rate, due to neutrons plus gamma radiation, against the integral discriminator level (as in Fig. 163), (2) noting the point where gamma radiation causes a sharp rise in the curve, (3) extrapolating the neutron curve for pulse level below this point, and (4) transferring the entire neutron curve to a linear scale and determining the full area under this curve.

The graphical method outlined above is necessary for precise measurement only when the gamma radiation dose rate is high (greater than 10 r/hr), and when the fast neutron dose rate is low (< 100 mrad/hr). In other cases the binary pulse integrators give adequate accuracy and require less time and effort.

Calculations of Energy Loss Under the Bias in Fast Neutron Dosimetry. – The energy loss under the bias in an integrating fast neutron dosimeter has been considered by Wagner and Hurst.[103,104]

[103] E. B. Wagner and G. S. Hurst, *Rev. Sci. Instr.* **29**, 153 (1958).

[104] E. B. Wagner and G. S. Hurst, to be published in *Health Phys;* see also this report, Table 44.

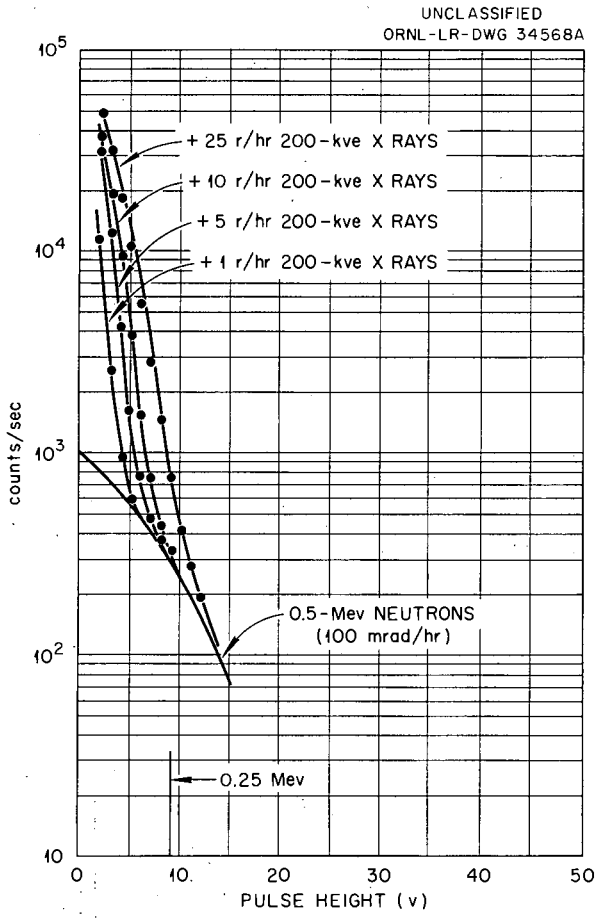

Fig. 162. Response of the Fast-Neutron Dosimeter to 200-kve X Rays Plus 0.5-Mev Neutrons.

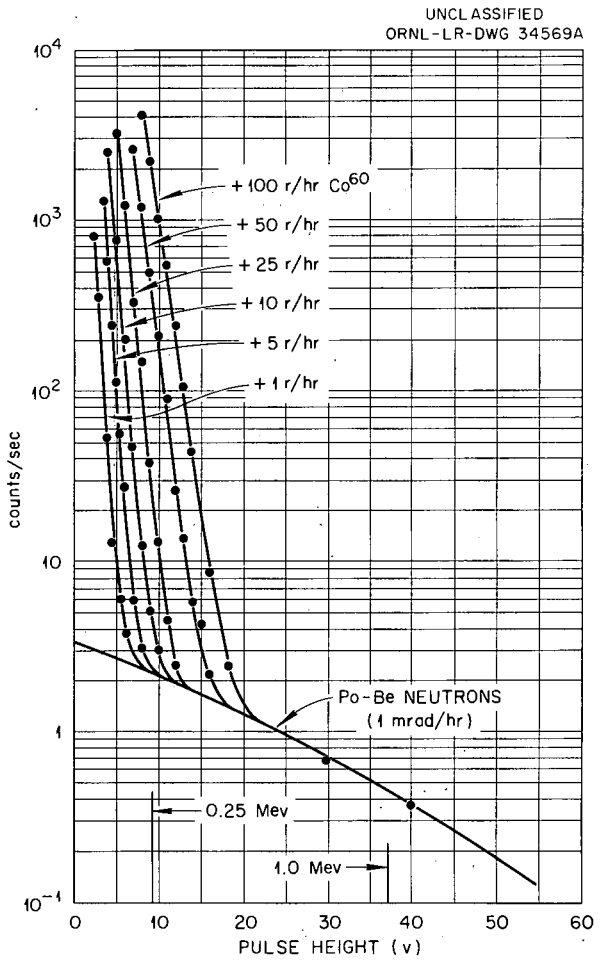

Fig. 163. Response of the Fast-Neutron Dosimeter to Co^{60} Gamma Rays Plus Po-Be Neutrons.

They find experimentally that the fractional energy loss under the bias is always much less than unity for the bias values necessary in practical cases; usually it is only a few per cent. Petrov,[105] on the other hand, considers losses in an idealized parallel-plate dosimeter and finds that they may be much larger than the experimentally determined values. It is the purpose of this paper to reconsider the problem treated by Petrov and to show that his model in reality yields smaller losses below the bias than the values quoted by him. This error is apparently due to a misconception on his part as to the exact function of the binary integrator.

[105] I. I. Petrov, *Atomnaya Energ.* 3, 326 (1957).

The model considered by Petrov is that of neutrons incident normally on a plane-parallel radiator of thickness greater than the range of the most energetic protons generated therein. Protons are ejected from the radiator into a narrow gas-filled gap (see Fig. 164). Both radiator and gap are considered to be effectively infinite in lateral extension. One wishes to calculate the total energy deposited in such a chamber by protons generated in the walls and gas and expending energy in the gas at least as great as the bias energy. Clearly, a realistic chamber of finite lateral extent will have generated in it a distribution of proton energies which will be more heavily populated in the low-energy region than in the case of an infinite chamber. Hence the bias losses calculated for

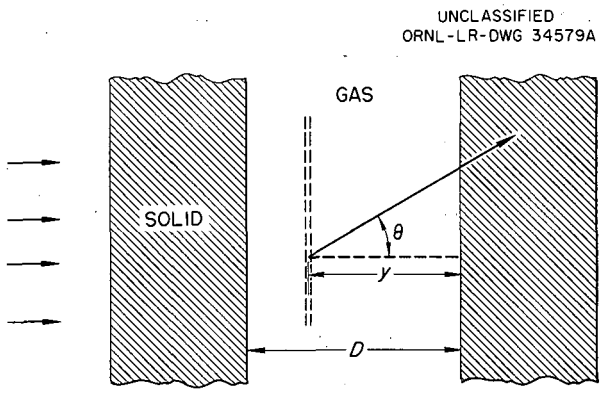

Fig. 164. Schematic Representation of a Parallel-Plate Fast-Neutron Dosimeter.

this idealized model should always be less than one would calculate for an actual chamber.

The following notation is employed:

D = gap spacing,

A = area of radiator normal to the neutron beam,

N_g = number of hydrogen atoms per cm^3 of gas,

N_R = number of hydrogen atoms per cm^3 in radiator,

ϕ = incident neutron flux,

E = energy of incident neutrons,

$E_p(\theta)$ = energy of protons recoiling at the angle θ relative to the beam direction,

E_e = energy lost in gap by a proton,

$\mu = \cos\theta$,

y = distance from gap wall at which proton recoil may occur.

A range–energy relation of the form $R = kE^n$ will be assumed for protons in both gas and radiator. Following Hurst, Ritchie, and Wilson,[106] and Petrov,[105] n will be taken to be 1.73. Clearly, if $N_g k_g = N_R k_R$, where k_g and k_R refer to gas and radiator, respectively, one may neglect the difference in density between radiator and gas in this simple one-dimensional case. Since this is true to a good approximation in the gas-wall combinations considered in refs 105 and 106, and in any chamber designed in accordance with the Bragg-Gray principle, the equivalent problem of the energy deposited between parallel planes a distance D apart in an infinite medium of gas is considered.

Consider protons recoiling at the angle θ from an n-p collision occurring at a distance y from the far wall of the gap (Fig. 164). Since

$$E_p(\theta) = E\mu^2 \qquad (\mu \geqq 0) \ ,$$

and the fraction of recoils occurring at y in the interval $d\mu$ at μ is $2\mu\, d\mu$, the number of protons liberated in dy at y and $d\mu$ at μ which lose the energy E_e in the gap is

$$d^2N = \phi\, N_g \sigma A\, 2\mu\, d\mu\, dy \ . \qquad (1)$$

Equation (1) may be rewritten conveniently in terms of the dimensionless variables, $\eta = y/kE^n$, and $\xi = 2\phi\, N_g \sigma A\, k_g E^n$. One then has

$$d^2N = \xi\mu\, d\mu\, d\eta \ . \qquad (1a)$$

The energy deposited in the gap by a given proton at μ and η, $E_e = x_e E$, may be written in terms of η and μ from the range–energy relation.

One finds that the fractional part of the total energy loss below the bias energy $B = xE$ is given by

$$f(x) = x^2 + \frac{4}{d} g(x) \ , \ \text{if} \ x < 1 - (1-d)^{1/n} , \qquad (2)$$

where $d = D/kE^n$, and

$$g(x) = \frac{n}{3(n+1)} x^{n+1} + \left[\frac{2n+3}{3} \sum_{r=0}^{\infty} \frac{(-1)^r (n)(n+1)\ldots(n-r+1)}{r!\,(2n+5-2r)} - \frac{1}{(2n+5)(n+1)} - \frac{n}{3(n+1)} \right] + x^2 \sum_{r=0}^{\infty} \frac{n(n-1)\ldots(n-r)(-x)^r}{r!\,(r+2)(2n+1-2r)} \ . \qquad (3)$$

[106] G. S. Hurst, R. H. Ritchie, and H. N. Wilson, *Rev. Sci. Instr.* **22**, 981 (1951).

For the case under consideration, where $n = 1.73$,

$$g(x) = 0.211233x^{2.73} - 0.153314x^{4.23} + 0.193946x^2 - \\ -0.171125x^3 - 0.092658x^4 + 0.009373x^5 + \\ +0.001928x^6 + 0.000691x^7 + 0.000316x^8 .$$

Figure 165 shows a plot of $g(x)$. The values of $1 - f$ given in Table 45 were calculated from Eq. (2). Also shown are values given by Petrov for this quantity. The constant k_g has been taken the same as that used by Petrov for the purposes of comparison, namely, 1.91 cm $(\text{Mev})^{-1.73}$, and is appropriate to acetylene at 15°C and 760 mm Hg (ref 105). Apparently, as suggested by Wagner and Hurst,[104] Petrov has assumed that the fast-neutron integrator pulse misses not only those pulses having energies less than the bias but misses also that part of a given pulse which lies below the bias value.

Assistance to Other Installations

The Dosimetry Techniques Group has assisted several other organizations in their fast-neutron instrumentation and measurement problems. Chemical Warfare Services built their own integrator and counter patterned after the Radsan and counter Q-1696. They shipped these instruments to ORNL where they were reworked, debugged, and put in operating condition by the Dosimetry Techniques

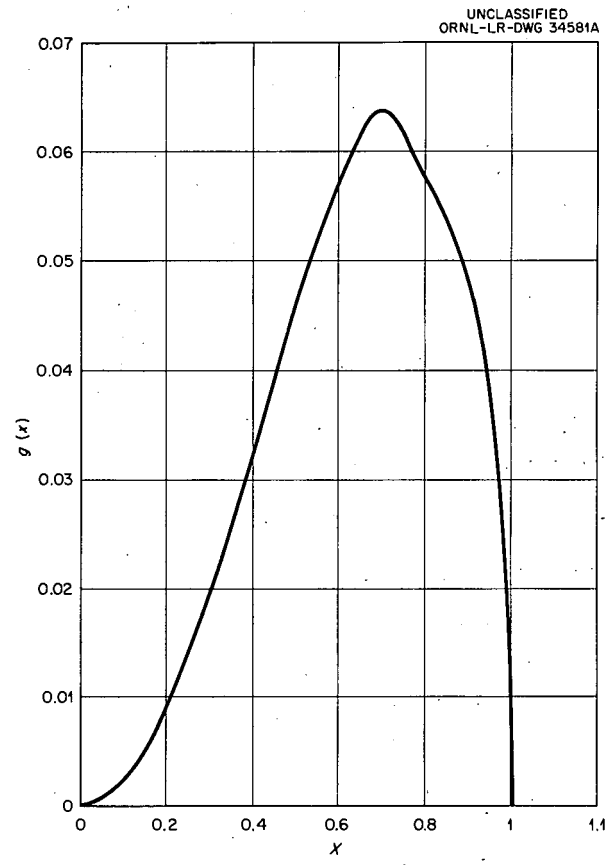

Fig. 165. Plot of a Function Occurring in the Expression for Energy Loss Under the Bias, Eq. (2).

Table 45. Comparisons of Losses Under the Bias in the Idealized Dosimeter

D	E (Mev)	B (Mev)	d	x	$(1-f)_{\text{Petrov}}$	$(1-f)_{\text{Eq. (2)}}$*
1	1	0.05	0.524	0.05	0.884	0.993
	1	0.10	0.524	0.10	0.767	0.974
1	2	0.05	0.158	0.25	0.875	0.997
	2	0.10	0.158	0.05	0.748	0.984
1	3	0.05	0.075	0.0167	0.845	0.998
	3	0.10	0.075	0.0333	0.691	0.988
4	2	0.10	0.633	0.05	0.890	0.994
	2	0.20	0.633	0.10	0.780	0.977
4	5	0.10	0.129	0.02	0.885	0.997
	5	0.20	0.129	0.04	0.770	0.988

*$f(x) = x^2 + \frac{4}{d} g(x)$, if $x < 1 - (1-d)^{1/n}$, where $d = D/kE^n$.

Group and the Counter Laboratory of the Instrumentation Division.

At the request of the Westinghouse Naval Reactors Facility at Idaho Falls, fast-neutron doses were measured with the Radsan at approximately 100 points around their reactor to aid in the shielding design.

Gamma Dosimetry Developments

A gamma dosimeter is being developed with the Phillips 18509/01 miniature halogen-filled Geiger counter. Although the bare counter has a high energy dependence, as shown by Fig. 166, with the proper amount of tin and lead shielding it can be made to have a satisfactory energy dependence down to 150 kev, as shown by Fig. 167. Preliminary data of the relative neutron-to-gamma response was determined by using Po-Be and Po-B neutron sources. It appears that with equal dose rates of gamma and fast neutron radiation the neutron response is about 7% of that due to gamma. When the counter is operated as a pulse device, the response is essentially linear from 0.1 mr/hr to 5 r/hr, and when operated as a current device the response is logarithmic from 5 to 200 r. It is adaptable to simple circuitry since it requires only about 400 v anode voltage, has output pulses on the order of 20 v, and exhibits good stability and reproducibility. An electronic circuit is being designed to utilize the counter for a gamma dosimeter.

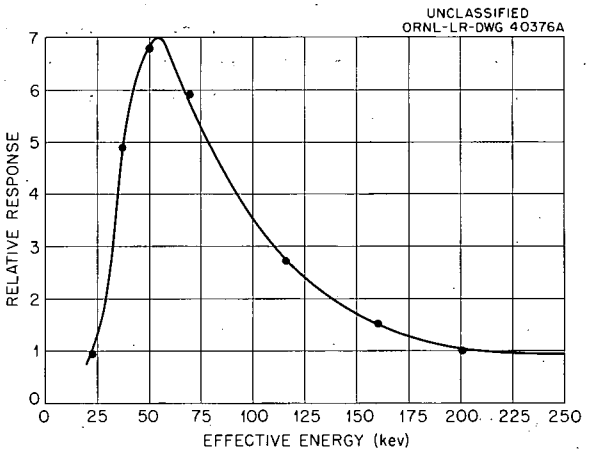

Fig. 166. G-M Counter Without Any Shielding.

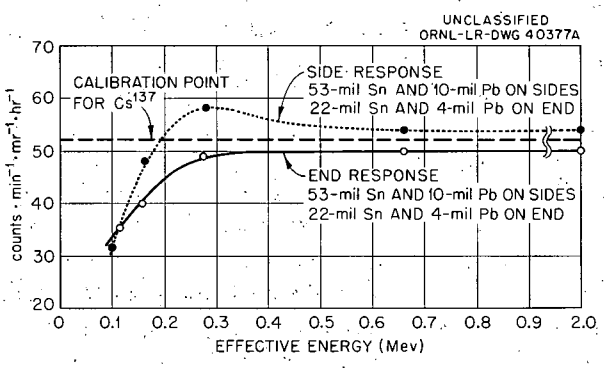

Fig. 167. G-M Counter with Tin and Lead Shielding.

INTERNAL DOSIMETRY

APPLIED RADIOBIOLOGY

B. R. Fish

Inhalation Studies

G. W. Royster, Jr.

U. S. Davis, Jr.
G. J. Dodson
M. B. Edwards
E. S. Jones
C. A. Markarian[1]
J. A. Payne[2]
H. E. Stokinger[3]
J. L. Thompson

Single Acute Inhalation of U_3O_8 Aerosol. – Data from 25 dogs exposed to single inhalations of U_3O_8 fumes obtained from burning enriched uranium metal were examined to determine the biological half life and per cent retention in the lungs. The exposure method and apparatus have been described in previous progress reports.[4,5] This study is related to accidental inhalation exposures to all types of uranium fumes, including those generated by machining and grinding operations.[6]

The aerosol particle size of 0.35 μ remained constant within reasonable limits; however, the concentration varied by a factor of 10. Most of the variation in aerosol concentration was between exposures to different animals, the variation during a single exposure being less than a factor of 2. The average radioactivity concentration was 680 $d \cdot min^{-1} \cdot liter^{-1}$. It was noted that when the aerosol concentration was high the relative number of chain-like aggregates increased. A new fume-generating device which may provide better control of aerosol concentration is being fabricated.

The animals were serially sacrificed at 1 hr and 1, 2, 4, 8, 16, 32, 64, and 128 days following exposure. After sacrifice the lungs and other tissues were removed and assayed for uranium content. Autoradiograms were made by using sections of lung and pulmonary lymph nodes from the dogs sacrificed at 2 and 128 days. The autoradiograms showed a large number of alpha tracks in lung tissue and few in the lymph nodes of the "2 day" dogs; in the "128 day" dogs slightly more uranium was found in lymphatic tissue than in the same quantity of lung tissue. Radiochemical analysis showed that the ratio of the uranium concentration in the lymph node to the uranium concentration in lung tissue increased from 0.13 at 1 day to 1.2 at 128 days.

The data indicate a biological half life in the lung of approximately 100 days. It has been estimated that the half life of insoluble uranium compounds in the lung is between 50 and 200 days.[7-9] Lung burden, in terms of percentage retained of the dose to which the dogs were exposed, may be described by $14\ t^{-0.18}$ for t in days (Fig. 168).

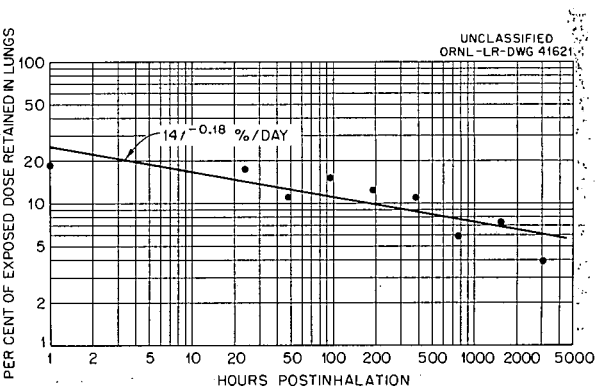

Fig. 168. Lung Retention of Uranium in Dogs After an Acute Inhalation of Uranium Metal Fumes (U_3O_8).

Each point on the graph represents the average data from two to four animals. The observed urinary uranium excretion rates represent the removal of about 2% of the lung burden per day.

Chronic Inhalation of Uranium Aerosols. – Studies have been initiated to determine more accurately the retention, distribution, and excretion of uranium in chronic exposure cases. Adult female beagles are being used in these studies. The exposure

[1] U.S. Air Force.

[2] Co-op student.

[3] Consultant, USPHS.

[4] S. R. Bernard *et al.*, *H-P Semiann. Prog. Rep. July 31, 1956*, ORNL-2151, p 1–8.

[5] S. R. Bernard *et al.*, *H-P Semiann. Prog. Rep. July 31, 1957*, ORNL-2384, p 3–6.

[6] J. D. McLendon *et al.*, *An Uranium Inhalation Exposure Case History*, Y-B94-54 (1958).

[7] H. C. Hodge *et al.*, *Suggested Maximum Allowable Concentration of Insoluble Uranium Compounds in Air*, UR-67, p 41–49 (1949).

[8] H. C. Hodge and R. G. Thomas, *Proc. UN Intern. Conf. Peaceful Uses Atomic Energy, 2nd, Geneva, 1958* **23**, *302–5 (1958)*.

[9] C. E. Miller, *Progr. in Nuclear Energy. Ser. VII* **2**, 87–104 (1959).

equipment (Fig. 169) consists of a Lucite box, approximately 1 m^3 in volume, and an attached breathing apparatus.[10] The aerosol is introduced to the system from a modified ball mill[11] and the uranium concentration is regulated by controlling the air flow. During the time of inhalation, samples are taken to determine the uranium oxide concentration and particle size. Each of four dogs has received 15 weekly inhalations of U_3O_8 dust having a mass median particle size of 0.7 μ with a limited size range and average concentration of 70 $d \cdot min^{-1} \cdot liter^{-1}$. Four additional dogs have received three inhalations each and more dogs will be added to the weekly schedule. The animals breathe 50 liters each during an inhalation, and the resulting dose of 3500 $d \cdot min^{-1} \cdot week^{-1}$ is comparable with the Y-12 plant exposure limit.

Samples of excreta are collected on a 24-hr basis for the sixth and seventh days following every exposure. Uranium content of the urine and feces is measured in order to establish excretion patterns. Serial sacrifices are scheduled for three-month intervals.

Aerosol Project

B. R. Fish M. B. Edwards

G. J. Ellis III[12] F. G. Karioris[12]

J. M. Garner, Jr. C. Orr, Jr.[13]

Preparation and Analysis of Aerosols. – A Bahco micro particle classifier has been used to separate enriched uranium oxide into several size fractions

[10] S. R. Bernard *et al.*, *H-P Semiann. Prog. Rep. July 31, 1956*, ORNL-2151, p 4.

[11] H. E. Stokinger, *Natl. Nuclear Energy Ser. Div. VI* 1 (Part 1), 441 (1949).

[12] Temporary employee.

[13] Consultant, Georgia Institute of Technology.

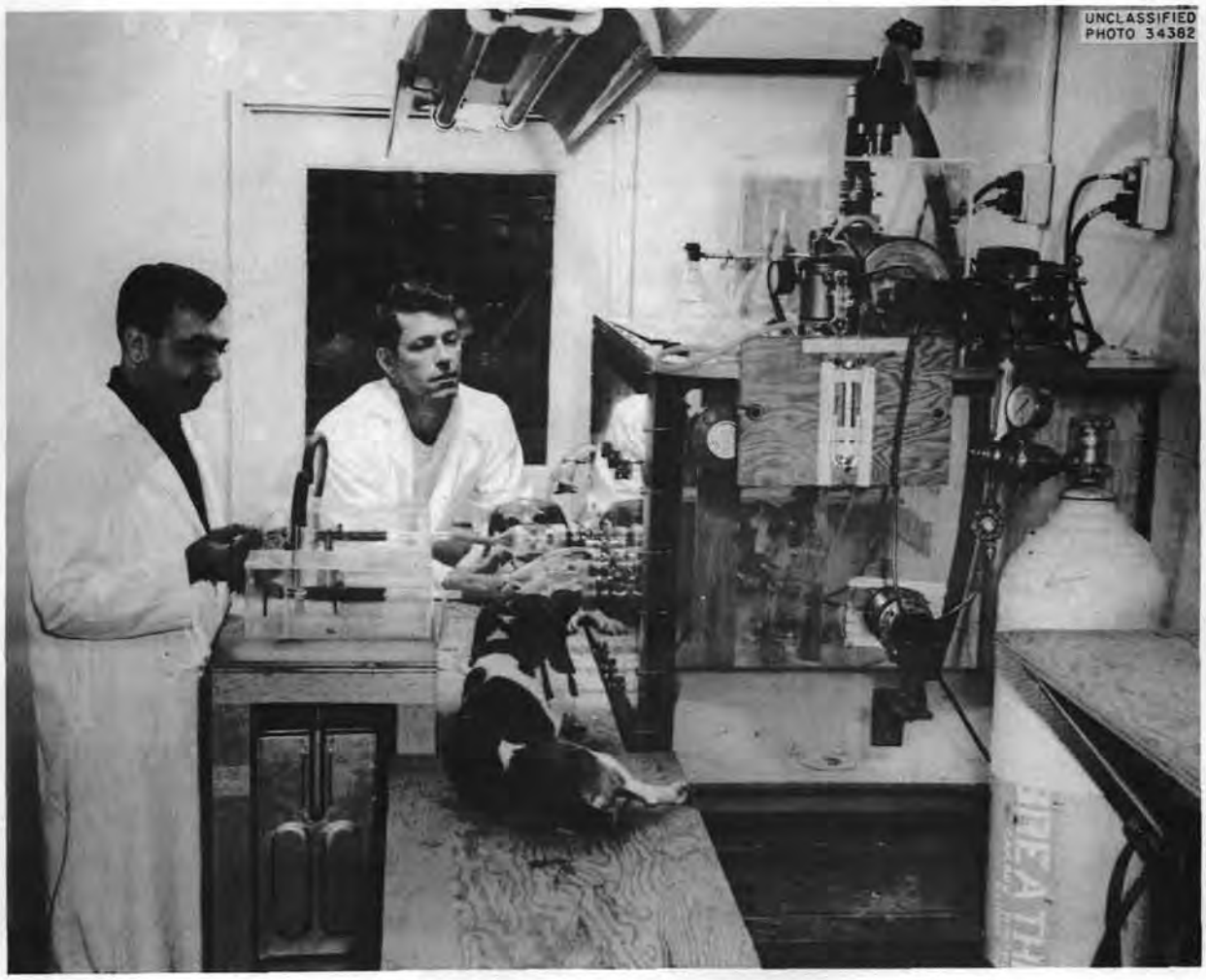

Fig. 169. Chronic Inhalation Equipment.

for use in inhalation exposures. The first batch of separated material is now being used for chronic exposures of dogs as described in this report (see preceding section, "Inhalation Studies"). The capabilities of the classifier are illustrated in Figs. 170 and 171. Figure 170 shows an unrefined material, and Fig. 171 shows the composition after a single pass through the classifier. It should be noted that for any given run the feed material is separated into two size fractions, coarse and fine.

Fig. 170. Electron Photomicrograph of Bulk Uranium Oxide (U_3O_8). 8000X.

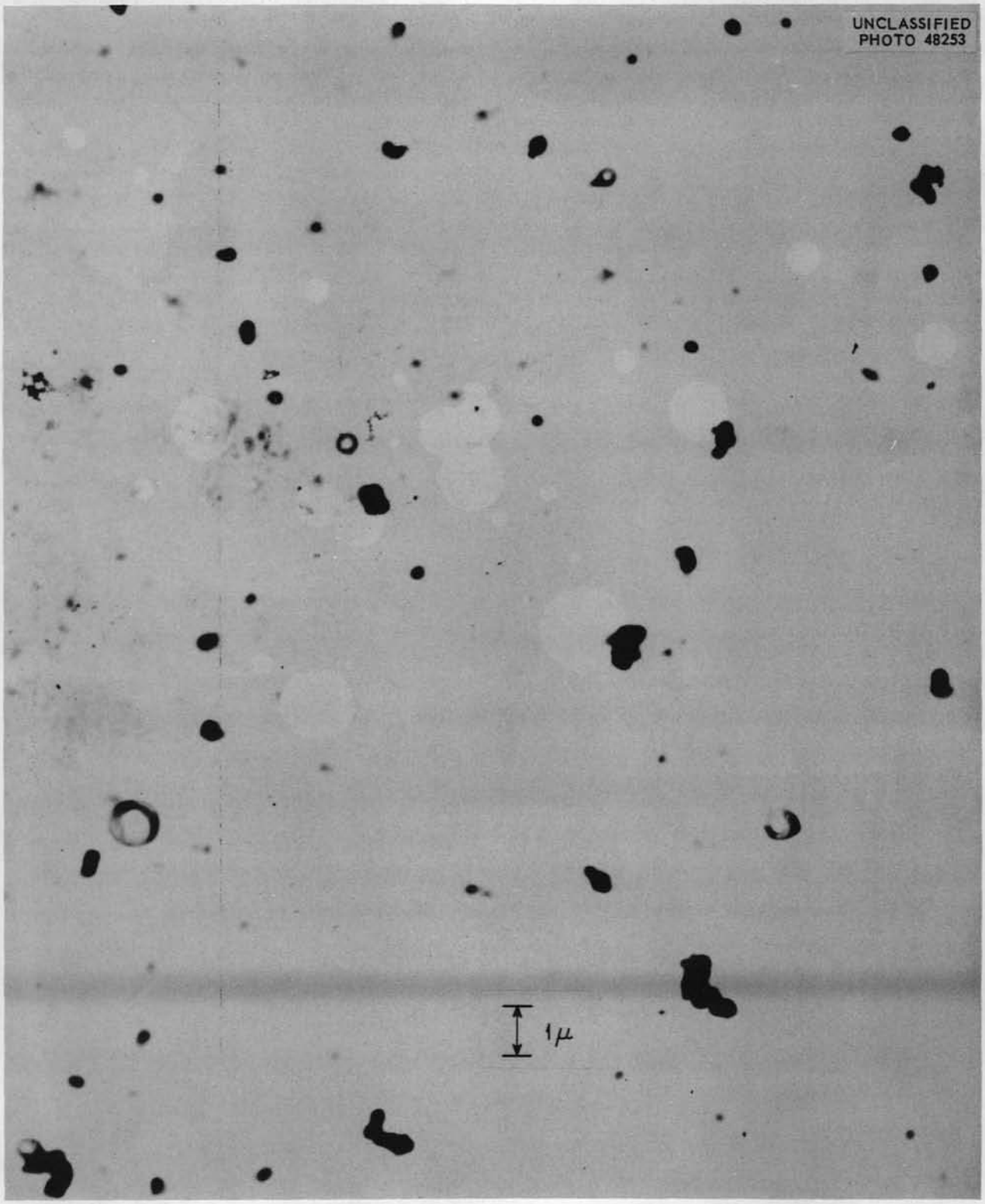

Fig. 171. Electron Photomicrograph of Uranium Oxide (U_3O_8) After a Single Pass Through the Classifier.

The fine fraction contains only particles smaller than some upper limit as controlled by the density of the material and the operating conditions of the instrument. Some fine particles are included in the coarse fraction although their relative number is reduced. The range of sizes in any particular fraction may be narrowed by recycling the coarse fraction or by changing the operating conditions and recycling the fine fraction.

A preliminary survey[14] has been completed in the Y-12 enriched uranium processing facilities to determine the air-borne radioactivity and particle size to which the workers in these areas may be exposed. This information will be used in the design of experiments which simulate industrial exposures.

Six batches of depleted thorium dioxide having size ranges from 0.13 to 10.0 μ have been obtained. Figure 172 shows the size range for four of these batches compared with a typical particle size distribution from an area in the survey described above. This material will be further classified into suitable fractions for use in inhalation studies.

Aerosol Exposure Chamber. – An inhalation chamber for the exposure of mice (Fig. 173) to radioactive aerosols is under development. This chamber is similar to one used at the U.S. Naval Radiological Defense Laboratory.[15] It consists of a cylinder in which a constant concentration of aerosol is maintained by continuous feed. The mice are contained in tubes, tapered at the chamber ends, which are inserted through holes in the walls of the exposure chamber in such a way that only the nose of the animal is exposed to the aerosol. These holes, 84 in number, are staggered in seven circles of 12 holes each. By boring the holes on 2-in. centers there is enough room to position the tubes containing the mice. Each hole in the chamber is fitted with a rubber liner which serves to support the mouse tube and prevent leakage of the aerosol. The mice are secured in the extreme forward position by means of a suitable amount of facial tissue placed between the animal and the rubber stopper which seals the rear opening of each tube (Fig. 174).

[14] M. B. Edwards and B. R. Fish, *Particle Size Survey of Enriched Uranium Processing Facilities – Y-12 Plant*, ORNL CF-59-5-129 (May 20, 1959).

[15] S. H. Cohn *et al.*, *Radiotoxicity Resulting from Exposure to Fallout Simulant. Part II*, USNRDL-TR-118, p 4 (Jan. 11, 1957).

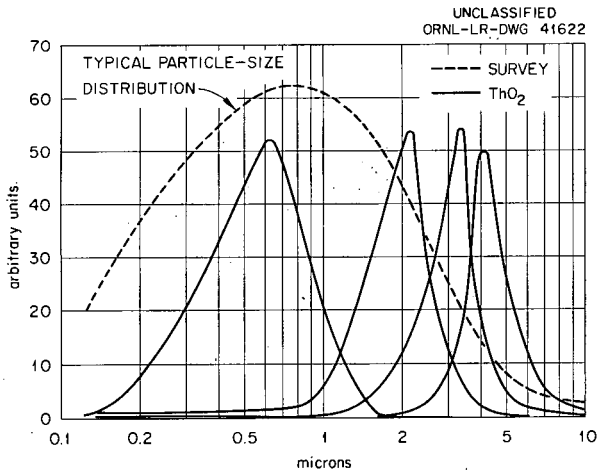

Fig. 172. Particle-Size Distribution of Four Thorium Dioxide Batches and Distribution Found in a Preliminary Survey of Enriched Uranium Processing Areas.

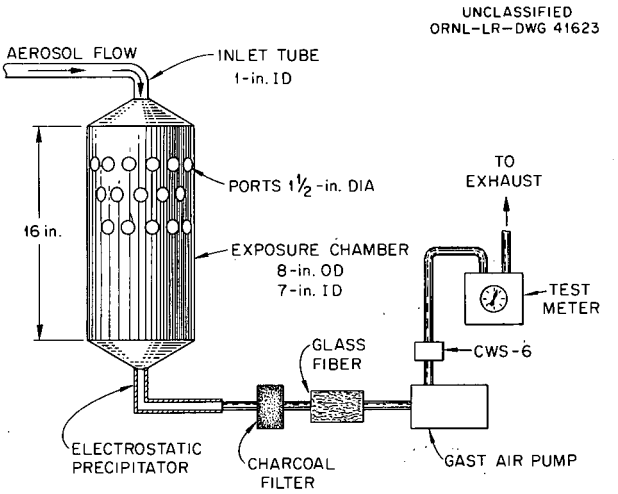

Fig. 173. Mouse Exposure Chamber.

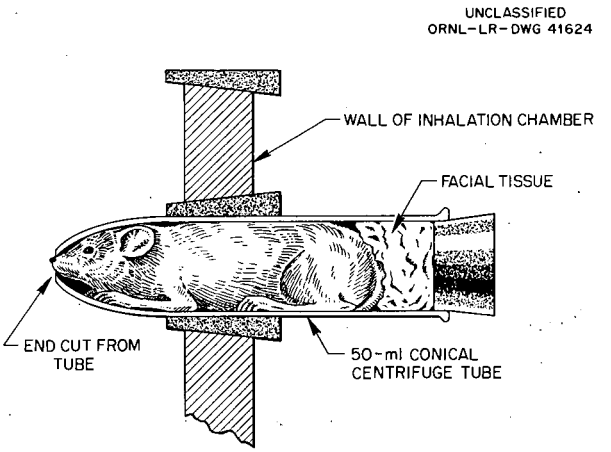

Fig. 174. Mouse Container.

The radioactive dust in the chamber will be collected on Millipore filters and counted in a proportional counter to determine its concentration. A thermal precipitator will be used to sample particulates for size determination in the electron microscope. The chamber can be attached to one of the existing aerosol generators. A Gast air pump will be used to draw the aerosol through the chamber. An electrostatic precipitator, a charcoal filter, and a glass filter trap, in that order, will be placed between the chamber and the pump. The pump exhaust will be passed through a CWS-6 filter and then into an existing exhaust system.

Portable Air Sampler. – The first model of a portable air sampler for personnel monitoring has been completed. This unit is similar to a sampler designed by Lippman.[16] The monitor will be strapped to the back of a person working in the areas to be tested. The air intake and filter are mounted on a shoulder strap and can be positioned as desired to obtain breathing zone samples. The unit weighs 10 lb and consists of a Lucite carrying case, battery pack, motor pump assembly, rotameter, and filter holder (Fig. 175). In order that the equipment might be carried more comfortably, the backing plate is hinged for flexibility and covered with ½-in. foam rubber. The batteries have sufficient capacity to power the equipment for 8 hr without recharging.

The maximum flow rates for this air sampler[16] using AA Millipore, glass filter, and Whatman No.

[16] M. Lippman, E. E. Christofano, and R. T. Graveson, "Lightweight Air Sample Pumps for Field Use," *American Industrial Hygiene Association Abstracts, 1959 Industrial Health Conference, Chicago, Ill.*

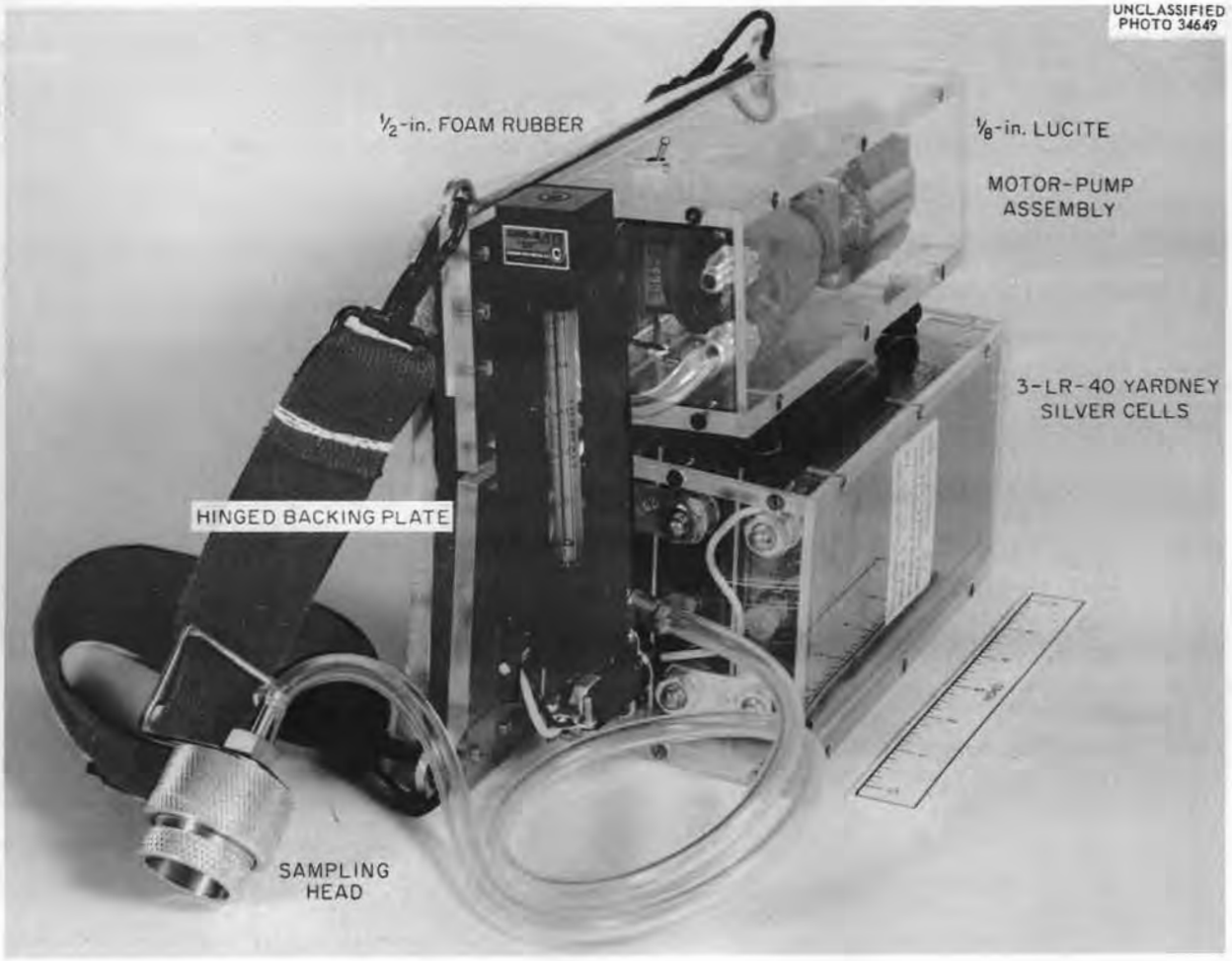

Fig. 175. Portable Air Sampler.

41 filter papers are 10.5, 11.5, and 12.7 liters/min, respectively. These flow rates are well within the desired range for air monitoring.

Distribution and Excretion Studies

J. R. Muir

B. R. Fish
N. L. Gillum
E. S. Jones
H. A. Ludeman[17]
J. A. Payne
J. L. Thompson

Distribution and Excretion of Uranium. – The study of the deposition of soluble uranium compounds in the animal body previously reported[18] has been extended to an additional species. Female white rats of the CD strain were injected on a body weight basis at one of three dose levels: 0.01, 0.1, and 1.0 milligram of uranium per kilogram of body weight. In order to make the radiation doses relatively uniform, the uranyl nitrate injection solutions were composed of a constant amount of U^{233} buffered with one of three quantities of depleted uranium. The concentrations used were 5 μg of U^{233} + 495 μg of U^{D} (depleted uranium) per ml, 5 μg of U^{233} + 45 μg of U^{D} per ml, and 5 μg of U^{233} + 0 μg of U^{D} per ml.

Sixty rats which received single intravenous injections were serially sacrificed at 1, 2, 4, 8, and 12 weeks. The rate of excretion is generally the same for all dose levels (Fig. 176). The points for each level are connected by straight-line segments, and each point represents the average excretion rate of from 4 to 20 animals. Autoradiograms of kidneys from two rats which received the two highest dose levels show alpha tracks in the cortex, primarily from epithelial cells in proximal convoluted tubules and from tubular debris. The percentage deposition in the kidneys varies directly with gravimetric dose (Fig. 177). The indicated dose dependence may help to explain apparent anomalies in the retention of uranium in the kidneys of humans receiving a similar range of injection doses.[19]

Studies with Protoporphyrin. – The possible use of porphyrins to modify or prevent uranium toxicity

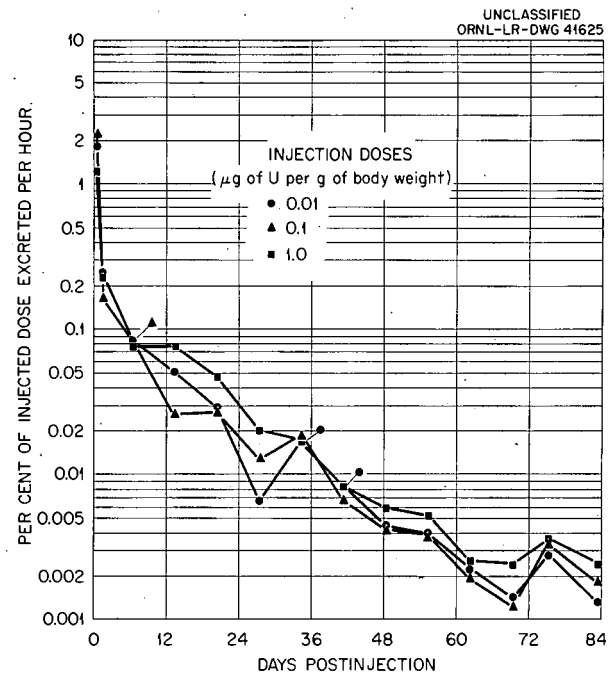

Fig. 176. Urinary Excretion of Uranium by Female White Rats Following Intravenous Injection.

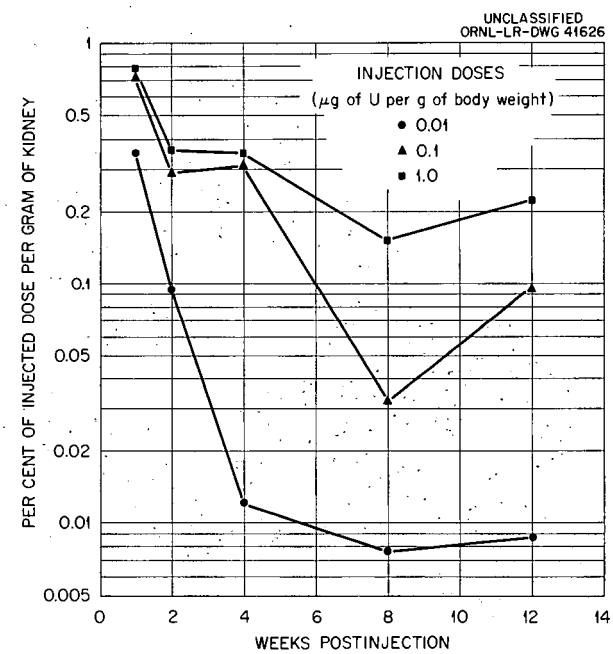

Fig. 177. Percentage Deposition of Uranium in Kidneys of Female White Rats Following Intravenous Injection.

[17] ORINS research participant.

[18] J. R. Muir *et al.*, *H-P Ann. Prog. Rep. July 31, 1958*, ORNL-2590, p 145.

[19] S. R. Bernard, *Health Phys.* 1, 288–305 (1958).

in man by internal decontamination has been suggested by Bases.[20] He has shown that much larger amounts of uranyl protoporphyrin than of inorganic uranium salts can be maintained in the body without apparent kidney or liver damage. It has been speculated that uranium as uranyl protoporphyrin would be excreted into the feces via the bile – that is, a fate similar to that of protoporphyrin.[20–22] If uranium can be made to complex with protoporphyrin injected into the body, this may reduce the assault on the critical organ, kidney, following an acute exposure to uranium. This laboratory is currently investigating the properties of uranyl protoporphyrin to evaluate the application of protoporphyrin to this problem.

A study is being made of the optimum pH at which the uranyl protoporphyrin can be prepared in the largest yield and of the conditions at which it can be stored in stable form over a period of time. Protoporphyrin is increasingly more soluble in dilute NaOH at pH 6.8 to 9.2. Upon the addition of uranyl nitrate the insoluble uranyl protoporphyrin is formed. The washed precipitate is soluble in dilute NaOH at pH 7.4 and then is reprecipitated by dilute HCl at pH 4.6. The insoluble uranyl protoporphyrin is washed with distilled water until the gamma count of the filtrate is indistinguishable from background. Most of the uranyl ions have reacted with the protoporphyrin, as indicated by the low gamma count of the first filtrate. The filtrates obtained in washing the dry product periodically over the first four weeks have shown no deviation from background when counted. During that time the dry product was stored at room temperature in closed containers. A continuation of these tests over a longer period of time will give further evidence of the stability of uranyl protoporphyrin. Since this complex is soluble near a pH of 7, it seems probable that solutions can be used to study its stability and distribution in animal tissues and fluids.

Applications of the Analog Computer to Distribution and Excretion Models. – A small electronic analog computer has been assembled in our laboratory to analyze simple biological models of the distribution and excretion of uranium. It will be used to test the utility of such equipment in the laboratory and to aid in the design of experiments for evaluating biological and mathematical parameters.

The computer is composed of three FLEPAC[23] units (obtained on temporary loan from the Instrumentation and Controls Division) and a control panel designed for flexibility of operation. Two strip-chart recorders are used for making permanent records of output, and a zero-centered voltmeter is used for monitoring operating conditions. Additional input and output devices, such as function generator, *X-Y* plotter, and oscilloscope, may be used. The entire unit (Fig. 178) is enclosed in a rack and mounted on casters for mobility. Tests of operating characteristics are being conducted.

Instrumentation

J. M. Garner, Jr. S. J. Wode[24]

Small-Animal Counter (*in Vivo*). – A special scintillation counter for measuring the radioactivity of small animals and other samples has been developed. Samples are enclosed in thin-wall plastic boxes to prevent contamination of the counter. The containers are selected to conform closely to the size of the specimen. The box is fitted onto a suitable positioning tray (Fig. 179), which is then placed in a guide rack that holds the assembly in a fixed position with respect to the lower crystal. The upper crystal is then lowered, by means of the hand wheel (Fig. 180), to within $\frac{1}{32}$ in. of the top of the box to obtain a large solid angle. Plastic boxes up to 5 in. in diameter and 4 in. in height may be used.

Signals from the photomultiplier tubes are fed to a preamplifier and then to a DD-2 linear amplifier and pulse-height selector. The signals from the pulse-height selector are fed to a counting rate meter–recorder unit and also to a scaler. An external pulse-height selector driven by the chart drive motor is provided for use when a gamma-ray spectrum is desired. This technique is used to aid in presetting the internal pulse-height selector for optimum counting with the scaler. Either differential or integral counts may be made.

[20] R. E. Bases, *Science* 126, 164–65 (1957).

[21] R. E. Bases, *Brookhaven National Laboratory Quarterly Progress Report (1 Oct.–31 Dec. 1954)*, BNL-326, p 45.

[22] R. E. Bases, *Cancer* 11, 259–63 (1958).

[23] F. P. Green, *The ORNL FLEPAC Computing Device*, ORNL CF-58-10-124 (October 1958).

[24] Temporary employee.

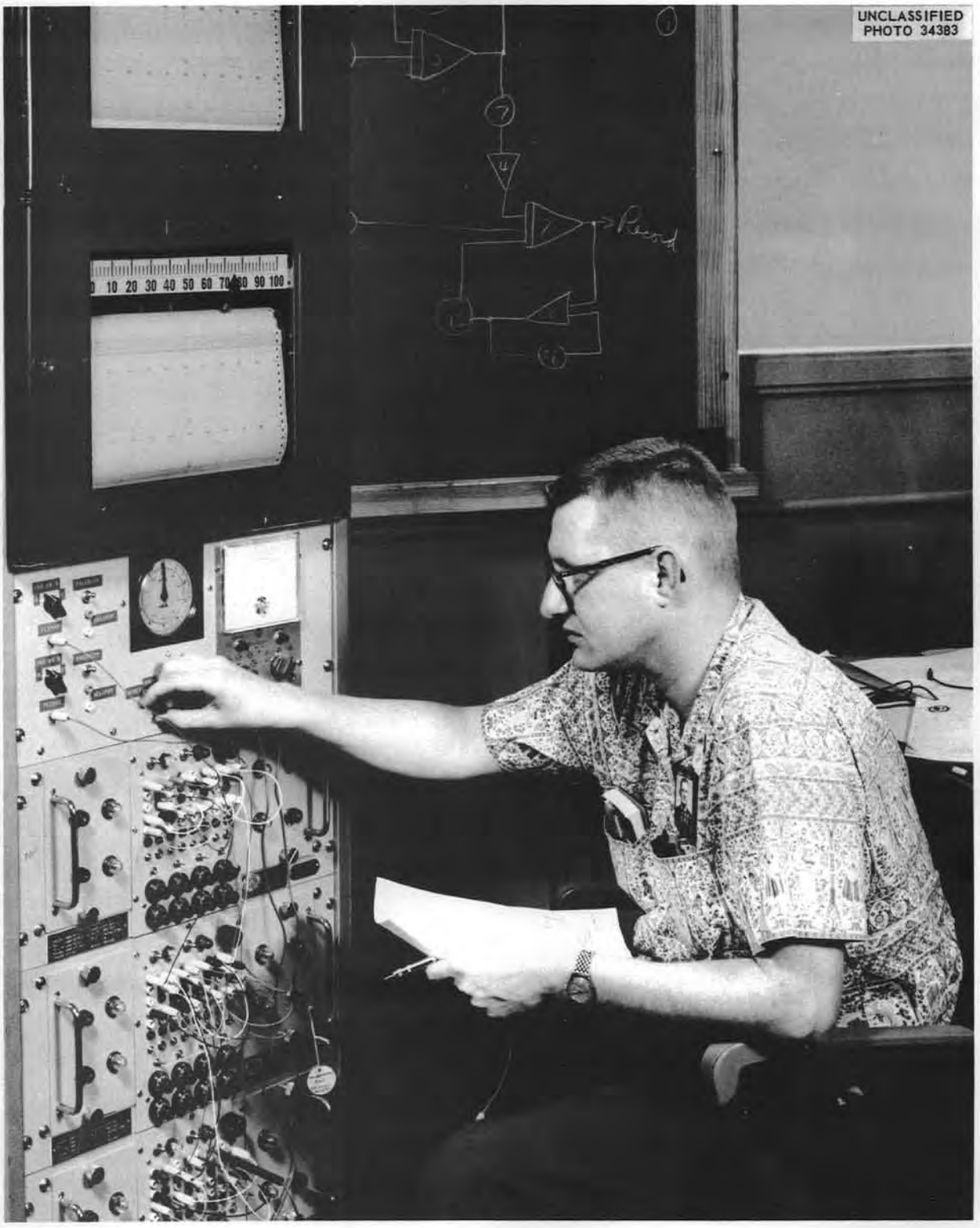

Fig. 178. Small Electronic Analog Computer.

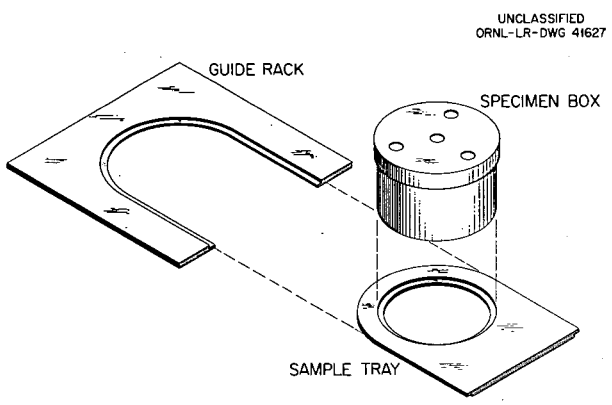

Fig. 179. Positioning Assembly.

Autoradiographic Studies

E. S. Jones

M. A. Kastenbaum[25] J. L. Thompson
J. A. Payne A. C. Upton[26]

Nonuniform Distribution of Internally Deposited Radioisotopes. – The usefulness of autoradiography in studying localization within tissues of internally deposited radionuclides has been previously demonstrated,[27] but additional information is needed especially concerning nonuniform distribution of radioisotopes within tissues or organs. A laboratory for autoradiography has been established, and methods suitable to our needs have been developed.

Localized deposition of uranium in rat kidneys is being examined in detail by means of autoradiographic and histological techniques. In addition to the application to the distribution and excretion studies, the investigation will provide data for establishing a nonuniform distribution factor, *N*. These data may be used in refining calculations of radiation dose to the kidneys from internally deposited uranium. The amounts of uranium in kidney will be measured by ashing cortex and medulla separately[28] and by counting the alpha tracks.

Female CD rats are injected intravenously with known amounts of uranium. The animals are sacrificed at various intervals after injection, and the kidneys are removed and weighed. Each kidney is bisected; the cortex and medulla of the anterior half of one kidney and the posterior half of the other are separated from each other with sharp needles.[29,30] Cortex and medulla are then separately weighed and ashed for radiochemical analysis. After the remaining half is weighed, the kidneys are embedded and cut into serial sections at 5 μ, and every fortieth and forty-first section used for autoradiograms.

Using an eye micrometer, tracks are counted in two rows of five fields each in both medulla and cortex in the histological units of the kidney, including the proximal tubules, distal tubules, collecting tubules, glomeruli, and Henle's loop. The nonuniform distribution factor for radiation dose may be determined directly from the relative track density in the critical portion of the tissue. The average ratio of track counts in the cortex to that in the medulla may be checked against the ratio derived from the ashing procedure. Histological damage related to internal deposits of uranium is being studied on the stained sections cut adjacent to those used for autoradiography.

INTERNAL DOSE ESTIMATION

Inorganic Analysis of Human Tissue

M. J. Cook K. K. McDaniel
E. L. Grove[31] I. H. Tipton[32]

Analysis of human tissue by emission spectroscopy and flame photometry has continued. The emission spectroscopy has been done under subcontract in the Physics Department of the University of Tennessee. Because the amount of data is voluminous, a series of memorandums have been issued which contain the data for the tissues from each city. The fifth in the series has been issued and gives the data from tissue received from Seattle and Tacoma, Washington.[33] The analyses of tissues from Richmond, Virginia, have been completed,[34] and a report will be issued soon. In

[25] Mathematics Panel.

[26] Biology Division.

[27] W. B. Looney and L. A. Woodruff, *A.M.A. Arch. Pathol.* **56**, 1 (1953).

[28] A. Tannenbaum and H. Silverstone, *Natl. Nuclear Energy Ser. Div. IV* **23**, 1 (1951).

[29] M. Arataki, *Am. J. Anat.* **36**, 399–436 (1926).

[30] K. Fischermann, *Acta Pathol. Microbiol. Scand.* 44(1), 48–53 (1958).

[31] Consultant, University of Alabama.

[32] Consultant, University of Tennessee.

[33] I. H. Tipton *et al.*, *Spectrographic Analysis of Normal Human Tissue from Seattle and Tacoma, Washington*, ORNL CF-58-10-15 (Oct. 6, 1958).

[34] I. H. Tipton *et al.*, *Spectrographic Analysis of Normal Human Tissue from Richmond, Virginia* (CF memo to be published).

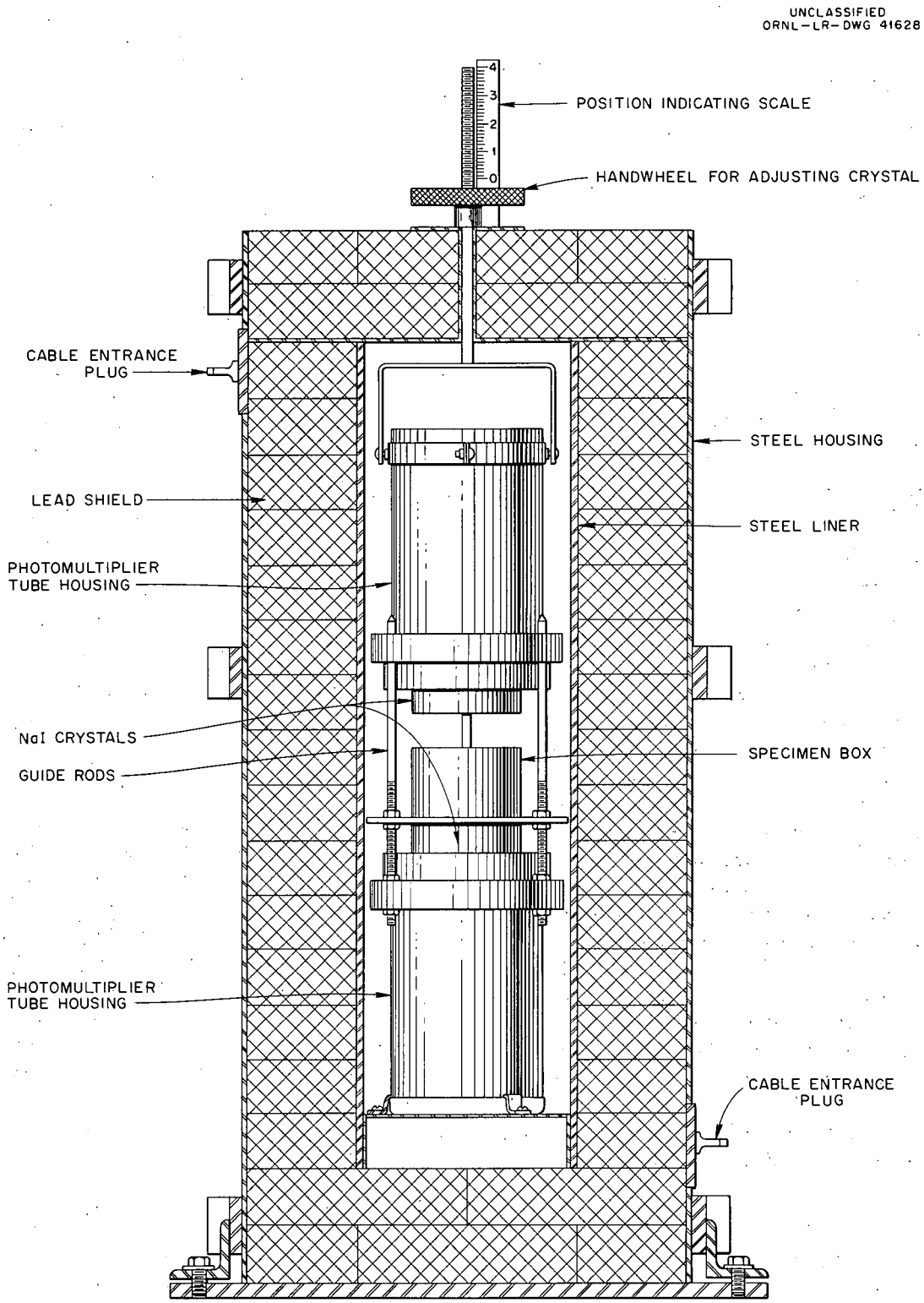

Fig. 180. Small-Animal Counter.

addition to samples from the United States, samples have been received and analyzed from 18 locations throughout the world.

During the past year the scope of the program for spectrographic analysis of human tissue was broadened to include a classification and study of the data obtained over the past eight years. The data have been grouped according to the geographical origin of the subject from whom the tissues were taken, as well as to the cause of death and age of subject at death.

Even though most of the American subjects were supposed to have been "normal" (i.e., victims of instantaneous death by traumatic accident), some died suddenly of heart disease and others were known to have conditions (alcoholism, epilepsy, cerebral atrophy) which were not normal. Listed below is the number of samples analyzed according to the classification of death – accident, heart, other:

Tissue	Number of Samples Analyzed		
	Accident	Heart	Other
Aorta	65	13	6
Brain	75	14	11
Heart	86	19	11
Kidney	87	18	12
Liver	88	19	12
Lung	87	19	12
Ovary	9	3	1
Pancreas	85	14	10
Prostate	26	6	3
Spleen	84	20	12
Testis	42	10	5

The per cent occurrence and order of magnitude of concentration of trace elements in 11 soft tissues from U.S. adults are indicated in Fig. 181. For convenience the elements studied are grouped according to their known function in the body and the specificity they exhibit for a particular organ. Those with a known function are grouped as "essential" and those with no known function as "abnormal." The median, range, and 90% range for zinc, cadmium, and lead in 11 tissues are shown in Fig. 182.

Another variation observed is the relationship between the concentration of the element and the age of the subject. In Fig. 183 this variation is shown for certain elements in kidney, liver, and lung. The subjects were divided into three age groups: 0 to 45 days, 45 days to 12 years, and 12 to 20 years. The number of samples analyzed from each age group is given below:

	Number of Samples Analyzed		
	0 to 45 Days	45 Days to 12 Years	12 to 20 Years
Kidney	16	30	12
Liver	22	30	11
Lung	10	9	10

In the lungs of stillborns and infants, there was either very little aluminum and titanium or none at all, but the concentration of both increases with age; the same was true for cadmium in the kidney. Chromium is the only minor element which appears to decrease with age.

Comparison of tissues from U.S. adults with those of adults from Europe, Africa, and Asia also revealed differences in some elements. Figure 184 shows medians and ranges of tissues of all American and all foreign adults for lead, cadmium, and zinc in kidney, liver, and lung. The foreign group included a greater proportion of subjects who had died of disease than the U.S. group and a greater variety of diseases as well. The cause of death of these subjects was classified as accident, heart, cancer, and infection. A comparison of tissues from U.S. and foreign accident subjects is shown in Fig. 185. For cadmium in kidney and liver there is a marked difference between the Mongoloid Asians and Africans, the Mongoloid Asians having a much higher median concentration of cadmium than U.S. adults, and the Africans a lower median concentration. The Caucasian Asians have a somewhat lower median for cadmium in the kidney and liver than the U.S. adults but not as low as that of the African. The median for zinc in the kidney and liver was approximately the same for all groups.

The differences between tissues from diseased individuals and those from victims of accidental death are more striking in the foreign group (Fig. 186) than in the U.S. group. This is not surprising, because all of the U.S. group died instantly, whereas many of the foreign group had been hospitalized for periods of time long enough to reflect any change in trace element patterns which might occur

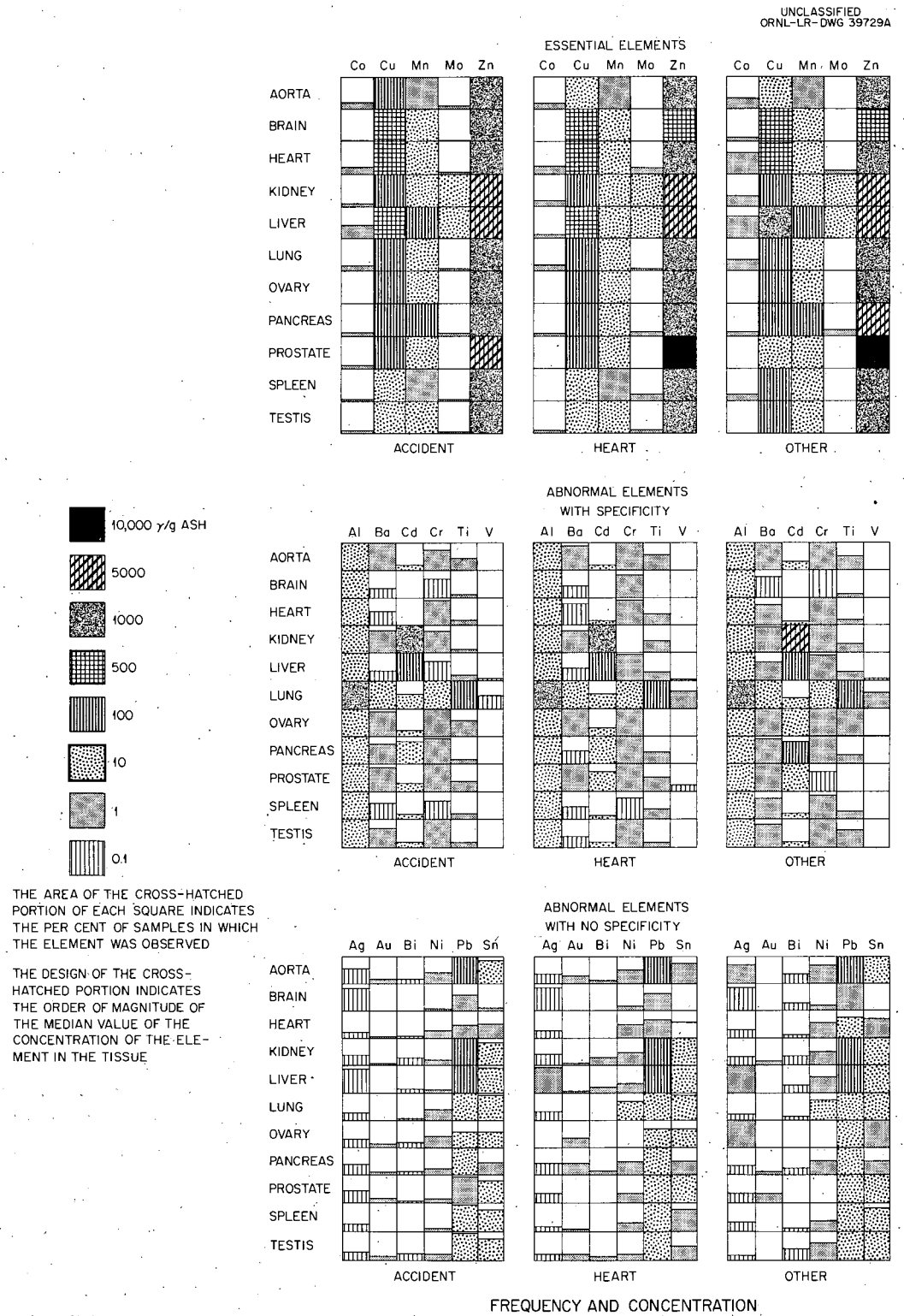

Fig. 181. Per Cent Occurrence and Order of Magnitude of Concentration of Elements in 11 Soft Tissues.

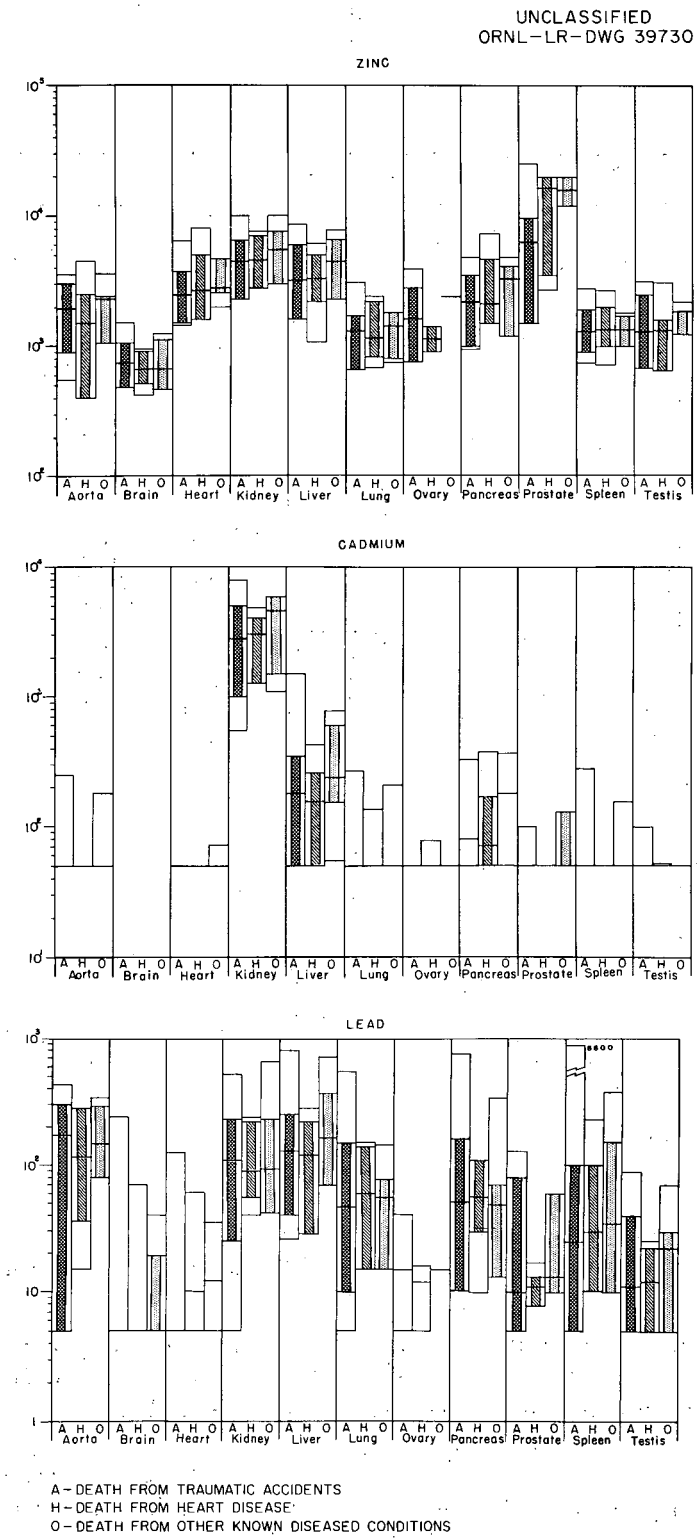

Fig. 182. Median, Range, and 90% Range for Zn, Cd, and Pb in 11 Soft Tissues. All values fell between the limits of the full bar, and 90% fell between the limits of the cross-hatched bar. The heavy horizontal line indicates the median line.

UNCLASSIFIED
ORNL-LR-DWG 39736A

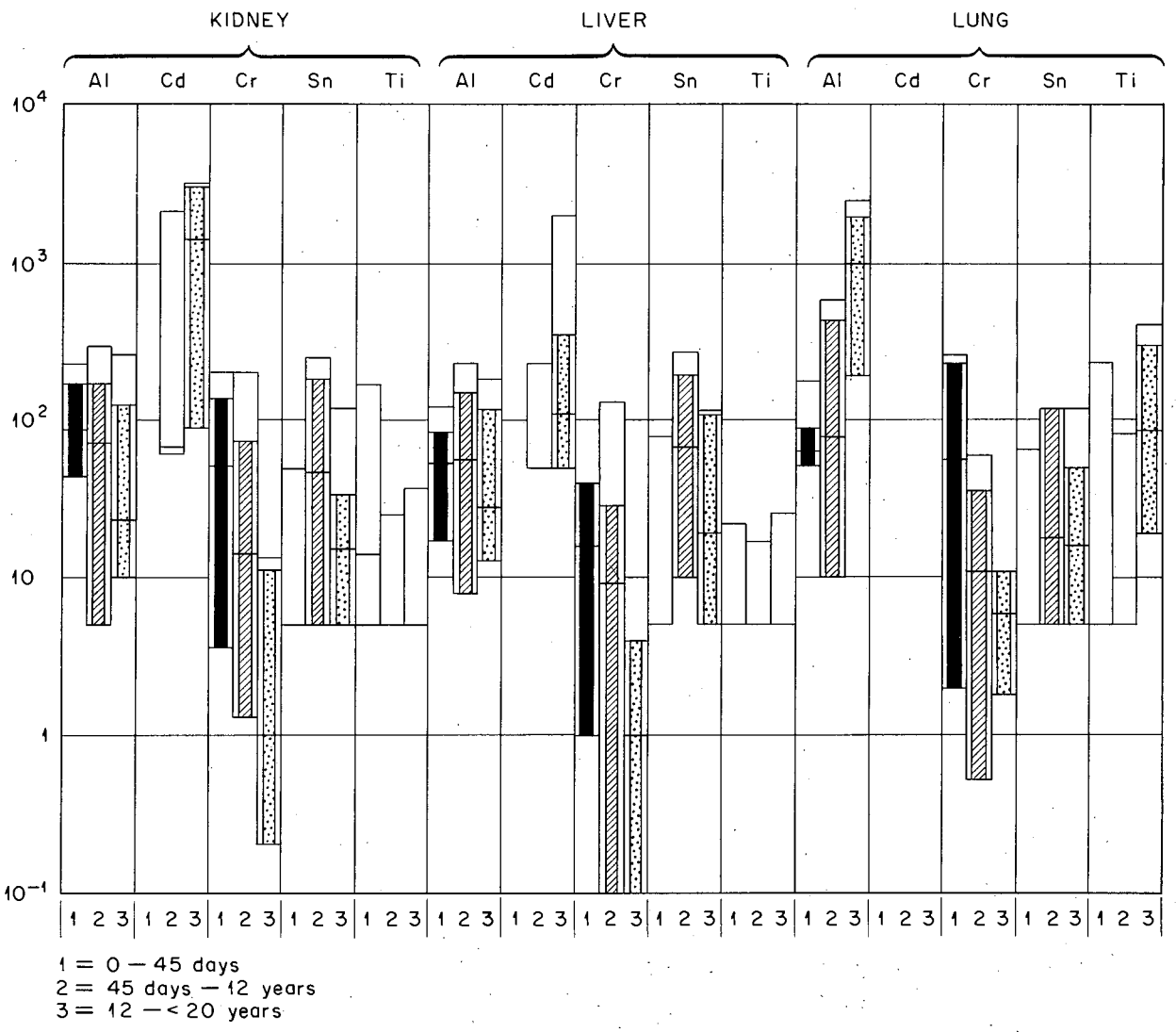

Fig. 183. Examples of Variation with Age. All values fell between the limits of the full bar, and 90% fell between the limits of the shaded bar. The heavy horizontal line indicates the median value.

in a diseased state or result from prolonged medication.

Further statistical analyses are being made on the 25 elements commonly seen in all the different tissues which have been analyzed.

In addition to determining sodium and potassium by flame photometry, a correlative study to evaluate the dry ashing techniques used in tissue preparation has been conducted under subcontract by the School of Chemistry of the University of Alabama. Beef serum and rabbit blood samples were ashed at fixed temperatures within the range of 300 to 900°C and allowed to remain at the fixed temperature for 24 or 72 hr.

The results are plotted for sodium in Figs. 187 and 188 and for potassium in Figs. 189 and 190. There is apparently little loss of sodium due to ashing below 700°C, but a safe temperature for ashing is probably 600°C. Since for potassium there is a definite loss above 550°C, 500°C is probably the safe upper limit for ashing.

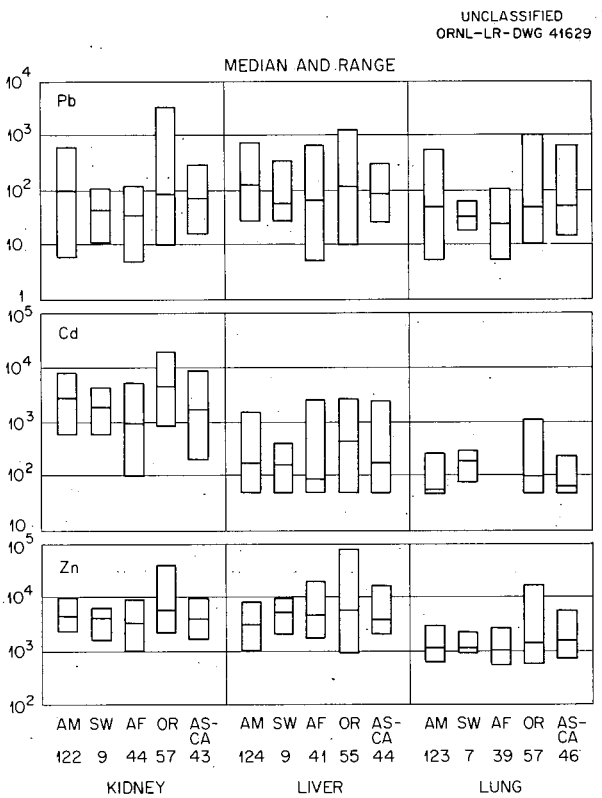

Fig. 184. Comparison of Tissues from All American and Foreign Adults. The number under the symbol denoting the geographical origin indicates the number of samples from this location.

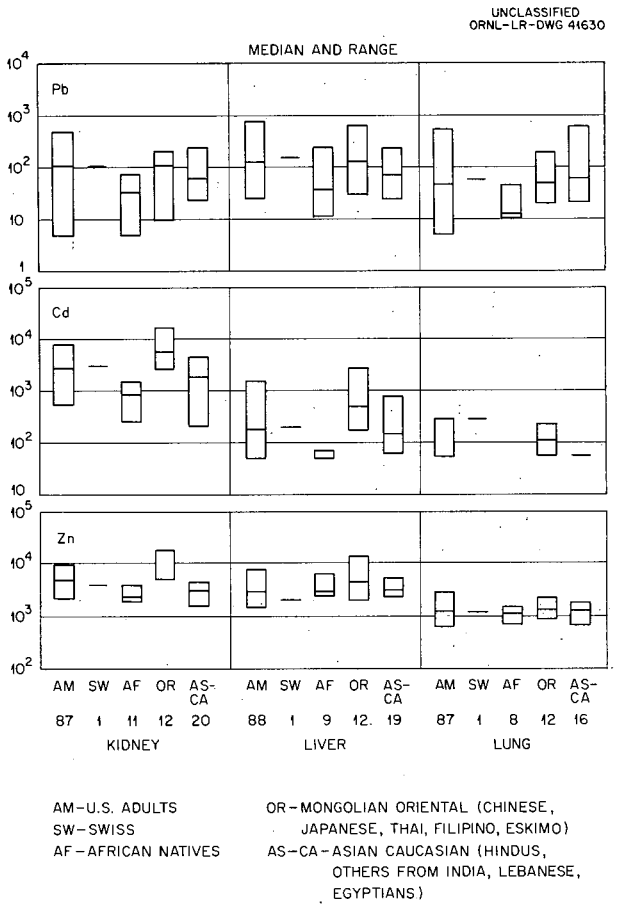

Fig. 185. Comparison of Tissues from American and Foreign Accidents.

An ARL quantometer with 33 fixed and 9 movable channels has been purchased and installed in the Spectrochemical Section of the Analytical Chemistry Division. Within the next year the routine analytical part of this program will be transferred to this section.

Dose to Gastrointestinal Tract from Ingested Radionuclides

W. S. Snyder H. B. Eldridge M. R. Ford

The dose delivered by an isotope and its daughter elements as it passes through the gastrointestinal tract is given by

$$D(t) = \sum_{i=1}^{n} C_i X_i(t) \quad , \qquad (1)$$

where $X_i(t)$ is the number of μc of the ith daughter element present at time t and C_i is a constant. Except for gamma emitters, the dose may be considered to be absorbed locally, and thus (1) represents the dose to a certain section of the tract, namely, the portion of the tract reached at time t. For the dose to the stomach the approximate formula is

$$D_s(t) = \sum_{i=1}^{n} C_i \int_0^{T_s} X_i(t)\, dt \quad , \qquad (2)$$

where T_s is the total time that the material spends in the stomach and C_i is the appropriate constant.

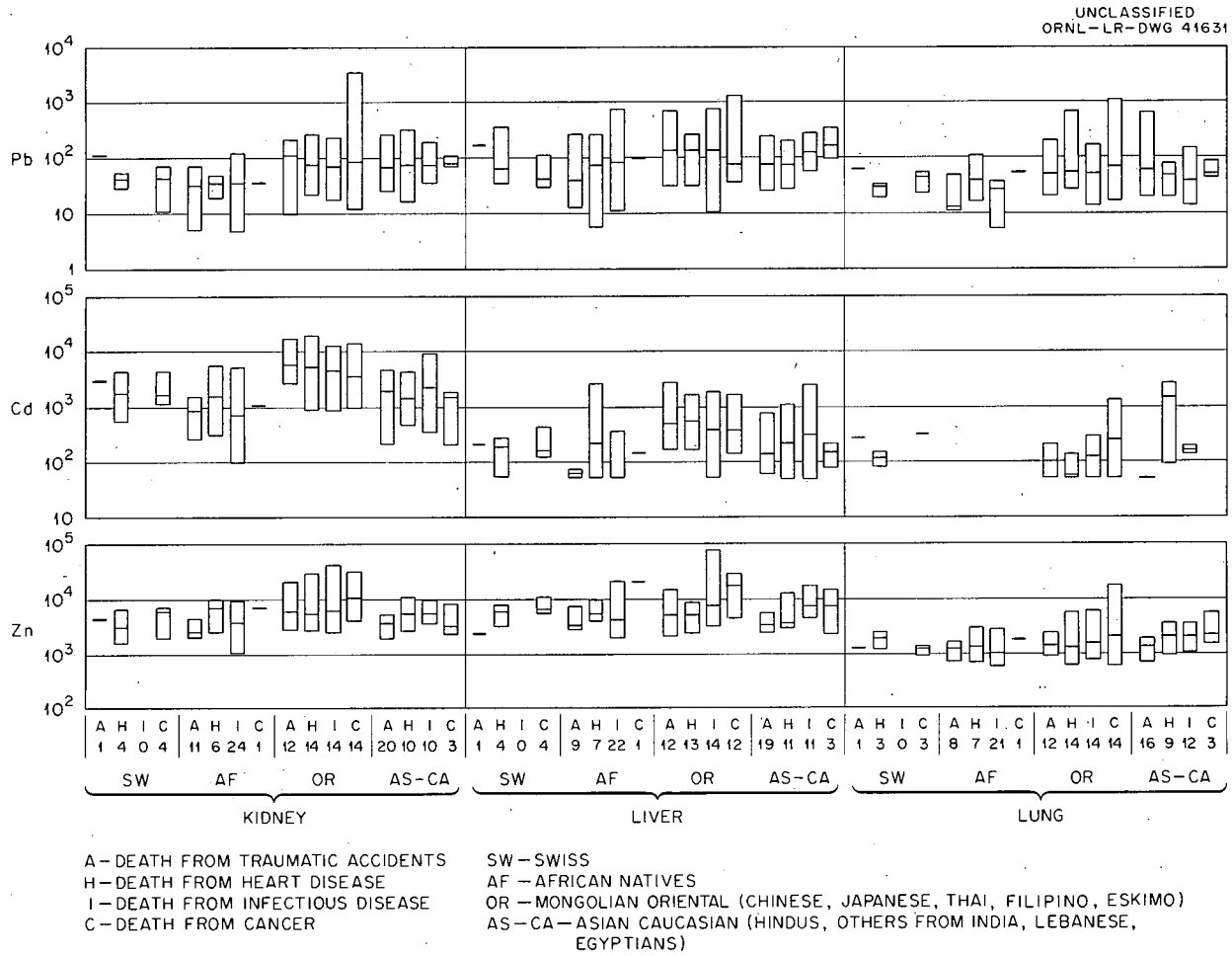

Fig. 186. Foreign Accidents and Disease. The numbers above the symbol denoting the geographical origin indicate the number of samples from this location.

The amount of ith daughter isotope present at time t is governed by the following differential equation:

$$\frac{dX_i}{dt} = \sum_{j=1}^{i} A_{ij} X_j(t) \ , \qquad i = 1,2, \ldots , n \ . \quad (3)$$

A code for the Oracle has been developed which computes over- and underapproximations of $D(t)$ and $D_s(t)$ and also their maximum values and the time of occurrence of such maxima.

With a slight modification of the code it can be used to compute the relative amounts F_i of parent and daughter elements that accumulate in body organs according to the formulas given in the ICRP Report of Committee II on permissible dose for internal radiation.[35] This report also contains the appropriate constants to be used in formulas (1), (2), and (3) for the calculation of MPC values for occupational exposure.

Dose to the Gonads from Radionuclides Present in Food or Water

W. S. Snyder C. F. Taylor[36] M. R. Ford

The gonads absorb energy released by radionuclides that are present in the gonads, and they

[35] *Report of Committee II on Permissible Dose for Internal Radiation — 1958 Revision*, Pergamon, London (in press).

[36] Summer participant.

are irradiated also by x or gamma rays released from nuclides present in other organs. Since the gastrointestinal (GI) tract and the urinary system are principal routes by which the isotope may enter or be eliminated from the body, the GI tract and the bladder are two large reservoirs from which x- or gamma-ray emitters may irradiate the gonads.

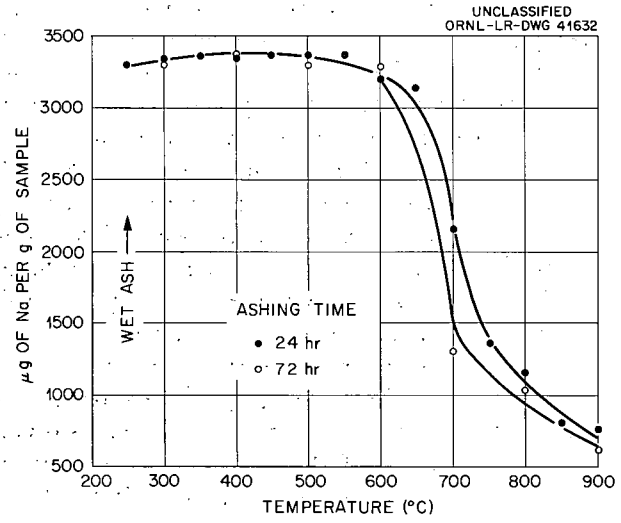

Fig. 187. Loss of Sodium with Temperature. Dry ash of beef serum; source, slaughterhouse.

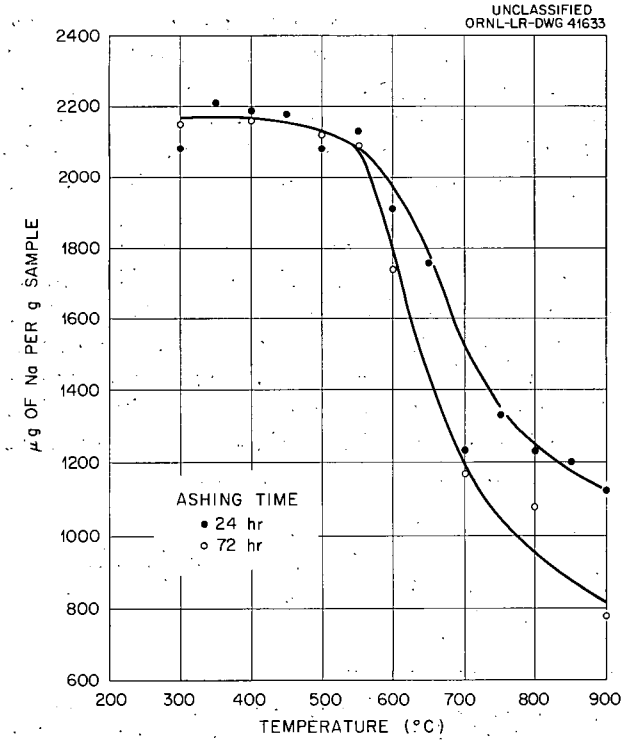

Fig. 188. Loss of Sodium with Temperature. Dry ash of rabbit blood.

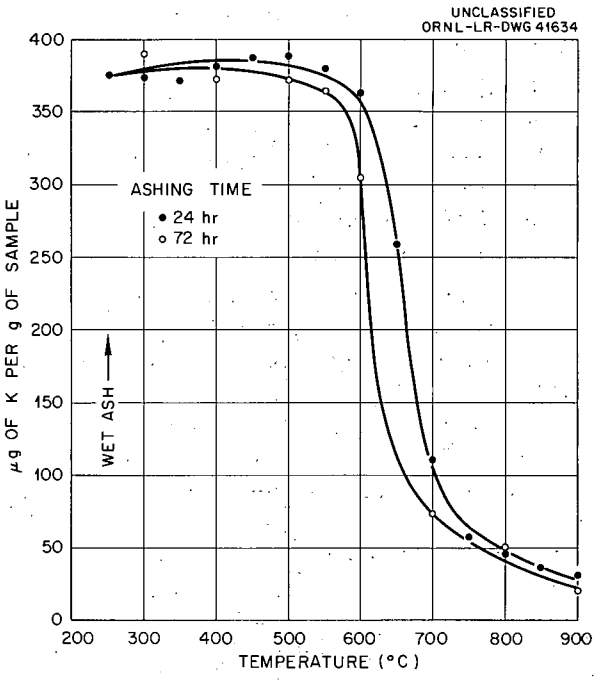

Fig. 189. Loss of Potassium with Temperature. Dry ash of beef serum; source, slaughterhouse.

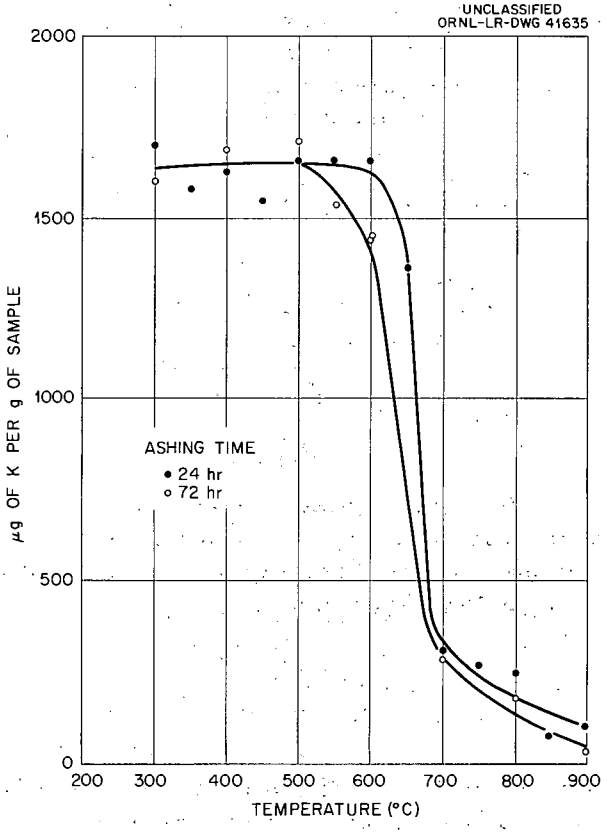

Fig. 190. Loss of Potassium with Temperature. Dry ash of rabbit blood.

Thus the dose to the gonads has been estimated in three parts:

1. the dose to the gonads from x- or gamma-ray emitters present in the GI tract,
2. the dose to the gonads from gamma emitters present in the bladder,
3. the dose due to the presence of the radionuclides in the gonads.

Although the methods used are general, only the dose to the ovary is discussed here.

The ovary is considered as a spherical mass with a radius of 0.5 cm, and the precursors of the ova are considered to lie primarily in the periphery or cortex. Thus it is the average dose to a spherical shell that is of principal interest. The bladder and the GI tract also will be considered as spherical in shape. Consequently, it is the dose from a sphere to a spherical shell that is computed. The source sphere and the target shell are assumed to be embedded in a homogeneous medium of 1 g/cm^3 density. The scattering cross section of this material is denoted by σ_{scatt}, and σ_{ab} denotes the absorption cross section of this material.

The first collision dose is denoted by D_1 and is given by Eq. (1). It gives the average dose in rads per year in a thin spherical shell of radius R cm, due to a gamma emitter which is distributed in a solid sphere of radius r cm:

$$D_1 = \frac{kIE\,\sigma_{ab}}{4\sigma^3 RD}\Big(\sigma r\{E_3[\sigma(D+r-R)] + E_3[\sigma(D-r-R)] - E_3[\sigma(D+r+R)] - E_3[\sigma(D-r+R)]\} + \{E_4[\sigma(D+r-R)] - E_4[\sigma(D-r-R)] - E_4[\sigma(D+r+R)] + E_4[\sigma(D-r+R)]\}\Big)\,, \qquad (1)$$

where D is the distance between centers, k is a units conversion constant, I is photons·cm^{-3}·year^{-1}, σ is the total cross section, and E is the photon energy in Mev. The functions

$$E_n(x) = \int_1^\infty \frac{e^{-xt}}{t^n}\,dt$$

entering here for $n = 3$ and 4 are related to $E_1(x)$ by a simple recursion formula, and $E_1(x)$ has been tabulated.[37] Clearly, D_1 underestimates the dose since it neglects multiple collisions of the photons. Since buildup factors are not currently available for many energies of interest, other models are used for estimating the magnitude of this effect.

If σ_{ab} is replaced by σ in (1), a second estimate is obtained which can be interpreted in physical terms. It amounts to assuming that the entire energy of the photon is absorbed whenever a collision occurs. The importance of this approximation lies in the fact that it gives an overestimate of the dose near a point source and an underestimate of the dose far from a point source. Also, it does make some allowance for multiple scattering since the total energy of the photon is taken into account. This estimate is termed the single-hit annihilation estimate. It is shown in Fig. 191 and, as expected, is the highest of the estimates and is to be considered as an upper approximation.

Replacement of σ by σ_{ab} in (1) results in the straight-ahead approximation. This replacement amounts to using $e^{-\sigma_{ab}x}$ as the attenuation factor for distance x instead of $e^{-\sigma x}$, and this would be true if the scattered photons were to scatter straight ahead, that is, remain in the beam. This approximation underestimates the dose near a point source and overestimates it at a large distance from the source. In general, this is the best approximation to the actual dose available without extensive computation. In Fig. 191, it lies between the first-collision approximation and the single-hit annihilation approximation. This estimate of dose is used in all the calculations that follow.

The dose from material in the bladder is estimated by assuming a spherical bladder whose volume expands at a constant rate. Allowing 3.75 voidings per day and 1500 cm^3 as the volume of urine excreted per day, the radius of the bladder increases until the volume $4\pi r^3/3 = 1500/3.75$ is reached after a time lapse of 24/3.75 hr. Thus the dose per void is

$$\int_0^{24/3.75} \frac{D_1(r)}{24\times 365}\,dt = \int_0^{4.6} \frac{D_1(r)}{24\times 365}\,\frac{96\pi r^2 dr}{1500}\,.$$

[37] *Tables of Sine, Cosine and Exponential Integrals*, vol 1, prepared by the Federal Works Agency, WPA, for City of New York, A. N. Lowan, Technical Director, 1940.

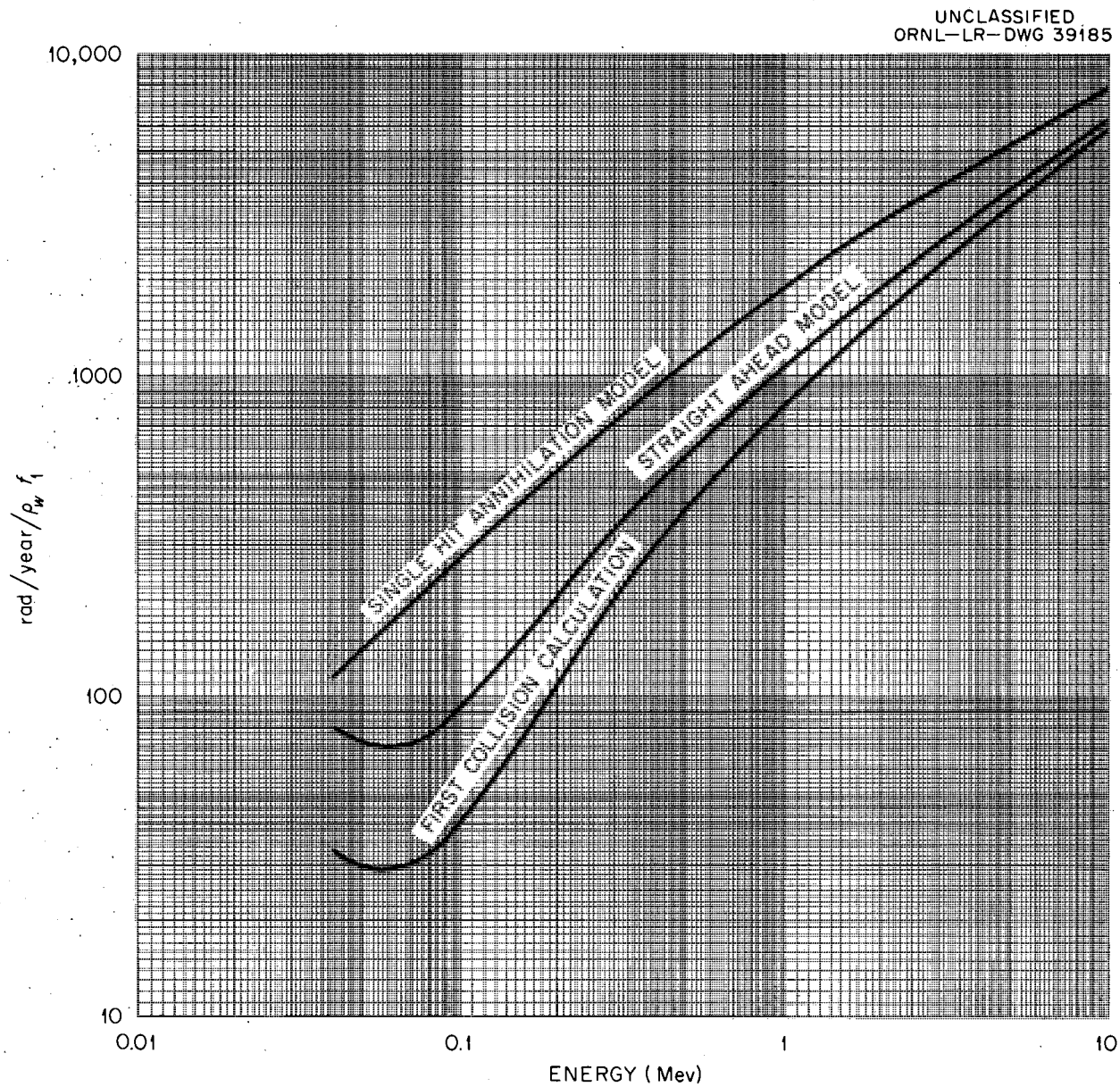

Fig. 191. Dose from GI Tract to Ovary (Solid Sphere to Spherical Shell).

Since the number of voids per year is 3.75 × 365,

$$D_2(r) = 10^{-2}\pi \int_0^{4.6} r^2 D_1(r)\, dr \text{ rads/year} \quad . \qquad (2)$$

The integration was performed, but since the formula is rather lengthy, only the graph is shown in Fig. 192, using the same three approximate treatments as before. Biological data used in these formulas are listed below:

Organ	Radius (cm)	Volume (cm^3)	Time (hr)
GI tract	9.7	3500	31 (average time)
Bladder (filled)	4.6	400	24/3.75 (per filling)
Ovary	0.5	0.4	

Finally, the dose to the ovary from the concentration of the isotope in this organ must be considered. Available biological data are scarce

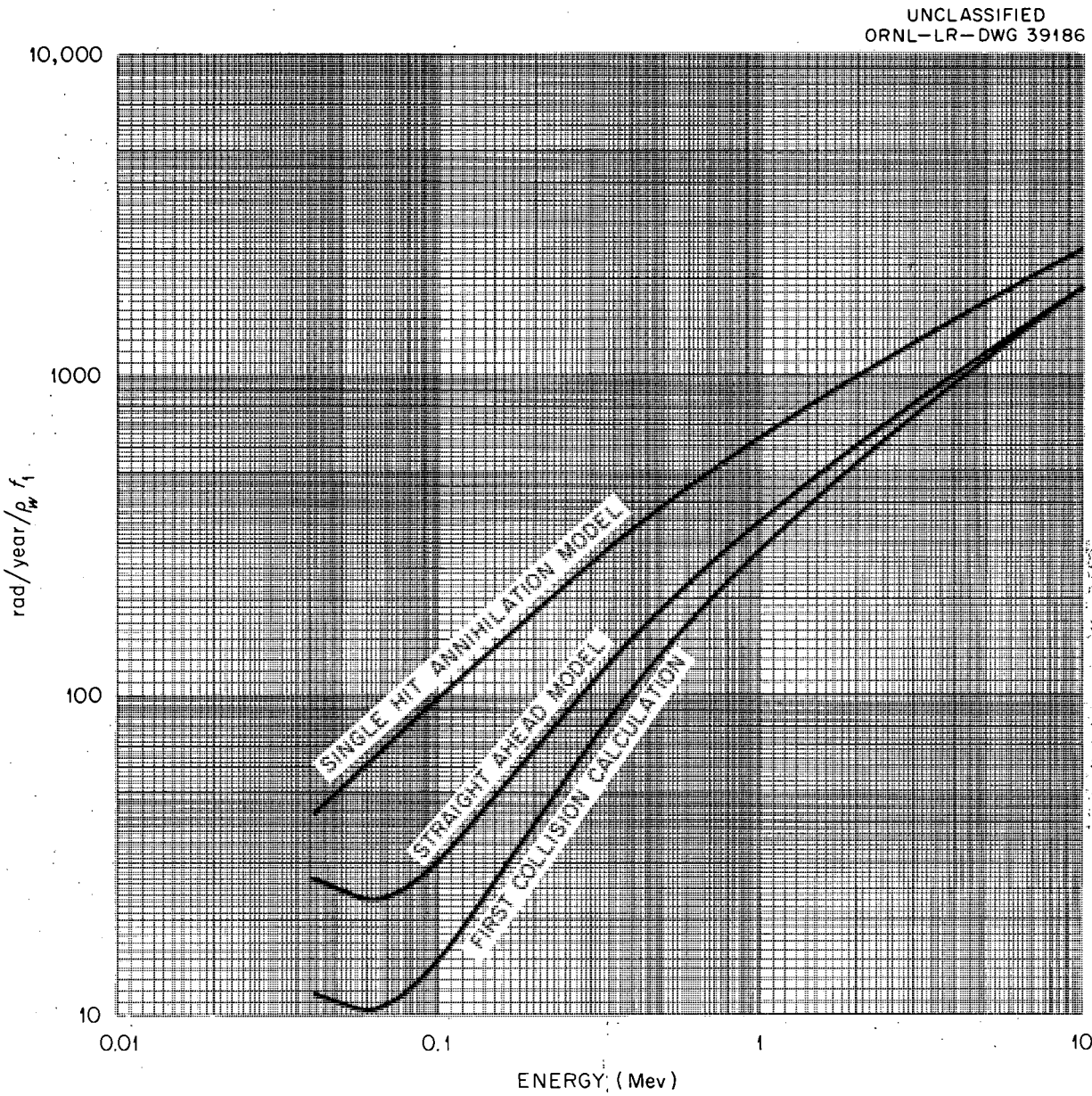

Fig. 192. Dose from Bladder to Ovary (Expanding Sphere to Spherical Shell).

indeed. By using small-animal data as well as average concentrations in other soft tissues or in the total body, it is possible to get a rough indication of what this dose might be. The biological data used to estimate the concentration of the isotope in any of these organs are taken from ref 35.

As an illustration of the use of these equations, results are listed in Table 46 for some of the isotopes that are gamma emitters and are of greatest long-term yield in fission material. A concentration of the radioisotope in the water intake of standard man of 1 $\mu c/cm^3$ has been assumed. A blank entry means that the amount of dose contributed is considered to be small on the basis of the available data. Thus if the recommended limit of internal genetic dose, 0.05 rem/year, given by the ICRP is taken as the standard, the MPC in $\mu c/cm^3$ for whole population exposure in the case

Table 46. Dose to the Ovary

A concentration of 1 $\mu c/cm^3$ in drinking water was assumed

Fission Products	Dose (rem/year)			
	GI Tract to Ovary	Bladder to Ovary	Ovary	Total
$Cs^{137} + Ba^{137m}$		200	25,000	25,000
$Ce^{144} + Pr^{144}$	70		17	87
Sm^{151}	80		2.5	83
Nb^{95}	830		1.3	830
$Ru^{106} + Rh^{106}$	250	2.6	250	500
$Zr^{95} + Nb^{95}$	780		5	790
Y^{91}	2.4		2.5	4.9
Ce^{141}	94		0.5	95
$Ru^{103} + Rh^{103m}$	610	6.5	63	680
$Ba^{140} + La^{140}$	550	42	1,000	1,600
$Nd^{147} + Pm^{147}$	250		0.5	250
I^{131}		150	2,500	2,700

of any individual isotope is 0.05/(total dose), where the total dose in rem per year is as given in Table 46. In actual fallout material, these and other radioisotopes will occur together in various amounts, and this must be taken into account. The relative amounts of each of the fission products listed in Table 46 will vary with the spacing of weapon tests as well as with meteorological and geographical factors.

It is seen from Table 46 that the bladder usually does not contribute significantly to the dose; but in most of the cases reviewed the GI tract does make a significant contribution to the total dose, and in seven of these cases it accounts for most of the dose. The greater importance of the GI tract, especially in the case of insoluble radioactive materials, is undoubtedly due to its much greater size and the greater length of time that the material must spend in passing through it as compared with the corresponding quantities for the bladder.

Further work along the lines sketched here is in progress.

Internal Dose Handbooks

K. Z. Morgan M. J. Cook
W. S. Snyder M. R. Ford

The preliminary revision of the National[38] and International[39] handbooks on internal dose prepared as a joint publication of the NCRP (National Committee on Radiation Protection and Measurements) and the ICRP (International Commission on Radiological Protection) was reviewed by the various committees concerned. Coordination of opinions regarding basic philosophy, formulas, and parameters used in determining the final recommended values resulted in an extensive interchange of ideas. In addition the committees were furnished memoranda containing review studies

[38] Report of National Committee on Radiation Protection, National Bureau of Standards Handbook 52 (1953), *Maximum Permissible Amounts of Radioisotopes in the Human Body and Maximum Permissible Concentrations in Air and Water*, GPO, Washington.

[39] "Recommendations of the International Commission on Radiological Protection" (1955), *Brit. J. Radiol.*, Suppl. 6 (Meeting of the International Congress of Radiology held in Copenhagen, Denmark, July 1953).

and calculations for the more controversial permissible levels for the radionuclides considered. These included Ra, Sr, U, Pu, Th, Rn, H^3, and P.

MPC values based on the GI tract were listed for the various radionuclides. These values are based on the assumption that the dose to the GI tract is proportional to the time spent in each segment of the GI tract. For long parent-daughter chains, this calculation has been programed for a digital computer calculation. In the case of alpha emitters there is no significant irradiation of the mucosal layer, and as a result it is assumed that only 1% of the rad dose is effective.

In the case of natural thorium and Th^{232} the calculated MPC values were listed in the tables even though they are very low and essentially the same as the values listed for Pu^{239}. Some committee members believed that the occupational exposure with thorium justified the assumption that it is no more hazardous than natural uranium. As a consequence a footnote was added to the tables stating that pending further investigation the value for natural uranium (a value 17 times larger) may be used. Unfortunately no conclusive experimental evidence exists or is expected to be available in the near future that will resolve this vital issue.

Calculations were made to determine the MPC values for isotopes of Pu, U, Th, Ra, and Sr based on the power function. The resulting formulas and MPC values are listed for reference in the ICRP publication but are not given as the recommended values because the majority of committee members believed that the exponential formulation gave values more consistent with the values listed for other radionuclides and in these cases just as reasonable as those obtained by means of the power function.

After decisions were obtained from the committees on the above illustrative problems and many similar ones, the results were incorporated in the *Report*. The final version of the ICRP *Report* has been approved by the Publications Committee of the ICRP, and it is now in press.[40]

The NCRP has published an abbreviated version of the above *Report*. This report, entitled *Maximum Permissible Body Burdens and Maximum Permissible Concentrations of Radionuclides in Air and in Water for Occupational Exposure*, is Handbook 69 (ref 41) (superseding Handbook 52) in the series of National Bureau of Standards handbooks. It contains the same table of MPC and body burden values as well as most of the text material dealing with the basic approach and philosophy found in the ICRP *Report*, but it makes reference to the ICRP *Report* for details regarding calculations, formulas, and supplementary tables.

Additions to the bibliography from which biological data for the handbooks were taken have increased the number of references listed to approximately 2000. This compilation is being published by Pergamon Press as a separate handbook of ICRP and will be reprinted in the journal *Health Physics*.

---

[40] *Report of Committee II on Permissible Dose for Internal Radiation — 1958 Revision*, Pergamon, London (in press).

[41] *Natl. Bur. Standards (U.S.) Handbook 69* (1959).

EDUCATION, TRAINING, AND CONSULTATION

E. E. Anderson

AEC FELLOWSHIP PROGRAM

E. E. Anderson M. F. Fair

Forty-three students completed the course in radiological physics at Vanderbilt University in May 1959. Thirty-three of these were AEC Fellows, six were from the Vanderbilt University Reactor School, two were Air Force officers, and two were from the Newport News Shipbuilding Company. Thirty people reported to ORNL in June for their applied health physics training. Twenty-seven were AEC Fellows and three were Air Force officers. Eleven of the Fellows were granted extensions to their Fellowship to complete the requirements for the MS degree. Four of the Fellows chose to do their research at the Health Physics Division, ORNL, and six returned to Vanderbilt Univeristy; one declined his Fellowship extension because of a teaching commitment. The AEC Fellows for the 1959–60 program were selected in March 1959, and a group of 13 will enroll at Vanderbilt University in September 1959.

OTHER ACTIVITIES

E. E. Anderson M. F. Fair K. Z. Morgan

A five-week course in Health Physics was conducted at Bombay, India, from November 17, 1958, to December 19, 1958. There were 31 students enrolled in the course from seven countries – India, Formosa, Indonesia, Japan, Thailand, the Philippine Islands, and Australia. This was the third international course conducted by this group. The first was in Stockholm, Sweden, in 1955, and the second was in Mol, Belgium, in 1957.

A 60-hr course in Health Physics was presented by the Division for the foreign ORSORT program. This was a combined lecture and laboratory course covering all aspects of applied health physics and waste disposal. A 10-hr lecture course was given to new members of the Applied Health Physics Group. Two trainees from Holland spent two months with the Division.

Lectures and discussion periods on particular phases of health physics were given for the following:

1. U.S. Public Health Service,
2. ORNL Orientation Program,
3. MIT Practice School,
4. ORINS Radioisotope Techniques Course,
5. ORINS UT-AEC Military Veterinary Radiological Health Course.

PUBLICATIONS

H. H. Abee and D. M. Davis, *Use of Light Aircraft for Surveying for Radioactive Ground Contamination*, ORNL CF-58-5-98 (June 25, 1958).

S. I. Auerbach, "The Soil Ecosystem and Radioactive Waste Disposal to the Ground," *Ecology* **39**, 522–29 (1958).

S. I. Auerbach and D. A. Crossley, Jr., "Strontium-90 and Cesium-137 Uptake by Vegetation Under Natural Conditions," *Proc. U.N. Intern. Conf. Peaceful Uses Atomic Energy, 2nd, Geneva, 1958* **18**, 494 (1958).

J. A. Auxier, J. O. Buchanan, C. Eisenhauer, and H. E. Menker, *Experimental Evaluation of the Radiation Protection Afforded by Residential Structures Against Distributed Sources*, CEX-58.1 (Jan. 19, 1959).

R. D. Birkhoff, "Interpretation of Experiments Utilizing a Stopping Potential," *Bull. Am. Phys. Soc.* Ser. II, 3(4), 300 (1958).

R. D. Birkhoff and R. H. Ritchie, "Finite Source Consideration for the Spherical Condenser Spectrometer," *Bull. Am. Phys. Soc.* Ser. II, 3(3), 181 (1958).

F. N. Browder (ed.), H. H. Abee, K. E. Cowser, D. M. Davis, W. G. Stockdale, and E. J. Witkowski, *Radioactive Waste Management at Oak Ridge National Laboratory*, ORNL-2601 (Apr. 14, 1959).

K. E. Cowser, *Statistical Procedure for Grouping Jobs of Similar Difficulty*, Masters Thesis, University of Tennessee (June 1959).

K. E. Cowser and R. J. Morton, "Treatment Plant for Removal of Radioactive Contaminants from Process Waste Water, Part II: Evaluation of Performance," *J. Sanit. Engr. Div., Proc. Am. Soc. Civil Engrs.* SA **3**, 55–76 (1959).

K. E. Cowser, R. J. Morton, and E. J. Witkowski, "The Treatment of Large Volume, Low-Level Waste by the Lime-Soda Softening Process," *Proc. U.N. Intern. Conf. Peaceful Uses Atomic Energy, 2nd, Geneva, 1958* **18**, 161–73 (1958).

K. E. Cowser and F. L. Parker, "Soil Disposal of Radioactive Wastes at ORNL: Criteria and Techniques of Site Selection and Monitoring," *Health Phys.* **1**, 152–63 (1958).

D. M. Davis, *Personnel Monitoring Around a Reactor*, ORNL CF-58-5-40 (May 2, 1958).

D. M. Davis, J. C. Hart, and K. Z. Morgan, *Personnel Meters*, ORNL CF-58-12-39 (Jan. 2, 1959).

W. de Laguna, "What Is Safe Waste Disposal?" *Bull. Atomic Scientists* **15**, 35–43 (1959).

W. de Laguna, K. E. Cowser, and F. L. Parker, "Disposal of High Level Radioactive Liquid Wastes in Terrestrial Pits – A Sequel," *Proc. U.N. Intern. Conf. Peaceful Uses Atomic Energy, 2nd, Geneva, 1958* **18**, 101–15 (1958).

W. D. Dillow, J. A. Auxier, and R. D. Birkhoff, *A Study of Cavity Ionization as a Function of Atomic Number by Use of a Miniature Counter*, ORNL-2724 (June 3, 1959).

M. B. Edwards and B. R. Fish, *Particle Size Survey of Enriched Uranium Processing Facilities – Y-12 Plant*, ORNL CF-59-5-129 (May 1959).

F. M. Empson and I. R. Higgins, *Physical Characterization of Acidic and Neutralized Synthetic Fuel Reprocessing Waste Solutions on Evaporation and Calcination*, ORNL-2566 (Feb. 17, 1959).

B. R. Fish, "Applications of an Analog Computer to Analysis of Distribution and Excretion Data," *Health Phys.* **1**, 276–81 (1958).

E. R. Graham, "Uptake of Waste Sr^{90} and Cs^{137} by Soil and Vegetation," *Soil Sci.* **86**, 91–97 (1958).

G. S. Hurst and T. E. Bortner, "Negative Ions of Oxygen," *Radiation Research* Suppl. **1**, 547 (1959).

G. S. Hurst and T. E. Bortner, *Capture of Electrons in Molecular Oxygen,* ORNL-2670 (July 6, 1959).

G. S. Hurst and T. E. Bortner, "Attachment of Low Energy Electrons in Mixtures Containing Oxygen," *Phys. Rev.* **114**, 116 (1959).

T. A. Lincoln and E. D. Gupton, "Radiation Dose to Gonads from Diagnostic X-Ray Exposure," *J. Am. Med. Assoc.* **166**, 233 (1958).

K. Z. Morgan, "Current Status of Internal Dose Problem" *Health Phys.* **1**(2), 125–34 (1958).

K. Z. Morgan, "Programs of ORNL Health Physics Division Relating to Civil Defense," p 37–44 in *Proceedings of Conference on Research in Radiobiology and Radiation Medicine* (ed. by H. E. Cohen), Office of Civil and Defense Mobilization, Washington, Feb. 28, 1959.

K. Z. Morgan, "Health Physics," sec 7-2, 22-59, *Nuclear Engineering Handbook* (ed. by H. Etherington), McGraw-Hill, New York, 1958.

K. Z. Morgan, "Determination of Exposures," sec 14, *Radiation Hygiene Handbook* (H. Blatz, Editor-in-Chief), McGraw-Hill, New York, 1959.

K. Z. Morgan, "Health Physics," chap. V, *International Series of Monographs on Nuclear Energy* (R. A. Charpie and J. V. Dunworth, eds.), Pergamon, London, 1959.

K. Z. Morgan, "Waste Management Program at ORNL," testimony and formal statement before Special Subcommittee on Radiation of Joint Committee on Atomic Energy, Congress of United States, Eighty-Sixth Congress, Jan. 29, 1959, First Session, vol 1, p 428–53, Washington, D.C.

K. Z. Morgan, "Summary and Evaluation of Environmental Factors That Must Be Considered in the Disposal of Radioactive Waste," testimony and formal statement before Special Subcommittee on Radiation of Joint Committee on Atomic Energy, Congress of United States, Eighty-Sixth Congress, Feb. 2, 1959, First Session, vol 3, p 2372–93, Washington, D.C.

K. Z. Morgan, I. H. Tipton, and M. J. Cook, "Summary of Data Used in Revision of Internal Dose Recommendations of the International Commission on Radiological Protection," *Proc. U.N. Intern. Conf. Peaceful Uses Atomic Energy, 2nd, Geneva, 1958* **21**, 8–14 (1958).

R. J. Morton, "Consolidation for Strength," *Am. J. Public Health* **48**, 1571–77 (1958).

R. J. Morton, *Backflow Preventers for Cross-Connection Control at Oak Ridge National Laboratory,* ORNL CF-59-5-27 (May 7, 1959).

D. R. Nelson, R. D. Birkhoff, R. H. Ritchie, and H. H. Hubbell, Jr., *Measurement of Electron Flux in Media Bombarded by X-Rays,* ORNL-2521 (Oct. 13, 1958).

W. O. Olson, H. H. Hubbell, Jr., and R. D. Birkhoff, *A Study of Preacceleration in Beta-Ray Spectroscopy,* ORNL-2569 (Sept. 19, 1958).

F. L. Parker, L. Hemphill, and J. Crowell, *Status Report on Waste Disposal in Natural Salt Formations,* ORNL-2560 (Aug. 14, 1958).

F. L. Parker (ed.), W. J. Boegly, Jr., R. L. Bradshaw, J. Crowell, E. R. Eastwood, F. M. Empson, B. D. Gunter, L. Hemphill, O. H. Myers, and E. G. Struxness, *Status Report on Waste Disposal in Natural Salt Formations: II,* ORNL-2700 (Apr. 9, 1959).

R. H. Ritchie, "Interaction of Charged Particles with a Degenerate Fermi-Dirac Electron Gas," *Phys. Rev.* **114**, 644 (1959).

W. S. Snyder, "Calculation of Radiation Dose," *Health Phys.* **1**, 51 (1958).

E. G. Struxness and J. O. Blomeke, "Multipurpose Processing and Ultimate Disposal of Radioactive Wastes," *Proc. U.N. Intern. Conf. Peaceful Uses Atomic Energy, 2nd, Geneva, 1958* **18**, 43–55 (1958).

D. G. Thomas and J. V. Hilyer, *Detection of ThO_2 Contamination in Simulated Cuts and Abrasions,* ORNL CF-59-1-35 (Jan. 15, 1959).

J. C. Villforth, H. H. Hubbell, Jr., and R. D. Birkhoff, "Calibration of a Scintillation Spectrometer at Low Energies," *Bull. Am. Phys. Soc.* Ser. II, **3**(4), 303 (1958).

PAPERS

S. I. Auerbach

Fission Product Uptake by Trees in the Vicinity of ORNL Waste Pits, Health Physics Society, Fourth Annual Meeting, June 17–20, 1959, Gatlinburg, Tennessee.

R. D. Birkhoff

Dosimetry of Beta-Rays and Electrons, Ninth International Congress for Radiology, July 23–31, Munich, Germany.

R. D. Birkhoff, R. A. Finston, W. G. Stone, and H. H. Hubbell, Jr.

A-C Measurements of Electron Flux in Media Irradiated by X-Rays, Southeastern Section Meeting of the American Physical Society, April 9–11, 1959, New Orleans, Louisiana.

R. D. Birkhoff, F. Kalil, W. G. Stone, and H. H. Hubbell, Jr.

Measurement of Stopping Power by Calorimetric Methods, I. Calorimeter Design and Scattering Effects, Health Physics Society, Fourth Annual Meeting, June 17–20, 1959, Gatlinburg, Tennessee.

T. E. Bortner

An Improved Method for Measuring Electron Attachment, Health Physics Society, Fourth Annual Meeting, June 17–20, 1959, Gatlinburg, Tennessee.

K. E. Cowser and R. J. Morton

Radioactive Contaminant Removal from Process Waste Water: Evaluation of Performance, Annual Meeting of American Society of Civil Engineers, October 13–17, 1958, New York, New York.

Treatment of Large-Volume, Low Level Waste at ORNL, I. Design Features of Plant and Evaluation of Performance, Health Physics Society, Fourth Annual Meeting, June 17–20, 1959, Gatlinburg, Tennessee.

P. B. Dunaway

Field Studies on Mammals at Oak Ridge National Laboratory, Annual Meeting of the Society of Mammalogists, June 22–24, 1959, Washington, D.C.

B. R. Fish

Estimation of Body Burden and Internal Dose Based upon Urinary Uranium, and Urinalysis Summary, Symposium on Health Protection Criteria for Uranium Processing Operations, New York University Bellevue Medical Center, October 15–17, 1958, New York, New York.

Applied Research on Inhalation Problems in the ORNL Health Physics Division, Conference on Pulmonary Toxicology, June 15–16, 1959, Washington, D.C.

Applied Radiobiology Program on Uranium at Oak Ridge, Meeting of the U.S. Public Health Service Advisory Committee on Health Problems in the Uranium Mining and Milling Industry, July 21–22, 1959, Brighton, Utah.

B. R. Fish and G. R. Patterson

An Inhalation Exposure to U_3O_8, Fourth Annual Meeting of the Bioassay and Analytical Chemistry Group, November 3–4, 1958, Rochester, New York; also presented (by M. B. Edwards) at the American Industrial Hygiene Association Conference, April 25–May 1, 1959, Chicago, Illinois.

D. A. Gardiner and K. E. Cowser

Treatment of Large-Volume, Low-Level Waste at ORNL, II. An Application of Response Surface Methodology for Optimizing Treatment Efficiency, Health Physics Society, Fourth Annual Meeting, June 17–20, 1959, Gatlinburg, Tennessee.

J. M. Garner, Jr., and R. L. Bradshaw
Radiation Monitoring Utilizing Average Current from Halogen-Quenched G-M Tubes, Health Physics Society, Fourth Annual Meeting, June 17–20, 1959, Gatlinburg, Tennessee.

L. Hemphill, W. J. Boegly, Jr., R. L. Bradshaw, F. M. Empson, and F. L. Parker
Preliminary Studies of the Disposal of Radioactive Wastes in Natural Salt Formations, Health Physics Society, Fourth Annual Meeting, June 17–20, 1959, Gatlinburg, Tennessee.

H. H. Hubbell, Jr., R. A. Finston, and R. D. Birkhoff
Measurement of Electron Flux in Tissue-Like Media Bombarded by X-Rays, Health Physics Society, Fourth Annual Meeting, June 17–20, 1959, Gatlinburg, Tennessee.

H. H. Hubbell, Jr., W. O. Olson, and R. D. Birkhoff
Preacceleration in Beta-Ray Spectroscopy, Southeastern Section Meeting of the American Physical Society, April 9–11, 1959, New Orleans, Louisiana.

G. S. Hurst
Formation of Negative Ions of Oxygen, International Congress of Radiation Research, August 10–16, 1958, Burlington, Vermont.

Some Examples of Radiation Dosimetry Activities at the Oak Ridge National Laboratory Health Physics Division, Sixth Tripartite Instrumentation Conference, April 20–24, 1959, Chalk River, Canada.

"Sticky" Collisions as a Mechanism for Three-Body Stabilization of O_2^{-*}, Health Physics Society, Fourth Annual Meeting, June 17–20, 1959, Gatlinburg, Tennessee.

Mixed Dosimetry and Its Application in Determining the Dose Received by the Japanese at Hiroshima and Nagasaki, Ninth International Congress for Radiology, July 23–31, 1959, Munich, Germany.

G. S. Hurst and T. D. Strickler
Alpha Particle Ionization of Binary Gas Mixtures, Conference on the Penetration of Charged Particles in Matter, September 15–18, 1958, Gatlinburg, Tennessee.

D. G. Jacobs
The Desorption of Cesium from Conasauga Shale, the 135th National Meeting of the American Chemical Society, April 5–10, 1959, Boston, Massachusetts.

D. G. Jacobs and W. J. Lacy
Adsorption and Ion Exchange of Radioactive Waste Liquor by Shale, the 135th National Meeting of the American Chemical Society, April 5–10, 1959, Boston, Massachusetts.

Sorption of ORNL Intermediate-Level Wastes by Conasauga Shale, Health Physics Society, Fourth Annual Meeting, June 17–20, 1959, Gatlinburg, Tennessee.

R. M. Johnson, P. L. Ziemer, F. Kalil, and R. D. Birkhoff
Measurement of Stopping Power by Calorimetric Methods, II. Foil Preparation and Results for Al, Cu, and Au, Health Physics Society, Fourth Annual Meeting, June 17–20, 1959, Gatlinburg, Tennessee.

W. J. Lacy, F. M. Empson, and I. R. Higgins (presented by F. M. Empson)
Physical and Chemical Properties of Nuclear Power Reactor Waste Solutions, American Chemical Society, Southeastern Regional Meeting, University of Florida, December 11–13, 1958, Gainesville, Florida.

K. Z. Morgan

Maximum Permissible Exposure of the Population-at-Large to Sources of Ionizing Radiation, presented at hearing held before the Joint Committee on Atomic Energy, May 7, 1959, Washington, D.C.

Immediate Evaluation of Doses from External Radiation and from Internal Contaminations in the Event of a Radiation Accident, and *Some Problems in the Control of Criticality,* OEEC Symposium on Health Physics at Risø, Denmark, May 25–29, 1959.

Growth and Development of Health Physics and Responsibilities in the Field of Radiation Protection, Ninth International Congress of Radiology, July 24–30, 1959, Munich, Germany.

L. B. O'Kelly

Attachment of Electrons in O_2-CO_2 and O_2-CH_4 Mixtures, Health Physics Society, Fourth Annual Meeting, June 17–20, 1959, Gatlinburg, Tennessee.

F. L. Parker

Dispersion in the Hydrosphere, U.S. Public Health Service, Conference on Radionuclide Disposal to the Hydrosphere, Robert A. Taft Sanitary Engineering Center, February 5–6, 1959, Cincinnati, Ohio.

Dispersal of Radiocontaminants in Streams, Health Physics Society, Fourth Annual Meeting, June 17–20, 1959, Gatlinburg, Tennessee.

F. L. Parker, L. Hemphill, and W. J. Boegly, Jr.

Statement on the Disposal of Radioactive Wastes in Salt Formations, presented before the Committee on Waste Disposal of the Division of Earth Sciences of the National Academy of Sciences, National Research Council, October 13, 1958, Washington, D.C.

R. H. Ritchie

Dosimetry of the Y-12 Accident, Health Physics Society, Fourth Annual Meeting, June 17–20, 1959, Gatlinburg, Tennessee.

W. S. Snyder

Interspecies Correlations of Published Uranium Data, Symposium on Health Protection Criteria for Uranium Processing Operations, October 15–17, 1958, New York, New York.

The Scientific Basis for the Permissible Levels of Internal Contamination, OEEC Symposium on Health Physics, May 25–29, 1959, Risø, Denmark.

W. S. Snyder and J. Neufeld

On the Stopping Power of Ions in Tissue, Health Physics Society, Fourth Annual Meeting, June 17–20, 1959, Gatlinburg, Tennessee.

W. T. Thornton and J. A. Auxier

Silver Phosphate Glass Dosimetry: Fluorescence Method, Health Physics Society, Fourth Annual Meeting, June 17–20, 1959, Gatlinburg, Tennessee.

T. Tamura

Structural Implications in Cesium Sorption, Health Physics Society, Fourth Annual Meeting, June 17–20, 1959, Gatlinburg, Tennessee.

Treatment of High Level Waste By Sintering, Meeting on Waste Disposal, Brookhaven National Laboratory, January 8–9, 1959, Upton, Long Island, New York.

W. K. Willard

Avian Uptake of Fission Products, Association of Southeastern Biologists Meeting, April 16–18, 1959, Knoxville, Tennessee.

LECTURES

E. E. Anderson

Hospital Health Physics Practices, U. S. Naval Medical Center, September 24, 1958, and April 17, 1959, Bethesda, Maryland.

Opportunities in Health Physics, Health Physics Society Chapter, September 30, 1958, Aiken, South Carolina.

Critical Manpower Shortage, Regional Symposia, October 30–31, 1958, Idaho Falls, Idaho; Brookhaven National Laboratory, November 4–5, 1958, Upton, L. I., New York.

Radiation Hazards and Current Practices in Radiation Protection, Vanderbilt University, February 10, 1959, Nashville, Tennessee; Marion Institute, February 19, 1959, Marion, Alabama; Alabama Polytechnic Institute, February 20, 1959, Auburn, Alabama; Bethany College, March 17, 1959 Bethany, West Virginia; George Washington University, March 20, 1959, Washington, D. C.; The A & T College of North Carolina, April 8, 1959, Greensboro, North Carolina; Flora MacDonald College, April 9, 1959, Red Springs, North Carolina; University of Florida, April 14, 1959, Gainesville, Florida; Florida Southern College, April 15, 1959, Lakeland, Florida; Memphis State University, April 20, 1959, Memphis, Tennessee; Oklahoma State University, April 22, 1959. Stillwater, Oklahoma; University of Arkansas, April 24, 1959, Fayetteville, Arkansas; Iowa State Teachers College, May 11–12, 1959, Cedar Falls, Iowa; University of Chattanooga, June 24, 1959, Chattanooga, Tennessee; University of Wyoming, July 9–10, 1959, Laramie, Wyoming (four lectures); Brigham Young University, July 13–14, 1959, Provo, Utah (three lectures); Purdue University, July 23–24, 1959, Lafayette, Indiana (four lectures); Tuskegee Institute, July 29, 1959, Tuskegee Institute, Alabama.

Fundamental Principles of Health Physics, ORINS, February 27, 1959, Oak Ridge, Tennessee.

Certification of Health Physicists, Baltimore-Washington Health Physics Society Chapter, March 18, 1959, Washington, D. C.

Maximum Permissible Exposures, Medical College of Virginia, March 19, 1959, Richmond, Virginia.

S. I. Auerbach

Ecology and Radiation Ecology, ORSORT students, May 19, 1959, ORNL, and Health Physics Radiological Physics Course, ORNL, June 1959, Oak Ridge, Tennessee.

Ecological Studies in Radioactive Waste Areas, Botany Department, Duke University, December 3, 1958, Durham, North Carolina; Biology, Chemistry, and Physics Departments, Bethany College, February 3, 1959, Bethany, West Virginia; Biology Department, University of Louisville, February 11, 1959, Louisville, Kentucky; Biology Department, Florida Southern College, March 18, 1959, Lakeland, Florida; Biology Department, Florida State University, March 19, 1959, Tallahassee, Florida; Biology Department, Southern University, March 20, 1959, Baton Rouge, Louisiana; Beta Beta Beta Biological Society, Howard College, March 24, 1959, Birmingham, Alabama.

W. J. Boegly

Exposures to Ionizing Radiations and Their Control, College of Education, University of Tennessee, May 25 and July 14, 1959, Knoxville, Tennessee.

K. E. Cowser

Waste Handling, Treatment, and Disposal at ORNL, Oak Ridge Institute of Nuclear Studies, Veterinary Radiological Health Course, October 1, 1958, Oak Ridge Tennessee; and U.S. Public Health Service Course on Environmental Health Aspects of Nuclear Reactor Operations, March 24, 1959, Oak Ridge, Tennessee.

Process Waste Water Treatment, Health Physics Course for ORSORT foreign students, April 17, 1959, Oak Ridge, Tennessee.

ORNL Waste Pits and Burial Grounds, Health Physics Course for ORSORT foreign students, May 5, 1959, Oak Ridge, Tennessee.

D. A. Crossley, Jr.

Research in Insect Ecology at Oak Ridge National Laboratory, Biology Department, Texas Technological College, December 11–12, 1958, Lubbock, Texas.

L. C. Emerson

Health Physics, series of lectures in Third International Course in Health Physics, Atomic Energy Establishment Trombay, November 17–December 19, 1958, Bombay, India.

Reactor Safety, Vanderbilt University, May 11–12, 1959, Nashville, Tennessee.

Waste Disposal, Vanderbilt University, May 18–19, 1959, Nashville, Tennessee.

F. M. Empson

Tank Disposal and Calcination of Reactor Fuel Reprocessing Wastes, Health Physics Course for ORSORT foreign students, April 21, 1959, Oak Ridge, Tennessee.

M. F. Fair

Radiation Hazards, Lenoir City Civitan Club, September 16, 1958, Lenoir City, Tennessee; Oak Ridge Institute of Nuclear Studies Medical School, September 22, 1958, and April 30, 1959; Oak Ridge, Tennessee; Bell Telephone Company, September 26, 1958, Oak Ridge, Tennessee; Oak Ridge High School, November 10, 1958, Oak Ridge, Tennessee; Lenoir City High School, December 4, 1958, Lenoir City, Tennessee; Lenoir City Civic Clubs, February 19, 1959, Lenoir City, Tennessee; Vanderbilt Medical School, April 13, 1959, Nashville, Tennessee.

Health Physics, MIT students, September 17, 1958, Oak Ridge, Tennessee.

Principles of Health Physics, Oak Ridge Institute of Nuclear Studies, Oak Ridge, Tennessee; September 18 and October 2, 1958; January 14, February 20, April 16, and May 6, 1959.

L. Hemphill

Nature and Composition of Chemical Processing Wastes, U.S. Public Health Service Course on Environmental Health Aspects of Nuclear Reactor Operations, March 24, 1959, Oak Ridge, Tennessee; and National Science Foundation Summer Institute, North Texas State College, June 12, 1959, Denton, Texas.

D. G. Jacobs

Geochemical Research in Waste Disposal, Sanitary Engineering Seminar, Harvard University, April 6, 1959, Cambridge, Massachusetts.

Ion Exchange in Soil, Health Physics Course for ORSORT foreign students, April 24, 1959, Oak Ridge, Tennessee.

K. Z. Morgan

Dosimetry of Y-12 Accident, Conference for AEC Industrial Physicians, Oak Ridge Institute of Nuclear Studies, August 25, 1958, Oak Ridge, Tennessee.

Windscale Accident, Local "Hams," September 23, 1958, Oak Ridge, Tennessee.

The Control of Radiation by the Health Physicist, E.P.A. Mission on Protection of Workers Against Radiation Hazards, ORNL, September 24, 1958, Oak Ridge, Tennessee.

Criticality Accident at the Oak Ridge Y-12 Plant on June 17, 1958, Advisory Committee for Biology and Medicine, October 17–18, 1958, Germantown, West Virginia.

History and Development of Radiation Protection, Eurochemic Group, ORNL, October 23, 1958, Oak Ridge, Tennessee.

Dosimetry of June Criticality Accident at Y-12, AEC Industrial Physicians, Health Physicists, and Industrial Hygienists, October 29, 1958, Cincinnati, Ohio.

Emergency Permissible Levels, A Discussion, Analytical Chemistry Group, November 3, 1958, Rochester, New York.

Remarks on Exposure Evaluation, United Kingdom Team Meeting for Discussions on Criticality, November 12–14, 1958, Oak Ridge, Tennessee.

Programs of ORNL Health Physics Division Relating to Civil Defense, Conference on Research Activities in Radiobiology and Radiation Medicine, OCD, December 1–2, 1958, Washington, D.C.

Health Physics Tenth Annual Nuclear Sciences Seminar, U.S. Naval Reserve, Oak Ridge Institute of Nuclear Studies, December 4, 1958, Oak Ridge Tennessee; National Science Foundation Students, June 25, 1959, Vanderbilt University, Nashville, Tennessee.

New Levels of Maximum Permissible Exposure to Ionizing Radiation, Chemical Technology Seminar, January 20, 1959, Oak Ridge, Tennessee.

Internal Dose, Nuclear Training Short Course, April 16–17, 1959, North Carolina State College, Raleigh, North Carolina; AEC Fellowship students, April 27–28, May 4–5, 1959, Vanderbilt University, Nashville, Tennessee; Health Physics Course for ORSORT foreign students, May 12, 15, 1959, Oak Ridge, Tennessee; AEC Inspection Meeting, Radiation Hazards, June 15, 1959, Oak Ridge, Tennessee.

The Criteria Imposed on Instrumentation by the MPE and MPC Levels, ORNL, Discussion of Health Physics Instrumentation, June 24, 1959, Oak Ridge, Tennessee.

R. J. Morton

Radioactive Waste Disposal at ORNL, Conference Session, Japanese Radioisotope Industrial Use Study Team, ORNL, August 15, 1958, Oak Ridge, Tennessee.

Waste Management Facilities at ORNL (field tour and lecture), U.S. Public Health Service Course on Environmental Health Aspects of Reactor Operations, ORNL, August 31, 1958, and March 24, 1959, Oak Ridge, Tennessee.

Low- and Intermediate-Level Radioactive Wastes, Conference Session, Mission on Protection of Workers Against Radiation Hazards, European Productivity Agency, ORNL, September 24, 1958, Oak Ridge, Tennessee.

Treatment and Disposal of Low-Level Radioactive Waste, ORSORT students, ORNL, January 6, 1959, Oak Ridge, Tennessee.

J. S. Olson

Sand Dunes and the Idea of Ecological Succession, University of Tennessee, Botany Department Seminar, February 12, 1959, Knoxville, Tennessee.

Random and Contagious Spatial Distributions of Organisms, with an Example of Monte Carlo Study of Colony Growth, Statistics Seminar, ORNL, April 21, 1959, Oak Ridge, Tennessee.

F. L. Parker

Hydraulic Studies Using Radiotracers, U.S. Public Health Service Course on Radioactive Pollutants in Water, November 17–21, 1958, Cincinnati, Ohio.

Environmental Surveillance, U.S. Public Health Service Course on Environmental Health Aspects of Nuclear Reactor Operation, ORNL, March 24, 1959, Oak Ridge, Tennessee.

Disposal into Salt, Health Physics Course for ORSORT foreign students, ORNL, April 29, 1959, Oak Ridge, Tennessee.

E. G. Struxness

Recent Developments in Waste Disposal, Annual Meeting of the Tennessee Academy of Science, December 5, 1958, Oak Ridge, Tennessee.

Summary of ORNL Waste Research Program, Health Physics Course for ORSORT foreign students, ORNL, May 4, 1959, Oak Ridge, Tennessee.

T. Tamura

Structural Implications in Ion Exchange, University of Wisconsin, Soils Department, June 5, 1959, Madison, Wisconsin.

Disposal Using Clay Minerals, Health Physics Course for ORSORT foreign students, May 1, 1959, Oak Ridge, Tennessee.

INTERNAL DISTRIBUTION

1. C. E. Center
2. Biology Library
3. Health Physics Library
4–6. Central Research Library
7. Reactor Experimental Engineering Library
8–24. Laboratory Records Department
25. Laboratory Records, ORNL R.C.
26. L. B. Emlet (K-25)
27. J. P. Murray (Y-12)
28. A. M. Weinberg
29. J. A. Swartout
30. E. D. Shipley
31. K. Z. Morgan
32. M. L. Nelson
33. C. P. Keim
34. S. C. Lind
35. A. S. Householder
36. C. S. Harrill
37. C. E. Winters
38. A. H. Snell
39. E. H. Taylor
40. W. H. Jordan
41. T. A. Lincoln
42. A. Hollaender
43. F. L. Culler
44. H. E. Seagren
45. D. Phillips
46. M. T. Kelley
47. E. E. Anderson
48. R. S. Livingston
49. R. A. Charpie
50. K. E. Cowser
51. C. D. Susano
52. L. B. Farabee
53. F. J. Davis
54. R. J. Morton
55. C. E. Haynes
56. Hugh F. Henry (K-25)
57. E. G. Struxness
58. W. E. Cohn
59. H. H. Hubbell
60. D. E. Arthur
61. J. Neufeld
62. M. L. Randolph
63. P. M. Reyling
64. G. C. Williams
65. M. J. Skinner
66. J. C. Hart
67. T. H. J. Burnett
68. W. J. Lacy
69. M. J. Cook
70. G. S. Hurst
71. T. E. Bortner
72. J. A. Lane
73. W. S. Snyder
74. L. Hemphill
75. L. B. Holland
76. J. L. Gabbard
77. G. Jacobs
78. R. L. Bradshaw
79. A. C. Upton
80. L. C. Emerson (Y-12)
81. D. M. Davis
82. P. E. Brown
83. E. D. Gupton
84. J. C. Ledbetter
85. R. L. Clark
86. G. C. Cain
87. L. C. Johnson
88. W. Ogg
89. O. D. Teague
90. E. L. Sharp
91. E. J. Kuna
92. H. H. Abee
93. C. R. Guinn
94. A. D. Warden
95. E. B. Wagner
96. D. A. Crossley, Jr.
97. J. R. Muir
98. J. A. Auxier
99. M. F. Fair
100. S. I. Auerbach
101. G. W. Royster, Jr.
102. R. R. Dickison
103. J. D. McLendon
104. F. W. Sanders
105. F. C. Maienschein
106. W. J. Boegly, Jr.
107. F. L. Parker
108. W. E. Lotz
109. B. Fish
110. M. B. Edwards

111. F. M. Empson
112. R. D. Birkhoff
113. R. H. Ritchie
114. J. A. Harter
115. W. G. Stone
116. J. S. Cheka
117. P. N. Hensley
118. R. W. Peelle
119. P. B. Dunaway
120. T. Tamura
121. J. S. Olson
122. J. C. Frye (consultant)
123. W. H. Langham (consultant)
124. A. Wolman (consultant)
125. R. E. Zirkle (consultant)
126. L. S. Taylor (consultant)
127. R. L. Platzman (consultant)
128. ORNL – Y-12 Technical Library, Document Reference Section

EXTERNAL DISTRIBUTION

129. C. P. Straub, Public Health Service, Robert A. Taft Sanitary Engineering Center
130. R. M. Collier, University of Florida
131. Physics and Engineering Group, Balcones Research Center, RFD 4, Box 189, Austin, Texas
132. G. E. Thoma, St. Louis University Hospital, 135 South Grand Boulevard, St. Louis, Missouri
133. H. J. McAlduff, AEC, Oak Ridge
134. Vanderbilt University (Physics Library)
135. Massachusetts Institute of Technology (Department of Electrical Engineering)
136. University of California (Gerhard Klein)
137. R. M. Richardson, U.S. Geological Survey, 2-C P. O. Building, Knoxville, Tennessee
138. C. V. Theis, U.S. Geological Survey, Box 433, Albuquerque, New Mexico
139. Lola Lyons, Librarian, Olin Industries, Inc., East Alton, Illinois
140. Jack Story, Health Physicist, North Carolina State College, Raleigh, North Carolina
141. J. H. Ebersole, USSS Nautilus, c/o Fleet Post Office, New York, New York
142. David S. Smith, Health and Safety Division, U.S. Atomic Energy Commission, Chicago Operations Office, P. O. Box 59, Lemont, Illinois
143. Division of Research and Development, AEC, ORO
144. S. C. Sigoloff, Edgerton, Germeshausen and Grier, Inc., P. O. Box 1912, Las Vegas, Nevada
145. Robert Wood, Department of Physics, Memorial Center, 444 E. 68th St., New York 21, New York
146. Robert E. Yoder, Harvard School of Public Health, 55 Shattuck Street, Boston, Massachusetts
147. John Wolfe, Division of Biology and Medicine, U.S. Atomic Energy Commission, Washington, D.C.
148. Orlando Park, Department of Biology, Northwestern University, Evanston, Illinois
149. Eugene Odum, Department of Zoology, University of Georgia, Athens, Georgia
150. W. T. Ham, Medical College of Virginia, Richmond, Virginia
151. F. H. W. Noll, Department of Physics, Berea College, Berea, Kentucky
152. S. R. Bernard, Committee on Mathematical Biology, University of Chicago, 5741 Drexel Avenue, Chicago 37, Illinois
153. Herbert E. Stokinger, Bureau of State Service, Department of Health Education and Welfare, Penn 14 Broadway, Cincinnati 2, Ohio
154. J. B. Lackey, University of Florida, Gainesville, Florida
155. J. J. Davis, Biology Operation, Hanford Atomic Power Operations, Seattle, Washington
156. Royal Shanks, Department of Botany, University of Tennessee, Knoxville, Tennessee
157. Robert B. Platt, Department of Biology, Emory University, Atlanta, Georgia
158. C. H. Bernard, Physics Department, Texas A&M College, College Station, Texas
159. H. M. Borella, Edgerton, Germeshausen and Grier, Inc., P. O. Box 1912, Las Vegas, Nevada
160. D. R. Nelson, St. John's University, Collegeville, Minn.
161. J. S. Mendell, Rensselaer Polytechnic Institute, Troy, N. Y.
162. H. P. Yockey, Aerojet-General Nucleonics, San Ramon, Calif.
163. C. E. Dady, Watertown Arsenal, Ordnance Material Research Office, Watertown, Mass.
164–794. Given distribution as shown in TID-4500 (15th ed.) under Health and Safety category (100 copies – OTS)